

Many-Body Methods in Chemistry and Physics

MBPT and Coupled-Cluster Theory

Isaiah Shavitt and Rodney J. Bartlett



CAMBRIDGE

This page intentionally left blank

MANY-BODY METHODS IN CHEMISTRY AND PHYSICS

Written by two leading experts in the field, this book explores the many-body methods that have become the dominant approach in determining molecular structure, properties, and interactions. With a tight focus on the highly popular many-body perturbation theory (MBPT) and coupled-cluster (CC) methods, the authors present a simple, clear, unified approach to describe the mathematical tools and diagrammatic techniques employed. Using this book the reader will be able to understand, derive, and confidently implement the relevant algebraic equations for current and even new CC methods. Hundreds of diagrams throughout the book enhance reader understanding through visualization of computational procedures, and the extensive referencing and detailed index allow further exploration of this evolving area. This book provides a comprehensive treatment of the subject for graduates and researchers within quantum chemistry, chemical physics and nuclear, atomic, molecular, and solid-state physics.

ISAIAH SHAVITT, Emeritus Professor of Ohio State University and Adjunct Professor of Chemistry at the University of Illinois at Urbana-Champaign, developed efficient methods for multireference configuration-interaction calculations, including the graphical unitary-group approach (GUGA), and perturbation-theory extensions of such treatments. He is a member of the International Academy of Quantum Molecular Science and a Fellow of the American Physical Society, and was awarded the Morley Medal of the American Chemical Society (2000).

RODNEY J. BARTLETT, Graduate Research Professor at the Quantum Theory Project, University of Florida, pioneered the development of CC theory in quantum chemistry to offer highly accurate solutions of the Schrödinger equation for molecular structure and spectra. He is a member of the International Academy of Quantum Molecular Sciences and a Fellow of the American Physical Society (1986). He was awarded a Guggenheim Fellowship (1986), the ACS Award in Theoretical Chemistry (2007) and the Schrödinger Medal of WATOC (2008).

Cambridge Molecular Science

As we enter the twenty-first century, chemistry has positioned itself as the central science. Its subject matter, atoms and the bonds between them, is now central to so many of the life sciences on the one hand, as biological chemistry brings the subject to the atomic level, and to condensed matter and molecular physics on the other. Developments in quantum chemistry and in statistical mechanics have also created a fruitful overlap with mathematics and theoretical physics. Consequently, boundaries between chemistry and other traditional sciences are fading and the term *molecular science* now describes this vibrant area of research.

Molecular science has made giant strides in recent years. Bolstered both by instrumental and theoretical developments, it covers the temporal scale down to femtoseconds, a time scale sufficient to define atomic dynamics with precision, and the spatial scale down to a small fraction of an Ångström. This has led to a very sophisticated level of understanding of the properties of small-molecule systems, but there has also been a remarkable series of developments in more complex systems. These include: protein engineering; surfaces and interfaces; polymers colloids; and biophysical chemistry. This series provides a vehicle for the publication of advanced textbooks and monographs introducing and reviewing these exciting developments.

Series editors

Professor Richard Saykally
University of California, Berkeley

Professor Ahmed Zewail
California Institute of Technology

Professor David King
University of Cambridge

MANY-BODY METHODS
IN CHEMISTRY
AND PHYSICS

MBPT and Coupled-Cluster Theory

ISAIAH SHAVITT

*Professor Emeritus
The Ohio State University
and
Adjunct Professor of Chemistry
University of Illinois at Urbana-Champaign*

and

RODNEY J. BARTLETT

*Graduate Research Professor of Chemistry and Physics
University of Florida*



CAMBRIDGE
UNIVERSITY PRESS

CAMBRIDGE UNIVERSITY PRESS
Cambridge, New York, Melbourne, Madrid, Cape Town, Singapore,
São Paulo, Delhi, Dubai, Tokyo

Cambridge University Press
The Edinburgh Building, Cambridge CB2 8RU, UK

Published in the United States of America by Cambridge University Press, New York

www.cambridge.org

Information on this title: www.cambridge.org/9780521818322

© I. Shavitt and R. J. Bartlett 2009

This publication is in copyright. Subject to statutory exception and to the provision of relevant collective licensing agreements, no reproduction of any part may take place without the written permission of Cambridge University Press.

First published in print format 2009

ISBN-13 978-0-511-59643-8 eBook (NetLibrary)

ISBN-13 978-0-521-81832-2 Hardback

Cambridge University Press has no responsibility for the persistence or accuracy of urls for external or third-party internet websites referred to in this publication, and does not guarantee that any content on such websites is, or will remain, accurate or appropriate.

To Vera and Beverly

Contents

<i>Preface</i>	<i>page</i> xi
1 Introduction	1
1.1 Scope	1
1.2 Conventions and notation	2
1.3 The independent-particle approximation	3
1.4 Electron correlation	7
1.5 Configuration interaction	9
1.6 Motivation	10
1.7 Extensivity	11
1.8 Disconnected clusters and extensivity	15
2 Formal perturbation theory	18
2.1 Background	18
2.2 Classical derivation of Rayleigh–Schrödinger perturbation theory	18
2.3 Projection operators	27
2.4 General derivation of formal time-independent perturbation theories	29
2.5 Similarity transformation derivation of the formal perturbation equations and quasidegenerate PT	46
2.6 Other approaches	53
3 Second quantization	54
3.1 Background	54
3.2 Creation and annihilation operators	55
3.3 Normal products and Wick’s theorem	67
3.4 Particle–hole formulation	71
3.5 Partitioning of the Hamiltonian	75

3.6	Normal-product form of the quantum-mechanical operators	80
3.7	Generalized time-independent Wick's theorem	85
3.8	Evaluation of matrix elements	86
4	Diagrammatic notation	90
4.1	Time ordering	90
4.2	Slater determinants	91
4.3	One-particle operators	92
4.4	Two-particle operators	111
5	Diagrammatic expansions for perturbation theory	130
5.1	Resolvent operator and denominators	130
5.2	First-order energy	131
5.3	Second-order energy	131
5.4	Third-order energy	132
5.5	Conjugate diagrams	134
5.6	Wave-function diagrams	135
5.7	Fourth-order energy	138
5.8	Linked-diagram theorem	152
5.9	Numerical example	153
5.10	Unlinked diagrams and extensivity	156
6	Proof of the linked-diagram theorem	165
6.1	The factorization theorem	165
6.2	The linked-diagram theorem	172
7	Computational aspects of MBPT	177
7.1	Techniques of diagram summation	177
7.2	Factorization of fourth-order quadruple-excitation diagrams	180
7.3	Spin summations	182
8	Open-shell and quasidegenerate perturbation theory	185
8.1	Formal quasidegenerate perturbation theory (QDPT)	185
8.2	The Fermi vacuum and the model states	192
8.3	Normal-product form of the generalized Bloch equations	194
8.4	Diagrammatic notation for QDPT	195
8.5	Schematic representation of the generalized Bloch equation	198
8.6	Level-shift and wave-operator diagrams	203
8.7	Incomplete model space	227
9	Foundations of coupled-cluster theory	251
9.1	Coupled-cluster theory for noninteracting He atoms	251
9.2	The coupled-cluster wave function	254

9.3	The coupled-cluster doubles (CCD) equations	258
9.4	Exponential <i>Ansatz</i> and the linked-diagram theorem of MBPT	272
9.5	Diagrammatic derivation of the CCD equations	279
10	Systematic derivation of the coupled-cluster equations	292
10.1	The connected form of the CC equations	292
10.2	The general form of CC diagrams	295
10.3	Systematic generation of CC diagrams	297
10.4	The coupled-cluster singles and doubles (CCSD) equations	299
10.5	Coupled-cluster singles, doubles and triples (CCSDT) equations	308
10.6	Coupled-cluster singles, doubles, triples and quadruples (CCSDTQ) equations	321
10.7	Coupled-cluster effective-Hamiltonian diagrams	328
10.8	Results of various CC methods compared with full CI	340
11	Calculation of properties in coupled-cluster theory	347
11.1	Expectation value for a CC wave function	347
11.2	Reduced density matrices	352
11.3	The response treatment of properties	361
11.4	The CC energy functional	366
11.5	The Λ equations	367
11.6	Effective-Hamiltonian form of the Λ equations	376
11.7	Response treatment of the density matrices	381
11.8	The perturbed reference function	385
11.9	The CC correlation-energy derivative	396
12	Additional aspects of coupled-cluster theory	406
12.1	Spin summations and computational considerations	406
12.2	Coupled-cluster theory with an arbitrary single-determinant reference function	411
12.3	Generalized many-body perturbation theory	415
12.4	Brueckner orbitals and alternative treatments of \hat{T}_1	418
12.5	Monitoring multiplicities in open-shell coupled-cluster calculations	422
12.6	The A and B response matrices from the viewpoint of CCS	425
12.7	Noniterative approximations based on the CC energy functional	427
12.8	The nature of the solutions of CC equations	429
13	The equation-of-motion coupled-cluster method for excited, ionized and electron-attached states	431
13.1	Introduction	431

13.2	The EOM-CC <i>Ansatz</i>	432
13.3	Diagrammatic treatment of the EE-EOM-CC equations	437
13.4	EOM-CC treatment of ionization and electron attachment	445
13.5	EOM-CC treatment of higher-order properties	449
13.6	EOM-CC treatment of frequency-dependent properties	454
14	Multireference coupled-cluster methods	462
14.1	Introduction	462
14.2	Hilbert-space state-universal MRCC	465
14.3	Hilbert-space state-specific MRCC	471
14.4	Fock-space valence-universal MRCC	475
14.5	Intermediate-Hamiltonian Fock-space MRCC	490
	<i>References</i>	496
	<i>Author index</i>	521
	<i>Subject index</i>	524

Preface

“What are the electrons really doing in molecules?” This famous question was posed by R. A. Mulliken over a half-century ago. Accurate quantitative answers to this question would allow us, in principle, to know all there is to know about the properties and interactions of molecules. Achieving this goal, however, requires a very accurate solution of the quantum-mechanical equations, primarily the Schrödinger equation, a task that was not possible for most of the past half-century. This situation has now changed, primarily due to the development of numerically accurate many-body methods and the emergence of powerful supercomputers.

Today it is well known that the many-body instantaneous interactions of the electrons in molecules tend to keep electrons apart; this is manifested as a correlation of their motions. Hence a correct description of *electron correlation* has been the focal point of atomic, molecular and solid state theory for over 50 years. In the last two decades the most prominent methods for providing accurate quantum chemical wave functions and using them to describe molecular structure and spectra are *many-body perturbation theory* (MBPT) and its *coupled-cluster* (CC) generalizations. These approaches have become the methods of choice in quantum chemistry, owing to their accuracy and their correct scaling with the number of electrons, a property known as *extensivity* (or *size-extensivity*). This property distinguishes *many-body* methods from the configuration-interaction (CI) tools that have commonly been used for many years. However, maintaining extensivity – a critical rationale for all such methods – requires many-body methods that employ quite different mathematical tools for their development than those that have been customary in quantum chemistry. In particular, diagrammatic techniques are found to be extremely powerful, offering a unified, transparent and precise approach to the derivation and implementation of the relevant algebraic equations. For many readers, however, diagrammatic

methods have seemed to be used arbitrarily, making it difficult to understand with confidence the detailed one-to-one correspondence between the diagrams and the various terms of the operable algebraic equations.

In order to address this situation, this book presents a unified, detailed account of the highly popular MBPT and CC quantum mechanical methods. It introduces direct, completely unambiguous procedures to derive all the relevant algebraic equations diagrammatically, in one simple, easily applied and unified approach. The ambiguity associated with some diagrammatic approaches is completely eliminated. Furthermore, in order for a quantum-chemical approach to be able to describe molecular structure, excited states and properties derived from expectation values and from response methods, new theory has had to be developed. This book also addresses the theory for each of these topics, including the *equation-of-motion CC (EOM-CC)* method for excited, ionized and electron attached states as well as the *analytical gradient* theory for determining structure, vibrational spectra and density matrices. Finally, the recent developments in multireference approaches, *quasidegenerate perturbation theory (QDPT)* and *multireference CC (MRCC)*, are also presented. All these equations are readily developed from the same simple diagrammatic arguments used throughout the book. With a modest investment of time and effort, this book will teach anyone to understand and confidently derive the relevant algebraic equations for current CC methods and even the new CC methods that are being introduced regularly. Selected numerical illustrations are also presented to assess the performance of the various approximations to MBPT and CC.

This book is directed at graduate students in quantum chemistry, chemical physics, physical chemistry and atomic, molecular, solid-state and nuclear physics. It can serve as a textbook for a two-semester course on many-body methods for electronic structure and as a useful resource for university faculty and professional scientists. For this purpose, an extensive bibliography and a detailed index are included. Useful introductory material for the book, including detailed treatments of self-consistent field theory and configuration interaction, can be found in parts of the book by Szabo and Ostlund (1982). Additional useful sources include, among others, the monograph by Lindgren and Morrison (1986), which emphasizes atomic structure and includes the treatment of angular momentum and spin coupling, and the book focusing on diagrammatic many-body methods by Harris, Monkhorst and Freeman (1992). An interesting historical account of the development of coupled-cluster theory was provided by Paldus (2005), whose unpublished (but widely distributed) Nijmegen lectures introduced many researchers to this methodology.

Many colleagues, students and others have helped us in various ways during the writing of this book. In particular we would like to thank the following: Erik Deumens, Jürgen Gauss, Tom Hughes, Joshua McClellan, Monika Musiał, Marcel Nooijen, Josef Paldus, Steven Parker, Ajith Perera, John Stanton, Peter Szalay, Andrew Taube and John Watts.

The graphics in this book were generated in LaTeX, using the package *pstricks* 97. We are grateful to its author, Timothy van Zandt, and editors, Denis Girou and Sebastian Rahtz, for providing such a versatile graphics facility.

1

Introduction

1.1 Scope

The book focuses primarily on many-body (or better, many-electron) methods for electron correlation. These include *Rayleigh–Schrödinger perturbation theory (RSPT)*, particularly in its diagrammatic representation (referred to as *many-body perturbation theory*, or *MBPT*), and *coupled-cluster (CC)* theory; their relationship to *configuration interaction (CI)* is included. Further extensions address properties other than the energy, and also excited states and multireference CC and MBPT methods.

The many-body algebraic and diagrammatic methods used in electronic structure theory have their origin in quantum field theory and in the study of nuclear matter and nuclear structure. The second-quantization formalism was first introduced in a treatment of quantized fields by Dirac (1927) and was extended to fermion systems by Jordan and Klein (1927) and by Jordan and Wigner (1928). This formalism is particularly useful in field theory, in scattering problems and in the study of infinite systems because it easily handles problems involving infinite, indefinite or variable numbers of particles. The diagrammatic approach was introduced into field theory by Feynman (1949a,b) and applied to many-body systems by Hugenholtz (1957) and by Goldstone (1957). Many-body perturbation theory and its linked-diagram formalism were first introduced by Brueckner and Levinson (1955) and by Brueckner (1955), and were formalized by Goldstone (1957). Other important contributions to the methodology, first in field theory and then in the theory of nuclear structure, are due to Dyson (1949a,b), Wick (1950), Hubbard (1957, 1958a,b) and Frantz and Mills (1960). Applications to the electronic structure of atoms and molecules began with the work of Kelly (1963, 1964a,b, 1968), and molecular applications using finite analytical basis sets appeared in the work of Bartlett and Silver (1974a,b).

More complete accounts of the history of these methods have been given by Lindgren and Morrison (1986) and by Lindgren (1998).

The coupled-cluster method also has origins in nuclear structure theory, with the seminal papers of Coester (1958) and Coester and Kümmel (1960). It was introduced to electronic structure theory and formalized by Čížek (1966, 1969) and Čížek and Paldus (1971). A historical account of its origins and development was given by Paldus (2005).

Additional references to the development and extensions of the many-body methods are given in the relevant chapters.

The rest of this chapter provides some background material, including a brief discussion of the independent-particle model and the configuration-interaction method. We discuss the limitations of these methods and the need for the perturbation-theoretical and many-body methods that form the subject of the rest of this book. We also provide a preliminary introduction to the cluster ideas that form the basis of coupled-cluster theory. Readers in need of a more extensive introduction are referred to the excellent book by Szabo and Ostlund (1982).

A detailed exposition of formal perturbation theory is given in Chapter 2. A number of different derivations and approaches are included in this exposition in order to provide a broad foundation for the terminology and techniques employed in this field. The many-body technique of second quantization is introduced in Chapter 3, and the diagrammatic representation is described in Chapter 4. The application of the many-body and diagrammatic techniques to perturbation theory is described in Chapter 5, and this is followed by proof of the crucial linked-diagram theorem in Chapter 6 and a discussion of some practical aspects of many-body perturbation-theory calculations in Chapter 7. Open-shell and quasidegenerate perturbation theory is presented in Chapter 8. Coupled-cluster theory is discussed in Chapters 9 and 10, again including several forms of the derivations in order to provide better understanding. The calculation of properties in the coupled-cluster method is described in Chapter 11. Several additional aspects of coupled-cluster theory are discussed in Chapter 12, and the equation-of-motion (EOM) coupled-cluster method for excited-state calculations is described in Chapter 13. Finally, multireference coupled-cluster methods are presented in Chapter 14.

1.2 Conventions and notation

Throughout this book we use atomic units, setting $m = e = \hbar = 1$ where m and $-e$ are the mass and charge of the electron and $\hbar = h/2\pi$ is Planck's

Table 1.1. *Terminology for excitation levels*

Level	Symbol	Name	Alternative
1	S	singles	mono-excited
2	D	doubles	bi-excited
3	T	triples	tri-excited
4	Q	quadruples	tetra-excited
5	P	pentuples	penta-excited
6	H	hextuples	hexa-excited

constant. As is customary in quantum chemistry, these constants are omitted from the expressions in this book but their implied presence is needed for proper dimensionality.

With a few exceptions, lower-case letters ($a, b, \dots, \phi, \psi, \dots$, etc.) are used for one- and two-particle entities, and upper-case letters ($A, B, \dots, \Phi, \Psi, \dots$, etc.) are used for many-particle entities. Operators are designated by a caret over a roman letter ($\hat{a}, \hat{i}, \hat{F}, \hat{H}$, etc.), by a script upper-case letter (\mathcal{H}, \mathcal{P} , etc.) or by an Greek upper-case letter (Λ, Ω , etc.). Vectors and matrices are represented by boldface lower- and upper-case letters, respectively.

The acronyms used to specify excitation-level combinations included in the different computational models have evolved, first in configuration interaction (CI) and then in coupled-cluster (CC) theory, using a mixture of English, Greek and Latin roots, in view of the need to provide a unique initial letter for each level, as listed in Table 1.1. For example, a CI calculation that includes all single, double and triple excitations is described as CISDT. The fourth column in Table 1.1 lists some alternative excitation-level names that have been used.

1.3 The independent-particle approximation

In this section we briefly summarize several aspects of the procedures used to obtain starting approximations for correlated molecular electronic structure calculations. For more complete discussions and detailed derivations the reader is referred to other sources, such as Szabo and Ostlund (1982) or standard textbooks.

Most electronic structure calculations begin with a relatively simple approximation based on the independent-particle model. The wave function

for such a model is a single Slater determinant (SD),

$$\begin{aligned}\Phi &= \frac{1}{\sqrt{N!}} \begin{vmatrix} \psi_1(1) & \psi_2(1) & \cdots & \psi_N(1) \\ \psi_1(2) & \psi_2(2) & \cdots & \psi_N(2) \\ \vdots & \vdots & \ddots & \vdots \\ \psi_1(N) & \psi_2(N) & \cdots & \psi_N(N) \end{vmatrix} \\ &= \mathcal{A}\psi_1\psi_2\ldots\psi_N,\end{aligned}\tag{1.1}$$

where $\psi_i(\mu)$ is a spinorbital, a function of the space and spin coordinates of the μ th electron (typically a product of a spatial orbital and a spin function), and \mathcal{A} is the antisymmetrizer. The most commonly used independent-particle model is the *Hartree–Fock* (HF) or *self-consistent field* (SCF) wave function,[†] in which the spinorbitals are varied to minimize the energy expectation value of the single-determinant wave function. The minimization can be achieved by solving a set of coupled one-electron eigenvalue equations for the spinorbitals,

$$\hat{f}\psi_i = \varepsilon_i\psi_i,\tag{1.2}$$

in which the Fock operator \hat{f} depends on all the spinorbitals (this dependence is given explicitly later in this section). Iterative procedures are required to obtain consistency between the spinorbitals used to define \hat{f} and the spinorbitals obtained as its eigenfunctions.

Because a determinant is invariant to unitary transformations of its columns or rows, the SD wave function (1.1) is invariant under unitary transformations of the occupied spinorbitals $\{\psi_i, i = 1, 2, \dots, N\}$ among themselves. Therefore, any unitary transformation of the occupied spinorbitals provides an alternative representation of the *same SD wave function*. The particular representation of the wave function in which the spinorbitals are solutions of (1.2), i.e., are eigenfunctions of \hat{f} (so that the matrix representation of \hat{f} in terms of these spinorbitals is diagonal, $\langle\psi_i|\hat{f}|\psi_j\rangle = \varepsilon_i\delta_{ij}$), is called the *canonical HF wave function*; the corresponding spinorbitals (including

[†] It was common to distinguish between the original type of *Hartree–Fock* solution, which achieves the absolute minimum of the energy of an SD wave function (1.1) with respect to any variation of the spinorbitals (subject only to appropriate restrictions in the restricted HF case) and usually require numerical (finite difference) methods of solution as employed by Hartree and others for atomic wave functions, and the *self-consistent field* form (also known as *Hartree–Fock–Roothaan* or *matrix Hartree–Fock*), in which the spinorbitals are expanded in a basis set and the lowest energy solution within the space generated by that basis set is sought. This second approach converts the operator eigenvalue equation (1.2) to a matrix eigenvalue equation for the eigenvectors of expansion coefficients. The HF solution is thus the limiting result (the *HF limit*) of the self-consistent field procedure as the basis set approaches completeness. In current usage, however, the distinction has unfortunately been lost, and the terms Hartree–Fock and self-consistent field are used interchangeably, both commonly referring to the basis-set expansion approach. We shall follow this practice in this book.

the unoccupied or *virtual* spinorbitals obtained as additional eigenfunctions of \hat{f} that are not used in the SD wave function) are the *canonical spinorbitals*. All other representations of the HF solution are called *noncanonical* and produce a block-diagonal matrix representation of \hat{f} with two internally non-diagonal blocks representing the occupied and virtual spinorbital spaces, respectively. The orbital energies ε_i , which are the eigenfunctions of \hat{f} , are invariant under unitary transformations but are associated one-to-one with the canonical spinorbitals only.

The degree of freedom provided by the invariance of the HF wave function under unitary transformations of the occupied spinorbitals (and, separately, of the unoccupied spinorbitals) is sometimes used to transform the spinorbitals to a localized form, in which the individual spinorbitals are localized to the regions of individual atoms or bonds. Such localized forms of the solution often offer advantages of simpler interpretation and provide a basis for more compact descriptions of correlated wave functions.

Several variants of the Hartree–Fock approach are in common use; these are defined by the restrictions, if any, that are placed on the spinorbitals $\{\psi_i\}$. In the usual form of the *unrestricted Hartree–Fock (UHF)* model there are no restrictions other than that each spinorbital is a product of a spatial orbital and a spin-up (α) or spin-down (β) spin function. This form is often used for open-shell states and sometimes for the description of bond dissociation. The most common restriction constrains pairs of spinorbitals to share the same spatial orbital, leading to the *restricted Hartree–Fock (RHF)* model in which each spatial orbital can accommodate at most two electrons. The RHF model is most commonly used for closed-shell molecules near their equilibrium geometry. When applied to open-shell cases, in which one or more spinorbitals are unpaired, it is often referred to as *restricted open-shell Hartree–Fock (ROHF)*. For closed-shell molecules near their equilibrium geometry the UHF and RHF solutions are generally equivalent and produce the same set of doubly occupied spatial orbitals.†

Independently of whether spin restrictions are used, restrictions can be placed on the symmetry properties of the spatial orbitals requiring them to belong to irreducible representations (*irreps*) of the point group of the molecule. Such restrictions can often cause difficulties in the descriptions of potential-energy surfaces, when symmetry-restricted solutions at high-symmetry points may be higher in energy than symmetry-unrestricted solutions at the same points (a phenomenon referred to as *symmetry breaking*)

† Except where stated explicitly otherwise, the treatment in this book is in terms of unrestricted spinorbitals, and the terms orbitals and Hartree–Fock (or SCF) generally refer to spinorbitals and UHF.

and thus do not connect continuously with the solutions for distorted (lower-symmetry) structures.

In most cases, a Hartree–Fock solution provides an excellent initial approximation for the electronic wave function and energy of a molecular system, often accounting for more than 99% of the total electronic energy and 95% of the wave function. Nevertheless, because the energy differences of interest in chemical and spectroscopic processes are a fraction of one percent of the total electronic energy and because the accuracy of the HF model tends to vary considerably between different structures and different electronic states, this model does not usually provide adequately accurate solutions by itself. In most cases, though, it provides a satisfactory zero-order solution that can then be used as the starting point for the *post-Hartree–Fock* methods discussed in this book. There are however cases in which HF does not provide an adequate zero-order function; these are due primarily to near degeneracies between several Slater-determinantal contributions to the wave function. In such cases a multideterminantal (“multiconfigurational”) function can provide a better zero-order wave function. The *multiconfigurational Hartree–Fock* (MCHF) model, also referred to as *multiconfigurational SCF* (MCSCF), can be particularly effective in providing good zero-order solutions in such cases, but the use of such multiconfigurational zero-order functions requires *multireference* methods in the post-HF stage and introduces additional complications for the many-body methods that are the principal topic of this book.

It is instructive to consider an alternative derivation of the Hartree–Fock model that provides physical insight into the reasons for its success and introduces some important concepts. We shall do this in terms of the unrestricted model, because of its generality and its relatively simple notation. Instead of invoking the variational principle and minimizing the energy of a single-determinant wave function with respect to the spinorbitals, the same Fock equation (1.2) can be obtained by a physically motivated argument.

The difficulty in the solution of the electronic Schrödinger equation is principally due to the interelectron repulsion terms $1/r_{\mu\nu}$ in the Hamiltonian. Those terms couple the motions of the different electrons and prevent separation of the equation into individual one-electron equations. It is therefore natural to seek an approximate solution in which the instantaneous interelectron interaction terms are replaced by averaged interactions, describing the motion of each electron in the time-averaged field of the other electrons. The averaged interaction energy of an electron in spinorbital ψ_i , when the total electron distribution is described by the single-SD wave function (1.1),

is obtained as

$$\begin{aligned}\langle \psi_i | \hat{u} | \psi_i \rangle &= \sum_{j \ (j \neq i)}^N \left\langle \psi_i(1) \psi_j(2) \left| \frac{1}{r_{12}} \right| \psi_i(1) \psi_j(2) - \psi_j(1) \psi_i(2) \right\rangle \\ &= \sum_{j=1}^N \langle \psi_i(1) | \hat{J}_j - \hat{K}_j | \psi_i(1) \rangle,\end{aligned}\tag{1.3}$$

where the restriction on the summation in the first line can be ignored because of the cancellation between the first (*Coulomb* or *direct*) term and the second (*exchange*) term when $i = j$. The *Coulomb* and *exchange operators* are defined by

$$\begin{aligned}\hat{J}_i(1)\phi(1) &= \left\langle \psi_i(2) \left| \frac{1}{r_{12}} \right| \psi_i(2) \right\rangle_2 \phi(1), \\ \hat{K}_i(1)\phi(1) &= \left\langle \psi_i(2) \left| \frac{1}{r_{12}} \right| \phi(2) \right\rangle_2 \psi_i(1),\end{aligned}\tag{1.4}$$

the integration being over the coordinates of electron 2 only. With the replacement of the instantaneous electron repulsion by the average form, the Schrödinger equation becomes separable, the equation for each electron takes the form (1.2) and the Fock operator is given by

$$\hat{f} = \hat{h} + \sum_{i=1}^N (\hat{J}_i - \hat{K}_i),\tag{1.5}$$

where \hat{h} is the one-electron operator in the Hamiltonian. Because of the cancellation of the Coulomb and exchange terms in (1.3) when $i = j$, and thus the removal of the restriction on the summation, the Fock operators for all the spinorbitals are equal and we have only one eigenvalue equation for the spinorbitals, with the different spinorbitals obtained as different eigenfunctions of that operator. The iterative and coupled nature of the equations is due to the dependence of the Coulomb and exchange operators on all the occupied orbitals.

The average-interaction approach leads to exactly the same equations as the energy-minimization approach and serves to provide a physical rationale for the Hartree–Fock model. It also provides the basis for defining the concept of *electron correlation*, as discussed in the next section.

1.4 Electron correlation

The purpose of all many-body methods is to describe *electron correlation*, defined as representing the difference between the Hartree–Fock description

of the electronic wave function and the exact solution of the nonrelativistic time-independent Schrödinger equation (Löwdin 1959, Kutzelnigg 2003). (Note that this definition is not necessarily unique, because of the different types of Hartree–Fock model that can be used as the reference point.) We are interested in the correlation correction to the energy, called the *correlation energy*,

$$\Delta E_{\text{corr}} = E_{\text{exact}} - E_{\text{HF}} \quad (1.6)$$

(where E_{HF} implies the exact solution of the Hartree–Fock problem, i.e., in an infinite, complete, basis set), and also in the correction to the wave function,

$$\Psi_{\text{exact}} = \Phi_{\text{HF}} + \chi_{\text{corr}}, \quad (1.7)$$

which determines the electron density and all other properties of molecules.

The naming of the correlation correction reflects the fact that the Hartree–Fock model describes the motion of the electrons in the average field of the other electrons, neglecting the instantaneous correlation in the motions of the electrons due to their mutual repulsion. However, this dynamic effect is not the only type of error in the Hartree–Fock model. In many cases, especially for excited states and other open-shell states and even for ground-state closed-shell molecules when bonds are stretched to near breaking (if the RHF model is used as the reference), near degeneracies between single-configuration descriptions cause the single-configuration Hartree–Fock model to be deficient even as a zero-order approximation for the wave function and energy. Therefore we distinguish between the two components of the correlation effect: *dynamic correlation*, reflecting the instantaneous correlation in electron motions due to their mutual repulsion, and *nondynamic correlation*, reflecting the effect of near degeneracies and other substantial inadequacies of the single-configuration model. While it is difficult to provide a quantitative separation between these two components of the correlation error, the understanding provided by these concepts is important in designing methods for obtaining satisfactory solutions of the Schrödinger equation.

The two components of the correlation error respond best to two different types of treatment. Nondynamic correlation is handled most efficiently by using a multiconfigurational zero-order description such as multiconfigurational SCF (MCSCF). Dynamical correlation is handled efficiently by the perturbation methods and coupled cluster approaches described in the rest of this book. Unfortunately, unlike the situation in the configuration interaction model, the *multireference* extension of the perturbation and coupled-

cluster models is quite difficult, and general methods for this type of approach are still not widely available. Nevertheless, single-reference coupled-cluster theory, when carried to a high enough level, has proved to be capable of overcoming the nondynamic correlation problem to a considerable extent.

1.5 Configuration interaction

The simplest approach to treating electron correlation is by the *configuration-interaction* (CI) method. If we start with the *self-consistent field* (SCF) wave function and orbitals (the Hartree–Fock solution limited to the space spanned by a given basis set), we can write the CI expansion of an N -electron wave function in the (unnormalized) form

$$\Psi = \Phi_{\text{SCF}} + \sum_{i,a} C_i^a \Phi_i^a + \sum_{i < j, a < b} C_{ij}^{ab} \Phi_{ij}^{ab} + \cdots \quad (\text{up to } N \text{ excitations}), \quad (1.8)$$

where Φ_i^a is a *singly excited* configuration in which an occupied orbital ϕ_i of the SCF wave function has been replaced by a virtual orbital ϕ_a (an orbital not occupied in the SCF function, which can also be chosen to be an eigenfunction of the Fock operator, $\hat{f}\phi_a = \varepsilon_a\phi_a$), Φ_{ij}^{ab} is a *double-excitation* configuration etc.

If m is the number of SCF occupied orbitals and n is the number of virtual orbitals ($m + n$ equals the number of basis functions) then the number of k -fold excited configurations is $O(m^k n^k)$ (as long as $k \ll m$). This number grows very rapidly with k , so that a complete solution is impractical and the CI expansion needs to be truncated. Usually the truncation is made after the double-excitation level, producing CISD, i.e. CI with single (S) and double (D) excitations. Because Φ_{SCF} is (usually) a reasonable starting approximation to Ψ and because the Hamiltonian \hat{H} has no more than two-electron operators (so that $\langle \Phi_{\text{SCF}} | \hat{H} | \Phi_{ij}^{ab} \rangle = 0$ for higher than double excitations), this represents a reasonable approximation in most cases.

The contribution of single excitations to a CI expansion (1.8) based on an SCF function (unrestricted or closed-shell restricted) as the initial term is quite small. This is due to the *Brillouin theorem*, which states that the Hamiltonian matrix element between the SCF function and a single excitation vanishes,

$$\langle \Phi_{\text{SCF}} | \hat{H} | \Phi_i^a \rangle = 0. \quad (1.9)$$

This theorem holds for both canonical and noncanonical forms of the SCF function and is a consequence of the block-diagonal nature of the Fock operator \hat{f} (Section 1.3) given by $f_{ia} = \langle \Phi_{\text{SCF}} | \hat{H} | \Phi_i^a \rangle = 0$ (see Chapter 3). As a

consequence of the Brillouin theorem, a CI expansion with single excitations only (CIS) based on an unrestricted or closed-shell restricted SCF function provides no improvement over SCF. It is only through the interaction of the single excitations with the doubles (and, to a much smaller extent, triples) that the singles acquire nonzero coefficients C_i^a in the expansion. These arguments do not apply to the restricted open-shell SCF (ROHF) case, for which the \hat{f} matrix is not block diagonal, the Brillouin theorem does not hold, and a CIS wave function can provide a useful improvement over SCF.

The contribution of single excitations to the CI expansion (as well as to perturbation expansions and coupled-cluster wave functions) can be eliminated completely by a suitable transformation of the orbitals. Such a transformation involves some mixing of occupied and virtual orbitals and therefore the initial term in the transformed expansion is no longer exactly equivalent to the SCF function. The resulting orbitals are called *Brueckner orbitals* and can be obtained by an iterative procedure in which, in each iteration, pairs of occupied and virtual orbitals are mixed to eliminate the corresponding single-excitation contributions in first order. This process must be applied to an expansion that includes at least double excitations, because it is the interaction of the single excitations with the doubles that is responsible for almost all of the contribution of the single excitations to the expansion.

Natural orbitals (NOs) are very similar to Brueckner orbitals; they are obtained by transforming the orbitals so as to diagonalize the one-particle density matrix of the correlated wave function. For two-electron systems, the natural orbitals are the same as the Brueckner orbitals, making it relatively easy to eliminate single excitations from correlated two-electron wave functions. In natural-orbital-based expansions for systems of more than two electrons the contribution of single excitations tends to be very small, in fact much smaller than even the small contributions in the SCF case.

The exact solution, within the given basis set, is obtained by using all terms of the CI expansion, up to N excitations. This is called *full CI* and is invariant under any linear transformation of the orbitals.

1.6 Motivation

The motivation for studying perturbation theory (PT) and other many-body (MB) techniques comes from the following principal sources.

1. Unlike truncated CI, most PT formulations provide properly *extensive* descriptions. These concepts are discussed in Section 1.7; briefly,

a method is extensive if the energy of a system computed by this method scales correctly with system size. An example illustrating the lack of extensivity of truncated CI is presented in Section 1.7.

2. Perturbation theory formulations can incorporate the most important higher-excitation effects at a relatively low order (e.g., they can combine the most important quadruple-excitation contributions with the double excitations), but by leaving out the relatively unimportant parts of these higher excitations they avoid the labor that would be required if we tried to include these higher-excitation effects in full, as we would have to do in CI, which cannot separate these different components of the higher excitations.
3. Systematic diagrammatic techniques allow high-efficiency organization of the calculations. This aspect is closely related to point 2 above and allows, in principle, improved results, at comparable levels of effort, compared with CI.

There also are disadvantages of such methods.

1. The PT and related MB techniques are generally *nonvariational*, so that we have no bounds on the energy.
2. The PT series does not always converge and thus cannot be applied in certain situations, and in many other cases convergence can be slow. These problems can be circumvented in some cases by reorganization of the series, including the summation of some types of term to infinite order; this is done, for example, in coupled-cluster (CC) methods. Alternatively, these convergence problems can be circumvented by going to a *multireference* (MR) version such as QDPT or MRCC but, as we shall see, this introduces additional complications.

1.7 Extensivity

In thermodynamics, a system property is called *extensive* if its value for a uniformly distributed system is proportional to the size of the system. A quantum-mechanical model is said to be *extensive* (commonly, although redundantly, *size-extensive*) if the energy of a system computed with this model scales correctly with the size of the system (Bartlett and Purvis 1978, Bartlett 1981). This property is most easily understood for a system such as a uniform electron gas or a system of noninteracting unis, such as N He atoms, for which $E(N\text{He}) = NE(\text{He})$. For arbitrary systems a precise definition is more difficult (Nooijen, Shamasundar and Mukherjee 2005) and will be dealt with more fully in Sections 5.10 and 9.2.1.

A closely related concept is that of *size-consistency*. As defined by Pople, Binkley and Seeger (1976), a model is size-consistent if the energies of two systems A and B and of the combined system AB with A and B very far apart, computed in equivalent ways, satisfy

$$E(AB) = E(A) + E(B) . \quad (1.10)$$

These two properties of the computed energy are not quite the same, but in many cases they go hand-in-hand. We shall discuss this question in more detail later, but now we use a simple example to demonstrate the lack of extensivity of truncated CI. We shall consider a model system of N noninteracting He atoms (or, equivalently, N H_2 molecules) as examples of electron-pair bonds and examine the behavior of the energy as a function of N (Sasaki 1977, Davidson and Silver 1977).

First we shall examine the case of one He atom with Hamiltonian \hat{h} , wave function ψ and energy ε , for which

$$\hat{h}\psi = \varepsilon\psi . \quad (1.11)$$

Since this is a two-electron system, its exact wave function can be written in terms of natural orbitals as a linear combination of a *reference function* ϕ_0 and all double excitations relative to it, without single-excitation terms (see Section 1.5). Let us express the wave function in the unnormalized form

$$\psi = \phi_0 + c\chi , \quad (1.12)$$

where

$$\begin{aligned} \langle \phi_0 | \phi_0 \rangle &= 1 , \\ \langle \chi | \chi \rangle &= 1 , \\ \langle \phi_0 | \chi \rangle &= 0 \end{aligned} \quad (1.13)$$

(intermediate normalization), and χ is the appropriate normalized aggregate of all double excitations relative to ϕ_0 ; alternatively, we could consider a calculation within the space spanned by just two basis functions, in which case χ would be the *only* double-excitation configuration. The elements of the corresponding *Hamiltonian matrix* will be written in the form

$$\begin{aligned} \langle \phi_0 | \hat{h} | \phi_0 \rangle &= \varepsilon_0 , \\ \langle \phi_0 | \hat{h} | \chi \rangle &= \beta , \\ \langle \chi | \hat{h} | \chi \rangle &= \alpha , \end{aligned} \quad (1.14)$$

and the CI eigenvalue equation is

$$\begin{pmatrix} \varepsilon_0 & \beta \\ \beta^* & \alpha \end{pmatrix} \begin{pmatrix} 1 \\ c \end{pmatrix} = \varepsilon \begin{pmatrix} 1 \\ c \end{pmatrix}, \quad (1.15)$$

which can be solved for the exact energy ε and the coefficient c . The first equation in the 2×2 system is

$$\varepsilon_0 + \beta c = \varepsilon, \quad \Delta\varepsilon \equiv \varepsilon - \varepsilon_0 = \beta c. \quad (1.16)$$

The second equation is

$$\beta^* + \alpha c = \varepsilon c, \quad \frac{\beta^*}{c} = \varepsilon - \alpha = \varepsilon_0 + \Delta\varepsilon - \alpha. \quad (1.17)$$

Substituting $c = \Delta\varepsilon/\beta$ from the first equation gives

$$\frac{|\beta|^2}{\Delta\varepsilon} = \varepsilon_0 + \Delta\varepsilon - \alpha, \quad \Delta\varepsilon^2 - (\alpha - \varepsilon_0)\Delta\varepsilon - |\beta|^2 = 0, \quad (1.18)$$

which is a quadratic equation for the correlation energy $\Delta\varepsilon$.

Now consider a system of N noninteracting He atoms, with Hamiltonian

$$\hat{H} = \sum_{i=1}^N \hat{h}(i), \quad (1.19)$$

where $\hat{h}(i)$ is the Hamiltonian for the i th atom. The reference function can be written

$$\Phi_0 = \mathcal{A}\phi_0(1)\phi_0(2)\cdots\phi_0(N), \quad (1.20)$$

where the arguments $1, 2, \dots, N$ identify the atoms. The antisymmetrizer \mathcal{A} exchanges electrons between different two-electron factors ϕ_0 ; because of the lack of interaction, it can actually be ignored. The double-excitation functions are of the form

$$\Phi_i = \mathcal{A}\phi_0(1)\phi_0(2)\cdots\phi_0(i-1)\chi(i)\phi_0(i+1)\cdots\phi_0(N). \quad (1.21)$$

(We do not need to consider mixed double excitations, or single excitations, because of the lack of interaction among the atoms and between ϕ_0 and any single excitation from it.) The CI doubles (CID) wave function is then

$$\Psi_{\text{CID}} = \Phi_0 + \sum_{i=1}^N C_i \Phi_i \quad (1.22)$$

(it is unnormalized, and all the $C_i = C$ are equal by symmetry). We obtain the following matrix elements:

$$\begin{aligned}
 \langle \Phi_0 | \Phi_0 \rangle &= 1, \\
 \langle \Phi_0 | \Phi_i \rangle &= 0, \\
 \langle \Phi_i | \Phi_j \rangle &= \delta_{ij}, \\
 \langle \Phi_0 | \hat{H} | \Phi_0 \rangle &= N\varepsilon_0 = E_0, \\
 \langle \Phi_0 | \hat{H} | \Phi_i \rangle &= \langle \phi_0 | \hat{h} | \chi \rangle = \beta, \\
 \langle \Phi_i | \hat{H} | \Phi_j \rangle &= \delta_{ij}[(N-1)\varepsilon_0 + \alpha] \\
 &= \delta_{ij}(E_0 + \alpha - \varepsilon_0).
 \end{aligned} \tag{1.23}$$

The CI equations are given by

$$\begin{pmatrix} E_0 & \beta & \beta & \dots & \beta \\ \beta^* & E_0 + \alpha - \varepsilon_0 & 0 & \dots & 0 \\ \beta^* & 0 & E_0 + \alpha - \varepsilon_0 & \dots & 0 \\ \vdots & \vdots & \vdots & \ddots & \vdots \\ \beta^* & 0 & 0 & \dots & E_0 + \alpha - \varepsilon_0 \end{pmatrix} \begin{pmatrix} 1 \\ C \\ C \\ \vdots \\ C \end{pmatrix} = E \begin{pmatrix} 1 \\ C \\ C \\ \vdots \\ C \end{pmatrix}. \tag{1.24}$$

From the first equation we get

$$E_0 + N\beta C = E$$

or

$$\Delta E \equiv E - E_0 = N\beta C. \tag{1.25}$$

From the other (equivalent) equations we get

$$\beta^* + (E_0 + \alpha - \varepsilon_0)C = EC$$

or

$$\frac{\beta^*}{C} = \varepsilon_0 + \Delta E - \alpha. \tag{1.26}$$

Substituting $C = \Delta E / N\beta$ from (1.25) gives

$$\frac{N|\beta|^2}{\Delta E} = \varepsilon_0 + \Delta E - \alpha,$$

$$\Delta E^2 - (\alpha - \varepsilon_0)\Delta E - N|\beta|^2 = 0. \tag{1.27}$$

Equation (1.27) is quadratic in the correlation energy ΔE , with solution

$$\Delta E = \frac{\alpha - \varepsilon_0}{2} \pm \sqrt{\left(\frac{\alpha - \varepsilon_0}{2}\right)^2 + N|\beta|^2}. \tag{1.28}$$

The behavior of ΔE as $N \rightarrow \infty$ is then found to be

$$\Delta E \xrightarrow{N \rightarrow \infty} -|\beta|\sqrt{N} = \frac{\Delta\varepsilon}{|c|}\sqrt{N} \quad (1.29)$$

(using $\Delta\varepsilon = \beta c$ from (1.16)), instead of the correct answer $\Delta E = N\Delta\varepsilon$. Therefore this truncated CI expansion is not extensive.

Of course, in this case we know the correct answer. If we define

$$\Phi_{ij} = \mathcal{A}\phi_0(1) \cdots \phi_0(i-1)\chi(i)\phi_0(i+1) \cdots \phi_0(j-1)\chi(j)\phi_0(j+1) \cdots \phi_0(N) \quad (1.30)$$

etc. then

$$\begin{aligned} \Psi &= \mathcal{A}\psi(1)\psi(2) \cdots \psi(N) \\ &= \mathcal{A}[\phi_0(1) + c\chi(1)][\phi_0(2) + c\chi(2)] \cdots [\phi_0(N) + c\chi(N)] \\ &= \Phi_0 + \sum_{i=1}^N c\Phi_i + \sum_{i<j} c^2\Phi_{ij} + \cdots + c^N\Phi_{123\dots N}, \end{aligned} \quad (1.31)$$

which can also be written as

$$\Psi = \Phi_0 + \sum_i c\Phi_i + \frac{1}{2} \sum_{i,j} c^2\Phi_{ij} + \frac{1}{3!} \sum_{i,j,k} c^3\Phi_{ijk} + \cdots \quad (1.32)$$

Thus the coefficients of the higher than double excitations are not independent parameters but are closely related to the coefficients of the doubles. Obviously, the larger the system becomes the poorer will be the truncated CI expansion Ψ_{CID} . The relative contributions to $|\Psi|^2$ of different excitation levels are:

$$\begin{aligned} \text{zero excitations,} & \quad 1; \\ \text{doubles,} & \quad Nc^2; \\ \text{quadruples,} & \quad \frac{1}{2}N(N-1)c^4 \sim \frac{1}{2}N^2c^4; \\ \text{sextuples,} & \quad \frac{1}{3!}N(N-1)(N-2)c^6 \sim \frac{1}{6}N^3c^6; \end{aligned} \quad (1.33)$$

etc. No matter how small c^2 is, if N is large enough then the higher-excitation contributions eventually become dominant. We shall return to this example in the discussions of other computational models.

1.8 Disconnected clusters and extensivity

The N -He-atoms example provides a simple explanation of the lack of extensivity of CID in terms of separated pairs (disconnected clusters). As previously stated, the coefficients of the higher-excitation configurations

(quadruples, sextuples, etc.) in this example are not independent parameters, so that if we knew the *correct* double-excitation coefficients c , i.e. those obtained from a *full* CI calculation, not from CID, we would know the complete wave function and would be able to obtain the exact energy. While a double-excitation configuration represents the correlation of a pair of electrons (a *two-electron cluster*), a quadruple excitation represents the correlation of four electrons at a time, etc. But the four-electron correlations in this example really represent two separate two-electron correlations occurring simultaneously. This type of four-electron cluster is called a *disconnected cluster*, being made up of two simultaneous but independent two-electron clusters. In the language of coupled-cluster theory, the two-electron clusters are represented by an operator \hat{T}_2 corresponding to a linear combination of double-excitation operators and the higher-order disconnected clusters are represented by products of connected-cluster operators, such as $\frac{1}{2}\hat{T}_2^2$ for disconnected quadruple excitations, obtained from the expansion of an exponential operator $e^{\hat{T}}$ (where \hat{T} may be limited to \hat{T}_2 or may contain additional connected-cluster operators \hat{T}_1, \hat{T}_3 etc.).

If we bring the N He atoms closer and let them interact, the full CI wave function will no longer be represented *exactly* as a product of one-atom wave functions

$$(1 + \hat{T}_2 + \frac{1}{2!}\hat{T}_2^2 + \frac{1}{3!}\hat{T}_2^3 + \cdots)\Phi_0 = e^{\hat{T}_2}\Phi_0 \quad (1.34)$$

equivalent to the expansion (1.32); it will have additional *connected* cluster contributions $\hat{T}_1, \hat{T}_3, \hat{T}_4, \dots$ as well as additional disconnected cluster contributions $\frac{1}{2}\hat{T}_1^2, \hat{T}_1\hat{T}_2, \hat{T}_1\hat{T}_3, \hat{T}_2\hat{T}_3, \frac{1}{3!}\hat{T}_1^3, \frac{1}{2}\hat{T}_1^2\hat{T}_2, \dots$, obtained from the expansion of $e^{\hat{T}}$ (where $\hat{T} = \hat{T}_1 + \hat{T}_2 + \cdots$). The CI quadruple excitation contribution is represented by the operator

$$\hat{C}_4 = \hat{T}_4 + \frac{1}{2}\hat{T}_2^2 + \frac{1}{4!}\hat{T}_1^4 + \hat{T}_1\hat{T}_3 + \frac{1}{2}\hat{T}_1^2\hat{T}_2. \quad (1.35)$$

In the noninteracting case $\frac{1}{2}\hat{T}_2^2$ is the only contribution to \hat{C}_4 , but even in the interacting case it will still be by far the most important. In fact, the order of importance, based upon the order of PT in which the contribution first appears (for an SCF reference state), is generally

$$\hat{T}_2, \frac{1}{2}\hat{T}_2^2, \hat{T}_1, \hat{T}_3, \frac{1}{3!}\hat{T}_2^3, \hat{T}_4, \dots \quad (1.36)$$

In CI we cannot compute the individual components of (1.35) separately but in PT and CC we can, and \hat{T}_2^2 is much easier to compute than \hat{T}_4 . Thus we can obtain the major effect of the quadruple excitations $\frac{1}{2}\hat{T}_2^2$ more easily in PT and CC, because in these methods it is not combined with the much more difficult \hat{T}_4 . Furthermore, it is the disconnected clusters that are the key for extensivity (as is clear from the N -He-atoms example).

2

Formal perturbation theory

2.1 Background

There are two stages in the study of perturbation theory and related techniques (although they are mixed intimately in most derivations in the literature). The first is the *formal development*, carried out in terms of the total Hamiltonian and total wave function (and total zero-order wave function), without attempt to express anything in terms of one- and two-body quantities (components of \hat{H} , orbitals, integrals over orbitals etc.). We can make a considerable amount of progress in this way before considering the detailed form of \hat{H} . The second is the *many-body development*, where all expressions are obtained in terms of orbitals (one-electron states) and one- and two-electron integrals. We shall try to keep these separate for a while and begin with a consideration of formal perturbation theory.

Another aspect of the study of many-body techniques is the large variety of approaches, notations and derivations that have been used. Each different approach has contributed to the lore and the language of many-body theory, and each tends to illuminate some aspects better than the other approaches. If we want to be able to read the literature in this field, we should be familiar with several alternative formulations. Therefore, we shall occasionally derive some results in more than one way and, in particular, we shall derive the basic perturbation-theory equations and their many-body representations in several complementary ways.

2.2 Classical derivation of Rayleigh–Schrödinger perturbation theory

2.2.1 The *perturbation Ansatz*

We begin with a classical textbook derivation of formal Rayleigh–Schrödinger perturbation theory (RSPT). We separate the Hamiltonian into a zero-order

part and a perturbation,

$$\hat{H} = \hat{H}_0 + \hat{V} . \quad (2.1)$$

When convenient, we shall write this in the form

$$\hat{H} = \hat{H}_0 + \lambda \hat{V} , \quad (2.2)$$

where λ is an “order parameter” that is used to classify the various contributions by their order and set to $\lambda = 1$ at the end. The exact (unknown) solutions will be written

$$\hat{H}\Psi_n = E_n\Psi_n , \quad (2.3)$$

while for the zero-order problem (assumed soluble) we write

$$\hat{H}_0\Phi_n = E_n^{(0)}\Phi_n , \quad (2.4)$$

with

$$\langle \Phi_m | \Phi_n \rangle = \delta_{mn} . \quad (2.5)$$

If Φ_n is nondegenerate, it is possible to number the solutions in such a way that

$$\begin{aligned} \lim_{\lambda \rightarrow 0} \Psi_n &= \Phi_n , \\ \lim_{\lambda \rightarrow 0} E_n &= E_n^{(0)} . \end{aligned} \quad (2.6)$$

(If there are degeneracies, it is possible to choose the zero-order solutions so that (2.6) is still satisfied.) Let us define the differences

$$\begin{aligned} \chi_n &= \Psi_n - \Phi_n , \\ \Delta E_n &= E_n - E_n^{(0)} , \end{aligned} \quad (2.7)$$

and then rewrite the Schrödinger equation in the forms

$$\begin{aligned} \hat{H}(\Phi_n + \chi_n) &= E_n(\Phi_n + \chi_n) , \\ \hat{H}_0\Phi_n + \hat{V}\Phi_n + \hat{H}\chi_n &= E_n^{(0)}\Phi_n + \Delta E_n\Phi_n + E_n\chi_n , \\ (\hat{H} - E_n)\chi_n &= (\Delta E_n - \hat{V})\Phi_n . \end{aligned} \quad (2.8)$$

2.2.2 Indeterminacy of the solution

If we assume for the moment that ΔE_n (and thus E_n) is known then (2.8) is an inhomogeneous linear differential equation for χ_n , since the right-hand side is known. If we have a particular solution for such an equation, we can add to it any multiple of the solution of the corresponding homogeneous equation,

$$(\hat{H} - E_n)f = 0, \quad (2.9)$$

and still have a solution. For example, if the inhomogeneous equation is

$$\hat{A}f = g,$$

where \hat{A} is a linear operator, g is a known function and f is the unknown function and if f_0 is a particular solution, satisfying

$$\hat{A}f_0 = g$$

while h is a solution of the homogeneous equation

$$\hat{A}h = 0$$

then

$$f = f_0 + ch$$

(where c is an arbitrary constant) is also a solution of the original equation, since

$$\begin{aligned} \hat{A}f &= \hat{A}f_0 + c\hat{A}h \\ &= g + 0 = g. \end{aligned}$$

Thus χ_n is not fully determined, since we can add to it an arbitrary multiple of $\Psi_n = \Phi_n + \chi_n$, the *only* solution of (2.9) that is consistent with E_n .

This degree of freedom can be used to force χ_n to be orthogonal to Φ_n ,

$$\langle \chi_n | \Phi_n \rangle = 0. \quad (2.10)$$

This choice means that we extract only that part of the correction χ_n to Φ_n that is essentially different from Φ_n . In other words, we partition Ψ_n into two parts, one parallel (i.e. proportional) to Φ_n and the other orthogonal to it. As the choice of normalization is arbitrary, it is convenient to use *intermediate normalization*:

$$\begin{aligned} \langle \Phi_n | \Phi_n \rangle &= 1, & \langle \chi_n | \Phi_n \rangle &= 0, \\ \langle \Psi_n | \Phi_n \rangle &= \langle \Phi_n + \chi_n | \Phi_n \rangle = 1 + 0 = 1, \\ \langle \Psi_n | \Psi_n \rangle &= 1 + \langle \chi_n | \chi_n \rangle. \end{aligned} \quad (2.11)$$

2.2.3 Energy expressions

From the intermediate-normalization assumption (2.11) we get

$$\begin{aligned}\langle \Phi_n | \hat{H} | \Psi_n \rangle &= E_n \langle \Phi_n | \Psi_n \rangle = E_n, \\ \langle \Phi_n | \hat{H}_0 | \Psi_n \rangle &= \langle \hat{H}_0 \Phi_n | \Psi_n \rangle = E_n^{(0)} \langle \Phi_n | \Psi_n \rangle = E_n^{(0)}.\end{aligned}\tag{2.12}$$

Subtracting the second equation from the first, we have

$$\begin{aligned}\Delta E_n &= E_n - E_n^{(0)} = \langle \Phi_n | \hat{H} - \hat{H}_0 | \Psi_n \rangle \\ &= \langle \Phi_n | \hat{V} | \Psi_n \rangle.\end{aligned}$$

Thus

$$\begin{aligned}\Delta E_n &= \langle \Phi_n | \hat{V} | \Psi_n \rangle, \\ E_n &= \langle \Phi_n | \hat{H} | \Psi_n \rangle.\end{aligned}\tag{2.13}$$

The last equation is sometimes referred to as the *transition matrix element form* (or *projected form*) for the energy. When Ψ_n is exact this E_n is also exact but if Ψ_n is approximate, with an error of order ϵ , then the error in E_n is also of order ϵ and may be greater than the error in the *variational* estimate

$$E_n = \frac{\langle \Psi_n | \hat{H} | \Psi_n \rangle}{\langle \Psi_n | \Psi_n \rangle}\tag{2.14}$$

(which has an error of order ϵ^2 for a wave function error of order ϵ). (Note that if Ψ_n is a *full CI* expansion based on Φ_n and its excitations then only the coefficients of the single and double excitations are needed to determine the exact energy from (2.13).)

2.2.4 Order-by-order expansion

To proceed further, we use the order parameter λ and expand:

$$\begin{aligned}\Psi_n &= \Phi_n + \chi_n = \Psi_n^{(0)} + \lambda \Psi_n^{(1)} + \lambda^2 \Psi_n^{(2)} + \dots \quad (\Psi_n^{(0)} \equiv \Phi_n), \\ E_n &= E_n^{(0)} + \Delta E_n = E_n^{(0)} + \lambda E_n^{(1)} + \lambda^2 E_n^{(2)} + \dots\end{aligned}\tag{2.15}$$

Substituting into the Schrödinger equation

$$(\hat{H} - E_n) \Psi_n = 0\tag{2.16}$$

with $\hat{H} = \hat{H}_0 + \lambda \hat{V}$, we get

$$(\hat{H}_0 + \lambda \hat{V} - E_n^{(0)} - \lambda E_n^{(1)} - \lambda^2 E_n^{(2)} - \dots)(\Psi_n^{(0)} + \lambda \Psi_n^{(1)} + \lambda^2 \Psi_n^{(2)} + \dots) = 0.\tag{2.17}$$

Equating coefficients of powers of λ gives for λ^0 , λ^1 and λ^2 , respectively:

$$(\hat{H}_0 - E_n^{(0)})\Psi_n^{(0)} = 0 \quad (\text{zero order}), \quad (2.18)$$

$$(\hat{H}_0 - E_n^{(0)})\Psi_n^{(1)} = (E_n^{(1)} - \hat{V})\Psi_n^{(0)} \quad (\text{first order}), \quad (2.19)$$

$$(\hat{H}_0 - E_n^{(0)})\Psi_n^{(2)} = (E_n^{(1)} - \hat{V})\Psi_n^{(1)} + E_n^{(2)}\Psi_n^{(0)} \quad (\text{second order}) \quad (2.20)$$

and in general, for λ^m , the m th-order equation

$$(\hat{H}_0 - E_n^{(0)})\Psi_n^{(m)} = (E_n^{(1)} - \hat{V})\Psi_n^{(m-1)} + \sum_{l=0}^{m-2} E_n^{(m-l)}\Psi_n^{(l)},$$

which becomes

$$(E_n^{(0)} - \hat{H}_0)\Psi_n^{(m)} = \hat{V}\Psi_n^{(m-1)} - \sum_{l=0}^{m-1} E_n^{(m-l)}\Psi_n^{(l)}. \quad (2.21)$$

In order to get expressions for $E_n^{(m)}$ we apply $\langle \Phi_n |$ to each equation and integrate. For λ^1 we get

$$\langle \Phi_n | \hat{H}_0 - E_n^{(0)} | \Psi_n^{(1)} \rangle = \langle \Phi_n | E_n^{(1)} - \hat{V} | \Phi_n \rangle. \quad (2.22)$$

By the Hermitian property of \hat{H}_0 we have

$$\underbrace{\langle (\hat{H}_0 - E_n^{(0)})\Phi_n | \Psi_n^{(1)} \rangle}_{=0} = E_n^{(1)} - \underbrace{\langle \Phi_n | \hat{V} | \Phi_n \rangle}_{\equiv V_{nn}}$$

and so

$$E_n^{(1)} = \langle \Phi_n | \hat{V} | \Phi_n \rangle = V_{nn}, \quad (2.23)$$

where we set

$$V_{ij} = \langle \Phi_i | \hat{V} | \Phi_j \rangle. \quad (2.24)$$

Thus we have obtained $E_n^{(1)}$ without knowledge of $\Psi_n^{(1)}$ and can now solve the inhomogeneous differential equation for $\Psi_n^{(1)}$. We are free to require $\langle \Phi_n | \Psi_n^{(1)} \rangle = 0$, the intermediate-normalization condition. This is equivalent to adding an arbitrary multiple of Φ_n (the solution of the corresponding homogeneous equation $(\hat{H}_0 - E_n^{(0)})f = 0$) to $\Psi_n^{(1)}$. The same can be done for each order m :

$$\underbrace{\langle \Phi_n | E_n^{(0)} - \hat{H}_0 | \Psi_n^{(m)} \rangle}_{=0} = \langle \Phi_n | \hat{V} | \Psi_n^{(m-1)} \rangle - \sum_{l=0}^{m-1} E_n^{(m-l)} \underbrace{\langle \Phi_n | \Psi_n^{(l)} \rangle}_{=\delta_{l0}},$$

giving

$$E_n^{(m)} = \langle \Phi_n | \hat{V} | \Psi_n^{(m-1)} \rangle. \quad (2.25)$$

Thus, in principle, we can obtain each $E_n^{(m)}$ from the previous $\Psi_n^{(m-1)}$ and then solve for $\Psi_n^{(m)}$ etc., while always maintaining $\langle \Phi_n | \Psi_n^{(m)} \rangle = 0$ ($m > 0$).

2.2.5 Expansion in zero-order functions

The inhomogeneous differential equations for $\Psi_n^{(m)}$ are not easy to solve, though they are easier than eigenvalue equations. One way to proceed is to expand the unknown $\Psi_n^{(m)}$ in terms of the known zero-order solutions Φ_k . This exploits the fact that the set of eigenfunctions of any semibounded Hermitian operator form a complete set:

$$\begin{aligned} \Psi_n^{(m)} &= \sum_k a_{kn}^{(m)} \Phi_k = \sum_k |\Phi_k\rangle \langle \Phi_k | \Psi_n^{(m)} \rangle, \\ a_{kn}^{(m)} &= \langle \Phi_k | \Psi_n^{(m)} \rangle \quad (\text{to be determined}). \end{aligned} \quad (2.26)$$

To obtain $a_{kn}^{(m)}$ we multiply the m th-order equation by $\langle \Phi_k |$ and integrate:

$$\begin{aligned} \underbrace{\langle \Phi_k | E_n^{(0)} - \hat{H}_0 | \Psi_n^{(m)} \rangle}_{=(E_n^{(0)} - E_k^{(0)}) \langle \Phi_k |} &= \underbrace{\langle \Phi_k | \hat{V} | \Psi_n^{(m-1)} \rangle}_{\sum_j \langle \Phi_k | \hat{V} | \Phi_j \rangle \langle \Phi_j | \Psi_n^{(m-1)} \rangle} - \sum_{l=0}^{m-1} E_n^{(m-l)} \underbrace{\langle \Phi_k | \Psi_n^{(l)} \rangle}_{=a_{kn}^{(l)}}. \end{aligned}$$

Thus

$$(E_n^{(0)} - E_k^{(0)}) a_{kn}^{(m)} = \sum_j V_{kj} a_{jn}^{(m-1)} - \sum_{l=0}^{m-1} E_n^{(m-l)} a_{kn}^{(l)}. \quad (2.27)$$

In this equation the $l = 0$ contributions are to be interpreted as $a_{kn}^{(0)} = \langle \Phi_k | \Phi_n \rangle = \delta_{kn}$.

This result provides a system of equations for the $a_{kn}^{(m)}$ coefficients, to be solved order by order, but the first thing to notice is that we have no equation for $a_{nn}^{(m)}$; this coefficient is arbitrary, corresponding to the arbitrariness of adding any multiple of the zero-order solution Φ_n (of the zero-order homogeneous equation for the same n). This arbitrariness appears for each order $\Psi_n^{(m)}$ separately. The following choice of intermediate normalization can thus be made for each order:

$$\begin{aligned} \langle \Phi_n | \Psi_n^{(m)} \rangle &= 0 \quad (m > 0), \\ a_{nn}^{(m)} &= 0 \quad (m > 0). \end{aligned}$$

Consequently

$$a_{nn}^{(m)} = \delta_{m0}. \quad (2.28)$$

Since $a_{kn}^{(0)} = \delta_{kn}$, the first-order equation becomes:

$$(E_n^{(0)} - E_k^{(0)})a_{kn}^{(1)} = V_{kn} - E_n^{(1)}a_{kn}^{(0)} = V_{kn} \quad (n \neq k),$$

so that

$$a_{kn}^{(1)} = \frac{V_{kn}}{E_n^{(0)} - E_k^{(0)}} \quad (n \neq k). \quad (2.29)$$

Thus we have the well-known result

$$\Psi_n^{(1)} = \sum_k' \frac{V_{kn}}{E_n^{(0)} - E_k^{(0)}} \Phi_k \quad (2.30)$$

where $\sum_k' \equiv \sum_k (k \neq n)$. From this we get the second-order energy,

$$\begin{aligned} E_n^{(2)} &= \langle \Phi_n | \hat{V} | \Psi_n^{(1)} \rangle = \sum_k a_{kn}^{(1)} V_{nk} \\ &= \sum_k' \frac{V_{nk} V_{kn}}{E_n^{(0)} - E_k^{(0)}} = \sum_k' \frac{|V_{kn}|^2}{E_n^{(0)} - E_k^{(0)}}, \end{aligned} \quad (2.31)$$

which is also well known.

This process can be continued in the same manner to higher orders, e.g.,

$$\begin{aligned} a_{kn}^{(2)} &= (E_n^{(0)} - E_k^{(0)})^{-1} \left\{ \sum_j' a_{jn}^{(1)} V_{kj} - E_n^{(1)} a_{kn}^{(1)} - E_n^{(2)} a_{kn}^{(0)} \right\} \\ &= \sum_j' \frac{V_{kj} V_{jn}}{(E_n^{(0)} - E_k^{(0)})(E_n^{(0)} - E_j^{(0)})} - \frac{V_{kn} V_{nn}}{(E_n^{(0)} - E_k^{(0)})^2} \quad (k \neq n). \end{aligned} \quad (2.32)$$

However, it is somewhat cumbersome and not very convenient for the many-body techniques that we shall want to use, so we will look at more systematic techniques. However, before we do that, we will consider two more aspects of this analysis, the Wigner $2n + 1$ rule and the Hylleraas variational principle for the first-order wave function.

2.2.6 Wigner's $2n + 1$ rule

Wigner's rule (Wigner 1935) says that knowledge of $\Psi_n^{(l)}$ for $l = 1, 2, \dots, m$ allows us to determine directly the $E_n^{(l)}$ for $l = 1, 2, \dots, 2m + 1$. This result can be obtained by a series of transformations of the m th-order energy contribution (2.25), $E_n^{(m)} = \langle \Phi_n | \hat{V} | \Psi_n^{(m-1)} \rangle$, using the differential equations for $\Psi_n^{(l)}$, to raise the order of the “bra” part while lowering the order of the “ket” part, repeatedly until the two orders are equal (if m is odd) or differ by unity (if m is even).

We shall work out one step of this repetitive sequence explicitly, using the first-order equation (2.19) in the form

$$\hat{V}\Phi_n = (E_n^{(0)} - \hat{H}_0)\Psi_n^{(1)} + E_n^{(1)}\Phi_n \quad (2.33)$$

and then the $(m-1)$ th-order equation in its usual form (2.21):

$$\begin{aligned} E_n^{(m)} &= \langle \Phi_n | \hat{V} | \Psi_n^{(m-1)} \rangle \\ &= \langle \hat{V}\Phi_n | \Psi_n^{(m-1)} \rangle \\ &= \langle (E_n^{(0)} - \hat{H}_0)\Psi_n^{(1)} | \Psi_n^{(m-1)} \rangle + E_n^{(1)} \langle \Phi_n | \Psi_n^{(m-1)} \rangle \\ &= \langle \Psi_n^{(1)} | E_n^{(0)} - \hat{H}_0 | \Psi_n^{(m-1)} \rangle + 0 \\ &= \langle \Psi_n^{(1)} | \hat{V} | \Psi_n^{(m-2)} \rangle - \sum_{l=0}^{m-2} E_n^{(m-l-1)} \langle \Psi_n^{(1)} | \Psi_n^{(l)} \rangle \\ &= \langle \Psi_n^{(1)} | \hat{V} | \Psi_n^{(m-2)} \rangle - \sum_{l=1}^{m-2} E_n^{(m-l-1)} \langle \Psi_n^{(1)} | \Psi_n^{(l)} \rangle \end{aligned} \quad (2.34)$$

(since the $l=0$ term vanishes). If this is repeated k times we get

$$E_n^{(m)} = \langle \Psi_n^{(k)} | \hat{V} | \Psi_n^{(m-k-1)} \rangle - \sum_{j=1}^k \sum_{l=1}^{m-k-1} E_n^{(m-j-l)} \langle \Psi_n^{(j)} | \Psi_n^{(l)} \rangle. \quad (2.35)$$

Taking the cases in which m is replaced by $2m$ or $2m+1$ and k by $m-1$ or m , respectively, we get Wigner's results:

$$E_n^{(2m)} = \langle \Psi_n^{(m-1)} | \hat{V} | \Psi_n^{(m)} \rangle - \sum_{j=1}^{m-1} \sum_{l=1}^m E_n^{(2m-j-l)} \langle \Psi_n^{(j)} | \Psi_n^{(l)} \rangle, \quad (2.36)$$

$$E_n^{(2m+1)} = \langle \Psi_n^{(m)} | \hat{V} | \Psi_n^{(m)} \rangle - \sum_{j=1}^m \sum_{l=1}^m E_n^{(2m-j-l+1)} \langle \Psi_n^{(j)} | \Psi_n^{(l)} \rangle. \quad (2.37)$$

2.2.7 The Hylleraas variation principle for the first-order wave function

Instead of expanding $\Psi_n^{(1)}$ in the zero-order functions Φ_k , the first-order wave function and the second-order energy can also be obtained by a variational method due to Hylleraas (1930) (see, e.g., Bethe and Salpeter (1957), pp. 122–3).

We begin by multiplying the first-order equation (2.19) by $\langle \Psi_n^{(1)} |$ and integrating:

$$\langle \Psi_n^{(1)} | \hat{H}_0 - E_n^{(0)} | \Psi_n^{(1)} \rangle = \langle \Psi_n^{(1)} | E_n^{(1)} - \hat{V} | \Phi_n \rangle$$

or

$$0 = \langle \Psi_n^{(1)} | \hat{V} - E_n^{(1)} | \Phi_n \rangle + \langle \Psi_n^{(1)} | \hat{H}_0 - E_n^{(0)} | \Psi_n^{(1)} \rangle.$$

To this equation we add the equation for the second-order energy,

$$E_n^{(2)} = \langle \Phi_n | \hat{V} - E_n^{(1)} | \Psi_n^{(1)} \rangle$$

(note that we have not invoked $\langle \Phi_n | \Psi_n^{(1)} \rangle = 0$). The result is

$$\begin{aligned} E_n^{(2)} &= \langle \Psi_n^{(1)} | \hat{V} - E_n^{(1)} | \Phi_n \rangle + \langle \Phi_n | \hat{V} - E_n^{(1)} | \Psi_n^{(1)} \rangle + \langle \Psi_n^{(1)} | \hat{H}_0 - E_n^{(0)} | \Psi_n^{(1)} \rangle \\ &= 2 \operatorname{Re} \langle \Psi_n^{(1)} | \hat{V} - E_n^{(1)} | \Phi_n \rangle + \langle \Psi_n^{(1)} | \hat{H}_0 - E_n^{(0)} | \Psi_n^{(1)} \rangle. \end{aligned} \quad (2.38)$$

If we define a functional

$$J_2[\Psi] = 2 \operatorname{Re} \langle \Psi | \hat{V} - E_n^{(1)} | \Phi_n \rangle + \langle \Psi | \hat{H}_0 - E_n^{(0)} | \Psi \rangle, \quad (2.39)$$

then obviously

$$J_2[\Psi_n^{(1)}] = E_n^{(2)}. \quad (2.40)$$

The variation of this functional is

$$\begin{aligned} \delta J_2[\Psi] &= \langle \delta \Psi | \hat{V} - E_n^{(1)} | \Phi_n \rangle + \langle \Phi_n | \hat{V} - E_n^{(1)} | \delta \Psi \rangle \\ &\quad + \langle \delta \Psi | \hat{H}_0 - E_n^{(0)} | \Psi \rangle + \langle \Psi | \hat{H}_0 - E_n^{(0)} | \delta \Psi \rangle. \end{aligned} \quad (2.41)$$

Requiring that $\delta J_2[\Psi] = 0$ for *any* $\delta \Psi$ (including $\delta \Psi^*$) results in

$$(\hat{V} - E_n^{(1)})\Phi_n + (\hat{H}_0 - E_n^{(0)})\Psi = 0,$$

for which $\Psi = \Psi_n^{(1)}$ is a solution (since the above relation is equivalent to the first-order equation). Thus $\Psi_n^{(1)}$ and $E_n^{(2)}$ can be obtained by making $J_2[\Psi]$ stationary. It is easily verified that

$$J_2[\Psi + c\Phi_n] = J_2[\Psi]$$

for any constant c , and this degree of freedom can be used to enforce $\langle \Psi | \Phi_n \rangle = 0$. If the function Ψ is constrained at the outset to be orthogonal to Φ_n then $J_2[\Psi]$ can be written in the form

$$J_2[\Psi] = 2 \operatorname{Re} \langle \Psi | \hat{V} | \Phi_n \rangle + \langle \Psi | \hat{H}_0 - E_n^{(0)} | \Psi \rangle \quad (\langle \Psi | \Phi_n \rangle = 0). \quad (2.42)$$

Next we show that if $E_n^{(0)}$ is the lowest eigenvalue of \hat{H}_0 then $J_2[\Psi]$ is an upper bound for $E_n^{(2)}$. We write Ψ in the form

$$\Psi = \Psi_n^{(1)} + \chi. \quad (2.43)$$

Then

$$\begin{aligned} J_2[\Psi] &= J_2[\Psi_n^{(1)}] + 2 \operatorname{Re} \langle \chi | \hat{V} - E_n^{(1)} | \Phi_n \rangle \\ &\quad + 2 \operatorname{Re} \langle \chi | \hat{H}_0 - E_n^{(0)} | \Psi_n^{(1)} \rangle + \langle \chi | \hat{H}_0 - E_n^{(0)} | \chi \rangle. \end{aligned} \quad (2.44)$$

Using the first-order equation, we find that the third term can be written as the negative of the second term, canceling it, so that we have

$$J_2[\Psi] = E_n^{(2)} + \langle \chi | \hat{H}_0 - E_n^{(0)} | \chi \rangle. \quad (2.45)$$

If $E_n^{(0)}$ is the lowest eigenvalue of \hat{H}_0 then the integral $\langle \chi | \hat{H}_0 - E_n^{(0)} | \chi \rangle$ is nonnegative and is zero if, and only if, χ is the corresponding eigenfunction. Therefore

$$J_2[\Psi] \geq E_n^{(2)} \quad (E_n^{(0)} \leq E_k^{(0)} \text{ for all } k \neq n). \quad (2.46)$$

Thus $J_2[\Psi]$, with an arbitrary trial function Ψ containing adjustable parameters, can be used in a variational approach for finding approximations to the first-order wave function and second-order energy, and this provides an upper bound to $E_n^{(2)}$ in the case of a state having the lowest zero-order energy (provided that Φ_0 is an exact eigenfunction of \hat{H}_0).

2.3 Projection operators

Before we proceed to alternative derivations of the perturbation theory equations, we shall introduce two *projection operators*. To simplify the notation, we shall use the index 0, instead of n , to indicate the state in which we are interested (regardless of whether it is the ground state or some excited state). We shall omit this index entirely when there is no danger of confusion, and particularly when we refer to the exact wave function $\Psi_0 \equiv \Psi$, the exact energy $E_0 \equiv E$ and their order-by-order contributions $\Psi^{(m)}$ and $E^{(m)}$.

We define the projection operators in terms of the orthonormal zero-order functions:

$$\begin{aligned} \hat{P} &= |\Phi_0\rangle\langle\Phi_0|, \\ \hat{Q} &= \hat{1} - \hat{P} = \sum_{i \neq 0} |\Phi_i\rangle\langle\Phi_i| = \sum_i' |\Phi_i\rangle\langle\Phi_i| \end{aligned} \quad (2.47)$$

(where $\sum'_i \equiv \sum_{i \neq 0}$). These operators are *linear*, *Hermitian* and *idempotent*:

$$\begin{aligned}\hat{P}^2 &= |\Phi_0\rangle\langle\Phi_0|\Phi_0\rangle\langle\Phi_0| = |\Phi_0\rangle\langle\Phi_0| = \hat{P}, \\ \hat{Q}^2 &= (\hat{1} - \hat{P})^2 = \hat{1} - \hat{P} - \hat{P} + \hat{P}^2 = \hat{1} - \hat{P} = \hat{Q}, \\ \hat{P}\hat{Q} &= \hat{Q}\hat{P} = \hat{0},\end{aligned}\tag{2.48}$$

as required for projection operators. (A more general expression for these operators, applicable to nonorthonormal zero-order functions as long as Φ_0 is orthogonal to all the other Φ_i , is given by the form

$$\begin{aligned}\hat{P} &= |\Phi_0\rangle\langle\Phi_0|\Phi_0\rangle^{-1}\langle\Phi_0|, \\ \hat{Q} &= |\mathbf{h}\rangle\langle\mathbf{h}|\mathbf{h}\rangle^{-1}\langle\mathbf{h}|,\end{aligned}\tag{2.49}$$

where $|\mathbf{h}\rangle$ is a row vector consisting of all the functions $|\Phi_i\rangle$ ($i \neq 0$) and $\langle\mathbf{h}|$ is its adjoint column vector. Note that $\langle\mathbf{h}|\mathbf{h}\rangle^{-1} = \mathbf{S}^{-1}$ is the inverse of the overlap matrix $\mathbf{S} = \langle\mathbf{h}|\mathbf{h}\rangle$. It is easy to see that this form of the operators satisfies the projection operator conditions.)

When \hat{P} operates on a general function Ψ expressed in terms of the Φ_i , i.e.

$$\Psi = \sum_i a_i \Phi_i,\tag{2.50}$$

then

$$\hat{P}\Psi = \sum_i a_i |\Phi_0\rangle\langle\Phi_0|\Phi_i\rangle = \sum_i a_i |\Phi_0\rangle\delta_{0i} = a_0 \Phi_0,\tag{2.51}$$

so that \hat{P} extracts the Φ_0 component from Ψ . Similarly, \hat{Q} annihilates the Φ_0 component,

$$\hat{Q}\Psi = (\hat{1} - \hat{P})\Psi = \Psi - a_0 \Phi_0 = \sum'_i a_i \Phi_i.\tag{2.52}$$

The operator \hat{Q} projects out the *orthogonal complement* to Φ_0 . Any function can then be written as a sum of the two projections:

$$\Psi = \hat{1}\Psi = (\hat{P} + \hat{Q})\Psi = \hat{P}\Psi + \hat{Q}\Psi.\tag{2.53}$$

This is often termed the “resolution of the identity” into its components. Similarly, any operator can be resolved into four components,

$$\begin{aligned}\hat{A} &= (\hat{P} + \hat{Q})\hat{A}(\hat{P} + \hat{Q}) \\ &= \underbrace{\hat{P}\hat{A}\hat{P} + \hat{Q}\hat{A}\hat{Q}}_{\hat{A}_D} + \underbrace{\hat{P}\hat{A}\hat{Q} + \hat{Q}\hat{A}\hat{P}}_{\hat{A}_X},\end{aligned}\tag{2.54}$$

where $\hat{A}_D = \hat{P}\hat{A}\hat{P} + \hat{Q}\hat{A}\hat{Q}$ is the block-diagonal part of \hat{A} (also called \hat{A}_E , or the *even* part) and $\hat{A}_X = \hat{P}\hat{A}\hat{Q} + \hat{Q}\hat{A}\hat{P}$ is the cross- or off-diagonal part (also called \hat{A}_O , or the *odd* part). Note that

$$\begin{aligned}(\hat{A}\hat{B})_D &= \hat{A}_D\hat{B}_D + \hat{A}_X\hat{B}_X, \\ (\hat{A}\hat{B})_X &= \hat{A}_D\hat{B}_X + \hat{A}_X\hat{B}_D.\end{aligned}\tag{2.55}$$

The projection operators \hat{P} and \hat{Q} commute with \hat{H}_0 . For a general function f expanded in the zero-order functions Φ_i ,

$$f = \sum_i c_i \Phi_i, \tag{2.56}$$

we have

$$\begin{aligned}\hat{P}\hat{H}_0 f &= \sum_i c_i \hat{P}\hat{H}_0 \Phi_i = \sum_i c_i E_i^{(0)} \hat{P}\Phi_i = c_0 E_0^{(0)} \Phi_0, \\ \hat{H}_0 \hat{P} f &= \sum_i c_i \hat{H}_0 \hat{P}\Phi_i = c_0 \hat{H}_0 \Phi_0 = c_0 E_0^{(0)} \Phi_0.\end{aligned}\tag{2.57}$$

Thus $\hat{P}\hat{H}_0 = \hat{H}_0\hat{P}$ (since f is arbitrary), so that $[\hat{P}, \hat{H}_0] = 0$. Similarly $[\hat{Q}, \hat{H}_0] = 0$ (to see this, set $\hat{Q} = \hat{1} - \hat{P}$).

2.4 General derivation of formal time-independent perturbation theories

2.4.1 General formalism

Now we turn to a more general, and somewhat more elegant, derivation of the perturbation equations. We shall use $\lambda = 1$ and determine the ordering of the contributions to E_n and Ψ_n on the basis of the number of \hat{V} factors and other considerations. We shall continue to use the index 0, instead of n , to indicate the state in which we are interested (regardless of whether it is the ground state or some excited state), and shall omit this index altogether whenever there is no danger of confusion.

To be more general, we shall not always require that all the functions Φ_i , in terms of which the solutions are to be expanded, are eigenfunctions of \hat{H}_0 . The only requirements are that these functions are orthonormal, that Φ_0 is an eigenfunction of \hat{H}_0 and that all other Φ_i span the orthogonal complement of Φ_0 . The case in which all the Φ_i are eigenfunctions of \hat{H}_0 , in which some simplifications are possible, will be referred to as the *diagonal case*, because in terms of these functions the matrix representation of \hat{H}_0 is diagonal.

We begin the derivation with the Schrödinger equation in the form

$$(\hat{H}_0 + \hat{V})\Psi = E\Psi, \quad (2.58)$$

with zero-order solution

$$\hat{H}_0\Phi_0 = E_0^{(0)}\Phi_0. \quad (2.59)$$

Operating on (2.58) with $\langle\Phi_0|$ we obtain

$$\underbrace{\langle\Phi_0|\hat{H}_0|}_{=E_0^{(0)}\langle\Phi_0|}\Psi\rangle + \langle\Phi_0|V|\Psi\rangle = E\langle\Phi_0|\Psi\rangle, \quad (2.60)$$

where we have used the Hermitian property of \hat{H}_0 . With intermediate normalization this gives

$$E_0^{(0)} + \langle\Phi_0|V|\Psi\rangle = E,$$

so that

$$\Delta E = \langle\Phi_0|V|\Psi\rangle, \quad (2.61)$$

as we already know. Next, we write Ψ in the form

$$\begin{aligned} \Psi &= \hat{P}\Psi + \hat{Q}\Psi = |\Phi_0\rangle\langle\Phi_0|\Psi\rangle + \sum_i' |\Phi_i\rangle\langle\Phi_i|\Psi\rangle \\ &= \Phi_0 + \chi, \end{aligned} \quad (2.62)$$

whence

$$\Phi_0 = \hat{P}\Psi, \quad \chi = \hat{Q}\Psi. \quad (2.63)$$

Rearranging the Schrödinger equation (2.58) as

$$-\hat{H}_0\Psi = (\hat{V} - E)\Psi, \quad (2.64)$$

we introduce an arbitrary parameter ζ by adding $\zeta\Psi$ to each side:

$$(\zeta - \hat{H}_0)\Psi = (\hat{V} - E + \zeta)\Psi. \quad (2.65)$$

This parameter is a convenience that will allow us to obtain different perturbation expansions from the same development by different choices of ζ (e.g., $\zeta = E$ or $\zeta = E_0^{(0)}$).

We next apply \hat{Q} to both sides:

$$\hat{Q}(\zeta - \hat{H}_0)\Psi = \hat{Q}(\hat{V} - E + \zeta)\Psi. \quad (2.66)$$

Using the idempotency of \hat{Q} and its commutation with \hat{H}_0 , the operator on the left-hand side can be rewritten as

$$\hat{Q}(\zeta - \hat{H}_0)\Psi = \hat{Q}^2(\zeta - \hat{H}_0)\Psi = \hat{Q}(\zeta - \hat{H}_0)\hat{Q}\Psi. \quad (2.67)$$

The operator $\hat{Q}(\zeta - \hat{H}_0)\hat{Q}$ operates entirely in Q -space and in terms of the zero-order functions has the expansion

$$\hat{Q}(\zeta - \hat{H}_0)\hat{Q} = \sum_i' \sum_j' |\Phi_i\rangle \langle \Phi_i | \zeta - \hat{H}_0 | \Phi_j\rangle \langle \Phi_j|, \quad (2.68)$$

which simplifies in the diagonal case to

$$\hat{Q}(\zeta - \hat{H}_0)\hat{Q} = \sum_i' |\Phi_i\rangle (\zeta - E_i^{(0)}) \langle \Phi_i|. \quad (2.69)$$

Going back to the rewritten Schrödinger equation (2.66), we now have

$$\hat{Q}(\zeta - \hat{H}_0)\hat{Q}\Psi = \hat{Q}(\hat{V} - E + \zeta)\Psi. \quad (2.70)$$

We restrict the possible choices of ζ to those that do not coincide with any of the eigenvalues of \hat{H}_0 in Q -space, so that the inverse of $\hat{Q}(\zeta - \hat{H}_0)\hat{Q}$ in Q -space exists. (If $E_0^{(0)}$ is a well-separated eigenvalue of \hat{H}_0 then a choice of ζ in the neighborhood of $E_0^{(0)}$ would be satisfactory.) This inverse is written in the form

$$\hat{R}_0(\zeta) = \frac{\hat{Q}}{\zeta - \hat{H}_0} \equiv \sum_i' \sum_j' |\Phi_i\rangle \langle \Phi_i | (\zeta - \hat{H}_0)^{-1} | \Phi_j\rangle \langle \Phi_j| \quad (2.71)$$

and is called the *resolvent* of \hat{H}_0 . In the diagonal case it can be expressed as

$$\hat{R}_0(\zeta) = \sum_i' \sum_j' |\Phi_i\rangle \langle \Phi_i | (\zeta - E_j^{(0)})^{-1} | \Phi_j\rangle \langle \Phi_j| = \sum_i' \frac{|\Phi_i\rangle \langle \Phi_i|}{(\zeta - E_i^{(0)})}, \quad (2.72)$$

which rationalizes the notation

$$\frac{\hat{Q}}{\zeta - \hat{H}_0}.$$

(If $\hat{H}\phi = \varepsilon\phi$ then $f(\hat{H})\phi = f(\varepsilon)\phi$; here $f(\hat{H}_0) = (\zeta - \hat{H}_0)^{-1}$.)

It is easy to see that $\hat{R}_0(\zeta)$ as given in the previous equation is the inverse of $\hat{Q}(\zeta - \hat{H}_0)\hat{Q}$ in Q -space, since

$$\begin{aligned}
& \frac{\hat{Q}}{\zeta - \hat{H}_0} \hat{Q}(\zeta - \hat{H}_0) \hat{Q} \\
&= \left(\sum'_{i,j} |\Phi_i\rangle \langle \Phi_i| (\zeta - \hat{H}_0)^{-1} |\Phi_j\rangle \langle \Phi_j| \right) \left(\sum'_{k,l} |\Phi_k\rangle \langle \Phi_k| (\zeta - \hat{H}_0) |\Phi_l\rangle \langle \Phi_l| \right) \\
&= \sum'_{i,l} |\Phi_i\rangle \left\langle \Phi_i \left| (\zeta - \hat{H}_0)^{-1} \left(\sum'_j |\Phi_j\rangle \langle \Phi_j| \right) (\zeta - \hat{H}_0) \right| \Phi_l \right\rangle \\
&= \sum'_{i,l} |\Phi_i\rangle \left\langle \Phi_i \left| (\zeta - \hat{H}_0)^{-1} (1 - |\Phi_0\rangle \langle \Phi_0|) (\zeta - \hat{H}_0) \right| \Phi_l \right\rangle \langle \Phi_l| \\
&= \sum'_i |\Phi_i\rangle \langle \Phi_i| = \hat{Q}, \tag{2.73}
\end{aligned}$$

because the sums exclude $i = 0$, $l = 0$. (Note that the inverse of an operator \hat{A} in Q -space is any operator \hat{B} that satisfies $\hat{A}\hat{B} = \hat{B}\hat{A} = \hat{Q}$. It is not necessarily a general inverse, i.e. in the complete Hilbert space. Projection operators have no inverses outside the space onto which they project; within that space they are their own inverses, since, e.g., $\hat{Q}\hat{Q} = \hat{Q}$.)

Applying $\hat{R}_0(\zeta) = \frac{\hat{Q}}{\zeta - \hat{H}_0}$ to both sides of (2.70), we get

$$\hat{Q}\Psi = \hat{R}_0(\zeta)(\hat{V} - E + \zeta)\Psi, \tag{2.74}$$

and thus, substituting in $\Psi = \Phi_0 + \hat{Q}\Psi$, we have

$$\Psi = \Phi_0 + \hat{R}_0(\zeta)(\hat{V} - E + \zeta)\Psi. \tag{2.75}$$

This can be seen as an iterative equation for Ψ . For example, substituting the entire right-hand side of (2.75) into the Ψ on the right-hand side of the same equation, we have

$$\begin{aligned}
\Psi &= \Phi_0 + \hat{R}_0(\zeta)(\hat{V} - E + \zeta)\Phi_0 \\
&\quad + \hat{R}_0(\zeta)(\hat{V} - E + \zeta)\hat{R}_0(\zeta)(\hat{V} - E + \zeta)\Psi
\end{aligned} \tag{2.76}$$

and, if we continue in the same manner,

$$\Psi = \sum_{m=0}^{\infty} \{ \hat{R}_0(\zeta)(\hat{V} - E + \zeta) \}^m \Phi_0 \tag{2.77}$$

(provided that the series converges). This would be a formal solution to the problem except that the unknown E appears on the right-hand side. For the same reason, the m th term in the sum does not simply correspond to the

m th-order correction to the wave function, since E contains contributions of different orders. In any case, using $\Delta E = \langle \Phi_0 | \hat{V} | \Psi \rangle$ we have, formally,

$$\Delta E = \sum_{m=0}^{\infty} \langle \Phi_0 | \hat{V} \left[\hat{R}_0(\zeta)(\hat{V} - E + \zeta) \right]^m | \Phi_0 \rangle, \quad (2.78)$$

which is an implicit equation for $E = E_0^{(0)} + \Delta E$.

2.4.2 Brillouin–Wigner perturbation theory

Different choices of ζ can now be made in order to obtain different types of perturbation theory (PT) expansions. The first is the choice $\zeta = E$, which produces *Brillouin–Wigner* PT (BWPT) (Brillouin 1932, Wigner 1935). This choice cancels $-E + \zeta$ in $\hat{R}_0(\zeta)(\hat{V} - E + \zeta)^m$ and leads to

$$\begin{aligned} \Psi &= \sum_{m=0}^{\infty} \{ \hat{R}_0(E) \hat{V} \}^m \Phi_0 \\ \Delta E &= \sum_{m=0}^{\infty} \langle \Phi_0 | \hat{V} \{ \hat{R}_0(E) \hat{V} \}^m | \Phi_0 \rangle \end{aligned} \quad (\text{BWPT}). \quad (2.79)$$

More explicitly, the energy expansion becomes

$$\begin{aligned} \Delta E &= \langle \Phi_0 | \hat{V} | \Phi_0 \rangle + \langle \Phi_0 | \hat{V} \hat{R}_0(E) \hat{V} | \Phi_0 \rangle \\ &\quad + \langle \Phi_0 | \hat{V} \hat{R}_0(E) \hat{V} \hat{R}_0(E) \hat{V} | \Phi_0 \rangle + \cdots, \end{aligned} \quad (2.80)$$

but the equations are still implicit, since the unknown E appears on the r.h.s. In principle, they can be solved iteratively. Put in an estimate for E , such as the first-order result $E_0^{(0)} + \langle \Phi_0 | \hat{V} | \Phi_0 \rangle$ and then compute the second-order correction. Use the corrected E to compute a better second- (and/or third-) order correction, etc., until self-consistency is obtained. However, this procedure is generally too cumbersome to be very practical.

It is instructive to see how the BWPT equations would be evaluated (ignoring the problem with E), assuming the diagonal case for simplicity. In this case

$$\hat{R}_0(E) = \frac{\hat{Q}}{E - \hat{H}_0} = \sum_i' |\Phi_i\rangle \frac{1}{E - E_i^{(0)}} \langle \Phi_i|, \quad (2.81)$$

and the second-order energy becomes

$$\begin{aligned}
 E^{(2)} &= \langle \Phi_0 | \hat{V} \hat{R}_0(E) \hat{V} | \Phi_0 \rangle \\
 &= \sum_i' \langle \Phi_0 | \hat{V} | \Phi_i \rangle (E - E_i^{(0)})^{-1} \langle \Phi_i | \hat{V} | \Phi_0 \rangle \\
 &= \sum_i' \frac{V_{0i} V_{i0}}{E - E_i^{(0)}}, \tag{2.82}
 \end{aligned}$$

which is similar to the RSPT result except for the presence of E rather than $E_0^{(0)}$ in the denominator. Similarly, for third order:

$$\begin{aligned}
 E^{(3)} &= \sum_{i,j}' \langle \Phi_0 | \hat{V} | \Phi_i \rangle (E - E_i^{(0)})^{-1} \langle \Phi_i | \hat{V} | \Phi_j \rangle (E - E_j^{(0)})^{-1} \langle \Phi_j | \hat{V} | \Phi_0 \rangle \\
 &= \sum_{i,j}' \frac{V_{0i} V_{ij} V_{j0}}{(E - E_i^{(0)})(E - E_j^{(0)})} \tag{BWPT} \tag{2.83}
 \end{aligned}$$

etc.

The form of these equations is actually simpler than that of the RSPT equations (ignoring the problem of the unknown E in the denominators), because of the absence of the so-called *renormalization terms* – the additional sums $\sum_{l=0}^{m-1}$ involving the lower-order energies in RSPT. However, it does not provide a true order-by-order expansion for the energy (because of the presence of the infinite-order E), and related to this is a very fundamental problem with BWPT, its lack of extensivity when stopped at any finite order. In fact, BWPT resembles CI in many respects, and successive orders of the BWPT calculation are closely related to the successive iterations used to solve the matrix eigenvalue problem in some CI procedures.

2.4.3 Demonstration of non-extensivity of finite-order BWPT

We shall consider again the model problem of N noninteracting He atoms, and take the second-order energy as an example:

$$E^{(2)} = \sum_i' \frac{|V_{i0}|^2}{E - E_i^{(0)}}, \tag{2.84}$$

where E is the exact ground-state energy and $E_0^{(0)}, E_i^{(0)}, \dots$ are the zero-order energies associated with the zero-order functions Φ_0, Φ_i, \dots . We shall use a basis of two configurations per atom, $\phi_0(i)$ and $\chi(i)$ for the i th atom, as in Section 1.7. In this basis the complete Hamiltonian for one atom is

$$\hat{h} = (\hat{P} + \hat{Q})\hat{h}(\hat{P} + \hat{Q}) = \hat{P}\hat{h}\hat{P} + \hat{P}\hat{h}\hat{Q} + \hat{Q}\hat{h}\hat{P} + \hat{Q}\hat{h}\hat{Q} \tag{2.85}$$

(here $\hat{P} = |\phi_0\rangle\langle\phi_0|$, $\hat{Q} = |\chi\rangle\langle\chi|$) and, using the notation of Section 1.7,

$$\hat{h} = |\phi_0\rangle\varepsilon_0\langle\phi_0| + |\phi_0\rangle\beta\langle\chi| + |\chi\rangle\beta^*\langle\phi_0| + |\chi\rangle\alpha\langle\chi|. \quad (2.86)$$

The zero-order Hamiltonian for the atom can be taken as the diagonal part,

$$\hat{h}_0 = |\phi_0\rangle\varepsilon_0\langle\phi_0| + |\chi\rangle\alpha\langle\chi|, \quad (2.87)$$

and the perturbation \hat{v} is

$$\hat{v} = |\phi_0\rangle\beta\langle\chi| + |\chi\rangle\beta^*\langle\phi_0|. \quad (2.88)$$

Note that ϕ_0 and χ are eigenfunctions of \hat{h}_0 with eigenvalues ε_0 and α , respectively:

$$\begin{aligned} \hat{h}_0|\phi_0\rangle &= |\phi_0\rangle\varepsilon_0 \underbrace{\langle\phi_0|\phi_0\rangle}_{=1} + |\chi\rangle\alpha \underbrace{\langle\chi|\phi_0\rangle}_{=0} = \varepsilon_0|\phi_0\rangle, \\ \hat{h}_0|\chi\rangle &= |\phi_0\rangle\varepsilon_0\langle\phi_0|\chi\rangle + |\chi\rangle\alpha\langle\chi|\chi\rangle = \alpha|\chi\rangle. \end{aligned} \quad (2.89)$$

The basis for N atoms is the set of functions

$$\begin{aligned} \Phi_0 &= \mathcal{A}\phi_0(1)\phi_0(2)\cdots\phi_0(N), \\ \Phi_i &= \mathcal{A}\phi_0(1)\cdots\chi(i)\cdots\phi_0(N), \\ \Phi_{ij} &= \mathcal{A}\phi_0(1)\cdots\chi(i)\cdots\chi(j)\cdots\phi_0(N), \end{aligned} \quad (2.90)$$

etc. The zero-order Hamiltonian is $\hat{H}_0 = \sum_i \hat{h}_0(i)$, also given as

$$\begin{aligned} \hat{H}_0 &= |\Phi_0\rangle\langle\Phi_0|\hat{H}|\Phi_0\rangle\langle\Phi_0| + \sum_i |\Phi_i\rangle\langle\Phi_i|\hat{H}|\Phi_i\rangle\langle\Phi_i| \\ &\quad + \sum_{i<j} |\Phi_{ij}\rangle\langle\Phi_{ij}|\hat{H}|\Phi_{ij}\rangle\langle\Phi_{ij}| + \dots \\ &= |\Phi_0\rangle E_0^{(0)}\langle\Phi_0| + \sum_i |\Phi_i\rangle E_i^{(0)}\langle\Phi_i| + \sum_{i<j} |\Phi_{ij}\rangle E_{ij}^{(0)}\langle\Phi_{ij}| + \dots \end{aligned} \quad (2.91)$$

(note that the sums exclude $i = 0$, $j = 0$, etc.), in which (see Section 1.7)

$$E_i^{(0)} = E_0^{(0)} + \alpha - \varepsilon_0, \quad E_{ij}^{(0)} = E_0^{(0)} + 2\alpha - 2\varepsilon_0, \dots \quad (2.92)$$

This zero-order Hamiltonian has the above basis functions as eigenfunctions:

$$\begin{aligned} \hat{H}_0|\Phi_0\rangle &= |\Phi_0\rangle E_0^{(0)}\langle\Phi_0|\Phi_0\rangle + 0 = E_0^{(0)}|\Phi_0\rangle, \\ \hat{H}_0|\Phi_i\rangle &= \sum_j |\Phi_j\rangle E_j^{(0)} \underbrace{\langle\Phi_j|\Phi_i\rangle}_{\delta_{ij}} + 0 = (E_0^{(0)} + \alpha - \varepsilon_0)|\Phi_i\rangle, \end{aligned} \quad (2.93)$$

etc. The perturbation consists of the cross terms:

$$\begin{aligned} \hat{V} = & \sum_i |\Phi_0\rangle \beta \langle \Phi_i| + \sum_{i < j} |\Phi_i\rangle \beta \langle \Phi_{ij}| + \sum_{i < j} |\Phi_j\rangle \beta \langle \Phi_{ij}| \\ & + \sum_i |\Phi_i\rangle \beta^* \langle \Phi_0| + \sum_{i < j} |\Phi_{ij}\rangle \beta^* \langle \Phi_i| + \sum_{i < j} |\Phi_{ij}\rangle \beta^* \langle \Phi_j| + \dots \end{aligned} \quad (2.94)$$

In all nonzero terms $|\Phi \dots\rangle \dots \langle \Phi \dots|$ in \hat{V} the number of excited atoms in the ket and bra differs by exactly unity, and all other indices are identical in the two $\Phi \dots$ functions. In all other cases the corresponding matrix elements vanish, e.g., $\langle \Phi_i | \hat{H} | \Phi_{jk} \rangle = \sum_l \langle \Phi_i | \hat{h}(l) | \Phi_{jk} \rangle = 0$ ($i \neq j, i \neq k$).

The only matrix elements we need for the second-order energy are

$$V_{0i} = \langle \Phi_0 | \hat{V} | \Phi_i \rangle = \beta \quad (2.95)$$

(which are independent of N). The denominators are

$$E - E_i^{(0)} = E - (E_0^{(0)} + \alpha - \varepsilon_0) = \Delta E - \alpha + \varepsilon_0. \quad (2.96)$$

We can proceed in one of two ways, as follows.

1. We can use our knowledge of the exact $E = N\varepsilon$, or $\Delta E = E - E_0^{(0)} = N\varepsilon - N\varepsilon_0 = N\Delta\varepsilon$, giving the second-order energy

$$E^{(2)} = \sum_i \frac{|V_{0i}|^2}{N\Delta\varepsilon - \alpha + \varepsilon_0} = \sum_{i=1}^N \frac{|\beta|^2}{N\Delta\varepsilon - \alpha + \varepsilon_0} = \frac{N|\beta|^2}{N\Delta\varepsilon - \alpha + \varepsilon_0};$$

thus

$$\lim_{N \rightarrow \infty} E^{(2)} = \frac{|\beta|^2}{\Delta\varepsilon} = \text{constant}. \quad (2.97)$$

2. We can use $E^{(2)}$ instead of $E - E_0^{(0)} = \Delta E$ (note that $E^{(1)} = V_{00} = 0$ in this example):

$$E^{(2)} = \frac{N|\beta|^2}{E^{(2)} - \alpha + \varepsilon_0}, \quad (E^{(2)})^2 + (\varepsilon_0 - \alpha)E^{(2)} - N|\beta|^2 = 0;$$

thus

$$E^{(2)} = \frac{1}{2}(\alpha - \varepsilon_0) \pm \frac{1}{2}\sqrt{(\alpha - \varepsilon_0)^2 + 4N|\beta|^2}, \quad (2.98)$$

just as in CID, with the same limiting behavior as $N \rightarrow \infty$, $E^{(2)} \rightarrow -|\beta|\sqrt{N}$.

In neither case have we obtained the extensive result, $E^{(2)} \propto N$. It is the fact that we have E rather than $E^{(0)}$ in the denominator that is responsible for the lack of extensivity.

2.4.4 Formal Rayleigh–Schrödinger perturbation theory

Returning to the general results (2.77), (2.78), we will now derive the *Rayleigh–Schrödinger* perturbation theory (RSPT) (Rayleigh 1894, Schrödinger 1926) by setting

$$\zeta = E_0^{(0)} \quad (\text{RSPT}), \quad (2.99)$$

so that

$$\zeta - E = -\Delta E. \quad (2.100)$$

We then have

$$\begin{aligned} \Psi &= \sum_{m=0}^{\infty} \left[\hat{R}_0(E_0^{(0)})(\hat{V} - \Delta E) \right]^m \Phi_0 \\ \Delta E &= \sum_{m=0}^{\infty} \langle \Phi_0 | \hat{V} \left[\hat{R}_0(E_0^{(0)})(\hat{V} - \Delta E) \right]^m | \Phi_0 \rangle \end{aligned} \quad (\text{RSPT}). \quad (2.101)$$

Thus we have removed the unknown E in the denominators in \hat{R}_0 , but we still have ΔE in $\hat{V} - \Delta E$. Because of the presence of ΔE we do not yet have a true expansion in orders of λ (or orders of \hat{V}). This presence can be removed by substituting the formula in 2.101 for each ΔE on the r.h.s., iteratively, and collecting terms of each order of λ by counting the number of \hat{V} factors in each term.

We shall now proceed to do that, simplifying the notation further by omitting the argument $E_0^{(0)}$ from the resolvent $\hat{R}_0(E_0^{(0)}) \equiv \hat{R}_0$ and omitting the subscript 0 from Φ_0 . We then have

$$\begin{aligned} \Psi &= \sum_{m=0}^{\infty} \left[\hat{R}_0(\hat{V} - \Delta E) \right]^m \Phi \\ \Delta E &= \sum_{m=0}^{\infty} \langle \Phi | \hat{V} \left[\hat{R}_0(\hat{V} - \Delta E) \right]^m | \Phi \rangle \end{aligned} \quad (\text{RSPT}). \quad (2.102)$$

We will examine the energy expression first, since ΔE appears on the r.h.s. in both equations. Expanding the first few orders for ΔE , we get

$$\begin{aligned} \Delta E &= \langle \Phi | \hat{V} | \Phi \rangle + \langle \Phi | \hat{V} \hat{R}_0(\hat{V} - \Delta E) | \Phi \rangle \\ &\quad + \langle \Phi | \hat{V} \hat{R}_0(\hat{V} - \Delta E) \hat{R}_0(\hat{V} - \Delta E) | \Phi \rangle \\ &\quad + \langle \Phi | \hat{V} \hat{R}_0(\hat{V} - \Delta E) \hat{R}_0(\hat{V} - \Delta E) \hat{R}_0(\hat{V} - \Delta E) | \Phi \rangle + \dots \end{aligned} \quad (2.103)$$

First we note that the final ΔE in each term can be ignored, because

$$\hat{R}_0 \Delta E | \Phi \rangle = \Delta E \hat{R}_0 | \Phi \rangle = 0 \quad (2.104)$$

(since \hat{R}_0 contains \hat{Q}). Thus

$$\begin{aligned}
\Delta E &= \langle \Phi | \hat{V} | \Phi \rangle + \langle \Phi | \hat{V} \hat{R}_0 \hat{V} | \Phi \rangle + \langle \Phi | \hat{V} \hat{R}_0 (\hat{V} - \Delta E) \hat{R}_0 \hat{V} | \Phi \rangle \\
&\quad + \langle \Phi | \hat{V} \hat{R}_0 (\hat{V} - \Delta E) \hat{R}_0 (\hat{V} - \Delta E) \hat{R}_0 \hat{V} | \Phi \rangle + \dots \\
&= \langle \Phi | \hat{V} | \Phi \rangle + \langle \Phi | \hat{V} \hat{R}_0 \hat{V} | \Phi \rangle + \langle \Phi | \hat{V} \hat{R}_0 \hat{V} \hat{R}_0 \hat{V} | \Phi \rangle \\
&\quad - \langle \Phi | \hat{V} \hat{R}_0 \langle \Phi | \hat{V} | \Phi \rangle \hat{R}_0 \hat{V} | \Phi \rangle - \langle \Phi | \hat{V} \hat{R}_0 \langle \Phi | \hat{V} \hat{R}_0 \hat{V} | \Phi \rangle \hat{R}_0 \hat{V} | \Phi \rangle - \dots \\
&\quad + \langle \Phi | \hat{V} \hat{R}_0 \hat{V} \hat{R}_0 \hat{V} \hat{R}_0 \hat{V} | \Phi \rangle \\
&\quad - \langle \Phi | \hat{V} \hat{R}_0 \hat{V} \hat{R}_0 \langle \Phi | \hat{V} | \Phi \rangle \hat{R}_0 \hat{V} | \Phi \rangle - \langle \Phi | \hat{V} \hat{R}_0 \langle \Phi | \hat{V} | \Phi \rangle \hat{R}_0 \hat{V} \hat{R}_0 \hat{V} | \Phi \rangle \\
&\quad + \langle \Phi | \hat{V} \hat{R}_0 \langle \Phi | \hat{V} | \Phi \rangle \hat{R}_0 \langle \Phi | \hat{V} | \Phi \rangle \hat{R}_0 \hat{V} | \Phi \rangle + \dots
\end{aligned} \tag{2.105}$$

Arranging this result according to the number of \hat{V} factors (i.e., in orders of λ) we have

$$\begin{aligned}
\Delta E &= \langle \Phi | \hat{V} | \Phi \rangle + \langle \Phi | \hat{V} \hat{R}_0 \hat{V} | \Phi \rangle \\
&\quad + \langle \Phi | \hat{V} \hat{R}_0 \hat{V} \hat{R}_0 \hat{V} | \Phi \rangle - \langle \Phi | \hat{V} | \Phi \rangle \langle \Phi | \hat{V} \hat{R}_0^2 \hat{V} | \Phi \rangle \\
&\quad + \langle \Phi | \hat{V} \hat{R}_0 \hat{V} \hat{R}_0 \hat{V} \hat{R}_0 \hat{V} | \Phi \rangle - \langle \Phi | \hat{V} \hat{R}_0 \hat{V} | \Phi \rangle \langle \Phi | \hat{V} \hat{R}_0^2 \hat{V} | \Phi \rangle \\
&\quad - \langle \Phi | \hat{V} | \Phi \rangle \langle \Phi | \hat{V} \hat{R}_0 (\hat{V} \hat{R}_0 + \hat{R}_0 \hat{V}) \hat{R}_0 \hat{V} | \Phi \rangle \\
&\quad + \langle \Phi | \hat{V} | \Phi \rangle^2 \langle \Phi | \hat{V} \hat{R}_0^3 \hat{V} | \Phi \rangle + \dots
\end{aligned} \tag{2.106}$$

Thus

$$\begin{aligned}
E^{(1)} &= \langle \Phi | \hat{V} | \Phi \rangle = V_{00}, \\
E^{(2)} &= \langle \Phi | \hat{V} \hat{R}_0 \hat{V} | \Phi \rangle, \\
E^{(3)} &= \langle \Phi | \hat{V} \hat{R}_0 (\hat{V} - \langle \Phi | \hat{V} | \Phi \rangle) \hat{R}_0 \hat{V} | \Phi \rangle = \langle \Phi | \hat{V} \hat{R}_0 (\hat{V} - E^{(1)}) \hat{R}_0 \hat{V} | \Phi \rangle, \\
E^{(4)} &= \langle \Phi | \hat{V} \hat{R}_0 (\hat{V} - E^{(1)}) \hat{R}_0 (\hat{V} - E^{(1)}) \hat{R}_0 \hat{V} | \Phi \rangle - E^{(2)} \langle \Phi | \hat{V} \hat{R}_0^2 \hat{V} | \Phi \rangle.
\end{aligned} \tag{2.107}$$

The combination $\hat{V} - E^{(1)}$ appears very frequently, and it is convenient to use a special symbol for it,

$$\hat{W} = \hat{V} - E^{(1)}, \tag{2.108}$$

so that

$$W_{ij} = V_{ij} - \delta_{ij} E^{(1)}, \tag{2.109}$$

and we have

$$\begin{aligned}
E^{(3)} &= \langle \Phi | \hat{V} \hat{R}_0 \hat{W} \hat{R}_0 \hat{V} | \Phi \rangle \\
E^{(4)} &= \langle \Phi | \hat{V} \hat{R}_0 \hat{W} \hat{R}_0 \hat{W} \hat{R}_0 \hat{V} | \Phi \rangle - E^{(2)} \langle \Phi | \hat{V} \hat{R}_0^2 \hat{V} | \Phi \rangle,
\end{aligned} \tag{2.110}$$

etc. In the diagonal case we can make these equations more explicit. Using the abbreviation

$$D_{0i} = E_0^{(0)} - E_i^{(0)} \quad (2.111)$$

for the denominators in the resolvent, the various orders of the energy can be written in the diagonal case in the form:

$$\begin{aligned} E^{(1)} &= V_{00}, \\ E^{(2)} &= \sum_i' \frac{V_{0i} V_{i0}}{D_{0i}}, \\ E^{(3)} &= \sum_{ij} \frac{V_{0i} W_{ij} V_{j0}}{D_{0i} D_{0j}}, \\ E^{(4)} &= \sum_{ijk} \frac{V_{0i} W_{ij} W_{jk} V_{k0}}{D_{0i} D_{0j} D_{0k}} - E^{(2)} \sum_i' \frac{V_{0i} V_{i0}}{D_{0i}^2}. \end{aligned} \quad (2.112)$$

We see that each $E^{(m)}$ contains a *principal term*,

$$\langle \Phi | \hat{V} \hat{R}_0 \hat{W} \hat{R}_0 \hat{W} \cdots \hat{W} \hat{R}_0 \hat{V} | \Phi \rangle = \sum_{ijk \cdots yz} \frac{V_{0i} W_{ij} W_{jk} \cdots W_{yz} V_{z0}}{D_{0i} D_{0j} D_{0k} \cdots D_{0y} D_{0z}}, \quad (2.113)$$

with m factors \hat{V} , \hat{W} , $m-1$ factors \hat{R}_0 and some *renormalization terms*; these contain lower-order energies $E^{(l)}$ ($2 \leq l \leq m-2$) and factors involving powers \hat{R}_0^k ($k > 1$). (It is convenient not to consider the $E^{(1)}$ terms in \hat{W} as renormalization terms, since they are simply accommodated by a shift of origin for \hat{V} , replacing \hat{V} by \hat{W} , as shown at the end of this subsection.)

Similarly, for the wave function we obtain (the general form is followed by the diagonal-case formula in each equation):

$$\begin{aligned} \Psi^{(1)} &= \hat{R}_0 \hat{V} | \Phi \rangle = \sum_i' | \Phi_i \rangle \frac{V_{i0}}{D_{0i}}, \\ \Psi^{(2)} &= \hat{R}_0 \hat{W} \hat{R}_0 \hat{V} | \Phi \rangle = \sum_{ij} | \Phi_i \rangle \frac{W_{ij} V_{j0}}{D_{0i} D_{0j}}, \\ \Psi^{(3)} &= \hat{R}_0 \hat{W} \hat{R}_0 \hat{W} \hat{R}_0 \hat{V} | \Phi \rangle - \langle \Phi | \hat{V} \hat{R}_0 \hat{V} | \Phi \rangle \hat{R}_0^2 \hat{V} | \Phi \rangle \\ &= \sum_{ijk} | \Phi_i \rangle \frac{W_{ij} W_{jk} V_{k0}}{D_{0i} D_{0j} D_{0k}} - E^{(2)} \sum_i' | \Phi_i \rangle \frac{V_{i0}}{D_{0i}^2}, \end{aligned} \quad (2.114)$$

etc. If we now look back at $E^{(4)}$ we see that the renormalization term there can be written as

$$E^{(2)} \langle \Phi | \hat{V} \hat{R}_0 \hat{R}_0 \hat{V} | \Phi \rangle = E^{(2)} \langle \hat{R}_0 \hat{V} \Phi | \hat{R}_0 \hat{V} \Phi \rangle = E^{(2)} \langle \Psi^{(1)} | \Psi^{(1)} \rangle, \quad (2.115)$$

so that

$$\begin{aligned} E^{(4)} &= \langle \Phi | \hat{V} \hat{R}_0 \hat{W} \hat{R}_0 \hat{W} \hat{R}_0 \hat{V} | \Phi \rangle - E^{(2)} \langle \Psi^{(1)} | \Psi^{(1)} \rangle \\ &= \sum_{ijk}' \frac{V_{0i} W_{ij} W_{jk} V_{k0}}{D_{0i} D_{0j} D_{0k}} - E^{(2)} \langle \Psi^{(1)} | \Psi^{(1)} \rangle \quad (\text{RSPT}). \end{aligned} \quad (2.116)$$

This is a well-known form for $E^{(4)}$.

Note that $E^{(1)} = V_{00}$ could be eliminated completely from the analysis if \hat{H}_0 shifted by V_{00} , as follows:

$$\begin{aligned} \hat{H} &= \hat{H}_0 + \hat{V} \\ &= (\hat{H}_0 + V_{00}) + (\hat{V} - V_{00}) \\ &= \hat{\hat{H}}_0 + \hat{W}, \end{aligned} \quad (2.117)$$

where

$$\hat{\hat{H}}_0 = \hat{H}_0 + V_{00}, \quad \hat{W} = \hat{V} - V_{00}, \quad V_{00} = \langle \Phi_0 | \hat{V} | \Phi_0 \rangle = E_0^{(1)}. \quad (2.118)$$

In this form $\hat{\hat{H}}_0$ is the new zero-order Hamiltonian and \hat{W} is the perturbation. In the diagonal case the original zeroth-order functions Φ_i are still eigenfunctions of the new $\hat{\hat{H}}_0$, with eigenvalues $V_{00} + E_i^{(0)}$. The factors D_{0i} in the denominators, which are differences of eigenvalues, are unchanged. With this new splitting of the Hamiltonian we have

$$\tilde{E}_0^{(0)} = \langle \Phi | \hat{\hat{H}}_0 + V_{00} | \Phi \rangle = E_0^{(0)} + V_{00} \quad (2.119)$$

(which equals E_{SCF} if Φ is the SCF wave function) and

$$\tilde{E}_0^{(1)} = \langle \Phi | \hat{V} - V_{00} | \Phi \rangle = V_{00} - V_{00} = 0, \quad (2.120)$$

i.e., the first-order energy vanishes,

$$W_{00} = 0. \quad (2.121)$$

Higher orders remain unchanged.

2.4.5 The general (non-diagonal) case

In the general case, in which the representation of \hat{H}_0 is non-diagonal, the resolvent \hat{R}_0 is not given explicitly in terms of the zeroth-order energies $E_i^{(0)}$, but it can be obtained by inversion of the matrix representation of $\hat{Q}(E_0^{(0)} - \hat{H}_0)\hat{Q}$. However, explicit inversion of that matrix is not actually required since the quantities needed are matrix elements of $\hat{R}_0\hat{W}$. If we write

$$\hat{X} = \hat{R}_0\hat{W} \quad (2.122)$$

then

$$\hat{Q} \left(E_0^{(0)} - \hat{H}_0 \right) \hat{Q} \hat{X} = \hat{Q} \hat{W}, \quad (2.123)$$

and the matrix representation \mathbf{X} of \hat{X} can be obtained by the solution of the system of linear equations

$$(E_0^{(0)} \mathbf{1} - \mathbf{H}_0) \mathbf{X} = \mathbf{W} \quad (2.124)$$

or, explicitly,

$$\sum_j' (E_0^{(0)} \delta_{ij} - (\hat{H}_0)_{ij}) X_{jk} = W_{ik}. \quad (2.125)$$

If the matrix representation of \hat{H}_0 is sparse (as often happens in actual applications), the iterative solution of the linear equation system is relatively easy. Note that only the $k = 0$ column of \mathbf{X} is required for $\hat{R}_0 \hat{V} |\Phi\rangle$, in which case we have $W_{i0} = V_{i0}$ ($i \neq 0$).

Once \mathbf{X} has been obtained, the energy expressions can be determined from

$$\begin{aligned} E^{(2)} &= \langle \Phi | \hat{V} \hat{X} | \Phi \rangle, \\ E^{(3)} &= \langle \Phi | \hat{V} \hat{X}^2 | \Phi \rangle, \\ E^{(4)} &= \langle \Phi | \hat{V} \hat{X}^3 | \Phi \rangle - E^{(2)} \langle \Psi^{(1)} | \Psi^{(1)} \rangle, \end{aligned} \quad (2.126)$$

with similar equations for the wave function.

Obviously, in the diagonal case,

$$X_{ij} = \frac{W_{ij}}{E_0^{(0)} - E_i^{(0)}} = \frac{W_{ij}}{D_{0i}}. \quad (2.127)$$

2.4.6 Bracketing procedure for RSPT

If the process of deriving the terms in the series (2.106) for ΔE is continued, a general result emerges (Brueckner 1955, Huby 1961, Paldus and Čížek 1975). To show this result, we first simplify the notation further, writing

$$\langle \hat{V} \hat{R}_0 \hat{V} \hat{R}_0 \cdots \hat{R}_0 \hat{V} \rangle \equiv \langle \Phi | \hat{V} \hat{R}_0 \hat{V} \hat{R}_0 \cdots \hat{R}_0 \hat{V} | \Phi \rangle \quad (2.128)$$

(i.e. omitting the $\Phi |$ from the bra and $| \Phi$ from the ket). Then the principal term for $E^{(m)}$ is

$$\langle \hat{V} \hat{R}_0 \hat{V} \hat{R}_0 \hat{V} \cdots \hat{R}_0 \hat{V} \rangle$$

and contains m operators \hat{V} . All the other terms are obtained by inserting bracket pairs in all possible valid ways around \hat{V} operators and around $\hat{V}\hat{R}_0\cdots\hat{V}$ products in the principal term, always excluding the \hat{V} s at the two ends but including multiple brackets and brackets within brackets (properly nested). Each term is given a sign factor $(-1)^l$, where l is the number of inserted bracket pairs. Thus, at fourth order we obtain

$$\begin{aligned} E^{(4)} = & \langle \hat{V}\hat{R}_0\hat{V}\hat{R}_0\hat{V}\hat{R}_0\hat{V} \rangle \\ & - \langle \hat{V}\hat{R}_0\langle\hat{V}\rangle\hat{R}_0\hat{V}\hat{R}_0\hat{V} \rangle - \langle \hat{V}\hat{R}_0\hat{V}\hat{R}_0\langle\hat{V}\rangle\hat{R}_0\hat{V} \rangle \\ & + \langle \hat{V}\hat{R}_0\langle\hat{V}\rangle\hat{R}_0\langle\hat{V}\rangle\hat{R}_0\hat{V} \rangle - \langle \hat{V}\hat{R}_0\langle\hat{V}\hat{R}_0\hat{V}\rangle\hat{R}_0\hat{V} \rangle. \end{aligned} \quad (2.129)$$

At fifth order there are already 14 terms (a principal term plus 13 bracketings) that include nested bracketings such as

$$\begin{aligned} \langle \hat{V}\hat{R}_0\langle\hat{V}\hat{R}_0\langle\hat{V}\rangle\hat{R}_0\hat{V}\rangle\hat{R}_0\hat{V} \rangle &= \langle \hat{V} \rangle \langle \hat{V}\hat{R}_0^2\hat{V} \rangle \langle \hat{V}\hat{R}_0^2\hat{V} \rangle \\ &= E^{(1)} \langle \Psi^{(1)} | \Psi^{(1)} \rangle^2. \end{aligned} \quad (2.130)$$

It can be shown that the total number of terms at the n th order is

$$\frac{(2n-2)!}{n!(n-1)!}.$$

We can reduce the proliferation of terms substantially by using the \hat{W} operator for all interior positions and omitting all single- \hat{V} or single- \hat{W} bracketings. We should also remember that any \hat{W} that appears next to a bra or ket (on its inside) may then be replaced by \hat{V} :

$$\langle \hat{W} \cdots = \langle \hat{V} \cdots, \quad \cdots \hat{W} \rangle = \cdots \hat{V} \rangle. \quad (2.131)$$

For example, for the fifth order contribution to the energy we get

$$\begin{aligned} E^{(5)} = & \langle \hat{V}\hat{R}_0\hat{W}\hat{R}_0\hat{W}\hat{R}_0\hat{W}\hat{R}_0\hat{V} \rangle - \langle \hat{V}\hat{R}_0\langle\hat{V}\hat{R}_0\hat{V}\rangle\hat{R}_0\hat{W}\hat{R}_0\hat{V} \rangle \\ & - \langle \hat{V}\hat{R}_0\hat{W}\hat{R}_0\langle\hat{V}\hat{R}_0\hat{V}\rangle\hat{R}_0\hat{V} \rangle - \langle \hat{V}\hat{R}_0\langle\hat{V}\hat{R}_0\hat{W}\hat{R}_0\hat{V}\rangle\hat{R}_0\hat{V} \rangle \\ = & \langle \hat{V}\hat{R}_0\hat{W}\hat{R}_0\hat{W}\hat{R}_0\hat{W}\hat{R}_0\hat{V} \rangle - \langle \hat{V}\hat{R}_0\hat{V} \rangle \langle \hat{V}\hat{R}_0(\hat{R}_0\hat{W} + \hat{W}\hat{R}_0)\hat{R}_0\hat{V} \rangle \\ & - \langle \hat{V}\hat{R}_0\hat{W}\hat{R}_0\hat{V} \rangle \langle \hat{V}\hat{R}_0^2\hat{V} \rangle \\ = & \langle \hat{V}\hat{R}_0\hat{W}\hat{R}_0\hat{W}\hat{R}_0\hat{W}\hat{R}_0\hat{V} \rangle - E^{(2)} \{ \langle \Psi^{(1)} | \Psi^{(2)} \rangle + \langle \Psi^{(2)} | \Psi^{(1)} \rangle \} \\ & - E^{(3)} \langle \Psi^{(1)} | \Psi^{(1)} \rangle; \end{aligned} \quad (2.132)$$

note that we have here just four terms.

2.4.7 Summary of formal RSPT results

We shall now collect the results for several orders of RSPT, giving both the general result (in terms of \hat{R}_0) and the diagonal-case explicit formulas. The first three orders of the wave-function contributions are:

$$\Psi^{(1)} = \hat{R}_0 \hat{V} |\Phi\rangle = \sum_i' |\Phi_i\rangle \frac{V_{i0}}{D_{0i}}, \quad (2.133)$$

$$\Psi^{(2)} = \hat{R}_0 \hat{W} \hat{R}_0 \hat{V} |\Phi\rangle = \sum_{i,j}' |\Phi_i\rangle \frac{W_{ij} V_{j0}}{D_{0i} D_{0j}}, \quad (2.134)$$

$$\begin{aligned} \Psi^{(3)} &= \hat{R}_0 \hat{W} \hat{R}_0 \hat{W} \hat{R}_0 \hat{V} |\Phi\rangle - \langle \Phi | \hat{V} \hat{R}_0 \hat{V} | \Phi \rangle \hat{R}_0^2 \hat{V} |\Phi\rangle \\ &= \sum_i' |\Phi_i\rangle \left(\sum_{j,k}' \frac{W_{ij} W_{jk} V_{k0}}{D_{0i} D_{0j} D_{0k}} - E^{(2)} \frac{V_{i0}}{D_{0i}^2} \right). \end{aligned} \quad (2.135)$$

The energy formulas satisfy $E^{(m)} = \langle \Phi | \hat{V} | \Psi^{(m-1)} \rangle$, and the first six orders are:

$$E^{(1)} = \langle \Phi | \hat{V} | \Phi \rangle = V_{00}, \quad (2.136)$$

$$E^{(2)} = \langle \Phi | \hat{V} \hat{R}_0 \hat{V} | \Phi \rangle = \sum_i' \frac{V_{0i} V_{i0}}{D_{0i}}, \quad (2.137)$$

$$E^{(3)} = \langle \Phi | \hat{V} \hat{R}_0 \hat{W} \hat{R}_0 \hat{V} | \Phi \rangle = \sum_{i,j}' \frac{V_{0i} W_{ij} V_{j0}}{D_{0i} D_{0j}}, \quad (2.138)$$

$$\begin{aligned} E^{(4)} &= \langle \Phi | \hat{V} \hat{R}_0 \hat{W} \hat{R}_0 \hat{W} \hat{R}_0 \hat{V} | \Phi \rangle - E^{(2)} \langle \Psi^{(1)} | \Psi^{(1)} \rangle \\ &= \sum_{ijk}' \frac{V_{0i} W_{ij} W_{jk} V_{k0}}{D_{0i} D_{0j} D_{0k}} - E^{(2)} \sum_i' \frac{V_{0i} V_{i0}}{D_{0i}^2} \end{aligned} \quad (2.139)$$

$$\begin{aligned} E^{(5)} &= \langle \Phi | \hat{V} \hat{R}_0 \hat{W} \hat{R}_0 \hat{W} \hat{R}_0 \hat{W} \hat{R}_0 \hat{V} | \Phi \rangle \\ &\quad - E^{(2)} \{ \langle \Psi^{(1)} | \Psi^{(2)} \rangle + \langle \Psi^{(2)} | \Psi^{(1)} \rangle \} - E^{(3)} \langle \Psi^{(1)} | \Psi^{(1)} \rangle \\ &= \sum_{ijkl}' \frac{V_{0i} W_{ij} W_{jk} W_{kl} V_{l0}}{D_{0i} D_{0j} D_{0k} D_{0l}} \\ &\quad - E^{(2)} \sum_{ij}' \frac{V_{0i} W_{ij} V_{j0}}{D_{0i} D_{0j}} \left(\frac{1}{D_{0i}} + \frac{1}{D_{0j}} \right) - E^{(3)} \sum_i' \frac{V_{0i} V_{i0}}{D_{0i}^2}, \end{aligned} \quad (2.140)$$

$$\begin{aligned}
E^{(6)} &= \langle \Phi | \hat{V} \hat{R}_0 \hat{W} \hat{R}_0 \hat{W} \hat{R}_0 \hat{W} \hat{R}_0 \hat{W} \hat{R}_0 \hat{V} | \Phi \rangle \\
&\quad - E^{(2)} \left\{ \langle \Psi^{(1)} | \Psi^{(3)} \rangle + \langle \Psi^{(2)} | \Psi^{(2)} \rangle + \langle \Psi^{(3)} | \Psi^{(1)} \rangle \right\} \\
&\quad - E^{(3)} \left\{ \langle \Psi^{(1)} | \Psi^{(2)} \rangle + \langle \Psi^{(2)} | \Psi^{(1)} \rangle \right\} - E^{(4)} \langle \Psi^{(1)} | \Psi^{(1)} \rangle \\
&\quad + (E^{(2)})^2 \langle \Psi^{(1)} | \hat{R}_0 | \Psi^{(1)} \rangle \\
&= \sum_{ijklm} ' \frac{V_{0i} W_{ij} W_{jk} W_{kl} W_{lm} V_{m0}}{D_{0i} D_{0j} D_{0k} D_{0l} D_{0m}} \\
&\quad - E^{(2)} \sum_{ijk} ' \frac{V_{0i} W_{ij} W_{jk} V_{k0}}{D_{0i} D_{0j} D_{0k}} \left(\frac{1}{D_{0i}} + \frac{1}{D_{0j}} + \frac{1}{D_{0k}} \right) \\
&\quad - E^{(3)} \sum_{ij} ' \frac{V_{0i} W_{ij} V_{j0}}{D_{0i} D_{0j}} \left(\frac{1}{D_{0i}} + \frac{1}{D_{0j}} \right) \\
&\quad - E^{(4)} \sum_i ' \frac{V_{0i} V_{i0}}{D_{0i}^2} + (E^{(2)})^2 \sum_i ' \frac{V_{0i} V_{i0}}{D_{0i}^3}.
\end{aligned} \tag{2.141}$$

The steps in the derivation of the formula for $E^{(6)}$ are shown in Fig. 2.1.

The wave functions and energies at each order can also be expressed in terms of lower-order quantities by substitution of the formulas for the lower-order wave functions and energies. In the case of the energies the most convenient forms are based on the Wigner formulas (2.36), (2.37). The corresponding results take the forms:

$$\Psi^{(2)} = \hat{R}_0 \hat{W} | \Psi^{(1)} \rangle, \tag{2.142}$$

$$\Psi^{(3)} = \hat{R}_0 \hat{W} | \Psi^{(2)} \rangle - E^{(2)} \hat{R}_0 | \Psi^{(1)} \rangle, \tag{2.143}$$

$$\Psi^{(4)} = \hat{R}_0 \hat{W} | \Psi^{(3)} \rangle - E^{(2)} \hat{R}_0 | \Psi^{(2)} \rangle - E^{(3)} \hat{R}_0 | \Psi^{(1)} \rangle, \tag{2.144}$$

$$E^{(2)} = \langle \Phi | \hat{V} | \Psi^{(1)} \rangle, \tag{2.145}$$

$$E^{(3)} = \langle \Psi^{(1)} | \hat{W} | \Psi^{(1)} \rangle, \tag{2.146}$$

$$E^{(4)} = \langle \Psi^{(1)} | \hat{W} | \Psi^{(2)} \rangle - E^{(2)} \langle \Psi^{(1)} | \Psi^{(1)} \rangle, \tag{2.147}$$

$$\begin{aligned}
E^{(5)} &= \langle \Psi^{(2)} | \hat{W} | \Psi^{(2)} \rangle - E^{(2)} \left\{ \langle \Psi^{(1)} | \Psi^{(2)} \rangle + \langle \Psi^{(2)} | \Psi^{(1)} \rangle \right\} \\
&\quad - E^{(3)} \langle \Psi^{(1)} | \Psi^{(1)} \rangle,
\end{aligned} \tag{2.148}$$

$$\begin{aligned}
E^{(6)} &= \langle \Psi^{(2)} | \hat{W} | \Psi^{(3)} \rangle - E^{(2)} \left\{ \langle \Psi^{(1)} | \Psi^{(3)} \rangle + \langle \Psi^{(2)} | \Psi^{(2)} \rangle \right\} \\
&\quad - E^{(3)} \left\{ \langle \Psi^{(1)} | \Psi^{(2)} \rangle + \langle \Psi^{(2)} | \Psi^{(1)} \rangle \right\} - E^{(4)} \langle \Psi^{(1)} | \Psi^{(1)} \rangle.
\end{aligned} \tag{2.149}$$

$$\begin{aligned}
E^{(6)} &= \langle \hat{V} \hat{R}_0 \hat{W} \hat{R}_0 \hat{W} \hat{R}_0 \hat{W} \hat{R}_0 \hat{V} \rangle - \langle \hat{V} \hat{R}_0 \langle \hat{V} \hat{R}_0 \hat{V} \rangle \hat{R}_0 \hat{W} \hat{R}_0 \hat{W} \hat{R}_0 \hat{V} \rangle \\
&\quad \langle \hat{V} \hat{R}_0 \hat{W} \hat{R}_0 \langle \hat{V} \hat{R}_0 \hat{V} \rangle \hat{R}_0 \hat{W} \hat{R}_0 \hat{V} \rangle - \langle \hat{V} \hat{R}_0 \hat{W} \hat{R}_0 \hat{W} \hat{R}_0 \langle \hat{V} \hat{R}_0 \hat{V} \rangle \hat{R}_0 \hat{V} \rangle \\
&\quad \langle \hat{V} \hat{R}_0 \langle \hat{V} \hat{R}_0 \hat{W} \hat{R}_0 \hat{V} \rangle \hat{R}_0 \hat{W} \hat{R}_0 \hat{V} \rangle - \langle \hat{V} \hat{R}_0 \hat{W} \hat{R}_0 \langle \hat{V} \hat{R}_0 \hat{W} \hat{R}_0 \hat{V} \rangle \hat{R}_0 \hat{V} \rangle \\
&\quad - \langle \hat{V} \hat{R}_0 \langle \hat{V} \hat{R}_0 \hat{W} \hat{R}_0 \hat{W} \hat{R}_0 \hat{V} \rangle \hat{R}_0 \hat{V} \rangle + \langle \hat{V} \hat{R}_0 \langle \hat{V} \hat{R}_0 \hat{V} \rangle \hat{R}_0 \langle \hat{V} \hat{R}_0 \hat{V} \rangle \hat{R}_0 \hat{V} \rangle \\
&\quad + \langle \hat{V} \hat{R}_0 \langle \hat{V} \hat{R}_0 \langle \hat{V} \hat{R}_0 \hat{V} \rangle \hat{R}_0 \hat{V} \rangle \hat{R}_0 \hat{V} \rangle \\
&= \langle \hat{V} \hat{R}_0 \hat{W} \hat{R}_0 \hat{W} \hat{R}_0 \hat{W} \hat{R}_0 \hat{W} \hat{R}_0 \hat{V} \rangle \\
&\quad - \langle \hat{V} \hat{R}_0 \hat{V} \rangle \{ \langle \hat{V} \hat{R}_0 | \hat{R}_0 \hat{W} \hat{R}_0 \hat{W} \hat{R}_0 \hat{V} \rangle + \langle \hat{V} \hat{R}_0 \hat{W} \hat{R}_0 | \hat{R}_0 \hat{W} \hat{R}_0 \hat{V} \rangle \\
&\quad \quad + \langle \hat{V} \hat{R}_0 \hat{W} \hat{R}_0 \hat{W} \hat{R}_0 | \hat{R}_0 \hat{V} \rangle \} \\
&\quad - \langle \hat{V} \hat{R}_0 \hat{W} \hat{R}_0 \hat{V} \rangle \{ \langle \hat{V} \hat{R}_0 | \hat{R}_0 \hat{W} \hat{R}_0 \hat{V} \rangle + \langle \hat{V} \hat{R}_0 \hat{W} \hat{R}_0 | \hat{R}_0 \hat{V} \rangle \} \\
&\quad - \langle \hat{V} \hat{R}_0 \hat{W} \hat{R}_0 \hat{W} \hat{R}_0 \hat{V} \rangle \langle \hat{V} \hat{R}_0 | \hat{R}_0 \hat{V} \rangle + \langle \hat{V} \hat{R}_0 \hat{V} \rangle^2 \langle \hat{V} \hat{R}_0^3 \hat{V} \rangle \\
&\quad + \langle \hat{V} \hat{R}_0 \hat{V} \rangle \langle \hat{V} \hat{R}_0 | \hat{R}_0 \hat{V} \rangle^2 \\
&= \langle \hat{V} \hat{R}_0 \hat{W} \hat{R}_0 \hat{W} \hat{R}_0 \hat{W} \hat{R}_0 \hat{W} \hat{R}_0 \hat{V} \rangle \\
&\quad - E^{(2)} \{ \langle \Psi^{(1)} | \Psi^{(3)} \rangle + E^{(2)} \hat{R}_0 \Psi^{(1)} \rangle \\
&\quad \quad + \langle \Psi^{(2)} | \Psi^{(2)} \rangle + \langle \Psi^{(3)} + E^{(2)} \hat{R}_0 \Psi^{(1)} | \Psi^{(1)} \rangle \} \\
&\quad - E^{(3)} \{ \langle \Psi^{(1)} | \Psi^{(2)} \rangle + \langle \Psi^{(2)} | \Psi^{(1)} \rangle \} - \{ E^{(4)} + E^{(2)} \langle \Psi^{(1)} | \Psi^{(1)} \rangle \} \langle \Psi^{(1)} | \Psi^{(1)} \rangle \\
&\quad + (E^{(2)})^2 \langle \Psi^{(1)} | \hat{R}_0 | \Psi^{(1)} \rangle + E^{(2)} \langle \Psi^{(1)} | \Psi^{(1)} \rangle^2 .
\end{aligned}$$

Fig. 2.1. Steps in the derivation of the formula for $E^{(6)}$.

2.4.8 Extensivity of Rayleigh–Schrödinger perturbation theory

Rayleigh–Schrödinger perturbation theory (RSPT) is extensive order by order. This is related to the fact that RSPT is a true order-by-order expansion, unlike BWPT, which has the infinite-order energy in all denominators. If we consider again the example of N noninteracting He atoms and take the second-order energy expression obtained in subsection 2.4.3 for BWPT, but replace the BWPT denominator (2.96)

$$E - E_i^{(0)} = \Delta E - \alpha + \varepsilon_0 \quad (2.150)$$

by the corresponding RSPT denominator,

$$E_0^{(0)} - E_i^{(0)} = \varepsilon_0 - \alpha, \quad (2.151)$$

the second-order energy becomes

$$E^{(2)} = \frac{N|\beta|^2}{\varepsilon_0 - \alpha}, \quad (2.152)$$

which is proportional to N .

A more complete demonstration of the extensivity of RSPT will await development of its many-body form but, basically, this extensivity is due to the fact that in a true order-by-order expansion the exact relationship

$$E(A+B) = E(A) + E(B) \quad (2.153)$$

for the energy of a system made up of noninteracting subsystems A and B must hold in each order.

2.5 Similarity transformation derivation of the formal perturbation equations and quasidegenerate PT

The following alternative derivation of the RSPT equations (Van Vleck 1929, Shavitt and Redmon 1980) is of interest because it is most easily generalized to quasidegenerate PT (QDPT) and thus to a form of multireference PT (MRPT).

Finding the eigenvalues and eigenfunctions of an operator \hat{H} is equivalent to finding a basis $\{\Psi_i\}$ in which \hat{H} is diagonal:

$$\langle \Psi_i | \hat{H} | \Psi_j \rangle = E_i \delta_{ij}. \quad (2.154)$$

If we have a representation of \hat{H} in some other basis,

$$H_{ij} = \langle \Phi_i | \hat{H} | \Phi_j \rangle, \quad (2.155)$$

then we need the transformation operator \hat{U} that transforms the basis $\{\Phi_i\}$ into the basis $\{\Psi_i\}$,

$$|\Psi_i\rangle = \hat{U}|\Phi_i\rangle = \sum_j |\Phi_j\rangle \langle \Phi_j | \hat{U} | \Phi_i \rangle = \sum_j |\Phi_j\rangle U_{ji}. \quad (2.156)$$

The inverse transformation is

$$|\Phi_i\rangle = \hat{U}^{-1}|\Psi_i\rangle, \quad (2.157)$$

so that, if the $\{\Phi_i\}$ basis is orthonormal, we have

$$\begin{aligned} \langle \Phi_i | \hat{U}^{-1} \hat{H} \hat{U} | \Phi_j \rangle &= \langle \Phi_i | \hat{U}^{-1} \hat{H} | \Psi_j \rangle \\ &= \langle \Phi_i | \hat{U}^{-1} | \Psi_j \rangle E_j \\ &= \langle \Phi_i | \Phi_j \rangle E_j = \delta_{ij} E_j. \end{aligned} \quad (2.158)$$

Thus we can obtain the eigenvalues of \hat{H} as the elements of the (diagonal) representation in the known orthonormal basis $\{\Phi_i\}$ of the *effective Hamiltonian*

$$\hat{H}^{\text{eff}} = \hat{U}^{-1} \hat{H} \hat{U}, \quad (2.159)$$

which is a *similarity transformation* of the original Hamiltonian \hat{H} . If both the $\{\Phi_i\}$ and $\{\Psi_i\}$ bases are orthonormal then the transformation connecting them is unitary, $\hat{U}^\dagger = \hat{U}^{-1}$, and the diagonalized representation of \hat{H} can be written in the form

$$E_i \delta_{ij} = \langle \Psi_i | \hat{H} | \Psi_j \rangle = \langle \hat{U} \Phi_i | \hat{H} | \hat{U} \Phi_j \rangle = \langle \Phi_i | \hat{U}^\dagger \hat{H} \hat{U} | \Phi_j \rangle, \quad (2.160)$$

so that the effective Hamiltonian can be expressed as

$$\hat{H}^{\text{eff}} = \hat{U}^\dagger \hat{H} \hat{U}. \quad (2.161)$$

Note that the original basis is any basis we choose, i.e., a known basis, while the transformed basis is the desired set of eigenfunctions of \hat{H} and is unknown. Thus the problem of finding the eigenfunctions and eigenvalues of \hat{H} is equivalent to that of finding an operator \hat{U} such that the representation of $\hat{U}^{-1} \hat{H} \hat{U}$ in some given basis $\{\Phi_i\}$ is diagonal. If we succeed then $\langle \Phi_i | \hat{U}^{-1} \hat{H} \hat{U} | \Phi_i \rangle$ are the eigenvalues and $\hat{U} | \Phi_i \rangle$ are the corresponding eigenfunctions.

If we are only interested in one particular eigensolution E_0 , $|\Psi_0\rangle$, it is enough to find a transformation \hat{U} that *block-diagonalizes* \hat{H}^{eff} , so that

$$\begin{aligned} \langle \Phi_0 | \hat{U}^{-1} \hat{H} \hat{U} | \Phi_i \rangle &= \langle \Phi_i | \hat{U}^{-1} \hat{H} \hat{U} | \Phi_0 \rangle = 0 \quad (i \neq 0), \\ \langle \Phi_0 | \hat{U}^{-1} \hat{H} \hat{U} | \Phi_0 \rangle &= E_0, \end{aligned} \quad (2.162)$$

without being concerned about how \hat{U} transforms the other Φ_i among themselves. In this case there is considerable arbitrariness in the choice of \hat{U} . To be more specific we shall use the projection operators of Section 2.3,

$$\hat{P} = |\Phi_0\rangle\langle\Phi_0|, \quad \hat{Q} = \hat{1} - \hat{P} = \sum_i' |\Phi_i\rangle\langle\Phi_i|, \quad (2.163)$$

and write \hat{U} in the form

$$\begin{aligned} \hat{U} &= \hat{P} \hat{U} \hat{P} + \hat{P} \hat{U} \hat{Q} + \hat{Q} \hat{U} \hat{P} + \hat{Q} \hat{U} \hat{Q} \\ &= |\Phi_0\rangle U_{00} \langle\Phi_0| + \hat{P} \hat{U} \hat{Q} + \hat{Q} \hat{U} \hat{P} + \hat{Q} \hat{U} \hat{Q}, \end{aligned} \quad (2.164)$$

where $U_{00} = \langle\Phi_0| \hat{U} | \Phi_0\rangle$.

The U_{00} and $\hat{Q} \hat{U} \hat{Q}$ parts of \hat{U} are arbitrary, since they do not affect the block diagonalization (U_{00} changes only the normalization of Ψ_0 , while $\hat{Q} \hat{U} \hat{Q}$

merely mixes the other Ψ_i ($i \neq 0$) among themselves). If we wish \hat{U} to make the minimum change (in the basis or in the effective Hamiltonian) essential to achieve block diagonalization, it is natural to choose $\hat{P}\hat{U}\hat{P} = \hat{P}$ (i.e., $U_{00} = 1$), $\hat{Q}\hat{U}\hat{Q} = \hat{Q}$, so that

$$\hat{P}\hat{U}\hat{P} + \hat{Q}\hat{U}\hat{Q} = \hat{1}. \quad (2.165)$$

Then

$$\hat{U} = \hat{1} + \hat{P}\hat{U}\hat{Q} + \hat{Q}\hat{U}\hat{P} \quad (2.166)$$

and

$$\Psi_0 = \hat{U}\Phi_0 = \hat{U}\hat{P}\Phi_0 = \Phi_0 + \hat{Q}\hat{U}\hat{P}\Phi_0, \quad (2.167)$$

so that $\hat{Q}\hat{U}\hat{P}\Phi_0$ is the perturbative correction to Φ_0 (using intermediate normalization).

The operator that, when operating on a zero-order function Φ_0 , produces the corresponding perturbed function Ψ_0 is called the *wave operator* and is commonly denoted by Ω . (A more general definition relevant to quasi-degenerate PT will be given at the end of this section.) Only the $\Omega\hat{P}$ part of Ω is of interest, the $\Omega\hat{Q}$ part being left undefined. In the present case we have

$$\Omega\hat{P} = \hat{U}\hat{P} = \hat{P} + \hat{Q}\hat{U}\hat{P}. \quad (2.168)$$

When $\Omega\hat{P}$ operates on any function Φ that is not orthogonal to Φ_0 we obtain a function proportional to Ψ_0 ,

$$\Omega\hat{P}|\Phi\rangle = \hat{U}\hat{P}|\Phi\rangle = \hat{U}|\Phi_0\rangle\langle\Phi_0|\Phi\rangle = |\Psi_0\rangle\langle\Phi_0|\Phi\rangle. \quad (2.169)$$

Using the notation of (2.54), \hat{U} can be written in the form

$$\begin{aligned} \hat{U} &= \hat{U}_D + \hat{U}_X, \\ \hat{U}_D &= \hat{1}, \quad \hat{U} = \hat{1} + \hat{U}_X, \end{aligned} \quad (2.170)$$

and so we are looking for \hat{U}_X such that

$$\hat{H}^{\text{eff}} = \hat{U}^{-1}\hat{H}\hat{U} = \hat{H}_D^{\text{eff}}, \quad \hat{H}_X^{\text{eff}} = \hat{0} \quad (2.171)$$

(i.e. such that \hat{H}^{eff} is block diagonal). To proceed further, we first partition the Hamiltonian as

$$\hat{H} = \hat{H}_0 + \hat{V}, \quad (2.172)$$

where \hat{H}_0 is diagonal ($\langle\Phi_i|\hat{H}_0|\Phi_j\rangle = E_i^{(0)}\delta_{ij}$), and then set

$$\begin{aligned} \hat{H}_0 &= (\hat{H}_0)_D, & (\hat{H}_0)_X &= 0, \\ \hat{H}_D &= \hat{H}_0 + \hat{V}_D, & \hat{H}_X &= \hat{V}_X. \end{aligned} \quad (2.173)$$

It is also convenient to define an operator \hat{W} as the correction to \hat{H}_0 needed to obtain \hat{H}^{eff} :

$$\hat{H}^{\text{eff}} = \hat{H}_0 + \hat{W}. \quad (2.174)$$

(This notation is unrelated to $\hat{W} = \hat{V} - E^{(1)}$ in previous sections.) We have

$$\begin{aligned} \hat{W} &= \hat{W}_D, \quad \hat{W}_X = 0, \\ \hat{P}\hat{W}\hat{P} &= \hat{P}\hat{H}^{\text{eff}}\hat{P} - \hat{P}\hat{H}_0\hat{P} = (E_0 - E_0^{(0)})\hat{P} = \Delta E_0\hat{P}, \end{aligned} \quad (2.175)$$

and $\hat{P}\hat{W}\hat{P}$, called the *level-shift operator*, provides the desired energy correction.

In order to solve for \hat{U} and \hat{W} we rewrite Eq. (2.159) for \hat{H}^{eff} in the form

$$\hat{U}\hat{H}^{\text{eff}} = \hat{H}\hat{U}, \quad (2.176)$$

or

$$\hat{U}\hat{H}_0 + \hat{U}\hat{W} = \hat{H}_0\hat{U} + \hat{V}\hat{U}. \quad (2.177)$$

Using $\hat{U} = \hat{1} + \hat{U}_X$, we get

$$\hat{H}_0 + \hat{U}_X\hat{H}_0 + \hat{W} + \hat{U}_X\hat{W} = \hat{H}_0 + \hat{H}_0\hat{U}_X + \hat{V} + \hat{V}\hat{U}_X,$$

that is,

$$\hat{H}_0\hat{U}_X - \hat{U}_X\hat{H}_0 = -\hat{V} - \hat{V}\hat{U}_X + \hat{W} + \hat{U}_X\hat{W}. \quad (2.178)$$

The diagonal part of this equation is

$$\hat{0} = -\hat{V}_D - \hat{V}_X\hat{U}_X + \hat{W}$$

or

$$\hat{W} = \hat{V}_D + \hat{V}_X\hat{U}_X, \quad (2.179)$$

while the off-diagonal part is

$$[\hat{H}_0, \hat{U}_X] = -\hat{V}_X - \hat{V}_D\hat{U}_X + \hat{U}_X\hat{W}. \quad (2.180)$$

If we expand in orders of \hat{V} ,

$$\hat{U}_X = \hat{U}_X^{(1)} + \hat{U}_X^{(2)} + \dots, \quad \hat{W} = \hat{W}^{(1)} + \hat{W}^{(2)} + \dots \quad (2.181)$$

(the zero-order parts are zero, since they have been left out of $\hat{U}_X = \hat{U} - \hat{1}$ and $\hat{W} = \hat{H}^{\text{eff}} - \hat{H}_0$), we have

$$\begin{aligned} [\hat{H}_0, \hat{U}_X^{(1)}] &= -\hat{V}_X, \\ [\hat{H}_0, \hat{U}_X^{(m)}] &= -\hat{V}_D\hat{U}_X^{(m-1)} + \sum_{l=1}^{m-1} \hat{U}_X^{(l)}\hat{W}^{(m-l)} \quad (m \geq 2), \end{aligned} \quad (2.182)$$

and

$$\begin{aligned}\hat{W}^{(1)} &= \hat{V}_D, \\ \hat{W}^{(m)} &= \hat{V}_X \hat{U}_X^{(m-1)} \quad (m \geq 2).\end{aligned}\tag{2.183}$$

Equation (2.182) for $\hat{U}_X^{(m)}$ can be rewritten, using $\hat{W}^{(1)} = \hat{V}_D$, in the form

$$\left[\hat{H}_0, \hat{U}_X^{(m)} \right] = - \left[\hat{V}_D, \hat{U}_X^{(m-1)} \right] + \sum_{l=1}^{m-2} \hat{U}_X^{(l)} \hat{W}^{(m-l)} \quad (m \geq 2) \tag{2.184}$$

(where the sum is empty for $m = 2$).

In order to solve an equation of the form

$$[\hat{H}_0, \hat{U}_X] = \hat{A}, \tag{2.185}$$

where \hat{A} is any operator expression satisfying $\hat{A} = \hat{A}_X$, we proceed as follows:

$$\begin{aligned}\hat{Q} \hat{A} \hat{P} &= \hat{Q} [\hat{H}_0, \hat{U}_X] \hat{P}, \\ &= \hat{Q} \hat{H}_0 \hat{Q} \hat{U} \hat{P} - \hat{Q} \hat{U} \hat{P} \hat{H}_0 \hat{P}, \\ &= (\hat{Q} \hat{H}_0 \hat{Q})(\hat{Q} \hat{U} \hat{P}) - (\hat{Q} \hat{U} \hat{P}) E_0^{(0)},\end{aligned}$$

so that

$$\begin{aligned}\hat{Q} \hat{U} \hat{P} &= -\hat{Q} (E_0^{(0)} - \hat{Q} \hat{H}_0 \hat{Q})^{-1} \hat{Q} \hat{A} \hat{P} \\ &= -\hat{R}_0 \hat{A} \hat{P},\end{aligned}\tag{2.186}$$

where \hat{R}_0 is the zero-order resolvent operator $\hat{R}_0(E_0^{(0)})$ for state 0,

$$\hat{R}_0 = \hat{Q} (E_0^{(0)} - \hat{Q} \hat{H}_0 \hat{Q})^{-1} \hat{Q} = \frac{\hat{Q}}{E_0^{(0)} - \hat{H}_0}. \tag{2.187}$$

Applying this result to (2.180), i.e. putting $\hat{A} = -\hat{V}_X - \hat{V}_D \hat{U}_X + \hat{U}_X \hat{W}$, we have

$$\begin{aligned}\hat{Q} \hat{U} \hat{P} &= \hat{R}_0 (\hat{V}_X + \hat{V}_D \hat{U}_X - \hat{U}_X \hat{W}) \hat{P} \\ &= \hat{R}_0 \hat{V} \hat{P} + \hat{R}_0 \hat{V} \hat{Q} \hat{U} \hat{P} - \hat{R}_0 \hat{U} \hat{P} \hat{W} \hat{P}.\end{aligned}\tag{2.188}$$

Equating equal orders of the perturbation on both sides, we can now write (2.182) and (2.183) in the form

$$\begin{aligned}\hat{Q} \hat{U}^{(1)} \hat{P} &= \hat{R}_0 \hat{V} \hat{P}, \\ \hat{Q} \hat{U}^{(m)} \hat{P} &= \hat{R}_0 \hat{V} \hat{Q} \hat{U}^{(m-1)} \hat{P} - \sum_{l=1}^{m-1} \hat{R}_0 \hat{U}^{(l)} \hat{P} \hat{W}^{(m-l)} \hat{P} \quad (m \geq 2)\end{aligned}\tag{2.189}$$

and

$$\begin{aligned}\hat{P}\hat{W}^{(1)}\hat{P} &= \hat{P}\hat{V}\hat{P}, \\ \hat{P}\hat{W}^{(m)}\hat{P} &= \hat{P}\hat{V}\hat{Q}\hat{U}^{(m-1)}\hat{P} \quad (m \geq 2).\end{aligned}\tag{2.190}$$

These equations for $\hat{Q}\hat{U}\hat{P}$ and $\hat{P}\hat{W}\hat{P}$ determine the perturbed wave function through

$$\Psi_0 = \Phi_0 + \hat{Q}\hat{U}\hat{P}\Phi_0 \tag{2.191}$$

and the perturbed energy through (2.175). Using (2.188), the wave operator is determined from (cf. (2.168))

$$\Omega\hat{P} = \hat{P} + \hat{R}_0(\hat{V} + \hat{V}\hat{Q}\hat{U} - \hat{U}\hat{P}\hat{W})\hat{P}. \tag{2.192}$$

Only the $\hat{Q}\hat{U}^{(m)}\hat{P}$ part (corresponding to a column) of $\hat{U}_X^{(m)}$ and the $\hat{P}\hat{W}^{(m)}\hat{P}$ part (corresponding to an element) of $\hat{W}^{(m)}$ are ever needed. Repeated substitution of the lower-order $\hat{Q}\hat{U}\hat{P}$ equations into the higher-order \hat{U} and \hat{W} equations gives the usual perturbation theory expressions, for example,

$$\hat{P}\hat{W}^{(2)}\hat{P} = \hat{P}\hat{V}\hat{Q}\hat{U}^{(1)}\hat{P} = \hat{P}\hat{V}\hat{R}_0\hat{V}\hat{P}, \tag{2.193}$$

which corresponds to

$$E_0^{(2)} = \langle \Phi_0 | \hat{V} \hat{R}_0 \hat{V} | \Phi_0 \rangle. \tag{2.194}$$

The principal merit of this derivation is that it can easily be generalized to a case in which more than one zero-order states are to be handled together as part of the \hat{P} block, i.e. in *degenerate* or *quasidegenerate perturbation theory* (QDPT). In that case

$$\hat{P} = \sum_{\alpha} |\Phi_{\alpha}\rangle\langle\Phi_{\alpha}|, \quad \hat{Q} = \hat{1} - \hat{P} = \sum_i |\Phi_i\rangle\langle\Phi_i|, \tag{2.195}$$

where the Greek subscripts sum over the *model states* (the quasidegenerate set of zero-order states) and the Roman subscripts over all others. The PT equations then have the same form as before (but with the modified definition of \hat{P} , \hat{Q}) and they define a model-space *matrix* $\hat{P}\hat{W}\hat{P}$, from which we may obtain the (non-Hermitian) *effective Hamiltonian matrix*

$$\hat{P}\hat{H}^{\text{eff}}\hat{P} = \hat{P}\hat{H}_0\hat{P} + \hat{P}\hat{W}\hat{P}, \tag{2.196}$$

the *transformation matrix* $\hat{Q}\hat{U}\hat{P}$ and the *wave operator* $\Omega\hat{P} = \hat{P} + \hat{Q}\hat{U}\hat{P}$.

A more familiar form of the QDPT equations, known as the *generalized Bloch equation* (Lindgren 1974, Kvasnička 1974, 1977b, Lindgren 1978, Lindgren and Morrison 1986), is easily recovered from (2.179), (2.180):

$$\begin{aligned} [\hat{U}_X, \hat{H}_0] &= (\hat{V}_X + \hat{V}_D \hat{U}_X) - \hat{U}_X (\hat{V}_D + \hat{V}_X \hat{U}_X), \\ \hat{Q}[\Omega, \hat{H}_0] \hat{P} &= \hat{Q}(\hat{V} \Omega) \hat{P} - \hat{Q} \Omega \hat{P} (\hat{V} \Omega) \hat{P}, \end{aligned} \quad (2.197)$$

using $\Omega \hat{P} = \hat{U} \hat{P} = \hat{P} + \hat{Q} \hat{U} \hat{P}$. Also, since $\hat{P} \Omega \hat{P} = \hat{P}$ and $\hat{P}[\Omega, \hat{H}_0] \hat{P} = 0$, we may add

$$\hat{P}[\Omega, \hat{H}_0] \hat{P} = \hat{P} \hat{V} \Omega \hat{P} - \hat{P} \Omega \hat{P} \hat{V} \Omega \hat{P}$$

to (2.197) to get the generalized Bloch equation in the form

$$[\Omega, \hat{H}_0] \hat{P} = \hat{V} \Omega \hat{P} - \Omega \hat{P} \hat{V} \Omega \hat{P} \quad (2.198)$$

(see Lindgren and Morrison 1986). This equation is a generalization of the original Bloch equation (Bloch 1958, Bloch and Horowitz 1958) of degenerate perturbation theory, in which the model states are exactly degenerate in zero order, which is often the case for calculations on open-shell states. The QDPT approach and the generalized Bloch equations are discussed in detail in Chapter 8.

While the PT equations (2.182), (2.183) have the same general form in the quasidegenerate and degenerate cases as in the nondegenerate case, their solution in the quasidegenerate case is complicated by the fact that instead of a single resolvent \hat{R}_0 we now have a set of resolvents

$$\hat{R}_0(E_\alpha^{(0)}) \equiv \hat{R}_\alpha = \frac{\hat{Q}}{E_\alpha^{(0)} - \hat{H}_0} \quad (2.199)$$

for all the model states. The solutions are given by (compare Eqs. (2.189, 2.190))

$$\begin{aligned} U_{i\alpha}^{(1)} &= R_\alpha^i V_{i\alpha}, \\ U_{i\alpha}^{(m)} &= \sum_j R_\alpha^i V_{ij} U_{j\alpha}^{(m-1)} - \sum_{l=1}^{m-1} \sum_\beta R_\alpha^i U_{i\beta}^{(l)} W_{\beta\alpha}^{(m-l)} \quad (m \geq 2), \end{aligned} \quad (2.200)$$

and

$$\begin{aligned} W_{\alpha\beta}^{(1)} &= V_{\alpha\beta}, \\ W_{\alpha\beta}^{(m)} &= \sum_i V_{\alpha i} U_{i\beta}^{(m-1)} \quad (m \geq 2). \end{aligned} \quad (2.201)$$

In (2.200) we have

$$R_\alpha^i = \langle \Phi_i | \hat{R}_\alpha | \Phi_i \rangle. \quad (2.202)$$

When the $\hat{Q}\hat{U}\hat{P}$ and $\hat{P}\hat{W}\hat{P}$ matrices have been determined to satisfactory accuracy, the final solutions of the quasidegenerate (or degenerate) problem are determined by solving the non-Hermitian eigenvalue problem.

$$\sum_{\beta} \hat{H}_{\alpha\beta}^{\text{eff}} C_{\beta\gamma} = C_{\alpha\gamma} E_{\gamma}, \quad (2.203)$$

to complete the diagonalization of the P -space. This gives the final energies E_{γ} and the transformation matrix \mathbf{C} . The wave functions are then

$$\begin{aligned} |\Psi_{\gamma}\rangle &= \sum_{\beta} \hat{U} |\Phi_{\beta}\rangle C_{\beta\gamma} \\ &= \sum_{\beta} \left(|\Phi_{\beta}\rangle + \sum_i |\Phi_i\rangle U_{i\beta} \right) C_{\beta\gamma}. \end{aligned} \quad (2.204)$$

It is therefore clear that the wave operator can be more generally defined as the operator that, when it operates on the manifold of model states, generates the manifold of perturbed states; a diagonalization of the effective Hamiltonian $\hat{P}\hat{H}^{\text{eff}}\hat{P}$ is then needed to obtain the transformation that converts the states generated by $\Omega\Phi_{\alpha}$ into the exact eigenstates of \hat{H} .

2.6 Other approaches

At this point it is appropriate to begin consideration of the *many-body* form of RSPT, where some important simplifications and cancellations will appear through the use of *diagrammatic techniques*. Actually, there is another important variant of the derivation of the formal equations of PT: this uses *time-dependent PT* (see e.g. Raimes (1972) or March, Young and Sampanthar (1967)). This variant was in fact used in the original derivation of the many-body form of perturbation theory (Brueckner 1955, Goldstone 1957), but this derivation cannot be presented without the introduction of several additional concepts that complicate the presentation considerably and so it will not be discussed further in this book.

3

Second quantization

3.1 Background

Second-quantization techniques evolved primarily for problems in which the number of particles is not fixed or known and in the context of *independent-particle models* (such as the Hartree–Fock model). Such techniques provide a method of representing independent-particle-model wave functions (i.e. Slater determinants) and operators in a compact convenient notation and also provide an efficient way of manipulating such functions and operators.

The second-quantization notation assumes the existence of an unspecified number of functions in a given fixed *one-particle basis*, say

$$\{\phi_i\} = \{\phi_1, \phi_2, \dots\}. \quad (3.1)$$

In general, the functions $\{\phi_i\}$ are *spinorbitals*, very often the Hartree–Fock spinorbitals. To avoid complications, we assume that the basis is *orthonormal*,

$$\langle \phi_i | \phi_j \rangle = \delta_{ij}. \quad (3.2)$$

The number of functions in the basis need not appear explicitly in the formalism (but of course will affect any computation). The given one-particle basis generates *Hilbert spaces* for $N = 1, 2, \dots$ particles, for which the basis functions are products of N one-particle basis functions. However, since we are dealing with fermions, we will restrict the many-particle functions to be antisymmetric and thus assume a many-particle basis constructed of *Slater determinants* made up of the one-particle basis functions. The totality of the antisymmetric Hilbert spaces for $N = 1, 2, \dots$ is often referred to as a *Fock space* (Kutzelnigg 1982, 1984, Kutzelnigg and Koch 1983), and we are looking for a representation of functions and operators in this Fock space, without explicitly specifying N . Obviously, the ordinary form

of the Hamiltonian,

$$\hat{H} = \sum_{\mu=1}^N \hat{h}_{\mu} + \sum_{\mu<\nu}^N \hat{v}_{\mu\nu} \quad (3.3)$$

where \hat{h}_{μ} and $\hat{v}_{\mu\nu}$ are the one-particle and two-particle terms in \hat{H} and μ, ν are particle labels, does not satisfy this requirement because N appears in the summation limits.

3.2 Creation and annihilation operators

3.2.1 Definitions

We begin by considering the representation of a normalized Slater determinant

$$\Phi = \Phi_{ijk\dots z} \equiv \mathcal{A}\phi_i\phi_j\phi_k\dots\phi_z \equiv |\phi_i\phi_j\phi_k\dots\phi_z\rangle \equiv |ijk\dots z\rangle, \quad (3.4)$$

where \mathcal{A} is the antisymmetrizer and each ϕ is a spinorbital in our one-particle basis. The various forms of (3.4) are equivalent notations for the same function, and we shall normally use one of the last two forms. The Slater determinant (SD) Φ is represented in *second-quantized form* by specifying the *occupancies* (or *occupation numbers*) n_1, n_2, \dots of the basis spinorbitals ϕ_1, ϕ_2, \dots in the determinant. Obviously,

$$n_i(\Phi) = \begin{cases} 0 & \text{if } \phi_i \text{ is empty (not present) in the SD } \Phi \\ 1 & \text{if } \phi_i \text{ is occupied (present) in the SD } \Phi \end{cases} \quad (i = 1, 2, \dots). \quad (3.5)$$

The determinant itself (and various operators on it) are represented in terms of a set of *creation and annihilation operators*. The notation for these varies:

$$\begin{aligned} &\text{creation operator for spinorbital } \phi_i, & \hat{X}_i^{\dagger}, \hat{a}_i^{\dagger}; \hat{c}_i^{\dagger}, \hat{i}^{\dagger}; \\ &\text{annihilation operator for spinorbital } \phi_i, & \hat{X}_i, \hat{a}_i, \hat{c}_i, \hat{i}. \end{aligned}$$

Here we shall use $\hat{a}_i^{\dagger}, \hat{a}_i$ and, when there is no possibility of confusion, $\hat{i}^{\dagger}, \hat{i}$. They are defined in terms of their action on SDs:

$$\begin{aligned} \hat{a}_i^{\dagger}|ijk\dots z\rangle &= |ijk\dots z\rangle, \\ \hat{a}_i|ijk\dots z\rangle &= |jk\dots z\rangle. \end{aligned} \quad (3.6)$$

It is convenient to arrange the spinorbitals in an SD in lexical order as

$$|ijk\dots z\rangle, \quad \text{where } i < j < k < \dots < z,$$

and therefore it is necessary to determine the effects of the creation and annihilation operators when the affected orbital is not (or is not being placed) at the beginning of the SD. Then, because

$$\hat{P}|ijk \cdots z\rangle = (-1)^{\sigma(\hat{P})}|ijk \cdots z\rangle, \quad (3.7)$$

where \hat{P} permutes the i, j, k, \dots, z and $\sigma(\hat{P})$ is the parity of the permutation \hat{P} , we have

$$\begin{aligned} \hat{a}_p^\dagger |ijk \cdots z\rangle &= (-1)^{\eta_p} |ijk \cdots p \cdots z\rangle, \\ \hat{a}_p |ijk \cdots p \cdots z\rangle &= (-1)^{\eta_p} |ijk \cdots z\rangle, \end{aligned} \quad (3.8)$$

where η_p is the number of orbitals preceding ϕ_p in the SD (after the operation, for \hat{a}_p^\dagger , and before the operation, for \hat{a}_p). We also have

$$\begin{aligned} \hat{a}_i^\dagger |\Phi\rangle &= 0 & \text{if } n_i(\Phi) = 1, \\ \hat{a}_i |\Phi\rangle &= 0 & \text{if } n_i(\Phi) = 0. \end{aligned} \quad (3.9)$$

We can now describe an SD as the result of the successive operation of several \hat{a}_p^\dagger on the *vacuum* SD, $|\rangle$, which contains no spinorbitals ($N = 0$):

$$\hat{a}_i^\dagger \hat{a}_j^\dagger \hat{a}_k^\dagger \cdots \hat{a}_z^\dagger |\rangle = |ijk \cdots z\rangle. \quad (3.10)$$

Next, consider the matrix elements of \hat{a}_p^\dagger and \hat{a}_p between two SDs Φ and Φ' . It is clear (owing to the orthonormality of the spinorbitals) that

$$\langle \Phi' | \hat{a}_p | \Phi \rangle = \begin{cases} \pm 1 & \text{if } n_p(\Phi) = 1, n_p(\Phi') = 0, n_i(\Phi) = n_i(\Phi') \quad (i \neq p), \\ 0 & \text{otherwise.} \end{cases} \quad (3.11)$$

That is, the matrix element is nonzero only if Φ and Φ' have the same orbital occupancies except that ϕ_p has an electron in Φ but not in Φ' (thus Φ' has one fewer electron than Φ). The sign depends on the relative order of the spinorbitals in the two SDs. Let us order the orbitals the same way in Φ and Φ' , except that in Φ we put ϕ_p at the beginning,

$$\begin{aligned} \Phi &= |pij \cdots z\rangle, \\ \Phi' &= |ij \cdots z\rangle \end{aligned} \quad (3.12)$$

(at most, this introduces a factor of -1 in the matrix element). Then the matrix element is

$$\langle ij \cdots z | \hat{a}_p | pij \cdots z \rangle = \langle ij \cdots z | ij \cdots z \rangle = 1. \quad (3.13)$$

We get the same answer by operating with \hat{a}_p^\dagger on the bra:

$$\langle \hat{a}_p^\dagger ij \cdots z | pij \cdots z \rangle = \langle pij \cdots z | pij \cdots z \rangle = 1. \quad (3.14)$$

If Φ and Φ' do not satisfy the above occupancy conditions then both matrix elements will vanish. Therefore, in all cases,

$$\langle \Phi' | \hat{a}_p | \Phi \rangle = \langle \hat{a}_p^\dagger \Phi' | \Phi \rangle \quad (3.15)$$

and similarly

$$\langle \Phi' | \hat{a}_p^\dagger | \Phi \rangle = \langle \hat{a}_p \Phi' | \Phi \rangle. \quad (3.16)$$

This shows that \hat{a}_p^\dagger is the operator *adjoint* to \hat{a}_p and so justifies the notation. In general, we can write

$$\begin{aligned} \langle ij \cdots z | \hat{a}_p &= \langle \hat{a}_p^\dagger ij \cdots z | = \langle pij \cdots z |, \\ \langle pij \cdots z | \hat{a}_p^\dagger &= \langle \hat{a}_p pij \cdots z | = \langle ij \cdots z |, \end{aligned} \quad (3.17)$$

so that \hat{a}_p^\dagger and \hat{a}_p act as annihilation and creation operators, respectively, when acting to the left.

The operator product $\hat{a}_p^\dagger \hat{a}_p$ is particularly interesting:

$$\hat{a}_p^\dagger \hat{a}_p | \Phi \rangle = n_p(\Phi) | \Phi \rangle = \begin{cases} | \Phi_p \rangle & \text{if } \phi_p \text{ is in } \Phi, \\ 0 & \text{otherwise.} \end{cases} \quad (3.18)$$

This combination is called the *number operator* for orbital (or spinorbital) ϕ_p , is written \hat{n}_p , so that

$$\hat{n}_p = \hat{a}_p^\dagger \hat{a}_p, \quad (3.19)$$

and has all the SDs as eigenfunctions, with eigenvalues equal to the corresponding occupation numbers (0 or 1).

3.2.2 Anticommutation relations

Now we shall derive *anticommutation relations* for the creation and annihilation operators. Consider the following:

$$\begin{aligned} \hat{a}_p^\dagger \hat{a}_q^\dagger |ijk \cdots \rangle &= |pqijk \cdots \rangle \\ \hat{a}_q^\dagger \hat{a}_p^\dagger |ijk \cdots \rangle &= |qpijk \cdots \rangle = -|pqijk \cdots \rangle. \end{aligned} \quad (3.20)$$

This is true for any SD $|ijk \cdots \rangle$; if ϕ_p or ϕ_q already exists in $|ijk \cdots \rangle$, both products will give zero. Therefore, in general,

$$\begin{aligned} \hat{a}_p^\dagger \hat{a}_q^\dagger &= -\hat{a}_q^\dagger \hat{a}_p^\dagger, \\ [\hat{a}_p^\dagger, \hat{a}_q^\dagger]_+ &\equiv \hat{a}_p^\dagger \hat{a}_q^\dagger + \hat{a}_q^\dagger \hat{a}_p^\dagger = \hat{0}, \end{aligned} \quad (3.21)$$

where $[\hat{A}, \hat{B}]_+ \equiv \hat{A}\hat{B} + \hat{B}\hat{A}$ is the *anticommutator* of \hat{A} and \hat{B} and is sometimes written as $\{\hat{A}, \hat{B}\}$. Note that if $p = q$ the relation still holds, since

then $\hat{a}_p^\dagger \hat{a}_p^\dagger = \hat{0}$ and thus $[\hat{a}_p^\dagger, \hat{a}_p^\dagger]_+ = \hat{0}$. Note also that $[\hat{A}, \hat{B}]_+ = [\hat{B}, \hat{A}]_+$, unlike the ordinary commutator, for which $[\hat{A}, \hat{B}] = -[\hat{B}, \hat{A}]$.

Next consider the following:

$$\begin{aligned}\hat{a}_p \hat{a}_q |qpj \cdots\rangle &= \hat{a}_p |pij \cdots\rangle = |ij \cdots\rangle, \\ \hat{a}_q \hat{a}_p |qpj \cdots\rangle &= -\hat{a}_q \hat{a}_p |pqij \cdots\rangle = -\hat{a}_q |qij \cdots\rangle = -|ij \cdots\rangle.\end{aligned}\tag{3.22}$$

If ϕ_p and/or ϕ_q are in the interior of the SD then they can always be brought forward to the beginning with, at most, a change of sign, the same change in both cases. Furthermore, if ϕ_p and/or ϕ_q are not present in the SD then both lines give zero. Thus, in general,

$$\hat{a}_p \hat{a}_q = -\hat{a}_q \hat{a}_p \tag{3.23}$$

or

$$[\hat{a}_p, \hat{a}_q]_+ = \hat{0}.\tag{3.24}$$

Now consider \hat{a}_p^\dagger and \hat{a}_q :

$$\hat{a}_p^\dagger \hat{a}_q |qij \cdots\rangle = \hat{a}_p^\dagger |ij \cdots\rangle = |pij \cdots\rangle.\tag{3.25}$$

This operator product replaces ϕ_q by ϕ_p , even if ϕ_p was in the interior of the SD, since

$$\hat{a}_p^\dagger \hat{a}_q |ij \cdots q \cdots\rangle = (\pm 1)^2 |ij \cdots p \cdots\rangle = |ij \cdots p \cdots\rangle.\tag{3.26}$$

However,

$$\hat{a}_q \hat{a}_p^\dagger |qij \cdots\rangle = \hat{a}_q |pqij \cdots\rangle = -\hat{a}_q |qpj \cdots\rangle = -|pij \cdots\rangle \quad (p \neq q)\tag{3.27}$$

(this combination also replaces ϕ_q by ϕ_p , but with a change of sign), and thus

$$[\hat{a}_p^\dagger, \hat{a}_q]_+ = \hat{0} \quad (p \neq q).\tag{3.28}$$

If $p = q$ we have

$$\begin{aligned}\hat{a}_p^\dagger \hat{a}_p |pij \cdots\rangle &= |pij \cdots\rangle, \\ \hat{a}_p \hat{a}_p^\dagger |pij \cdots\rangle &= 0,\end{aligned}\tag{3.29}$$

and if ϕ_p does not appear in the SD,

$$\begin{aligned}\hat{a}_p^\dagger \hat{a}_p |ij \cdots\rangle &= 0, \\ \hat{a}_p \hat{a}_p^\dagger |ij \cdots\rangle &= \hat{a}_p |pij \cdots\rangle = |ij \cdots\rangle.\end{aligned}\tag{3.30}$$

Thus in all cases

$$(\hat{a}_p^\dagger \hat{a}_p + \hat{a}_p \hat{a}_p^\dagger) |\cdots\rangle = |\cdots\rangle,\tag{3.31}$$

and therefore

$$\left[\hat{a}_p^\dagger, \hat{a}_p\right]_+ = \left[\hat{a}_p, \hat{a}_p^\dagger\right]_+ = \hat{1}. \quad (3.32)$$

To summarize, the anticommutation relations for the creation and annihilation operators are:

$$\begin{aligned} [\hat{a}_p, \hat{a}_q]_+ &= \hat{0}, \\ [\hat{a}_p^\dagger, \hat{a}_q^\dagger]_+ &= \hat{0}, \\ [\hat{a}_p^\dagger, \hat{a}_q]_+ &= [\hat{a}_p, \hat{a}_q^\dagger]_+ = \hat{\delta}_{pq}, \end{aligned} \quad (3.33)$$

where $\hat{\delta}_{pq}$ is the Kronecker-delta operator. (More generally, if the spinor-bitals are not orthonormal then one obtains $[\hat{a}_p^\dagger, \hat{a}_q]_+ = \langle p|q \rangle$.)

3.2.3 Representation of operators

Next we want to consider the representation of general operators and matrix elements. As previously noted, any SD can be represented as the result of the operation of a string of creation operators on the vacuum state,

$$|ij \cdots \rangle = \hat{a}_i^\dagger \hat{a}_j^\dagger \cdots | \rangle, \quad (3.34)$$

we also have (using the adjointness of \hat{a}_i^\dagger and \hat{a}_i),

$$\langle ij \cdots | = \langle a_i^\dagger a_j^\dagger \cdots | = \langle | \cdots \hat{a}_j \hat{a}_i. \quad (3.35)$$

Any annihilation operator operating on the vacuum state gives zero,

$$\hat{a}_i | \rangle = 0, \quad (3.36)$$

and similarly

$$\langle | \hat{a}_i^\dagger = \langle \hat{a}_i | = 0. \quad (3.37)$$

For consistency, the vacuum state is taken to be normalized,

$$\langle | \rangle = 1, \quad (3.38)$$

as seen, for example, from

$$\begin{aligned} 1 = \langle i|i \rangle &= | \hat{a}_i \hat{a}_i^\dagger | \rangle \\ &= \langle | ([\hat{a}_i, \hat{a}_i^\dagger]_+ - \hat{a}_i^\dagger \hat{a}_i) | \rangle \\ &= \langle | \hat{1} | \rangle - \langle | \hat{a}_i^\dagger \hat{a}_i | \rangle \\ &= \langle | \rangle - 0 = \langle | \rangle. \end{aligned} \quad (3.39)$$

In general, if we have two SDs

$$\begin{aligned} |I\rangle &= |i_1 i_2 \cdots i_N\rangle = \hat{i}_1^\dagger \hat{i}_2^\dagger \cdots \hat{i}_N^\dagger | \rangle, \\ |J\rangle &= |j_1 j_2 \cdots j_N\rangle = \hat{j}_1^\dagger \hat{j}_2^\dagger \cdots \hat{j}_N^\dagger | \rangle \end{aligned} \quad (3.40)$$

then, using the more compact notation \hat{i} for \hat{a}_i and \hat{i}^\dagger for \hat{a}_i^\dagger ,

$$\langle I|J\rangle = \langle | \hat{i}_N \cdots \hat{i}_2 \hat{i}_1 \hat{j}_1^\dagger \hat{j}_2^\dagger \cdots \hat{j}_N^\dagger | \rangle. \quad (3.41)$$

If we now move \hat{i}_1 all the way to the right (N transpositions), there are two possible outcomes:

1. No j_p is the same as i_1 , and therefore

$$\langle I|J\rangle = \langle | \hat{i}_N \cdots \hat{i}_2 \hat{j}_1^\dagger \hat{j}_2^\dagger \cdots \hat{j}_N^\dagger \hat{i}_1 | \rangle (-1)^N = 0, \quad (3.42)$$

since $\hat{i}_1 | \rangle = 0$.

2. One of the j 's, say j_p , is the same as i_1 , so that

$$\hat{i}_1 \hat{j}_p^\dagger = [\hat{i}_1, \hat{j}_p^\dagger]_+ - \hat{j}_p^\dagger \hat{i}_1 = \delta_{i_1 j_p} - \hat{j}_p^\dagger \hat{i}_1 = \hat{1} - \hat{j}_p^\dagger \hat{i}_1 \quad (i_1 = j_p) \quad (3.43)$$

and

$$\langle I|J\rangle = \langle | \hat{i}_N \cdots \hat{i}_2 \hat{j}_1^\dagger \hat{j}_2^\dagger \cdots \hat{j}_{p-1}^\dagger \hat{j}_{p+1}^\dagger \cdots \hat{j}_N^\dagger | \rangle (-1)^{p-1} - 0 \quad (3.44)$$

(the last term is zero because we have an \hat{i}_1 left over that goes all the way to the right).

If we next do this for \hat{i}_2 and then \hat{i}_3 etc., we get either zero, if there are any i_q without a matching j_p , or $(-1)^\tau$, if the two sets of indices i_1, i_2, \dots, i_N and j_1, j_2, \dots, j_N are identical except possibly for their order, in which case τ is the parity of the *line-up permutation*, which permutes, say, the j 's to match the i 's.

The foregoing provides a demonstration of how matrix elements involving creation and annihilation operators can be manipulated. An important element of such manipulations is commuting enough operators to bring all annihilation operators to the right of all creation operators, since

$$\langle | \hat{a}_i^\dagger \hat{a}_j^\dagger \cdots \hat{a}_p \hat{a}_q | \rangle = 0. \quad (3.45)$$

Now consider a *symmetric one-electron operator*

$$\hat{F} = \sum_{\mu=1}^N \hat{f}_\mu, \quad (3.46)$$

where μ identifies the electron on which \hat{f}_μ operates, and the \hat{f}_μ 's are identical except for the identity of the electron on which each operates (thus \hat{F}

operates in the same way on all electrons, which is why it is called a *symmetric* one-electron operator). Now consider a matrix element of \hat{F} between two SDs:

$$\begin{aligned}
 \langle I|\hat{F}|J\rangle &= \langle i_1 i_2 \cdots i_N | \hat{F} | j_1 j_2 \cdots j_N \rangle \\
 &= \sum_{\mu} \langle i_1 i_2 \cdots i_N | \hat{f}_{\mu} | j_1 j_2 \cdots j_N \rangle \\
 &= \sum_{\mu} \langle \phi_{i_1}(1) \phi_{i_2}(2) \cdots \phi_{i_N}(N) | \hat{f}_{\mu} \sum_{\hat{P}} (-1)^{\sigma(\hat{P})} | \hat{P} \phi_{j_1}(1) \phi_{j_2}(2) \cdots \phi_{j_N}(N) \rangle,
 \end{aligned} \tag{3.47}$$

where the bra and ket in the last line each comprise a specific spinorbital product, not a determinant, and where \hat{P} permutes the j 's and $\sigma(\hat{P})$ is the parity of \hat{P} . The well-known result is that

$$\begin{aligned}
 \langle I|\hat{F}|J\rangle &= \sum_{k=1}^N \langle i_k | \hat{f} | i_k \rangle (-1)^{\sigma(\hat{P})} && \text{if there exists a permutation } \hat{P} \\
 &&& \text{such that } \hat{P} j_1 j_2 \cdots j_N = i_1 i_2 \cdots i_N, \\
 \langle I|\hat{F}|J\rangle &= \langle i_k | \hat{f} | i'_k \rangle (-1)^{\sigma(\hat{P})} && \text{if there exists a permutation } \hat{P} \text{ such that} \\
 &&& \hat{P} j_1 j_2 \cdots j_N = i_1 i_2 \cdots i'_k \cdots i_N \quad (i'_k \neq i_k) \\
 &&& \text{(one noncoincidence),} \\
 \langle I|\hat{F}|J\rangle &= 0 && \text{otherwise (two or more noncoincidences).}
 \end{aligned} \tag{3.48}$$

It is easy to verify that the same result will be obtained for the operator

$$\sum_{k,l} \langle k | \hat{f} | l \rangle \hat{a}_k^{\dagger} \hat{a}_l = \sum_{k,l} f_{kl} \hat{a}_k^{\dagger} \hat{a}_l, \tag{3.49}$$

where the sums are over all the spinorbitals in the basis. For simplicity, let us assume that the two sets of indices i_1, i_2, \dots, i_N and j_1, j_2, \dots, j_N have been “lined-up” in such a way that $i_p = j_p$ for as many $p = 1, 2, \dots, N$ as possible. Then, if there are *zero noncoincidences*,

$$\begin{aligned}
 \left\langle I \left| \sum_{k,l} f_{kl} \hat{a}_k^{\dagger} \hat{a}_l \right| I \right\rangle &= \sum_{k,l} f_{kl} \langle I | \hat{a}_k^{\dagger} \hat{a}_l | I \rangle \\
 &= \sum_{k,l} f_{kl} \delta_{kl} n_l(I) \\
 &= \sum_{k \in I} f_{kk} = \sum_{p=1}^N \langle i_p | \hat{f} | i_p \rangle,
 \end{aligned} \tag{3.50}$$

since $k \neq l$ creates a noncoincidence between $\langle I |$ and $\hat{a}_k^{\dagger} \hat{a}_l | I \rangle$. For one

noncoincidence $i_p \neq j_p$, the only term in the k, l sum that will make $\langle I |$ coincide with $\hat{a}_k^\dagger \hat{a}_l | J \rangle$ will be $l = j_p$, $k = i_p$, so that

$$\begin{aligned} \left\langle I \left| \sum_{k,l} f_{kl} \hat{a}_k^\dagger \hat{a}_l \right| J \right\rangle &= \sum_{k,l} f_{kl} \langle I | \hat{a}_k^\dagger \hat{a}_l | J \rangle \\ &= f_{i_p j_p} \langle I | \hat{i}_p^\dagger \hat{j}_p | J \rangle \\ &= f_{i_p j_p} = \langle i_p | f | j_p \rangle. \end{aligned} \quad (3.51)$$

For two or more noncoincidences there is no single pair $\hat{a}_k^\dagger \hat{a}_l$ that will render $\langle I | \hat{a}_k^\dagger \hat{a}_l | J \rangle \neq 0$, so we get zero for the matrix element. Thus, all matrix elements of $\hat{F} = \sum_{\mu=1}^N \hat{f}_\mu$ within the Fock space generated by the one-electron basis are the same as those of $\sum_{k,l} f_{kl} \hat{a}_k^\dagger \hat{a}_l$ and *within that space* we can write

$$\hat{F} = \sum_{\mu=1}^N \hat{f}_\mu = \sum_{k,l} \langle k | f | l \rangle \hat{a}_k^\dagger \hat{a}_l. \quad (3.52)$$

Similarly, for a *symmetric two-electron operator*

$$\hat{G} = \sum_{\mu < \nu}^N \hat{g}_{\mu\nu} = \frac{1}{2} \sum_{\mu \neq \nu}^N \hat{g}_{\mu\nu}$$

we obtain

$$\hat{G} = \frac{1}{2} \sum_{i,j,k,l} \langle i(1)j(2) | \hat{g}_{12} | k(1)l(2) \rangle \hat{a}_i^\dagger \hat{a}_j^\dagger \hat{a}_l \hat{a}_k. \quad (3.53)$$

Noting the order of the arguments (1, 2) in the matrix element and the order of the annihilation operators $\hat{a}_l \hat{a}_k$, we have

$$\hat{a}_i^\dagger \hat{a}_j^\dagger \hat{a}_l \hat{a}_k = (\hat{a}_i^\dagger (\hat{a}_j^\dagger \hat{a}_l) \hat{a}_k) = (\hat{a}_i^\dagger \hat{a}_k) (\hat{a}_j^\dagger \hat{a}_l) - \delta_{jk} \hat{a}_i^\dagger \hat{a}_l, \quad (3.54)$$

using the anticommutation relations (3.33) with two transpositions. This form of the operators is independent of N .

To show that this form for the two-body operator is correct, consider first the zero-noncoincidence case (perfectly lined up),

$$\langle I | \hat{G} | I \rangle = \frac{1}{2} \sum_{ijkl} \langle ij | \hat{g} | kl \rangle \langle I | \hat{a}_i^\dagger \hat{a}_j^\dagger \hat{a}_l \hat{a}_k | I \rangle. \quad (3.55)$$

The only nonzero contributions will be for l and k values that appear in $|I\rangle$, say $k = i_p$, $l = i_q$ ($p < q$):

$$\begin{aligned} & \langle ij|\hat{g}|i_p i_q\rangle \langle I|\hat{a}_i^\dagger \hat{a}_j^\dagger \hat{a}_{i_p} \hat{a}_{i_q}|i_1 i_2 \cdots i_p \cdots i_q \cdots\rangle \\ &= \langle ij|\hat{g}|i_p i_q\rangle \langle I|\hat{a}_i^\dagger \hat{a}_j^\dagger|i_1 i_2 \cdots\rangle (-1)^{(p-1)+(q-2)}. \end{aligned} \quad (3.56)$$

To get a nonzero result, $\hat{a}_i^\dagger \hat{a}_j^\dagger \hat{a}_{i_p} \hat{a}_{i_q}$ must restore i_p and i_q to their proper places; this can be done in two ways:

1. set $i = i_p$, $j = i_q$, resulting in

$$\begin{aligned} & \langle i_p i_q|\hat{g}|i_p i_q\rangle \langle I|i_1 i_2 \cdots i_p \cdots i_q \cdots\rangle (-1)^{(p-1)+(q-2)} (-1)^{(p-1)+(q-2)} \\ &= \langle i_p i_q|\hat{g}|i_p i_q\rangle; \end{aligned} \quad (3.57)$$

2. set $i = i_q$, $j = i_p$, resulting in

$$\begin{aligned} & \langle i_q i_p|\hat{g}|i_p i_q\rangle \langle I|i_1 i_2 \cdots i_p \cdots i_q \cdots\rangle (-1)^{(p-1)+(q-2)} (-1)^{(p-1)+(q-1)} \\ &= -\langle i_q i_p|\hat{g}|i_p i_q\rangle = -\langle i_p i_q|\hat{g}|i_q i_p\rangle. \end{aligned} \quad (3.58)$$

This same pair of contributions will also be obtained for $k = i_q$, $l = i_p$. The total matrix element can be written in either of two forms

$$\begin{aligned} \langle I|\hat{G}|I\rangle &= \frac{1}{2} \sum_{i \in I} \sum_{j \in I} (\langle ij|\hat{g}|ij\rangle - \langle ij|\hat{g}|ji\rangle) \\ &= \sum_{\substack{i < j \\ (i \in I, j \in I)}} (\langle ij|\hat{g}|ij\rangle - \langle ij|\hat{g}|ji\rangle). \end{aligned} \quad (3.59)$$

The case $i = j$ does not contribute because of the cancellation of the direct and exchange terms in this case. It is convenient to define the *antisymmetric integral*

$$\langle ij|\hat{g}|kl\rangle_A \equiv \langle ij|\hat{g}|kl\rangle - \langle ij|\hat{g}|lk\rangle, \quad (3.60)$$

so that

$$\langle I|\hat{G}|I\rangle = \frac{1}{2} \sum_{i \in I} \sum_{j \in I} \langle ij|\hat{g}|ij\rangle_A. \quad (3.61)$$

This is, of course, the same as the ordinary result (the Slater–Condon rules) obtained by first-quantized techniques.

Similarly, for a single noncoincidence $i_p \neq i'_p$, i.e. for

$$\begin{aligned} |I\rangle &= |i_1 i_2 \cdots i_p \cdots\rangle, \\ |I'\rangle &= |i_1 i_2 \cdots i'_p \cdots\rangle, \end{aligned} \quad (3.62)$$

we get contributions to $\langle I' | \hat{G} | I \rangle$ from $\hat{a}_i^\dagger \hat{a}_j^\dagger \hat{a}_l \hat{a}_k$ as follows:

$$\begin{aligned}
&\text{for } i = i'_p, \quad k = i_p, \quad j = l = i_q \quad (q \neq p), & \langle i'_p i_q | i_p i_q \rangle; \\
&\text{for } i = i'_p, \quad l = i_p, \quad j = k = i_q \quad (q \neq p), & -\langle i'_p i_q | i_q i_p \rangle; \\
&\text{for } j = i'_p, \quad l = i_p, \quad i = k = i_q \quad (q \neq p), & \langle i_q i'_p | i_q i_p \rangle; \\
&\text{for } j = i'_p, \quad k = i_p, \quad i = l = i_q \quad (q \neq p), & -\langle i_q i'_p | i_p i_q \rangle.
\end{aligned} \tag{3.63}$$

Here the first two terms are equal to the last two terms, respectively. So the total result is

$$\begin{aligned}
\langle I' | \hat{G} | I \rangle &= 2 \times \frac{1}{2} \sum_{j \in I} (\langle i'_p j | \hat{g} | i_p j \rangle - \langle i'_p j | \hat{g} | j i_p \rangle) \\
&= \sum_{j \in I} \langle i'_p j | \hat{g} | i_p j \rangle_A \quad (\text{single noncoincidence}).
\end{aligned} \tag{3.64}$$

Again, the terms in which $j = i_p$ or $j = i'_p$ will cancel, since

$$\begin{aligned}
\langle i'_p i_p | \hat{g} | i_p i_p \rangle_A &= \langle i'_p i_p | \hat{g} | i_p i_p \rangle - \langle i'_p i_p | \hat{g} | i_p i_p \rangle = 0, \\
\langle i'_p i'_p | \hat{g} | i_p i'_p \rangle_A &= \langle i'_p i'_p | \hat{g} | i_p i'_p \rangle - \langle i'_p i'_p | \hat{g} | i'_p i_p \rangle = 0,
\end{aligned} \tag{3.65}$$

and the result agrees with the Slater–Condon rules for a single noncoincidence. For two noncoincidences $j_p \neq i'_p, j_q \neq i'_q$ we get

$$\langle I' | \hat{G} | I \rangle = \langle i'_p i'_q | \hat{g} | i_p i_q \rangle_A \quad (\text{two noncoincidences}), \tag{3.66}$$

and for more than two noncoincidences we get zero, also in agreement with the Slater–Condon rules.

The electronic Hamiltonian consists of one- and two-electron parts,

$$\hat{H} = \hat{H}_1 + \hat{H}_2, \tag{3.67}$$

with

$$\hat{H}_1 = \sum_{\mu} \hat{h}_{\mu}, \quad \hat{H}_2 = \sum_{\mu < \nu} \hat{v}_{\mu\nu}, \tag{3.68}$$

where (using atomic units)

$$\hat{h}_{\mu} = -\frac{1}{2} \nabla_{\mu}^2 - \sum_A \frac{Z_A}{r_{\mu A}}, \quad \hat{v}_{\mu\nu} = \frac{1}{r_{\mu\nu}}. \tag{3.69}$$

The *second-quantized form* of the Hamiltonian is then

$$\hat{H} = \hat{H}_1 + \hat{H}_2 = \sum_{i,j} \langle i | \hat{h} | j \rangle \hat{a}_i^\dagger \hat{a}_j + \frac{1}{2} \sum_{ijkl} \langle ij | \hat{v} | kl \rangle \hat{a}_i^\dagger \hat{a}_j^\dagger \hat{a}_l \hat{a}_k, \tag{3.70}$$

where

$$\langle ij|\hat{v}|kl\rangle \equiv \langle i(1)j(2)|\hat{v}_{12}|k(1)l(2)\rangle. \quad (3.71)$$

The antisymmetric two-electron integral for \hat{v} is often abbreviated as follows:

$$\langle ij|\hat{v}|kl\rangle - \langle ij|\hat{v}|lk\rangle = \langle ij|\hat{v}|kl\rangle_A \equiv \langle ij||kl\rangle. \quad (3.72)$$

Since

$$\langle ij||kl\rangle = -\langle ij||lk\rangle, \quad \hat{a}_l\hat{a}_k = -\hat{a}_k\hat{a}_l, \quad (3.73)$$

we can also write the second-quantized Hamiltonian in the form

$$\hat{H} = \sum_{ij} h_{ij} \hat{a}_i^\dagger \hat{a}_j + \frac{1}{4} \sum_{ijkl} \langle ij||kl\rangle \hat{a}_i^\dagger \hat{a}_j^\dagger \hat{a}_l \hat{a}_k. \quad (3.74)$$

This form is the one we shall find most convenient to use in the subsequent development.

The second-quantized forms of the operators are the second-quantization analogs of the forms

$$\hat{A} = \sum_{I,J} |I\rangle \langle I| \hat{A} |J\rangle \langle J| = \sum_{I,J} |I\rangle A_{IJ} \langle J|, \quad (3.75)$$

except that in the first-quantized form the number of electrons appears through the number of spin orbitals in each of $|I\rangle$ and $|J\rangle$, while the second-quantized form is independent of N .

3.2.4 Invariance under unitary transformations

Next we wish to show the invariance of the second-quantized form of an operator under a unitary transformation of the basis. Let the transformation be effected by a unitary operator \hat{U} , so that

$$\begin{aligned} |\phi'_i\rangle &= \hat{U}|\phi_i\rangle = \sum_j |\phi_j\rangle \langle \phi_j|\hat{U}|\phi_i\rangle \\ &= \sum_j |\phi_j\rangle U_{ji}, \end{aligned} \quad (3.76)$$

where

$$\begin{aligned} U_{ji} &= \langle \phi_j|\hat{U}|\phi_i\rangle, \\ \hat{U}^{-1} &= \hat{U}^\dagger, \\ (\hat{U}^{-1})_{ij} &= U_{ji}^*. \end{aligned} \quad (3.77)$$

Define the *row vectors*

$$\begin{aligned} |\phi\rangle &= (|\phi_1\rangle \ |\phi_2\rangle \ \cdots), \\ |\phi'\rangle &= (|\phi'_1\rangle \ |\phi'_2\rangle \ \cdots) \end{aligned} \quad (3.78)$$

and a *matrix* \mathbf{U} with elements U_{ij} . Then the transformation can be written in the form

$$|\phi'\rangle = |\phi\rangle \mathbf{U}, \quad (3.79)$$

the inverse transformation being

$$|\phi\rangle = |\phi'\rangle \mathbf{U}^{-1} = |\phi'\rangle \mathbf{U}^\dagger \quad (3.80)$$

or

$$|\phi_j\rangle = \sum_i |\phi'_i\rangle U_{ij}^\dagger = \sum_i |\phi'_i\rangle U_{ji}^*. \quad (3.81)$$

The corresponding bras are organized as *column vectors*

$$\begin{aligned} \langle\phi| &= \begin{pmatrix} \langle\phi_1| \\ \langle\phi_2| \\ \vdots \end{pmatrix} = |\phi\rangle^\dagger, \\ \langle\phi'| &= \begin{pmatrix} \langle\phi'_1| \\ \langle\phi'_2| \\ \vdots \end{pmatrix} = |\phi'\rangle^\dagger, \end{aligned} \quad (3.82)$$

with the transformation

$$\begin{aligned} \langle\phi_j| &= \sum_i U_{ji} \langle\phi'_i|, \\ \langle\phi| &= \mathbf{U} \langle\phi'|, \quad \langle\phi'| = \mathbf{U}^\dagger \langle\phi|. \end{aligned} \quad (3.83)$$

Now consider the one-electron operator

$$\begin{aligned} \hat{F} &= \sum_{kl} \langle\phi_k|\hat{f}|\phi_l\rangle \hat{a}_k^\dagger \hat{a}_l \\ &= \sum_{kl} \sum_{ij} U_{ki} \langle\phi'_i|\hat{f}|\phi'_j\rangle U_{jl}^\dagger \hat{a}_k^\dagger \hat{a}_l \\ &= \sum_{ij} \langle\phi'_i|\hat{f}|\phi'_j\rangle \left(\sum_k \hat{a}_k^\dagger U_{ki} \right) \left(\sum_l U_{jl}^\dagger \hat{a}_l \right) \\ &= \sum_{ij} \langle\phi'_i|\hat{f}|\phi'_j\rangle \hat{a}_i'^\dagger \hat{a}_j', \end{aligned} \quad (3.84)$$

where

$$\hat{a}'_i{}^\dagger = \sum_k \hat{a}_k^\dagger U_{ki}, \quad \hat{a}'_j = \sum_l U_{jl}^\dagger \hat{a}_l. \quad (3.85)$$

Again, we can organize the creation and annihilation operators as row and column vectors, respectively:

$$\begin{aligned} \hat{\mathbf{a}}^\dagger &= (\hat{a}_1^\dagger \hat{a}_2^\dagger \cdots), \\ \hat{\mathbf{a}} &= \begin{pmatrix} \hat{a}_1 \\ \hat{a}_2 \\ \vdots \end{pmatrix} \end{aligned} \quad (3.86)$$

(note the consistency of the adjoint notation). Then

$$\begin{aligned} \hat{\mathbf{a}}'^\dagger &= \hat{\mathbf{a}}^\dagger \mathbf{U} & \text{or} & & \hat{\mathbf{a}}^\dagger &= \hat{\mathbf{a}}'^\dagger \mathbf{U}^\dagger & \text{(as for the kets),} \\ \hat{\mathbf{a}}' &= \mathbf{U}^\dagger \hat{\mathbf{a}} & \text{or} & & \hat{\mathbf{a}} &= \mathbf{U} \hat{\mathbf{a}}' & \text{(as for the bras).} \end{aligned} \quad (3.87)$$

These definitions of the transformed creation and annihilation operators are consistent with their usual definitions. For example,

$$\hat{a}'_j{}^\dagger |\cdots\rangle = |j' \cdots\rangle = \sum_i |i \cdots\rangle U_{ij} = \sum_i \hat{a}_i^\dagger |\cdots\rangle U_{ij}. \quad (3.88)$$

3.3 Normal products and Wick's theorem

3.3.1 Normal products of operators

The following definitions and analyses are designed to help in the evaluation of matrix elements, in particular of *vacuum expectation values* $\langle |\hat{A}\hat{B}\cdots| \rangle$ of products of creation and annihilation operators (see Harris, Monkhorst and Freeman 1992).

Let \hat{A} , \hat{B} , \hat{C} , ... stand for various creation and annihilation operators. Then the *normal product* (or normal-ordered product) of such operators, relative to the physical vacuum, is written $n[\hat{A}\hat{B}\hat{C}\cdots]$ and is defined as the rearranged product of operators such that all creation operators are to the left of all annihilation operators with a phase factor corresponding to the parity of the permutation producing the rearrangement:

$$n[\hat{A}\hat{B}\hat{C}\cdots] = (-1)^{\sigma(\hat{P})} \hat{a}^\dagger \hat{b}^\dagger \cdots \hat{u} \hat{v}, \quad (3.89)$$

where

$$\hat{a}^\dagger \hat{b}^\dagger \cdots \hat{u} \hat{v} = \hat{P}(\hat{A}\hat{B}\hat{C}\cdots), \quad (3.90)$$

\hat{P} being a permutation acting on the operators \hat{A} , \hat{B} , ... and $\sigma(\hat{P})$ its parity. This definition is not unique, since any rearrangement of the creation operators among themselves and/or the annihilation operators among themselves is permissible but would always be accompanied by an appropriate change in the phase factor; thus all forms of a normal product are equivalent. Examples are as follows:

$$\begin{aligned} n[\hat{a}^\dagger \hat{b}] &= \hat{a}^\dagger \hat{b}, & n[\hat{a} \hat{b}^\dagger] &= -\hat{b}^\dagger \hat{a}, \\ n[\hat{a} \hat{b}] &= \hat{a} \hat{b} = -\hat{b} \hat{a}, \\ n[\hat{a}^\dagger \hat{b} \hat{c}^\dagger \hat{d}] &= -\hat{a}^\dagger \hat{c}^\dagger \hat{b} \hat{d} = \hat{c}^\dagger \hat{a}^\dagger \hat{b} \hat{d} = \hat{a}^\dagger \hat{c}^\dagger \hat{d} \hat{b} = -\hat{c}^\dagger \hat{a}^\dagger \hat{d} \hat{b}. \end{aligned} \quad (3.91)$$

In general, $n[\hat{A}\hat{B}\hat{C}\cdots] \neq \hat{A}\hat{B}\hat{C}\cdots$, since permuting an annihilation operator \hat{a} with a creation operator \hat{b}^\dagger adds a term δ_{ab} in addition to the change in sign,

$$\hat{a}\hat{b}^\dagger = [\hat{a}, \hat{b}^\dagger]_+ - \hat{b}^\dagger \hat{a} = \delta_{ab} - \hat{b}^\dagger \hat{a}, \quad (3.92)$$

and the δ -term is not present in the definition of the normal product, $n[\hat{a}\hat{b}^\dagger] = -\hat{b}^\dagger \hat{a}$.

Note that in writing the second-quantized forms of quantum mechanical operators (including the Hamiltonian) in the previous section, we have actually put them into normal-product form, so that we have

$$\hat{H} = \sum_{ij} h_{ij} n[\hat{a}_i^\dagger \hat{a}_j] + \frac{1}{4} \sum_{ijkl} \langle ij || kl \rangle n[\hat{a}_i^\dagger \hat{a}_j^\dagger \hat{a}_l \hat{a}_k]. \quad (3.93)$$

The usefulness of the normal-product form is that its vacuum expectation value is zero:

$$\langle |n[\hat{A}\hat{B}\cdots]| \rangle = 0 \quad \text{if } [\hat{A}\hat{B}\cdots] \text{ is not empty.} \quad (3.94)$$

3.3.2 Contractions

In order to be able to compute expectation values of general operator strings, we will take advantage of *Wick's theorem* (Wick 1950). In order to be able to formulate this we need to define the *contraction* (or *pairing*) of operators. For a pair of creation or annihilation operators \hat{A} , \hat{B} , we define their contraction as

$$\hat{\sqcup} \hat{A} \hat{B} \equiv \hat{A} \hat{B} - n[\hat{A} \hat{B}]. \quad (3.95)$$

Specifically, the four possibilities are:

$$\begin{aligned}
 \hat{a}^\dagger \hat{b}^\dagger &= \hat{a}^\dagger \hat{b}^\dagger - \hat{a}^\dagger \hat{b}^\dagger = 0, \\
 \hat{a} \hat{b} &= \hat{a} \hat{b} - \hat{a} \hat{b} = 0, \\
 \hat{a}^\dagger \hat{b} &= \hat{a}^\dagger \hat{b} - \hat{a}^\dagger \hat{b} = 0, \\
 \hat{a} \hat{b}^\dagger &= \hat{a} \hat{b}^\dagger - (-\hat{b}^\dagger \hat{a}) = [\hat{a}, \hat{b}^\dagger]_+ = \delta_{ab}.
 \end{aligned} \tag{3.96}$$

Thus, the contraction of two operators is equal to a number (zero or one).

A *normal product with contractions* is defined as follows:

$$n[\hat{A}\hat{B}\hat{C}\cdots\underbrace{\hat{R}\cdots\hat{S}\cdots\hat{T}\cdots\hat{U}\cdots}] = (-1)^\sigma \hat{R}\hat{T}\hat{S}\hat{U}\cdots n[\hat{A}\hat{B}\hat{C}\cdots] \tag{3.97}$$

where all the contracted pairs have been put in front of the normal product and σ is the parity of the permutation indicated by

$$\begin{pmatrix} \hat{A}\hat{B}\hat{C}\cdots\hat{R}\cdots\hat{S}\cdots\hat{T}\cdots\hat{U}\cdots \\ \hat{R}\hat{T}\hat{S}\hat{U}\cdots\hat{A}\hat{B}\hat{C}\cdots \end{pmatrix}.$$

The result is obviously either zero or plus or minus the normal product with all the contracted pairs omitted.

3.3.3 Time-independent Wick's theorem

The time-independent form of Wick's theorem states: *A product of a string of creation and annihilation operators is equal to their normal product plus the sum of all possible normal products with contractions.* Symbolically,

$$\begin{aligned}
 &\hat{A}\hat{B}\hat{C}\hat{D}\cdots \\
 &= n[\hat{A}\hat{B}\hat{C}\hat{D}\cdots] + n[\hat{A}\hat{B}\hat{C}\hat{D}\cdots] + n[\hat{A}\hat{B}\hat{C}\hat{D}\cdots] + n[\hat{A}\hat{B}\hat{C}\hat{D}\cdots] \\
 &\quad + \cdots + n[\hat{A}\hat{B}\hat{C}\hat{D}\cdots] + n[\hat{A}\hat{B}\hat{C}\hat{D}\cdots] + \cdots + n[\hat{A}\hat{B}\hat{C}\hat{D}\cdots] + \cdots \\
 &\quad + n[\hat{A}\hat{B}\hat{C}\hat{D}\cdots] + n[\hat{A}\hat{B}\hat{C}\hat{D}\cdots] + n[\hat{A}\hat{B}\hat{C}\hat{D}\cdots] + \cdots
 \end{aligned} \tag{3.98}$$

Thus, all possible contractions of one pair, two pairs etc. are included. This expression is also written symbolically in the form

$$\hat{A}\hat{B}\hat{C}\hat{D}\cdots = n[\hat{A}\hat{B}\hat{C}\hat{D}\cdots] + \sum \underbrace{n[\hat{A}\hat{B}\hat{C}\hat{D}\cdots]}, \tag{3.99}$$

the sum being over all possible contractions. An outline of the proof is given in the next subsection. While the complete proof is somewhat tedious, it is essentially straightforward (see, e.g. March, Young and Sampanthar 1967).

The importance of the above result is that the vacuum expectation value of any normal product with contractions is zero unless all operators are contracted. The reason is that each contraction contributes a factor of zero or ± 1 and, if an uncontracted normal product remains, its vacuum expectation value is zero. Thus,

$$\langle |\hat{A} \cdots \hat{B} \cdots \hat{C} \cdots \hat{D} \cdots| \rangle = \sum \langle |n[\underbrace{\hat{A} \cdots \hat{B} \cdots \hat{C} \cdots \hat{D} \cdots}]| \rangle, \quad (3.100)$$

where the sum is over all possible fully contracted normal products. For example,

$$\begin{aligned} \hat{a}^\dagger \hat{b} \hat{c}^\dagger \hat{d} \hat{e}^\dagger \hat{f} &= n[\hat{a}^\dagger \hat{b} \hat{c}^\dagger \hat{d} \hat{e}^\dagger \hat{f}] + n[\hat{a}^\dagger \hat{b} \hat{c}^\dagger \hat{d} \hat{e}^\dagger \hat{f}] + n[\hat{a}^\dagger \hat{b} \hat{c}^\dagger \hat{d} \hat{e}^\dagger \hat{f}] \\ &\quad + n[\hat{a}^\dagger \hat{b} \hat{c}^\dagger \hat{d} \hat{e}^\dagger \hat{f}] + n[\hat{a}^\dagger \hat{b} \hat{c}^\dagger \hat{d} \hat{e}^\dagger \hat{f}], \end{aligned} \quad (3.101)$$

where we have omitted all contractions except those of the form $\hat{u} \hat{v}^\dagger$, since they vanish. Since no fully contracted term survives, the vacuum expectation value of this operator product is zero, as is obvious from

$$\underbrace{\langle |\hat{a}^\dagger \hat{b} \hat{c}^\dagger \hat{d} \hat{e}^\dagger \hat{f}| \rangle}_{=0} = 0. \quad (3.102)$$

A more complex example is given by:

$$\begin{aligned} \hat{a} \hat{b}^\dagger \hat{c} \hat{d}^\dagger \hat{e} \hat{f}^\dagger &= n[\hat{a} \hat{b}^\dagger \hat{c} \hat{d}^\dagger \hat{e} \hat{f}^\dagger] + n[\hat{a} \hat{b}^\dagger \hat{c} \hat{d}^\dagger \hat{e} \hat{f}^\dagger] + n[\hat{a} \hat{b}^\dagger \hat{c} \hat{d}^\dagger \hat{e} \hat{f}^\dagger] + n[\hat{a} \hat{b}^\dagger \hat{c} \hat{d}^\dagger \hat{e} \hat{f}^\dagger] \\ &\quad + n[\hat{a} \hat{b}^\dagger \hat{c} \hat{d}^\dagger \hat{e} \hat{f}^\dagger] + n[\hat{a} \hat{b}^\dagger \hat{c} \hat{d}^\dagger \hat{e} \hat{f}^\dagger] + n[\hat{a} \hat{b}^\dagger \hat{c} \hat{d}^\dagger \hat{e} \hat{f}^\dagger] + n[\hat{a} \hat{b}^\dagger \hat{c} \hat{d}^\dagger \hat{e} \hat{f}^\dagger] \\ &\quad + n[\hat{a} \hat{b}^\dagger \hat{c} \hat{d}^\dagger \hat{e} \hat{f}^\dagger] + n[\hat{a} \hat{b}^\dagger \hat{c} \hat{d}^\dagger \hat{e} \hat{f}^\dagger] + n[\hat{a} \hat{b}^\dagger \hat{c} \hat{d}^\dagger \hat{e} \hat{f}^\dagger] + n[\hat{a} \hat{b}^\dagger \hat{c} \hat{d}^\dagger \hat{e} \hat{f}^\dagger] \\ &\quad + n[\hat{a} \hat{b}^\dagger \hat{c} \hat{d}^\dagger \hat{e} \hat{f}^\dagger] + n[\hat{a} \hat{b}^\dagger \hat{c} \hat{d}^\dagger \hat{e} \hat{f}^\dagger] + n[\hat{a} \hat{b}^\dagger \hat{c} \hat{d}^\dagger \hat{e} \hat{f}^\dagger], \end{aligned} \quad (3.103)$$

for which the vacuum expectation value is

$$\langle |\hat{a} \hat{b}^\dagger \hat{c} \hat{d}^\dagger \hat{e} \hat{f}^\dagger| \rangle = \langle |n[\hat{a} \hat{b}^\dagger \hat{c} \hat{d}^\dagger \hat{e} \hat{f}^\dagger]| \rangle = \delta_{ab} \delta_{cd} \delta_{ef}. \quad (3.104)$$

These examples demonstrate the power of Wick's theorem.

3.3.4 Outline of proof of Wick's theorem

In a normal-ordered product $\hat{p}^\dagger \hat{q}^\dagger \cdots \hat{u} \hat{v}$ all contractions vanish since in such a product there can be no $\cdots \hat{s} \cdots \hat{t}^\dagger \cdots$ contractions. Thus, if a string of

operators is already in normal product form we have

$$\begin{aligned} \hat{p}^\dagger \hat{q}^\dagger \cdots \hat{u} \hat{v} &= n[\hat{p}^\dagger \hat{q}^\dagger \cdots \hat{u} \hat{v}] \\ &= n[\hat{p}^\dagger \hat{q}^\dagger \cdots \hat{u} \hat{v}] + \sum_{\substack{\text{all} \\ \text{contractions}}} n[\hat{p}^\dagger \hat{q}^\dagger \cdots \hat{u} \hat{v}], \end{aligned} \quad (3.105)$$

since all terms in the sum vanish. Thus Wick's theorem holds in this case.

Consider next the case where one pair of operators is out of normal order:

$$\begin{aligned} \hat{p}^\dagger \hat{q}^\dagger \cdots \hat{r} \hat{s}^\dagger \cdots \hat{u} \hat{v} &= \hat{p}^\dagger \hat{q}^\dagger \cdots \left([\hat{r}, \hat{s}^\dagger]_+ - \hat{s}^\dagger \hat{r} \right) \cdots \hat{u} \hat{v} \\ &= \hat{p}^\dagger \hat{q}^\dagger \cdots \delta_{rs} \cdots \hat{u} \hat{v} - \hat{p}^\dagger \hat{q}^\dagger \cdots \hat{s}^\dagger \hat{r} \cdots \hat{u} \hat{v} \\ &= n[\hat{p}^\dagger \hat{q}^\dagger \cdots \hat{r} \hat{s}^\dagger \cdots \hat{u} \hat{v}] + n[\hat{p}^\dagger \hat{q}^\dagger \cdots \hat{r} \hat{s}^\dagger \cdots \hat{u} \hat{v}]. \end{aligned} \quad (3.106)$$

All other contractions vanish, so Wick's theorem still holds.

Now consider the case where we have two annihilation operators to the left of one of the creation operators:

$$\begin{aligned} \hat{p}^\dagger \hat{q}^\dagger \cdots \hat{r} \hat{s} \hat{t}^\dagger \cdots \hat{u} \hat{v} &= \hat{p}^\dagger \hat{q}^\dagger \cdots \hat{r} \hat{s} \hat{t}^\dagger \cdots \hat{u} \hat{v} - \hat{p}^\dagger \hat{q}^\dagger \cdots \hat{r} \hat{t}^\dagger \hat{s} \cdots \hat{u} \hat{v} \\ &= \hat{p}^\dagger \hat{q}^\dagger \cdots \hat{r} \hat{s} \hat{t}^\dagger \cdots \hat{u} \hat{v} - \hat{p}^\dagger \hat{q}^\dagger \cdots \hat{r} \hat{t}^\dagger \hat{s} \cdots \hat{u} \hat{v} + \hat{p}^\dagger \hat{q}^\dagger \cdots \hat{t}^\dagger \hat{r} \hat{s} \cdots \hat{u} \hat{v} \\ &= n[\hat{p}^\dagger \hat{q}^\dagger \cdots \hat{r} \hat{s} \hat{t}^\dagger \cdots \hat{u} \hat{v}] + n[\hat{p}^\dagger \hat{q}^\dagger \cdots \hat{r} \hat{s} \hat{t}^\dagger \cdots \hat{u} \hat{v}] + n[\hat{p}^\dagger \hat{q}^\dagger \cdots \hat{r} \hat{s} \hat{t}^\dagger \cdots \hat{u} \hat{v}], \end{aligned} \quad (3.107)$$

again satisfying Wick's theorem, since all other contractions vanish.

This procedure can be continued for all pairs of operators out of normal order.

3.4 Particle-hole formulation

3.4.1 The reference state

Instead of referring all SDs and their matrix elements back to the vacuum state

$$|I\rangle = |i_1 i_2 \cdots i_N\rangle = \hat{i}_1^\dagger \hat{i}_2^\dagger \cdots \hat{i}_N^\dagger | \rangle, \quad (3.108)$$

it is more convenient to begin with a fixed *reference state*

$$|0\rangle \equiv |\Phi_0\rangle = |ijk \cdots n\rangle, \quad (3.109)$$

and define other SD's relative to it, e.g.

$$\begin{aligned}
 |\Phi_i^a\rangle &\equiv \hat{a}^\dagger \hat{i} |\Phi_0\rangle = |ajk \cdots n\rangle && \text{(single excitation)}, \\
 |\Phi_{ij}^{ab}\rangle &\equiv \hat{a}^\dagger \hat{b}^\dagger \hat{j} \hat{i} |\Phi_0\rangle = |abk \cdots n\rangle && \text{(double excitation)}, \\
 |\Phi_i\rangle &\equiv \hat{i} |\Phi_0\rangle = |jk \cdots n\rangle && \text{(electron removal)}, \\
 |\Phi^a\rangle &\equiv \hat{a}^\dagger |\Phi_0\rangle = |aijk \cdots n\rangle && \text{(electron attachment)}
 \end{aligned} \tag{3.110}$$

etc. Note also that

$$|\Phi_{ij}^{ab}\rangle = |\Phi_{ji}^{ba}\rangle = -|\Phi_{ij}^{ba}\rangle = -|\Phi_{ji}^{ab}\rangle. \tag{3.111}$$

The reference state $|0\rangle$ is also called the *Fermi vacuum* (corresponding to the Fermi level, the level of the highest occupied orbital in the reference function), in contrast with the *physical vacuum* $|\rangle$. (Some sources use $|0\rangle$ for the physical vacuum and $|\Phi\rangle$ or $|\Phi_0\rangle$ for the Fermi vacuum.) The spinorbitals i, j, k, \dots, n that are occupied in $|0\rangle$ are called *hole states* (they appear explicitly only when an electron is excited out of them by, e.g. \hat{i} , creating a hole in the reference state), while the other spinorbitals a, b, \dots are called *particle states*. We shall use the letters i, j, k, \dots to indicate indices restricted to hole states, the letters a, b, c, \dots to indicate indices restricted to particle states and the letters p, q, r, \dots to indicate any state (either hole or particle, without restriction). (Other common notations are: $\alpha, \beta, \gamma, \dots$ for holes, a, b, c, \dots for particles, p, q, r, \dots for either; λ, μ, ν, \dots for holes, p, q, r, \dots for particles, m, n, \dots for either; and other variations thereof.)

Using this notation we find that

$$\begin{aligned}
 \hat{i}^\dagger |0\rangle &= 0, & \hat{a} |0\rangle &= 0, \\
 \langle 0 | \hat{i} &= 0, & \langle 0 | \hat{a}^\dagger &= 0.
 \end{aligned} \tag{3.112}$$

It is convenient to define a new set of operators, sometimes called pseudo-creation and pseudo-annihilation operators (or quasi-operators), via

$$\begin{aligned}
 \hat{b}_i &= \hat{a}_i^\dagger, & \hat{b}_i^\dagger &= \hat{a}_i, \\
 \hat{b}_a &= \hat{a}_a, & \hat{b}_a^\dagger &= \hat{a}_a^\dagger.
 \end{aligned} \tag{3.113}$$

Thus \hat{b}_i^\dagger creates a vacancy in state i while \hat{b}_i eliminates such a vacancy. The particle pseudo-operators are identical to the ordinary particle operators, while the hole pseudo-creation and pseudo-annihilation operators are equivalent to the ordinary hole annihilation and creation operators, respectively. The motivation for this notation is that all pseudo-annihilation operators

operating to the right on the Fermi vacuum state give zero and all pseudo-creation operators operating to the left on the Fermi vacuum state also give zero,

$$\hat{b}_p|0\rangle = 0, \quad \langle 0|\hat{b}_p^\dagger = 0. \quad (3.114)$$

Here we will continue to use the ordinary creation and annihilation operator notation relative to the physical vacuum but our particle and hole states will be defined relative to the Fermi vacuum.

The energy of the reference state can be computed as follows:

$$\begin{aligned} E_{\text{ref}} &= \langle ijk \cdots n | \hat{H} | ijk \cdots n \rangle \\ &= \sum_{pq} \langle ijk \cdots n | \hat{p}^\dagger \hat{q} | ijk \cdots n \rangle h_{pq} \\ &\quad + \frac{1}{2} \sum_{pqrs} \langle ijk \cdots n | \hat{p}^\dagger \hat{q}^\dagger \hat{s} \hat{r} | ijk \cdots n \rangle \langle pq | \hat{v} | rs \rangle \\ &= \sum_l \langle ijk \cdots n | \hat{l}^\dagger \hat{l} | ijk \cdots n \rangle h_{ll} \\ &\quad + \frac{1}{2} \sum_{l \neq m} \langle ijk \cdots n | \hat{l}^\dagger \hat{m}^\dagger \hat{m} \hat{l} | ijk \cdots n \rangle \langle lm | \hat{v} | lm \rangle \\ &\quad + \frac{1}{2} \sum_{l \neq m} \langle ijk \cdots n | \hat{l}^\dagger \hat{m}^\dagger \hat{l} \hat{m} | ijk \cdots n \rangle \langle lm | \hat{v} | ml \rangle \\ &= \sum_l h_{ll} + \frac{1}{2} \sum_{lm} \langle lm | \hat{v} | lm \rangle - \frac{1}{2} \sum_{lm} \langle lm | \hat{v} | ml \rangle, \\ &= \sum_l h_{ll} + \frac{1}{2} \sum_{lm} \langle lm || lm \rangle. \end{aligned} \quad (3.115)$$

Note that we have used $\hat{l}^\dagger \hat{m}^\dagger \hat{l} \hat{m} = -\hat{l}^\dagger \hat{m}^\dagger \hat{m} \hat{l}$, that the summations are over the hole states only and that the sum over l and m includes both $l > m$ and $l < m$, as well as $l = m$, in the last two rows (since $\langle lm || nn \rangle = \langle ll || mn \rangle = 0$). We may also write E_{ref} in the more familiar form

$$E_{\text{ref}} = \sum_l h_{ll} + \sum_{l < m} \langle lm || lm \rangle, \quad (3.116)$$

where the restriction $l < m$ cancels the factor $\frac{1}{2}$.

3.4.2 Normal products and Wick's theorem relative to the Fermi vacuum

Now we are in a position to modify the concepts of normal products, contractions and Wick's theorem so that they relate to a *reference state* (the Fermi vacuum) instead of the physical vacuum.

A product of creation and/or annihilation operators is said to be in normal order relative to the Fermi vacuum $|0\rangle = |ijk \cdots n\rangle$ if all pseudo-creation operators \hat{a}^\dagger, \dots and \hat{i}, \dots are to the left of all pseudo-annihilation operators \hat{a}, \dots and \hat{i}^\dagger, \dots . Using the notation

$$\begin{aligned}\hat{b}_i^\dagger &= \hat{a}_i = \hat{i}, \\ \hat{b}_i &= \hat{a}_i^\dagger = \hat{i}^\dagger, \\ \hat{b}_a^\dagger &= \hat{a}_a^\dagger = \hat{a}^\dagger, \\ \hat{b}_a &= \hat{a}_a = \hat{a},\end{aligned}\tag{3.117}$$

the product is in normal order if all the \hat{b}_p^\dagger operators are to the left of all the \hat{b}_p operators. Since

$$\hat{b}_p|0\rangle = 0, \quad \langle 0|\hat{b}_p^\dagger = 0,\tag{3.118}$$

the Fermi-vacuum expectation value of a normal-ordered product of such operators vanishes.

To distinguish the new type of normal product from the previous type, it is often written as

$$N[ABC \cdots] = (-1)^{\sigma(\hat{P})} \hat{b}_p^\dagger \hat{b}_q^\dagger \cdots \hat{b}_u \hat{b}_v,\tag{3.119}$$

instead of $n[ABC \cdots]$ when the ordering is relative to the physical vacuum. The power $\sigma(\hat{P})$ of the phase factor is the parity of the permutation from $ABC \cdots$ to $\hat{b}_p^\dagger \hat{b}_q^\dagger \cdots \hat{b}_u \hat{b}_v$. Here we shall use the alternative notation $\{ABC \cdots\}$ for the normal product relative to the Fermi vacuum. Contractions relative to the Fermi vacuum will be denoted by brackets above the operators instead of below, and we have

$$\overline{\hat{A}\hat{B}} = \hat{A}\hat{B} - \{\hat{A}\hat{B}\}.\tag{3.120}$$

We then find that the *only nonzero contractions* are

$$\overline{\hat{i}^\dagger \hat{j}} = \delta_{ij}, \quad \overline{\hat{a} \hat{b}^\dagger} = \delta_{ab}.\tag{3.121}$$

A normal product with contractions is also defined in the same way as in the case where it is relative to the physical vacuum:

$$\{\hat{A}\hat{B}\hat{C}\cdots\overbrace{\hat{R}\cdots\hat{S}\cdots\hat{T}\cdots\hat{U}\cdots}\} = (-1)^\sigma \overbrace{\hat{R}\hat{T}}\overbrace{\hat{S}\hat{U}}\cdots\{\hat{A}\hat{B}\hat{C}\cdots\}. \quad (3.122)$$

Here σ is the parity of the permutation, as given below:

$$\begin{pmatrix} \hat{A}\hat{B}\hat{C}\cdots\hat{R}\cdots\hat{S}\cdots\hat{T}\cdots\hat{U}\cdots \\ \hat{R}\hat{T}\hat{S}\hat{U}\cdots\hat{A}\hat{B}\hat{C}\cdots \end{pmatrix}.$$

Wick's theorem has exactly the same form in this system as in the physical vacuum system,

$$\hat{A}\hat{B}\hat{C}\hat{D}\cdots = \{\hat{A}\hat{B}\hat{C}\hat{D}\cdots\} + \sum_{\substack{\text{all} \\ \text{contractions}}} \{\overbrace{\hat{A}\hat{B}}\overbrace{\hat{C}\hat{D}}\cdots\}; \quad (3.123)$$

as indicated, the sum is over all possible contractions of one pair, two pairs etc. Obviously, the usefulness of this theorem is at least partly due to the fact that *the Fermi vacuum expectation value of a normal product vanishes unless it is fully contracted*, so that

$$\langle 0|\hat{A}\cdots\hat{B}\cdots\hat{C}\cdots\hat{D}\cdots|0\rangle = \sum \langle 0|\overbrace{\hat{A}\cdots\hat{B}\cdots\hat{C}\cdots\hat{D}\cdots}\rangle|0\rangle, \quad (3.124)$$

where the sum is over all fully contracted normal products. From here on, unless explicitly stated otherwise, whenever we talk of the vacuum we will be referring to the Fermi vacuum and whenever we talk of normal products or contractions, we are referring to these concepts relative to the Fermi vacuum.

3.5 Partitioning of the Hamiltonian

The most convenient form for the zero-order part of the Hamiltonian is that of a diagonal one-electron operator,

$$\hat{H}_0 = \sum_p \varepsilon_p \hat{p}^\dagger \hat{p}. \quad (3.125)$$

In principle, the choice of the energy parameters $\{\varepsilon_p, p = 1, 2, \dots\}$, which we shall call *orbital energies*, is arbitrary and can be made independently of the choice of the set of orthonormal spinorbitals $\{\phi_p, p = 1, 2, \dots\}$ used in the construction of the Slater determinants, but both choices strongly affect the convergence of the perturbation series. With the total Hamiltonian split

into a one-electron and a two-electron part according to (3.67) and (3.74), the perturbation is given by

$$\begin{aligned}\hat{V} &= (\hat{H}_1 - \hat{H}_0) + \hat{H}_2 \\ &= \sum_{pq} (h_{pq} - \varepsilon_p \delta_{pq}) \hat{p}^\dagger \hat{q} + \frac{1}{4} \sum_{pqrs} \langle pq || rs \rangle \hat{p}^\dagger \hat{q}^\dagger \hat{s} \hat{r}.\end{aligned}\quad (3.126)$$

Most commonly the orbital energies are chosen as the diagonal elements

$$\varepsilon_p = f_{pp} \quad (3.127)$$

of a *Fock operator* (shown here in both first- and second-quantized forms)

$$\hat{F} = \sum_{\mu=1}^N \hat{f}_\mu = \sum_{pq} f_{pq} \hat{p}^\dagger \hat{q}. \quad (3.128)$$

The Fock operator \hat{F} is defined in terms of an auxiliary one-electron operator

$$\hat{U} = \sum_{\mu=1}^N \hat{u}_\mu = \sum_{pq} u_{pq} \hat{p}^\dagger \hat{q} \quad (3.129)$$

by

$$\hat{F} = \hat{H}_1 + \hat{U} = \sum_{pq} (h_{pq} + u_{pq}) \hat{p}^\dagger \hat{q} = \sum_{pq} f_{pq} \hat{p}^\dagger \hat{q}, \quad (3.130)$$

$$f_{pq} = \langle p | \hat{f} | q \rangle = h_{pq} + u_{pq}. \quad (3.131)$$

While \hat{U} could, in principle, be chosen arbitrarily, it is generally chosen in a particular way designed to generate an appropriate zero-order Hamiltonian and, at the same time, simplify the perturbation operator by canceling certain contributions to \hat{H}_2 . Using the Coulomb and exchange operators defined in (1.4), we define \hat{u} as in (1.3),

$$\hat{u} = \sum_i (\hat{J}_i - \hat{K}_i), \quad (3.132)$$

or, explicitly,

$$u_{pq} = \langle p | \hat{u} | q \rangle = \sum_i \langle pi || qi \rangle. \quad (3.133)$$

The sums in (3.132), (3.133) are over the hole-state spinorbitals that define the reference state $|0\rangle$ used as the zero-order function for the perturbation treatment.

Defining the operator

$$\hat{F}' = \sum_{pq} f'_{pq} \hat{p}^\dagger \hat{q}, \quad (3.134)$$

$$f'_{pq} = \langle p | \hat{f}' | q \rangle = f_{pq} - \varepsilon_p \delta_{pq}, \quad (3.135)$$

the perturbation (3.126) becomes

$$\begin{aligned} \hat{V} &= \hat{F}' - \hat{U} + \hat{H}_2 \\ &= \sum_{pq} (f'_{pq} - u_{pq}) \hat{p}^\dagger \hat{q} + \frac{1}{2} \sum_{pqrs} \langle pq | \hat{v} | rs \rangle \hat{p}^\dagger \hat{q}^\dagger \hat{s} \hat{r}. \end{aligned} \quad (3.136)$$

In these definitions we have not assumed that the spinorbitals are Hartree–Fock spinorbitals for the state being studied or for any other state, neither have we assumed that the orbital energies are equal to the diagonal elements of the Fock operator, (3.127). However, when a Hartree–Fock function is used as the reference function, and if (3.127) holds, this choice makes the \hat{F} operator equal to the Fock operator of Hartree–Fock theory and makes the reference energy E_{ref} , (3.115), equal to the HF energy E_{HF} . Furthermore, in the canonical Hartree–Fock case this Fock operator is diagonal and is given completely in terms of the orbital energies

$$f_{pq} = \varepsilon_p \delta_{pq} \quad (\text{canonical HF}) \quad (3.137)$$

and

$$\varepsilon_p = h_{pp} + \sum_i \langle pi | | pi \rangle. \quad (3.138)$$

In the noncanonical HF case, \hat{F} is block diagonal in terms of the occupied and virtual spinorbital blocks:

$$f_{ia} = 0 \quad (\text{noncanonical HF}). \quad (3.139)$$

When the orbital energies are given by (3.127) (this is the most common practice), the operator \hat{F}' , (3.134), becomes equal to the off-diagonal part \hat{F}° of \hat{F} :

$$\hat{F} = \hat{F}^{\text{d}} + \hat{F}^\circ, \quad \hat{f} = \hat{f}^{\text{d}} + \hat{f}^\circ, \quad (3.140)$$

$$\hat{F}^{\text{d}} = \sum_p f_{pp} \hat{p}^\dagger \hat{p} = \sum_{pq} f_{pq}^{\text{d}} \hat{p}^\dagger \hat{q}, \quad (3.141)$$

$$\hat{F}^\circ = \sum_{p \neq q} f_{pq} \hat{p}^\dagger \hat{q} = \sum_{pq} f_{pq}^\circ \hat{p}^\dagger \hat{q}, \quad (3.142)$$

where

$$f_{pq}^d = \langle p | \hat{f}^d | q \rangle = f_{pp} \delta_{pq}, \quad f_{pq}^o = \langle p | \hat{f}^o | q \rangle = (1 - \delta_{pq}) f_{pq}. \quad (3.143)$$

In this case

$$\hat{H}_0 = \hat{F}^d \quad (3.144)$$

and

$$\begin{aligned} \hat{V} &= \hat{F}^o - \hat{U} + \hat{H}_2 \\ &= \sum_{pq} (f_{pq}^o - u_{pq}) \hat{p}^\dagger \hat{q} + \frac{1}{2} \sum_{pqrs} \langle pq | \hat{v} | rs \rangle \hat{p}^\dagger \hat{q}^\dagger \hat{s} \hat{r}. \end{aligned} \quad (3.145)$$

The perturbation thus consists of one-electron and two-electron parts,

$$\begin{aligned} \hat{V}_1 &= \hat{F}^o - \hat{U} = \sum_{pq} (f_{pq}^o - u_{pq}) \hat{p}^\dagger \hat{q}, \\ \hat{V}_2 &= \hat{H}_2 = \frac{1}{2} \sum_{pqrs} \langle pq | \hat{v} | rs \rangle \hat{p}^\dagger \hat{q}^\dagger \hat{s} \hat{r} = \frac{1}{4} \sum_{pqrs} \langle pq || rs \rangle \hat{p}^\dagger \hat{q}^\dagger \hat{s} \hat{r}. \end{aligned} \quad (3.146)$$

Unless stated otherwise, it will generally be assumed that the orbital energies are given by (3.127) and that the auxiliary operator \hat{U} is determined by (3.133).

The definition of \hat{u} according to (3.133) will lead, as we shall see later, to the cancellation of $-\hat{U}$ with certain contributions to the two-electron part \hat{V}_2 , leaving just \hat{F}^o (or, more generally, \hat{F}') as the one-electron part of the perturbation. In the canonical Hartree–Fock representation, in which $\hat{F}^o = 0$, all the one-electron part \hat{V}_1 is canceled. Ultimately, the choices of the one-particle basis, the orbital energies and the operators \hat{U} and \hat{F} are motivated by the desire to make the perturbation \hat{V} small, and the Hartree–Fock scheme is usually a good way of achieving this goal.

The use of a diagonal zero-order Hamiltonian is motivated by the convenience of having a known complete set of eigenfunctions of \hat{H}_0 , leading to the diagonal case of PT. Indeed, using (3.125) we find that all possible Slater determinants made up of the spinorbitals $\{\phi_1, \phi_2, \dots\} = \{p\} = \{i, j, \dots, a, b, \dots\}$ are eigenfunctions of \hat{H}_0 , and the eigenvalues are sums of the corresponding orbital energies,

$$\hat{H}_0 |rst \dots\rangle = \sum_p \varepsilon_p \hat{p}^\dagger \hat{p} |rst \dots\rangle = (\varepsilon_r + \varepsilon_s + \varepsilon_t + \dots) |rst \dots\rangle \quad (3.147)$$

(for any number of electrons).

If the *reference state* is

$$|\Phi_0\rangle = |jk \dots n\rangle \quad (3.148)$$

then

$$\hat{H}_0|\Phi_0\rangle = E_0^{(0)}|\Phi_0\rangle = (\varepsilon_j + \varepsilon_k + \cdots + \varepsilon_n)|\Phi_0\rangle, \quad E_0^{(0)} = \sum_i \varepsilon_i \quad (3.149)$$

(the sum is over the hole states). This zero-order energy is not the same as E_{ref} . In fact, from (3.115),

$$\begin{aligned} E_{\text{ref}} &= \sum_i h_{ii} + \frac{1}{2} \sum_{ij} \langle ij || ij \rangle \\ &= \sum_i (f_{ii} - u_{ii}) + \frac{1}{2} \sum_{ij} \langle ij || ij \rangle \\ &= \sum_i \varepsilon_i - \sum_i u_{ii} + \frac{1}{2} \sum_{ij} \langle ij || ij \rangle \\ &= \sum_i \varepsilon_i - \frac{1}{2} \sum_{ij} \langle ij || ij \rangle, \end{aligned} \quad (3.150)$$

using (3.133). Combining the first and last line of (3.150), we can also write the reference energy in the form

$$E_{\text{ref}} = \frac{1}{2} \sum_i (h_{ii} + \varepsilon_i). \quad (3.151)$$

The various sums in (3.150), (3.151) are the traces of matrix representations over the occupied spinorbital space and thus are invariant under unitary transformations of the occupied spinorbitals.

Following the same analysis as in (3.115), we have

$$\begin{aligned} \langle \Phi_0 | \hat{V} | \Phi_0 \rangle &= \left\langle \Phi_0 \left| \sum_{pq} (f_{pq}^o - u_{pq}) \hat{p}^\dagger \hat{q} + \frac{1}{2} \sum_{pqrs} \langle pq || \hat{v} || rs \rangle \hat{p}^\dagger \hat{q}^\dagger \hat{s} \hat{r} \right| \Phi_0 \right\rangle \\ &= - \sum_i u_{ii} + \frac{1}{2} \sum_{ij} \langle ij || ij \rangle = -\frac{1}{2} \sum_{ij} \langle ij || ij \rangle \end{aligned} \quad (3.152)$$

(since $f_{ii}^o = 0$), and so we find that (3.150) is consistent with

$$E_{\text{ref}} = \langle \Phi_0 | \hat{H} | \Phi_0 \rangle = \langle \Phi_0 | \hat{H}_0 + \hat{V} | \Phi_0 \rangle = E^{(0)} + E^{(1)}. \quad (3.153)$$

(In the more general case, in which (3.127) is not assumed, (3.150)–(3.152) have the additional contribution $\sum_i f_{ii}'$.) For any other SD $|\Phi_{ij\cdots}^{ab\cdots}\rangle$ we have

$$\hat{H}_0|\Phi_{ij\cdots}^{ab\cdots}\rangle = \left(E^{(0)} + \varepsilon_a + \varepsilon_b + \cdots - \varepsilon_i - \varepsilon_j - \cdots \right) |\Phi_{ij\cdots}^{ab\cdots}\rangle. \quad (3.154)$$

The partitioning of the Hamiltonian based on an HF reference function and Fock operator, particularly in the canonical HF case, is often referred to

as *Møller–Plesset (MP) partitioning* (Møller and Plesset 1934). The RSPT expansion based on MP partitioning and Hartree–Fock orbitals has been referred to as *Møller–Plesset perturbation theory* (Binkley and Pople 1975, Pople, Binkley and Seeger 1976).

Other partitionings of the Hamiltonian can also be used as a basis for an RSPT expansion. In particular, the diagonal part of the Hamiltonian in any convenient Hilbert-space representation can be used as the zero-order Hamiltonian \hat{H}_0 :

$$\begin{aligned}\hat{H}_0 &= \sum_i |\Phi_i\rangle\langle\Phi_i|\hat{H}|\Phi_i\rangle\langle\Phi_i| = \sum_i |\Phi_i\rangle H_{ii}\langle\Phi_i|, \\ \hat{V} &= \hat{H} - \hat{H}_0 = \sum_{i \neq j} |\Phi_i\rangle\langle\Phi_i|\hat{H}|\Phi_j\rangle\langle\Phi_j|. \end{aligned} \quad (3.155)$$

Obviously, the Hilbert-space basis functions $|\Phi_i\rangle$ are eigenfunctions of this \hat{H}_0 , with eigenvalues H_{ii} :

$$\hat{H}_0|\Phi_i\rangle = \sum_j |\Phi_j\rangle H_{jj}\langle\Phi_j|\Phi_i\rangle = |\Phi_i\rangle H_{ii}. \quad (3.156)$$

This type of partitioning is called *Epstein–Nesbet (EN) partitioning* (Epstein 1926, Nesbet 1955) and leads to a perturbation expansion in which the denominators contain differences of diagonal matrix elements of the full Hamiltonian $H_{00} - H_{ii}$. In this case \hat{H}_0 is not a one-electron operator, and the H_{ii} are not expressible as sums of orbital energies. The Epstein–Nesbet perturbation expansion can also be obtained as a result of infinite-order summations of certain classes of terms in the Møller–Plesset series though unlike the MP choice, the EN expansion is not invariant under rotations among the occupied or the unoccupied orbitals. The effect of these two types of partitioning on PT convergence was examined by Bartlett and Shavitt (1977b).

3.6 Normal-product form of the quantum-mechanical operators

3.6.1 One-electron operators

Let us consider a one-electron operator

$$\hat{F} = \sum_{pq} \langle p|\hat{f}|q\rangle \hat{p}^\dagger \hat{q}. \quad (3.157)$$

Using Wick's theorem,

$$\hat{p}^\dagger \hat{q} = \{\hat{p}^\dagger \hat{q}\} + \overline{\hat{p}^\dagger \hat{q}}. \quad (3.158)$$

The contracted term vanishes unless p and q are the same hole state (call it i), when it is equal to 1, and thus

$$\begin{aligned}\hat{F} &= \sum_{pq} \langle p | \hat{f} | q \rangle \{ \hat{p}^\dagger \hat{q} \} + \sum_i \langle i | \hat{f} | i \rangle \\ &= \hat{F}_N + \sum_i \langle i | \hat{f} | i \rangle ,\end{aligned}\quad (3.159)$$

where F_N is the normal-product form of the operator (3.157),

$$\hat{F}_N = \sum_{pq} \langle p | \hat{f} | q \rangle \{ \hat{p}^\dagger \hat{q} \} . \quad (3.160)$$

Since $\langle 0 | \hat{F}_N | 0 \rangle = 0$, we have

$$\langle 0 | \hat{F} | 0 \rangle = \sum_i \langle i | \hat{f} | i \rangle , \quad \hat{F} = \hat{F}_N + \langle 0 | \hat{F} | 0 \rangle , \quad (3.161)$$

so that \hat{F}_N represents the difference between \hat{F} and its Fermi-vacuum expectation value,

$$\hat{F}_N = \hat{F} - \langle 0 | \hat{F} | 0 \rangle . \quad (3.162)$$

Note that \hat{F}_N contains hole-hole, particle-particle and hole-particle terms,

$$\begin{aligned}\hat{F}_N &= \sum_{ij} f_{ij} \{ \hat{i}^\dagger \hat{j} \} + \sum_{ab} f_{ab} \{ \hat{a}^\dagger \hat{b} \} + \sum_{ia} f_{ia} \{ \hat{i}^\dagger \hat{a} \} + \sum_{ia} f_{ai} \{ \hat{a}^\dagger \hat{i} \} \\ &= - \sum_{ij} f_{ij} \hat{j} \hat{i}^\dagger + \sum_{ab} f_{ab} \hat{a} \hat{b}^\dagger + \sum_{ia} f_{ia} \hat{i}^\dagger \hat{a} + \sum_{ia} f_{ai} \hat{a}^\dagger \hat{i} ,\end{aligned}\quad (3.163)$$

and can be separated into diagonal and off-diagonal parts:

$$\begin{aligned}\hat{F}_N &= \hat{F}_N^d + \hat{F}_N^o , \\ \hat{F}_N^d &= \sum_p f_{pp} \{ \hat{p}^\dagger \hat{p} \} = \hat{F}^d - \langle 0 | \hat{F}^d | 0 \rangle , \\ \hat{F}_N^o &= \sum_{p \neq q} f_{pq} \{ \hat{p}^\dagger \hat{q} \} = \hat{F}^o - \langle 0 | \hat{F}^o | 0 \rangle = \hat{F}^o ,\end{aligned}\quad (3.164)$$

since $\langle 0 | \hat{F}^o | 0 \rangle = 0$.

3.6.2 Two-electron operators

Next consider a two-electron operator,

$$\hat{G} = \frac{1}{2} \sum_{pqrs} \langle pq | \hat{g} | rs \rangle \hat{p}^\dagger \hat{q}^\dagger \hat{s} \hat{r} . \quad (3.165)$$

Noting that

$$\overline{\hat{p}^\dagger \hat{q}^\dagger} = \overline{\hat{p} \hat{q}} = 0, \quad \overline{\hat{i}^\dagger \hat{j}} = \delta_{ij}, \quad \overline{\hat{a}^\dagger \hat{b}} = 0, \quad (3.166)$$

we obtain

$$\begin{aligned} \hat{p}^\dagger \hat{q}^\dagger \hat{s} \hat{r} &= \{\hat{p}^\dagger \hat{q}^\dagger \hat{s} \hat{r}\} + \overline{\{\hat{p}^\dagger \hat{q}^\dagger \hat{s} \hat{r}\}} + \overline{\{\hat{p}^\dagger \hat{q}^\dagger \hat{s} \hat{r}\}} \\ &\quad + \overline{\{\hat{p}^\dagger \hat{q}^\dagger \hat{s} \hat{r}\}} + \overline{\{\hat{p}^\dagger \hat{q}^\dagger \hat{s} \hat{r}\}} + \overline{\{\hat{p}^\dagger \hat{q}^\dagger \hat{s} \hat{r}\}} + \overline{\{\hat{p}^\dagger \hat{q}^\dagger \hat{s} \hat{r}\}} \\ &= \{\hat{p}^\dagger \hat{q}^\dagger \hat{s} \hat{r}\} + \overline{\hat{p}^\dagger \hat{r} \{\hat{q}^\dagger \hat{s}\}} + \overline{\hat{q}^\dagger \hat{s} \{\hat{p}^\dagger \hat{r}\}} \\ &\quad - \overline{\hat{p}^\dagger \hat{s} \{\hat{q}^\dagger \hat{r}\}} - \overline{\hat{q}^\dagger \hat{r} \{\hat{p}^\dagger \hat{s}\}} + \overline{\hat{p}^\dagger \hat{r} \hat{q}^\dagger \hat{s}} - \overline{\hat{p}^\dagger \hat{s} \hat{q}^\dagger \hat{r}}, \end{aligned} \quad (3.167)$$

and therefore

$$\begin{aligned} \hat{G} &= \frac{1}{2} \sum_{pqrs} \langle pq|\hat{g}|rs\rangle \{\hat{p}^\dagger \hat{q}^\dagger \hat{s} \hat{r}\} + \frac{1}{2} \sum_{ipq} \langle ip|\hat{g}|iq\rangle \{\hat{p}^\dagger \hat{q}\} \\ &\quad + \frac{1}{2} \sum_{ipq} \langle pi|\hat{g}|qi\rangle \{\hat{p}^\dagger \hat{q}\} - \frac{1}{2} \sum_{ipq} \langle ip|\hat{g}|qi\rangle \{\hat{p}^\dagger \hat{q}\} \\ &\quad - \frac{1}{2} \sum_{ipq} \langle pi|\hat{g}|iq\rangle \{\hat{p}^\dagger \hat{q}\} + \frac{1}{2} \sum_{ij} \langle ij|\hat{g}|ij\rangle - \frac{1}{2} \sum_{ij} \langle ij|\hat{g}|ji\rangle. \end{aligned} \quad (3.168)$$

The second and fourth terms are equal to the third and fifth, respectively, thus removing the factor $\frac{1}{2}$, so

$$\begin{aligned} \hat{G} &= \frac{1}{2} \sum_{pqrs} \langle pq|\hat{g}|rs\rangle \{\hat{p}^\dagger \hat{q}^\dagger \hat{s} \hat{r}\} + \sum_{ipq} \langle pi|\hat{g}|qi\rangle \{\hat{p}^\dagger \hat{q}\} \\ &\quad - \sum_{ipq} \langle pi|\hat{g}|iq\rangle \{\hat{p}^\dagger \hat{q}\} + \frac{1}{2} \sum_{ij} \langle ij|\hat{g}|ij\rangle - \frac{1}{2} \sum_{ij} \langle ij|\hat{g}|ji\rangle \\ &= \hat{G}_N + \sum_{pq} \left(\sum_i \langle pi|\hat{g}|qi\rangle_A \right) \{\hat{p}^\dagger \hat{q}\} + \frac{1}{2} \sum_{ij} \langle ij|\hat{g}|ij\rangle_A, \end{aligned} \quad (3.169)$$

where

$$\hat{G}_N = \frac{1}{2} \sum_{pqrs} \langle pq|\hat{g}|rs\rangle \{\hat{p}^\dagger \hat{q}^\dagger \hat{s} \hat{r}\} = \frac{1}{4} \sum_{pqrs} \langle pq|\hat{g}|rs\rangle_A \{\hat{p}^\dagger \hat{q}^\dagger \hat{s} \hat{r}\} \quad (3.170)$$

and

$$\langle pq|\hat{g}|rs\rangle_A = \langle pq|\hat{g}|rs\rangle - \langle pq|\hat{g}|sr\rangle. \quad (3.171)$$

Since the Fermi-vacuum expectation value of \hat{G} is

$$\langle 0|\hat{G}|0\rangle = \frac{1}{2} \sum_{ij} \langle ij|\hat{g}|ij\rangle_A, \quad (3.172)$$

we have

$$\begin{aligned}\hat{G} &= \hat{G}_N + \sum_{pq} \left(\sum_i \langle pi | \hat{g} | qi \rangle_A \right) \{ \hat{p}^\dagger \hat{q} \} + \langle 0 | \hat{G} | 0 \rangle \\ &= \hat{G}_N + \hat{G}'_N + \langle 0 | \hat{G} | 0 \rangle,\end{aligned}\quad (3.173)$$

where \hat{G}'_N is a normal-product one-particle operator:

$$\begin{aligned}\hat{G}'_N &= \sum_{pq} \left(\sum_i \langle pi | \hat{g} | qi \rangle_A \right) \{ \hat{p}^\dagger \hat{q} \} = \sum_{pq} g'_{pq} \{ \hat{p}^\dagger \hat{q} \}, \\ g'_{pq} &= \sum_i \langle pi | \hat{g} | qi \rangle_A.\end{aligned}\quad (3.174)$$

3.6.3 The normal-product Hamiltonian

Next we look at the Hamiltonian operator, as partitioned in Section 3.5. For the zero-order part, using (3.125) and Wick's theorem we have

$$(\hat{H}_0)_N = \hat{H}_0 - E^{(0)} = \sum_p \varepsilon_p \hat{p}^\dagger \hat{p} - \sum_i \varepsilon_i = \sum_p \varepsilon_p \{ \hat{p}^\dagger \hat{p} \}.\quad (3.175)$$

The one-electron part of the perturbation is given by (see (3.146), (3.128))

$$\begin{aligned}\hat{V}_1 &= (\hat{V}_1)_N + \langle 0 | \hat{V}_1 | 0 \rangle, \\ (\hat{V}_1)_N &= \hat{F}_N^o - \hat{U}_N = \sum_{pq} (\hat{f}_{pq}^o - u_{pq}) \{ \hat{p}^\dagger \hat{q} \}, \\ \langle 0 | \hat{V}_1 | 0 \rangle &= - \sum_i u_{ii} = - \sum_{ij} \langle ij || ij \rangle = - \langle 0 | \hat{U} | 0 \rangle.\end{aligned}\quad (3.176)$$

The two-electron part, using (3.173), (3.174), is

$$\hat{V}_2 = (\hat{V}_2)_N + \hat{V}'_N + \langle 0 | \hat{V}_2 | 0 \rangle,\quad (3.177)$$

where

$$\begin{aligned}(\hat{V}_2)_N &= \frac{1}{4} \sum_{pqrs} \langle pq || rs \rangle \{ \hat{p}^\dagger \hat{q}^\dagger \hat{s} \hat{r} \}, \\ \hat{V}'_N &= \sum_{pq} v'_{pq} \{ \hat{p}^\dagger \hat{q} \}, \\ v'_{pq} &= \sum_i \langle pi || qi \rangle, \\ \langle 0 | \hat{V}_2 | 0 \rangle &= \frac{1}{2} \sum_{ij} \langle ij || ij \rangle,\end{aligned}\quad (3.178)$$

so that

$$v'_{pq} = u_{pq}, \quad \hat{V}'_N = \hat{U}_N. \quad (3.179)$$

The operator $(\hat{V}_2)_N$ will play a very important role in the formalism, and will be denoted by \hat{W}_N or simply \hat{W} ,

$$\hat{W} = \hat{W}_N = \frac{1}{4} \sum_{pqrs} \langle pq || rs \rangle \{ \hat{p}^\dagger \hat{q}^\dagger \hat{s} \hat{r} \}. \quad (3.180)$$

The total perturbation is then given by

$$\begin{aligned} \hat{V} &= \hat{F}_N^o - \hat{U}_N + \langle 0 | \hat{V}_1 | 0 \rangle + \hat{W}_N + \hat{V}'_N + \langle 0 | \hat{V}_2 | 0 \rangle \\ &= \hat{F}_N^o + \hat{W}_N + \langle 0 | \hat{V} | 0 \rangle, \end{aligned} \quad (3.181)$$

using the cancellation between \hat{V}'_N and $-\hat{U}_N$, (3.179) (this is the cancellation alluded to before (3.147), in Section 3.5). The shifted perturbation operator, which we define as

$$\hat{V}_N = \hat{V} - \langle 0 | \hat{V} | 0 \rangle \quad (3.182)$$

(this is the operator denoted by \hat{W} in Chapter 2), is then found to be a normal-product operator (relative to the Fermi vacuum):

$$\begin{aligned} \hat{V}_N &= \hat{F}_N^o + \hat{W}_N \\ &= \sum_{p \neq q} f_{pq} \{ \hat{p}^\dagger \hat{q} \} + \frac{1}{4} \sum_{pqrs} \langle pq || rs \rangle \{ \hat{p}^\dagger \hat{q}^\dagger \hat{s} \hat{r} \}. \end{aligned} \quad (3.183)$$

As seen in Chapter 2, the matrix elements of the shifted perturbation operator (3.182) are of central importance in the perturbation expansion, and the normal-product property of \hat{V}_N will greatly facilitate the computation of its matrix elements.

In the canonical HF case, in which the Fock operator is diagonal, \hat{V}_N is made up of the two-particle normal-product operator only:

$$\hat{V}_N = \hat{W} = \frac{1}{4} \sum_{pqrs} \langle pq || rs \rangle \{ \hat{p}^\dagger \hat{q}^\dagger \hat{s} \hat{r} \} \quad (\text{canonical HF}). \quad (3.184)$$

In this case, the operator \hat{W} defined in (3.180) is indeed the same as the \hat{W} operator of Chapter 2.

In the more general case, in which (3.127) is not assumed, we have (using $f'_{pq} = f_{pq} - \varepsilon_p \delta_{pq}$)

$$\begin{aligned} \hat{V}_N &= \hat{F}'_N + \hat{W}_N \\ &= \sum_{pq} f'_{pq} \{ \hat{p}^\dagger \hat{q} \} + \frac{1}{4} \sum_{pqrs} \langle pq || rs \rangle \{ \hat{p}^\dagger \hat{q}^\dagger \hat{s} \hat{r} \} \end{aligned} \quad (3.185)$$

and

$$\langle 0|\hat{V}|0\rangle = \sum_i f'_{ii} - \frac{1}{2} \sum_{ij} \langle ij||ij\rangle. \quad (3.186)$$

It is also possible to rewrite the Hamiltonian in a form that eliminates the first-order energy correction, leaving \hat{V}_N as the total perturbation, analogously to the last paragraph of subsection 2.4.4. Starting with $\hat{H} = \hat{H}_0 + \hat{V}$, we subtract

$$\langle 0|\hat{H}|0\rangle = \langle 0|\hat{H}_0|0\rangle + \langle 0|\hat{V}|0\rangle \quad (3.187)$$

from both sides, obtaining

$$\begin{aligned} \hat{H} - \langle 0|\hat{H}|0\rangle &= (\hat{H}_0 - \langle 0|\hat{H}_0|0\rangle) + (\hat{V} - \langle 0|\hat{V}|0\rangle), \\ (\hat{H} - E_{\text{ref}}) &= (\hat{H}_0 - E^{(0)}) + \hat{V}_N. \end{aligned} \quad (3.188)$$

In this scheme $\hat{H}_0 - E^{(0)} = (\hat{H}_0)_N$ is the zero-order Hamiltonian, \hat{V}_N is the perturbation and $\hat{H} - E_{\text{ref}} = \hat{H}_N$ is the full Hamiltonian and is a normal-product operator. The Schrödinger equation for this operator is

$$\hat{H}_N \Psi = \Delta E \Psi, \quad (3.189)$$

and the computed energy is

$$\Delta E = E - E_{\text{ref}} \quad (3.190)$$

(the *correlation energy* in the Hartree–Fock case). We also find that the zero- and first-order energies vanish in this form since they are vacuum expectation values of normal-product operators; the first nonvanishing contribution is the second-order energy.

Finally, we can write the total normal-product Hamiltonian as

$$\hat{H}_N = \hat{F}_N + \hat{W} = \hat{F}_N^{\text{d}} + \hat{F}^{\text{o}} + \hat{W} = \hat{F}_N^{\text{d}} + \hat{V}_N. \quad (3.191)$$

Most of the discussion in this book is based on the normal-product Schrödinger equation (3.189) and the decompositions (3.191) of the normal-product Hamiltonian.

3.7 Generalized time-independent Wick's theorem

To complete this phase of the analysis we need one more theorem, the *generalized Wick's theorem* dealing with products of normal products of operators. This is needed since we shall have to evaluate matrix elements of the

normal-product operator \hat{W} between various Slater determinants (not just the reference SD), as for example in

$$\langle \Phi_{ij\dots}^{ab\dots} | \hat{W} | \Phi_{lm\dots}^{de\dots} \rangle = \langle 0 | \hat{i}^\dagger \hat{j}^\dagger \dots \hat{b} \hat{a} \hat{W} \hat{d}^\dagger \hat{e}^\dagger \dots \hat{m} \hat{l} | 0 \rangle. \quad (3.192)$$

Here we have a vacuum expectation value of a product of three operator strings, each of which separately is in normal-product form, since

$$\begin{aligned} \{\hat{i}^\dagger \hat{j}^\dagger \dots \hat{b} \hat{a}\} &= \hat{i}^\dagger \hat{j}^\dagger \dots \hat{b} \hat{a}, \\ \{\hat{d}^\dagger \hat{e}^\dagger \dots \hat{m} \hat{l}\} &= \hat{d}^\dagger \hat{e}^\dagger \dots \hat{m} \hat{l}. \end{aligned} \quad (3.193)$$

The generalized Wick's theorem states that a general product of creation and annihilation operators in which some operator strings are already in normal-product form is given as the overall normal product of all the creation and annihilation operators plus the sum of all overall normal products with contractions except that, since contractions of pairs of operators that are already in normal order vanish (as seen from the definition (3.120) of a contraction), no contractions between pairs of operators within the same original normal product need be included:

$$\begin{aligned} &\{\hat{A}_1 \hat{A}_2 \dots\} \{\hat{B}_1 \hat{B}_2 \dots\} \{\hat{C}_1 \hat{C}_2 \dots\} \dots \\ &= \{\hat{A}_1 \hat{A}_2 \dots \hat{B}_1 \hat{B}_2 \dots \hat{C}_1 \hat{C}_2 \dots\} + \sum' \{\hat{A}_1 \hat{A}_2 \dots \overline{\hat{B}_1 \hat{B}_2} \dots \overline{\hat{C}_1 \hat{C}_2} \dots\}, \end{aligned} \quad (3.194)$$

where the sum is over contractions of one pair at a time, two pairs, etc., and the prime on the summation sign indicates that no "internal" contractions, such as $\overline{\hat{A}_i \hat{A}_j}$, $\overline{\hat{B}_i \hat{B}_j}$, etc., are to be included.

Note that the case in which the original product contains some individual creation or annihilation operators not within any normal product is also included in the scope of the generalized Wick's theorem, since for such operators $\hat{A} = \{\hat{A}\}$.

3.8 Evaluation of matrix elements

As a first example we shall use the generalized Wick's theorem to evaluate a matrix element of a normal-product one-electron operator between two singly excited determinants,

$$\begin{aligned} \langle \Phi_i^a | \hat{F}_N | \Phi_j^b \rangle &= \langle 0 | \hat{i}^\dagger \hat{a} \hat{F}_N \hat{b}^\dagger \hat{j} | 0 \rangle \\ &= \sum_{pq} \langle p | \hat{f} | q \rangle \langle 0 | \{\hat{i}^\dagger \hat{a}\} \{\hat{p}^\dagger \hat{q}\} \{\hat{b}^\dagger \hat{j}\} | 0 \rangle, \end{aligned} \quad (3.195)$$

where we have used $\hat{i}^\dagger \hat{a} = \{\hat{i}^\dagger \hat{a}\}$, $\hat{b}^\dagger \hat{j} = \{\hat{b}^\dagger \hat{j}\}$. In this case the only non-zero contractions are of the type

$$\begin{aligned} \overline{\hat{i}^\dagger \hat{j}} &= \delta_{ij}, & \overline{\hat{i}^\dagger \hat{q}} &= \delta_{iq}, & \overline{\hat{p}^\dagger \hat{j}} &= \delta_{pj}, \\ \overline{\hat{a} \hat{b}^\dagger} &= \delta_{ab}, & \overline{\hat{a} \hat{p}^\dagger} &= \delta_{ap}, & \overline{\hat{q} \hat{b}^\dagger} &= \delta_{qb}. \end{aligned} \quad (3.196)$$

Noting that only fully contracted terms survive in the (Fermi) vacuum expectation value, the only ways in which such terms are obtained through contractions between *different* normal products are as follows:

1. one of \hat{i}^\dagger and \hat{a} with one of \hat{q} , \hat{p}^\dagger ,
2. the remaining \hat{a} or \hat{i}^\dagger with \hat{b}^\dagger or \hat{j} , respectively; and
3. the remaining \hat{q} or \hat{p}^\dagger with the remaining \hat{b}^\dagger or \hat{j} .

The only two possibilities then are $\overline{\hat{i}^\dagger \hat{a} \hat{p}^\dagger \hat{q} \hat{b}^\dagger \hat{j}}$, and $\overline{\hat{i}^\dagger \hat{a} \hat{p}^\dagger \hat{q} \hat{b}^\dagger \hat{j}}$, giving

$$\langle \Phi_i^a | \hat{F}_N | \Phi_j^b \rangle = -\langle j | \hat{f} | i \rangle \delta_{ab} + \langle a | \hat{f} | b \rangle \delta_{ij}. \quad (3.197)$$

Specifically,

$$\begin{aligned} \langle \Phi_i^a | \hat{F}_N | \Phi_j^a \rangle &= -\langle j | \hat{f} | i \rangle & (i \neq j), \\ \langle \Phi_i^a | \hat{F}_N | \Phi_i^b \rangle &= \langle a | \hat{f} | b \rangle & (a \neq b), \\ \langle \Phi_i^a | \hat{F}_N | \Phi_i^a \rangle &= \langle a | \hat{f} | a \rangle - \langle i | \hat{f} | i \rangle. \end{aligned} \quad (3.198)$$

The last case leads to the obvious result

$$\begin{aligned} \langle \Phi_i^a | \hat{F} | \Phi_i^a \rangle &= \langle 0 | \hat{F} | 0 \rangle + \langle \Phi_i^a | \hat{F}_N | \Phi_i^a \rangle \\ &= \sum_j \langle j | \hat{f} | j \rangle + \langle a | \hat{f} | a \rangle - \langle i | \hat{f} | i \rangle = \sum_{j \neq i} \langle j | \hat{f} | j \rangle + \langle a | \hat{f} | a \rangle. \end{aligned} \quad (3.199)$$

As another example we shall evaluate the matrix element of \hat{W} between the same two configurations,

$$\begin{aligned} \langle \Phi_i^a | \hat{W} | \Phi_j^b \rangle &= \langle 0 | \hat{i}^\dagger \hat{a} \hat{W} \hat{b}^\dagger \hat{j} | 0 \rangle \\ &= \frac{1}{2} \sum_{pqrs} \langle pq | \hat{v} | rs \rangle \langle 0 | \{ \hat{i}^\dagger \hat{a} \} \{ \hat{p}^\dagger \hat{q}^\dagger \hat{s} \hat{r} \} \{ \hat{b}^\dagger \hat{j} \} | 0 \rangle. \end{aligned} \quad (3.200)$$

Noting again that the only non-zero contractions are of the types $\overline{\hat{i}^\dagger \hat{j}} = \delta_{ij}$ and $\overline{\hat{a} \hat{b}^\dagger} = \delta_{ab}$ and that only fully contracted terms survive in the (Fermi) vacuum expectation value, we must contract two of the $\hat{p}^\dagger \hat{q}^\dagger \hat{s} \hat{r}$ operators with each of the pairs to the left and right. The options for non-zero contractions then are:

$$\begin{aligned}
 \langle \Phi_i^a | \hat{W} | \Phi_j^b \rangle &= \frac{1}{2} \sum_{pqrs} \langle pq | \hat{v} | rs \rangle \left\{ \overbrace{\langle 0 | \hat{i}^\dagger \hat{a} \hat{p}^\dagger \hat{q}^\dagger \hat{s} \hat{r} \hat{b}^\dagger \hat{j} | 0 \rangle} + \overbrace{\langle 0 | \hat{i}^\dagger \hat{a} \hat{p}^\dagger \hat{q}^\dagger \hat{s} \hat{r} \hat{b}^\dagger \hat{j} | 0 \rangle} \right. \\
 &\quad \left. + \overbrace{\langle 0 | \hat{i}^\dagger \hat{a} \hat{p}^\dagger \hat{q}^\dagger \hat{s} \hat{r} \hat{b}^\dagger \hat{j} | 0 \rangle} + \overbrace{\langle 0 | \hat{i}^\dagger \hat{a} \hat{p}^\dagger \hat{q}^\dagger \hat{s} \hat{r} \hat{b}^\dagger \hat{j} | 0 \rangle} \right\} \\
 &= -\frac{1}{2} \langle aj | \hat{v} | bi \rangle + \frac{1}{2} \langle aj | \hat{v} | ib \rangle + \frac{1}{2} \langle ja | \hat{v} | bi \rangle - \frac{1}{2} \langle ja | \hat{v} | ib \rangle \\
 &= \langle aj | \hat{v} | ib \rangle - \langle aj | \hat{v} | bi \rangle = \langle aj || ib \rangle. \tag{3.201}
 \end{aligned}$$

It can be verified that the sign factor for a fully contracted product of creation and annihilation operators is $(-1)^x$, where x is the number of intersections of the contraction lines. Obviously x is not unique in general, since the contraction lines can be drawn with different intersection patterns, but for any particular contracted product the number of intersections is either always even, giving a sign factor of $+1$, or always odd, giving a factor of -1 .

A more difficult example is the matrix element between a single excitation and a double excitation:

$$\langle \Phi_i^a | \hat{W} | \Phi_{jk}^{bc} \rangle = \frac{1}{2} \sum_{pqrs} \langle pq | \hat{v} | rs \rangle \langle 0 | \{ \hat{i}^\dagger \hat{a} \} \{ \hat{p}^\dagger \hat{q}^\dagger \hat{s} \hat{r} \} \{ \hat{b}^\dagger \hat{c}^\dagger \hat{k} \hat{j} \} | 0 \rangle. \tag{3.202}$$

The only way in which we can fully contract the operators in the vacuum matrix element without internal contractions inside each of the three normal products is to contract the two operators in the first normal product with one operator each in the second and third products respectively, and introduce three contractions between the latter two products. The possibilities are:

1. \hat{i}^\dagger with \hat{s} or \hat{r} , \hat{a} with \hat{b}^\dagger or \hat{c}^\dagger , \hat{r} or \hat{s} with \hat{c}^\dagger or \hat{b}^\dagger , \hat{p}^\dagger and \hat{q}^\dagger with \hat{k} and \hat{j} ;
2. \hat{i}^\dagger with \hat{k} or \hat{j} , \hat{a} with \hat{p}^\dagger or \hat{q}^\dagger , \hat{j} or \hat{k} with \hat{q}^\dagger or \hat{p}^\dagger , \hat{s} and \hat{r} with \hat{b}^\dagger and \hat{c}^\dagger .

Thus we get

$$\begin{aligned}
 \langle \Phi_i^a | \hat{W} | \Phi_{jk}^{bc} \rangle = \frac{1}{2} \sum_{pqrs} \langle pq | \hat{v} | rs \rangle & \left(\begin{array}{l} \text{Diagram 1} \\ \text{Diagram 2} \\ \text{Diagram 3} \\ \text{Diagram 4} \\ \text{Diagram 5} \\ \text{Diagram 6} \\ \text{Diagram 7} \\ \text{Diagram 8} \\ \text{Diagram 9} \\ \text{Diagram 10} \\ \text{Diagram 11} \\ \text{Diagram 12} \\ \text{Diagram 13} \\ \text{Diagram 14} \\ \text{Diagram 15} \\ \text{Diagram 16} \\ \text{Diagram 17} \\ \text{Diagram 18} \\ \text{Diagram 19} \\ \text{Diagram 20} \\ \text{Diagram 21} \\ \text{Diagram 22} \\ \text{Diagram 23} \\ \text{Diagram 24} \\ \text{Diagram 25} \\ \text{Diagram 26} \\ \text{Diagram 27} \\ \text{Diagram 28} \\ \text{Diagram 29} \\ \text{Diagram 30} \\ \text{Diagram 31} \\ \text{Diagram 32} \\ \text{Diagram 33} \\ \text{Diagram 34} \\ \text{Diagram 35} \\ \text{Diagram 36} \\ \text{Diagram 37} \\ \text{Diagram 38} \\ \text{Diagram 39} \\ \text{Diagram 40} \\ \text{Diagram 41} \\ \text{Diagram 42} \\ \text{Diagram 43} \\ \text{Diagram 44} \\ \text{Diagram 45} \\ \text{Diagram 46} \\ \text{Diagram 47} \\ \text{Diagram 48} \\ \text{Diagram 49} \\ \text{Diagram 50} \\ \text{Diagram 51} \\ \text{Diagram 52} \\ \text{Diagram 53} \\ \text{Diagram 54} \\ \text{Diagram 55} \\ \text{Diagram 56} \\ \text{Diagram 57} \\ \text{Diagram 58} \\ \text{Diagram 59} \\ \text{Diagram 60} \\ \text{Diagram 61} \\ \text{Diagram 62} \\ \text{Diagram 63} \\ \text{Diagram 64} \\ \text{Diagram 65} \\ \text{Diagram 66} \\ \text{Diagram 67} \\ \text{Diagram 68} \\ \text{Diagram 69} \\ \text{Diagram 70} \\ \text{Diagram 71} \\ \text{Diagram 72} \\ \text{Diagram 73} \\ \text{Diagram 74} \\ \text{Diagram 75} \\ \text{Diagram 76} \\ \text{Diagram 77} \\ \text{Diagram 78} \\ \text{Diagram 79} \\ \text{Diagram 80} \\ \text{Diagram 81} \\ \text{Diagram 82} \\ \text{Diagram 83} \\ \text{Diagram 84} \\ \text{Diagram 85} \\ \text{Diagram 86} \\ \text{Diagram 87} \\ \text{Diagram 88} \\ \text{Diagram 89} \\ \text{Diagram 90} \\ \text{Diagram 91} \\ \text{Diagram 92} \\ \text{Diagram 93} \\ \text{Diagram 94} \\ \text{Diagram 95} \\ \text{Diagram 96} \\ \text{Diagram 97} \\ \text{Diagram 98} \\ \text{Diagram 99} \\ \text{Diagram 100} \end{array} \right) \\
 & + \text{eight more terms from possibility 2} \Big), \tag{3.203}
 \end{aligned}$$

from which we obtain

$$\begin{aligned}
 \langle \Phi_i^a | \hat{W} | \Phi_{jk}^{bc} \rangle = \frac{1}{2} & \left(-\langle kj | \hat{v} | ci \rangle \delta_{ab} + \langle jk | \hat{v} | ci \rangle \delta_{ab} + \langle kj | \hat{v} | ic \rangle \delta_{ab} - \langle jk | \hat{v} | ic \rangle \delta_{ab} \right. \\
 & + \langle kj | \hat{v} | bi \rangle \delta_{ac} - \langle jk | \hat{v} | bi \rangle \delta_{ac} - \langle kj | \hat{v} | ib \rangle \delta_{ac} + \langle jk | \hat{v} | ib \rangle \delta_{ac} \\
 & + \langle aj | \hat{v} | cb \rangle \delta_{ik} - \langle aj | \hat{v} | bc \rangle \delta_{ik} - \langle ja | \hat{v} | cb \rangle \delta_{ik} + \langle ja | \hat{v} | bc \rangle \delta_{ik} \\
 & - \langle ak | \hat{v} | cb \rangle \delta_{ij} + \langle ak | \hat{v} | bc \rangle \delta_{ij} + \langle ka | \hat{v} | cb \rangle \delta_{ij} - \langle ka | \hat{v} | bc \rangle \delta_{ij} \Big) \\
 & = -\langle jk || ic \rangle \delta_{ab} - \langle jk || bi \rangle \delta_{ac} + \langle aj || cb \rangle \delta_{ik} + \langle ak || bc \rangle \delta_{ij}. \tag{3.204}
 \end{aligned}$$

Thus we can get a non-zero result only if at least one hole or particle in Φ_{jk}^{bc} matches the hole or particle in Φ_i^a , for example

$$\begin{aligned}
 \langle \Phi_i^a | \hat{W} | \Phi_{ik}^{bc} \rangle &= \langle ak || bc \rangle & (a \neq b, c), \\
 \langle \Phi_i^a | \hat{W} | \Phi_{jk}^{ac} \rangle &= -\langle jk || ic \rangle & (i \neq j, k), \\
 \langle \Phi_i^a | \hat{W} | \Phi_{ik}^{ac} \rangle &= \langle ak || ac \rangle - \langle ik || ic \rangle.
 \end{aligned} \tag{3.205}$$

Obviously, we need some help with the detailed evaluation of these formulas, and this help is provided by the diagrammatic representation described in the following chapter.

4

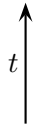
Diagrammatic notation

4.1 Time ordering

As we saw in Section 3.8, the second-quantization treatment can be cumbersome and error-prone. The generation and manipulation of the various expressions in this treatment are made much easier by the introduction of a systematic diagrammatic representation. The purposes of the diagrammatic notation are thus:

1. to make it easy to list all non vanishing distinct terms in the perturbation sums;
2. to elucidate certain cancellations in these sums;
3. to provide certain systematics for the discussion and manipulation of the various surviving terms, including classifications that allow us to group together various types of contribution, perform some partial summations etc.

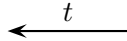
Diagrammatic notation originated in quantum field theory, in the form of *Feynman diagrams* or *graphs*, in an explicit time-dependent format. Initial applications to RSPT were also in time-dependent form, but in them the time dependence was introduced artificially by a gradual switching-on of the perturbation from $t = -\infty$ to $t = 0$ using a switching-on function $e^{\alpha t}$ (with $\alpha > 0$). This function takes the place of λ in $\hat{H} = \hat{H}_0 + \lambda \hat{V}$ and varies from 0 as $t \rightarrow -\infty$ to 1 as $t \rightarrow 0$. It leads to a *time sequence* in the application of various operators, and this is indicated in the diagrams by means of a *time axis*



for the sequence of events. The actual time at which each event occurs (i.e. an operator acts) is irrelevant; only the sequence is significant.

We shall continue to use the time-independent formulation, but the sequence in which operators act (i.e. from right to left) still furnishes us with a time axis. Thus, if we want to represent the result of the operation of an operator \hat{U} on a function $|\Phi_{ij}^{ab}\rangle$, we begin with a representation of Φ_{ij}^{ab} at the bottom, followed by a representation of the operator \hat{U} above it, leading to a representation of the result $\hat{U}|\Phi_{ij}^{ab}\rangle$ at the top.

Another common arrangement is to place the time axis horizontally, from right to left,



corresponding to the way in which we normally write a sequence of operators acting on a function, as mentioned above. This was used, for example, by Paldus and Čížek (1975), but we shall use the more common vertical arrangement. The only difference is a 90° rotation of the diagrams.

4.2 Slater determinants

We begin with the representation of a *Slater determinant* (SD). The *reference state* (the Fermi vacuum) is represented by *nothing*, i.e. by a position on the time axis at which there are no lines or other symbols. Any other SD, say Φ_i^a , is represented by vertical or diagonal (see the next section) directed lines, pointing upward for particles and downward for holes, with labels identifying the spinorbitals:

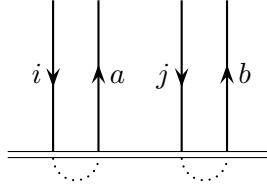
$$\Phi_i^a = \begin{array}{c} \downarrow \\ i \end{array} \begin{array}{c} \uparrow \\ a \end{array} \quad \Phi_{ij}^{ab} = \begin{array}{c} \downarrow \\ i \end{array} \begin{array}{c} \uparrow \\ a \end{array} \begin{array}{c} \downarrow \\ j \end{array} \begin{array}{c} \uparrow \\ b \end{array}$$

(the horizontal position of the lines has no significance). If we want to indicate specifically the *ket* and *bra* forms, the following (non-standard) notation may be used:

$$|\Phi^a\rangle = \hat{a}^\dagger|0\rangle = \begin{array}{c} \uparrow \\ a \end{array} \quad |\Phi_i\rangle = \hat{i}|0\rangle = \begin{array}{c} \downarrow \\ i \end{array}$$

$$\begin{aligned}
|\Phi_i^a\rangle &= \{\hat{a}^\dagger \hat{i}\}|0\rangle = \begin{array}{c} \downarrow i \quad \uparrow a \\ \hline \hline \end{array} & \langle \Phi_i^a| &= \langle 0|\{\hat{i}^\dagger \hat{a}\} = \begin{array}{c} \hline \hline \downarrow i \quad \uparrow a \end{array} \\
|\Phi_{ij}^{ab}\rangle &= \{\hat{a}^\dagger \hat{b}^\dagger \hat{j} \hat{i}\}|0\rangle = \{(\hat{a}^\dagger \hat{i})(\hat{b}^\dagger \hat{j})\}|0\rangle = \begin{array}{c} \downarrow i \quad \uparrow a \quad \downarrow j \quad \uparrow b \\ \hline \hline \end{array}
\end{aligned}$$

etc. The horizontal double line represents the point of operation of the normal-product operator, and below or above it we have the Fermi vacuum. Note that there is a phase ambiguity in the last example, since this diagram could equally represent $|\Phi_{ij}^{ab}\rangle$ or $|\Phi_{ij}^{ba}\rangle$. However, the way in which we shall use the diagrams will be independent of this choice of phase, provided reasonable consistency is maintained. If we want to be more specific, we can indicate which particle index appears above which hole index:



4.3 One-particle operators

4.3.1 Representation of one-particle operators and contractions

Next we consider the representation of operators. We begin with a one-electron operator in normal product form, say

$$\hat{U}_N = \sum_{pq} \langle p|\hat{u}|q\rangle \{\hat{p}^\dagger \hat{q}\}, \quad (4.1)$$

acting on a singly excited Slater determinant

$$|\Phi_i^a\rangle = \{\hat{a}^\dagger \hat{i}\}|0\rangle. \quad (4.2)$$

The action and representation of the individual terms in the sum over p, q in (4.1) will depend on whether p and q are particle or hole indices. We begin with a *particle-particle* (pp) term,

$$\langle b|\hat{u}|c\rangle \{\hat{b}^\dagger \hat{c}\}, \quad (4.3)$$

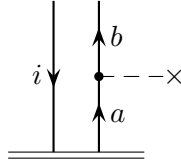
for which we obtain (using the generalized Wick's theorem)

$$\begin{aligned}
 \langle b|\hat{u}|c\rangle\{\hat{b}^\dagger\hat{c}\}\{\hat{a}^\dagger\hat{i}\}|0\rangle &= \langle b|\hat{u}|c\rangle\{\hat{b}^\dagger\hat{c}\hat{a}^\dagger\hat{i}\}|0\rangle + \langle b|\hat{u}|c\rangle\{\hat{b}^\dagger\hat{c}\hat{a}^\dagger\hat{i}\}|0\rangle \\
 &= \langle b|\hat{u}|c\rangle\hat{b}^\dagger\hat{a}^\dagger\hat{i}\hat{c}|0\rangle + \langle b|\hat{u}|c\rangle\delta_{ac}\{\hat{b}^\dagger\hat{i}\}|0\rangle \\
 &= 0 + \langle b|\hat{u}|c\rangle\delta_{ac}|\Phi_i^b\rangle.
 \end{aligned} \tag{4.4}$$

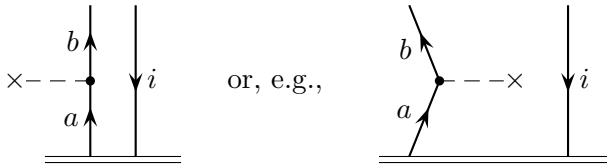
Thus we get a non-zero contribution only from particle–particle terms of the type

$$\langle b|\hat{u}|a\rangle\{\hat{b}^\dagger\hat{a}\}|\Phi_i^a\rangle = \langle b|\hat{u}|a\rangle|\Phi_i^b\rangle, \tag{4.5}$$

which is represented by the diagram

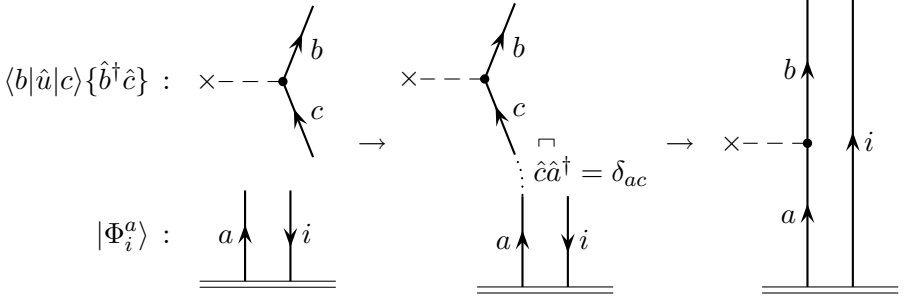


Note that the case $b = a$ is included. Represented at the bottom is $|\Phi_i^a\rangle$ and at the top $|\Phi_i^b\rangle$, the resulting determinant. The point of action of the operator is marked by the *interaction line* (or *vertex*) $\bullet---\times$, the \times being a *marker* for the particular operator \hat{u} . Different one-electron operators can be represented by using different markers, e.g. $\bullet---\#$, $\bullet---\triangle$, $\bullet---\square$ etc. Again, the horizontal arrangement has no significance and we could equally well have used

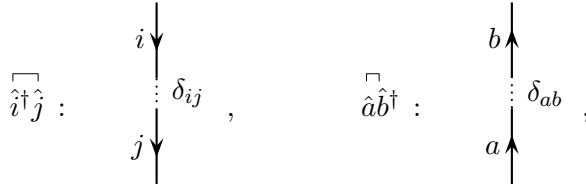


We associate the integral $\langle b|\hat{u}|a\rangle$ with the vertex $\bullet---\times$ as a multiplicative factor. Note that the *bra* spinorbital in the integral corresponds to the line *leaving* the vertex, while the *ket* corresponds to the *entering* line.

We can view this diagram as a graphical representation of the contraction process:



The only non-zero contractions are then represented as follows:



where the left-right order of the operators corresponds to the top-bottom order of the directed lines, and where a *creation* operator is represented by an arrow *leaving* its point of action (a vertex $\bullet - - \times$ or double line \equiv) and an *annihilation* operator is represented by an arrow *entering* its point of action. This representation of contractions tells us automatically which pairs of lines may be contracted ($\hat{i}^\dagger \hat{j}$ or $\hat{a} \hat{b}^\dagger$). Any line that is not contracted or terminated by a vertex (or by the double line) must proceed unchanged in the appropriate direction throughout the diagram.

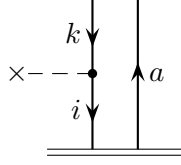
Next we consider a *hole-hole* (hh) term, $\langle j|\hat{u}|k\rangle\{\hat{j}^\dagger\hat{k}\}$, in (4.1), acting on $|\Phi_i^a\rangle$. Using the generalized Wick's theorem, we obtain:

$$\begin{aligned}
 \langle j|\hat{u}|k\rangle\{\hat{j}^\dagger\hat{k}\}\{\hat{a}^\dagger\hat{i}\}|0\rangle &= \langle j|\hat{u}|k\rangle\{\hat{j}^\dagger\hat{k}\hat{a}^\dagger\hat{i}\}|0\rangle + \langle j|\hat{u}|k\rangle\{\hat{j}^\dagger\hat{k}\hat{a}^\dagger\hat{i}\}|0\rangle \\
 &= -\langle j|\hat{u}|k\rangle\hat{k}\hat{a}^\dagger\hat{i}\hat{j}^\dagger|0\rangle + \delta_{ij}\langle j|\hat{u}|k\rangle\{\hat{k}\hat{a}^\dagger\}|0\rangle \\
 &= 0 - \delta_{ij}\langle j|\hat{u}|k\rangle\{\hat{a}^\dagger\hat{k}\}|0\rangle \\
 &= -\delta_{ij}\langle j|\hat{u}|k\rangle|\Phi_k^a\rangle.
 \end{aligned} \tag{4.6}$$

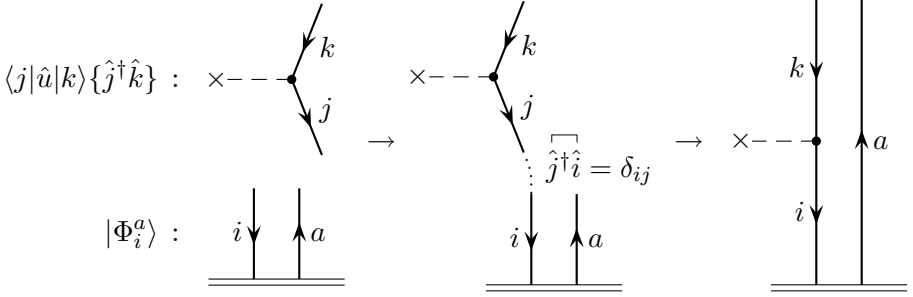
The only nonvanishing term of this type is

$$\langle i|\hat{u}|k\rangle\{\hat{i}^\dagger\hat{k}\}|\Phi_i^a\rangle = -\langle i|\hat{u}|k\rangle|\Phi_k^a\rangle, \tag{4.7}$$

which is represented by



This term originates in the contraction

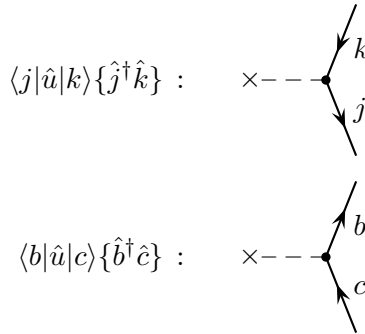


Note that, in the representation of the operator, $\{\hat{j}^\dagger\hat{k}\} = -\hat{k}\hat{j}^\dagger$; hence the k line (the annihilation operator, entering the vertex) is above the j line (the creation operator, leaving the vertex) and a minus sign appears.

4.3.2 Rules of interpretation

We should note the following rules for the interpretation of the one-particle vertices.

1. For both the pp and hh cases, the *bra* in the integral associated with the vertex corresponds to the *outgoing* line (and the *creation* operator) while the *ket* corresponds to the *incoming* line (and the *annihilation* operator):



2. Similarly, the *creation* operator associated with \hat{U}_N corresponds to an *outgoing* line (a line leaving the vertex) and the *annihilation* operator corresponds to an *incoming* line (a line terminating at the vertex). Again, this is true for both the pp and hh cases.
3. We have to associate a *phase factor* -1 with the case in which one hole is replaced by another (the hh case).
4. The case $k = i$ is included in the hh diagram, since this gives

$$\langle i|\hat{u}|i\rangle\{\hat{i}^\dagger\hat{i}\}|\Phi_i^a\rangle = -\langle i|\hat{u}|i\rangle\hat{i}\hat{i}^\dagger|\Phi_i^a\rangle = -\langle i|\hat{u}|i\rangle|\Phi_i^a\rangle : \quad \times \text{---} \text{---} \begin{array}{c} \downarrow i \\ \bullet \\ \downarrow i \\ \uparrow a \end{array} \quad \text{---} \text{---}$$

In formalisms that do not take advantage of normal ordering and Wick's theorem and that therefore compute terms for \hat{U} rather than \hat{U}_N , the contribution of the $\langle i|\hat{u}|i\rangle$ integral is

$$\langle i|\hat{u}|i\rangle\hat{i}^\dagger\hat{i}|\Phi_i^a\rangle = 0, \quad (4.8)$$

and the corresponding diagram is called an *exclusion-principle-violating* (EPV) diagram. The contribution $-\langle i|\hat{u}|i\rangle|\Phi_i^a\rangle$, according to the ordinary interpretation of the diagram, is included nevertheless; one is relying on its cancellation with another EPV diagram that results from contractions within the creation and annihilation operators of \hat{U} (which are excluded if we use \hat{U}_N). So in this case we have the additional hh terms

$$\langle j|\hat{u}|k\rangle\{\hat{j}^\dagger\hat{k}\hat{a}^\dagger\hat{i}\}|0\rangle = \delta_{jk}\langle j|\hat{u}|k\rangle|\Phi_i^a\rangle, \quad (4.9)$$

namely, terms of the type $+\langle k|\hat{u}|k\rangle|\Phi_i^a\rangle$ ($k \neq i$), represented by a diagram with a “bubble”,

$$\times \text{---} \text{---} \begin{array}{c} \circlearrowleft k \\ \bullet \end{array} \begin{array}{c} \downarrow i \\ \uparrow a \end{array} \quad (k \neq i).$$

This diagram represents the difference between $\hat{U}|\Phi_i^a\rangle$ and $\hat{U}_N|\Phi_i^a\rangle$. Note that the case $k = i$ should be excluded, since it corresponds to $\hat{i}^\dagger\hat{i}\hat{a}^\dagger\hat{i}|0\rangle = 0$

and is an EPV term (containing two holes i at the same time), but if we leave it in, it cancels the previously mentioned EPV diagram exactly:

$$\begin{array}{c}
 \times \text{---} \bullet \begin{array}{c} \downarrow i \\ \uparrow a \end{array} \\
 \downarrow i \\
 \hline
 -\langle i|\hat{u}|i\rangle|\Phi_i^a\rangle
 \end{array}
 +
 \begin{array}{c}
 \times \text{---} \bullet \begin{array}{c} \text{loop } i \end{array} \\
 \downarrow i \quad \uparrow a \\
 \hline
 +\langle i|\hat{u}|i\rangle|\Phi_i^a\rangle
 \end{array}
 = 0. \quad (4.10)$$

Therefore we eliminate the $k \neq i$ restriction in both cases and include EPV diagrams in the summation. However, if we consistently use the normal-product form of operators, the first EPV diagram (on the left in the above figure) is all right as it stands, since it originates in $\{\hat{i}^\dagger \hat{i}\}|\Phi_i^a\rangle = -\hat{i}\hat{i}^\dagger|\Phi_i^a\rangle = -|\Phi_i^a\rangle$, and so we do not need to include bubble diagrams; they would just provide the added term

$$\left(\sum_k \langle k|\hat{u}|k\rangle \right) |\Phi_i^a\rangle = \langle 0|\hat{U}|0\rangle |\Phi_i^a\rangle = (\hat{U} - \hat{U}_N)|\Phi_i^a\rangle, \quad (4.11)$$

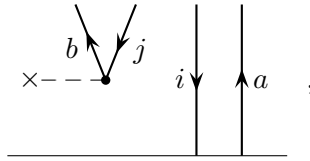
as noted above.

4.3.3 The complete one-particle operator

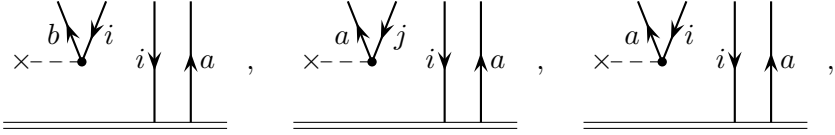
We have looked at the pp and hh terms of $\hat{U}_N|\Phi_i^a\rangle$. Next we will look at the ph and hp terms, beginning with ph:

$$\begin{aligned}
 \langle b|\hat{u}|j\rangle\{\hat{b}^\dagger\hat{j}\}\{\hat{a}^\dagger\hat{i}\}|0\rangle|\Phi_i^a\rangle &= \langle b|\hat{u}|j\rangle\{\hat{b}^\dagger\hat{j}\hat{a}^\dagger\hat{i}\}|0\rangle \\
 &= \langle b|\hat{u}|j\rangle\hat{a}^\dagger\hat{b}^\dagger\hat{j}\hat{i}|0\rangle \\
 &= \langle b|\hat{u}|j\rangle|\Phi_{ij}^{ab}\rangle
 \end{aligned}$$

(no contraction can contribute in this case), represented by



showing that the resulting determinant is $|\Phi_{ij}^{ab}\rangle$ (for the phase factor, we use the convention that a hole and a particle joined at the same vertex, i.e. on the same path, are in the same vertical position in $|\Phi_{ij\cdots}^{ab\cdots}\rangle$). In principle we should have omitted the cases $j = i$ and/or $b = a$, but it is not necessary to do this explicitly since EPV diagrams of this type,



give a vanishing SD anyway.

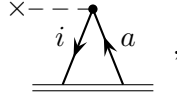
The hp term is

$$\begin{aligned}
 \langle j|\hat{u}|b\rangle\{\hat{j}^\dagger\hat{b}\}\{\hat{a}^\dagger\hat{i}\}|0\rangle &= \langle j|\hat{u}|b\rangle\{\hat{j}^\dagger\hat{b}\hat{a}^\dagger\hat{i}\}|0\rangle + \langle j|\hat{u}|b\rangle\overbrace{\{\hat{j}^\dagger\hat{b}\hat{a}^\dagger\hat{i}\}}^{|0\rangle}|0\rangle \\
 &\quad + \langle j|\hat{u}|b\rangle\overbrace{\{\hat{j}^\dagger\hat{b}\hat{a}^\dagger\hat{i}\}}^{|0\rangle}|0\rangle + \langle j|\hat{u}|b\rangle\overbrace{\{\hat{j}^\dagger\hat{b}\hat{a}^\dagger\hat{i}\}}^{|0\rangle}|0\rangle \quad (4.12) \\
 &= \langle j|\hat{u}|b\rangle\{0 + \delta_{ij} \times 0 + \delta_{ab} \times 0 + \delta_{ij}\delta_{ab}\}|0\rangle \\
 &= \delta_{ij}\delta_{ab}\langle j|\hat{u}|b\rangle|0\rangle
 \end{aligned}$$

and is nonzero only for

$$\langle i|\hat{u}|a\rangle\{\hat{i}^\dagger\hat{a}\}|\Phi_i^a\rangle = \langle i|\hat{u}|a\rangle|0\rangle, \quad (4.13)$$

which is represented by



showing clearly that the result of the operation involves the vacuum state $|0\rangle$.

For both the ph and hp terms, the integral associated with $\bullet---\times$ follows the same interpretation rules as for the pp and hh cases; note the mnemonics in parentheses:

incoming line	\leftrightarrow	annihilation operator	\leftrightarrow	ket state	(IAK)
outgoing line	\leftrightarrow	creation operator	\leftrightarrow	bra state	(OCB)

Of the four cases considered, only the hole-hole case requires a factor -1 .

The complete result for $\hat{U}_N|\Phi_i^a\rangle$ is

$$\begin{aligned}
 \sum_b \underbrace{i \downarrow \uparrow b}_{\langle b|\hat{u}|a\rangle|\Phi_i^b\rangle} + \sum_j \underbrace{\times - \downarrow \uparrow a}_{- \langle i|\hat{u}|j\rangle|\Phi_j^a\rangle} + \sum_{b,j} \underbrace{\times - \downarrow \uparrow j}_{\langle b|\hat{u}|j\rangle|\Phi_{ij}^{ab}\rangle} + \underbrace{\times - \downarrow \uparrow a}_{\langle i|\hat{u}|a\rangle|0\rangle}
 \end{aligned}$$

(without restrictions on any of the summation indices).

A very simple example is provided by the operation of \hat{U}_N on the Fermi vacuum state:

$$\hat{U}_N|0\rangle = \sum_{a,i} \begin{array}{c} i \searrow \nearrow a \\ \times \text{---} \bullet \end{array} = \sum_{a,i} \langle a|\hat{u}|i\rangle |\Phi_i^a\rangle. \quad (4.14)$$

Only the ph term contributes here, since this is the only term in which we can have the vacuum state below the interaction.

For another example, we consider the operation of \hat{U}_N on a doubly excited SD:

$$\begin{aligned} \hat{U}_N|\Phi_{ij}^{ab}\rangle = & \sum_c \begin{array}{c} i \downarrow \uparrow c \\ \times \text{---} \bullet \end{array} \begin{array}{c} j \downarrow \uparrow b \\ \times \text{---} \bullet \end{array} + \sum_k \begin{array}{c} k \downarrow \uparrow i \\ \times \text{---} \bullet \end{array} \begin{array}{c} j \downarrow \uparrow b \\ \times \text{---} \bullet \end{array} \\ & + \sum_c \begin{array}{c} i \downarrow \uparrow a \\ \times \text{---} \bullet \end{array} \begin{array}{c} j \downarrow \uparrow c \\ \times \text{---} \bullet \end{array} + \sum_k \begin{array}{c} i \downarrow \uparrow a \\ \times \text{---} \bullet \end{array} \begin{array}{c} k \downarrow \uparrow j \\ \times \text{---} \bullet \end{array} \\ & + \sum_{k,c} \begin{array}{c} i \downarrow \uparrow a \\ \times \text{---} \bullet \end{array} \begin{array}{c} j \downarrow \uparrow b \\ \times \text{---} \bullet \end{array} \begin{array}{c} k \downarrow \uparrow c \\ \times \text{---} \bullet \end{array} + \begin{array}{c} \times \text{---} \bullet \end{array} \begin{array}{c} i \downarrow \uparrow a \\ \times \text{---} \bullet \end{array} \begin{array}{c} j \downarrow \uparrow b \\ \times \text{---} \bullet \end{array} \\ & + \begin{array}{c} i \downarrow \uparrow a \\ \times \text{---} \bullet \end{array} \begin{array}{c} j \downarrow \uparrow b \\ \times \text{---} \bullet \end{array} + \begin{array}{c} \times \text{---} \bullet \end{array} \begin{array}{c} i \downarrow \uparrow b \\ \times \text{---} \bullet \end{array} \begin{array}{c} j \downarrow \uparrow a \\ \times \text{---} \bullet \end{array} + \begin{array}{c} i \downarrow \uparrow b \\ \times \text{---} \bullet \end{array} \begin{array}{c} j \downarrow \uparrow a \\ \times \text{---} \bullet \end{array}. \end{aligned} \quad (4.15)$$

In general, we can represent the operator \hat{U}_N as

$$\hat{U}_N = \sum_{a,b} \begin{array}{c} \times \text{---} \bullet \end{array} \begin{array}{c} b \\ \nearrow \\ a \end{array} + \sum_{i,j} \begin{array}{c} \times \text{---} \bullet \end{array} \begin{array}{c} j \\ \nearrow \\ i \end{array} + \sum_{i,a} \begin{array}{c} \times \text{---} \bullet \end{array} \begin{array}{c} i \searrow \nearrow a \end{array} + \sum_{i,a} \begin{array}{c} \times \text{---} \bullet \end{array} \begin{array}{c} i \searrow \nearrow a \end{array}. \quad (4.16)$$

For \hat{U} there is one more term:

$$\hat{U} = \hat{U}_N + \langle 0|\hat{U}|0\rangle = \hat{U}_N + \sum_i \begin{array}{c} \times \text{---} \bullet \end{array} \begin{array}{c} i \end{array}. \quad (4.17)$$

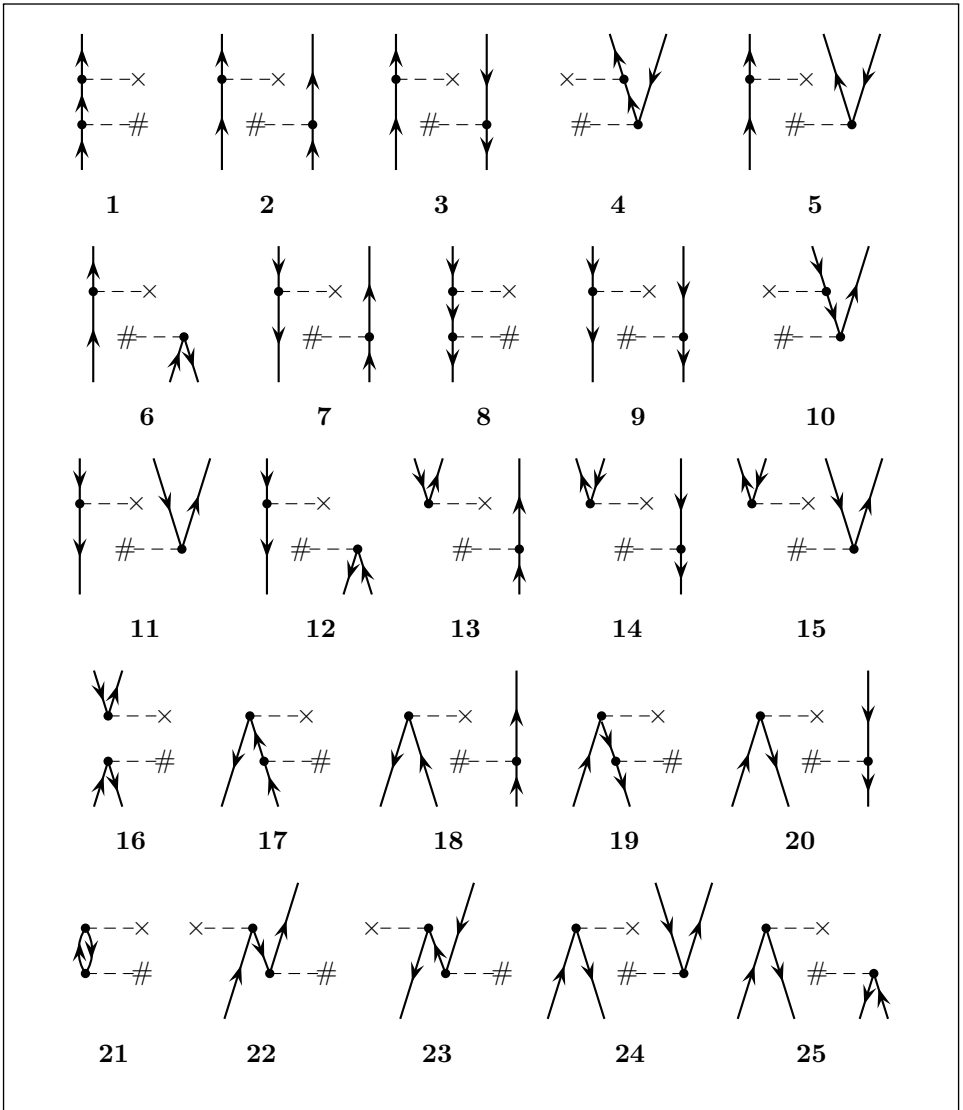
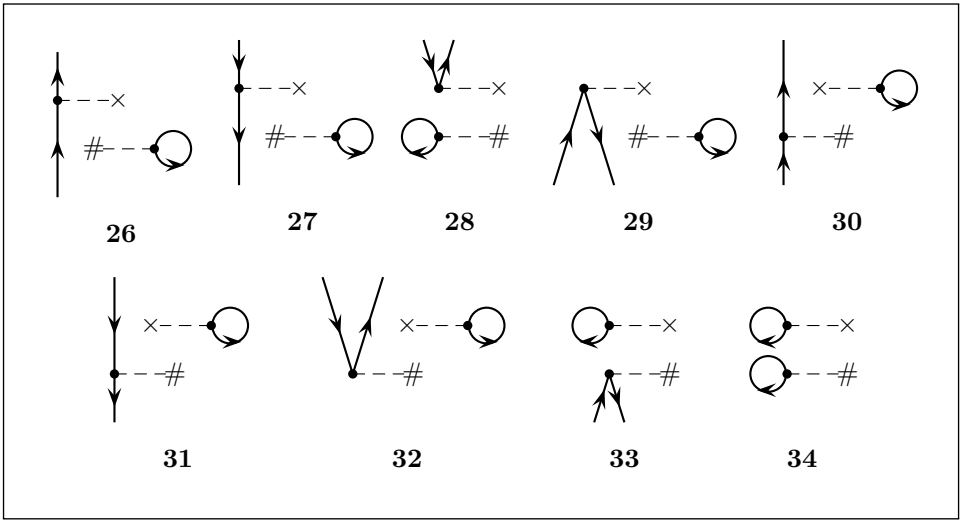


Fig. 4.1. Diagrams representing the operator product $\hat{U}_N \hat{Z}_N$.

where “Im” indicates the imaginary part. Obviously, if all the integrals are real then the vacuum expectation value of the commutator vanishes. This result is typical of the simplifications that are possible when working with commutators rather than with individual operator products.


In preparation for extending the treatment of phase factors, we shall consider several examples of the matrix elements of operator products. First,

Fig. 4.2. Additional diagrams for $\hat{U}\hat{Z}$.

let us take the relatively simple example of $\hat{U}_N\hat{Z}_N|0\rangle$, which can be represented by

$$\begin{aligned}
 \hat{U}_N\hat{Z}_N|0\rangle = & \begin{array}{c} \text{Diagram 28} \\ (i) \end{array} + \begin{array}{c} \text{Diagram 29} \\ (a) \end{array} \\
 & \sum_{abd} \langle a|\hat{u}|b\rangle \langle b|\hat{z}|i\rangle |\Phi_i^a\rangle - \sum_{aij} \langle j|\hat{u}|i\rangle \langle a|\hat{z}|j\rangle |\Phi_i^a\rangle \\
 & + \begin{array}{c} \text{Diagram 31} \\ (a) \end{array} + \begin{array}{c} \text{Diagram 32} \\ (j) \end{array} \\
 & \sum_{ia} \langle i|\hat{u}|a\rangle \langle a|\hat{z}|i\rangle |0\rangle + \sum_{abij} \langle a|\hat{u}|i\rangle \langle b|\hat{z}|j\rangle |\Phi_{ij}^{ab}\rangle \quad (4.24)
 \end{aligned}$$

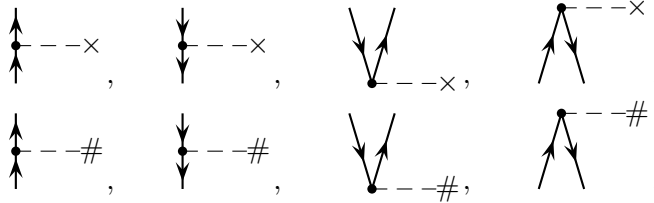
In this equation we introduce another (nonstandard) notational convention: *labels in parentheses identify the corresponding summation indices in the accompanying algebraic expressions*. The above result was obtained by contracting the $\begin{array}{c} \text{Diagram 28} \\ \bullet \end{array}$ diagram for Z_N (the only one with the vacuum state below it) with those U_N diagrams that can be attached to it without leaving

any lines extending to the bottom. The only minus sign is for the  combination in the second diagram, as noted in subsection 4.3.2. The phase of the resulting SD in the last diagram is obtained from the condition that surviving hole and particle lines at the top are paired vertically in $|\Phi_{ij\dots}^{ab\dots}\rangle$ if they are part of the same path.

Now consider the example $\langle \Phi_i^b | \hat{U}_N \hat{Z}_N | \Phi_i^a \rangle$. Here we have to connect the fragments



(note the same hole label i in both fragments) through the operator fragments



with the $\bullet - - x$ interaction line above the $\bullet - - \#$ line. The surviving terms are shown in Fig. 4.3. We have a total of nine diagrams, of which the last three contribute only in the special case $a = b$. Among these are some unusual cases. Diagram 4 is a true EPV case, in which the intermediate state (after the operation of \hat{Z}_N but before \hat{U}_N) has two holes in state i . Clearly this diagram should not contribute, but if we apply the diagram evaluation rules we do get a contribution, $\langle i | \hat{u} | a \rangle \langle b | \hat{z} | i \rangle$. At the same time, diagram 2 contains an EPV term when $j = i$, which should not contribute either (since it has two holes in i in the intermediate state), but the rules give $-\langle i | \hat{u} | a \rangle \langle b | \hat{z} | i \rangle$ (for $j = i$). Thus these two spurious contributions cancel exactly. We have the option either to

1. restrict the summation in diagram 2 to $j \neq i$ and leave out diagram 4, or to
2. use an unrestricted sum for 2 and include 4.

The result is the same, even though the second choice includes the evaluation of two terms that should have been left out. In diagrammatic many-body theory we always use option 2. Other examples of this choice will be encountered later.

We also need to re-emphasize that the horizontal arrangement in a diagram is not significant. Any diagrams that can be brought to congruence

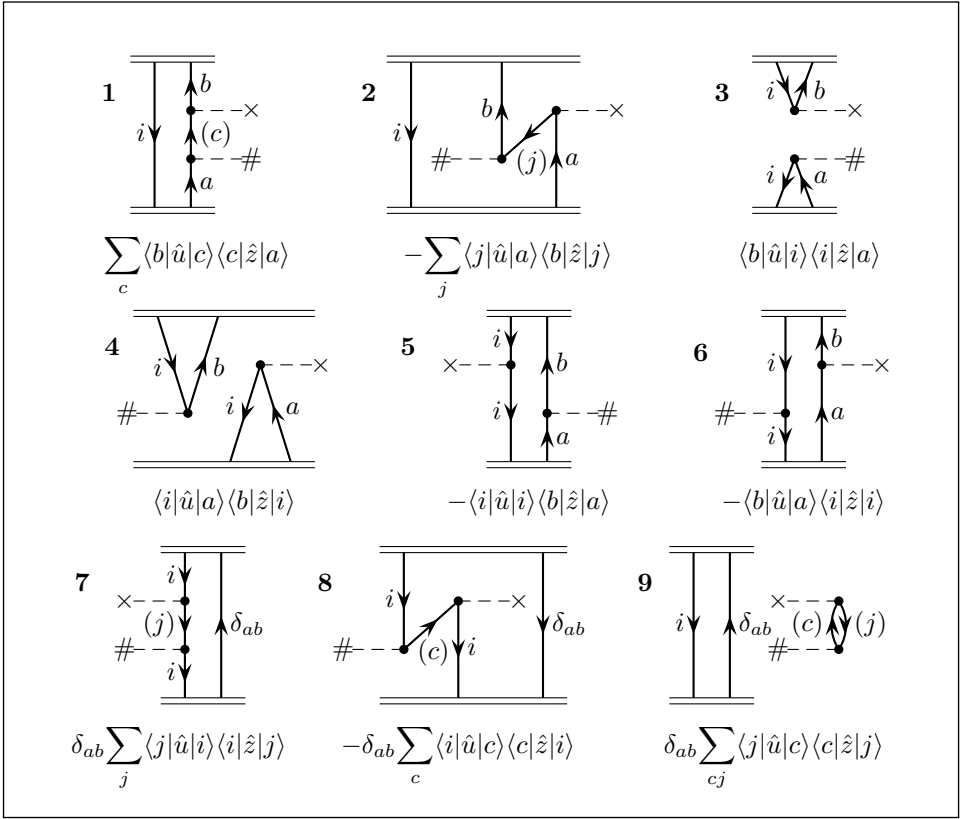
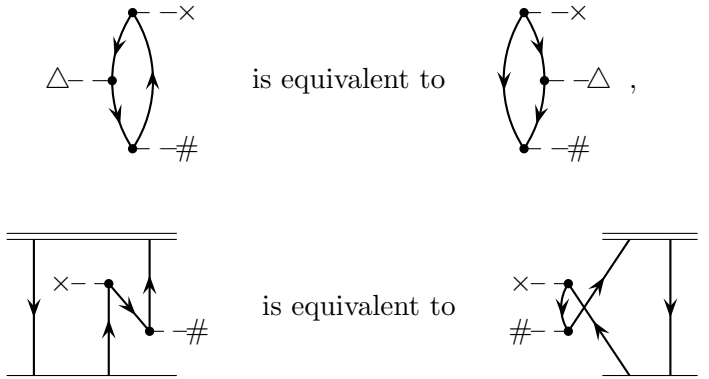


Fig. 4.3. Diagrams for the evaluation of the matrix element $\langle \Phi_i^b \hat{U}_N \hat{Z}_N \Phi_i^a \rangle$.

by changing the horizontal positions of lines and vertices are not distinct. For example,



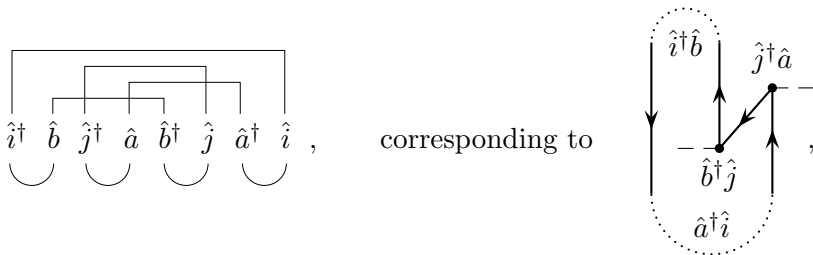
4.3.5 Phase factors

The example in Fig. 4.3 raises the important question of *phase factors*. We have put a minus sign in the expressions corresponding to diagrams 2 and 8, even though our current rule does not call for it. The need for a minus sign to be associated with diagram 2 can be seen from the following:

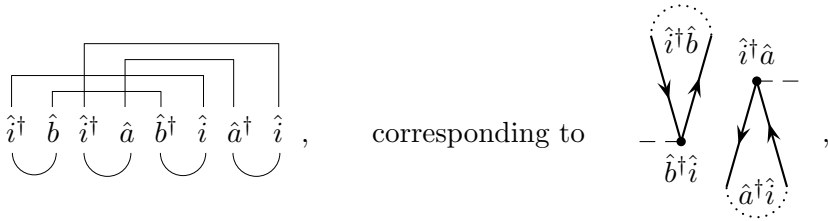
$$\begin{aligned}
 \langle 0 | \{\hat{i}^\dagger \hat{b}\} \{\hat{j}^\dagger \hat{a}\} \{\hat{b}^\dagger \hat{j}\} \{\hat{a}^\dagger \hat{i}\} | 0 \rangle &= \langle 0 | \overbrace{\{\hat{i}^\dagger \hat{b} \hat{j}^\dagger \hat{a} \hat{b}^\dagger \hat{j} \hat{a}^\dagger \hat{i}\}}^{\text{contraction lines}} | 0 \rangle \\
 &= -\langle 0 | \{\hat{i}^\dagger \hat{i} \hat{b} \hat{b}^\dagger \hat{j} \hat{j}^\dagger \hat{a} \hat{a}^\dagger\} | 0 \rangle = -1. \quad (4.25)
 \end{aligned}$$

Here we have unscrambled the operator product into a sequence of contracted pairs of operators, taking care that the order of the operators within each contracted pair is not changed. The parity of the unscrambling permutation provides the sign factor. As noted in Section 3.8, the sign factor can also be determined from the parity of the number of intersections of the contraction lines.

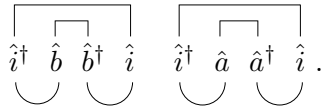
To be able to determine the sign associated with a particular diagram directly from the diagram we need a more general sign rule. In developing such a rule we consider the notion of a *path* in the diagram (see Paldus and Čížek 1975). A path is a sequence of connected lines, including any (external) connection $\overleftarrow{\downarrow} \overrightarrow{\uparrow}$ or $\overleftarrow{\uparrow} \overrightarrow{\downarrow}$ that indicates particle-hole pairs in the initial or final state. In the example of Fig. 4.3, diagrams 1, 2 and 5–8 each consist of a single closed path (or loop), while diagrams 3, 4 and 9 have two closed paths each. Each closed path represents a sequence of creation and annihilation operators connected alternately either by contraction or by belonging to the same original creation–annihilation pair (i.e., a vertex or external connection) in a normal product. For example, in diagram 2 the connection pattern is



while in diagram 4 we have

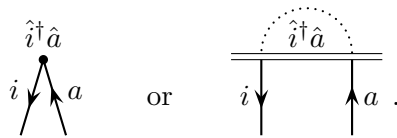


which rearranges to decouple the two loops without change of sign, since this only requires pairs of operators (vertices) to be moved past other pairs:

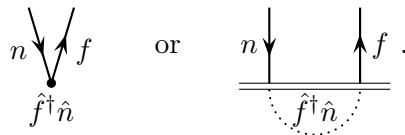


Entangled loops can always be disentangled with an even permutation moving pairs of operators (each corresponding to a vertex or an external connection) past other pairs. The sign factors can thus be computed separately for each loop and then multiplied together. We shall now show that the sign factor for each loop is $(-1)^{h-1}$, where h is the number of hole lines in the loop.

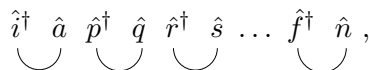
The left-most pair of creation–annihilation operators corresponding to any loop must be associated with the topmost feature of the loop, say



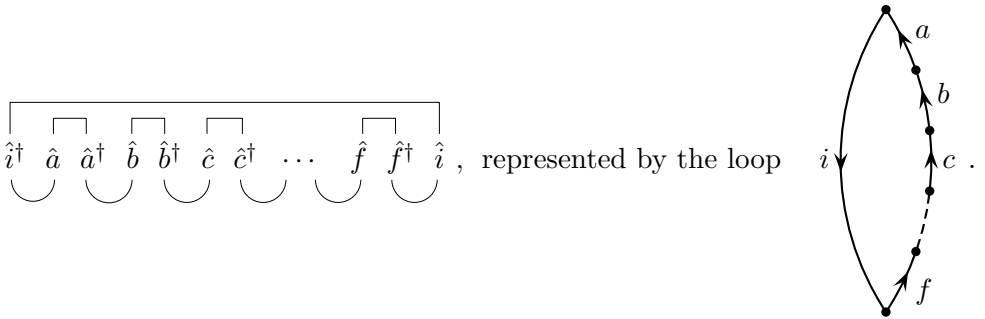
Similarly, the rightmost pair is associated with the bottom feature, say



The general form of the operator sequence is

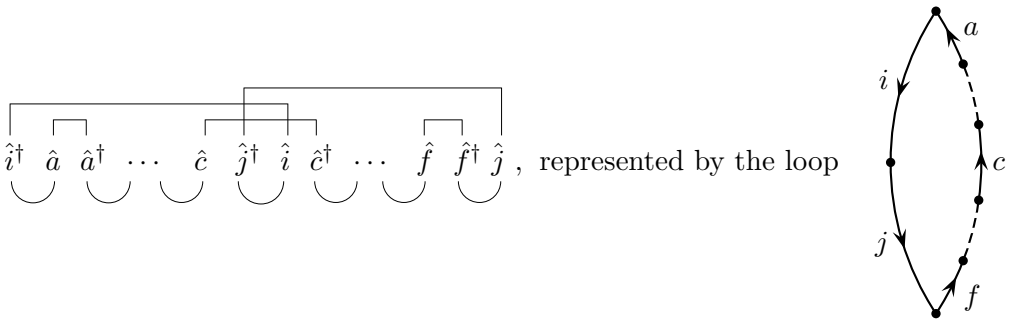


where each of p, q, r, s, \dots may refer to either a particle or a hole. To allow full contraction, the interior $\hat{p}^\dagger \hat{q} \hat{r}^\dagger \hat{s} \dots$ must contain an even number of hole operators \hat{k}^\dagger, \hat{k} as well as an even number of particle operators \hat{c}, \hat{c}^\dagger . We consider first the case of no interior hole operators. Then the diagram must have a contraction between \hat{i}^\dagger and \hat{n} (providing a factor δ_{in}) and, for a nonzero result, must have the general form

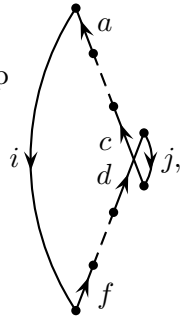
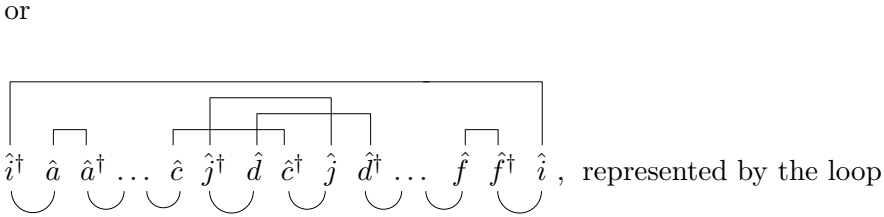
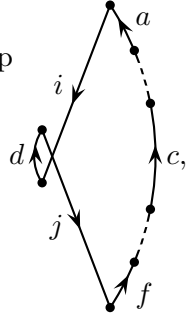
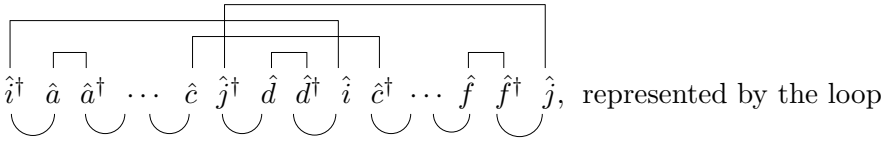


This example clearly has a $+$ sign. Thus, for a loop with one hole line ($h = 1$) we get the phase factor $+1 = (-1)^{h-1}$, as required.

Next we consider the case of two hole lines, i.e. two pairs of contracted hole operators. If the two interior hole operators are adjacent we have the pattern



Obviously unscrambling the contractions in this product produces a change of sign, so that we still have a phase factor (for $h = 2$) equal to $(-1)^{h-1} = -1$. If the two interior hole operators are not adjacent, but have some pairs of particle operators between them, as in



then we find the same sign factor as in the above simpler pattern. The same result is also obtained if more pairs of particle operators appear in between the hole operators.

Similarly, if more hole lines are introduced then we obtain another factor -1 for each additional hole line, giving a phase factor $(-1)^{h-1}$ for a loop with h hole lines. For l loops with h_1, h_2, \dots, h_l hole lines, respectively, we thus get

$$\prod_{i=1}^l (-1)^{h_i-1} = (-1)^{h-l}, \quad (4.26)$$

where $h = \sum_{i=1}^l h_i$ is the total number of hole lines.

Using the phase factor $(-1)^{h-l}$ we can easily see that alternative pairings of open lines (i.e. alternative external connections) produce equivalent results, so that we do not have to indicate the external connections explicitly.

For example,

$$\begin{array}{c}
 \begin{array}{c} \text{Diagram 1: } j \text{ and } b \text{ lines meeting at a vertex with a dashed line and a hash symbol. A dotted arc connects the vertex to itself.} \\ \text{Diagram 2: } i \text{ and } a \text{ lines meeting at a vertex with a dashed line and a cross symbol. A dotted arc connects the vertex to itself.} \end{array} = \begin{array}{c} \text{Diagram 3: } j \text{ and } b \text{ lines meeting at a vertex with a dashed line and a hash symbol. A dotted arc connects the vertex to a vertex where } i \text{ and } a \text{ lines meet with a dashed line and a cross symbol.} \end{array} = \begin{array}{c} \text{Diagram 4: } j \text{ and } b \text{ lines meeting at a vertex with a dashed line and a hash symbol. A dotted arc connects the vertex to a vertex where } i \text{ and } a \text{ lines meet with a dashed line and a cross symbol.} \end{array} \\
 \langle a | \hat{u} | i \rangle \langle b | \hat{z} | j \rangle | \Phi_{ij}^{ab} \rangle = - \langle a | \hat{u} | i \rangle \langle b | \hat{z} | j \rangle | \Phi_{ji}^{ab} \rangle \quad . \\
 (l = 2, h = 2) \qquad \qquad \qquad (l = 1, h = 2)
 \end{array} \tag{4.27}$$

Thus the results are independent of how the external connections are made, as long as the phase factors are calculated from the formula $(-1)^{h-l}$ for whichever connections are chosen. Therefore we can dispense henceforth with specifying external connections in open diagrams. We can also dispense, in general, with the unconventional double-bar notation, which we have used temporarily as a teaching tool.

Finally, we show how the phase-factor rule helps in demonstrating the cancellation of EPV diagrams. Again we use the example of Fig. 4.3, in the special case $a = b$, i.e. we evaluate the matrix element $\langle \Phi_i^a | \hat{U}_N \hat{Z}_N | \Phi_i^a \rangle$. We show the cancellation of the EPV components of diagram 9 with the EPV components of diagrams 2, 4 and 8:

$$\begin{array}{c}
 \begin{array}{c} \text{Diagram 9: } i \text{ and } a \text{ lines meeting at a vertex with a dashed line and a hash symbol. A dotted arc connects the vertex to itself.} \end{array} \quad (l = 2) \quad \text{cancels with} \quad \begin{array}{c} \text{Diagram 2: } i \text{ and } a \text{ lines meeting at a vertex with a dashed line and a cross symbol. A dotted arc connects the vertex to itself.} \end{array} \quad (l = 1), \\
 \begin{array}{c} \text{Diagram 9: } i \text{ and } a \text{ lines meeting at a vertex with a dashed line and a hash symbol. A dotted arc connects the vertex to itself.} \end{array} \quad (l = 2) \quad \text{cancels with} \quad \begin{array}{c} \text{Diagram 8: } a \text{ and } i \text{ lines meeting at a vertex with a dashed line and a cross symbol. A dotted arc connects the vertex to itself.} \end{array} \quad (l = 1), \\
 \begin{array}{c} \text{Diagram 9: } i \text{ and } a \text{ lines meeting at a vertex with a dashed line and a hash symbol. A dotted arc connects the vertex to itself.} \end{array} \quad (l = 2) \quad + \quad \begin{array}{c} \text{Diagram 4: } i \text{ and } a \text{ lines meeting at a vertex with a dashed line and a hash symbol. A dotted arc connects the vertex to itself.} \end{array} \quad (l = 2) \quad \text{cancels with}
 \end{array}$$

$$2 \quad (l = 1) + 8 \quad (l = 1).$$

In each case the integrals involved are the same and the number of hole lines is the same but the number of loops differs by one, so we get cancellation in each set.

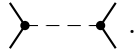
4.4 Two-particle operators

4.4.1 Goldstone diagrams for a two-particle operator

We now turn to a two-particle operator in normal-product form,

$$\hat{W} = \frac{1}{2} \sum_{pqrs} \langle pq|rs \rangle \{\hat{p}^\dagger \hat{q}^\dagger \hat{s} \hat{r}\} = \frac{1}{4} \sum_{pqrs} \langle pq||rs \rangle \{\hat{p}^\dagger \hat{q}^\dagger \hat{s} \hat{r}\}. \quad (4.28)$$

We shall first use the $\langle pq|rs \rangle$ form, with the factor $\frac{1}{2}$, and later go over to the antisymmetric form $\langle pq||rs \rangle$ with factor $\frac{1}{4}$. This operator will be denoted by an *interaction line* connecting two *half-vertices* at the same level (i.e. the same point on the time axis), for example



The two half-vertices and the interaction line constitute a single vertex. Each individual half-vertex will have one incoming and one outgoing line, each of which may be a particle line or a hole line. The association of line labels with the two-electron integral indices and the creation or annihilation operators follows the same rule as for one-body vertices:

bra index	\leftrightarrow	creation operator	\leftrightarrow	outgoing line
ket index	\leftrightarrow	annihilation operator	\leftrightarrow	incoming line

but with the added feature for the two-body case that

electron 1	\leftrightarrow	left half-vertex
electron 2	\leftrightarrow	right half-vertex

Thus for the term $\langle pq|rs \rangle \{\hat{p}^\dagger \hat{q}^\dagger \hat{s} \hat{r}\}$ we have the association

$$\begin{array}{llll} \hat{p}^\dagger & \leftrightarrow & \text{left outgoing line,} & \hat{q}^\dagger & \leftrightarrow & \text{right outgoing line,} \\ \hat{r} & \leftrightarrow & \text{left incoming line} & \hat{s} & \leftrightarrow & \text{right incoming line.} \end{array}$$

The integral indices associated with a two-body vertex are assigned according to the scheme

$$\langle \text{left-out} \text{ right-out} \mid \text{left-in} \text{ right-in} \rangle,$$

while the corresponding operator product can be described by

$$\{(\text{left-out})^\dagger(\text{right-out})^\dagger(\text{right-in})(\text{left-in})\}.$$

Diagrams employing this representation of the two-body interaction (which is based on non-antisymmetrized integrals) are called *Goldstone diagrams*.

Taking into consideration the different possible assignments of particle and hole lines, the \hat{W} operator is represented by

$$\begin{aligned} \hat{W} = & \begin{array}{c} \uparrow \\ \bullet \\ \uparrow \end{array} \text{---} \begin{array}{c} \uparrow \\ \bullet \\ \uparrow \end{array} + \begin{array}{c} \uparrow \\ \bullet \\ \downarrow \end{array} \text{---} \begin{array}{c} \downarrow \\ \bullet \\ \downarrow \end{array} + \begin{array}{c} \uparrow \\ \bullet \\ \uparrow \end{array} \text{---} \begin{array}{c} \swarrow \\ \bullet \\ \swarrow \end{array} + \begin{array}{c} \uparrow \\ \bullet \\ \uparrow \end{array} \text{---} \begin{array}{c} \searrow \\ \bullet \\ \searrow \end{array} + \begin{array}{c} \downarrow \\ \bullet \\ \downarrow \end{array} \text{---} \begin{array}{c} \downarrow \\ \bullet \\ \downarrow \end{array} \\ & + \begin{array}{c} \downarrow \\ \bullet \\ \downarrow \end{array} \text{---} \begin{array}{c} \swarrow \\ \bullet \\ \swarrow \end{array} + \begin{array}{c} \downarrow \\ \bullet \\ \downarrow \end{array} \text{---} \begin{array}{c} \searrow \\ \bullet \\ \searrow \end{array} + \begin{array}{c} \swarrow \\ \bullet \\ \swarrow \end{array} \text{---} \begin{array}{c} \swarrow \\ \bullet \\ \swarrow \end{array} + \begin{array}{c} \swarrow \\ \bullet \\ \swarrow \end{array} \text{---} \begin{array}{c} \searrow \\ \bullet \\ \searrow \end{array} + \begin{array}{c} \searrow \\ \bullet \\ \searrow \end{array} \text{---} \begin{array}{c} \searrow \\ \bullet \\ \searrow \end{array}, \end{aligned} \quad (4.29)$$

where summations over all appropriate indices are implied by the unlabeled lines. Note that we have left out diagrams that can be obtained from one of the above diagrams by interchanging the left and right half-vertices, which corresponds to exchanging the names of electrons 1 and 2, e.g.

$$\begin{array}{c} \swarrow \\ \bullet \\ \swarrow \end{array} \text{---} \begin{array}{c} \uparrow \\ \bullet \\ \uparrow \end{array} = \begin{array}{c} \uparrow \\ \bullet \\ \uparrow \end{array} \text{---} \begin{array}{c} \swarrow \\ \bullet \\ \swarrow \end{array}.$$

These equivalences will be taken care of by weight factors, as we discuss next.

So far we have ignored the factor $\frac{1}{2}$ in front of the sum for \hat{W} , as well as the collection of equivalent terms. As an example, take the diagram fragment

$$\begin{array}{c} (b) \uparrow \\ (a) \uparrow \end{array} \text{---} \begin{array}{c} \downarrow (j) \\ \downarrow (i) \end{array} = \frac{1}{2} \sum_{abij} \langle bi|aj \rangle \{ \hat{b}^\dagger \hat{i}^\dagger \hat{j} \hat{a} \}. \quad (4.30)$$

There is an equivalent fragment,

$$\begin{array}{c} (j) \downarrow \\ (i) \downarrow \end{array} \text{---} \begin{array}{c} \uparrow (b) \\ \uparrow (a) \end{array} = \frac{1}{2} \sum_{abij} \langle ib|ja \rangle \{ \hat{i}^\dagger \hat{b}^\dagger \hat{a} \hat{j} \}, \quad (4.31)$$

which is exactly equal to it, since $\langle ib|ja\rangle = \langle bi|aj\rangle$ and $\hat{b}^\dagger \hat{i}^\dagger = -\hat{i}^\dagger \hat{b}^\dagger$, $\hat{j}\hat{a} = -\hat{a}\hat{j}$. Thus we agree to use just one of the two equivalent fragments and so remove the factor $\frac{1}{2}$. However, if we consider the example

$$\begin{array}{c} (b) \uparrow \\ \bullet \\ (a) \uparrow \end{array} \text{---} \begin{array}{c} \uparrow (d) \\ \bullet \\ \uparrow (c) \end{array} = \frac{1}{2} \sum_{abcd} \langle bd|ac\rangle \{\hat{b}^\dagger \hat{d}^\dagger \hat{c} \hat{a}\}, \quad (4.32)$$

there is no other diagram equivalent to it since its mirror image in a vertical plane bisecting the vertex is congruent with it, and so the factor $\frac{1}{2}$ must be retained. However, a rigorous treatment of the weight factor problem cannot deal with diagram fragments, but must involve complete diagrams. This question will be dealt with further in the next subsection.

4.4.2 Vacuum expectation values of products of two-particle operators

Most of the diagrams with which we shall deal in many-body perturbation theory involve vacuum expectation values. In particular, the energy of a many-body system is given by sums of diagrams representing vacuum expectation values. To take a simple example, we shall consider the vacuum expectation value of \hat{W}^2 . (So far we have ignored the question of energy denominators, which represent the resolvent operators in the energy expressions; see (2.71). The diagrammatic representation of these denominators will be discussed in Chapter 5.) We shall first evaluate this quantity algebraically, using the generalized Wick's theorem, in order to make sure that we have the correct numerical factors and phases:

$$\begin{aligned} \langle 0|\hat{W}^2|0\rangle &= \frac{1}{2} \sum_{pqrs} \langle pq|rs\rangle \frac{1}{2} \sum_{tuvw} \langle tu|vw\rangle \langle 0|\{\hat{p}^\dagger \hat{q}^\dagger \hat{s} \hat{r}\} \{\hat{t}^\dagger \hat{u}^\dagger \hat{w} \hat{v}\}|0\rangle \\ &= \frac{1}{4} \sum_{pqrstuvw} \langle pq|rs\rangle \langle tu|vw\rangle \sum_{\text{contractions}} \langle 0|\{\hat{p}^\dagger \hat{q}^\dagger \hat{s} \hat{r} \hat{t}^\dagger \hat{u}^\dagger \hat{w} \hat{v}\}|0\rangle. \end{aligned} \quad (4.33)$$

Now we consider how the contractions are to be made. The only two possibilities for obtaining nonzero fully contracted terms without using internal contractions among the operators of either of the two original normal products $\{\hat{p}^\dagger \hat{q}^\dagger \hat{s} \hat{r}\}$ and $\{\hat{t}^\dagger \hat{u}^\dagger \hat{w} \hat{v}\}$ are:



1. contract \hat{p}^\dagger and \hat{q}^\dagger with \hat{w} and \hat{v} , in either order, which requires that p, q, w, v be hole indices,
2. contract \hat{s} and \hat{r} with \hat{t}^\dagger and \hat{u}^\dagger , in either order, which requires that s, r, t, u be particle indices.



Thus there are four distinct contractions,

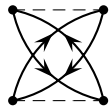
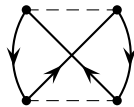
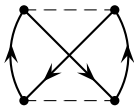
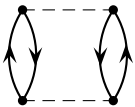
$$\begin{aligned}
 \langle 0 | \hat{W}^2 | 0 \rangle &= \frac{1}{4} \sum_{abcdijkl} \langle ij|ab \rangle \langle cd|kl \rangle \sum_{\text{contractions}} \langle 0 | \{ \hat{i}^\dagger \hat{j}^\dagger \hat{b} \hat{a} \hat{c}^\dagger \hat{d}^\dagger \hat{l} \hat{k} \} | 0 \rangle \\
 &= \frac{1}{4} \left\{ \sum_{abcdijkl} \langle ij|ab \rangle \langle cd|kl \rangle \langle 0 | \hat{i}^\dagger \hat{j}^\dagger \hat{b} \hat{a} \hat{c}^\dagger \hat{d}^\dagger \hat{l} \hat{k} | 0 \rangle \right. \\
 &\quad + \sum_{abcdijkl} \langle ij|ab \rangle \langle cd|kl \rangle \langle 0 | \hat{i}^\dagger \hat{j}^\dagger \hat{b} \hat{a} \hat{c}^\dagger \hat{d}^\dagger \hat{l} \hat{k} | 0 \rangle \\
 &\quad + \sum_{abcdijkl} \langle ij|ab \rangle \langle cd|kl \rangle \langle 0 | \hat{i}^\dagger \hat{j}^\dagger \hat{b} \hat{a} \hat{c}^\dagger \hat{d}^\dagger \hat{l} \hat{k} | 0 \rangle \\
 &\quad \left. + \sum_{abcdijkl} \langle ij|ab \rangle \langle cd|kl \rangle \langle 0 | \hat{i}^\dagger \hat{j}^\dagger \hat{b} \hat{a} \hat{c}^\dagger \hat{d}^\dagger \hat{l} \hat{k} | 0 \rangle \right\} \\
 &= \frac{1}{4} \left\{ \sum_{abij} \langle ij|ab \rangle \langle ab|ij \rangle - \sum_{abij} \langle ij|ab \rangle \langle ba|ij \rangle \right. \\
 &\quad \left. - \sum_{abij} \langle ij|ab \rangle \langle ab|ji \rangle + \sum_{abij} \langle ij|ab \rangle \langle ba|ji \rangle \right\}. \tag{4.34}
 \end{aligned}$$

The first and fourth terms are equal (by exchange of electrons 1 and 2 in the second integral), and so are the second and third. Thus the result is

$$\langle 0 | \hat{W}^2 | 0 \rangle = \frac{1}{2} \sum_{abij} \langle ij|ab \rangle (\langle ab|ij \rangle - \langle ab|ji \rangle). \tag{4.35}$$

The diagrammatic description of this matrix element involves two \hat{W} vertices, one above the other, with the vacuum at top and bottom. The two vertices must therefore have the forms   for the top vertex and

  for the bottom vertex and can be connected in four different ways, corresponding to the four contraction schemes in (4.34):



As in (4.34), the first and fourth diagrams are equivalent (by exchange of the two half-vertices at the top or bottom) and so are the second and third. Thus we are left with two diagrams, often referred to as the *direct* and *exchange* diagrams, respectively,

$$\begin{aligned}
 \langle 0 | \hat{W}^2 | 0 \rangle = & \quad \text{[Direct Diagram]} + \text{[Exchange Diagram]} , \\
 & \frac{1}{2} \sum_{abij} \langle ij | ab \rangle \langle ab | ij \rangle \quad - \frac{1}{2} \sum_{abij} \langle ij | ab \rangle \langle ab | ji \rangle \\
 & (l = 2, h = 2) \quad \quad \quad (l = 1, h = 2)
 \end{aligned} \tag{4.36}$$

in agreement with the algebraic derivation. The minus sign for the exchange diagram is obtained from our phase-factor rule $(-1)^{h-l}$, as shown. This rule, which we derived originally for diagrams with one-body vertices only, applies equally to diagrams containing two-body vertices. Note also that the EPV terms, in which $i = j$ and/or $a = b$, cancel between the direct and exchange terms, justifying the use of unrestricted summations.

The factor $\frac{1}{2}$ derives from the fact that each of these diagrams is (or can be redrawn to be) symmetric under reflection in a vertical plane through its middle. It compensates for the fact that terms such as

$$\begin{aligned}
 & \text{[Diagram 1]} \quad \text{and} \quad \text{[Diagram 2]} , \\
 & \frac{1}{2} \langle ij | ab \rangle \langle ab | ij \rangle \quad \quad \quad \frac{1}{2} \langle ji | ba \rangle \langle ba | ji \rangle
 \end{aligned}$$

which are equal, will be included separately in the unrestricted sum over i, j, a, b . More generally, we note that the original coefficient $\frac{1}{2}$ in the sum $\frac{1}{2} \sum_{pqrs} \langle pq | rs \rangle \{ \hat{p}^\dagger \hat{q}^\dagger \hat{r} \hat{s} \}$ was introduced because only distinct terms should be summed; a simultaneous exchange $p \leftrightarrow q, r \leftrightarrow s$ (which corresponds to the exchange of electron labels 1 and 2) does not produce a distinct term. The same situation holds for the diagrams. Each distinct term should be included once but, because of the unrestricted summations, some are included more than once and the weight factor is needed to compensate. The restriction to inequivalent diagrams eliminates the double counting for asymmetric diagrams, but we need a factor $\frac{1}{2}$ for each diagram or unlinked part of a diagram that can be written in a form symmetric under left-right reflection.

To provide further examples of diagram construction, and of rules for diagram interpretation and phase factor and weight factor determination, we next consider the vacuum expectation value of a product of three two-body

operators, $\langle 0|\hat{W}^3|0\rangle$. (We should note again that in this chapter we are leaving out an important diagram interpretation aspect relating to the use of these diagrams in perturbation theory, i.e. the incorporation of the resolvent operators and their concomitant denominators. This aspect will be introduced in Chapter 5.) Each diagram for this matrix element contains three two-body vertices, of which the top and bottom vertices must have the same form as in the $\langle 0|\hat{W}^2|0\rangle$ case. To allow full contraction with no open lines remaining, the middle vertex must have two lines above and two lines below the vertex, for which there are the four possibilities



The first choice produces two diagrams, referred to as *particle ladder* diagrams (shown with their algebraic interpretations),

$$(i) \begin{array}{c} \text{---} \text{---} \text{---} \\ \text{---} \text{---} \text{---} \\ \text{---} \text{---} \text{---} \end{array} (j) = \frac{1}{2} \sum_{abcdij} \langle ij|ab\rangle \langle ab|cd\rangle \langle cd|ij\rangle \quad \left(\begin{array}{l} l=2, h=2, \\ \text{symmetric} \end{array} \right),$$

$$(i) \begin{array}{c} \text{---} \text{---} \text{---} \\ \text{---} \text{---} \text{---} \\ \text{---} \text{---} \text{---} \end{array} (j) = -\frac{1}{2} \sum_{abcdij} \langle ij|ab\rangle \langle ab|dc\rangle \langle cd|ij\rangle \quad \left(\begin{array}{l} l=1, h=2, \\ \text{symmetric} \end{array} \right).$$

The second diagram is the *exchange* version of the first, obtained in this case by interchanging the endpoints of the incoming particle lines at the middle vertex (any alternative exchange produces an equivalent diagram).

Using the second choice for the middle vertex, we obtain the *hole ladder* diagrams,

$$(a) \begin{array}{c} \text{---} \text{---} \text{---} \\ \text{---} \text{---} \text{---} \\ \text{---} \text{---} \text{---} \end{array} (b) = \frac{1}{2} \sum_{abijkl} \langle ij|ab\rangle \langle kl|ij\rangle \langle ab|kl\rangle \quad \left(\begin{array}{l} l=2, h=4, \\ \text{symmetric} \end{array} \right),$$

$$(a) \begin{array}{c} \text{---} \text{---} \text{---} \\ \text{---} \text{---} \text{---} \\ \text{---} \text{---} \text{---} \end{array} (b) = -\frac{1}{2} \sum_{abijkl} \langle ij|ab\rangle \langle lk|ij\rangle \langle ab|kl\rangle \quad \left(\begin{array}{l} l=1, h=4, \\ \text{symmetric} \end{array} \right).$$

Here also, we have a direct and an exchange diagram.

The third and fourth choices for the middle vertex, taken together, produce eight diagrams, referred to as *ring* diagrams (the name is taken from the shape of the last diagram of this set),

$$(a) \begin{array}{c} \text{---} \text{---} \text{---} \text{---} \\ \text{---} \text{---} \text{---} \text{---} \\ \text{---} \text{---} \text{---} \text{---} \end{array} \begin{array}{c} (i) \quad (b) \\ \text{---} \text{---} \text{---} \text{---} \\ (k) \quad (c) \end{array} (j) = - \sum_{abcijk} \langle ij|ab \rangle \langle kb|ic \rangle \langle ac|kj \rangle \quad \left(\begin{array}{l} l=2, \ h=3, \\ \text{asymmetric} \end{array} \right),$$

$$(a) \begin{array}{c} \text{---} \text{---} \text{---} \text{---} \\ \text{---} \text{---} \text{---} \text{---} \\ \text{---} \text{---} \text{---} \text{---} \end{array} \begin{array}{c} (i) \\ \text{---} \text{---} \text{---} \text{---} \\ (j) \quad (k) \end{array} (b) = \sum_{abcijk} \langle ji|ab \rangle \langle kb|ic \rangle \langle ac|kj \rangle \quad \left(\begin{array}{l} l=1, \ h=3, \\ \text{asymmetric} \end{array} \right),$$

$$(a) \begin{array}{c} \text{---} \text{---} \text{---} \text{---} \\ \text{---} \text{---} \text{---} \text{---} \\ \text{---} \text{---} \text{---} \text{---} \end{array} \begin{array}{c} (i) \\ \text{---} \text{---} \text{---} \text{---} \\ (j) \quad (k) \end{array} (b) = \sum_{abcijk} \langle ij|ab \rangle \langle kb|ic \rangle \langle ac|jk \rangle \quad \left(\begin{array}{l} l=1, \ h=3, \\ \text{asymmetric} \end{array} \right),$$

$$(a) \begin{array}{c} \text{---} \text{---} \text{---} \text{---} \\ \text{---} \text{---} \text{---} \text{---} \\ \text{---} \text{---} \text{---} \text{---} \end{array} \begin{array}{c} (i) \\ \text{---} \text{---} \text{---} \text{---} \\ (k) \quad (c) \end{array} (b) = \sum_{abcijk} \langle ij|ab \rangle \langle bk|ic \rangle \langle ac|kj \rangle \quad \left(\begin{array}{l} l=1, \ h=3, \\ \text{asymmetric} \end{array} \right),$$

$$(a) \begin{array}{c} \text{---} \text{---} \text{---} \text{---} \\ \text{---} \text{---} \text{---} \text{---} \\ \text{---} \text{---} \text{---} \text{---} \end{array} \begin{array}{c} (i) \\ \text{---} \text{---} \text{---} \text{---} \\ (j) \quad (k) \end{array} (b) = - \sum_{abcijk} \langle ij|ab \rangle \langle bk|ic \rangle \langle ac|jk \rangle \quad \left(\begin{array}{l} l=2, \ h=3, \\ \text{asymmetric} \end{array} \right),$$

$$(a) \begin{array}{c} \text{---} \text{---} \text{---} \text{---} \\ \text{---} \text{---} \text{---} \text{---} \\ \text{---} \text{---} \text{---} \text{---} \end{array} \begin{array}{c} (j) \quad (i) \\ \text{---} \text{---} \text{---} \text{---} \\ (k) \quad (c) \end{array} (b) = - \sum_{abcijk} \langle ji|ab \rangle \langle kb|ci \rangle \langle ac|kj \rangle \quad \left(\begin{array}{l} l=2, \ h=3, \\ \text{asymmetric} \end{array} \right),$$

$$(a) \begin{array}{c} \text{---} \text{---} \text{---} \text{---} \\ \text{---} \text{---} \text{---} \text{---} \\ \text{---} \text{---} \text{---} \text{---} \end{array} \begin{array}{c} (i) \\ \text{---} \text{---} \text{---} \text{---} \\ (j) \quad (k) \end{array} (b) = - \sum_{abcijk} \langle ji|ab \rangle \langle kb|ic \rangle \langle ac|jk \rangle \quad \left(\begin{array}{l} l=2, \ h=3, \\ \text{asymmetric} \end{array} \right),$$

$$(a) \begin{array}{c} \text{---} \text{---} \text{---} \text{---} \\ \text{---} \text{---} \text{---} \text{---} \\ \text{---} \text{---} \text{---} \text{---} \end{array} \begin{array}{c} (i) \\ \text{---} \text{---} \text{---} \text{---} \\ (j) \quad (k) \end{array} (b) = \sum_{abcijk} \langle ji|ab \rangle \langle kb|ci \rangle \langle ac|jk \rangle \quad \left(\begin{array}{l} l=3, \ h=3, \\ \text{asymmetric} \end{array} \right).$$

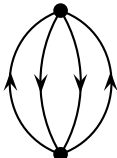
If the first of these eight diagrams is considered as the *direct* case then the next three are *single exchange*, the following three *double exchange* and the last one *triple exchange*. One could, in fact, take any of these eight as direct, and there would still be three single, three double and one triple exchange relative to it. In general, an exchange diagram is obtained by exchanging the terminating points of the two incoming lines *or* the starting points of the two outgoing lines at any two-body vertex.

4.4.3 Hugenholtz diagrams

The principal problem with the Goldstone representation is the rapid growth in the number of distinct diagrams as the number of interaction vertices increases, reflecting the individual listing of each possible exchange. There is also some difficulty in making sure that all those distinct possibilities have been listed exactly once, since it is not always easy to determine whether two diagrams are equivalent. However, the advantage of Goldstone diagrams is the straightforward determination of phase factors.

The difficulties associated with the use of the Goldstone representation can be overcome by basing the analysis on the antisymmetric integrals $\langle pq||rs \rangle$ (the final form in (4.28)). Since the exchange contribution is incorporated within each antisymmetrized integral, such an approach leads to a much smaller number of distinct diagrams. The diagrams using this representation of the \hat{W} operator are called *Hugenholtz diagrams* (Hugenholtz 1957). They maintain the usual (Goldstone) form for one-body operators but represent the two-body vertex as a single large dot with two incoming and two outgoing lines (each of which can be a particle or hole line). The labels on the outgoing lines appear in the bra part of the antisymmetrized integral, while the incoming labels appear in the ket part. The order of the labels in each part is indeterminate, and therefore the phase of the corresponding algebraic interpretation is indeterminate. (We shall deal with this phase-factor problem in the next subsection.) The correspondence between the Goldstone and Hugenholtz representations of the various terms in the \hat{W} operator, including the associated integrals (ignoring weight and phase factors) is shown in Fig. 4.4.

The Hugenholtz representation of the $\langle 0|\hat{W}^2|0 \rangle$ matrix element has just one distinct diagram instead of two,

$$\langle 0|\hat{W}^2|0 \rangle = \text{diagram} = \frac{1}{4} \sum_{abij} \langle ij||ab \rangle \langle ab||ij \rangle. \quad (4.37)$$


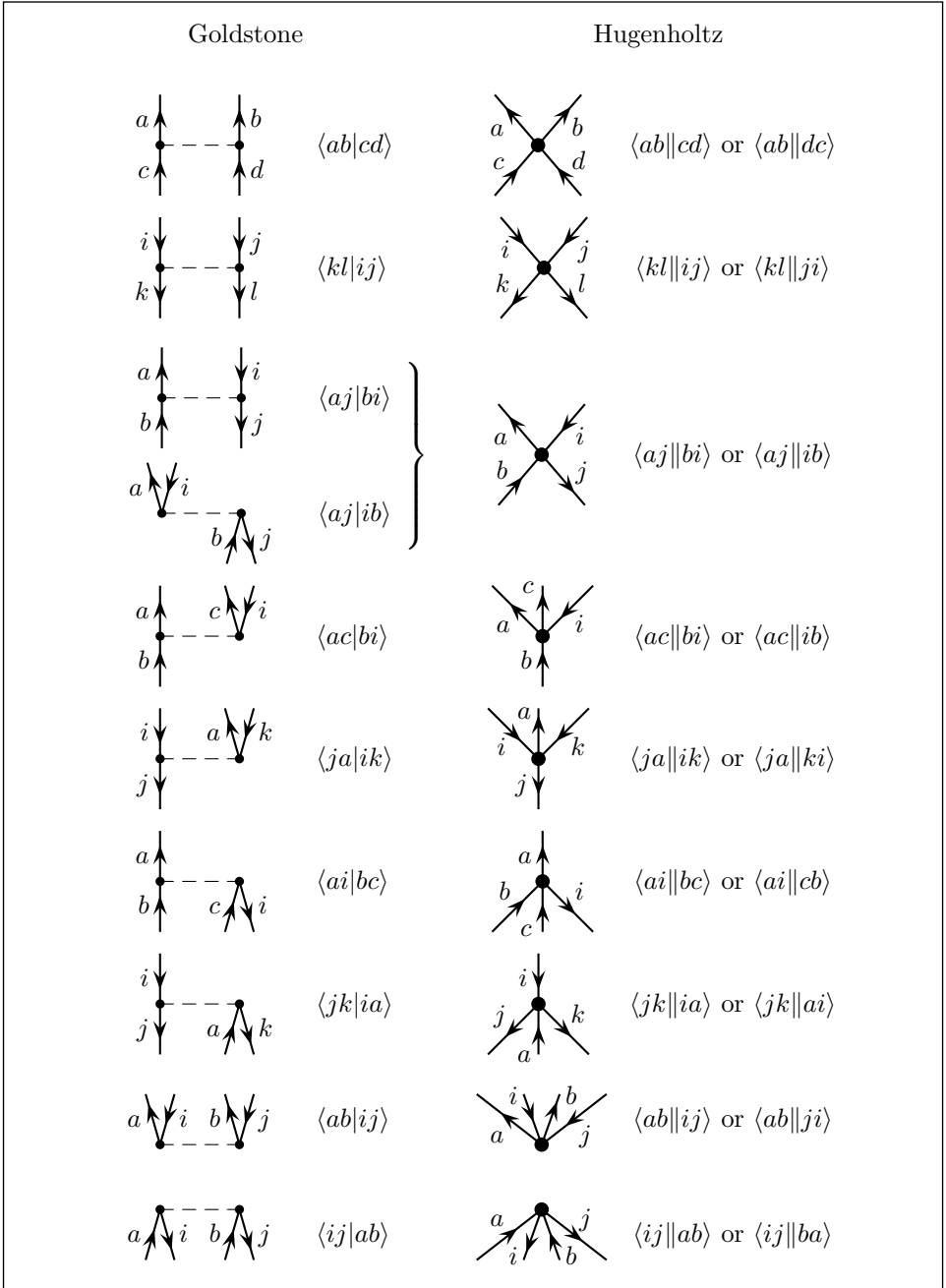


Fig. 4.4. The correspondence between the Goldstone and Hugenholtz diagrams for the \hat{W} operator and their associated integrals (the weights and phase factors have been left out).

Expansion of the antisymmetrized integrals in terms of ordinary integrals gives four terms, which are equal in pairs, reproducing the two-term result obtained with Goldstone diagrams, (4.36). The weight factor $\frac{1}{4}$ is obtained by counting the number of pairs of equivalent lines in the diagram: a pair of lines is *equivalent* if they connect the same pair of vertices in the same direction. Each pair of equivalent lines contributes a factor $\frac{1}{2}$. The diagram for $\langle 0|\hat{W}^2|0\rangle$ has two such pairs (two equivalent particle lines and two equivalent hole lines), resulting in a weight factor $\frac{1}{4}$.

The power of the Hugenholtz representation is easily seen in the evaluation of $\langle 0|\hat{W}^3|0\rangle$. Instead of the 12 diagrams of the Goldstone representation, we obtain just three, corresponding to the particle ladder, the hole ladder and the ring diagrams, respectively:

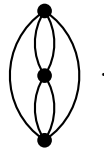
$$\begin{array}{c}
 \text{Diagram 1: A ring diagram with two vertices. The top arc has two arrows pointing right, labeled (a) and (b). The bottom arc has two arrows pointing left, labeled (c) and (d). External lines on the left and right are labeled (i) and (j) respectively, both pointing right.} \\
 (i) \rightarrow \text{---} (j) = \pm \frac{1}{8} \sum_{abcdij} \langle ij||ab\rangle \langle ab||cd\rangle \langle cd||ij\rangle,
 \end{array}$$

$$\begin{array}{c}
 \text{Diagram 2: A ring diagram with two vertices. The top arc has two arrows pointing left, labeled (i) and (j). The bottom arc has two arrows pointing right, labeled (k) and (l). External lines on the left and right are labeled (a) and (b) respectively, both pointing left.} \\
 (a) \leftarrow \text{---} (b) = \pm \frac{1}{8} \sum_{abijkl} \langle ij||ab\rangle \langle kl||ij\rangle \langle ab||kl\rangle,
 \end{array}$$

$$\begin{array}{c}
 \text{Diagram 3: A ring diagram with two vertices. The top arc has two arrows pointing left, labeled (b) and (j). The bottom arc has two arrows pointing right, labeled (c) and (k). External lines on the left and right are labeled (a) and (i) respectively, both pointing left.} \\
 (a) \leftarrow \text{---} (i) = \pm \sum_{abcijk} \langle ij||ab\rangle \langle kb||jc\rangle \langle ac||ik\rangle.
 \end{array}$$

The last diagram replaces all eight Goldstone ring diagrams.

It is obvious that the Hugenholtz representation reduces the number of diagrams considerably. Furthermore, it is much easier to list all the distinct diagrams in this scheme. The usual approach is first to list all Hugenholtz *skeletons*, which are diagrams without the arrows. For the $\langle 0|\hat{W}^3|0\rangle$ matrix element we have just one skeleton,



Arrows are then added in all distinct ways to produce all the distinct diagrams. It is quite easy to tell whether two diagrams are distinct: any two diagrams are equivalent if they have the same connection pattern, with the same senses of the arrows. In other words, two diagrams are equivalent if one can be deformed into the other without changing the vertical sequence of the vertices or the sense of the arrows. The weight factor is also easy to determine, by counting the number of equivalent line pairs. The major disadvantage is that Hugenholtz diagrams do not immediately specify the phase of the corresponding algebraic expression.

4.4.4 Antisymmetrized Goldstone diagrams

A solution to the phase problem of Hugenholtz diagrams is obtained by converting each distinct Hugenholtz diagram into *just one* Goldstone-like diagram and interpreting each two-body vertex in this Goldstone diagram in terms of antisymmetrized integrals $\langle pq||rs \rangle$ instead of ordinary integrals $\langle pq|rs \rangle$. These *antisymmetrized Goldstone* (ASG) diagrams (Brandow 1967) are obtained by expanding each large dot (two-body vertex) of the Hugenholtz representation into a Goldstone-type two-body vertex. This expansion is not unique, because the four lines connected to a Hugenholtz vertex can be assigned in different ways to the two half-vertices of the ASG diagram, but all possible expansions of a given Hugenholtz diagram give the same resulting algebraic expression provided that the signs are interpreted according to the rules for Goldstone diagrams. The weight factors are those of the corresponding Hugenholtz diagram, with a factor $\frac{1}{2}$ for each pair of equivalent lines. For example,

$$\begin{aligned}
 \text{Diagram 1} &= \text{Diagram 2} \quad \text{or} \quad \text{Diagram 3} \\
 &= \frac{1}{4} \sum_{abij} \langle ij||ab \rangle \langle ab||ij \rangle = -\frac{1}{4} \sum_{abij} \langle ij||ab \rangle \langle ab||ji \rangle \\
 &= \frac{1}{4} \sum_{abij} (\langle ij|ab \rangle - \langle ij|ba \rangle) (\langle ab|ij \rangle - \langle ab|ji \rangle) \\
 &= \frac{1}{2} \sum_{abij} \langle ij|ab \rangle (\langle ab|ij \rangle - \langle ab|ji \rangle).
 \end{aligned} \tag{4.38}$$

The procedure for generating and interpreting the antisymmetrized Goldstone diagrams can be summarized by the following rules:

1. Generate all distinct Hugenholtz skeletons.
2. For each skeleton assign arrows in all distinct ways to generate Hugenholtz diagrams.
3. Expand each Hugenholtz diagram into an ASG diagram in any of the possible equivalent ways.
4. Interpret each two-body vertex in each ASG diagram in terms of an antisymmetrized integral, with the usual $\langle \text{left-out right-out} || \text{left-in right-in} \rangle$ arrangement.
5. Interpret each one-body vertex in each ASG diagram as in ordinary Goldstone diagrams.
6. Assign a phase factor $(-1)^{h-l}$, as for ordinary Goldstone diagrams.
7. Assign a weight factor $(\frac{1}{2})^n$, where n is the number of equivalent line pairs; two lines are equivalent if they connect the same two vertices in the same direction.

Applying these rules to the $\langle 0 | \hat{W}^3 | 0 \rangle$ example, we obtain the matrix element as a sum of three diagrams:

$$\begin{array}{c} \text{Diagram 1} \end{array} = (i) \begin{array}{c} \text{Diagram 2} \end{array} (j) = \frac{1}{8} \sum_{abcdij} \langle ij || ab \rangle \langle ab || cd \rangle \langle cd || ij \rangle \\
 (h = 3, l = 2, n = 3)$$

$$\begin{array}{c} \text{Diagram 3} \end{array} = (a) \begin{array}{c} \text{Diagram 4} \end{array} (b) = \frac{1}{8} \sum_{abijkl} \langle ij || ab \rangle \langle kl || ij \rangle \langle ab || kl \rangle \\
 (h = 4, l = 2, n = 3),$$

$$\begin{array}{c} \text{Diagram 5} \end{array} = (a) \begin{array}{c} \text{Diagram 6} \end{array} (j) = - \sum_{abcijk} \langle ij || ab \rangle \langle kb || ic \rangle \langle ac || kj \rangle \\
 (h = 3, l = 2, n = 0).$$

Any other expansions of the Hugenholtz diagrams would give the same algebraic results. For example, the alternative expansion of the third diagram,

$$\begin{aligned}
& \text{Diagram 1} = (a) \text{ Diagram 2} = \sum_{abcijk} \langle ji || ab \rangle \langle bk || ic \rangle \langle ac || jk \rangle \\
& (h = 3, l = 3, n = 0),
\end{aligned}$$

obviously reduces to an equal algebraic expression.

From now on, except where stated otherwise, all the Goldstone-type diagrams we use will be ASG diagrams.

4.4.5 Representation of operators not in normal-product form

When we deal with a two-body operator

$$\hat{V}_2 = \frac{1}{2} \sum_{pqrs} \langle pq | \hat{v} | rs \rangle \hat{p}^\dagger \hat{q}^\dagger \hat{s} \hat{r} \quad (4.39)$$

that is not in normal-product form (cf.(4.28)), we must include internal contractions between the four creation or annihilation operators. Therefore the diagrammatic representation of such an operator includes contractions between the four lines attached to the same two-body vertex. Dealing first with the ordinary Goldstone representation, we obtain the following new diagrams, to be added to those of (4.29) (which we refer to as $(\hat{V}_2)_N$):

$$\begin{aligned} \hat{V}_2 = (\hat{V}_2)_N &+ \text{diagram 1} + \text{diagram 2} + \text{diagram 3} + \text{diagram 4} \\ &+ \text{diagram 5} + \text{diagram 6} + \text{diagram 7} + \text{diagram 8} \\ &+ \text{diagram 9} + \text{diagram 10} . \end{aligned} \quad (4.40)$$

In all but the last of these diagrams, the directions in which the lines leave and enter a vertex indicate that they are hole lines, to be summed over hole labels only, since only hole operators give nonzero contractions within products of creation and annihilation operators of the form $\hat{p}^\dagger \hat{q}^\dagger \hat{s} \hat{r}$. The last diagram, called an *oyster*, is drawn in this shape by convention, but also involves hole lines only. The last five diagrams (the “wiggles” and the oyster) are the exchange terms for the first five (the bubbles), and would

be left out in the ASG representation. For the purpose of weight-factor determination the oysters are considered symmetric, since it is immaterial which of the two hole lines is drawn above or below the vertex line.

The first four diagrams in (4.40) and the corresponding exchange diagrams in the second row represent the $\hat{V}'_N = \sum_{pq} \left(\sum_i (\langle pi|qi \rangle - \langle pi|i q \rangle) \right) \{ \hat{p}^\dagger \hat{q} \}$ operator of (3.178). The fifth and the remaining diagrams represent $\langle 0 | \hat{V}_2 | 0 \rangle = \frac{1}{2} \sum_{ij} (\langle ij|ij \rangle - \langle ij|ji \rangle)$.

The non-normal-product Goldstone diagrams in the representation of $\langle 0 | \hat{V}_2^2 | 0 \rangle$ are:

$$\begin{aligned}
 & \begin{array}{c} (j) \\ \text{---} \circ \text{---} \\ (i) \text{---} \circ \text{---} \\ (k) \text{---} \circ \text{---} \end{array} = \sum_{aijk} \langle ij|aj \rangle \langle ak|ik \rangle \quad \left(\begin{array}{c} l=3, \ h=3, \\ \text{asymmetric} \end{array} \right), \\
 & \begin{array}{c} (j) \\ \text{---} \circ \text{---} \\ (i) \text{---} \circ \text{---} \\ (k) \text{---} \circ \text{---} \end{array} = - \sum_{aijk} \langle ji|aj \rangle \langle ak|ik \rangle \quad \left(\begin{array}{c} l=2, \ h=3, \\ \text{asymmetric} \end{array} \right), \\
 & \begin{array}{c} (j) \\ \text{---} \circ \text{---} \\ (i) \text{---} \circ \text{---} \\ (k) \text{---} \circ \text{---} \end{array} = - \sum_{aijk} \langle ij|aj \rangle \langle ak|ki \rangle \quad \left(\begin{array}{c} l=2, \ h=3, \\ \text{asymmetric} \end{array} \right), \\
 & \begin{array}{c} (j) \\ \text{---} \circ \text{---} \\ (i) \text{---} \circ \text{---} \\ (k) \text{---} \circ \text{---} \end{array} = \sum_{aijk} \langle ji|aj \rangle \langle ak|ki \rangle \quad \left(\begin{array}{c} l=1, \ h=3, \\ \text{asymmetric} \end{array} \right), \\
 & \begin{array}{c} (i) \text{---} \circ \text{---} \text{---} \circ \text{---} (j) \\ (k) \text{---} \circ \text{---} \text{---} \circ \text{---} (l) \end{array} = \frac{1}{4} \sum_{ijkl} \langle ij|ij \rangle \langle kl|kl \rangle \quad \left(\begin{array}{c} l=4, \ h=4, \\ \text{symmetric} \end{array} \right), \\
 & \begin{array}{c} (i) \\ \text{---} \circ \text{---} \text{---} \circ \text{---} \\ (j) \\ (k) \text{---} \circ \text{---} \text{---} \circ \text{---} (l) \end{array} = -\frac{1}{4} \sum_{ijkl} \langle ij|ji \rangle \langle kl|kl \rangle \quad \left(\begin{array}{c} l=3, \ h=4, \\ \text{symmetric} \end{array} \right),
 \end{aligned}$$

$$\begin{aligned}
 & \begin{array}{c} (i) \text{---} \text{---} (j) \\ \text{---} (k) \text{---} \\ \text{---} (l) \end{array} = -\frac{1}{4} \sum_{ijkl} \langle ij|ij \rangle \langle kl|lk \rangle \quad \left(\begin{array}{l} l=3, \ h=4, \\ \text{symmetric} \end{array} \right), \\
 & \begin{array}{c} (i) \\ \text{---} (j) \text{---} \\ \text{---} (k) \text{---} \\ \text{---} (l) \end{array} = \frac{1}{4} \sum_{ijkl} \langle ij|ji \rangle \langle kl|lk \rangle \quad \left(\begin{array}{l} l=3, \ h=4, \\ \text{symmetric} \end{array} \right).
 \end{aligned}$$

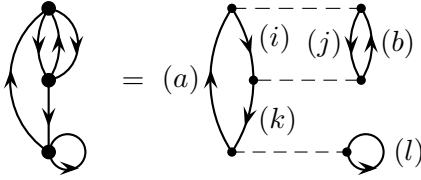
The weight factor $\frac{1}{4}$ for the last four diagrams arises from the factor $\frac{1}{2}$ for each of the two symmetric unlinked parts in each diagram. These unlinked diagrams have a *vacuum gap*, i.e., a Fermi vacuum intermediate state. Such diagrams are excluded from perturbation theory sums since the primed sums in perturbation theory exclude the reference state. As will be shown in Chapter 5, other unlinked diagrams also disappear from these sums because of cancellation with renormalization terms.

In the Hugenholtz and ASG representations the above eight Goldstone diagrams are replaced by just two diagrams, one for the four linked and one for the four unlinked Goldstone diagrams:

$$\begin{aligned}
 & \begin{array}{c} \text{---} \\ \text{---} \\ \text{---} \end{array} = \begin{array}{c} (a) \text{---} (j) \\ \text{---} (i) \text{---} \\ \text{---} (k) \end{array} = \sum_{aijk} \langle ij|aj \rangle \langle ak|ik \rangle \quad \left(\begin{array}{l} l=3 \\ h=3 \\ n=0 \end{array} \right), \\
 & \begin{array}{c} \text{---} \\ \text{---} \end{array} = \begin{array}{c} (i) \text{---} (j) \\ \text{---} (k) \text{---} (l) \end{array} = \frac{1}{4} \sum_{ijkl} \langle ij|ij \rangle \langle kl|kl \rangle \quad \left(\begin{array}{l} l=4 \\ h=4 \\ n=2 \end{array} \right).
 \end{aligned}$$

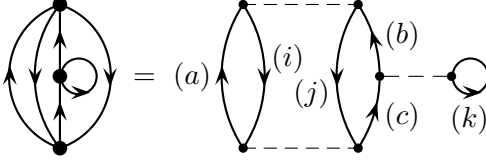
Finally, we give the non-normal-product terms for $\langle 0|\hat{V}_2^3|0\rangle$, in the Hugenholtz and ASG forms only:

$$\begin{aligned}
 & \begin{array}{c} \text{---} \\ \text{---} \\ \text{---} \end{array} = \begin{array}{c} (a) \text{---} (j) \text{---} (b) \\ \text{---} (i) \text{---} \text{---} (c) \text{---} (k) \end{array} = \frac{1}{2} \sum_{abcijk} \langle ij|ab \rangle \langle ab|cj \rangle \langle ck|ik \rangle \\
 & \quad (l=3, \ h=3, \ n=1),
 \end{aligned}$$



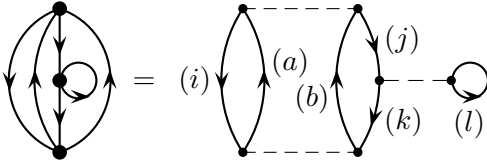
$$= -\frac{1}{2} \sum_{abijkl} \langle ij \| ab \rangle \langle kb \| ij \rangle \langle al \| kl \rangle$$

$(l = 3, h = 4, n = 1),$



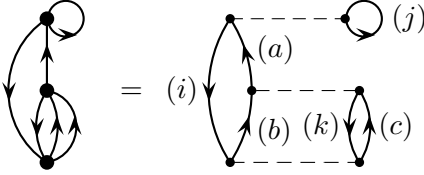
$$= \frac{1}{2} \sum_{abcijk} \langle ij \| ab \rangle \langle bk \| ck \rangle \langle ac \| ij \rangle$$

$(l = 3, h = 3, n = 1),$



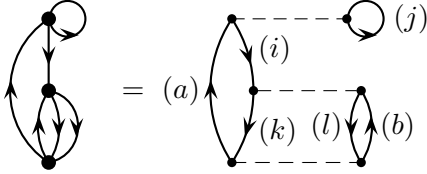
$$= -\frac{1}{2} \sum_{abijkl} \langle ij \| ab \rangle \langle kl \| jl \rangle \langle ab \| ik \rangle$$

$(l = 3, h = 4, n = 1),$



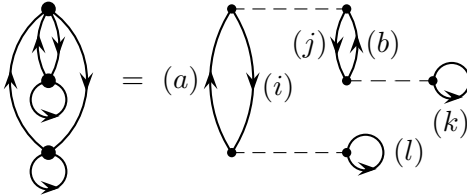
$$= \frac{1}{2} \sum_{abcijk} \langle ij \| aj \rangle \langle ak \| bc \rangle \langle bc \| ik \rangle$$

$(l = 3, h = 3, n = 1),$



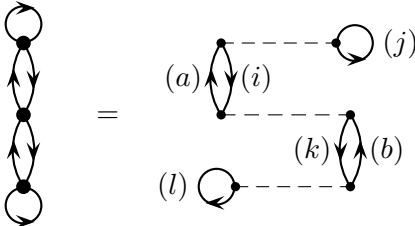
$$= -\frac{1}{2} \sum_{abijkl} \langle ij \| aj \rangle \langle kl \| ib \rangle \langle ab \| kl \rangle$$

$(l = 3, h = 4, n = 1),$



$$= \sum_{abijkl} \langle ij \| ab \rangle \langle bk \| jk \rangle \langle al \| il \rangle$$

$(l = 4, h = 4, n = 0),$



$$= \sum_{abijkl} \langle ij \| aj \rangle \langle ak \| ib \rangle \langle lb \| lk \rangle$$

$(l = 4, h = 4, n = 0),$

$$\begin{aligned}
 & \text{Diagram 1} = (a) \begin{array}{c} \text{Diagram 2} \\ \text{Diagram 3} \end{array} = \sum_{abijkl} \langle ij \| aj \rangle \langle kl \| bl \rangle \langle ab \| ik \rangle \\
 & (l = 4, h = 4, n = 0),
 \end{aligned}$$

$$\begin{aligned}
 & \text{Diagram 4} = (i) \begin{array}{c} \text{Diagram 5} \\ \text{Diagram 6} \end{array} = \sum_{abijkl} \langle ij \| aj \rangle \langle ak \| bk \rangle \langle bl \| il \rangle \\
 & (l = 4, h = 4, n = 0),
 \end{aligned}$$

$$\begin{aligned}
 & \text{Diagram 7} = (a) \begin{array}{c} \text{Diagram 8} \\ \text{Diagram 9} \end{array} = - \sum_{aijklm} \langle ij \| aj \rangle \langle lk \| ik \rangle \langle am \| lm \rangle \\
 & (l = 4, h = 5, n = 0),
 \end{aligned}$$

$$\begin{aligned}
 & \text{Diagram 10} = \begin{array}{c} \text{Diagram 11} \\ \text{Diagram 12} \end{array} = \frac{1}{8} \sum_{abijkl} \langle ij \| ab \rangle \langle ab \| ij \rangle \langle kl \| kl \rangle \\
 & (l = 4, h = 4, n = 3),
 \end{aligned}$$

$$\begin{aligned}
 & \text{Diagram 13} = (a) \begin{array}{c} \text{Diagram 14} \\ \text{Diagram 15} \end{array} = \frac{1}{8} \sum_{abijkl} \langle ij \| ab \rangle \langle kl \| kl \rangle \langle ab \| ij \rangle \\
 & (l = 4, h = 4, n = 3),
 \end{aligned}$$

$$\begin{aligned}
 & \text{Diagram 16} = \begin{array}{c} \text{Diagram 17} \\ \text{Diagram 18} \end{array} = \frac{1}{8} \sum_{abijkl} \langle ij \| ij \rangle \langle kl \| ab \rangle \langle ab \| kl \rangle \\
 & (l = 4, h = 4, n = 3),
 \end{aligned}$$

$$\begin{aligned}
 & \text{Diagram 19} = \begin{array}{c} \text{Diagram 20} \\ \text{Diagram 21} \end{array} = \frac{1}{2} \sum_{aijklm} \langle ij \| aj \rangle \langle ak \| ik \rangle \langle lm \| lm \rangle \\
 & (l = 5, h = 5, n = 1),
 \end{aligned}$$

$$\begin{aligned}
 & \text{Diagram 1} = (a) \begin{array}{c} \text{Diagram 2} \\ \text{Diagram 3} \end{array} = \frac{1}{2} \sum_{aijklm} \langle ij \| aj \rangle \langle kl \| kl \rangle \langle am \| im \rangle \\
 & \quad (l = 5, h = 5, n = 1), \\
 & \text{Diagram 4} = \begin{array}{c} (i) \text{Diagram 5} \\ (a) \text{Diagram 6} \end{array} = \frac{1}{2} \sum_{aijklm} \langle ij \| ij \rangle \langle kl \| al \rangle \langle am \| km \rangle \\
 & \quad (l = 5, h = 5, n = 1), \\
 & \text{Diagram 7} = (i) \text{Diagram 8} \\
 & \text{Diagram 9} = (k) \text{Diagram 10} = \frac{1}{8} \sum_{ijklmn} \langle ij \| ij \rangle \langle kl \| kl \rangle \langle mn \| mn \rangle \\
 & \quad (l = 6, h = 6, n = 3), \\
 & \text{Diagram 11} = (m) \text{Diagram 12}
 \end{aligned}$$

The last seven of these diagrams are unlinked. All 18 diagrams, taken together, represent the difference between $\langle 0 | \hat{V}_2^3 | 0 \rangle$ and the normal-product matrix element $\langle 0 | (\hat{V}_2)_N^3 | 0 \rangle$. The last diagram represents $\langle 0 | \hat{V}_2 | 0 \rangle^3$, while the others represent contributions involving the \hat{V}'_N operator of (3.178) and/or powers of $\langle 0 | \hat{V}_2 | 0 \rangle$. As will be seen in Chapter 5, all the unlinked diagrams will not contribute to the perturbation treatment and will not need to be considered.

4.4.6 The RSPT perturbation operator

As we saw in subsection 3.6.3, the normal-product perturbation operator $\hat{V}_N = \hat{V} - \langle 0 | \hat{V} | 0 \rangle$ can be written in the form

$$\begin{aligned}
 \hat{V}_N &= \hat{F}_N^o + \hat{W}_N \\
 &= \sum_{pq} f_{pq}^o + \frac{1}{4} \sum_{pqrs} \langle pq \| rs \rangle \{ \hat{p}^\dagger \hat{q}^\dagger \hat{s} \hat{r} \}, \quad (4.41)
 \end{aligned}$$

where we have used the cancellation between \hat{U}_N and \hat{V}'_N that arises from the choice $u_{pq} = -\sum_i \langle pi \| qi \rangle$. The one-electron part is represented diagrammatically by the $\blacktriangleright - \times$ vertex, while the two-electron part is represented by the standard two-body vertex. In the canonical Hartree–Fock case \hat{F}_N^o vanishes, and we are left with $\hat{W}_N = \hat{W}$ as the sole perturbation. In non-canonical Hartree–Fock the matrix elements f_{ia}, f_{ai} connecting hole states

with particle states also vanish, so that the one-electron perturbation operator has the diagrammatic expansion

$$\hat{F}_N^o = \begin{array}{c} \uparrow \\ | \\ \bullet \\ | \\ \uparrow \end{array} \text{---} \times + \begin{array}{c} \downarrow \\ | \\ \bullet \\ | \\ \downarrow \end{array} \text{---} \times \quad (\text{noncanonical HF}). \quad (4.42)$$

In the general (non-HF) case, the full expansion is required,

$$\hat{F}_N^o = \begin{array}{c} \uparrow \\ | \\ \bullet \\ | \\ \uparrow \end{array} \text{---} \times + \begin{array}{c} \downarrow \\ | \\ \bullet \\ | \\ \downarrow \end{array} \text{---} \times + \begin{array}{c} \swarrow \searrow \\ | \\ \bullet \\ | \\ \swarrow \searrow \end{array} \text{---} \times + \begin{array}{c} \swarrow \searrow \\ | \\ \bullet \\ | \\ \swarrow \searrow \end{array} \text{---} \times \quad (\text{general case}). \quad (4.43)$$

Even in the non-HF case it is possible to simplify the expansion of \hat{F}_N^o by performing a *semicanonical transformation* of the orbitals (Handy, Pople, Head-Gordon *et al.* 1989), which diagonalizes the hole-hole and particle-particle blocks of \hat{F} separately (leaving the reference function invariant), thus eliminating the first two diagrams in Eq. (4.43). This is the form of the partitioned Hamiltonian used in generalized MBPT (Bartlett 1995), to be discussed in Section 12.3.

More generally, the $\begin{array}{c} \swarrow \searrow \\ | \\ \bullet \\ | \\ \swarrow \searrow \end{array} \text{---} \times$ vertex represents the \hat{f}' operator of (3.135), which is equal to \hat{f}^o only if $\varepsilon_p = f_{pp}$ holds for all p .

5

Diagrammatic expansions for perturbation theory

5.1 Resolvent operator and denominators

In order to represent diagrammatically the various terms in the perturbation expansions for the energy and wave function, we need a diagrammatic representation of the resolvent \hat{R}_0 . We note that

$$\hat{R}_0 = \frac{\hat{Q}}{E_0^{(0)} - \hat{H}_0} = \sum_I' \frac{|\Phi_I\rangle\langle\Phi_I|}{E_0^{(0)} - E_I^{(0)}}, \quad (5.1)$$

the sum being over all states $|I\rangle \equiv |\Phi_I\rangle$ different from $|0\rangle$. When \hat{R}_0 operates on any state $|J\rangle$ other than $|0\rangle$ the result is

$$\hat{R}_0|J\rangle = \sum_I' \frac{|I\rangle\langle I|J\rangle}{E_0^{(0)} - E_I^{(0)}} = \sum_I' |I\rangle \frac{\delta_{IJ}}{E_0^{(0)} - E_I^{(0)}} = |J\rangle \frac{1}{E_0^{(0)} - E_J^{(0)}}. \quad (5.2)$$

Thus \hat{R}_0 does not change the state on which it operates, except for division by the energy denominator, and any particle or hole lines present below the point of action of \hat{R}_0 continue unchanged above it. This can be represented symbolically as follows:

$$\begin{array}{c} |\Phi_{ij\dots}^{ab\dots}\rangle \\ \hat{R}_0 \\ |\Phi_{ij\dots}^{ab\dots}\rangle \end{array} \begin{array}{c} \uparrow a \quad \downarrow i \quad \uparrow b \quad \downarrow j \quad \dots \\ \hline \uparrow a \quad \downarrow i \quad \uparrow b \quad \downarrow j \quad \dots \end{array} = \frac{|\Phi_{ij\dots}^{ab\dots}\rangle}{\varepsilon_{ij\dots}^{ab\dots}}, \quad (5.3)$$

where the energy denominator

$$\varepsilon_{ij\dots}^{ab\dots} = E_0^{(0)} - E_{|\Phi_{ij\dots}^{ab\dots}\rangle}^{(0)} = \varepsilon_i + \varepsilon_j + \dots - \varepsilon_a - \varepsilon_b - \dots, \quad (5.4)$$

is equal to the sum of the orbital energies of the hole lines crossed by the R_0 line minus those of the particle lines crossed by the \hat{R}_0 line. The only

exception to this result is $\hat{R}_0|0\rangle = 0$, so that we have no terms in which the resolvent line goes through a *vacuum gap*, as in

$$\hat{R}_0 \frac{\text{diagram with two vertical loops connected by two horizontal lines}}{\text{diagram with two vertical loops connected by two horizontal lines}} .$$

The convention is to omit the resolvent lines, it being understood that an energy denominator is to be read off the diagram between each successive pair of vertices. In wave function diagrams, which are open at the top, an additional resolvent line is implied above the highest vertex. We shall show the resolvent lines explicitly in some cases for pedagogical reasons.

5.2 First-order energy

The zero- and first-order energies (see Section 3.5) are given by

$$E^{(0)} = \sum_i \varepsilon_i, \quad (5.5)$$

$$E^{(1)} = \langle 0|\hat{V}|0\rangle = -\frac{1}{2} \sum_{ij} \langle ij||ij\rangle = - \text{diagram with two vertices connected by a horizontal line and each having a self-loop} \quad (5.6)$$

(using the ASG representation) and, of course, $E_{\text{ref}} = E^{(0)} + E^{(1)}$. More generally, if $\varepsilon_p = f_{pp}$ is not assumed, we have (see (3.186))

$$E^{(1)} = \sum_i f'_{ii} - \frac{1}{2} \sum_{ij} \langle ij||ij\rangle = \text{diagram with one vertex and a self-loop} - \text{diagram with two vertices connected by a horizontal line and each having a self-loop} \quad (5.7)$$

using the $\text{diagram with one vertex and a self-loop} - \times$ vertex to represent the \hat{f}' operator of (3.135).

5.3 Second-order energy

The correlation energy begins with second order, in the form (see (2.137))

$$E^{(2)} = \langle 0|\hat{V}\hat{R}_0\hat{V}|0\rangle = \langle 0|\hat{W}\hat{R}_0\hat{W}|0\rangle, \quad (5.8)$$

where we have used $\hat{W} = \hat{V} - \langle 0|\hat{V}|0\rangle$, as in Chapter 2, rather than the $\hat{W} = \hat{W}_N$ of Chapter 4. In the canonical Hartree–Fock case the two usages of \hat{W} are equivalent; otherwise, the \hat{W} in (5.8) includes a one-electron term, \hat{F}_N^0 . The equivalence of the two forms in (5.8) follows from $\hat{R}_0\hat{V}|0\rangle = \hat{R}_0\hat{W}|0\rangle$, because $\hat{R}_0|0\rangle = 0$.

The diagrammatic representation of the second-order energy $\langle 0|\hat{W}\hat{R}_0\hat{W}|0\rangle$ is very similar to that of $\langle 0|\hat{W}^2|0\rangle$, except for the addition of the resolvent

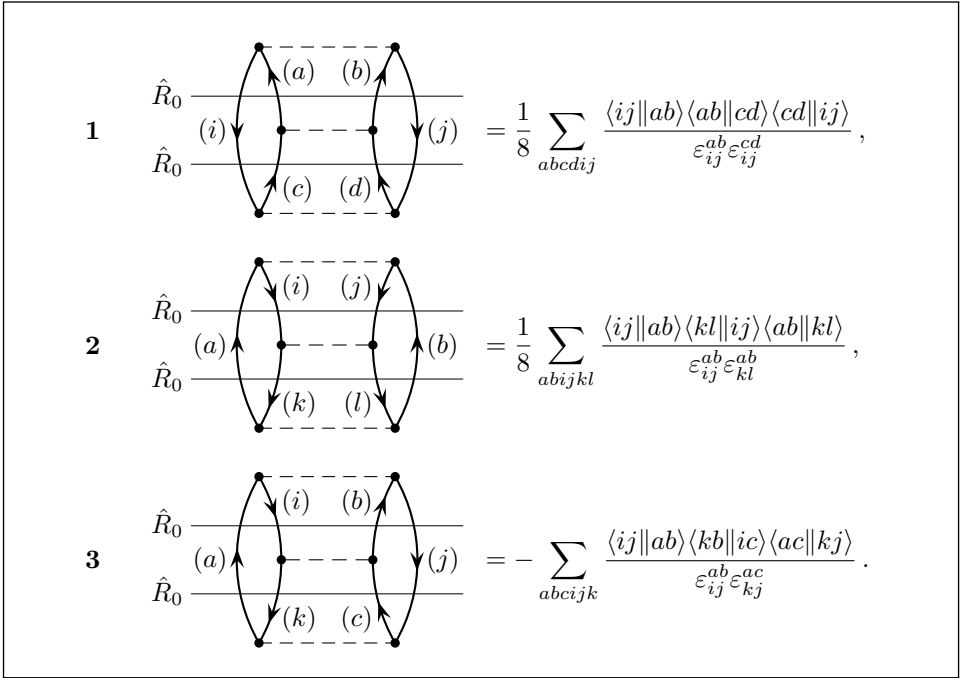


Fig. 5.1. Canonical HF-case ASG diagrams for the third-order energy.

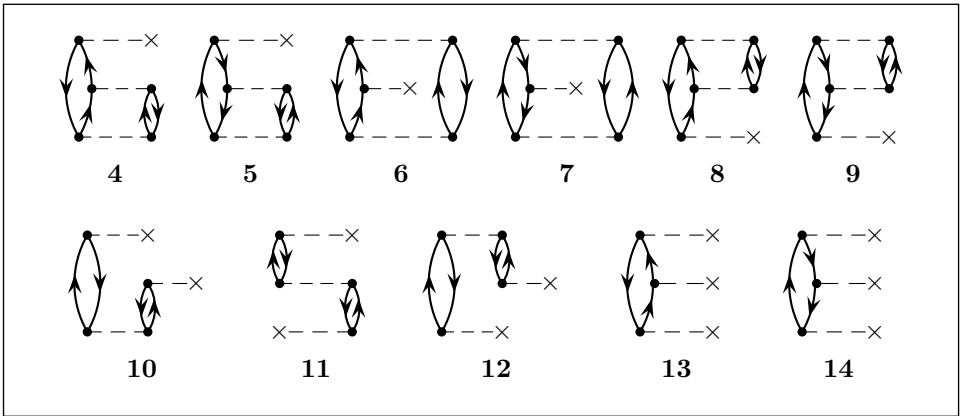


Fig. 5.2. Non-HF ASG diagrams for the third-order energy.

do not involve particle-hole one-electron integrals (such as $\langle a|\hat{f}|i \rangle$ or $\langle i|\hat{f}|a \rangle$) and contribute also in the noncanonical HF case; they involve doubly excited intermediate states only. The other diagrams contribute in the non-HF case only and involve some singly excited intermediate states.

The advantages of the Hartree–Fock case in simplifying the formalism seem obvious, but in fact have little computational significance beyond the proliferation of terms. The above non-HF diagrams have between three and five summation indices each, compared with six indices for the three HF-case diagrams, and thus require significantly less computational effort.

5.5 Conjugate diagrams

An interesting diagram symmetry operation consists of turning a diagram upside down (*time reversal*) followed by reversal of all arrow directions (*particle-hole inversion*) (Paldus and Čížek 1974). After these two operations each particle or hole line of the original diagram is again a particle or hole line, respectively, in its new position in the new diagram. The diagram resulting from this transformation (in any of its equivalent forms) is said to be *conjugate* to the original diagram.

An example of a pair of conjugate diagrams is given by the non-HF third-order energy diagrams 4 and 8 in Fig. 5.2. By carrying the original dummy summation label with each line to its new position in the transformed diagram, it is easy to see that the effect of the transformation on the algebraic interpretation of the diagram is an interchange of the bra and ket indices in each integral with no change in the values of the denominator or the numerical coefficient:

$$\begin{aligned}
 & \begin{array}{c} \text{Diagram 4: A third-order energy diagram with two horizontal lines labeled } \hat{R}_0. \text{ It features two vertical loops. The left loop has an upward arrow labeled } (a) \text{ and a downward arrow labeled } (i). \text{ The right loop has an upward arrow labeled } (b) \text{ and a downward arrow labeled } (j). \text{ Dashed lines connect the vertices of the loops.} \end{array} \\
 &= \frac{1}{2} \sum_{abci j} \frac{\langle i | \hat{f} | a \rangle \langle a j | bc \rangle \langle bc | i j \rangle}{\varepsilon_i^a \varepsilon_{ij}^{bc}}, \\
 & \begin{array}{c} \text{Diagram 8: The conjugate of Diagram 4, obtained by time reversal and particle-hole inversion. It has the same structure but with arrows reversed: the left loop has a downward arrow labeled } (i) \text{ and an upward arrow labeled } (a), \text{ and the right loop has a downward arrow labeled } (j) \text{ and an upward arrow labeled } (b). \end{array} \\
 &= \frac{1}{2} \sum_{abci j} \frac{\langle i j | bc \rangle \langle bc | a j \rangle \langle a | \hat{f} | i \rangle}{\varepsilon_{ij}^{bc} \varepsilon_i^a}.
 \end{aligned} \tag{5.13}$$

Consequently, the numerical values of the two diagrams are the complex conjugates of each other.

Each MBPT energy diagram is either *self-conjugate* (i.e. *Hermitian*), in which case its value is necessarily real, or conjugate to another energy diagram of the same order, in which case the sum of the two diagrams is equal to twice the real part of the value of either. Thus it is enough to evaluate just one of each pair of conjugate diagrams, taking twice the real part of its value as the total value of the pair.

The three HF-case diagrams for the third-order energy, Fig. 5.1, are all self-conjugate. Among the non-HF third-order diagrams, Fig. 5.2, the pairs 4 and 8, 5 and 9 and 10 and 12 are mutually conjugate, while the rest are self-conjugate. We shall see many more examples of conjugate diagrams in the fourth-order energy.

5.6 Wave-function diagrams

5.6.1 First-order wave function

Before proceeding to higher orders for the energy, we will digress to look at the diagrammatic representation of the wave function.

The first-order wave function is given by (2.133),

$$|\Psi^{(1)}\rangle = \hat{R}_0 \hat{W} |0\rangle, \quad (5.14)$$

where, in the sense of Chapter 2, we have used $\hat{W} = \hat{V} - \langle 0 | \hat{V} | 0 \rangle$. In the Hartree–Fock case this is the same as the two-electron normal-product operator \hat{W}_N and we have just one diagram, representing double-excitation contributions:

$$|\Psi^{(1)}\rangle = \hat{R}_0 \begin{array}{c} \text{(a)} \quad \text{(i)} \quad \text{(j)} \quad \text{(b)} \\ \text{Diagram: A horizontal line with two vertices. From each vertex, two lines go upwards to dashed loops. The left loop is labeled (a) and (i), and the right loop is labeled (j) and (b).} \end{array} = \frac{1}{4} \sum_{abij} \frac{\langle ab || ij \rangle}{\varepsilon_{ij}^{ab}} |\Phi_{ij}^{ab}\rangle. \quad (5.15)$$

For the purpose of counting loops we consider the open lines to be paired at the top according to the pairing pattern in the corresponding slater determinant, $|\Phi_{ij}^{ab}\rangle$ in this case, thus forming two *quasi-loops*. In regard to the determination of the weight factor, two unlabeled open lines are considered equivalent if they both begin at the same vertex or both end at the same vertex. The diagram in (5.15) has two quasi-loops, two hole lines and two pairs of equivalent lines, hence the factor $\frac{1}{4}$ (as usual the labels in parentheses are included only as a convenience to identify dummy summation indices in the corresponding algebraic expression, and all lines in this diagram are to be taken as unlabeled). As stated in Section 5.1, according to the convention one omits the resolvent line, with the understanding that in open diagrams

there is one such line above the highest vertex as well as between each pair of successive vertices.

In the non-HF case we need to include a one-electron vertex, leading to the additional diagram

$$\hat{R}_0 \begin{array}{c} \text{(a)} \nearrow \\ \text{(i)} \searrow \\ \bullet \text{---} \text{---} \times \end{array} = \sum_{ai} \frac{\langle a | \hat{f} | i \rangle}{\varepsilon_i^a} |\Phi_i^a\rangle \quad (5.16)$$

(since $f_{ai} = f_{ai}^o$ because a and i cannot be equal) which adds contributions from singly excited states. Here we have one quasiloop, one hole line and no equivalent lines, hence the factor $+1$. This diagram does not contribute in the noncanonical Hartree–Fock case because the f_{ai} integrals vanish in that case. Equation (5.16) still holds in the more general case in which \hat{f}' , (3.135), replaces \hat{f}^o because we have $f'_{ai} = f_{ai}^o$.

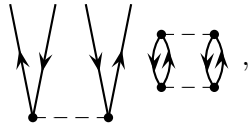
5.6.2 Second-order wave function

The second-order wave function is given by (2.134),

$$|\Psi^{(2)}\rangle = \hat{R}_0 \hat{W} \hat{R}_0 \hat{W} |0\rangle. \quad (5.17)$$

In the canonical HF case we have eight ASG diagrams, shown with their algebraic interpretation in Fig. 5.3. The first three diagrams represent doubly excited final states; they are followed by two singles, two triples and one quadruple.

The quadruple-excitation diagram 8 is an example of a *disconnected* diagram. As the name implies, such a diagram has two or more disconnected parts. If any part of a disconnected diagram is closed, i.e. has no open lines, as in



then the diagram is called *unlinked*. It will be shown later that unlinked diagrams cancel with the renormalization terms while *linked* disconnected diagrams remain in the wave function expansion. The second-order wave function expression has no renormalization terms, and no unlinked diagrams appear.

The non-HF contributions to $|\Psi^{(2)}\rangle$ are represented by the eleven diagrams in Fig. 5.4, which include five double excitations (9–12 and 19), four singles (13, 14, 17, 18) and two triples (15, 16). Diagrams 9 and 10 contribute in

$$\begin{aligned}
1 \quad & \begin{array}{c} \text{Diagram 1: Two vertical lines. Left line has incoming arrow (i) at bottom and outgoing arrow (a) at top. Right line has incoming arrow (j) at bottom and outgoing arrow (b) at top. A dashed horizontal line connects the two lines between two dots. The bottom dots are connected by a dashed line. The top dots are connected by a dashed line. The left dot is also connected to the right dot by a dashed line.} \end{array} = \frac{1}{8} \sum_{abcdij} \frac{\langle ab||cd \rangle \langle cd||ij \rangle}{\varepsilon_{ij}^{ab} \varepsilon_{ij}^{cd}} |\Phi_{ij}^{ab}\rangle, \\
2 \quad & \begin{array}{c} \text{Diagram 2: Two vertical lines. Left line has incoming arrow (a) at bottom and outgoing arrow (i) at top. Right line has incoming arrow (b) at bottom and outgoing arrow (j) at top. A dashed horizontal line connects the two lines between two dots. The bottom dots are connected by a dashed line. The top dots are connected by a dashed line. The left dot is also connected to the right dot by a dashed line.} \end{array} = \frac{1}{8} \sum_{abijkl} \frac{\langle kl||ij \rangle \langle ab||kl \rangle}{\varepsilon_{ij}^{ab} \varepsilon_{kl}^{ab}} |\Phi_{ij}^{ab}\rangle, \\
3 \quad & \begin{array}{c} \text{Diagram 3: Two vertical lines. Left line has incoming arrow (i) at bottom and outgoing arrow (a) at top. Right line has incoming arrow (b) at bottom and outgoing arrow (j) at top. A dashed horizontal line connects the two lines between two dots. The bottom dots are connected by a dashed line. The top dots are connected by a dashed line. The left dot is also connected to the right dot by a dashed line.} \end{array} = - \sum_{abcijk} \frac{\langle ak||cj \rangle \langle cb||ik \rangle}{\varepsilon_{ij}^{ab} \varepsilon_{ik}^{bc}} |\Phi_{ij}^{ab}\rangle, \\
4 \quad & \begin{array}{c} \text{Diagram 4: Two vertical lines. Left line has incoming arrow (i) at bottom and outgoing arrow (a) at top. Right line has incoming arrow (j) at bottom and outgoing arrow (b) at top. A dashed horizontal line connects the two lines between two dots. The bottom dots are connected by a dashed line. The top dots are connected by a dashed line. The left dot is also connected to the right dot by a dashed line.} \end{array} = \frac{1}{2} \sum_{abcij} \frac{\langle aj||cb \rangle \langle cb||ij \rangle}{\varepsilon_i^a \varepsilon_{ij}^{cb}} |\Phi_i^a\rangle, \\
5 \quad & \begin{array}{c} \text{Diagram 5: Two vertical lines. Left line has incoming arrow (a) at bottom and outgoing arrow (i) at top. Right line has incoming arrow (b) at bottom and outgoing arrow (j) at top. A dashed horizontal line connects the two lines between two dots. The bottom dots are connected by a dashed line. The top dots are connected by a dashed line. The left dot is also connected to the right dot by a dashed line.} \end{array} = -\frac{1}{2} \sum_{abijk} \frac{\langle kj||ib \rangle \langle ab||kj \rangle}{\varepsilon_i^a \varepsilon_{kj}^{ab}} |\Phi_i^a\rangle, \\
6 \quad & \begin{array}{c} \text{Diagram 6: Two vertical lines. Left line has incoming arrow (a) at bottom and outgoing arrow (i) at top. Right line has incoming arrow (j) at bottom and outgoing arrow (b) at top. A dashed horizontal line connects the two lines between two dots. The bottom dots are connected by a dashed line. The top dots are connected by a dashed line. The left dot is also connected to the right dot by a dashed line.} \end{array} = \frac{1}{4} \sum_{abcdijk} \frac{\langle bc||dk \rangle \langle ad||ij \rangle}{\varepsilon_{ijk}^{abc} \varepsilon_{ij}^{ad}} |\Phi_{ijk}^{abc}\rangle, \\
7 \quad & \begin{array}{c} \text{Diagram 7: Two vertical lines. Left line has incoming arrow (i) at bottom and outgoing arrow (a) at top. Right line has incoming arrow (b) at bottom and outgoing arrow (j) at top. A dashed horizontal line connects the two lines between two dots. The bottom dots are connected by a dashed line. The top dots are connected by a dashed line. The left dot is also connected to the right dot by a dashed line.} \end{array} = -\frac{1}{4} \sum_{abcijkl} \frac{\langle lc||jk \rangle \langle ab||il \rangle}{\varepsilon_{ijk}^{abc} \varepsilon_{il}^{ab}} |\Phi_{ijk}^{abc}\rangle, \\
8 \quad & \begin{array}{c} \text{Diagram 8: Two vertical lines. Left line has incoming arrow (a) at bottom and outgoing arrow (i) at top. Right line has incoming arrow (j) at bottom and outgoing arrow (b) at top. A dashed horizontal line connects the two lines between two dots. The bottom dots are connected by a dashed line. The top dots are connected by a dashed line. The left dot is also connected to the right dot by a dashed line.} \end{array} = \frac{1}{16} \sum_{abcdijkl} \frac{\langle cd||kl \rangle \langle ab||ij \rangle}{\varepsilon_{ijkl}^{abcd} \varepsilon_{ij}^{ab}} |\Phi_{ijkl}^{abcd}\rangle.
\end{aligned}$$

Fig. 5.3. Canonical HF-case ASG diagrams for the second-order wave function.

the noncanonical HF case but diagrams 11–19 do not because they involve integrals of the form $\langle a|\hat{f}|i \rangle$ or $\langle i|\hat{f}|a \rangle$, which vanish in this case. Diagrams 15, 16 and 19 are disconnected but not unlinked and are legitimate parts of the wave-function expansion.

As will be shown in Section 9.4, all disconnected wave-function diagrams can be re-expressed as products of connected wave-function diagrams each consisting of one of their disconnected parts. This factorization is at the

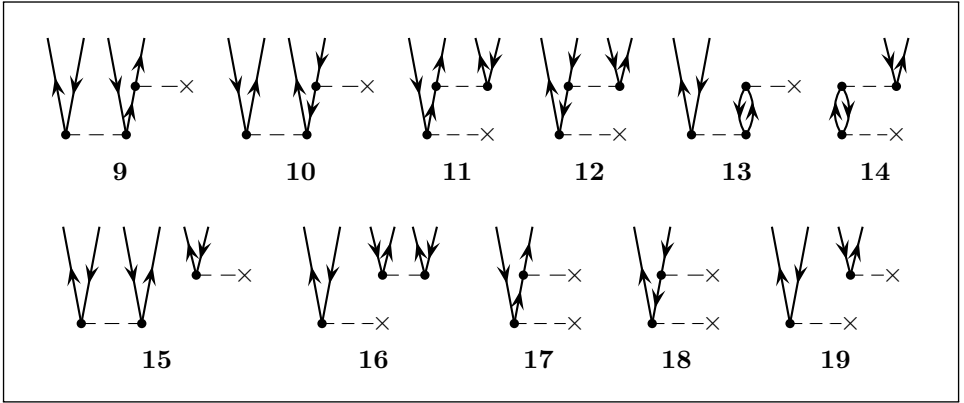


Fig. 5.4. non-HF ASG diagrams for the second-order wave function.

heart of the exponential *Ansatz* of coupled-cluster theory (Chapter 9). As an example we consider diagrams 15 and 16 of Fig. 5.4. These diagrams have equal numerators but, because of the different time sequences of the vertices, their denominators are different. Combining their denominator factors we get

$$\frac{1}{\varepsilon_{ijk}^{abc}\varepsilon_{ij}^{ab}} + \frac{1}{\varepsilon_{ijk}^{abc}\varepsilon_k^c} = \frac{1}{\varepsilon_{ijk}^{abc}} \left(\frac{1}{\varepsilon_{ij}^{ab}} + \frac{1}{\varepsilon_k^c} \right) = \frac{1}{\varepsilon_{ijk}^{abc}} \frac{\varepsilon_k^c + \varepsilon_{ij}^{ab}}{\varepsilon_{ij}^{ab}\varepsilon_k^c} = \frac{1}{\varepsilon_{ij}^{ab}\varepsilon_k^c}$$

because $\varepsilon_k^c + \varepsilon_{ij}^{ab} = \varepsilon_{ijk}^{abc}$. Thus the sum of these two second-order diagrams can be factored into a product of two independent sums corresponding to their two first-order disconnected parts:

$$\begin{array}{c} \text{Diagram 15} \end{array} - \times + \begin{array}{c} \text{Diagram 16} \end{array} - \times = \begin{array}{c} \text{Diagram 15} \end{array} \times \begin{array}{c} \text{Diagram 16} \end{array} - \times \quad (5.18)$$

(note that the upper cross on the r.h.s. of (5.18) is a multiplication sign). This is an example of a type of factorization that is very common in MBPT, and other examples will be seen in the discussion below of the fourth-order energy and in Chapters 6 and 7.

5.7 Fourth-order energy

5.7.1 Energy formula

Now we return to the energy expansion and look at $E^{(4)}$, (2.139), where new features will appear for the first time. This is the first case in which we have

a renormalization term. We have

$$\begin{aligned}
 E^{(4)} &= \langle 0 | \hat{W} \hat{R}_0 \hat{W} \hat{R}_0 \hat{W} \hat{R}_0 \hat{W} | 0 \rangle - E^{(2)} \langle \Psi^{(1)} | \Psi^{(1)} \rangle \\
 &= \langle 0 | \hat{W} \hat{R}_0 \hat{W} \hat{R}_0 \hat{W} \hat{R}_0 \hat{W} | 0 \rangle - \langle 0 | \hat{W} \hat{R}_0 \hat{W} | 0 \rangle \langle 0 | \hat{W} \hat{R}_0^2 \hat{W} | 0 \rangle \\
 &= \langle 0 | \hat{W} \hat{R}_0 \hat{W} \hat{R}_0 \hat{W} \hat{R}_0 \hat{W} | 0 \rangle - \langle 0 | \hat{W} \hat{R}_0 \langle 0 | \hat{W} \hat{R}_0 \hat{W} | 0 \rangle \hat{R}_0 \hat{W} | 0 \rangle, \quad (5.19)
 \end{aligned}$$

using $|\Psi^{(1)}\rangle = \hat{R}_0 \hat{W} | 0 \rangle$ and $E^{(2)} = \langle 0 | \hat{W} \hat{R}_0 \hat{W} | 0 \rangle$. In the last line of the equation the $E^{(2)}$ expression has been inserted between the two \hat{R}_0 operators in \hat{R}_0^2 (which derived from $\langle \Psi^{(1)} | \Psi^{(1)} \rangle$), showing the *bracket insertion* form of the renormalization term.

In the derivation of the diagrammatic expression for the principal term of $E^{(4)}$ we shall find some *unlinked diagrams* (diagrams that have disconnected closed parts) and will show that these exactly cancel the renormalization term. The *linked-diagram theorem*, to be proved in Chapter 6, generalizes this result to all orders, for both the energy and the wave function, so that the final expressions are sums of linked diagrams only. The bracket insertion form of the renormalization terms will help in demonstrating this cancellation.

5.7.2 Diagrams for $E^{(4)}$ in the canonical HF case

We shall now derive the diagrams that describe the principal term of the fourth-order energy. The renormalization term will be discussed in subsection 5.7.4, where it will be shown that it cancels with the unlinked diagrams of the principal term. The canonical HF case is discussed in the present subsection, and the additional diagrams for other cases are derived in subsection 5.7.3. Because of the greater complexity when dealing with four vertices, and in order to avoid missing some terms or including redundant equivalent terms, we shall follow the procedure outlined in subsection 4.4.4 and begin by listing all Hugenholtz skeletons.

To facilitate systematic generation of the Hugenholtz skeletons for the principal term of $E^{(4)}$, we classify them according to their connection patterns, using the designation k - l - m to describe a skeleton (or diagram) in which the top vertex is connected by k lines to the second vertex (counting from the top), l lines to the third vertex and m lines to the bottom vertex. Since we are dealing with the canonical HF case, each vertex must have four connecting lines, so $k + l + m = 4$. The same requirement of four lines at each vertex determines the remaining connections that do not involve the top vertex. The resulting 15 skeletons are shown in Fig. 5.5. Three of these skeletons (4-0-0, 0-4-0, 0-0-4) are unlinked. The first unlinked skeleton has

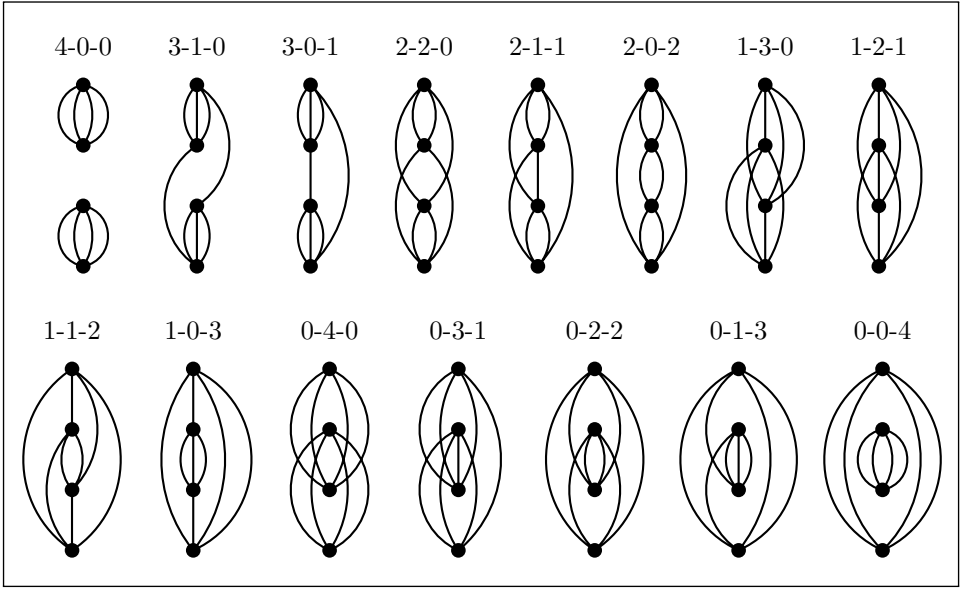
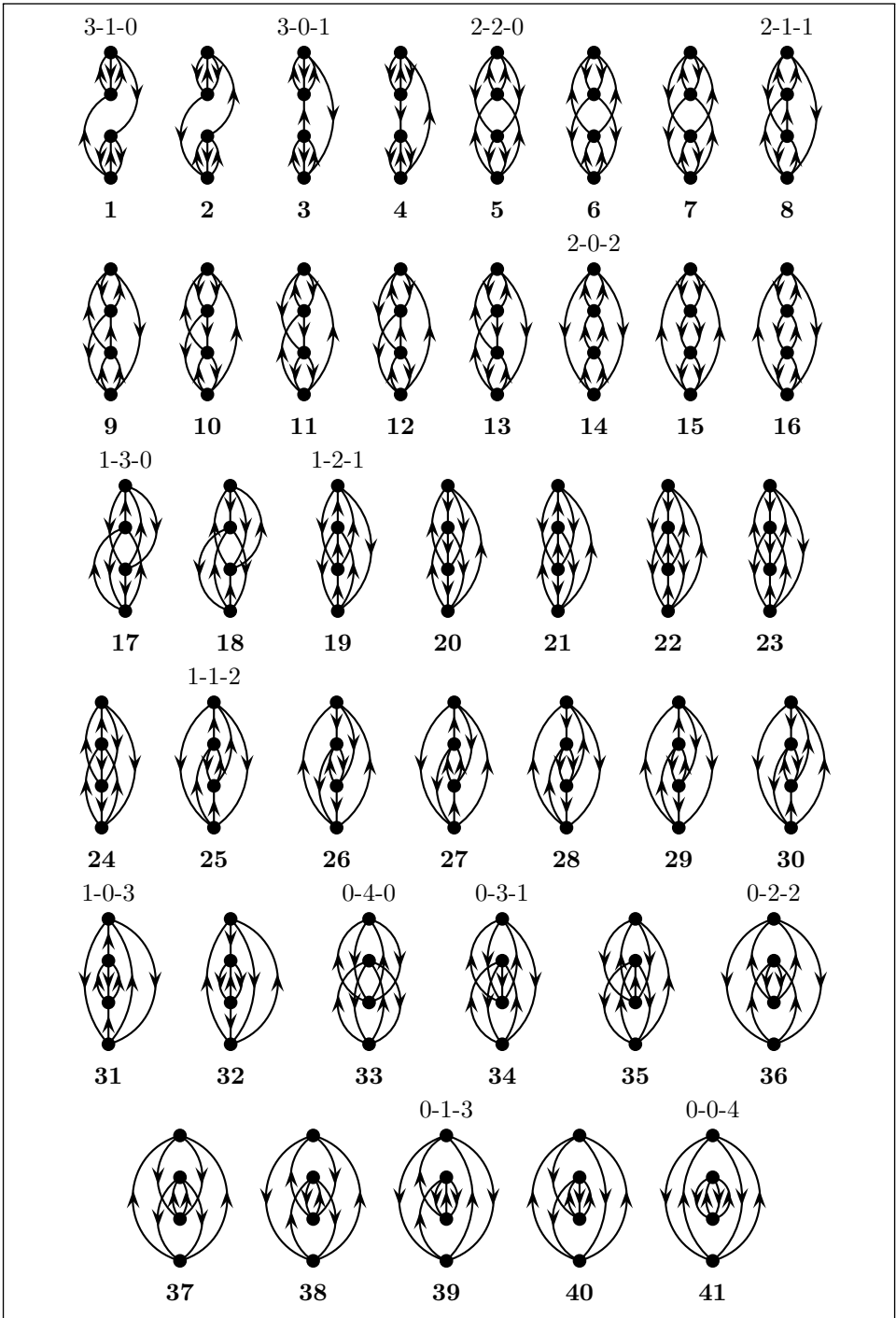


Fig. 5.5. Hugenholtz skeletons for the principal term of $E^{(4)}$ for canonical HF.

a vacuum gap and thus cannot contribute. The other two unlinked skeletons generate diagrams that cancel with the renormalization term, as will be shown in subsection 5.7.4.

Ignoring the vacuum-gap skeleton and inserting arrows in the other skeletons in all distinct ways, with two incoming and two outgoing lines at each vertex, we obtain the 41 Hugenholtz diagrams in Fig. 5.6. The two unlinked skeletons (33 and 41) generate just one diagram each, while the other (linked) skeletons generate from two to six distinct diagrams each.

The corresponding antisymmetrized Goldstone diagrams, using the same numbering as in Fig. 5.6, are shown in Figs. 5.7–5.10 classified by the type of intermediate states involved. These intermediate states are defined by the (omitted) resolvent lines that cross the diagrams between the vertices, and are represented by the denominators in the corresponding algebraic expressions. Only the middle intermediate state, between the second and third vertices, differs in its excitation level between the different classes of HF-case diagrams. The classification based on the intermediate state has important practical ramifications, because the diagrams for the different classes allow different factorization patterns for the corresponding sums, leading to substantial differences in the computational effort required for their evaluation. These factorizations and other computational considerations are discussed in Chapter 7.

Fig. 5.6. Hugenholtz diagrams for the principal term of $E^{(4)}$ for canonical HF.

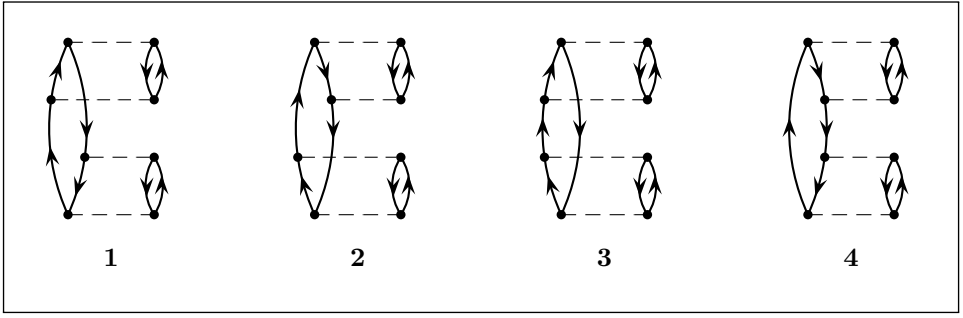


Fig. 5.7. Single-excitation ASG diagrams for the principal term of $E^{(4)}$.

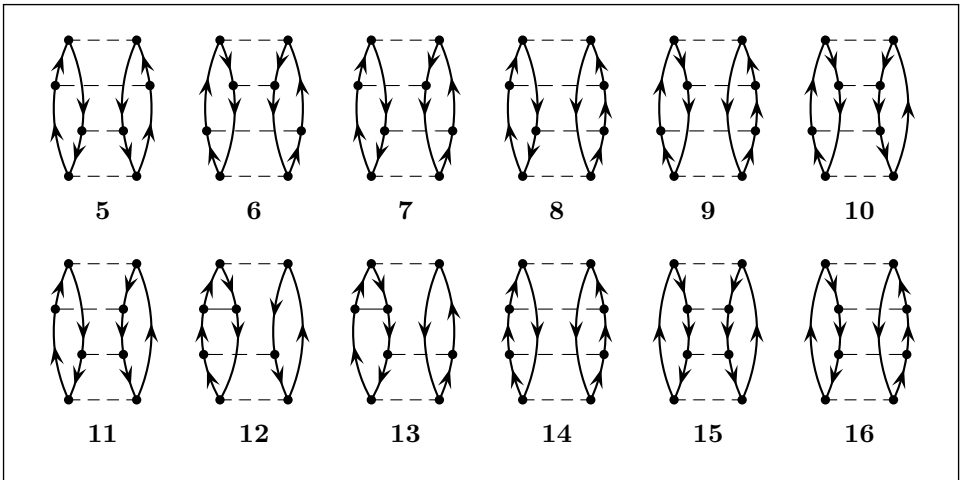


Fig. 5.8. Double-excitation ASG diagrams for the principal term of $E^{(4)}$.

The first four diagrams, shown in Fig. 5.7, include a singly excited intermediate state (between the second and third vertices). There are 12 diagrams with doubly excited intermediate states only (Fig. 5.8), 16 that include a triply excited intermediate state (Fig. 5.9) and nine that include a quadruply excited intermediate state (Fig. 5.10). The latter include the two unlinked diagrams, 33 and 41, which will be shown to cancel with the renormalization term. There are eight conjugate pairs: diagrams 1 and 2, 5 and 6, 8 and 9, 10 and 11, 17 and 18, 21 and 22, 23 and 24, 29 and 30. All other diagrams are self-conjugate.

The double-excitation diagrams 14 and 15 are particle and hole ladders, respectively. Diagrams 7 and 16 are usually referred to as ring diagrams,

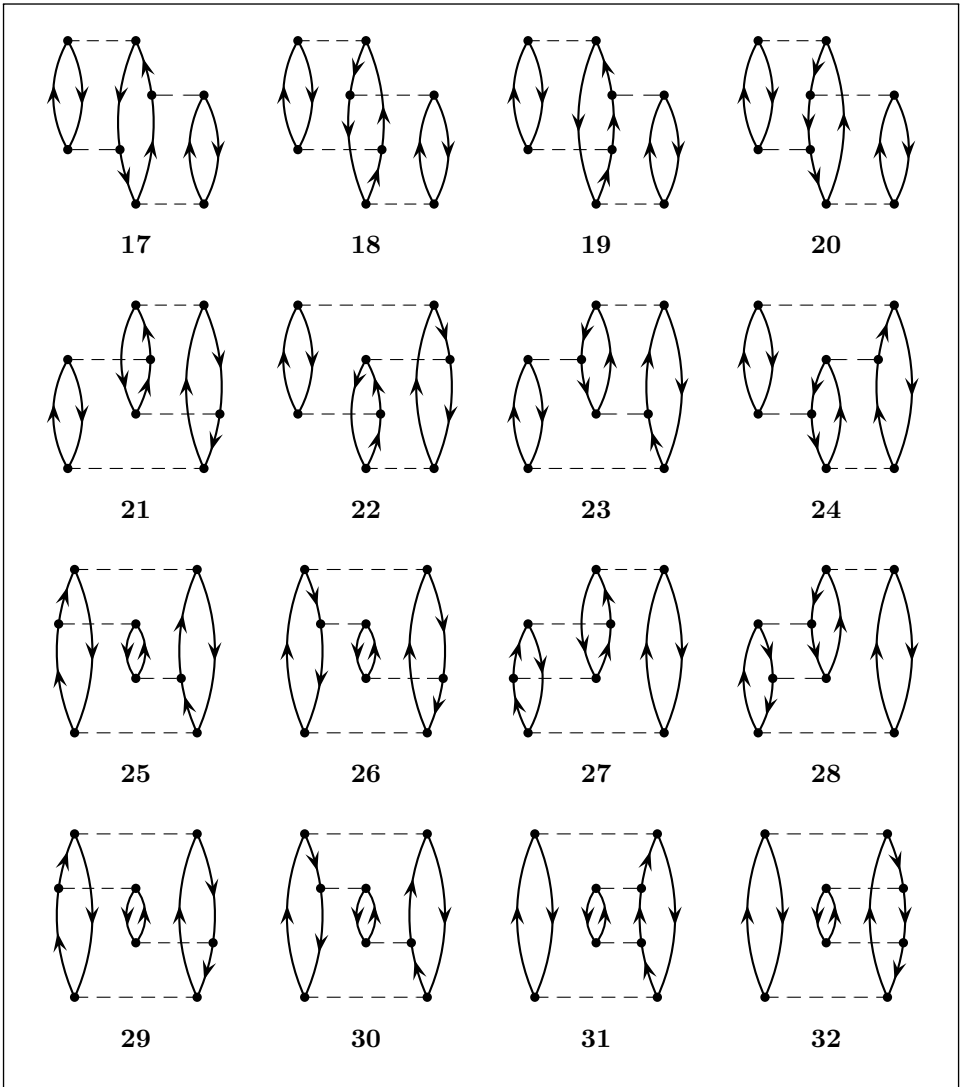
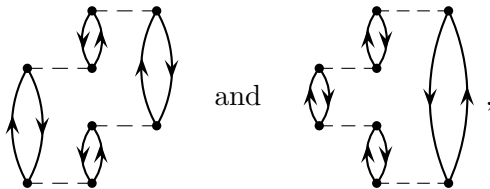


Fig. 5.9. Triple-excitation ASG diagrams for the principal term of $E^{(4)}$.

a designation that can be understood by considering their equivalent forms,



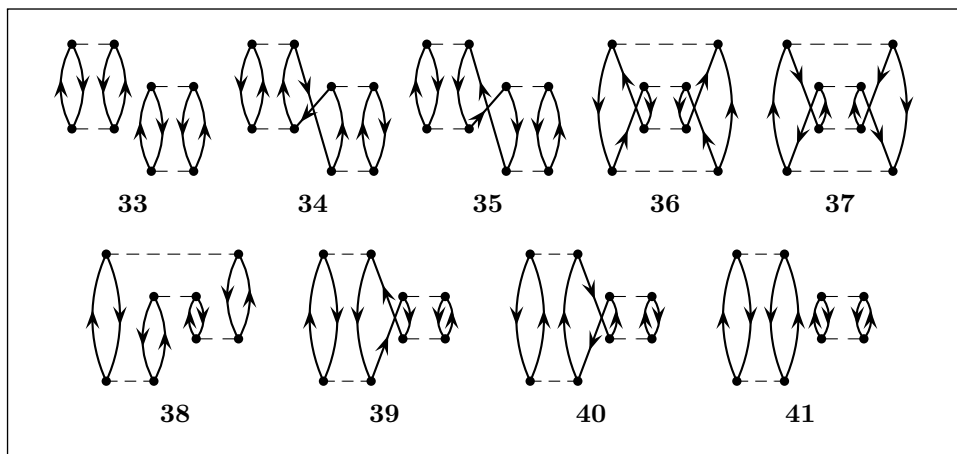


Fig. 5.10. Quadruple-excitation ASG diagrams for the principal term of $E^{(4)}$.

respectively. The other double-excitation diagrams involve more complicated connection patterns.

5.7.3 Non-HF diagrams for $E^{(4)}$

For the non-HF case we obtain the 69 additional linked Hugenholtz skeletons shown in Fig. 5.11. Each of these skeletons generates between one and four distinct diagrams, resulting in a total of 162 linked diagrams. Only six of these skeletons, generating 22 diagrams (those that do not involve a particle-hole one-electron integral of the form $\langle i|\hat{f}|a\rangle$ or $\langle a|\hat{f}|i\rangle$), contribute in the noncanonical HF case. It is left as an exercise for the reader to generate the non-HF diagrams from the skeletons.

(To generate ASG diagrams from Hugenholtz skeletons, the preferred sequence is to generate Hugenholtz diagrams first and then convert these to ASG diagrams, since each Hugenholtz diagram produces a single distinct ASG diagram. The alternative sequence through ASG skeletons is less straightforward, since a Hugenholtz skeleton may produce more than one distinct ASG skeleton.)

Some skeletons in Fig. 5.11 are equivalent to the upside-down image of other skeletons and these generate sets of pairs of conjugate diagrams. Thus the skeletons with a single one-electron vertex at the top (the first six in the first row) are equivalent, in order, to the upside-down images of those with a single one-electron vertex at the bottom (the first six in the third row), and generate 18 pairs of conjugate diagrams. Similarly, the six skeletons with a single one-electron vertex at the second level are symmetry related to the

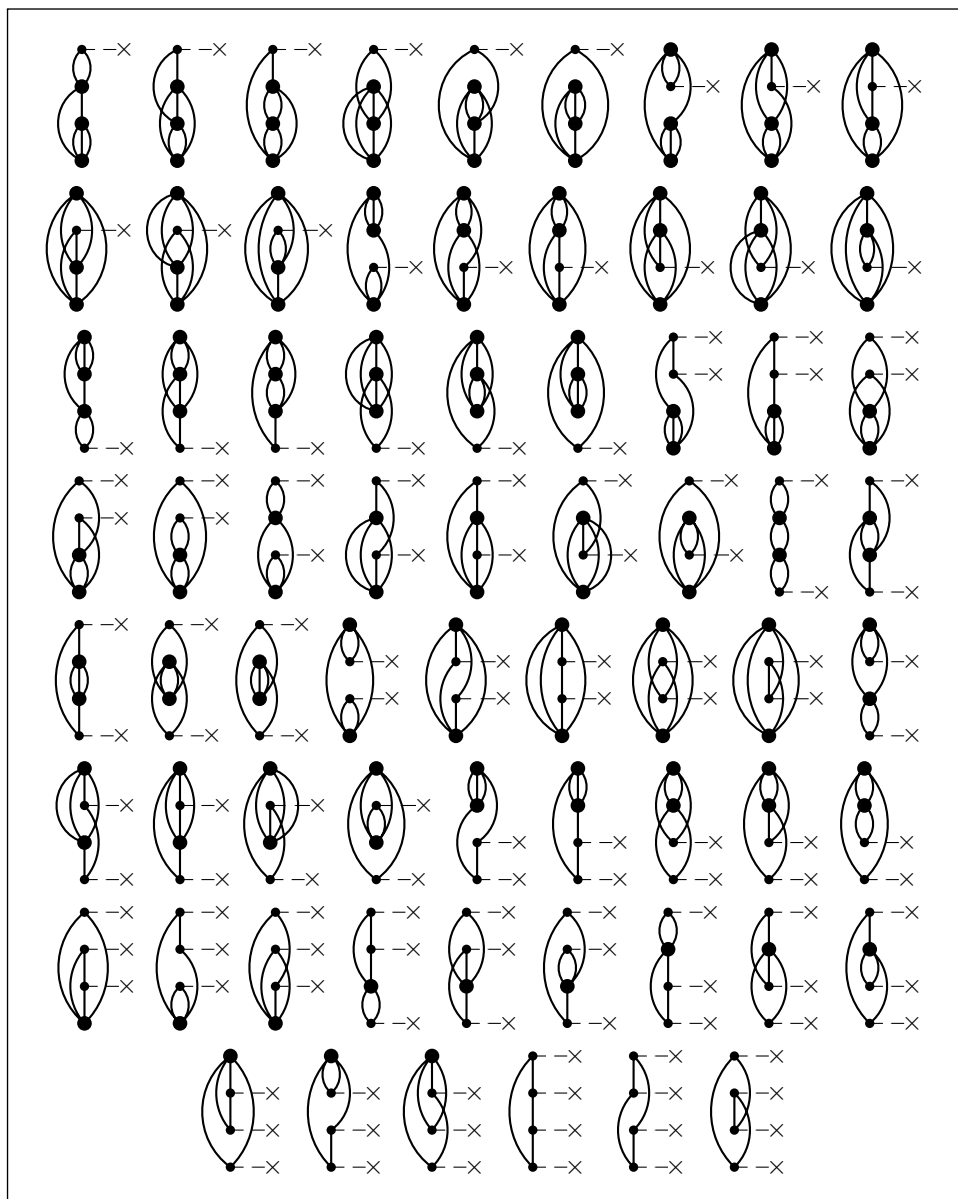


Fig. 5.11. Non-HF linked Hugenholtz skeletons for the principal term of $E^{(4)}$.

six diagrams with that vertex at the third level, generating another 18 pairs of conjugate diagrams. Among the skeletons with two one-electron vertices there are two sets of five skeletons that are symmetry related to two other sets, generating 10 pairs of conjugate diagrams each, while the skeletons

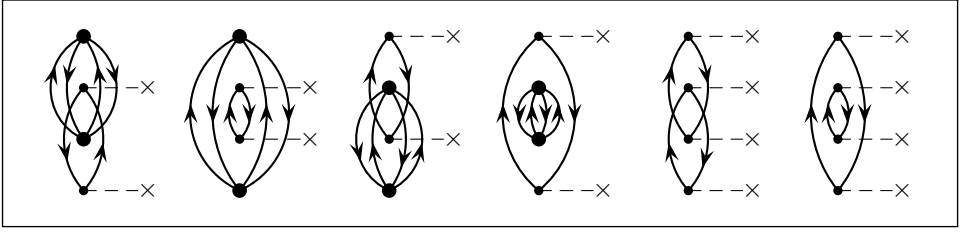


Fig. 5.12. Non-HF unlinked Hugenholtz diagrams for the principal term of $E^{(4)}$.

with three one-electron vertices consist of two sets of three skeletons that are symmetry related to two other sets, generating six pairs of conjugate diagrams each. There also are three pairs of conjugate diagrams generated from skeletons that are equivalent to their own upside-down image (two pairs with two one-electron vertices and one pair with four). In all, we obtain 71 pairs of conjugate diagrams and 20 self-conjugate diagrams.

There also are six unlinked non-HF skeletons (not counting three with a vacuum gap), each generating a single diagram. These diagrams are shown in Fig. 5.12. As will be shown later, they cancel with the non-HF part of the renormalization term.

The large number of non-HF diagrams re-emphasizes the advantages of the HF case in simplifying the formalism but, again, the computational effort involved in evaluating all the non-HF terms is small compared with the effort required for the HF terms.

5.7.4 Cancellation of the unlinked diagrams in $E^{(4)}$

We now proceed to show that the unlinked diagrams in the fourth-order energy cancel with the renormalization term. A formal proof of the cancellation of all unlinked diagrams in all MBPT energy and wave function expressions with the corresponding renormalization terms will be given in Chapter 6.

We begin with the canonical HF case. The two unlinked diagrams, 33 and 41 (Fig. 5.10), differ only in time ordering. Their algebraic expressions have the same numerators and differ only in one factor in the denominator:

$$\begin{aligned}
 & \hat{R}_0 \text{ (diagram 33)} - \hat{R}_0 \text{ (diagram 41)} = \frac{1}{16} \sum_{\substack{abcd \\ ijkl}} \frac{\langle ij || ab \rangle \langle kl || cd \rangle \langle ab || ij \rangle \langle cd || kl \rangle}{\varepsilon_{ij}^{ab} \varepsilon_{ijkl}^{abcd} \varepsilon_{kl}^{cd}}, \\
 & \hspace{15em} (5.20)
 \end{aligned}$$

$$= \frac{1}{16} \sum_{\substack{abcd \\ ijkl}} \frac{\langle ij || ab \rangle \langle ab || ij \rangle \langle kl || cd \rangle \langle cd || kl \rangle \langle ab || ij \rangle}{\epsilon_{ij}^{ab} \epsilon_{ijkl}^{abcd} \epsilon_{ij}^{ab}}. \quad (5.21)$$

Adding them together term by term we obtain

$$\frac{1}{16} \sum_{\substack{abcd \\ ijkl}} \frac{\langle ij || ab \rangle \langle ab || ij \rangle \langle kl || cd \rangle \langle cd || kl \rangle}{\epsilon_{ij}^{ab} \epsilon_{ijkl}^{abcd}} \left(\frac{1}{\epsilon_{kl}^{cd}} + \frac{1}{\epsilon_{ij}^{ab}} \right).$$

Noting that

$$\frac{1}{\epsilon_{kl}^{cd}} + \frac{1}{\epsilon_{ij}^{ab}} = \frac{1}{\epsilon_{ij}^{ab} \epsilon_{kl}^{cd}} (\epsilon_{ij}^{ab} + \epsilon_{kl}^{cd}) = \frac{\epsilon_{ijkl}^{abcd}}{\epsilon_{ij}^{ab} \epsilon_{kl}^{cd}},$$

the sum becomes

$$\begin{aligned} & \frac{1}{16} \sum_{\substack{abcd \\ ijkl}} \frac{\langle ij || ab \rangle \langle ab || ij \rangle \langle kl || cd \rangle \langle cd || kl \rangle}{\left(\epsilon_{ij}^{ab} \right)^2 \epsilon_{kl}^{cd}} \\ &= \left(\frac{1}{4} \sum_{abij} \frac{\langle ij || ab \rangle \langle ab || ij \rangle}{\left(\epsilon_{ij}^{ab} \right)^2} \right) \left(\frac{1}{4} \sum_{cdkl} \frac{\langle kl || cd \rangle \langle cd || kl \rangle}{\epsilon_{kl}^{cd}} \right). \end{aligned}$$

The second factor on the right-hand-side of this expression is just the second-order energy in the HF case,

$$E^{(2)} = \hat{R}_0 \frac{\langle kl || cd \rangle \langle cd || kl \rangle}{\epsilon_{kl}^{cd}}. \quad (5.22)$$

The first factor can be described diagrammatically in the form

$$\hat{R}_0 \frac{\langle ij || ab \rangle \langle ab || ij \rangle}{\left(\epsilon_{ij}^{ab} \right)^2},$$

which is equal to $\langle \Psi^{(1)} | \Psi^{(1)} \rangle$ in the HF case (the two resolvent lines represent the squared denominator). More explicitly, noting that

$$\begin{aligned} \sum_{cdkl} \langle \Phi_{ij}^{ab} | \Phi_{kl}^{cd} \rangle \frac{\langle cd || kl \rangle}{\varepsilon_{kl}^{cd}} &= \frac{\langle ij || ab \rangle}{\varepsilon_{ij}^{ab}} - \frac{\langle ba || ij \rangle}{\varepsilon_{ij}^{ba}} - \frac{\langle ab || ji \rangle}{\varepsilon_{ji}^{ab}} + \frac{\langle ba || ji \rangle}{\varepsilon_{ji}^{ba}} \\ &= \frac{\langle ij || ab \rangle}{\varepsilon_{ij}^{ab}} + \frac{\langle ij || ab \rangle}{\varepsilon_{ij}^{ab}} + \frac{\langle ij || ab \rangle}{\varepsilon_{ij}^{ab}} + \frac{\langle ij || ab \rangle}{\varepsilon_{ij}^{ab}} \\ &= 4 \frac{\langle ab || ij \rangle}{\varepsilon_{ij}^{ab}} \end{aligned} \quad (5.23)$$

(because $\langle \Phi_{ij}^{ab} | \Phi_{kl}^{cd} \rangle = \delta_{ik} \delta_{jl} \delta_{ac} \delta_{bd} - \delta_{ik} \delta_{jl} \delta_{ad} \delta_{bc} - \delta_{il} \delta_{jk} \delta_{ac} \delta_{bd} + \delta_{il} \delta_{jk} \delta_{ad} \delta_{bc}$), we can rewrite the first factor in the form

$$\left(\frac{1}{4} \sum_{abij} \frac{\langle ij || ab \rangle}{\varepsilon_{ij}^{ab}} \langle \Phi_{ij}^{ab} | \right) \left(\frac{1}{4} \sum_{cdkl} |\Phi_{kl}^{cd}\rangle \frac{\langle cd || kl \rangle}{\varepsilon_{kl}^{cd}} \right) = \langle \Psi^{(1)} | \Psi^{(1)} \rangle. \quad (5.24)$$

The sum of the two unlinked diagrams has thus been shown to be equal to $E^{(2)} \langle \Psi^{(1)} | \Psi^{(1)} \rangle$, exactly canceling the renormalization term.

This result can be represented diagrammatically in the form

The diagrammatic equation (5.25) shows two unlinked diagrams on the left, each consisting of two separate loops. The first diagram has two horizontal lines, each with a loop. The second diagram has two vertical lines, each with a loop. These are summed and equated to a diagram on the right. The right-hand side diagram consists of two horizontal lines, each with a loop, and a central vertex correction represented by a triangle with a dot, labeled \hat{R}_0 . The entire right-hand side is enclosed in a large angle bracket, also labeled \hat{R}_0 .

where “insertion” of the $E^{(2)}$ diagram simply means multiplication by $E^{(2)}$. Note that no denominator line spans both parts of this diagram.

In the non-HF case there are six additional unlinked diagrams, shown in their Hugenholtz form in Fig. 5.12. At the same time, there are additional diagrams in the expressions for $E^{(2)}$ and $\langle \Psi^{(1)} | \Psi^{(1)} \rangle$ in the renormalization term. The complete diagrammatic description of $E^{(2)}$ is

The diagrammatic equation (5.26) shows $E^{(2)}$ as the sum of two diagrams. The first diagram consists of two separate loops, each with a horizontal line. The second diagram consists of two separate loops, each with a horizontal line, and a central vertex correction represented by a triangle with a dot, labeled \hat{R}_0 .

while the first-order wave function is

The diagrammatic equation (5.27) shows $|\Psi^{(1)}\rangle$ as the sum of two diagrams. The first diagram consists of two separate loops, each with a horizontal line. The second diagram consists of two separate loops, each with a horizontal line, and a central vertex correction represented by a triangle with a dot, labeled \hat{R}_0 .

and its norm can be described by

The diagrammatic equation (5.28) shows $\langle \Psi^{(1)} | \Psi^{(1)} \rangle$ as the sum of two diagrams. The first diagram consists of two separate loops, each with a horizontal line. The second diagram consists of two separate loops, each with a horizontal line, and a central vertex correction represented by a triangle with a dot, labeled \hat{R}_0 .

(the repeated resolvent lines, one due to $\langle \Psi^{(1)} |$ and the other to $|\Psi^{(1)}\rangle$, must be shown explicitly in this equation to indicate the squared denominator). The complete renormalization term can therefore be described by

$$\begin{aligned}
 E^{(2)} \langle \Psi^{(1)} | \Psi^{(1)} \rangle = & \text{Diagram 1} + \text{Diagram 2} \\
 & + \text{Diagram 3} + \text{Diagram 4}, \quad (5.29)
 \end{aligned}$$

The diagrams represent various fourth-order energy contributions. Diagram 1 shows two loops on the left connected to a vertex, which then splits into two loops. Diagram 2 is similar but with different line connections. Diagrams 3 and 4 show more complex topologies with additional lines and vertices.

it being understood that there is a resolvent line both above and below each insertion.

The first term in (5.29) is the HF part, which is cancelled by the two HF-case unlinked diagrams, as shown earlier. The remaining three terms are canceled by the six non-HF unlinked diagrams of Fig. 5.12, as follows:

$$\begin{aligned}
 & \text{Diagram 5} + \text{Diagram 6} \\
 &= \frac{1}{4} \sum_{\substack{abc \\ ijk}} \frac{\langle ij || ab \rangle \langle k | \hat{f} | c \rangle \langle ab || ij \rangle \langle c | \hat{f} | k \rangle}{\varepsilon_{ij}^{ab} \varepsilon_{ijk}^{abc}} \left(\frac{1}{\varepsilon_k^c} + \frac{1}{\varepsilon_{ij}^{ab}} \right) \\
 &= \frac{1}{4} \sum_{\substack{abc \\ ijk}} \frac{\langle ij || ab \rangle \langle ab || ij \rangle \langle k | \hat{f} | c \rangle \langle c | \hat{f} | k \rangle}{(\varepsilon_{ij}^{ab})^2 \varepsilon_k^c} \\
 &= \text{Diagram 7}, \quad (5.30)
 \end{aligned}$$

The diagrams show the cancellation of terms. Diagram 5 and 6 are the terms from (5.29) that are being canceled. Diagram 7 is the resulting unlinked diagram after cancellation, showing two loops on the left connected to a vertex, which then splits into two loops.

and, similarly,

$$\text{Diagram 1} + \text{Diagram 2} = \text{Diagram 3}, \quad (5.31)$$

$$\text{Diagram 1} + \text{Diagram 2} = \text{Diagram 3}. \quad (5.32)$$

Thus we have obtained full cancellation of the unlinked diagrams with the renormalization term.

5.7.5 Role of the EPV terms

We shall now examine the cancellation of unlinked diagrams in more detail, focusing on the role of exclusion principle violating (EPV) terms.

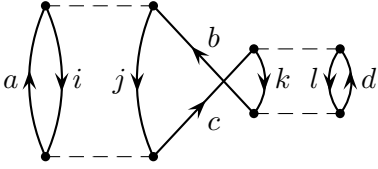
Consider two EPV quadruple-excitation terms, one linked and one unlinked, contributing to diagrams 39 and 41, respectively, of Fig. 5.10:

$$\text{Diagram} = - \frac{\langle ij || ab \rangle \langle kl || bd \rangle \langle bd || kl \rangle \langle ab || ij \rangle}{\varepsilon_{ij}^{ab} \varepsilon_{ijkl}^{ab} \varepsilon_{ij}^{ab}}, \quad (5.33)$$

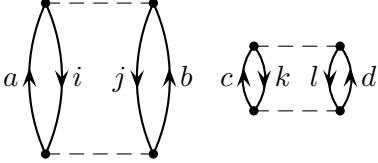
$$\text{Diagram} = + \frac{\langle ij || ab \rangle \langle kl || bd \rangle \langle bd || kl \rangle \langle ab || ij \rangle}{\varepsilon_{ij}^{ab} \varepsilon_{ijkl}^{ab} \varepsilon_{ij}^{ab}}. \quad (5.34)$$

We have not included the weight factors, since all lines are labeled. In unrestricted summations there would be a coefficient $\frac{1}{4}$ for the linked term and a coefficient $\frac{1}{16}$ for the unlinked term; however, there are four equivalent ways to assign the pair of equal particle labels in the latter diagram, so that the weight factors balance at the end. These two terms obviously cancel and this is as it should be, since both are EPV terms.

This same cancellation does not occur for the non-EPV terms ($b \neq c$):

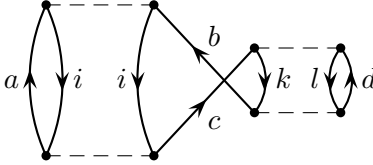


$$= - \frac{\langle ij||ab \rangle \langle kl||cd \rangle \langle bd||kl \rangle \langle ac||ij \rangle}{\varepsilon_{ij}^{ab} \varepsilon_{ijkl}^{abcd} \varepsilon_{ij}^{ac}}, \quad (5.35)$$

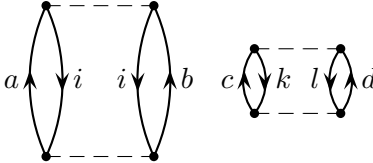


$$= + \frac{\langle ij||ab \rangle \langle kl||cd \rangle \langle cd||kl \rangle \langle ab||ij \rangle}{\varepsilon_{ij}^{ab} \varepsilon_{ijkl}^{abcd} \varepsilon_{ij}^{ab}}. \quad (5.36)$$

Note that having equal labels on equivalent lines produces vanishing contributions,



$$= - \frac{\langle ii||ab \rangle \langle kl||cd \rangle \langle bd||kl \rangle \langle ac||ii \rangle}{\varepsilon_{ii}^{ab} \varepsilon_{iikl}^{abcd} \varepsilon_{ii}^{ac}} = 0,$$



$$= + \frac{\langle ii||ab \rangle \langle kl||cd \rangle \langle cd||kl \rangle \langle ab||ii \rangle}{\varepsilon_{ii}^{ab} \varepsilon_{iikl}^{abcd} \varepsilon_{ii}^{ab}} = 0,$$

and thus such diagrams can be ignored in considering the cancellations.

Thus the unlinked EPV terms that are canceled by the renormalization term are not legitimate contributions in the first place and have only been included because of the presence of cancelling *linked* EPV terms. After cancellation of *all* the unlinked contributions, including the EPV terms, by the renormalization term, the “illegitimate” linked EPV terms in the principal term remain. We can divide up the renormalization term into two parts:

$$-E^{(2)} S_{11} = (-E^{(2)} S_{11})_{\text{CJ}} + (-E^{(2)} S_{11})_{\text{DJ}}, \quad (5.37)$$

where $S_{11} = \langle \Psi^{(1)} | \Psi^{(1)} \rangle$ and the subscript DJ (disjoint) indicates the sum of those contributions in which the diagrams for $E^{(2)}$ and S_{11} have no labels in common, while CJ (conjoint) indicates the sum of the contributions in which the two diagrams have one or more labels in common.

The disjoint part of the renormalization term cancels the non-EPV unlinked-diagram contributions,

$$(-E^{(2)}S_{11})_{\text{DJ}} = - \begin{array}{c} \text{Diagram 1: Two separate double-line loops, each with two vertices and two internal lines (one solid, one dashed).} \\ \text{Diagram 2: Two separate double-line loops, each with two vertices and two internal lines (one solid, one dashed).} \end{array} - \begin{array}{c} \text{Diagram 3: Two separate double-line loops, each with two vertices and two internal lines (one solid, one dashed).} \\ \text{Diagram 4: Two separate double-line loops, each with two vertices and two internal lines (one solid, one dashed).} \end{array} \quad \begin{array}{l} \text{(non-EPV} \\ \text{terms only),} \end{array} \quad (5.38)$$

while the conjoint part cancels the EPV unlinked-diagram contributions, leaving behind the *linked* EPV terms. Since either $(-E^{(2)}S_{11})_{\text{CJ}}$ or the sum of the linked EPV terms cancels the sum of the unlinked EPV contributions, they must be equal to each other,

$$\begin{aligned} (-E^{(2)}S_{11})_{\text{CJ}} = & \begin{array}{c} \text{Diagram 1: Two double-line loops connected by two internal lines labeled 'b'.} \\ \text{Diagram 2: Two double-line loops connected by two internal lines labeled 'j'.} \\ \text{Diagram 3: Two double-line loops connected by two internal lines labeled 'b'.} \end{array} \\ & + \begin{array}{c} \text{Diagram 4: Two double-line loops connected by two internal lines labeled 'j'.} \\ \text{Diagram 5: Two double-line loops connected by two internal lines labeled 'b'.} \\ \text{Diagram 6: Two double-line loops connected by two internal lines labeled 'j'.} \end{array} \\ & + \cdots \quad \text{(all the linked EPV terms),} \end{aligned} \quad (5.39)$$

so that these linked EPV terms can be regarded as the remnant of the renormalization term that was not canceled by “legitimate” (non-EPV) unlinked terms.

The total quadruple-excitation contribution can therefore be expressed in either of two ways:

$$\begin{aligned} E_Q^{(4)} &= (\text{non-EPV linked quadruple-excitation diagrams}) \\ &\quad + (\text{EPV linked quadruple-excitation diagrams}) \\ &= (\text{non-EPV linked quadruple-excitation diagrams}) \\ &\quad + (-E_2S_{11})_{\text{CJ}}. \end{aligned} \quad (5.40)$$

5.8 Linked-diagram theorem

The cancellation of all the unlinked diagrams against the renormalization terms in Rayleigh–Schrödinger perturbation theory is formalized by the *linked-diagram theorem* (Goldstone 1957), which states that the energy and

the wave function can be expressed, in each order, as a sum of linked diagrams only. Explicitly,

$$E^{(n)} = \langle 0 | \hat{W} (\hat{R}_0 \hat{W})^{n-1} | 0 \rangle_L, \quad (5.41)$$

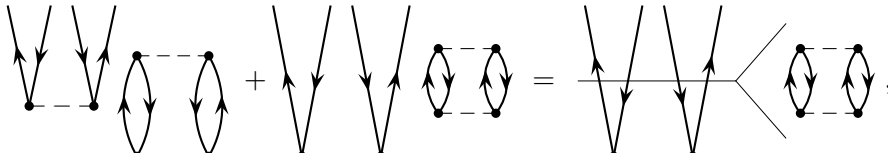
$$|\Psi^{(n)}\rangle = [(\hat{R}_0 \hat{W})^n | 0 \rangle]_L, \quad (5.42)$$

where the subscript L indicates the limitation to linked diagrams (which, in the case of the energy, is equivalent to a limitation to connected diagrams). Proof of this theorem is deferred to Chapter 6. The cancellation of the unlinked diagrams is closely related to the extensivity of the Rayleigh–Schrödinger perturbation theory, as will be discussed in Section 5.10.

As an example of the cancellation of unlinked diagrams in the wave function expansion, we shall consider the third-order wave function, the lowest wave-function order in which unlinked diagrams and a renormalization term occur (see (2.135)):

$$|\Psi^{(3)}\rangle = \hat{R}_0 \hat{W} \hat{R}_0 \hat{W} \hat{R}_0 \hat{W} | 0 \rangle - \hat{R}_0 \langle 0 | \hat{W} \hat{R}_0 \hat{W} \rangle \hat{R}_0 \hat{W} | 0 \rangle. \quad (5.43)$$

In the canonical HF case we find two unlinked diagrams, whose sum can be expressed as an insertion,



$$(5.44)$$

which is equal to the renormalization term. Again, it is understood that a resolvent line occurs both above and below the insertion. The non-HF case is left as an exercise for the reader.

5.9 Numerical example

In order to get a feel for the relative magnitudes of the various contributions to the energy, we shall look at an example from a set of calculations for the H_2O molecule at its equilibrium geometry in a (5s4p2d/3s1p) Slater-type basis (39-STO) (Bartlett, Shavitt and Purvis 1979, Wilson 1979, Bartlett 1981, Bartlett, Cole, Purvis *et al.* 1987). The correlation energy contributions for this example, through fourth order, are given in Table 5.1.

We see in the table that the fourth-order renormalization term cancels 61% of the principal term in this example. This cancellation is even more striking if we look just at the quadruple-excitation contribution. The sum of all quadruple-excitation diagrams in the principal term is $-13.910 \text{ m}E_h$;

Table 5.1. Contributions to the correlation energy in the water molecule in millihartrees (mE_h), using a 39-STO calculation (Bartlett, Shavitt and Purvis 1979, Wilson 1979, Bartlett 1981, Bartlett, Cole, Purvis *et al.* 1987)

$E^{(2)}$			-281.780
$E^{(3)}$			-3.241
$E^{(4)}$	singles	-2.033	
	doubles	-4.324	
	triples	-7.863	
	linked quadruples	+3.206	-11.014
$E^{(2)} + E^{(3)} + E^{(4)}$			-296.035
Another breakdown of $E^{(4)}$:			
	principal term		-28.130
	renormalization term		+17.116
	$E^{(4)}$		-11.014

deducting the value of the unlinked diagrams, -17.116 mE_h , leaves a linked-diagram contribution of $+3.206 \text{ mE}_h$. Thus removal of the unlinked quadruple-excitation diagrams in $E^{(4)}$ leads to a change in sign of the quadruple-excitation contribution.

It will be shown in Chapter 7 that the determination of the quadruple-excitation contribution to the fourth-order energy requires substantially less computational effort than the determination of the triple-excitation contribution. While the computational effort for the fourth-order quadruples is approximately proportional to the sixth power of the number of orbitals, the effort for the triples is approximately proportional to the seventh power. In fact, early fourth-order MBPT calculations (see e.g. Bartlett, Shavitt, Purvis *et al.* 1979) left out the triples, producing a result sometimes referred to as MBPT(4)SDQ or SDQ-MBPT(4). The results in Table 5.1 show not only that the triples' contribution may be greater in magnitude than that of the linked quadruples but also that the two contributions may be of opposite sign. In fact, including the quadruples without the triples may actually produce less accurate results than leaving both out.

We can use the H_2O 39-STO example to obtain a quantitative estimate of the role of the EPV terms in the cancellation of the unlinked diagrams, as discussed in subsection 5.7.5. Using an approximate evaluation of the conjoint part of the renormalization term based on a CEPA-3 estimate (Bartlett,

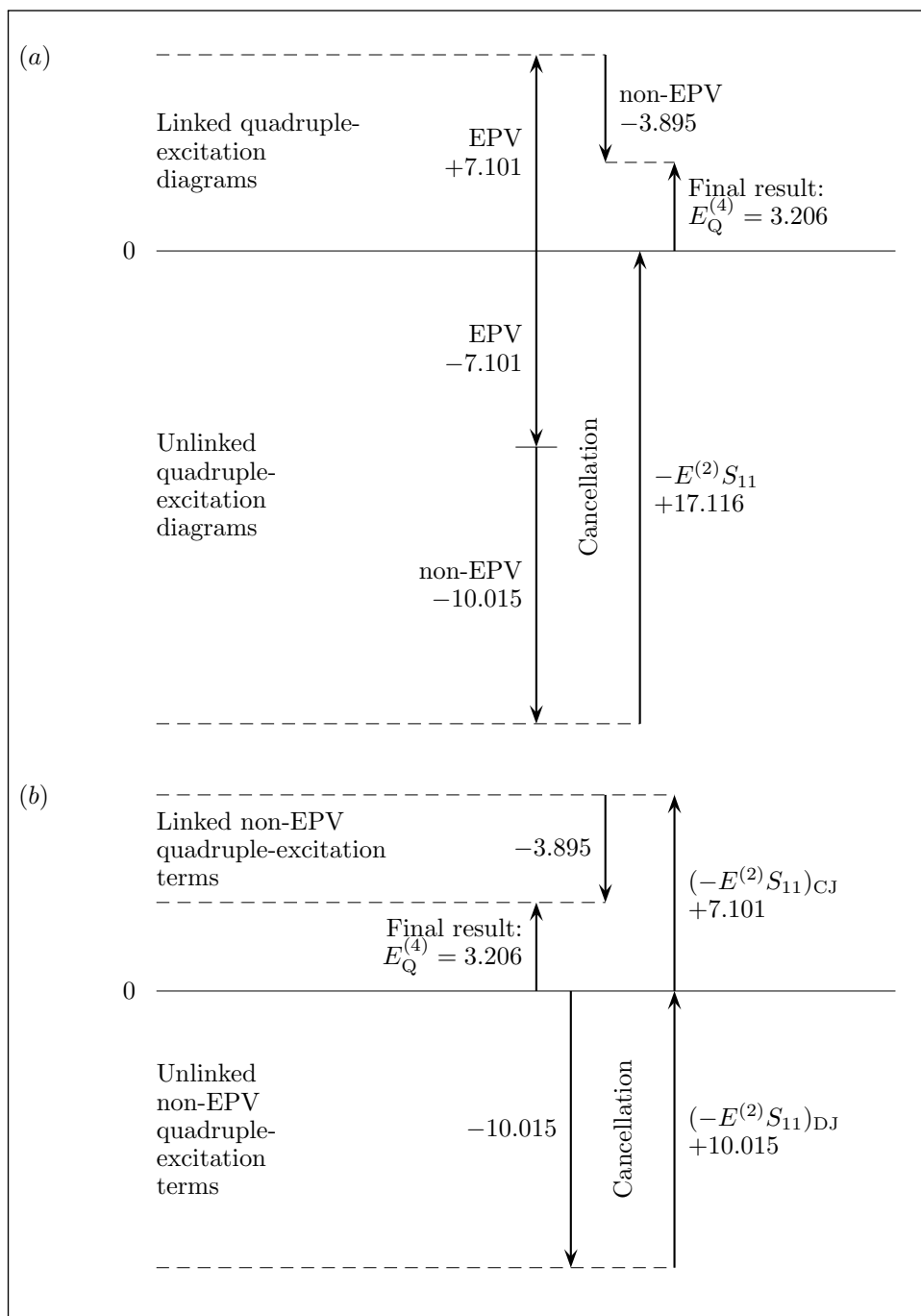


Fig. 5.13. Role of EPV terms in the cancellation of unlinked quadruple-excitation diagrams in $E^{(4)}$ for the 39-STO H_2O calculation (energies in millihartrees).

Shavitt and Purvis 1979), we find

$$\begin{aligned} (-E^{(2)}S_{11})_{\text{CJ}} &= 7.101 \text{ m}E_{\text{h}}, \\ (-E^{(2)}S_{11})_{\text{DJ}} &= 10.015 \text{ m}E_{\text{h}}, \end{aligned}$$

so that the linked quadruple-excitation contribution can be divided up as follows:

$$\begin{aligned} E_{\text{Q}}^{(4)} &= -3.895 \text{ m}E_{\text{h}} && \text{(linked non-EPV quadruple excitations)} \\ &+ 7.101 \text{ m}E_{\text{h}} && \text{(linked EPV quadruples} = (-E^{(2)}S_{11})_{\text{CJ}}) \\ &= 3.206 \text{ m}E_{\text{h}}. \end{aligned}$$

The two interpretations of the role of the EPV terms in the cancellation of the renormalization term and unlinked quadruple-excitation diagrams in fourth-order MBPT, as discussed in subsection 5.7.5, are given for the 39-STO H₂O calculation in Fig. 5.13. In part (a) of the figure all the unlinked quadruple-excitation diagrams (the EPV and non-EPV terms) are canceled by the complete renormalization term, leaving the linked diagrams (both EPV and non-EPV terms) as the final quadruple-excitation energy. In part (b) we leave out the EPV terms; here the unlinked non-EPV terms are canceled by the disjoint part of the renormalization term, leaving the linked non-EPV terms plus the conjoint part of the renormalization term as the final quadruple-excitation energy. This conjoint part can be re-expressed in the form of linked EPV terms, justifying the interpretation of the linked EPV terms as the uncanceled remnant of the renormalization term.

5.10 Unlinked diagrams and extensivity

5.10.1 Extensivity implications

For an extensive system, with size (extent) proportional to some count parameter N (the number of identical subunits), the total energy is, of course, proportional to N . If the Rayleigh–Schrödinger perturbation theory expansion, with $\hat{H} = \hat{H}_0 + \lambda\hat{V}$, converges for a range of values of λ then it must also provide a total converged energy that is proportional to N for each value of λ in that range. Thus, if the energy is expanded in powers of λ ,

$$E = E^{(0)} + \lambda E^{(1)} + \lambda^2 E^{(2)} + \dots, \quad (5.45)$$

then each order $E^{(n)}$ must be proportional to N so that the RSPT energy is extensive, order by order. (This does not hold for BWPT, in which E is not expanded in powers of λ , as demonstrated in subsection 2.4.3.)

Now consider the renormalization term in $E^{(4)}$, i.e. $-E^{(2)}S_{11}$. The factor $E^{(2)}$ is obviously proportional to N . To find the behavior of S_{11} we go back to the example of N noninteracting He atoms considered in subsections 2.4.3 and 2.4.8. For this example the RSPT first-order wave function is given by

$$|\Psi^{(1)}\rangle = \sum_i |\Phi_i\rangle \frac{\langle \Phi_i | \hat{V} | \Phi_0 \rangle}{E_0^{(0)} - E_i^{(0)}} = \sum_i |\Phi_i\rangle \frac{\beta^*}{\varepsilon_0 - \alpha}, \quad (5.46)$$

and thus

$$S_{11} = \langle \Psi^{(1)} | \Psi^{(1)} \rangle = \sum_{i,j} \frac{\beta}{\varepsilon_0 - \alpha} \langle \Phi_i | \Phi_j \rangle \frac{\beta^*}{\varepsilon_0 - \alpha} = N \frac{|\beta|^2}{(\varepsilon_0 - \alpha)^2} \quad (5.47)$$

or

$$S_{11} \propto N. \quad (5.48)$$

As a result of this analysis we find that

$$-E^{(2)}S_{11} \propto N^2, \quad (5.49)$$

which implies that the unlinked diagrams in $E^{(4)}$, with which the renormalization term cancels, are also proportional to N^2 . It is only by this cancellation that extensivity can be restored. In fact, as discussed below in subsection 5.10.2, it can be shown more generally that linked energy diagrams are always extensive (provided that the complete diagram is evaluated), and so any model for the energy that consists of a sum of linked diagrams is properly extensive.

5.10.2 The N -dependence of diagrams

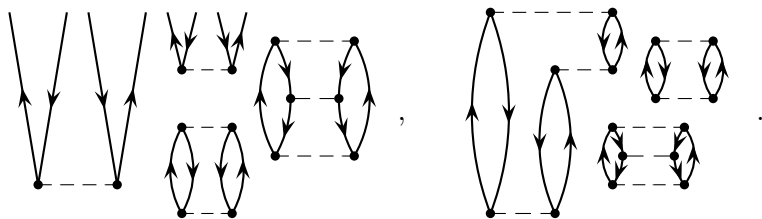
We can use the example of N noninteracting He atoms to examine the dependence of all MBPT diagrams on the size of the system, i.e. on the number of atoms N .

The key point is that, because the atoms do not interact, the integrals $\langle pq || rs \rangle$ and $\langle p | \hat{f} | q \rangle$ for this example vanish unless p, q, r, s (or p, q) all belong to the same atom. Thus nonzero contributions to the sum represented by any diagram are obtained only from terms in which the labels of the four or two lines connected to each vertex all belong to the same atom. In any connected piece of a diagram all vertices form a connected network, so nonzero contributions are obtained only from terms in which *all* labels in this connected piece belong to the same atom.

The *factorization theorem*, to be stated in detail and proved in Chapter 6, shows that different time-orderings of an unlinked and/or disconnected diagram can be collected into sets (defined by the relative positions of the top vertices of their separate connected pieces) whose sums are equal to connected diagrams with insertions, i.e. to products of the individual connected pieces (with an extra denominator for each insertion line). We have seen examples of this factorization in the demonstration of the cancellation of unlinked diagrams in the fourth-order energy (subsection 5.7.4) and in the third-order wave function (Section 5.8). The factorization decouples the connected pieces of the disconnected diagrams by eliminating denominators involving more than one connected piece. As a result, the sums over all disconnected diagrams can be rewritten in terms of sums of products of connected diagrams and insertions.

The sum of the terms of a connected diagram or insertion over the labels belonging to any He atom in our example is independent of the presence of the other atoms and therefore of N . For a closed linked diagram (or insertion) the sum over the labels of all atoms is thus proportional to N . For an open linked diagram, with fixed labels on the open lines (representing the coefficient of a given Slater determinant), a nonzero contribution requires all fixed and internal labels of each connected piece to belong to the same atom, so the sum over all internal labels is independent of N .

The factorization theorem therefore leads to the conclusion that the value of any MBPT diagram, for both the wave function and the energy, is proportional to N^k , where k is the number of closed connected pieces in the diagram. As examples we show two seventh-order unlinked diagrams, one open and one closed:



The first (open) diagram has two closed parts and its value (for the coefficient of any specific term in the wave function expansion) is proportional to N^2 while the second (closed) diagram has three closed parts and a value proportional to N^3 .

The linked-diagram theorem states that each order of the energy is given by a sum of closed linked (and therefore connected) diagrams only, i.e. diagrams each consisting of one closed part, while each order of the wave

function is given by a sum of open diagrams with no closed parts. It therefore implies that each order of the energy is proportional to N , again confirming the extensivity of RSPT. At the same time, the coefficient of each term $|\Phi_{ij,\dots}^{ab,\dots}\rangle$ in the expansion of the wave function, in each order, is independent of N (though the number of such terms is strongly dependent on N).

While the discussion of the N -dependence of diagrams has been presented here in terms of the example of N noninteracting He atoms, the result is much more general: the order-by-order extensivity property of Rayleigh–Schrödinger perturbation theory *requires* that the energy and wave function be expressed, in each order, as a sum of linked diagrams only.

5.10.3 Relationship to configuration interaction (CI)

Within any given basis set, the full-CI energy and the infinite-order converged PT energy $\sum_n E^{(n)}$ (if the PT series converges) are identical and provide the “exact” solution for the Schrödinger equation within the space generated by the given basis set. Thus the full-CI result provides a benchmark against which other methods using the same basis set can be measured. Truncated PT sums,

$$E_n = \sum_{m=2}^n E^{(m)}, \quad (5.50)$$

present successive approximations to the full-CI correlation energy $E_{\text{full-CI}}$.

The full-CI energy can also be approached by a sequence of CI calculations with increasing excitation-level configurations: E_{SCF} , E_{CID} (with all double-excitation configurations), E_{CISD} (singles and doubles), E_{CISDT} (triples added), E_{CISDTQ} (quadruples added), etc. (Note that if only singles are used then $E_{\text{CIS}} = E_{\text{SCF}}$ for SCF orbitals because of the Brillouin theorem.) In a certain sense, E_2 and E_3 can be seen as approximations to CID, or CISD in the non-HF case, since they involve only a sum over doubly excited configurations (singly excited configurations must be added for the non-HF case). In fact, for the H₂O 39-STO calculation we find (Bartlett and Shavitt 1977b),

$$\begin{aligned} E_2 &= E^{(2)} = -281.780 \text{ mE}_h, \\ E_3 &= E^{(2)} + E^{(3)} = -285.021 \text{ mE}_h, \\ E_{\text{CID}} &= -274.021 \text{ mE}_h, \\ E_{\text{CISD}} &= -275.576 \text{ mE}_h. \end{aligned}$$

We see that both E_2 and E_3 are lower than the CI energies. This behavior is not atypical for a nonvariational method like PT.

A better approximation for E_{CID} (or E_{CISD}) can be obtained, in principle, from fourth-order MBPT, but the latter contains contributions from single, triple and quadruple excitations as well. If we take the fourth-order RSPT formula

$$E^{(4)} = \langle 0 | \hat{W} \hat{R}_0 \hat{W} \hat{R}_0 \hat{W} \hat{R}_0 \hat{W} | 0 \rangle - E^{(2)} S_{11}$$

and limit the implied sums over intermediate states in \hat{R}_0 ,

$$\hat{R}_0 = \sum_I' \frac{|\Phi_I\rangle\langle\Phi_I|}{E_0^{(0)} - E_I^{(0)}},$$

so that they only span doubly excited states $|\Phi_I\rangle$, then we should get an approximation to CID only. In fact, this result can be worked out as follows (Bartlett and Shavitt 1977b, Bartlett, Shavitt and Purvis 1979):

double excitation diagrams in $E^{(4)}$	$-4.324 \text{ m}E_{\text{h}}$
+ renormalization term ($-E^{(2)}S_{11}$)	$17.116 \text{ m}E_{\text{h}}$
<hr/>	
total double-excitation part of $E^{(4)}$	$12.792 \text{ m}E_{\text{h}}$
$E^{(2)} + E^{(3)}$	$-285.021 \text{ m}E_{\text{h}}$
<hr/>	
fourth-order RSPT approximation to CID	$-272.229 \text{ m}E_{\text{h}}$
single excitation diagrams in $E^{(4)}$	$-2.033 \text{ m}E_{\text{h}}$
<hr/>	
fourth-order RSPT approximation to CISD	$-274.262 \text{ m}E_{\text{h}}$

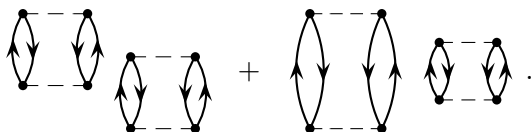
This result compares well with the values $E_{\text{CID}} = -274.021 \text{ m}E_{\text{h}}$, $E_{\text{CISD}} = -275.576 \text{ m}E_{\text{h}}$ given above. Note that the renormalization term is made up entirely of double-excitation contributions (in $E^{(2)}$ and in S_{11} , separately) and thus constitutes part of the RSPT approximation to CID.

This analysis is not meant to imply that CID or CISD is a more desirable approximation than any particular order of RSPT. In fact, while CI is inherently an infinite-order method, truncation at any excitation level sacrifices the important property of extensivity. The loss of extensivity is due to the presence of non-extensive terms at each truncation level of the CI energy. These terms are canceled in full CI but, because the cancellation involves contributions from different excitation levels, truncated CI at any level of truncation short of full CI necessarily retains non-extensive contributions. These non-extensive contributions reflect the implicit presence in the CI energy of the disjoint parts of renormalization terms, which are eventually canceled by higher-excitation non-EPV unlinked-diagram contributions (the EPV terms and the conjoint parts of the renormalization terms are absent

in CI calculations). These missing unlinked diagrams in the CI energy are a manifestation of the missing disconnected clusters in the CI wave function.

For example, the non-extensive contributions in the CISD energy reflect the implicit presence of the disjoint part of the fourth-order renormalization term $(-E^{(2)}S_{11})_{\text{DJ}}$; this arises from double, and possibly single, excitations. This contribution would be canceled in higher-level CI by non-EPV unlinked quadruple-excitation contributions, but it is retained in CISD and is primarily a manifestation of the lack of the disconnected $\frac{1}{2}\hat{T}_2^2$ clusters from the CISD wave function (see Section 1.8). Since the renormalization terms are expressible in terms of unlinked diagrams, the non-extensivity is commonly ascribed to uncanceled unlinked-diagram contributions retained in truncated CI. The non-extensivity effects in truncated CI increase rapidly with the size of the system, because of the higher N -dependence of the non-extensive terms.

A simple strategy to improve the CID (or CISD) energy is to add an estimate of the quadruple-excitation contribution. As a first try we can simply remove the $-E^{(2)}S_{11}$ renormalization-term contribution since this cancels the largest quadruples contribution in $E^{(4)}$, the unlinked quadruple-excitation diagrams (see Fig. 5.13). Thus adding $+E^{(2)}S_{11}$ is equivalent to adding the unlinked diagrams



In the above example this approach would give

E_{CISD}	$-275.576 \text{ m}E_{\text{h}}$
$E^{(2)}S_{11}$	$-17.116 \text{ m}E_{\text{h}}$
	$-292.692 \text{ m}E_{\text{h}}$
estimate of E_{CISDQ}	

This is a very reasonable value, though it is likely to overestimate the quadruple-excitation contribution somewhat (the true CISDQ correlation energy is probably about $-289 \text{ m}E_{\text{h}}$). This approach is, in fact, the basis for the *Davidson correction* (Davidson 1974, Langhoff and Davidson 1974)

$$\Delta E_{\text{Q}} \approx (1 - C_0^2)\Delta E_{\text{D}}, \quad (5.51)$$

where ΔE_{D} and ΔE_{Q} are the double- and quadruple-excitation contributions, respectively, in CI and C_0 is the coefficient of the SCF configuration in the normalized CID expansion. This correction is based on the assumption

(see Meunier, Levy and Berthier 1976, Bartlett and Shavitt 1977a) that

$$\Delta E_D \approx E^{(2)} \quad (5.52)$$

and

$$S_{11} = \langle \Psi^{(1)} | \Psi^{(1)} \rangle \approx \langle \chi_D | \chi_D \rangle = \frac{1 - C_0^2}{C_0^2} \approx 1 - C_0^2. \quad (5.53)$$

The denominator in the next-to-last form of (5.53) (Siegbahn 1978) signals the conversion from the full normalization of the CI wave function to the intermediate normalization appropriate for perturbation theory, $\Psi_{\text{CID}} = \Phi_{\text{SCF}} + \chi_D$, in which the coefficient of Φ_{SCF} is equal to 1; however, this denominator is usually ignored, giving the last form in the equation. Furthermore, ΔE_{SD} and C_0 from CISD are generally used instead of the CID values, providing an approximation for CISDQ.

The Davidson correction is one of a class of so-called *quadruples corrections* (see also Davidson and Silver 1977, Pople, Seeger and Krishnan 1977, Burton, Buenker, Bruna *et al.* 1983, Meissner 1988, Martin, François and Gijbels 1990) that constituted an attempt to account for the quadruple-excitation CI contributions on the basis of CISD data. Since the principal extensivity error in CISD is due to the implicit presence of the disjoint part of the fourth-order renormalization term and since those contributions can only be canceled by unlinked quadruple-excitation terms, these corrections go a long way toward restoring extensivity to CISD and are therefore also known as *extensivity corrections*.

Applying the Davidson-correction formula to the H₂O 39-STO CISD calculation gives

$$(1 - C_0^2)\Delta E_D = (1 - 0.972422^2)(-275.576) = -14.990 \text{ mE}_h, \quad (5.54)$$

which may be compared with

$$E^{(2)}S_{11} = -17.116 \text{ mE}_h. \quad (5.55)$$

If we had used $(1 - C_0^2)/C_0^2$ instead of $1 - C_0^2$ then we would have obtained a correction equal to -15.852 mE_h . Actually, $E^{(2)}S_{11}$ overestimates the correction, since only $(-E^{(2)}S_{11})_{\text{DJ}}$ is truly canceled by the non-EPV unlinked quadruple-excitation diagrams. A better correction would be

$$(E^{(2)}S_{11})_{\text{DJ}} = -10.015 \text{ mE}_h, \quad (5.56)$$

but we cannot easily obtain this value, or an estimate for it, from the CISD calculation. The various CEPA (coupled electron pairs approximation) models (CEPA- n , $n = 0-5$) (Kelly 1964a, Čížek 1966, Meyer 1974, Ahlrichs,

Table 5.2. *Correlation energy of H_2O in the 39-STO basis (energies are in millihartrees) (Rosenberg and Shavitt 1975, Rosenberg, Ermler and Shavitt 1976, Bartlett, Shavitt and Purvis 1979, Bartlett 1981, Bartlett, Cole, Purvis et al. 1987)*

	From D ^a calculation	From SD ^b calculation
CI correlation energy	-0.274021	-0.275576
Contribution of single excitations		-0.001555
C_0 (coefficient of Φ_{SCF} in normalized CI)	0.973176	0.972422
Davidson correction	-0.014504	-0.014990
CI correlation energy + correction	-0.288525	-0.290566
MBPT(2)	-0.281780	
MBPT(3)	-0.285021	
MBPT double excitations to infinite order	-0.28826	
MBPT(4)SDQ		-0.288172
MBPT(4)		-0.296035
CCD	-0.286210	
CCSD		-0.287858
CCSDT-1		-0.295408

^a Doubles

^b Singles and doubles.

Lischka, Staemmler *et al.* 1975, Kutzelnigg 1977, Koch and Kutzelnigg 1981) are various ways to estimate $(E^{(2)}S_{11})_{DJ}$ on the basis of pair energies (we shall not describe these methods here). Thus, if we could have used $(E^{(2)}S_{11})_{DJ}$ we would have obtained

$$\begin{aligned}
 E_{CISD} &= -275.576 \text{ m}E_h \\
 (E^{(2)}S_{11})_{DJ} &= -10.015 \text{ m}E_h \\
 \hline
 &= -285.591 \text{ m}E_h
 \end{aligned}$$

This analysis does not include the *full* quadruple-excitations contribution, since the remaining (uncancelled) true quadruples terms have been ignored. Including these terms would have added about $-3.9 \text{ m}E_h$; using $E^{(2)}S_{11}$ instead of $(E^{(2)}S_{11})_{DJ}$ compensates to some extent for this omission, giving about $-289.5 \text{ m}E_h$ compared with $-288.172 \text{ m}E_h$ for the fourth-order MBPT SDQ energy.

Various correlation-energy results for the H₂O 39-STO CISD calculation (Rosenberg and Shavitt 1975, Rosenberg, Ermler and Shavitt 1976, Bartlett, Shavitt and Purvis 1979, Bartlett 1981, Bartlett, Cole, Purvis *et al.* 1987) are summarized in Table 5.2; the CI, MBPT and coupled-cluster (CC) results are included. The coupled-cluster methods will be discussed in Chapters 9 and 10.

6

Proof of the linked-diagram theorem

6.1 The factorization theorem

As a first step in the formal proof of the linked-diagram theorem, we will derive a generalization of the factorization described in subsection 5.7.4, embodied in (5.25). This generalization, referred to as the *factorization theorem* (Hugenholtz 1957, Frantz and Mills 1960, Brandow 1967, 1977), states that a product of two connected open diagrams is equal to a sum of disconnected diagrams, each made up of the two diagrams of the original product with all possible time orderings of the vertices of one of the disconnected parts relative to those of the other.

We first give an example, using skeletons rather than full diagrams to reduce clutter since the validity of the factorization is independent of the arrow directions:

$$\begin{aligned}
 & \text{Diagram 1} \times \text{Diagram 2} = \text{Diagram 3} + \text{Diagram 4} + \text{Diagram 5} \\
 & \quad + \text{Diagram 6} + \text{Diagram 7} + \text{Diagram 8} + \text{Diagram 9} .
 \end{aligned}$$

The theorem can be extended straightforwardly to products of more than two open diagrams. It cannot be applied to a simple product of an open and a closed diagram or of two closed diagrams, because the total number of denominator factors would not be the same in the product and in the unlinked diagrams resulting from the expansion. However, it can be applied to a diagram with an insertion, which represents a product of two diagrams, at least one of which is closed, with a modification in the principal part due

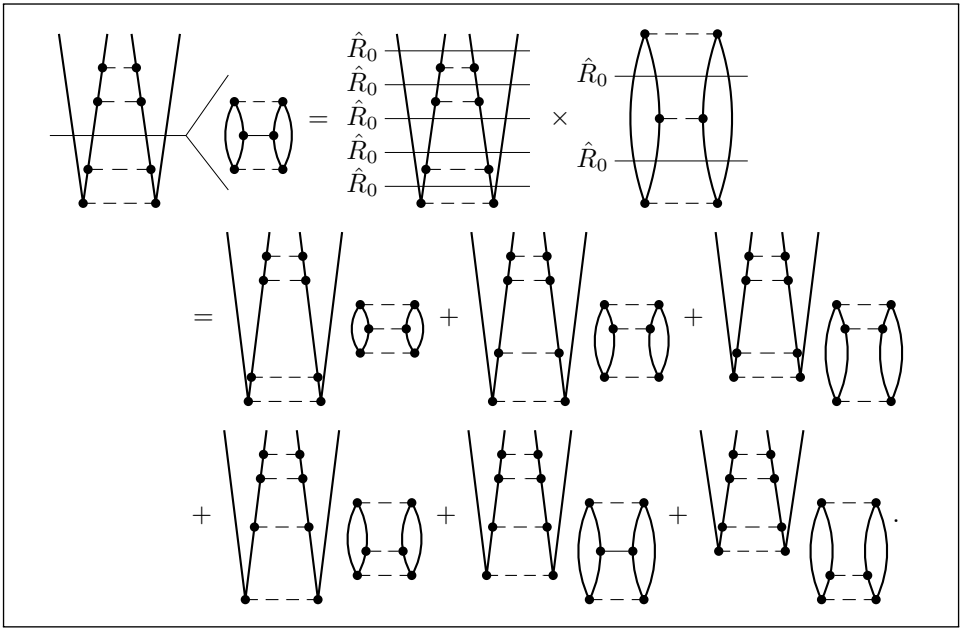


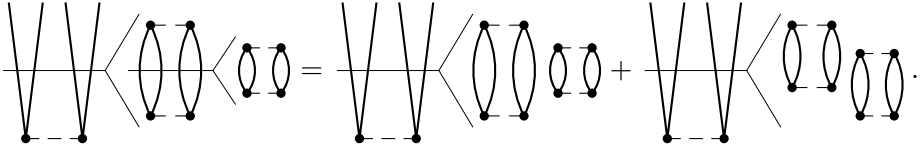
Fig. 6.1. A factorization-theorem example of the expansion of a diagram with an insertion as a sum of unlinked diagrams (resolvent lines are shown in the product form to show that a resolvent remains on each side of the original insertion).

to the presence of an extra resolvent line just above the insertion. In this case the sum over all time orderings is restricted to those orderings in which the top vertex of the inserted diagram remains at the level of the insertion. This form of the theorem is used to prove that the renormalization terms of RSPT cancel against the unlinked diagrams. An example is shown in Fig. 6.1.

Any structure that exists above the insertion remains unchanged in all diagrams in the sum. Therefore, any complex structure may be added above the insertion and we would still obtain a sum of the same number of unlinked diagrams. One obtains the modified theorem directly from the original theorem by cutting off the top of the principal part just above the insertion (including the extra resolvent) and the top vertex of the insertion before the expansion of the product, applying the original factorization theorem and then restoring the deleted parts in the product and in all the unlinked diagrams in the expansion. Obviously, restoring these parts does not affect the validity of the expansion.

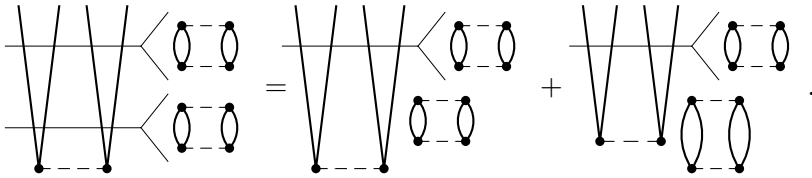
In the case of nested insertions the factorization theorem can be applied successively to the individual insertions, beginning with the innermost

insertion and proceeding outwards. For example, we have



When deriving the linked-diagram theorem we do not need to continue the expansion to the outer insertion, because the cancellation of the inner insertion with the corresponding unlinked terms within the outer insertion (shown on the right-hand side), owing to the sign change associated with each insertion, produces a zero factor.

Similarly, an extension of the expansion to multiple insertions in the same principal part can also be done sequentially, beginning with the lowest insertion. For example,



Again, it is unnecessary to proceed further because of the zero factor resulting from the first expansion.

To prove the factorization theorem we consider the product of two diagrams, both open at the top, following Frantz and Mills (1960) (see also Manne (1977) and Harris, Monkhorst and Freeman (1992), who deal specifically with the case of a diagram with an insertion) and note that the algebraic expressions for the diagram product and for all the different time orderings in the sum of the comparably labeled disconnected diagrams have the same numerator; then differ only in their denominators. Thus we have to show that the sum of the appropriate denominator factors ($1/\varepsilon_{ij}^{ab,\dots}$) for the disconnected diagrams is equal to the product of the denominator factors of the product.

Let the number of resolvent lines, and thus the number of denominator factors, in the two diagrams of the product be n and m , respectively, and let the corresponding denominators be written (from the bottom up) as D_1, D_2, \dots, D_n and D'_1, D'_2, \dots, D'_m , respectively. This is described

schematically by

$$\begin{array}{ccc}
 \begin{array}{c}
 \text{---} D_n \text{---} \\
 \text{---} D_{n-1} \text{---} \\
 \text{---} D_{n-2} \text{---} \\
 \vdots \\
 \text{---} D_3 \text{---} \\
 \text{---} D_2 \text{---} \\
 \text{---} D_1 \text{---} \\
 \text{---} \text{---} \text{---}
 \end{array}
 &
 \begin{array}{c}
 \text{vertex } n \\
 \text{vertex } n-1 \\
 \\
 \text{vertex } 3 \\
 \text{vertex } 2 \\
 \text{vertex } 1
 \end{array}
 &
 \begin{array}{ccc}
 \begin{array}{c}
 \text{---} D'_m \text{---} \\
 \text{---} D'_{m-1} \text{---} \\
 \text{---} D'_{m-2} \text{---} \\
 \vdots \\
 \text{---} D'_3 \text{---} \\
 \text{---} D'_2 \text{---} \\
 \text{---} D'_1 \text{---} \\
 \text{---} \text{---} \text{---}
 \end{array}
 &
 \begin{array}{c}
 \text{vertex } m \\
 \text{vertex } m-1 \\
 \\
 \text{vertex } 3 \\
 \text{vertex } 2 \\
 \text{vertex } 1
 \end{array}
 \end{array}
 \end{array}$$

The same scheme also applies to the case of a diagram with an insertion if we ignore all vertices and resolvents in the principal part above the insertion and add a fixed vertex above D'_m in the other part. We denote the sum of the denominator factors of the corresponding unlinked diagrams, summed over all possible relative orderings of their vertices without change of ordering within each disconnected part, by S_{nm} . We need to show that this sum is equal to the product of the denominator factors of the original diagram product, i.e.

$$S_{nm} = \frac{1}{D_1 D_2 \cdots D_n D'_1 D'_2 \cdots D'_m}. \quad (6.1)$$

As an example, we shall consider the case with $n = 3, m = 2$. The sum S_{32} consists of 10 terms, involving all possible time orderings of the two sets of vertices relative to each other:

$$\begin{array}{lcl}
 \hat{R}_0 \rightarrow & & \\
 \hat{R}_0 \rightarrow & D_3 & \text{---} \frac{D'_2}{D'_1} \text{---} \\
 \hat{R}_0 \rightarrow & & \frac{1}{D_1 D_2 D_3 (D_3 + D'_1)(D_3 + D'_2)} \\
 \hat{R}_0 \rightarrow & \text{---} \frac{D_2}{D_1} \text{---} & \\
 \hat{R}_0 \rightarrow & \text{---} \frac{D_1}{D_2} \text{---} & \\
 \hat{R}_0 \rightarrow & & \\
 \hat{R}_0 \rightarrow & D_3 & \text{---} \frac{D'_2}{D'_1} \text{---} \\
 \hat{R}_0 \rightarrow & \text{---} \frac{D_2}{D_1} \text{---} & \frac{1}{D_1 D_2 (D_2 + D'_1)(D_3 + D'_1)(D_3 + D'_2)} \\
 \hat{R}_0 \rightarrow & \text{---} \frac{D_1}{D_2} \text{---} & \\
 \hat{R}_0 \rightarrow & \text{---} \frac{D_1}{D_2} \text{---} &
 \end{array}$$

$$\begin{array}{rcl}
\hat{R}_0 \rightarrow & D_3 & -\underline{\underline{D'_2}}- \\
\hat{R}_0 \rightarrow & & \\
\hat{R}_0 \rightarrow & -\underline{\underline{D_2}}- & D'_1 \\
\hat{R}_0 \rightarrow & & \\
\hat{R}_0 \rightarrow & D_1 & -\underline{\underline{D'_2}}- \\
\hat{R}_0 \rightarrow & -\underline{\underline{D_1}}- &
\end{array}
\frac{1}{D_1(D_1 + D'_1)(D_2 + D'_1)(D_3 + D'_1)(D_3 + D'_2)}$$

$$\begin{array}{rcl}
\hat{R}_0 \rightarrow & D_3 & -\underline{\underline{D'_2}}- \\
\hat{R}_0 \rightarrow & & \\
\hat{R}_0 \rightarrow & -\underline{\underline{D_2}}- & \\
\hat{R}_0 \rightarrow & -\underline{\underline{D_1}}- & D'_1 \\
\hat{R}_0 \rightarrow & & \\
\hat{R}_0 \rightarrow & & -\underline{\underline{D'_2}}-
\end{array}
\frac{1}{D'_1(D_1 + D'_1)(D_2 + D'_1)(D_3 + D'_1)(D_3 + D'_2)}$$

$$\begin{array}{rcl}
\hat{R}_0 \rightarrow & -\underline{\underline{D_3}}- & D'_2 \\
\hat{R}_0 \rightarrow & & \\
\hat{R}_0 \rightarrow & D_2 & -\underline{\underline{D'_1}}- \\
\hat{R}_0 \rightarrow & & \\
\hat{R}_0 \rightarrow & -\underline{\underline{D_1}}- &
\end{array}
\frac{1}{D_1 D_2 (D_2 + D'_1)(D_2 + D'_2)(D_3 + D'_2)}$$

$$\begin{array}{rcl}
\hat{R}_0 \rightarrow & -\underline{\underline{D_3}}- & D'_2 \\
\hat{R}_0 \rightarrow & & \\
\hat{R}_0 \rightarrow & D_2 & -\underline{\underline{D'_1}}- \\
\hat{R}_0 \rightarrow & -\underline{\underline{D_1}}- & D'_1 \\
\hat{R}_0 \rightarrow & & \\
\hat{R}_0 \rightarrow & -\underline{\underline{D_1}}- &
\end{array}
\frac{1}{D_1(D_1 + D'_1)(D_2 + D'_1)(D_2 + D'_2)(D_3 + D'_2)}$$

$$\begin{array}{rcl}
\hat{R}_0 \rightarrow & -\underline{\underline{D_3}}- & D'_2 \\
\hat{R}_0 \rightarrow & & \\
\hat{R}_0 \rightarrow & D_2 & -\underline{\underline{D'_1}}- \\
\hat{R}_0 \rightarrow & -\underline{\underline{D_1}}- & D'_1 \\
\hat{R}_0 \rightarrow & & \\
\hat{R}_0 \rightarrow & -\underline{\underline{D_1}}- &
\end{array}
\frac{1}{D'_1(D_1 + D'_1)(D_2 + D'_1)(D_2 + D'_2)(D_3 + D'_2)}$$

and

$$S_{0m} = \frac{1}{D'_1 D'_2 \cdots D'_m}. \quad (6.3)$$

Our proof will be inductive, showing that if (6.1) holds for all n, m such that $n + m = k - 1$ then this equation holds also for $n + m = k$. Equations (6.2), (6.3) show that the equation holds for $n + m = 1$, as well as for S_{20} and S_{02} . It is also very easy to verify the S_{11} case:

$$S_{11} = \frac{1}{D_1(D_1 + D'_1)} + \frac{1}{D'_1(D_1 + D'_1)} = \frac{1}{D_1 + D'_1} \left(\frac{1}{D_1} + \frac{1}{D'_1} \right) = \frac{1}{D_1 D'_1}, \quad (6.4)$$

so that the theorem holds for all $n + m \leq 2$.

Now consider the case $n \geq 1, m \geq 1$, and divide the corresponding set of unlinked diagrams into two classes, those in which the top vertex occurs in the first part and those in which it occurs in the second part. The two classes can be described schematically by

$$\begin{array}{ccc} \hat{R}_0 \rightarrow & -\frac{D_n}{D_{n-1}} - & D'_m \\ \hat{R}_0 \rightarrow & \vdots & \vdots \\ & \vdots & \vdots \end{array} \quad \text{and} \quad \begin{array}{ccc} \hat{R}_0 \rightarrow & D_n - \frac{D'_m}{D'_{m-1}} - & \\ \hat{R}_0 \rightarrow & \vdots & \vdots \\ & \vdots & \vdots \end{array}$$

The contribution from the topmost level in both classes is the factor

$$\frac{1}{D_n + D'_m}.$$

In the diagram class on the left this factor is multiplied by $S_{n-1,m}$ (when we allow all possible relative orderings of the remaining vertices), while in the class on the right it is multiplied by $S_{n,m-1}$. Therefore

$$S_{nm} = \frac{1}{D_n + D'_m} (S_{n-1,m} + S_{n,m-1}). \quad (6.5)$$

If the theorem holds for $S_{n-1,m}$ and $S_{n,m-1}$, we can substitute the corresponding products and obtain

$$\begin{aligned} S_{n-1,m} + S_{n,m-1} &= \left(\frac{1}{D'_m} + \frac{1}{D_n} \right) \frac{1}{D_1 \cdots D_{n-1} D'_1 \cdots D'_{m-1}} \\ &= \frac{D_n + D'_m}{D_1 D_2 \cdots D_n D'_1 D'_2 \cdots D'_m}, \end{aligned} \quad (6.6)$$

so that

$$S_{nm} = \frac{1}{D_n + D'_m} (S_{n-1,m} + S_{n,m-1}) = \frac{1}{D_1 D_2 \cdots D_n D'_1 D'_2 \cdots D'_m}, \quad (6.7)$$

satisfying the theorem. Since the theorem holds for $n + m \leq 2$, it must hold for all n, m .

It should be emphasized that, for the factorization theorem to hold, all summations over internal lines must be unrestricted, including any EPV terms. The EPV terms in the disconnected or unlinked diagrams are counterbalanced in the MBPT expansions by the inclusion of such terms in the summations for the linked diagrams as well, as discussed in subsection 5.7.5.

6.2 The linked-diagram theorem

The linked-diagram theorem states that the wave function and the correlation energy are each given by a sum of linked diagrams only, provided that all EPV terms are included in the summations for each diagram. It was first stated by Brueckner (1955), who proved it explicitly for specific low orders of the perturbation expansion and also asserted that it must be true at all orders, because of the incorrect size dependence of the unlinked diagrams and the renormalization terms. It was proved formally for all orders by Goldstone (1957), in terms of both time-dependent and time-independent diagrammatic techniques.

An elegant time-independent derivation was presented by Manne (1977), who showed that all diagrams that contain unlinked parts or insertions, or any combinations of these, cancel mutually leaving an expansion in terms of linked diagrams only. This derivation is closely tied to the factorization theorem in the form applicable to diagrams with insertions.

The direct diagrammatic expansion of RSPT using the bracketing procedure described in subsection 2.4.6 (and see Fig. 2.1) includes diagrams that contain insertions, as well as unlinked diagrams, i.e. diagrams that contain separate closed parts. Each unlinked diagram may itself contain insertions and each insertion may contain unlinked diagrams and further insertions, to any depth.

We will consider first all unlinked wave function diagrams that contain a linked (but possibly disconnected) open part, one separate closed part and no insertions. Let us group together all those of a given order which have the same open part and the same closed part and for which the top vertex of the closed part is at the same level relative to the open part, with all possible relative orderings of the other vertices of the closed part relative to those of the open part, without change of ordering within each part (such as the set of unlinked diagrams in the expansion in Fig. 6.1). According to the factorization theorem, and because of the change of sign associated in the perturbation expansion with each insertion, the diagrams in such a

group cancel with the diagram in which the separate closed part is placed as an insertion into the open part at the original level of the top vertex of the closed part. The same procedure can be applied to groups of diagrams with the top vertex of the closed part at any other level relative to the open part; consequently *all* unlinked wave-function diagrams with one open part cancel with *all* linked wave-function diagrams with one insertion containing a single (i.e. linked) closed part.

The same procedure can be applied to unlinked energy diagrams consisting of two closed parts where the part with the higher top vertex plays the same role as the open part in the previous paragraph, thus proving the cancellation of all two-part unlinked closed diagrams with the corresponding insertions.

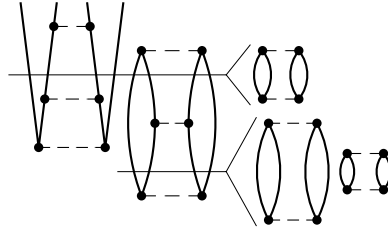
This approach can then be extended to diagrams with any combination of separate closed parts and insertions, including cases with insertions that contain unlinked diagrams or other insertions, as well as to unlinked diagrams that contain insertions, to any depth. For the purpose of this extension, following Manne we classify all the diagrams of a given order according to the nature of the lowest-level separate item they contain; here a separate item refers to an insertion at that level or to a separate closed part with top vertex at that level. We will refer to the original diagram minus the lowest separate item (but retaining the extra resolvent) as the remainder diagram. This remainder diagram may be linked or unlinked, may have any number of separate closed parts and may itself contain insertions.

If the lowest item is a separate closed part, we collect together all diagrams of a given order that have that same lowest closed part with top vertex at the same level relative to the remainder diagram, and the same remainder diagram. In this case all these diagrams cancel with a corresponding diagram with an insertion at the specified level.

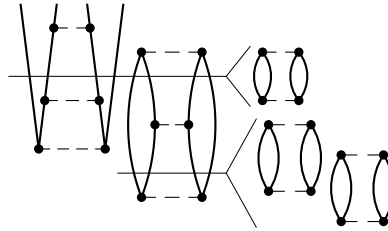
If the lowest item is an insertion that contains no further insertions or unlinked diagrams then, by the argument of the previous paragraph, it cancels against all the corresponding unlinked diagrams with a lowest unlinked part having a top vertex at the same level. If, however, this lowest-item insertion contains other insertions or unlinked diagrams then we consider the remainder diagram as a fixed multiplicative factor and apply the same procedure to the diagram within the insertion. Proceeding in this manner until we reach the innermost insertion we find that *all* unlinked diagrams and *all* diagrams that contain insertions cancel, leaving an expansion in terms of linked diagrams only.

As an example, consider the following twelfth-order wave-function diagram containing an unlinked principal part and two insertions, one of which

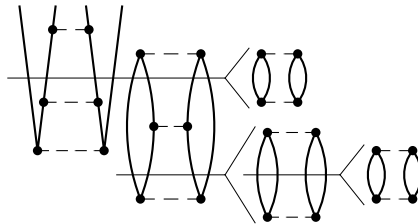
contains an unlinked diagram:



The lowest separate item in this diagram is the lower insertion. Since this insertion contains an unlinked diagram, we consider the rest of the diagram (which is itself unlinked and contains an insertion) as a multiplicative factor and focus our attention on the contents of the lower insertion. The lowest separate item within this insertion is the separate closed part at its right, because it has the lowest top vertex within the insertion. In this example there is only one other diagram that can be grouped with it, differing from it only in the relative levels of the lower vertices within the insertion:



According to the factorization theorem, the sum of these two diagrams cancels against the corresponding diagram with an inner insertion (which, like all insertions, comes in with a sign change), regardless of the value of the original remainder diagram:



All three of these diagrams would appear in the straightforward RSPT expansion of the twelfth-order wave function following the bracketing procedure and, provided that all summations in all diagrams are unrestricted, these and all other diagrams that contain unlinked parts or insertions can be left out of the expansion.

We shall consider briefly an alternative derivation of the linked-diagram theorem along the lines of Goldstone's time-independent derivation (Harris, Monkhorst and Freeman 1992). In this derivation the linked-diagram expansions for the wave function and energy are substituted into the recursive form (2.75) of the Schrödinger equation, and the factorization theorem is used to show that this expansion satisfies the equation.

To prove this assertion we first rewrite (2.75) in a form appropriate for RSPT,

$$|\Psi\rangle = |0\rangle + \hat{R}_0(\hat{W} - \Delta E)|\Psi\rangle \quad (6.8)$$

with

$$\Delta E = \langle 0|\hat{W}|\Psi\rangle, \quad (6.9)$$

where $\hat{R}_0 \equiv \hat{R}_0(E_0)$, $\hat{W} = \hat{V} - E^{(1)}$ and $\Delta E = E - E_{\text{ref}} = E - E_0 - E^{(1)}$. The implicit equations (6.8), (6.9) for $|\Psi\rangle$ and ΔE are entirely equivalent to the Schrödinger equation.

We need to prove that these equations are satisfied by the linked-diagram expansions

$$|\Psi\rangle = \sum_{n=0}^{\infty} [(\hat{R}_0\hat{W})^n|0\rangle]_{\text{L}}, \quad (6.10)$$

$$\Delta E = \sum_{n=1}^{\infty} \langle 0|\hat{W}(\hat{R}_0\hat{W})^n|0\rangle_{\text{L}}, \quad (6.11)$$

where the subscript L indicates that the summations are limited to linked diagrams only (note that the $n = 0$ term is missing in the summation for ΔE in (6.11) because $\langle 0|\hat{W}|0\rangle = 0$). We are going to prove this assertion by substituting (6.10), (6.11) into the recursive equations (6.8), (6.9) and showing that the latter are then satisfied.

We first substitute (6.10) in (6.9), obtaining

$$\Delta E = \sum_{n=1}^{\infty} \langle 0|\hat{W}[(\hat{R}_0\hat{W})^n|0\rangle]_{\text{L}}. \quad (6.12)$$

It is easy to verify that all the closed diagrams that can be formed by adding a new top vertex to the upwards-open linked n -vertex diagrams are linked (because all disconnected parts of the open diagram must be closed by the single added vertex) and constitute the complete set of all closed linked $(n + 1)$ -vertex diagrams. Therefore (6.12) is consistent with (6.9).

Next we substitute (6.10) in (6.8), resulting in

$$\begin{aligned} |\Psi\rangle &= |0\rangle + \sum_{n=0}^{\infty} \hat{R}_0(\hat{W} - \Delta E)[(\hat{R}_0\hat{W})^n|0\rangle]_{\text{L}} \\ &= |0\rangle + \sum_{n=0}^{\infty} \hat{R}_0\hat{W}[(\hat{R}_0\hat{W})^n|0\rangle]_{\text{L}} - \sum_{n=0}^{\infty} \Delta E \hat{R}_0[(\hat{R}_0\hat{W})^n|0\rangle]_{\text{L}}. \end{aligned} \quad (6.13)$$

Each term of the first sum over n in the second line of (6.13) consists of all the upwards-open $(n+1)$ -vertex diagrams that can be formed by adding one vertex (and the corresponding resolvent) to all upwards-open linked n -vertex diagrams. Each resulting diagram either is linked or is unlinked with a single separate closed part (if the added vertex closed a disconnected part of the n -vertex open diagram) and has the top vertex of the closed part as the top vertex of the entire diagram. We may therefore rewrite (6.13) in the form

$$\begin{aligned} |\Psi\rangle &= |0\rangle + \sum_{n=0}^{\infty} [\hat{R}_0\hat{W}(\hat{R}_0\hat{W})^n|0\rangle]_{\text{L}} + \sum_{n=0}^{\infty} [\hat{R}_0\hat{W}[(\hat{R}_0\hat{W})^n|0\rangle]_{\text{L}}]_{\text{U}} \\ &\quad - \sum_{n=0}^{\infty} \Delta E \hat{R}_0[(\hat{R}_0\hat{W})^n|0\rangle]_{\text{L}}, \end{aligned} \quad (6.14)$$

where the subscript U indicates restriction to unlinked terms. The factorization theorem can then be used to show the cancellation of the last two sums in this equation, because each term in the third sum can be described by an open diagram with an insertion above its top vertex; this diagram cancels the contributions to the second sum from the sum of corresponding unlinked two-part open diagrams in which the top vertex of the closed part is the top vertex of the entire diagram. The remaining terms of the right-hand side are equivalent to the linked-diagram expansion (6.10), proving that this expansion satisfies (6.8) and the Schrödinger equation.

The linked-diagram theorem accounts for the transition from RSPT to MBPT, and is a major simplification of ordinary RSPT. As a result of the linked-diagram requirement and the inclusion of EPV terms, there are no renormalization terms and no restricted summations in the MBPT expansions. In fact, MBPT assumes the simple, recursive form of BWPT while, unlike BWPT, maintaining extensivity. In this form, RSPT has been reduced to its essentials, providing both an efficient computational tool and a framework for the easy introduction of infinite-order summations of diagrams via the coupled-cluster methods described in Chapters 9 and 10.

Computational aspects of MBPT

7.1 Techniques of diagram summation

The straightforward summation of individual MBPT diagrams is usually an inefficient process. If the one-electron basis contains n_h hole states (orbitals occupied in Φ_0) and n_p particle states (virtual orbitals), the number of terms in the sum represented by a diagram with h internal hole lines and p internal particle lines is $n_h^h n_p^p$. Using symmetries with respect to permutation of the indices can reduce the number of distinct terms by some factor but the overall number of terms is still of order $n_h^h n_p^p$, which may often be too large for practical computation.

A variety of techniques are used to reduce the computational effort. The principal approach involves the evaluation and reuse of various intermediate quantities (partial sums). Another technique is the factorization of sums of certain classes of diagrams, using a procedure analogous to the use of the factorization theorem to factor sums of unlinked diagrams. The identification of conjugate diagrams (Section 5.5) can also serve to reduce the number of diagrams that need to be evaluated.

We will consider some examples from the fourth-order energy in discussing efficient summation techniques. We will focus on the canonical HF case, since diagrams containing one-particle vertices have fewer lines than the corresponding diagrams with only two-particle vertices. First we examine the double-excitation diagrams; see Fig. 5.8. Since typically $n_p \gg n_h$, the largest number of terms is represented by the particle ladder, diagram 14:

$$\begin{array}{c}
 (a) \text{---} \text{---} \text{---} (b) \\
 (c) \text{---} (i) \text{---} (j) \text{---} (d) \\
 (e) \text{---} \text{---} \text{---} (f)
 \end{array} = \frac{1}{16} \sum_{abcdefij} \frac{\langle ij || ab \rangle \langle ab || cd \rangle \langle cd || ef \rangle \langle ef || ij \rangle}{\varepsilon_{ij}^{ab} \varepsilon_{ij}^{cd} \varepsilon_{ij}^{ef}}. \quad (7.1)$$

The straightforward summation of (7.1) would involve $n_h^2 n_p^6$ terms (loosely referred to as an n^8 process). However, we can split this diagram into two parts, separated by the middle resolvent line:

$$\begin{array}{c}
 \begin{array}{c} (a) \quad \text{---} \quad (b) \\ \text{---} \quad \text{---} \quad \text{---} \quad \text{---} \\ c \quad i \quad j \quad d \\ \text{---} \quad \text{---} \quad \text{---} \quad \text{---} \end{array} \sim \sum_{ab} \frac{\langle ij || ab \rangle}{\varepsilon_{ij}^{ab}} \langle ab || cd \rangle = (S_{ij}^{cd})^* \\
 \hline
 \begin{array}{c} c \quad i \quad j \quad d \\ \text{---} \quad \text{---} \quad \text{---} \quad \text{---} \\ (e) \quad \text{---} \quad (f) \end{array} \sim \sum_{ef} \langle cd || ef \rangle \frac{\langle ef || ij \rangle}{\varepsilon_{ij}^{ef}} = S_{ij}^{cd}
 \end{array} \quad (7.2)$$

(noting that a, b, e, f are dummy summation indices). Summation of the product of these two partial sums over c, d, i, j after insertion of the denominator corresponding to the middle resolvent line produces the complete sum for the diagram,

$$\frac{1}{16} \sum_{cdij} \frac{|S_{ij}^{cd}|^2}{\varepsilon_{ij}^{cd}} = \frac{1}{4} \sum_{\substack{c>d \\ i>j}} \frac{|S_{ij}^{cd}|^2}{\varepsilon_{ij}^{cd}}.$$

The last form of this expression uses the relationships $S_{ij}^{cd} = -S_{ij}^{dc} = -S_{ji}^{cd} = S_{ji}^{dc}$ and $S_{ij}^{cc} = S_{ii}^{cd} = 0$, which arise from the use of antisymmetric two-electron integrals. The evaluation of S_{ij}^{cd} is proportional in effort to $n_h^2 n_p^4$ (there are $n_h^2 n_p^2$ sums to be computed, each requiring n_p^2 contributions). The final sum is much faster, being proportional to $n_h^2 n_p^2$. The complete procedure thus amounts to an $n_h^2 n_p^4$ process, loosely referred to as n^6 .

Note that each half-diagram in (7.2) is a second-order wave-function diagram, in either ket (bottom) or bra (top) form. As a wave-function diagram, each half would include a factor $\frac{1}{8}$ (for three pairs of equivalent lines) and its own ε_{ij}^{cd} denominator (see subsection 5.6.2). However, because the c, d, i, j lines and the resolvent line are actually common to the two parts, we have to remove a factor $\frac{1}{4}$ (for two common pairs of equivalent lines) and one denominator, leaving the above result. Note also that each term in the partial sums contains a first-order wave-function coefficient such as $\langle ef || ij \rangle / \varepsilon_{ij}^{ef}$, the coefficient of $|\Phi_{ij}^{ef}\rangle$ in $|\Psi^{(1)}\rangle$.

For another example, consider diagram 7 of Fig. 5.8:

$$\begin{array}{c}
 \begin{array}{c} (a) \quad \text{---} \quad (j) \\ \text{---} \quad \text{---} \quad \text{---} \quad \text{---} \\ (i) \quad \text{---} \quad (l) \\ \text{---} \quad \text{---} \quad \text{---} \quad \text{---} \\ (c) \quad \text{---} \quad (k) \end{array} \quad \begin{array}{c} (b) \\ \text{---} \quad \text{---} \quad \text{---} \quad \text{---} \\ d \end{array} \\
 \hline
 \end{array} = \sum_{abcdijkl} \frac{\langle ij || ab \rangle \langle al || cj \rangle \langle kb || id \rangle \langle cd || kl \rangle}{\varepsilon_{ij}^{ab} \varepsilon_{il}^{bc} \varepsilon_{kl}^{cd}}. \quad (7.3)$$

In this case the partial sum will be

$$T_{il}^{bc} = \sum_{dk} \langle kb || id \rangle \frac{\langle cd || kl \rangle}{\varepsilon_{kl}^{cd}}, \quad (7.4)$$

an $n_h^3 n_p^3$ process, and the complete sum is given by

$$\sum_{bcil} \frac{(T_{li}^{cb})^* T_{il}^{bc}}{\varepsilon_{il}^{bc}}.$$

For one more example of a double-excitation diagram, consider diagram 8 of Fig. 5.8:

$$= -\frac{1}{4} \sum_{abcdeijk} \frac{\langle ij || ab \rangle \langle ab || cd \rangle \langle kd || ie \rangle \langle ce || kj \rangle}{\varepsilon_{ij}^{ab} \varepsilon_{ij}^{cd} \varepsilon_{jk}^{ce}}. \quad (7.5)$$

Using the partial sums (7.2), (7.4) of the previous two examples, the complete sum for this diagram is given by

$$-\frac{1}{4} \sum_{cdij} \frac{(S_{ij}^{cd})^* T_{ij}^{dc}}{\varepsilon_{ij}^{cd}}.$$

These examples demonstrate how the same partial sum can be used in the evaluation of more than one diagram. Using the partial summation technique, the evaluation of all the double-excitation diagrams in fourth order involves at most an $n_h^2 n_p^4$ ($\sim n^6$) computational process.

Next we consider fourth-order triple-excitation diagrams, Fig. 5.9, and take diagram 25 as an example:

$$= \frac{1}{2} \sum_{abcdeijk} \frac{\langle ij || ab \rangle \langle ak || cd \rangle \langle db || ke \rangle \langle ce || ij \rangle}{\varepsilon_{ij}^{ab} \varepsilon_{ijk}^{bcd} \varepsilon_{ij}^{ce}}. \quad (7.6)$$

Because of the triple-excitation factor in the denominator, we are forced to use a six-index partial sum,

$$U_{ijk}^{bcd} = \sum_e \frac{\langle db || ke \rangle \langle ce || ij \rangle}{\varepsilon_{ij}^{ab}}, \quad (7.7)$$

requiring an $n_h^3 n_p^4$ ($\sim n^7$) computational process. The complete sum for

this diagram is then

$$\frac{1}{2} \sum_{bcdijk} \frac{(U_{jik}^{cbd})^* U_{ijk}^{bcd}}{\varepsilon_{ijk}^{bcd}}.$$

Applying the same approach to the fourth-order quadruple-excitation diagrams would have resulted in an n^8 process because of the quadruple-excitation factor in the denominator. However, as is shown below in Section 7.2, a factorization similar to that derived in the factorization theorem eliminates the quadruple-excitation denominator factor and reduces the computational effort for these diagrams to an n^6 process, leaving the triple-excitation contribution as the most computationally demanding part of a fourth-order energy calculation.

7.2 Factorization of fourth-order quadruple-excitation diagrams

As stated in Section 5.9, evaluation of the quadruple-excitation diagrams in the fourth-order energy (Fig. 5.10) requires less computational effort than needed for the triple-excitation contributions (Fig. 5.9). Both types of diagram involve summations over eight indices and, while partial summations reduce the computational effort for the triple-excitation diagrams to order n^7 , the quadruple-excitation diagrams can actually be evaluated in an at most n^6 process. This is accomplished by a technique similar to that used in the proof of the factorization theorem, adding together diagrams that differ only in the time ordering of their lowest two vertices.

Adding diagrams 34 and 40 in Fig. 5.10 we get

$$\begin{aligned}
 &= -\frac{1}{4} \sum_{abcdijkl} \langle ij || ab \rangle \langle kl || cd \rangle \langle ab || ik \rangle \langle cd || jl \rangle \frac{1}{\varepsilon_{ij}^{ab} \varepsilon_{ijkl}^{abcd}} \left(\frac{1}{\varepsilon_{jl}^{cd}} + \frac{1}{\varepsilon_{ik}^{ab}} \right) \\
 &= -\frac{1}{4} \sum_{abcdijkl} \langle ij || ab \rangle \langle kl || cd \rangle \langle ab || ik \rangle \langle cd || jl \rangle \frac{1}{\varepsilon_{ij}^{ab} \varepsilon_{jl}^{cd} \varepsilon_{ik}^{ab}}. \quad (7.8)
 \end{aligned}$$

As a result of this factorization the quadruple-excitation denominator is

eliminated, allowing the use of partial summation in the forms

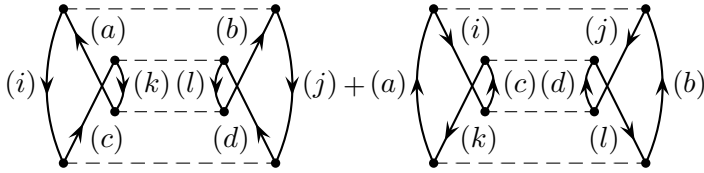
$$\begin{aligned} S_{jk} &= \sum_{cdl} \langle kl \| cd \rangle \frac{\langle cd \| jl \rangle}{\varepsilon_{jl}^{cd}}, \\ T_{jk} &= \sum_{abi} \frac{\langle ij \| ab \rangle}{\varepsilon_{ij}^{ab}} \frac{\langle ab \| ik \rangle}{\varepsilon_{ik}^{ab}}. \end{aligned} \quad (7.9)$$

This procedure is just an $n_h^3 n_p^2$ ($\sim n^5$) process for each partial sum. The final sum is an n_h^2 process,

$$\sum_{jk} T_{jk} S_{jk}.$$

The same procedure can be used for the sum of diagrams 35 and 39, which can be obtained from 34 and 40, respectively, by reversing the directions of all the arrows. The computation of the partial sums in this case is an $n_h^2 n_p^3$ process and the final sum is an n_p^2 process.

Next we consider the sum of diagrams 36 and 37:



$$\begin{aligned} &= \frac{1}{16} \sum_{abcdijkl} \langle ij \| ab \rangle \langle kl \| cd \rangle \langle ab \| kl \rangle \langle cd \| ij \rangle \frac{1}{\varepsilon_{ij}^{ab} \varepsilon_{ijkl}^{abcd}} \left(\frac{1}{\varepsilon_{ij}^{cd}} + \frac{1}{\varepsilon_{kl}^{ab}} \right) \\ &= \frac{1}{16} \sum_{abcdijkl} \langle ij \| ab \rangle \langle ab \| kl \rangle \langle kl \| cd \rangle \langle cd \| ij \rangle \frac{1}{\varepsilon_{ij}^{ab} \varepsilon_{ij}^{cd} \varepsilon_{kl}^{ab}}. \end{aligned} \quad (7.10)$$

In this case the partial sums involve n^6 processes:

$$\begin{aligned} S_{ijkl} &= \sum_{ab} \frac{\langle ij \| ab \rangle}{\varepsilon_{ij}^{ab}} \langle ab \| kl \rangle, \\ T_{ijkl} &= \sum_{cd} \frac{\langle kl \| cd \rangle}{\varepsilon_{kl}^{cd}} \frac{\langle cd \| ij \rangle}{\varepsilon_{ij}^{cd}}. \end{aligned} \quad (7.11)$$

The final sum is an n^4 process,

$$\frac{1}{16} \sum_{ijkl} T_{ijkl} S_{ijkl}.$$

The above factorizations take care of six of the seven HF-case linked

quadruple-excitation fourth-order diagrams (Fig. 5.10). The remaining diagram, number 38, can be handled by writing it as a sum of two equivalent diagrams and factoring the sum as before:

$$\begin{aligned}
 \text{Diagram 38} &= \frac{1}{2} (a) \text{Diagram 1} + \frac{1}{2} (a) \text{Diagram 2} \\
 &= \frac{1}{2} \sum_{abcdijkl} \langle ij || ab \rangle \langle kl || cd \rangle \langle db || lj \rangle \langle ac || ik \rangle \frac{1}{\varepsilon_{ij}^{ab} \varepsilon_{ijkl}^{abcd}} \left(\frac{1}{\varepsilon_{ik}^{ac}} + \frac{1}{\varepsilon_{jl}^{bd}} \right) \\
 &= \frac{1}{2} \sum_{abcdijkl} \langle ij || ab \rangle \langle kl || cd \rangle \langle bd || jl \rangle \langle ac || ik \rangle \frac{1}{\varepsilon_{ij}^{ab} \varepsilon_{ik}^{ac} \varepsilon_{jl}^{bd}}.
 \end{aligned} \tag{7.12}$$

The partial sums can be chosen as

$$\begin{aligned}
 S_{jk}^{bc} &= \sum_{dl} \langle kl || cd \rangle \frac{\langle bd || jl \rangle}{\varepsilon_{jl}^{bd}}, \\
 T_{jk}^{bc} &= \sum_{ai} \frac{\langle ij || ab \rangle}{\varepsilon_{ab}^{ij}} \frac{\langle ac || ik \rangle}{\varepsilon_{ik}^{ac}},
 \end{aligned} \tag{7.13}$$

which are n^6 processes, and the final sum is an n^4 process:

$$\frac{1}{2} \sum_{bcjk} T_{jk}^{bc} S_{jk}^{bc}.$$

The summation methods described here are not the only feasible processes, and the choice of procedure depends also on the maximum utilization of sums computed in lower orders (see e.g. Bartlett and Shavitt 1977b).

7.3 Spin summations

So far the formalism has been specified in terms of spinorbitals, and no attempt has been made to consider the effects of spin. However, since the non-relativistic Hamiltonian does not contain spin coordinates, integration over the spin variables is easily carried out and results in significant economies in the calculations.

The simplest way in which spin affects the PT summations is that some integrals vanish because of spin orthogonality. Thus if we indicate the spin factor of a spinorbital by putting a bar over β spinorbitals, and no bar over

$$\begin{aligned}
&= \frac{1}{2} \sum_{abij} \frac{1}{\varepsilon_{ij}^{ab}} [2\langle ij|\hat{v}|ab\rangle\langle ab|\hat{v}|ij\rangle + 2\langle ij|\hat{v}|ba\rangle\langle ba|\hat{v}|ij\rangle \\
&\quad - \langle ij|\hat{v}|ab\rangle\langle ba|\hat{v}|ij\rangle - \langle ij|\hat{v}|ba\rangle\langle ab|\hat{v}|ij\rangle],
\end{aligned}$$

where the summations are over the distinct spatial orbitals only and zero terms have been left out. Since a, b are dummy summation indices and can be interchanged, we find that the first two terms in the brackets are equal (after summation), and so are the third and fourth. Thus

$$\begin{aligned}
(a) \begin{array}{c} \curvearrowright \\ \curvearrowleft \end{array} (i) \begin{array}{c} \curvearrowright \\ \curvearrowleft \end{array} (j) (b) &= \sum_{abij} \frac{2\langle ij|\hat{v}|ab\rangle\langle ab|\hat{v}|ij\rangle - \langle ij|\hat{v}|ab\rangle\langle ba|\hat{v}|ij\rangle}{\varepsilon_{ij}^{ab}} \\
&= \sum_{abij} \frac{\langle ij|\hat{v}|ab\rangle}{\varepsilon_{ij}^{ab}} [2\langle ab|\hat{v}|ij\rangle - \langle ba|\hat{v}|ij\rangle]. \quad (7.16)
\end{aligned}$$

Similar treatments hold for other terms. More general diagram interpretation rules can be derived to obtain the spin-independent form directly from the diagram, at least for the Goldstone diagram case (see e.g. Paldus and Čížek 1975), for which we simply get an extra 2^l factor for the summation over spatial orbitals. This factor arises because in each closed loop of a Goldstone diagram all spin factors must be equal, and they may be either all α or all β . Thus a viable procedure for spin-adapted bases is to expand each ASG diagram into ordinary Goldstone diagrams and to sum them over orbital labels only, with a factor of 2^l for each diagram. Summing over spatial orbitals reduces the range of each summation by a factor of two, but even when summing over spinorbitals in a UHF-type treatment the number of nonzero contributions is reduced very substantially by spin orthogonality and by the requirement of spin continuity along each loop.

Open-shell and quasidegenerate perturbation theory

8.1 Formal quasidegenerate perturbation theory (QDPT)

As is well known, ordinary Rayleigh–Schrödinger perturbation theory breaks down when applied to a state that is degenerate in zero order, unless spin or symmetry restrictions eliminate all but one of the degenerate determinants from the expansion. The breakdown is due to singularities arising from the vanishing of denominators involving differences in energy between the reference determinant and determinants that are degenerate with it. Even when exact zero-order degeneracies are not present but two or more close-lying zero-order states contribute strongly to the wave function, as is the case for many excited states or in situations involving bond breaking, the RSPT expansions tend either to diverge or to converge very slowly.

These problems commonly arise in the case of open-shell states because different distributions of the open-shell electrons among the open-shell orbitals, all with the same or very similar total zero-order energies, are possible. Many open-shell high-spin states can be treated effectively with single-reference-determinant methods using either unrestricted or restricted open-shell HF reference determinants because the spin restrictions exclude alternative assignment of the electrons to the open-shell orbitals; however, low-spin states, such as open-shell singlets, require alternative approaches.

Several common series-extrapolation techniques can be used to speed up the convergence of a perturbation expansion or to obtain an approximate limit of a divergent series. The results of such an extrapolation usually improve as more of the early terms of the series become available. Approaches based on Padé approximants (closely related to continued fractions) have been applied in some studies (e.g. Reid 1967, Goscinski 1967, Brändas and Goscinski 1970, Bartlett and Brändas 1972, Bartlett and Shavitt 1977b,

Swain 1977). A more general solution to these problems is found in a multireference version of perturbation theory, called *open-shell* or *degenerate perturbation theory* in the case of exactly degenerate zero-order states and *quasidegenerate perturbation theory (QDPT)* in the more general case.

The equation governing degenerate perturbation theory is the Bloch equation (Bloch 1958, Bloch and Horowitz 1958),

$$(E_0 - \hat{H}_0)\Omega\hat{P} = \hat{V}\Omega\hat{P} - \Omega\hat{P}\hat{V}\Omega\hat{P}. \quad (8.1)$$

It is easily generalized to the quasidegenerate case (Lindgren 1974, Kvasnička 1974), in which no single E_0 is identified, in the form seen in (2.198):

$$[\Omega, \hat{H}_0]\hat{P} = \hat{V}\Omega\hat{P} - \Omega\hat{P}\hat{V}\Omega\hat{P}. \quad (8.2)$$

In these equations \hat{P} is the projector onto the *model space*, the space spanned by the reference functions (*model functions*) Φ_α ,

$$\hat{P} = \sum_\alpha |\Phi_\alpha\rangle\langle\Phi_\alpha| = \sum_\alpha \hat{P}_\alpha, \quad \hat{P}_\alpha = |\Phi_\alpha\rangle\langle\Phi_\alpha|, \quad (8.3)$$

and Ω is the wave operator, which, when operating on the model space, produces the space spanned by the perturbed wave functions

$$\Psi_\alpha = \Omega\Phi_\alpha = \Omega\hat{P}\Phi_\alpha. \quad (8.4)$$

The projector onto the *orthogonal* or *complementary space*, the space spanned by all the functions Φ_I that are not in the model space, is

$$\hat{Q} = \hat{1} - \hat{P} = \sum_I |\Phi_I\rangle\langle\Phi_I| = \sum_I \hat{Q}_I, \quad \hat{Q}_I = |\Phi_I\rangle\langle\Phi_I|. \quad (8.5)$$

Since the $\Omega\hat{Q}$ part of Ω is irrelevant it is convenient to set it to zero, so that

$$\Omega = \Omega\hat{P}. \quad (8.6)$$

With intermediate normalization Ω is split into two components,

$$\Omega = \hat{P} + \hat{Q}\Omega, \quad (8.7)$$

and it follows that

$$\hat{P}\Omega = \hat{P}. \quad (8.8)$$

As noted in Section 2.5, $\Omega = \hat{U}\hat{P}$, where \hat{U} is the transformation operator that block-diagonalizes the Hilbert space into a \hat{P} block and a \hat{Q} block.

The model functions Φ_α are eigenfunctions of \hat{H}_0 but, because of their degeneracy or quasidegeneracy, it is to be expected that each eigenfunction of the full Hamiltonian \hat{H} will contain sizable contributions from more

than one model function. The intermediately normalized wave operator cannot directly produce this mixing since, as seen from (8.7), it merely adds contributions from the \hat{Q} -space to each model function. As discussed in Section 2.5, a final transformation among the perturbed functions Ψ_α is required to produce the eigenfunctions $\tilde{\Psi}_\alpha$ of \hat{H} :

$$\tilde{\Psi}_\alpha = \sum_\beta \Psi_\beta C_{\beta\alpha} = \sum_\beta \Omega \Phi_\beta C_{\beta\alpha} = \Omega \tilde{\Phi}_\alpha, \quad (8.9)$$

where

$$\tilde{\Phi}_\alpha = \sum_\beta \Phi_\beta C_{\beta\alpha} \quad (8.10)$$

are the properly mixed zero-order functions for the problem, also called *bonnes fonctions* (Bloch 1958). The transformation matrix \mathbf{C} is determined, together with the energies, by a final diagonalization of the effective Hamiltonian \hat{H}^{eff} , as discussed further below.

The relationships between the different functions and the wave operator Ω can be summarized in the following set of equations:

$$\Psi_\alpha = \Phi_\alpha + \hat{Q}\Omega\Phi_\alpha, \quad \tilde{\Psi}_\alpha = \tilde{\Phi}_\alpha + \hat{Q}\Omega\tilde{\Phi}_\alpha, \quad (8.11)$$

$$\hat{P}\Psi_\alpha = \Phi_\alpha, \quad \hat{P}\tilde{\Psi}_\alpha = \tilde{\Phi}_\alpha, \quad (8.12)$$

$$\Omega\Psi_\alpha = \Omega\Phi_\alpha = \Psi_\alpha, \quad \Omega\tilde{\Psi}_\alpha = \Omega\tilde{\Phi}_\alpha = \tilde{\Psi}_\alpha, \quad (8.13)$$

$$\hat{P}\Omega\Phi_\alpha = \hat{P}\Psi_\alpha = \Phi_\alpha, \quad \hat{P}\Omega\tilde{\Phi}_\alpha = \hat{P}\tilde{\Psi}_\alpha = \tilde{\Phi}_\alpha. \quad (8.14)$$

Since the generalized Bloch equation contains the exactly degenerate case as a special case, we may confine our attention to the generalized equation. This equation was derived in Section 2.5 using a similarity transformation approach. A more conventional derivation, following the procedure of Lindgren and Morrison (1986) with some modifications, will now be given.

Using (8.9) for the exact eigenfunctions $\tilde{\Psi}_\alpha$ of \hat{H} , the Schrödinger equation can be written in the form

$$\hat{H}\Omega\tilde{\Phi}_\alpha = E_\alpha\Omega\tilde{\Phi}_\alpha. \quad (8.15)$$

Partitioning the Hamiltonian as $\hat{H} = \hat{H}_0 + \hat{V}$, with $\hat{H}_0\Phi_\alpha = E_\alpha^{(0)}\Phi_\alpha$, we can rewrite (8.15) in the form

$$(E_\alpha - \hat{H}_0)\Omega\tilde{\Phi}_\alpha = \hat{V}\Omega\tilde{\Phi}_\alpha. \quad (8.16)$$

Operating on (8.16) from the left with Ω and using (8.8) and the commutation of \hat{H}_0 and \hat{P} , we obtain

$$E_\alpha\Omega\tilde{\Phi}_\alpha - \Omega\hat{H}_0\tilde{\Phi}_\alpha = \Omega\hat{V}\Omega\tilde{\Phi}_\alpha. \quad (8.17)$$

Subtracting (8.17) from (8.16), we eliminate the term containing E_α and obtain an implicit equation for Ω ,

$$(-\hat{H}_0\Omega + \Omega\hat{H}_0)\tilde{\Phi}_\alpha = (\hat{V}\hat{\Omega} - \Omega\hat{V}\Omega)\tilde{\Phi}_\alpha. \quad (8.18)$$

This equation must be true for all $\tilde{\Phi}_\alpha$; furthermore, since the E_α no longer appear, it must be true for any linear combination of the $\tilde{\Phi}_\alpha$, so we may replace $\tilde{\Phi}_\alpha$ with \hat{P} , obtaining

$$[\Omega, H_0] = \hat{V}\Omega - \Omega\hat{V}\Omega, \quad (8.19)$$

which is the generalized Bloch equation (8.2) with $\Omega = \Omega\hat{P}$.

Operating on (8.15) from the left with \hat{P} , we obtain

$$\hat{P}\hat{H}\Omega\tilde{\Phi}_\alpha = E_\alpha\tilde{\Phi}_\alpha. \quad (8.20)$$

Defining an *effective Hamiltonian*

$$\hat{H}^{\text{eff}} \equiv \hat{P}\hat{H}\Omega\hat{P} = \hat{P}\hat{H}\Omega, \quad (8.21)$$

we find that

$$\hat{H}^{\text{eff}}\tilde{\Phi}_\alpha = E_\alpha\tilde{\Phi}_\alpha. \quad (8.22)$$

This equation operates entirely in \hat{P} -space and shows that the correctly mixed zero-order functions $\tilde{\Phi}_\alpha$ and thus the transformation coefficients $C_{\beta\alpha}$ of (8.9), (8.10), as well as the corresponding eigenenergies E_α of \hat{H} , can be obtained by solving the \hat{P} -space eigenvalue problem for the non-Hermitian effective Hamiltonian \hat{H}^{eff} .

The definition (8.21) of \hat{H}^{eff} has an appearance that is different from the definition (2.159) but these definitions are equivalent in \hat{P} -space, as will now be shown. As in Section 2.5, we split the effective Hamiltonian into a zero-order part and a correction by substituting $\hat{H} = \hat{H}_0 + \hat{V}$ into (8.21), obtaining

$$\begin{aligned} \hat{H}^{\text{eff}} &= \hat{P}\hat{H}_0\Omega + \hat{P}\hat{V}\Omega \\ &= \hat{H}_0\hat{P} + \hat{W}, \end{aligned} \quad (8.23)$$

where

$$\hat{W} = \hat{P}\hat{W}\hat{P} = \hat{P}\hat{V}\Omega \quad (8.24)$$

is the *level-shift operator*, also called the *reaction operator*. This equation for \hat{W} corresponds to (2.179).

As seen in (8.7), the $\hat{P}\Omega\hat{P}$ part of the wave operator is given simply by \hat{P} . In order to obtain the $\hat{Q}\Omega\hat{P}$ part we operate on the generalized Bloch equation (8.19) from the left with \hat{Q} and from the right with \hat{P}_α :

$$\hat{Q}[\Omega, \hat{H}_0]\hat{P}_\alpha = \hat{Q}\hat{V}\Omega\hat{P}_\alpha - \hat{Q}\hat{V}\Omega\hat{P}_\alpha. \quad (8.25)$$

Applying the procedure of (2.185), (2.186), the commutator equation is replaced by the following equation involving a resolvent:

$$\begin{aligned}\hat{Q}\Omega\hat{P}_\alpha &= \hat{R}_\alpha\hat{V}\Omega\hat{P}_\alpha - \hat{R}_\alpha\Omega\hat{V}\Omega\hat{P}_\alpha \\ &= \hat{R}_\alpha\hat{V}\Omega\hat{P}_\alpha - \hat{R}_\alpha\Omega\hat{W}\hat{P}_\alpha,\end{aligned}\quad (8.26)$$

where \hat{R}_α , the zero-order resolvent for the model function Φ_α , is given by

$$\hat{R}_\alpha = \hat{Q}(E_\alpha^{(0)} - \hat{Q}\hat{H}_0\hat{Q})^{-1}\hat{Q} \equiv \frac{\hat{Q}}{E_\alpha^{(0)} - \hat{H}_0}. \quad (8.27)$$

Expanding Ω and \hat{W} in orders of \hat{V} ,

$$\Omega = \hat{P} + \hat{Q}\Omega^{(1)} + \hat{Q}\Omega^{(2)} + \dots, \quad (8.28)$$

$$\hat{W} = \hat{W}^{(1)} + \hat{W}^{(2)} + \dots \quad (8.29)$$

(since $\hat{W}^{(0)} = 0$), we can solve (8.26) order by order, obtaining

$$\begin{aligned}\hat{Q}\Omega^{(1)}\hat{P}_\alpha &= \hat{R}_\alpha\hat{V}\hat{P}_\alpha, \\ \hat{Q}\Omega^{(n)}\hat{P}_\alpha &= \hat{R}_\alpha\hat{V}\hat{Q}\Omega^{(n-1)}\hat{P}_\alpha - \sum_{m=1}^{n-1} \hat{R}_\alpha\Omega^{(m)}\hat{W}^{(n-m)}\hat{P}_\alpha \quad (n \geq 2)\end{aligned}\quad (8.30)$$

and

$$\begin{aligned}\hat{W}^{(1)} &= \hat{P}\hat{V}\hat{P}, \\ \hat{W}^{(n)} &= \hat{P}\hat{V}\hat{Q}\Omega^{(n-1)} \quad (n \geq 2).\end{aligned}\quad (8.31)$$

These equations are equivalent to (2.189), (2.190), and are valid for both QDPT and nondegenerate RSPT, for which there is only one model state, $\Phi_\alpha = \Phi_0$.

A more explicit form of (8.30), (8.31) can be obtained by defining the matrix elements

$$W_{\beta\alpha} = \langle \Phi_\beta | \hat{W} | \Phi_\alpha \rangle, \quad (8.32)$$

$$\Omega_{I\alpha} = \langle \Phi_I | \Omega | \Phi_\alpha \rangle \quad (8.33)$$

etc., where the lower-case Greek indices run over model states and the upper-case Latin indices run over the orthogonal (\hat{Q} -space) states. The perturbed wave functions are then given by

$$|\Psi_\alpha\rangle = \Omega|\Phi_\alpha\rangle = |\Phi_\alpha\rangle + \sum_I |I\rangle\Omega_{I\alpha} = |\Phi_\alpha\rangle + |\chi_\alpha\rangle, \quad (8.34)$$

where

$$|\chi_\alpha\rangle = \sum_I |I\rangle\Omega_{I\alpha} \quad (8.35)$$

is the perturbation correction to $|\Phi_\alpha\rangle$. We also define

$$R_\alpha^I = \langle \Phi_I | \hat{R}_\alpha | \Phi_I \rangle = \langle \Phi_I | \hat{Q} (E_\alpha^{(0)} - \hat{Q} \hat{H}_0 \hat{Q})^{-1} \hat{Q} | \Phi_I \rangle \equiv \left\langle \Phi_I \left| \frac{\hat{Q}}{E_\alpha^{(0)} - H_0} \right| \Phi_I \right\rangle, \quad (8.36)$$

where the last form is short-hand notation for the more complete expression. In the diagonal case, in which \hat{H}_0 is diagonal in the space of all the Φ_I and Φ_α states, this expression simplifies to

$$R_\alpha^I = \frac{1}{E_\alpha^{(0)} - E_I^{(0)}} = \frac{1}{D_{\alpha I}}, \quad (8.37)$$

where

$$D_{\alpha I} = E_\alpha^{(0)} - E_I^{(0)}. \quad (8.38)$$

The diagonal case is assumed in the diagrammatic formulation that follows. In either the diagonal or the non-diagonal case we then have

$$\begin{aligned} \Omega_{I\alpha}^{(1)} &= R_\alpha^I V_{I\alpha}, \\ \Omega_{I\alpha}^{(n)} &= \sum_J R_\alpha^I V_{IJ} \Omega_{J\alpha}^{(n-1)} - \sum_{m=1}^{n-1} \sum_\beta R_\alpha^I \Omega_{I\beta}^{(m)} W_{\beta\alpha}^{(n-m)} \quad (n \geq 2) \end{aligned} \quad (8.39)$$

and

$$\begin{aligned} W_{\beta\alpha}^{(1)} &= V_{\beta\alpha}, \\ W_{\beta\alpha}^{(n)} &= \sum_I V_{\beta I} \Omega_{I\alpha}^{(n-1)} \quad (n \geq 2). \end{aligned} \quad (8.40)$$

The last term in (8.39) corresponds to the renormalization term in non-degenerate RSPT but, unlike the nondegenerate case, in which this term cancels unlinked-diagram contributions to the principal term in the many-body form of PT, certain parts of the renormalization term survive in the form of “folded diagrams” in the degenerate and quasidegenerate cases, as will be shown explicitly in the diagrammatic formulation that follows.

Successively replacing high-order terms on the right-hand sides of (8.39), (8.40) by expressions in terms of lower-order terms, these equations can be expressed fully in terms of resolvent operators and matrix elements of the

perturbation operator \hat{V} . The results for the second and third orders are

$$W_{\beta\alpha}^{(2)} = \sum_I V_{\beta I} R_{\alpha}^I V_{I\alpha}, \quad (8.41)$$

$$\Omega_{I\alpha}^{(2)} = \sum_J R_{\alpha}^I V_{IJ} R_{\alpha}^J V_{J\alpha} - \sum_{\beta} R_{\alpha}^I R_{\beta}^I V_{I\beta} V_{\beta\alpha}, \quad (8.42)$$

$$W_{\beta\alpha}^{(3)} = \sum_{IJ} V_{\beta I} R_{\alpha}^I V_{IJ} R_{\alpha}^J V_{J\alpha} - \sum_{I\gamma} V_{\beta I} R_{\alpha}^I R_{\gamma}^I V_{I\gamma} V_{\gamma\alpha}, \quad (8.43)$$

$$\begin{aligned} \Omega_{I\alpha}^{(3)} = & \sum_{JK} R_{\alpha}^I V_{IJ} R_{\alpha}^J V_{JK} R_{\alpha}^K V_{K\alpha} - \sum_{J\beta} R_{\alpha}^I V_{IJ} R_{\alpha}^J R_{\beta}^I V_{J\beta} V_{\beta\alpha} \\ & - \sum_{J\beta} R_{\alpha}^I R_{\beta}^I V_{I\beta} V_{\beta J} R_{\alpha}^J V_{J\alpha} - \sum_{J\beta} R_{\alpha}^I R_{\beta}^I V_{IJ} R_{\beta}^J V_{J\beta} V_{\beta\alpha} \\ & + \sum_{\beta\gamma} R_{\alpha}^I R_{\beta}^I R_{\gamma}^I V_{I\gamma} V_{\gamma\beta} V_{\beta\alpha}. \end{aligned} \quad (8.44)$$

The first two terms on the right-hand side of (8.44) result from substitution of (8.42) into the principal term of $\Omega_{I\alpha}^{(3)}$, which is found from (8.39). The third term corresponds to the $m = 1$ contribution to the renormalization term, while the last two terms correspond to the $m = 2$ contribution (since $\Omega_{I\beta}^{(2)}$ generates two terms). These explicit forms are easily connected to the diagrammatic representations, which are based on expressions in terms of resolvents and perturbation-operator components only.

Defining the cumulative n th-order effective Hamiltonian by

$$\hat{H}^{\text{eff}(n)} \equiv \hat{H}_0 + \sum_{m=1}^n \hat{W}^{(m)} \quad (n \geq 1), \quad (8.45)$$

so that

$$H_{\beta\alpha}^{\text{eff}(n)} = \langle \Phi_{\beta} | \hat{H}^{\text{eff}(n)} | \Phi_{\alpha} \rangle = \delta_{\beta\alpha} E_{\alpha}^{(0)} + \sum_{m=1}^n W_{\beta\alpha}^{(m)} \quad (n \geq 1), \quad (8.46)$$

the coefficients $C_{\beta\alpha}^{(n)}$ that define the transformation of the n th order perturbed functions to the proper eigenfunctions of the full Hamiltonian \hat{H} and also the corresponding n th order eigenvalues $E_{\alpha}^{(n)}$ are obtained by solving the non-Hermitian matrix eigenvalue problem

$$\sum_{\beta} \hat{H}_{\gamma\beta}^{\text{eff}(n)} C_{\beta\alpha}^{(n)} = C_{\gamma\alpha}^{(n)} E_{\alpha}^{(n)}. \quad (8.47)$$

8.2 The Fermi vacuum and the model states

The one-electron states (spinorbitals) in QDPT are divided into three classes. The *core states* are those spinorbitals that are occupied in all the reference determinants (model states), the *valence states* are occupied in some, but not all, model states and the *virtual states* are unoccupied in all the model states.

In nondegenerate many-body PT the Fermi vacuum state, which determines the Fermi level separating the one-electron states into particle and hole states, is the reference determinant. In QDPT there are multiple reference determinants, so the assignment of the Fermi vacuum is not immediately obvious. Commonly (Sandars 1969), the Fermi vacuum state in QDPT is chosen as a determinant made up of all the core states. Usually this is a closed-shell state, and obviously, it contains fewer electrons than the target states of the calculation. The Fermi level, the boundary between the particle and hole states, is then placed between the core and valence states, as shown schematically in the level diagram in Fig. 8.1. Here the labels u, v, w, \dots are used for the valence states while the labels i, j, k, \dots and a, b, c, \dots refer to the hole and particle states, respectively, as before. The model states are then described by the action of valence-state creation operators on the Fermi vacuum; for example,

$$|\Phi^{uvw}\rangle = \hat{u}^\dagger \hat{v}^\dagger \hat{w}^\dagger |0\rangle. \quad (8.48)$$

Other choices for the Fermi vacuum are possible, in which the boundary between the hole and particle states is put either within or at the top of the valence space. In these cases the model states are described by the action of valence-state annihilation (and possibly creation) operators on the Fermi vacuum. In the present treatment we shall limit ourselves to the first-mentioned choice for the Fermi vacuum, consisting of all the one-electron states shared by all the model states.

With the Fermi level placed at the bottom of the valence space, the Fermi vacuum state contains fewer electrons than the model states and so cannot be one of them. Nevertheless, with the second-quantization notation for operators, in which the number of electrons does not appear explicitly, the same operator definitions can still be used for the Fermi vacuum state and for the states of interest in the calculation.

With hole and particle states defined as in Fig. 8.1, the partitioning of the Hamiltonian and the normal-ordered form of its components are the same in QDPT as in nondegenerate PT (Section 3.5 and subsection 3.6.3). We shall also continue to use the same definition of the auxiliary operator \hat{U} , see (3.129), (3.132) and (3.133), as in nondegenerate PT, the summations

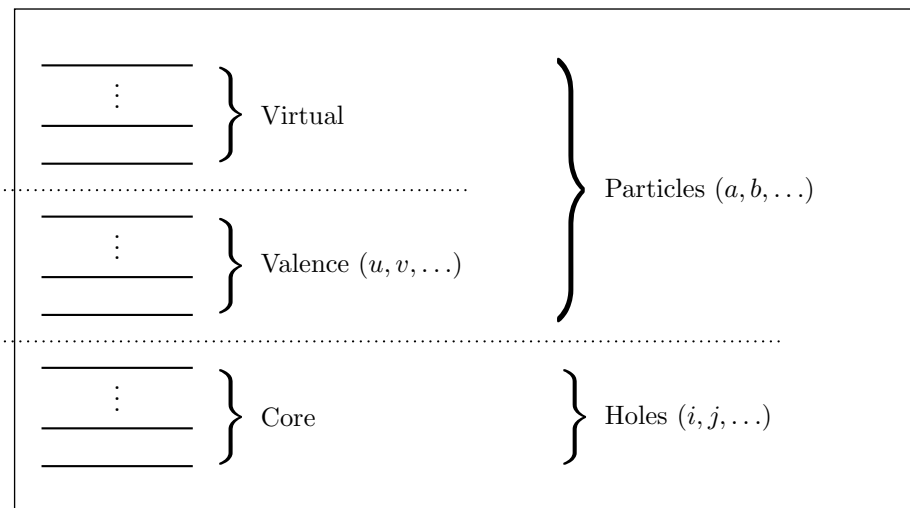


Fig. 8.1. Classification of one-electron states in QDPT.

in (3.132), (3.133) being over the hole (core) states; this choice retains the simplifications seen in subsection 3.6.3 in the normal-ordered form of the perturbation operator. The operator \hat{F} , (3.130), is the Fock operator for the Fermi vacuum state. If we want this operator to be diagonal (as in canonical HF) or block diagonal (as in noncanonical HF), in order to take advantage of the resulting elimination or reduction of diagrams involving one-electron operators, we need to use the HF wave function and one-electron states corresponding to the Fermi vacuum state. It should be realized that the HF spinorbitals of the Fermi vacuum state and their orbital energies may be less than optimal for rapid convergence of the perturbation expansion for the quasidegenerate states (an alternative choice may be the use of MCSCF spinorbitals of the model space), but they are often used because of the resulting simplifications.

In the most common form of diagrammatic QDPT the model space is chosen to be *complete*; i.e. all possible assignments of the valence electrons in the valence states are included in the model states. While the choice of a complete model space simplifies the formalism, it has two important disadvantages. First, such a model space is often inordinately large, adversely impacting the feasibility of the calculation. Second, even if the size of the model space is not excessive, a complete model space often includes many high-energy determinants that are not expected to contribute significantly to the wave function. Such high-energy determinants result when multiple valence electrons are placed in the highest valence orbitals, which are often

higher in energy than some of the external (\hat{Q} -space) determinants, leading to the phenomenon of *intruder states*. Intruder states are \hat{Q} -space states with zero-order energies lying within the range of model-state zero-order energies. Such states usually generate small denominators in the perturbation expansions, leading to divergence or extremely slow convergence. The convergence of a PT expansion is generally enhanced by having a wide gap, in the zero-order energies, between the model states and all the orthogonal-space states. Such a gap is usually not achievable with complete model spaces, even when they do not lead to intruder states.

As a result of these difficulties, complete-model-space methods rarely provide practical solutions for problems involving quasidegenerate states, and few applications of such methods to electronic structure problems have been made. Nevertheless the relative formal simplicity of this approach is instructive, and so the resulting diagrammatic methods will be described in detail in Sections 8.4–8.6. Formalisms for incomplete model spaces in QDPT are discussed in Section 8.7.

8.3 Normal-product form of the generalized Bloch equations

In order to use in degenerate MBPT the generalized Wick's theorem and the diagrammatic techniques employed so effectively in the nondegenerate case, it is most convenient to use the normal-product form of the perturbation operator (see subsection 3.6.3),

$$\hat{V}_N = \hat{V} - \langle 0|\hat{V}|0\rangle, \quad (8.49)$$

where $|0\rangle$ represents the Fermi vacuum, i.e. the core state. It is also convenient to define a modified level-shift operator

$$\hat{W}' \equiv \hat{W} - \langle 0|\hat{V}|0\rangle. \quad (8.50)$$

In the series expansion (8.29) for \hat{W} , only the first-order part is modified,

$$\hat{W}'^{(n)} = \hat{W}^{(n)} - \delta_{n1}\langle 0|\hat{V}|0\rangle, \quad (8.51)$$

and the effective Hamiltonian can be expanded as

$$\hat{H}^{\text{eff}} = \hat{H}_0 + \langle 0|\hat{V}|0\rangle + \hat{W}'^{(1)} + \hat{W}'^{(2)} + \hat{W}'^{(3)} + \dots. \quad (8.52)$$

The modified level-shift operator (8.50) is the analog of the correlation energy in the nondegenerate theory, while $\hat{H}_0 + \langle 0|\hat{V}|0\rangle$ is the analog of E_{ref} .

The other operators obtained by contractions based on the generalized Wick's theorem, i.e. the various components of the wave operator and the level-shift operator, will automatically be in normal order.

With these definitions, the order-by-order generalized Bloch equations (8.30), (8.31) remain valid if \hat{V} and $\hat{W}^{(1)}$ are replaced by \hat{V}_N and $\hat{W}'^{(1)}$. The relevant elements of these operators are given by

$$(\hat{V}_N)_{IJ} = V_{IJ} - \delta_{IJ} \langle 0 | \hat{V} | 0 \rangle, \quad (\hat{V}_N)_{\beta\alpha} = V_{\beta\alpha} - \delta_{\beta\alpha} \langle 0 | \hat{V} | 0 \rangle, \quad (\hat{V}_N)_{I\alpha} = V_{I\alpha}, \quad (8.53)$$

$$W'_{\beta\alpha}^{(1)} = W_{\beta\alpha}^{(1)} - \delta_{\beta\alpha} \langle 0 | \hat{V} | 0 \rangle. \quad (8.54)$$

The detailed forms of the generalized Bloch equations (8.39)–(8.44) also remain valid if the matrix elements in them are replaced by these modified versions. Note in particular that the equation in (8.40) for $W_{\beta\alpha}^{(n)}$, $n \geq 2$, is not affected by the modifications because the off-diagonal elements $V_{\alpha I}$ are not modified. In the equation in (8.39) for $\Omega_{I\alpha}^{(n)}$ the modifications in the principal and renormalization terms cancel.

In the rest of this chapter we shall assume that the various operators and their matrix elements have been replaced by their modified versions but, in order not to encumber the notation, we shall omit the N subscript and the prime on the perturbation and level-shift operators and their matrix elements. We shall therefore be able to use the normal-ordered perturbation operator in the form given in subsection 3.6.3 and to apply the contractions based on the generalized Wick's theorem in the diagrammatic development of QDPT.

8.4 Diagrammatic notation for QDPT

The diagrammatic notation for hole and particle states is the same in QDPT as in nondegenerate PT. However, since summations over particle states include the valence as well as the virtual states (using the arrangement in Fig. 8.1), we also need a notation for spinorbitals that are restricted to valence states. These are conventionally denoted by upward-pointing double arrows (Sandars 1969). For example, in a case with three valence electrons the model state Φ^{uvw} can be represented diagrammatically by

$$\begin{array}{c} \uparrow \\ | \\ u \end{array} \quad \begin{array}{c} \uparrow \\ | \\ v \end{array} \quad \begin{array}{c} \uparrow \\ | \\ w \end{array} .$$

Additional notation is required if the Fermi vacuum is chosen to include all or some of the valence orbitals.

Components of the level-shift operator \hat{W} (the QDPT analog of the energy) may be represented schematically by the diagram

$$|\beta\rangle\langle\beta|\hat{W}|\alpha\rangle\langle\alpha| = \begin{array}{c} \uparrow\beta \\ \boxed{\hat{W}} \\ \uparrow\alpha \end{array} \quad (8.55)$$

where the heavy lines represent many-electron states (in this case, the model states Φ_α and Φ_β) rather than one-electron states. To avoid confusion between the generic Φ_α notation and the specific Φ^{uvw} notation, we designate the many-electron basis states by $|\alpha\rangle$ etc. for model states and $|I\rangle$ etc. for \hat{Q} -space states. Clearly, the corresponding matrix element $W_{\beta\alpha}$ is recovered by placing this operator between the respective ket and bra states. It will sometimes be convenient to identify this diagram just with the matrix element $W_{\beta\alpha}$ instead of the full operator.

If the model states are $|\alpha\rangle = |\Phi^{uvw}\rangle = \hat{u}^\dagger\hat{v}^\dagger\hat{w}^\dagger|0\rangle$ and $|\beta\rangle = |\Phi^{xyz}\rangle = |\hat{x}^\dagger\hat{y}^\dagger\hat{z}^\dagger|0\rangle$ then the operator can be represented schematically by the diagram

$$\hat{x}^\dagger\hat{y}^\dagger\hat{z}^\dagger\langle\Phi^{xyz}|\hat{W}|\Phi^{uvw}\rangle\hat{w}\hat{v}\hat{u} = \langle\Phi^{xyz}|\hat{W}|\Phi^{uvw}\rangle\{\hat{x}^\dagger\hat{y}^\dagger\hat{z}^\dagger\hat{w}\hat{v}\hat{u}\} = \begin{array}{c} \uparrow x \quad \uparrow y \quad \uparrow z \\ \boxed{\hat{W}} \\ \uparrow u \quad \uparrow v \quad \uparrow w \end{array} . \quad (8.56)$$

Note that the creation and annihilation operator product is in normal order. Again, it will sometimes be convenient to identify this diagram just with the matrix element $\langle\Phi^{xyz}|\hat{W}|\Phi^{uvw}\rangle$. Obviously, all the labels on the incoming valence lines should be different from each other, and the same must apply to the outgoing valence lines, otherwise the corresponding determinants would describe null states. However, any labels on incoming valence lines may be equal to labels on the outgoing lines.

Some valence lines in a diagram may pass through it without interaction, as in

$$\hat{x}^\dagger\hat{y}^\dagger\hat{w}^\dagger\langle\Phi^{xy}|\hat{W}|\Phi^{uv}\rangle\hat{w}\hat{v}\hat{u} = \langle\Phi^{xy}|\hat{W}|\Phi^{uv}\rangle\{\hat{x}^\dagger\hat{y}^\dagger\hat{w}^\dagger\hat{w}\hat{v}\hat{u}\} = \begin{array}{c} \uparrow x \quad \uparrow y \quad | \\ \boxed{\hat{W}} \\ \uparrow u \quad \uparrow v \quad | \end{array} \uparrow w . \quad (8.57)$$

Such noninteracting valence lines, called *passive lines*, participate in determining the identity of the initial and final states involved but do not affect the matrix-element value. They are usually omitted from the diagram, with the understanding that the diagram represents all allowed assignments of valence labels to the omitted passive lines. For \hat{W} diagrams all open lines must be valence lines, with the number of outgoing lines equal to the number of incoming lines.

Wave-operator diagrams are the QDPT analogs of wave-function diagrams in nondegenerate PT. They can be represented schematically in the form

$$|I\rangle\langle I|\Omega|\alpha\rangle\langle\alpha| = |I\rangle\Omega_{I\alpha}\langle\alpha| = \begin{array}{c} \uparrow I \\ \boxed{\Omega} \\ \uparrow \alpha \end{array}, \quad (8.58)$$

where the top line designates a \hat{Q} -space state and may represent a mix of particle, hole and valence lines. Specifically, if \underline{n}_v is the number of entering valence lines at the bottom of the diagram and $\tilde{n}_v, \tilde{n}_p, \tilde{n}_h$ are the number of open valence, particle and hole lines, respectively, at the top then preservation of the number of electrons requires that

$$\tilde{n}_v + \tilde{n}_p - \tilde{n}_h = \underline{n}_v. \quad (8.59)$$

Usually wave-operator diagrams are summed over the outgoing \hat{Q} -space states $|I\rangle$, so that the diagram in (8.58) represents the perturbation correction $|\chi_\alpha\rangle$ to the model state $|\alpha\rangle$,

$$|\chi_\alpha\rangle\langle\alpha| = \sum_I |I\rangle\Omega_{I\alpha}\langle\alpha| = \begin{array}{c} \uparrow (I) \\ \boxed{\Omega} \\ \uparrow \alpha \end{array} = \begin{array}{c} \uparrow \\ \boxed{\Omega} \\ \uparrow \alpha \end{array}, \quad (8.60)$$

where a label in parentheses (or no label) indicates a dummy (summation) index. A specific matrix element $\Omega_{J\alpha}$ is obtained by placing the sum (8.60) between the bra state $\langle J|$ and the ket state $|\alpha\rangle$. To take a specific example, if $|\alpha\rangle = |\Phi^{uvw}\rangle$ and $|I\rangle = |\Phi_i^{abcx}\rangle = \hat{a}^\dagger \hat{i} \hat{b}^\dagger \hat{c}^\dagger \hat{x}^\dagger |0\rangle$ then

$$\sum_{aibcx} \langle \Phi_i^{abcx} | \Omega | \Phi^{uvw} \rangle \{ \hat{a}^\dagger \hat{i} \hat{b}^\dagger \hat{c}^\dagger \hat{x}^\dagger \hat{w} \hat{v} \hat{u} \} = \begin{array}{c} \begin{array}{ccccc} \uparrow (a) & \uparrow (i) & \downarrow & \uparrow (b) & \uparrow (c) & \uparrow (x) \end{array} \\ \boxed{\Omega} \\ \begin{array}{ccc} \uparrow u & \uparrow v & \uparrow w \end{array} \end{array}. \quad (8.61)$$

Here, too, the operator product is in normal order. As in the case of the \hat{W} diagrams, passive valence lines affect only the identity, not the value, of the matrix element and are usually omitted from the diagrams. The number of omitted passive lines is $N_v - \underline{n}_v$, where N_v is the number of valence electrons. Outgoing open lines (other than passive lines) in wave-operator diagrams may include valence lines in addition to general particle lines. As will be shown later, such lines have their origin in the secondary term of the generalized Bloch equation (8.2).

All QDPT diagrams can be classified according to the number of incoming valence lines \underline{n}_v . For a problem involving N_v valence electrons, the number of incoming valence lines is limited to the range $\underline{n}_v = 0, 1, \dots, N_v$; $\underline{n}_v = 0$ represents the diagrams of nondegenerate PT, all of which are included among the QDPT diagrams. It is understood that the balance of $N_v - \underline{n}_v$ valence lines in each diagram is made up of implied passive lines. In particular, in the case of the level-shift diagrams the nondegenerate PT ($\underline{n}_v = 0$) energy diagrams contribute equally to all diagonal elements of the effective Hamiltonian (and do not contribute to off-diagonal elements).

The definition of linked and unlinked diagrams needs to be broadened in QDPT. *A disconnected part of a diagram is considered unlinked if it has no open lines other than valence lines.* In other words, open valence lines are disregarded in determining the linked or unlinked status of a diagram. Using this broadened definition, the cancellation of unlinked diagrams holds in QDPT, assuming a complete model space, just as in nondegenerate PT. This linked-diagram theorem for QDPT was first proved by Brandow (1966, 1967); see also Sandars (1969) and Lindgren (1974).

8.5 Schematic representation of the generalized Bloch equation

The explicit form of the generalized Bloch equation (8.39) can be represented schematically by the two diagram equations

$$\begin{array}{c} \uparrow I \\ \boxed{\Omega^{(1)}} \\ \uparrow \alpha \end{array} = \hat{R}_\alpha^I \begin{array}{c} \uparrow I \\ \hat{V} \\ \bullet \\ \uparrow \alpha \end{array} \quad (8.62)$$

for the principal term $(\Omega^{(n)})_1$ in the $\Omega^{(n)}$ equation, the first term on the right-hand side of (8.63), we have

$$|I\rangle(\Omega_{I\alpha}^{(n)})_1\langle\alpha| = \text{Diagram} = \sum_J |I\rangle \frac{V_{IJ}}{D_{\alpha I}} \Omega_{J\alpha}^{(n-1)}\langle\alpha|. \quad (8.66)$$

Obviously, the folded valence lines of model state α will be crossed by any resolvent line within the $\Omega^{(n-1)}$ block (including its own top resolvent \hat{R}_α^J) and will contribute to the corresponding denominators. However, in the conventional drawing of QDPT diagrams the incoming valence lines are left unfolded; it is understood that these lines are to be folded only for the purpose of determining the appropriate denominators, not for the purpose of contracting successive operators in accordance with Wick's theorem. For the purpose of the latter contractions the valence lines continue to act as particle lines rather than hole lines. The term “folded diagrams” is applied instead to diagrams representing the secondary term in the Bloch equation for the wave operator, as will be shown next.

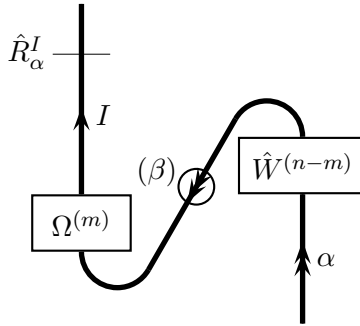
The secondary term $(\Omega^{(n)})_2$ in the wave-operator equation (8.63) represents new challenges specific to QDPT. In nondegenerate PT the $\hat{W}^{(n-m)}$ operator just equals the number $E^{(n-m)}$, and its diagrammatic representation has no open lines. Therefore this energy factor is disconnected from the wave-operator factor and can be represented as an insertion that cancels the unlinked diagrams in the principal term. In the QDPT case there will still be diagrams in which the $\hat{W}^{(n-m)}$ operator is disconnected and therefore unlinked, and these contributions will still cancel the unlinked diagrams in the principal term (using the broadened definition of unlinked diagrams in QDPT; see Section 8.4). But the terms in which the $\hat{W}^{(n-m)}$ operator is connected to the $\Omega^{(m)}$ operator survive and give rise to a new type of diagram specific to QDPT, called a *folded diagram*.

Looking at the schematic representation of the secondary term in (8.63), on the one hand we see that the resolvent that appears above the $\Omega^{(m)}$ block in that diagram refers not to the model states β that enter that block but to the model state α that enters the $\hat{W}^{(n-m)}$ block below it. On the other hand, any resolvent lines within the $\Omega^{(m)}$ block (including its top resolvent \hat{R}_β^I) must refer to the β state that enters that block. The correct denominators

can be recovered, employing the usual rule, by folding the valence lines connecting the two blocks, as well as the valence lines entering the $\hat{W}^{(n-m)}$ block, in the following way:

$$\begin{aligned}
 |I\rangle (\Omega_{I\alpha}^{(n)})_2 \langle \alpha| &= \sum_{m=1}^{n-1} \text{Diagram} \\
 &= -|I\rangle \sum_{m=1}^{n-1} \sum_{\beta} \Omega_{I\beta}^{(m)} \frac{W_{\beta\alpha}^{(n-m)}}{D_{\alpha I}} \langle \alpha|. \quad (8.67)
 \end{aligned}$$

However, conventionally this schematic diagram is drawn without folding the incoming α lines,

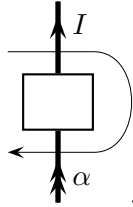


it being understood that the denominators are read from the fully folded diagram (8.67). The minus sign in the interpretation of the diagram originates from the minus sign in front of the secondary term in the generalized Bloch equation. In general, since the $\Omega^{(m)}$ and $\hat{W}^{(n-m)}$ blocks may contain folds of their own (originating from lower-order factors inside them), we have a -1 factor from each internal fold in a diagram.

Further points need to be made concerning the scope of the resolvent lines within the $\Omega^{(m)}$ and $\hat{W}^{(n-m)}$ blocks. Obviously, the resolvent lines within the $\Omega^{(m)}$ block are to be interpreted relative to the model state β entering it, ignoring the α state, as shown schematically by the thin horizontal lines in (8.67). Resolvent lines within the $\hat{W}^{(n-m)}$ block, however, are to be interpreted relative to model state α , ignoring the descending part of the

β folded line emerging from it, as also shown in (8.67). If any folded line is crossed twice by a resolvent line (once as the folded line descends and again as it ascends), its effects cancel in the corresponding denominator.

An alternative to the folding of the state lines in the QDPT diagrams was introduced by Kucharski and Bartlett (1988) in the context of the Hose–Kaldor approach for incomplete model spaces, to be described in Section 8.7; it consists of the folding of the resolvent lines instead of the state lines. This approach can be used just as well in the context of the diagrammatic representation discussed here for complete model spaces. It can replace the folding of the incoming valence lines in all diagrams as well as the folding of the intermediate valence lines in the folded diagrams that represent the renormalization terms. In this procedure a resolvent term such as R_α^I is represented by a directed line that crosses the state lines for state I from left to right and then curves down to cross the state lines for state α from right to left, as represented schematically by



The denominator $D_{\alpha I}$ is obtained from the orbital energies of the state lines crossed by the resolvent line according to

$$D_{\alpha I} = \sum_i^{\rightarrow} \varepsilon_i - \sum_a^{\rightarrow} \varepsilon_a - \sum_u^{\leftarrow} \varepsilon_u, \quad (8.68)$$

where the arrows on the summation signs limit the summations to the state lines crossed by the folded resolvent line in the indicated direction. The states crossed by the upper and lower parts of the resolvent line must be \hat{Q} - and \hat{P} -space states, respectively. Thus the lower part of the resolvent line crosses valence lines only and, while the state crossed by the upper part may include valence lines, the summation over particle labels in it has to be restricted in many diagrams to prevent it from becoming a model state.

With this notation the schematic form (8.62), (8.63) of the generalized Bloch equation can be rewritten as

$$\Omega^{(1)} = \text{diagram with a box labeled } \Omega^{(1)} \text{ and a resolvent line } \hat{V} \text{ crossing it} \quad (8.69)$$

and

$$\Omega^{(n)} = \Omega^{(n-1)} - \sum_{m=1}^{n-1} \Omega^{(m)} \quad (n \geq 2). \quad (8.70)$$

Note that the leading resolvents within the $\Omega^{(n-1)}$ and $\Omega^{(m)}$ blocks in (8.70) are represented by lines that fold down to cross the model states α and β , respectively. This notation is particularly effective in describing the renormalization terms without resort to folded state lines.

8.6 Level-shift and wave-operator diagrams

8.6.1 Zero and first order

The zero-order part of the effective Hamiltonian \hat{H}^{eff} is just the zero-order Hamiltonian \hat{H}_0 , which is diagonal in the model functions $\{\alpha\}$ and the orthogonal-space functions $\{I\}$,

$$\langle \beta | \hat{H}_0 | \alpha \rangle = \delta_{\beta\alpha} E_\alpha^{(0)}, \quad \langle J | \hat{H}_0 | I \rangle = \delta_{JI} E_I^{(0)}, \quad \langle I | \hat{H}_0 | \alpha \rangle = 0. \quad (8.71)$$

The zero-order energies of these functions are equal to the sum of the orbital energies of the one-particle states they contain:

$$\begin{aligned} E^{(0)}(\Phi^{uv\dots}) &= E_0 + \varepsilon_u + \varepsilon_v + \dots, \\ E^{(0)}(\Phi_{ij\dots}^{ab\dots}) &= E_0 + \varepsilon_a + \varepsilon_b + \dots - \varepsilon_i - \varepsilon_j - \dots, \end{aligned} \quad (8.72)$$

where

$$E_0 = \sum_i \varepsilon_i \quad (8.73)$$

is the zero-order energy of the Fermi-vacuum state.

The $\langle 0 | \hat{V} | 0 \rangle$ term in the effective Hamiltonian (8.52) is given by the first-order energy diagram (5.6) for the Fermi-vacuum state. The modified first-order level-shift operator $\hat{W}'^{(1)}$ is given by the ASG diagrams

$$\begin{aligned} & \begin{array}{c} w \uparrow \\ \bullet \\ u \uparrow \end{array} \text{---} \begin{array}{c} x \uparrow \\ \bullet \\ v \uparrow \end{array} + \begin{array}{c} w \uparrow \\ \bullet \\ u \uparrow \end{array} \text{---} \times, \end{aligned} \quad (8.74)$$

since the only open lines allowed in \hat{W} diagrams are valence lines. The second of these diagrams is the non-HF contribution, which vanishes if canonical HF spinorbitals of the Fermi-vacuum state are used. No resolvents are involved in these diagrams.

In all QDPT diagrams it is to be understood that additional passive valence lines are implied that make the total number of incoming valence lines equal to the number of valence electrons. However, diagrams in which the number of incoming valence lines exceeds the number of valence electrons are to be ignored. Specifically, the first diagram in (8.74), whose value is $\langle wx||uv\rangle\{\hat{w}^\dagger\hat{x}^\dagger\hat{v}\hat{u}\}$, provides a contribution $\langle wx||uv\rangle$ to the matrix elements $\langle\Phi^{wxyz\dots}|\hat{W}^{(1)}|\Phi^{uvyz\dots}\rangle$, including those cases in which one or both of the incoming line labels u, v are equal to the outgoing line labels w, x . The second diagram in (8.74), whose value is $\langle w|\hat{f}^o|u\rangle\{\hat{w}^\dagger\hat{u}\}$, provides a contribution $\langle w|\hat{f}^o|u\rangle$ to the matrix elements $\langle\Phi^{wxy\dots}|\hat{W}^{(1)}|\Phi^{uxy\dots}\rangle$, not including the case $u = w$ (because of the off-diagonal nature of the one-electron perturbation, subsection 4.4.6).

The first-order wave operator is given by the corresponding nondegenerate PT diagrams (5.15), (5.16), plus the ASG diagrams

$$(a) \begin{array}{c} \uparrow \\ \bullet \\ \uparrow \\ u \end{array} \text{---} \begin{array}{c} \uparrow \\ \bullet \\ \uparrow \\ v \end{array} (b) + (b) \begin{array}{c} \uparrow \\ \bullet \\ \uparrow \\ u \end{array} \text{---} \begin{array}{c} \swarrow \\ \bullet \\ \uparrow \\ \end{array} (a) \begin{array}{c} \swarrow \\ \bullet \\ \uparrow \\ \end{array} (i) + (a) \begin{array}{c} \uparrow \\ \bullet \\ \uparrow \\ u \end{array} \text{---} \times. \quad (8.75)$$

Again, the last of these is the non-HF contribution.

Because summations over particle labels include valence label values, it is important to restrict the summations over the outgoing particle labels in the first and third of these diagrams to prevent the upper state from becoming a model state. Thus labels a and b in the first diagram cannot be allowed to take on valence values at the same time, while the summation over a in the third diagram must be over virtual labels only.

The nondegenerate PT diagram (5.15) provides a contribution

$$\frac{1}{4} \sum_{abij} \frac{\langle ab||ij\rangle}{\varepsilon_{ij}^{ab}} \{\hat{a}^\dagger \hat{i} \hat{b}^\dagger \hat{j}\} = \frac{1}{4} \sum_{abij} \frac{\langle ab||ij\rangle}{\varepsilon_{ij}^{ab}} |\Phi_{ij}^{abxy\dots}\rangle \langle\Phi^{xy\dots}|$$

to $\Omega^{(1)}$, generating a first-order correction for the $|\Phi^{xy\dots}\rangle$ model states for all $x \neq y \neq \dots$, where x, y, \dots label an appropriate number of passive lines. Similarly, the diagram (5.16) provides a contribution

$$\sum_{ai} \frac{\langle a|\hat{f}|i\rangle}{\varepsilon_i^a} \{\hat{a}^\dagger \hat{i}\} = \sum_{ai} \frac{\langle a|\hat{f}|i\rangle}{\varepsilon_i^a} |\Phi_i^{axy\dots}\rangle \langle\Phi^{xy\dots}|$$

to the same first-order correction.

The first diagram in (8.75) provides a contribution

$$\frac{1}{2} \sum_{ab} \frac{\langle ab||uv\rangle}{\varepsilon_{uv}^{ab}} \{\hat{a}^\dagger \hat{b}^\dagger \hat{v} \hat{u}\} = \frac{1}{2} \sum_{ab} \frac{\langle ab||uv\rangle}{\varepsilon_{uv}^{ab}} |\Phi^{abxy\dots}\rangle \langle\Phi^{uvxy\dots}|$$

to $\Omega^{(1)}$ (terms in which both a and b take on valence values are excluded), generating a first-order correction for the model state $|\Phi^{uvxy}\rangle$. The second diagram in (8.75) provides a contribution

$$\frac{1}{2} \sum_{abi} \frac{\langle ba || ui \rangle}{\varepsilon_{iu}^{ab}} \{ \hat{a}^\dagger \hat{i} \hat{b}^\dagger \hat{u} \} = \frac{1}{2} \sum_{abi} \frac{\langle ba || ui \rangle}{\varepsilon_{iu}^{ab}} | \Phi_i^{abxy} \rangle \langle \Phi^{uvxy} |$$

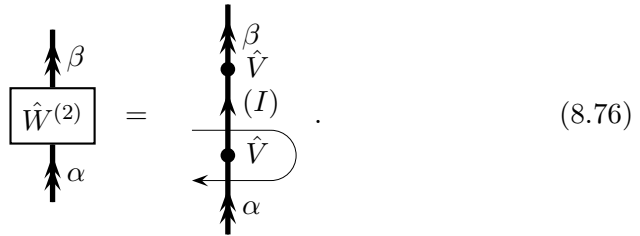
to $\Omega^{(1)}$, generating a first-order correction for the $|\Phi^{uvxy}\rangle$ model state, and the third diagram provides a contribution

$$\sum_a \frac{\langle a | \hat{f}^o | u \rangle}{\varepsilon_u^a} \{ \hat{a}^\dagger \hat{u} \} = \sum_a \frac{\langle a | \hat{f}^o | u \rangle}{\varepsilon_u^a} | \Phi^{axy} \rangle \langle \Phi^{uvxy} |$$

(in which the summation over a is restricted to virtual label values) to the same first-order correction.

8.6.2 Second-order level-shift operator

The matrix element of the second-order level-shift operator is given by (8.41). It can be expressed schematically in the folded-resolvent-line notation:



$$\boxed{\hat{W}^{(2)}} = \begin{array}{c} \uparrow \beta \\ \bullet \hat{V} \\ \text{---} (I) \text{---} \\ \bullet \hat{V} \\ \uparrow \alpha \end{array} \quad (8.76)$$

As in nondegenerate PT, a convenient way to generate higher-order QDPT ASG diagrams is to begin with Hugenholtz diagrams. This approach makes it easy to avoid redundant equivalent diagrams. The QDPT Hugenholtz diagrams for the second-order level-shift operator are given in Fig. 8.2. The first and second rows in this figure represent the canonical HF and non-HF diagrams, respectively.

The relevant ASG diagrams are shown in Fig. 8.3. As in other cases, the corresponding nondegenerate PT diagrams (5.9), (5.10), which are not shown here, are also to be included. Together, all these diagrams represent (8.41). In the diagrams in Fig. 8.3 without intermediate hole lines (diagrams 3, 6, 10, 11, 14), it is necessary to restrict the summations over the intermediate-particle labels so that not all these labels take on valence label values at the same time (because of the \hat{Q} projector in the resolvent).

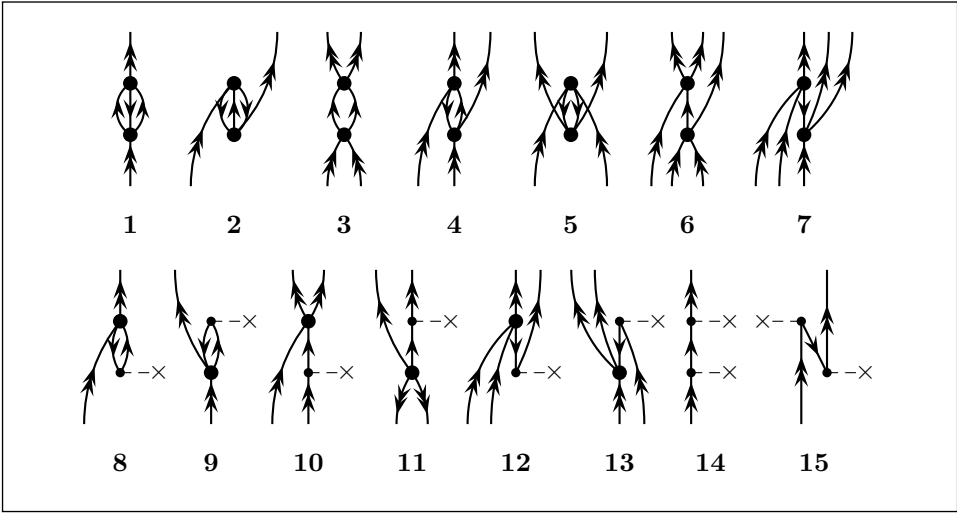


Fig. 8.2. Quasidegenerate PT Hugenholtz diagrams for the second-order level-shift operator.

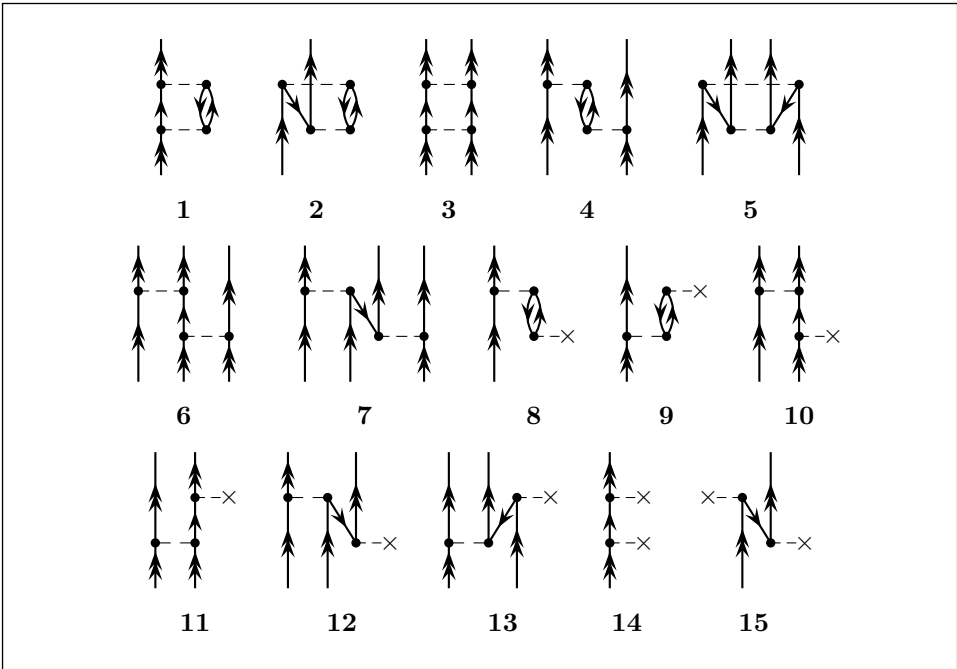


Fig. 8.3. Quasidegenerate PT ASG diagrams for the second-order level-shift operator.

For examples of the folded-resolvent-line notation for these diagrams we consider diagrams 1 and 2 of Fig. 8.3:

1

$$(a) \begin{array}{c} v \\ \uparrow \\ \text{---} \\ (i) \text{---} (b) \\ \text{---} \\ u \end{array} = \frac{1}{2} \sum_{iab} \frac{\langle vi || ab \rangle \langle ab || ui \rangle}{\varepsilon_{ui}^{ab}} \{ \hat{v}^\dagger \hat{u} \},$$

2

$$\begin{array}{c} v \\ \uparrow \\ \text{---} \\ (i) \text{---} (j) \text{---} (a) \\ \text{---} \\ u \end{array} = \begin{array}{c} v \\ \uparrow \\ \text{---} \\ (i) \text{---} (j) \text{---} (a) \\ \text{---} \\ u \end{array} = -\frac{1}{2} \sum_{ija} \frac{\langle ij || ua \rangle \langle va || ij \rangle}{\varepsilon_{ij}^{av}} \{ \hat{v}^\dagger \hat{u} \}.$$

The shortened resolvent line in the second form of diagram 2 reflects the fact that lines crossed twice by the folded resolvent line make no net contribution to the corresponding denominator. Obviously the same denominators are obtained with conventional resolvents and folded incoming valence lines. The weight factor is due to the presence of one pair of equivalent internal lines in each diagram.

8.6.3 Second-order wave operator

The matrix elements of the second-order wave operator are given by (8.42) and are represented schematically in the folded-resolvent-line notation by

$$\boxed{\Omega_L(2)} \begin{array}{c} I \\ \uparrow \\ \alpha \end{array} = \begin{array}{c} I \\ \uparrow \\ \text{---} \\ \hat{V}(J) \text{---} \\ \text{---} \\ \hat{V}(\beta) \text{---} \\ \text{---} \\ \alpha \end{array} - \begin{array}{c} I \\ \uparrow \\ \text{---} \\ \hat{V} \text{---} \\ \text{---} \\ \hat{V} \text{---} \\ \text{---} \\ \alpha \end{array}. \quad (8.77)$$

The corresponding ASG diagrams consist of the nondegenerate PT diagrams in Figs. 5.3 and 5.4 plus the diagrams in Figs. 8.4 and 8.5. This

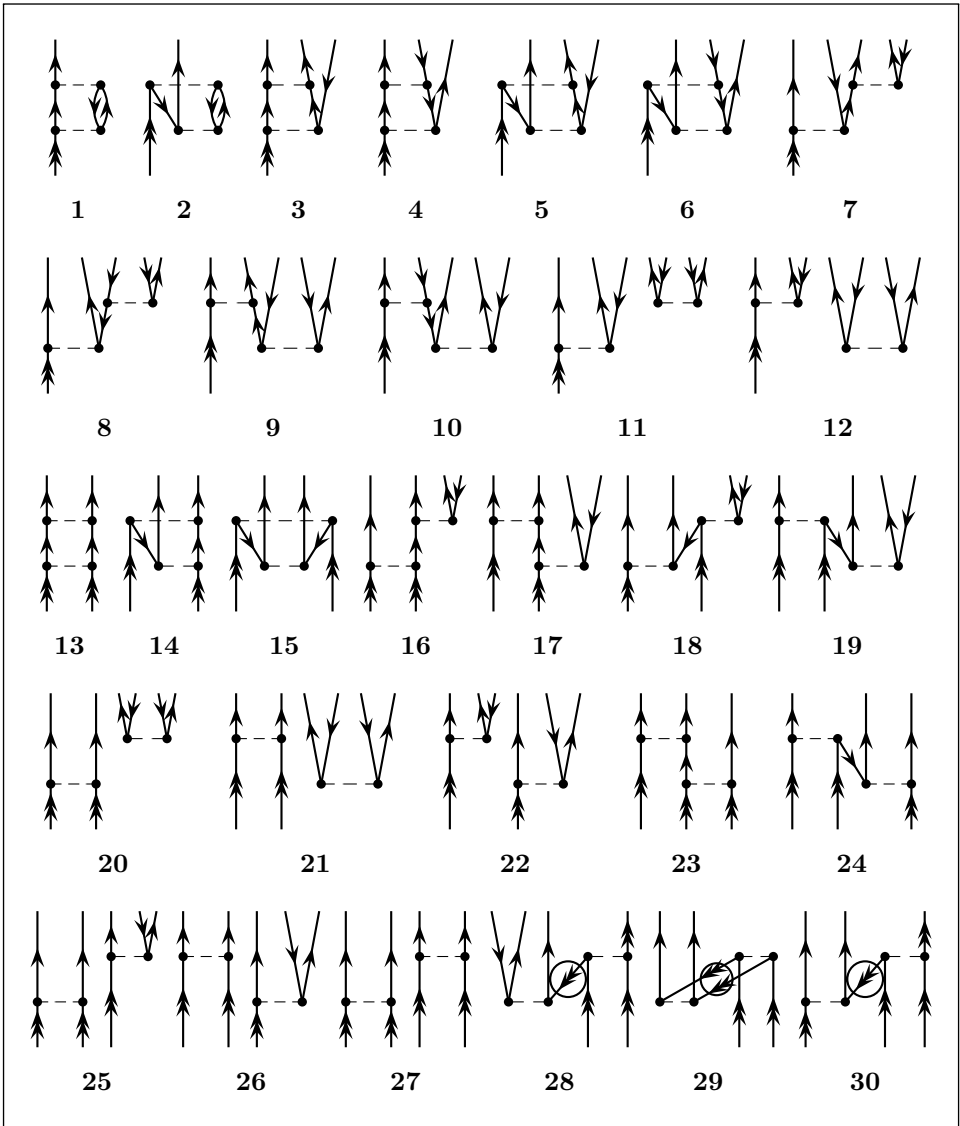


Fig. 8.4. Quasidegenerate PT ASG HF diagrams for the second-order wave operator.

set of diagrams is the first that contains folded diagrams (diagrams 28–30 in Fig. 8.4 and 58–61 in Fig. 8.5), representing the secondary contribution in (8.63). The diagrams in each of these figures are arranged in order of increasing number of incoming valence lines (separately for principal-term and folded diagrams). Diagrams 11, 12, 20–22, 25–27, 39–42, 45, 46, 51–57 are disconnected but not unlinked. The folded diagrams 28, 30, 60 are the

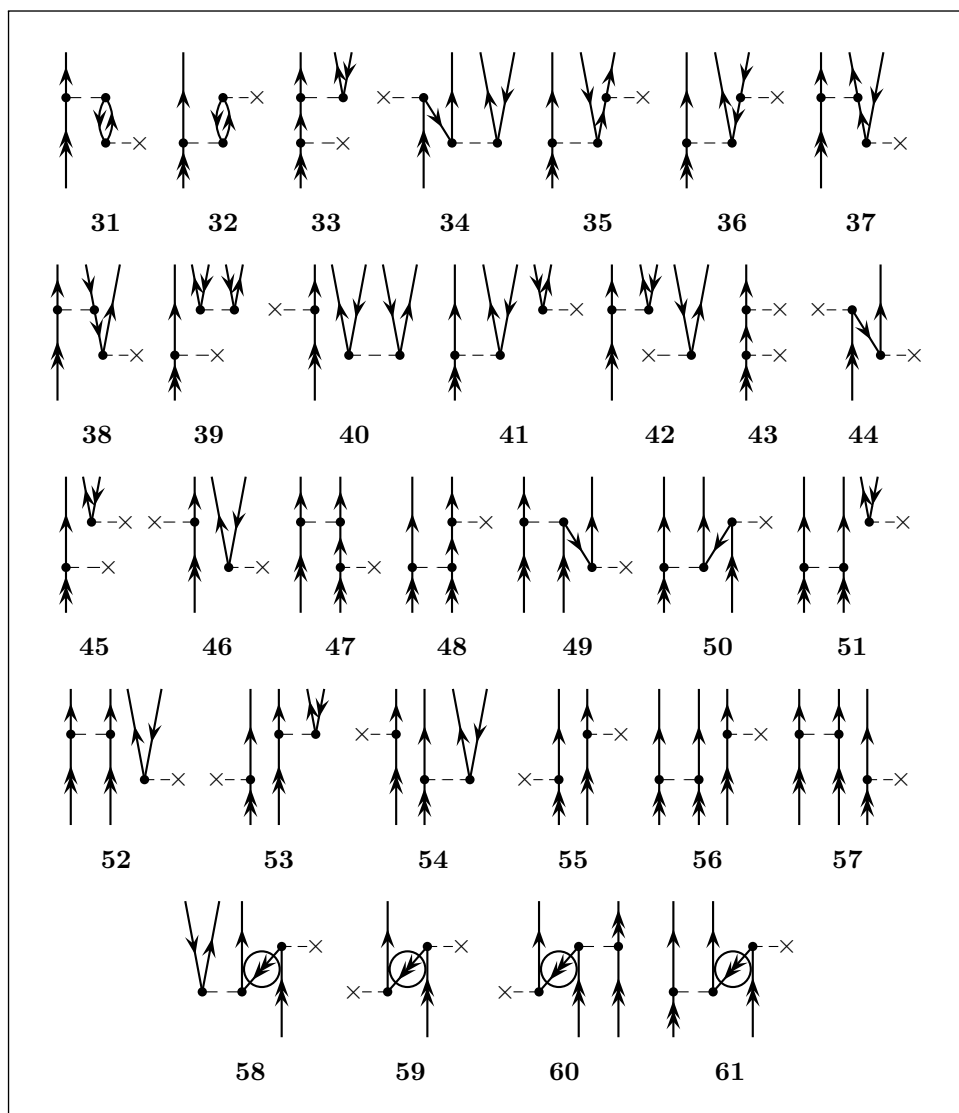


Fig. 8.5. Quasidegenerate PT ASG non-HF diagrams for the second-order wave operator.

first examples of wave-operator diagrams that contain outgoing valence lines (originating in the \hat{W} part of the secondary term). The summations over particle labels in many of these diagrams must be restricted to comply with the \hat{Q} projectors in the resolvents.

No disconnected folded diagrams have been included in Figs. 8.4 and 8.5, because all such diagrams for the second-order wave operator are unlinked

and cancel against certain contributions to disconnected principal-term diagrams. In fact, folding any of the disconnected principal-term diagrams for the second-order wave operator produces “folded” diagrams in which there are no folded lines that connect the \hat{W} part in the second term of the second equation in (8.39) with the rest of the diagram. The result is best described in the folded-resolvent-line notation.

An example of the folding process for these disconnected diagrams and of the relevant cancellations is provided by the folding of diagram 25 of Fig. 8.4:

$$= -\frac{1}{2} \sum_{iabxy} \frac{\langle ab||iu\rangle\langle xy||vw\rangle}{\varepsilon_{iuvw}^{abxy}\varepsilon_{iu}^{ab}} \{\hat{a}^\dagger\hat{b}^\dagger\hat{x}^\dagger\hat{y}^\dagger\hat{w}\hat{v}\hat{u}\}.$$

Comparing this diagram with the disconnected principal-term diagram 26 of Fig. 8.4,

$$= \frac{1}{2} \sum_{iabcd} \frac{\langle cd||vw\rangle\langle ab||iu\rangle}{\varepsilon_{iuvw}^{abcd}\varepsilon_{iu}^{ab}} \{\hat{a}^\dagger\hat{b}^\dagger\hat{c}^\dagger\hat{d}^\dagger\hat{w}\hat{v}\hat{u}\},$$

it is seen that the whole of the unlinked folded diagram cancels with those terms of the disconnected principal-term diagram in which c and d take on valence-label values (i.e. $c = x$, $d = y$). The canceled terms in the latter diagram represent unlinked contributions to that diagram.

Such cancellations occur between all unlinked folded diagrams and all unlinked contributions to the disconnected principal-term diagrams 21, 26, 27, 40, 46, 52, 54–57. The other disconnected diagrams have no unlinked contributions, either because both their disconnected parts contain hole lines (diagrams 11, 12, 22, 41, 42) or because the restriction that the intermediate state must not be a model state eliminates potential unlinked contributions to them (diagrams 20, 25, 39, 45, 51, 53). The result is that no unlinked diagrams or unlinked terms in disconnected diagrams survive. Thus the

summations over final states in the disconnected diagrams must be restricted to reflect that result.

As an example of the folded-resolvent-line notation for linked folded diagrams we consider diagram 28 of Fig. 8.4:

$$= -\frac{1}{2} \sum_{iabwx} \frac{\langle ab || ix \rangle \langle xw || uv \rangle}{\epsilon_{iuv}^{abw} \epsilon_{ix}^{ab}} \{ \hat{a}^\dagger \hat{i} \hat{b}^\dagger \hat{w}^\dagger \hat{v} \hat{u} \}.$$

No restriction over the a and b summations is needed here because of the presence of the hole line i .

The algebraic interpretation of QDPT diagrams, including weight factors, phase factors and more complex types of folded diagram, are discussed in detail in the next two subsections.

8.6.4 Weight factors and phases

When computing a specific matrix element of \hat{W} or Ω , the free lines have fixed labels and so may be ignored for the purpose of counting equivalent lines. Thus, in these cases the weight factor is $\frac{1}{2}$ for each pair of equivalent *internal* lines. However, when summing over the orthogonal-space states in wave-operator diagrams to obtain the perturbative corrections to the model states, as in

$$|\chi_\alpha^{(n)}\rangle = \sum_I |I\rangle \Omega_{I\alpha}^{(n)}, \quad (8.78)$$

open lines at the top of the Ω diagrams are included in the calculation of the weight factors. Each pair of open lines of the same type (hole, particle or valence) connected to the same vertex contributes a factor $\frac{1}{2}$. All open lines in \hat{W} diagrams and at the bottom of Ω diagrams are always valence lines that specify a model state and are never summed over; therefore they do not contribute to the weight factors.

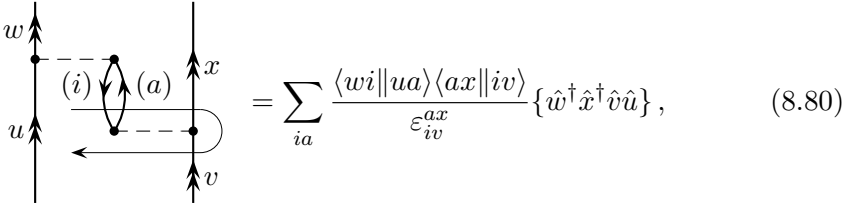
The phase factors in QDPT diagrams depend on the order of the creation and annihilation operators in the operator product associated with the diagrams. The case of \hat{W} diagrams is relatively simple, since all operators

are valence-state operators. Each pair of open-line labels on the same continuous path in the diagram is represented by a creation operator and an annihilation operator in corresponding positions (counting inwards from the two ends) in the operator product. With this ordering of the operators, the phase factor is given by the usual PT rule as $(-1)^{h-l}$, ignoring the open lines. The identity of the corresponding \hat{W} matrix element is determined from the operator product based on the constructions

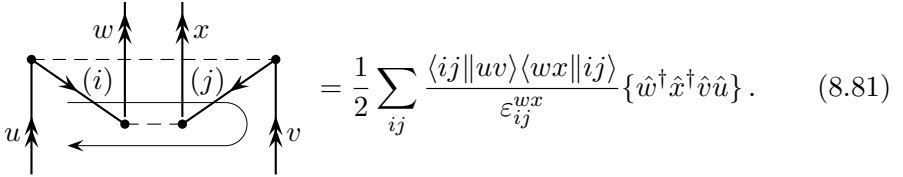
$$|\Phi^{uvw\dots}\rangle = \hat{u}^\dagger \hat{v}^\dagger \hat{w}^\dagger \dots |0\rangle, \quad \langle\Phi^{xyz\dots}| = \langle 0| \dots \hat{z} \hat{y} \hat{x}. \quad (8.79)$$

Indices representing the appropriate number of passive lines are added in corresponding positions. The same diagram value is assigned to matrix elements with all allowed values of the passive-line indices, i.e. all values which cause no duplication of indices in either the bra or ket states.

As examples, we consider diagrams 4 and 5 in Fig. 8.3, shown first in the folded-resolvent-line notation:

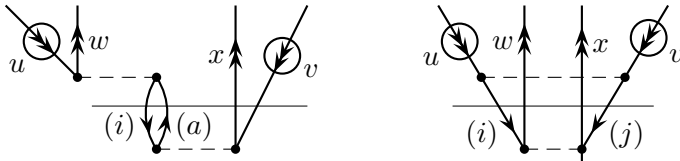


$$= \sum_{ia} \frac{\langle wi||ua\rangle \langle ax||iv\rangle}{\varepsilon_{iv}^{ax}} \{\hat{w}^\dagger \hat{x}^\dagger \hat{v} \hat{u}\}, \quad (8.80)$$



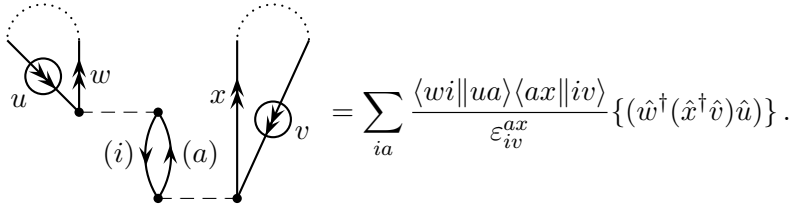
$$= \frac{1}{2} \sum_{ij} \frac{\langle ij||uv\rangle \langle wx||ij\rangle}{\varepsilon_{ij}^{wx}} \{\hat{w}^\dagger \hat{x}^\dagger \hat{v} \hat{u}\}. \quad (8.81)$$

Both diagrams contribute to the matrix element $\langle\Phi^{wxyz\dots}|\hat{W}^{(2)}|\Phi^{uvw\dots}\rangle$, where y, z, \dots label passive lines. In the first diagram we have one hole line and one loop, giving a phase factor $+1$, and no equivalent internal lines. In the second we have two hole lines and no loops, again giving a phase factor $+1$, and one pair of equivalent internal lines, giving a weight $\frac{1}{2}$. Alternatively, the denominators can be derived by folding the incoming valence lines:



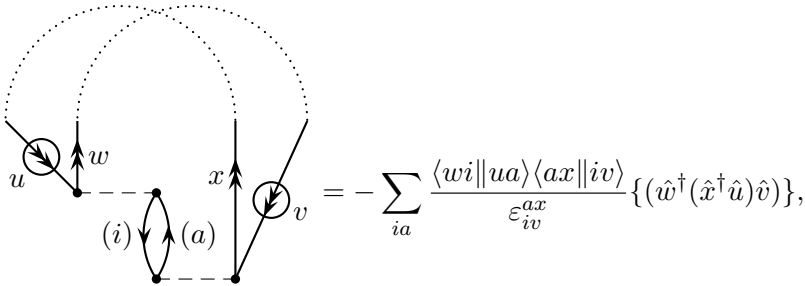
Alternative assignments of operator sequences and phase factors can be based on the folded form of these diagrams. Taking the first of the above

diagrams as an example, we can connect pairs of incoming and outgoing valence lines whose labels occupy corresponding positions in the initial and final model states with dotted lines, forming quasiloops, and pair the corresponding creation and annihilation operators:



$$= \sum_{ia} \frac{\langle wi || ua \rangle \langle ax || iv \rangle}{\varepsilon_{iv}^{ax}} \{(\hat{w}^\dagger(\hat{x}^\dagger\hat{v})\hat{u})\}.$$

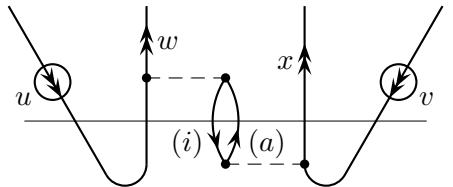
In this case we have included these quasiloops in the loop count and have counted the folded lines as holes (just as for the denominator determination), so this diagram now has three loops and three hole lines, and a phase factor +1, just as before. The alternative quasiloop connection,



$$= - \sum_{ia} \frac{\langle wi || ua \rangle \langle ax || iv \rangle}{\varepsilon_{iv}^{ax}} \{(\hat{w}^\dagger(\hat{x}^\dagger\hat{u})\hat{v})\},$$

has two loops and a phase factor -1 and is equal in value to the previous form because of the odd permutation of the operators. This form of the diagram can be considered as contributing to $\langle \Phi^{wxyz} | \hat{W} | \Phi^{vuyz} \rangle$, which is consistent with the previous assignment because of the odd permutation of the indices in the ket side of the matrix element. As in the case of nondegenerate PT diagrams, this analysis shows that the choice of quasiloop connections does not affect diagram values and justifies the omission of these connections from the diagrams.

The folding of the incoming valence lines could also have been done from the bottom of the diagram, as in



Since the resolvent line crosses the folded u line twice, the denominator is unaffected.

To specify the phase of an orthogonal-space state we define it by

$$|\Phi_{ij\dots m}^{ab\dots efg\dots}\rangle = (\hat{a}^\dagger \hat{i})(\hat{b}^\dagger \hat{j}) \cdots (\hat{e}^\dagger \hat{m}) \hat{f} \hat{g}^\dagger \cdots |0\rangle, \quad (8.82)$$

where the superscript indices may represent either particle or valence labels. The labels in an orthogonal-space state fall into two classes: there are zero or more pairs, each pair consisting of a particle (or valence) label vertically above a hole label in the state specification, such as (a, i) , (b, j) , (e, m) in (8.82), and there are unpaired (excess) particle (or valence) labels, such as f, g . In a wave-operator matrix element $\Omega_{I\alpha}$ each unpaired particle or valence label in the final state I is considered as paired with a valence label in the initial (model) state α if the two are in corresponding positions in the unpaired final-state labels and the initial-state labels (ignoring all the paired labels). Thus, in the matrix element $\langle \Phi_{ij\dots m}^{ab\dots efg\dots} | \Omega | \Phi^{uv\dots} \rangle$, f is paired with u and g is paired with v . Note that the operator product in (8.82) is in normal order and that creation and annihilation operator pairs such as $(\hat{a}^\dagger \hat{i})$ may be moved together freely across any other operators in the sequence without affecting the resulting function or the normal order.

In determining the phase factor for a wave-operator diagram, the simplest approach is to place paired labels on the same continuous path in the diagram. Each open hole line is then connected by a dotted line with its paired open particle line, creating a quasiloop, and the usual $(-1)^{h-l}$ rule for the phase factor is applied. As examples we consider diagrams 8 and 22 of Fig. 8.4,

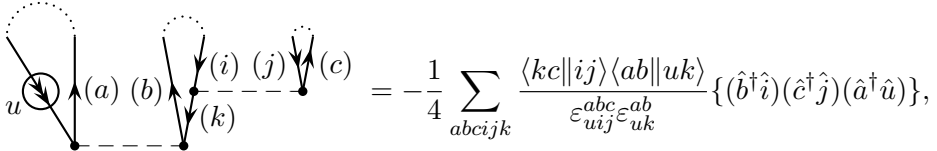
$$= -\frac{1}{4} \sum_{abcijk} \frac{\langle kc || ij \rangle \langle ab || uk \rangle}{\varepsilon_{uij}^{abc} \varepsilon_{uk}^{ab}} \{ (\hat{b}^\dagger \hat{i}) (\hat{c}^\dagger \hat{j}) (\hat{a}^\dagger \hat{u}) \},$$

$$= \frac{1}{4} \sum_{abcdij} \frac{\langle ab || ui \rangle \langle cd || vj \rangle}{\varepsilon_{uvij}^{abcd} \varepsilon_{vj}^{cd}} \{ (\hat{b}^\dagger \hat{i}) (\hat{d}^\dagger \hat{j}) (\hat{a}^\dagger (\hat{c}^\dagger \hat{v}) \hat{u}) \},$$

which contribute to $\langle \Phi_{ij}^{bcax\dots} | \Omega | \Phi^{ux\dots} \rangle$ and $\langle \Phi_{ij}^{bdacx\dots} | \Omega | \Phi^{uvx\dots} \rangle$, respectively, where x, \dots label passive lines. Each diagram has two pairs of equivalent

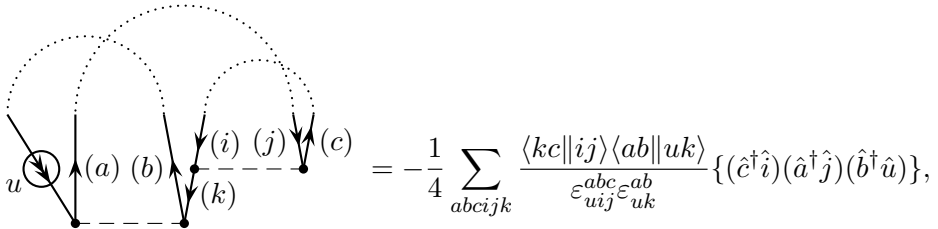
open lines, contributing a weight factor $\frac{1}{4}$. In the first diagram we have two loops and three hole lines, hence the phase factor -1 . The second diagram has two loops and two hole lines, and a phase factor of $+1$.

Alternatively, we can fold the incoming valence lines and connect all paired indices with dotted lines, counting the folded incoming valence lines as hole lines for the purpose of phase-factor determination as we have previously done for level-shift diagrams; thus



$$= -\frac{1}{4} \sum_{abcijk} \frac{\langle kc || ij \rangle \langle ab || uk \rangle}{\varepsilon_{uij}^{abc} \varepsilon_{uk}^{ab}} \{(\hat{b}^\dagger \hat{i})(\hat{c}^\dagger \hat{j})(\hat{a}^\dagger \hat{u})\},$$

or, using a different pairing scheme,



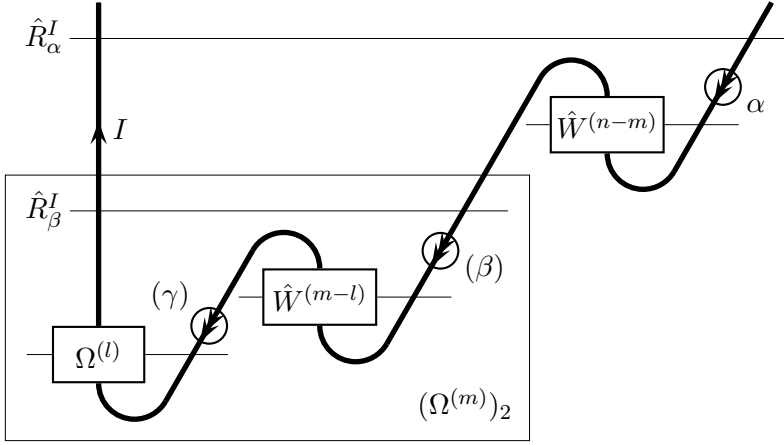
$$= -\frac{1}{4} \sum_{abcijk} \frac{\langle kc || ij \rangle \langle ab || uk \rangle}{\varepsilon_{uij}^{abc} \varepsilon_{uk}^{ab}} \{(\hat{c}^\dagger \hat{i})(\hat{a}^\dagger \hat{j})(\hat{b}^\dagger \hat{u})\},$$

which contribute to $\langle \Phi_{ij}^{bcax...} | \Omega | \Phi^{ux...} \rangle$ and $\langle \Phi_{ij}^{cabx...} | \Omega | \Phi^{ux...} \rangle$, respectively. These two forms now have three and one loops, respectively, and both have four hole lines, giving a phase factor -1 in both cases, corresponding to even permutations of the creation and annihilation operators and of the superscript indices in the bra state between the two forms. Normal order of the operator product is maintained as long as the valence annihilation operators are placed at the end of the operator string.

8.6.5 Folded diagrams

Folded diagrams, which represent the secondary term in the generalized Bloch equation, occur for both Ω and \hat{W} diagrams; the \hat{W} diagrams inherit their folds from their Ω component, (8.24) or (8.40). An additional phase factor -1 is required for each fold. The number of folds is not determined by the number of internal folded lines but by the number of nested secondary terms represented in the diagram. Repeated secondary terms, and thus multiple folds, arise when the $\Omega_{I\beta}^{(m)}$ factor and/or the $W_{\beta\alpha}^{(n-m)}$ factor contributing to the secondary term in (8.39) contain lower-order secondary-term contributions of their own. Thus, replacing the $\Omega^{(m)}$ factor in (8.67) by its own secondary term produces the doubly folded diagram shown here

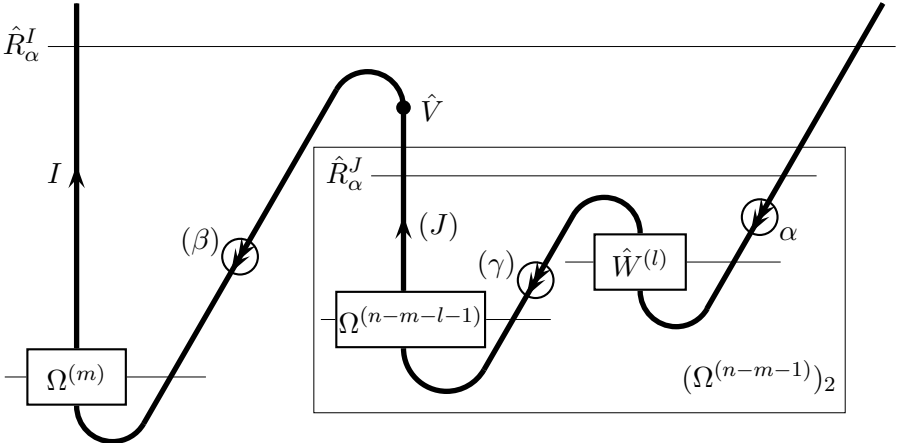
schematically in its fully folded form:



$$= \sum_{ml} \sum_{\beta\gamma} |I\rangle \Omega_{I\gamma}^{(l)} \frac{W_{\gamma\beta}^{(m-l)} W_{\beta\alpha}^{(n-m)}}{D_{\alpha I} D_{\beta I}} \langle \alpha|. \quad (8.83)$$

This type of doubly folded diagram first occurs in the third-order wave operator and the fourth-order level-shift operator diagrams.

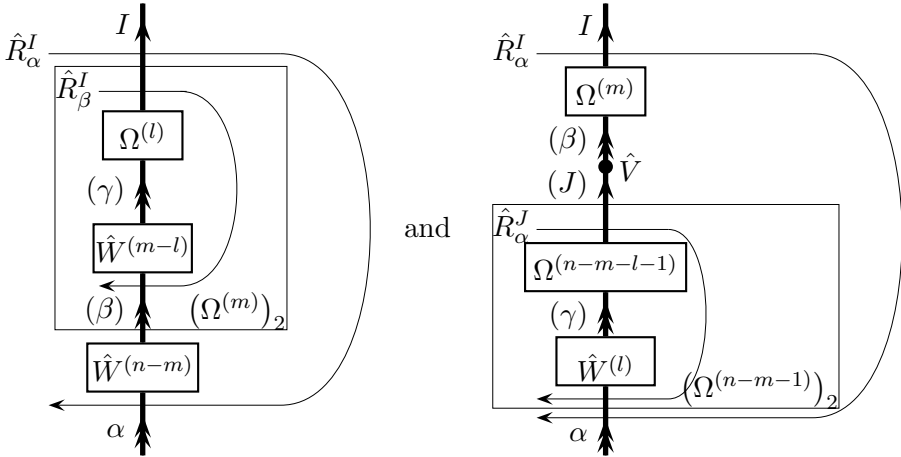
Similarly, replacing the $\hat{W}^{(n-m)} = \hat{P}\hat{V}\hat{Q}\Omega^{(n-m-1)}$ factor in (8.67) by its own secondary term produces the doubly folded diagram shown here schematically in its fully folded form:



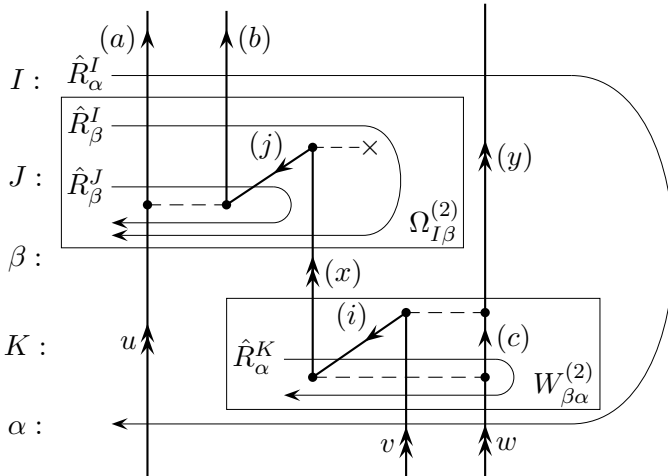
$$= \sum_{ml} \sum_{J\beta\gamma} |I\rangle \Omega_{I\beta}^{(m)} \frac{V_{\beta J} \Omega_{J\gamma}^{(n-m-l-1)} W_{\gamma\alpha}^{(l)}}{D_{\alpha I} D_{\alpha J}} \langle \alpha|. \quad (8.84)$$

This type of doubly folded diagram first occurs in the fourth-order wave operator and the fifth-order level-shift operator diagrams.

The folded-resolvent-line notation is particularly effective in representing all kinds of folded diagrams. We have seen its application to an $\Omega^{(2)}$ singly folded diagram in subsection 8.6.3. The doubly folded schematic diagrams of (8.83), (8.84) take the following forms in this notation:



An example of a singly folded diagram that illustrates some details of the interpretation of such diagrams is provided by the following fourth-order wave-operator diagram containing $\Omega^{(2)}$ and $\hat{W}^{(2)}$ components in the expression $-\hat{R}_\alpha^I \Omega_{I\beta}^{(2)} W_{\beta\alpha}^{(2)}$. We shall first display it in the folded-resolvent-line notation, in which the identity of the intermediate states at the various level is more apparent:

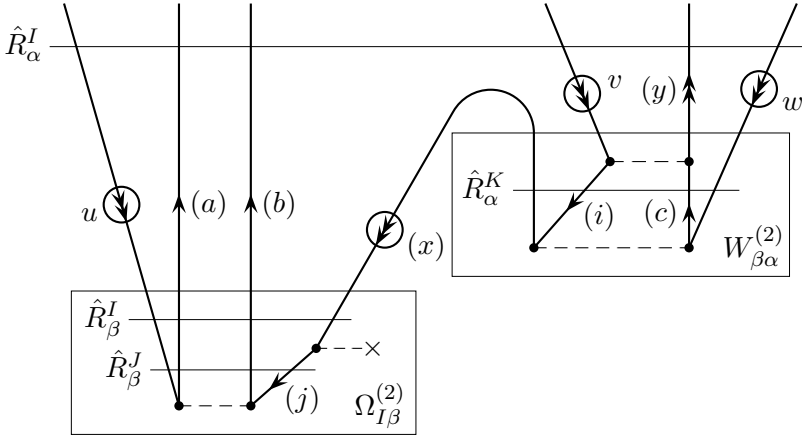


The initial, final and intermediate states are identified on the left-hand side, and the resolvents required are also indicated. Note that the y line is passive

for the $\Omega^{(2)}$ diagram while the u line is passive for the $\hat{W}^{(2)}$ diagram. The denominators generated by the various resolvents are:

$$\begin{aligned} D_{I\alpha} &= E_{\alpha}^{(0)} - E_I^{(0)} = \varepsilon_{uvw}^{aby}, \\ D_{I\beta} &= E_{\beta}^{(0)} - E_I^{(0)} = \varepsilon_{ux}^{ab}, \\ D_{J\beta} &= E_{\beta}^{(0)} - E_J^{(0)} = \varepsilon_{uj}^{ab}, \\ D_{K\alpha} &= E_{\alpha}^{(0)} - E_K^{(0)} = \varepsilon_{iw}^{xc}. \end{aligned}$$

It is easily seen that these denominators are correctly recovered from the fully folded form of the diagram:

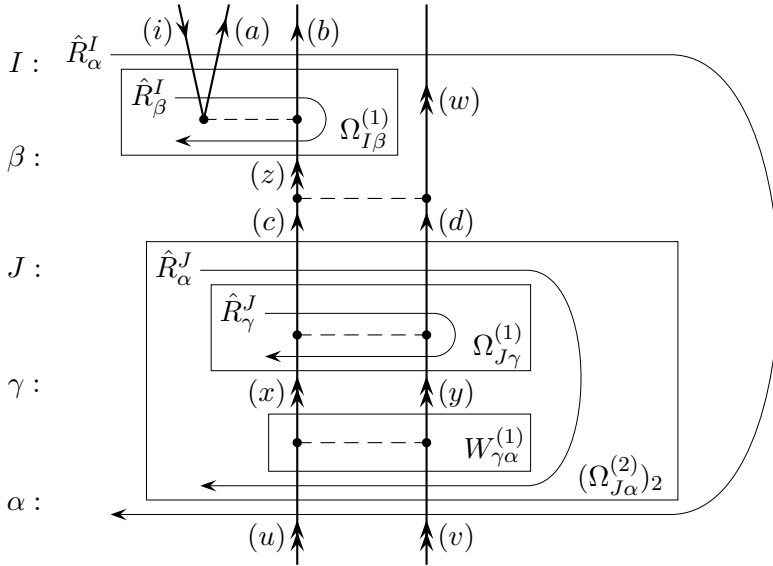


The x line must come out of the top of the $\hat{W}^{(2)}$ section rather than connecting its two end vertices with a straight line and the internal resolvent R_{α}^K within the $\hat{W}^{(2)}$ section crosses the ascending part of the x line but not the descending part nor any other line on the left-hand side of the diagram. The value of this diagram is given by

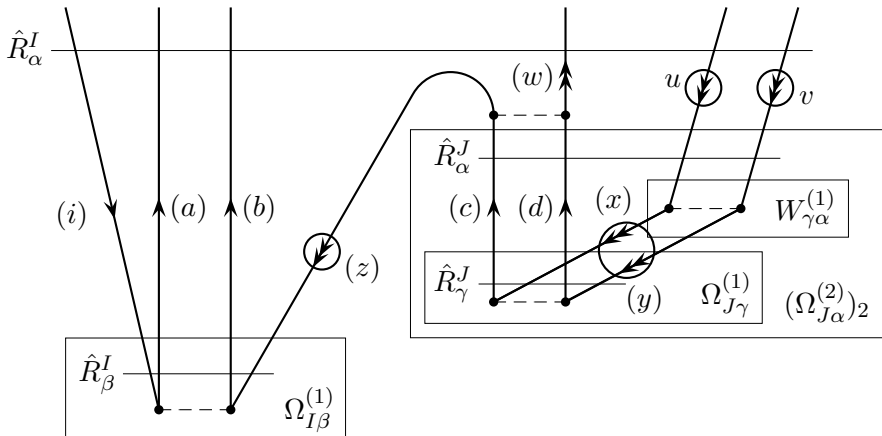
$$-\frac{1}{2} \sum_{ijxabcy} \frac{\langle ab||uj\rangle \langle j|f|x\rangle \langle iy||vc\rangle \langle xc||iw\rangle}{\varepsilon_{uvw}^{aby} \varepsilon_{ux}^{ab} \varepsilon_{uj}^{ab} \varepsilon_{iw}^{xc}} \{ \hat{a}^{\dagger} \hat{b}^{\dagger} \hat{y}^{\dagger} \hat{w} \hat{v} \hat{u} \}.$$

The factor $\frac{1}{2}$ is due to the pair of equivalent lines a, b . There are two hole lines and no loops. The negative sign is due to the single internal fold. Open-line labels on the same continuous path are associated with creation and annihilation operators in corresponding positions in the operator sequence (counting inwards from the two ends).

As an example of a doubly folded diagram we consider a fourth-order wave-operator diagram of the type described schematically in (8.84):



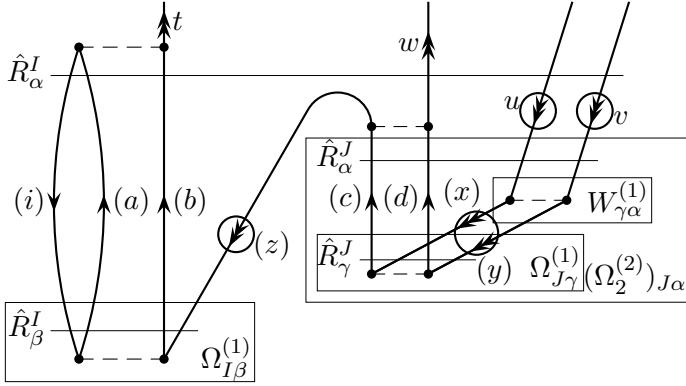
The many-electron states involved, corresponding to the designations in the schematic diagram (8.84), are identified on the left-hand side of the diagram. Specifically, these states are $|I\rangle = |\Phi_i^{abw}\rangle$, $|\beta\rangle = |\Phi^{zw}\rangle$, $|J\rangle = |\Phi^{cd}\rangle$, $|\gamma\rangle = |\Phi^{xy}\rangle$, $|\alpha\rangle = |\Phi^{uv}\rangle$. The upper parts of resolvent lines may not cross model states, so the labels c and d cannot both take valence index values at the same time. Each intermediate model state (β and γ in this diagram) corresponds to a fold and is crossed only by the lower parts of the folded resolvent lines. The fully folded form is



The whole right-hand side of this diagram, including the top \hat{V} vertex, represents $W_{\beta\alpha}^{(4)}$, justifying the designation of the open line emerging from that \hat{V} vertex as a valence line (w). This diagram has three equivalent pairs (a, b) , (c, d) , (x, y) , one hole line, one quasiloop involving the lines labeled a, i and two internal folds. Its value is given by

$$\frac{1}{8} \sum_{iwx yzabcd} \frac{\langle ab||iz\rangle\langle zw||cd\rangle\langle cd||xy\rangle\langle xy||uv\rangle}{\varepsilon_{iuv}^{abw}\varepsilon_{iz}^{ab}\varepsilon_{uv}^{cd}\varepsilon_{cd}^{xy}} \{\hat{a}^\dagger\hat{b}^\dagger\hat{w}^\dagger\hat{v}\hat{u}\}.$$

Finally, we consider a fifth-order level-shift-operator diagram obtained by adding an interaction vertex on top of the previous wave-operator diagram:



$$= \frac{1}{8} \sum_{ixyzabcd} \frac{\langle it||ab\rangle\langle ab||iz\rangle\langle zw||cd\rangle\langle cd||xy\rangle\langle xy||uv\rangle}{\varepsilon_{iuv}^{abw}\varepsilon_{iz}^{ab}\varepsilon_{uv}^{cd}\varepsilon_{cd}^{xy}} \{\hat{t}^\dagger\hat{w}^\dagger\hat{v}\hat{u}\}.$$

It provides a contribution to the matrix elements $\langle\Phi^{tw\dots}|\hat{W}^{(5)}|\Phi^{uv\dots}\rangle$.

8.6.6 Third-order level-shift operator

The number of distinct diagrams in QDPT grows very rapidly with the order of the treatment, making high-order calculations difficult. We shall restrict ourselves here to discussing the generation of third-order level-shift-operator diagrams. We shall consider principal-term diagrams (those without internal folds) and folded diagrams separately.

For the principal-term diagrams it is easiest to follow a similar procedure to that used for the second-order level-shift diagrams and begin with the Hugenholtz diagrams. We shall classify the diagrams according to the number of open valence lines that enter and leave each of the three vertices. The notation (ijk/lmn) will be used to describe a class of diagrams with i, j and k open valence lines entering the first, second and third vertices, respectively

Table 8.1. *Representative classes, numbers of distinct linked ASG diagrams in each class and set and total number of principal-term diagrams for the third-order level-shift operator*

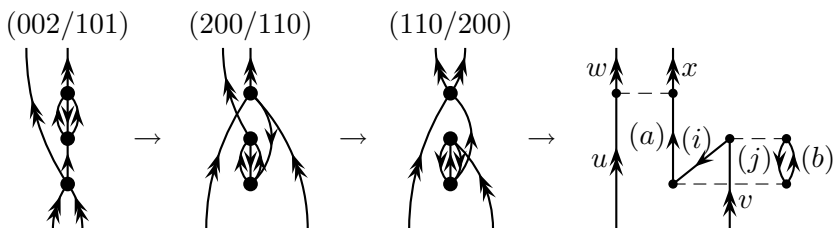
Valence electrons	Representative classes	Classes in set	Diagrams in class		Diagrams in set	
			HF	non-HF	HF	non-HF
0	(000/000)	1	3	11	3	11
1	(001/100)	6	2	7	12	42
	(001/001)	3	2	4	6	12
2	(002/200)	6	1	1	6	6
	(002/110)	6	1	3	6	18
	(002/101)	12	1	2	12	24
	(011/110)	6	2	3	12	18
	(011/011)	3	1	2	3	6
3	(012/210)	6	1	0	6	0
	(012/201)	6	1	1	6	6
	(012/111)	12	1	1	12	12
	(012/021)	6	0	1	0	6
	(111/111)	1	2	0	2	0
4	(022/211)	6	1	0	6	0
	(112/211)	6	1	0	6	0
Folded					10	20
Total					108	181

(counting downwards from the top vertex) and l, m and n open valence lines leaving these vertices, respectively. Obviously $i + j + k = l + m + n$. The closed-shell third-order energy diagrams of Figs. 5.1 and 5.2 correspond to the class (000/000) and are included in the expansions for the diagonal elements of the level-shift operator in the open-shell case.

The various classes of diagrams can be organized in sets. The different classes in a set all have the same number of diagrams and can be obtained from each other by permutation of the three vertices and/or by reversing all arrows (which includes converting all entering open valence lines to leaving open valence lines and vice versa). For example, the 12 classes (002/101), (002/011), (020/110), (020/011), (200/110), (200/101), (101/002), (011/002), (110/020), (011/020), (110/200) and (101/200) form one such set. We shall list the linked diagrams for just one *representative*

class from each set. Table 8.1 lists the representative classes, the number of distinct diagrams in each class and set and the total number of diagrams of HF and non-HF type. Clearly, the total number, 289, of third-order diagrams (including 30 folded diagrams, as shown later), in comparison with just 14 diagrams for the closed-shell case, demonstrates the difficulty of carrying out higher-order QDPT calculations.

The principal-term Hugenholtz diagrams for the representative classes are shown in Fig. 8.6 (apart from the closed-shell class (000/000)). No disconnected diagrams are included since such diagrams would be unlinked. Obtaining all other Hugenholtz diagrams from the representative classes, converting them to ASG diagrams and giving them an algebraic interpretation are straightforward. As an example we show the generation of a Hugenholtz diagram of the class (110/200) from the corresponding diagram in the representative class (002/101) by permutation of vertices ($1 \rightarrow 2 \rightarrow 3 \rightarrow 1$) and reversal of arrows, including the interconversion of entering and leaving open valence lines, followed by its conversion to an ASG diagram:



This ASG diagram represents the contribution

$$\begin{aligned}
 & -\frac{1}{2} \sum'_{ijab} \frac{\langle wx \| ua \rangle \langle ij \| vb \rangle \langle ab \| ij \rangle}{\varepsilon_v^a \varepsilon_{ij}^{ab}} \{ \hat{w}^\dagger \hat{x}^\dagger \hat{v} \hat{u} \} \\
 & = -\frac{1}{2} \sum'_{ijab} \frac{\langle wx \| ua \rangle \langle ij \| vb \rangle \langle ab \| ij \rangle}{\varepsilon_v^a \varepsilon_{ij}^{ab}} | \Phi^{wx\dots} \rangle \langle \Phi^{uv\dots} |
 \end{aligned}$$

to $\hat{W}^{(3)}$, contributing to the matrix elements $\langle \Phi^{wx\dots} | \hat{W}^{(3)} | \Phi^{uv\dots} \rangle$. The prime over the summation sign indicates that the sum over a exclude valence-index values in order to avoid intermediate model states. The denominator reflects the folding of the incoming valence lines u and v . The weight factor reflects the equivalence of the two hole lines i and j . The phase factor is due to the presence of two hole lines and one loop. The generation of the rest of the normal third-order diagrams and their interpretation are left as an exercise for the reader.

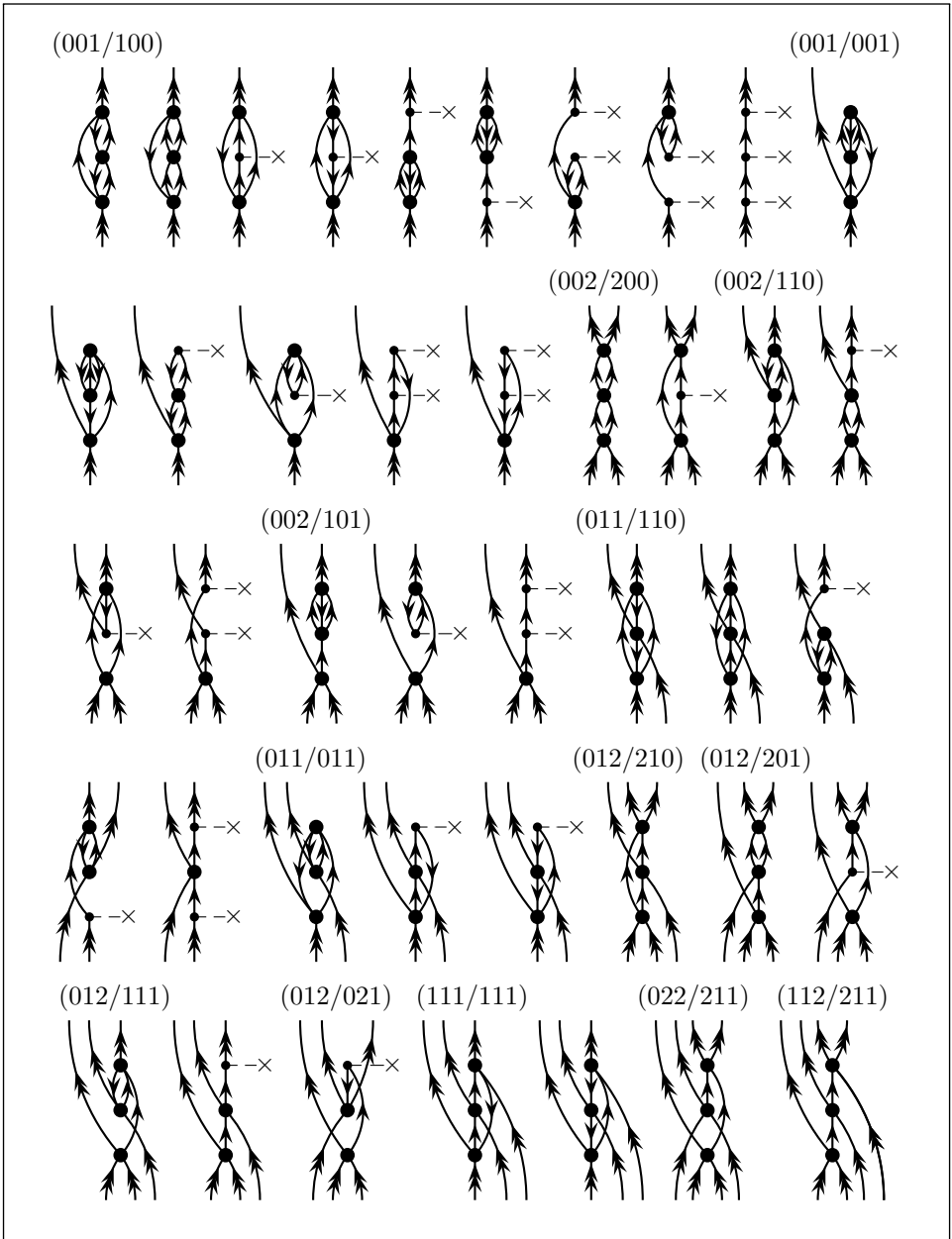


Fig. 8.6. Quasidegenerate PT Hugenholtz diagrams for representative classes of the principal term of the third-order level-shift operator.

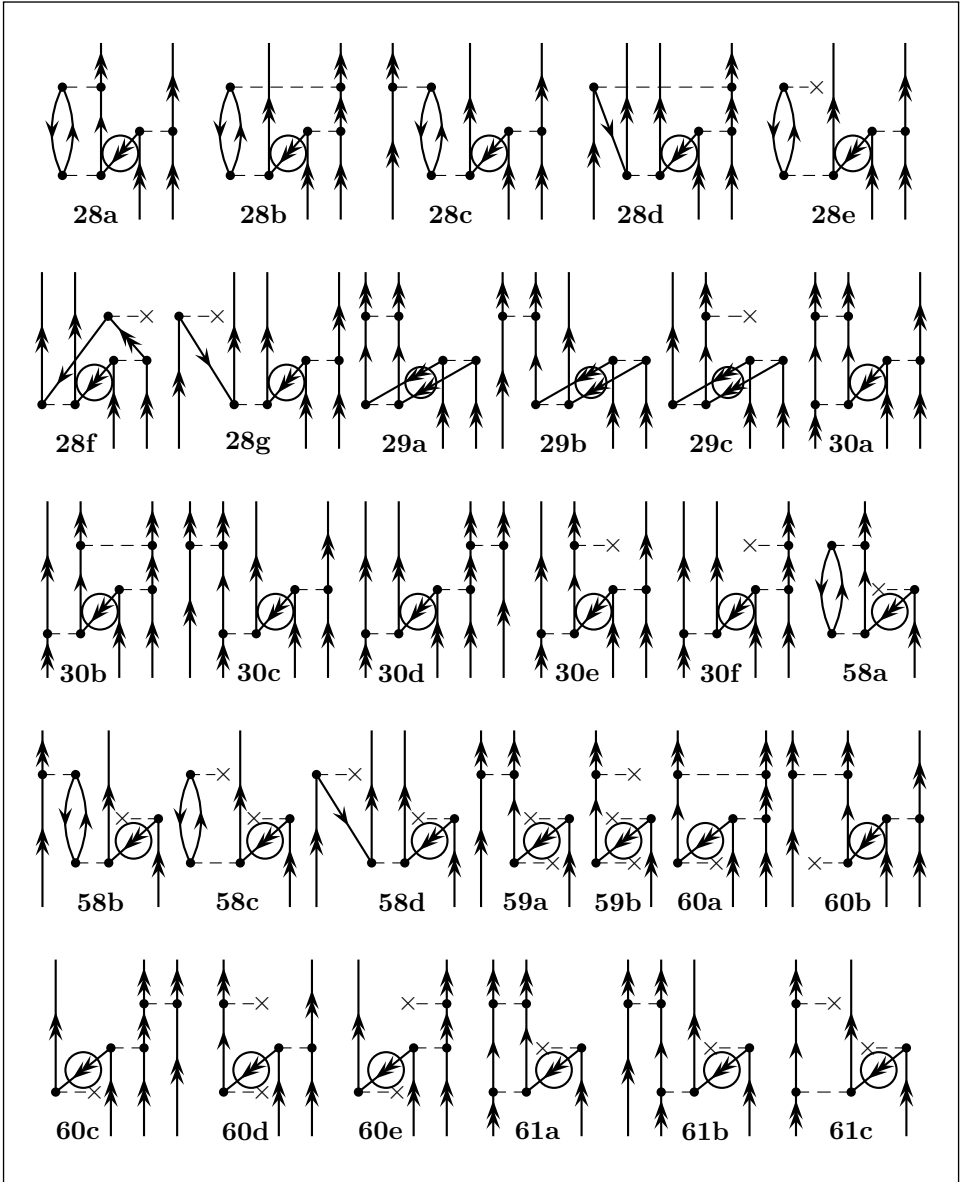


Fig. 8.7. Quasidegenerate PT ASG folded diagrams for the third-order level-shift operator.

The folded third-order level-shift diagrams are best obtained by adding an interaction vertex to the top of the folded second-order wave-operator diagrams (diagrams 28–30 and 58–61 of Figs. 8.4 and 8.5) in all allowed ways. To avoid generating equivalent diagrams, the Hugenholtz version should be examined in each case. The resulting set of folded ASG diagrams is

displayed in Fig. 8.7. The numbering of these diagrams identifies the folded second-order wave-operator diagrams from which they have been generated.

As an example of how to interpret the folded diagrams we shall consider diagram 28f, shown here in both conventional and folded-resolvent-line form:

$$= \sum_{iyz} \frac{\langle i | \hat{f} | z \rangle \langle xw || yi \rangle \langle yz || uv \rangle}{\varepsilon_{iuv}^{wxz} \varepsilon_{iy}^{wx}} \{ \hat{x}^\dagger \hat{w}^\dagger \hat{v} \hat{u} \}.$$

This diagram contributes to the matrix elements $\langle \Phi^{xwt...} | \hat{W}^{(3)} | \Phi^{uvt...} \rangle$, where the indices beginning with t represent passive lines. The minus sign due to the fold is canceled by the minus sign due to the presence of one hole line (i) and no loops. There are no equivalent internal lines.

8.6.7 Third-order wave operator

Because of the proliferation of the number of diagrams with increasing order, we shall not present actual diagrams for the third-order wave operator. Even the number of skeletons is too large to present conveniently. Instead, we shall just give a schematic description of the five different terms appearing in the expression for this operator in (8.44). This expression contains one principal term, three singly folded terms and one doubly folded term. Their schematic form in the folded-resolvent-line notation is

$$(8.85)$$

It can be seen that the expression for $\Omega^{(3)}$ contains all possible distributions of \hat{Q} -space and model-space states for the two internal state lines.

Furthermore, all possible arrangements of the three folded resolvent lines are included in which the upper part crosses a \hat{Q} -space state and the lower part crosses a model state, the resolvent lines do not cross each other, no two resolvent lines cross the same pair of states and each state is crossed by at least one resolvent line. An outer resolvent line that crosses the final and initial states is always present. Note that the second and fourth terms in (8.85) contain the same sequence of intermediate states but differ in the states that are crossed by the middle resolvent line.

A compact notation for these schematic diagrams can be obtained using sets of matched parentheses, paired according to the ordinary algebraic convention, interspersed with state labels. The opening and closing parentheses of each pair represent the upper and lower parts of the folded resolvent line, respectively:

$$\Omega_{I\alpha}^{(3)} = (I(J(K\alpha))) - (I((J\beta)\alpha)) - ((I\beta)(J\alpha)) - ((I(J\beta))\alpha) + (((I\gamma)\beta)\alpha). \quad (8.86)$$

Perturbation operators are implied between the state labels in such a way that each \hat{Q} -space-state label is immediately followed by a \hat{V} operator and each model-state label is immediately preceded by such an operator, without intervening parentheses. Summations over intermediate states are implied.

Using the conventional notation the same expression takes the following form, in which we have folded the incoming model-state line labeled α in each term in order to be able to show the scope of all resolvent lines:

$$\Omega_{I\alpha}^{(3)} = \text{Diagram 1} - \text{Diagram 2} - \text{Diagram 3} - \text{Diagram 4} + \text{Diagram 5} \quad (8.87)$$

Note the scope of the middle resolvent line in the third term (compare (8.67)). The difference in the operator sequences in the second and fourth terms is due to the fact that the second term represents the sum $\sum_J \hat{R}_\alpha^I V_{IJ} (\Omega_{J\alpha}^{(2)})_2$, in which $(\Omega_{J\alpha}^{(2)})_2 = \sum_\beta \hat{R}_\alpha^J \Omega_{J\beta}^{(1)} W_{\beta\alpha}^{(1)}$, while the fourth term represents $\sum_\beta \hat{R}_\alpha^I (\Omega_{I\beta}^{(2)})_1 W_{\beta\alpha}^{(1)}$ (the subscripts 1 and 2 refer to the principal and secondary terms, respectively, in (8.39)).

8.7 Incomplete model space

8.7.1 The Hose–Kaldor approach

A formalism for the use of incomplete model spaces in QDPT was introduced by Hose and Kaldor (1979, 1980, 1982). Their approach uses different Fermi vacuum states for the calculation of the different matrix elements of the wave and level-shift operators. The incoming model state is used as the Fermi vacuum for all matrix elements in which that state is the initial (ket) state. Thus all elements in the same column of the matrices for the wave and level-shift operators use the same Fermi vacuum, but different columns use different Fermi vacuums. A similar approach to multireference coupled-cluster theory was formulated by Jeziorski and Monkhorst (1981).

When the Hose–Kaldor (HK) approach is applied to a complete model space it generates the same results, order by order (but not diagram by diagram), as the approach presented in the previous sections because it solves the same generalized Bloch equation. However, because it can be applied easily to incomplete model spaces, it can partly overcome the problems of intruder states and of model spaces that are too large for practical applications. In such cases it results in incomplete cancellation of unlinked diagrams, as will be shown in the following analysis, but the procedure is nevertheless quite practical and has been used successfully for various applications (e.g. Kaldor 1984, Hose and Kaldor 1984, Kucharski and Bartlett 1988), although, like most QDPT applications, not beyond third order. In presenting this formalism we shall use the diagrammatic approach of Kucharski and Bartlett (1988), in which the folded-resolvent-line notation was first introduced.

The one-electron states in the HK formalism are classified into core, valence and virtual states, as in the previously described approach. However, for each different Fermi vacuum used, the valence orbitals are classified as valence holes (the valence states occupied in that particular Fermi vacuum) and valence particles. For each such Fermi vacuum, the hole states consist of the core states plus the valence hole states of that vacuum. Similarly, the

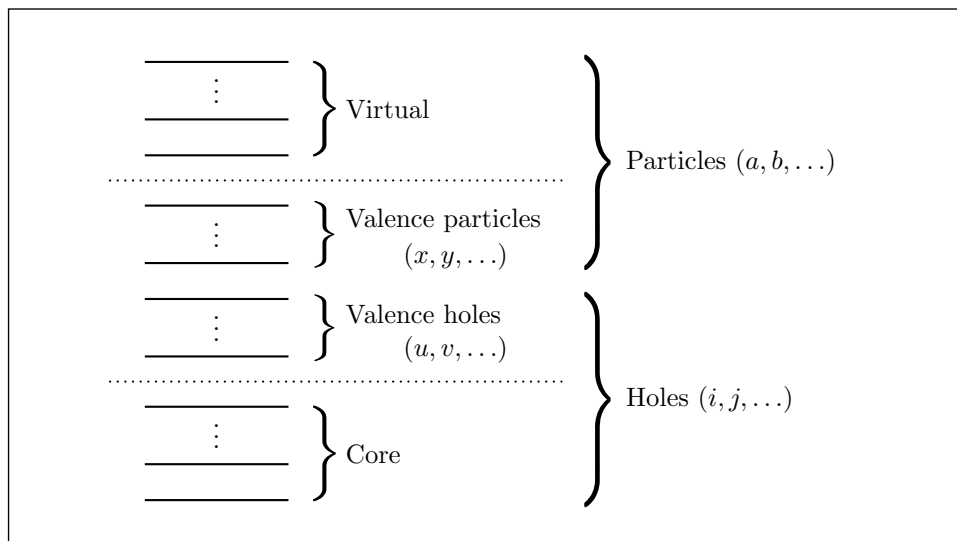


Fig. 8.8. Classification of one-electron states in the Hose–Kaldor approach.

particle states consist of the virtual states plus the valence particle states. This classification is shown schematically in Fig. 8.8, but it should be remembered that the sequence of the valence states in this figure does not reflect their energy order and that the classification of the valence states depends on the model state used as the Fermi vacuum. In the diagrammatic notation, valence states are distinguished by double arrows. In skeleton representations a bar across the state line is used to indicate lines restricted to valence states.

The selection of the model states is a major factor in determining the convergence behavior of the perturbation series. As noted in Section 8.2, a large energy gap between the model states on the one hand and all external (\hat{Q} -space) states on the other is desirable, because each denominator factor in the various terms contributing to the level-shift and wave-operator matrix elements represents an energy difference between a model state and an external state. Small denominator factors increase the magnitude of high-order contributions and retard (or even prevent) convergence.

8.7.2 The one-electron interaction

The cancellation between the \hat{U}_N and \hat{V}'_N operators that simplifies the expression for the perturbation in nondegenerate MBPT, (3.176)–(3.183), can

no longer be used in the same way in the HK formalism of quasidegenerate PT. The reason for this lies in the different summation ranges in the definitions of u_{pq} and v'_{pq} in the latter case, owing to the varying definitions of the Fermi vacuum for the different columns of the level-shift and wave-operator matrices and to the difference between these Fermi-vacuum definitions and the corresponding definition for the Fock operator.

The definition $u_{pq} = \sum_i \langle pi || qi \rangle$, (3.133), is part of the definition of the Fock operator (3.130) and therefore the summation over i runs over the occupied spinorbitals in the determinant used as the reference state for that Fock operator, regardless of whether this determinant is an HF wave function for any particular state. A typical choice for the reference determinant is just the core state, i.e. the determinant consisting of all the spinorbitals occupied in all the model states. However, in the definition $v'_{pq} = \sum_i \langle pi || qi \rangle$, given in (3.178), the summation over i is over the spinorbitals constituting the Fermi vacuum used for the definition of normal products for the current matrix element, which include the current valence hole states.

The one-electron component of the normal-product perturbation operator in the HK formalism is therefore given by the operator

$$\hat{G}_N = \hat{F}_N^o + \hat{V}'_N - \hat{U}_N = \sum_{pq} g_{pq} \{\hat{p}^\dagger \hat{q}\}, \quad (8.88)$$

where

$$g_{pq} = \langle p | \hat{g} | q \rangle = f_{pq}^o + v'_{pq} - u_{pq}. \quad (8.89)$$

More generally, if we do not require $\varepsilon_p = f_{pp}$, we use $f'_{pq} = f_{pq} - \varepsilon_p \delta_{pq} = h_{pq} + u_{pq} - \varepsilon_p \delta_{pq}$ and define

$$\begin{aligned} g_{pq} &= f'_{pq} + v'_{pq} - u_{pq} \\ &= h_{pq} - \varepsilon_p \delta_{pq} + \sum_i \langle pi || qi \rangle. \end{aligned} \quad (8.90)$$

The last form in (8.90), in which the summation is over the hole states of the current Fermi vacuum (core plus valence holes), is the most general, being independent of the definition of the Fock operator and its relationship to the orbital energies. Obviously the operators \hat{v}' and \hat{g} are different for the different columns of the level-shift and wave-operator matrices.

If the core determinant is used for the definition of the Fock operator, the difference between v'_{pq} and u_{pq} is given by

$$v'_{pq} - u_{pq} = \sum_u \langle pu || qu \rangle, \quad (8.91)$$

the sum over u running over the valence hole states for the current Fermi vacuum. In this case

$$g_{pq} = f_{pq}^o + \sum_u \langle pu || qu \rangle. \quad (8.92)$$

In the diagrams we shall designate the \hat{G} operator by the vertex $\bullet - - - \otimes$, it being understood that the definition of the corresponding interaction varies for the different columns of the level-shift and wave-operator matrices.

8.7.3 First-order diagrams

The zero-order energies for the various model states are given by the usual formula, $\sum_i \varepsilon_i$; the scope of the summation, however, depends upon the model state, reflecting the differences in the corresponding sets of hole states. Thus the zero-order energy values, which enter the diagonal elements of the effective Hamiltonian matrix \hat{H}^{eff} , usually differ between model states.

Since the initial (ket) state in each matrix element serves as its own Fermi vacuum in the HK formalism, the initial state in the generalized Bloch equations (8.39)–(8.44) is the current vacuum state, $|\alpha\rangle = |0\rangle$, and there are no lines below the lowest vertex in the diagrams of this formalism. The diagonal elements of the level-shift operator are vacuum expectation values and are represented by closed diagrams that are mostly similar to those of non-degenerate MBPT. However, there are open valence lines at the top of all diagrams for off-diagonal elements of the level-shift operator, reflecting the differences between the final and initial states. All wave-operator diagrams are open at the top, as in the nondegenerate theory. Summations over the final states in wave-operator diagrams must exclude model states.

In nondegenerate MBPT the first-order energy was given by (5.6) or (5.7), which benefited from the cancellation of half the sum $-\sum_i u_{ii}$ with $\frac{1}{2} \sum_{ij} \langle ij || ij \rangle = \frac{1}{2} \sum_i v'_{ii}$ (see (3.152)). In the present case \hat{v}' is not equal to \hat{u} (and is different for different model states), and thus the cancellation is incomplete. Instead we find that the diagonal elements of the first-order

level shift operator are given by

$$\begin{aligned} \sum_i (f'_{ii} - u_{ii} + \frac{1}{2}v'_{ii}) &= \sum_i (-v'_{ii} + \frac{1}{2}v'_{ii}) + \sum_i (f'_{ii} + v'_{ii} - u_{ii}) \\ &= -\frac{1}{2} \sum_{ij} \langle ij || ij \rangle + \sum_i g_{ii}, \end{aligned} \quad (8.93)$$

using (8.90). Diagrammatically this result is represented by (compare (5.7))

$$- \text{diagram 1} - \text{diagram 2} + \text{diagram 3} = -\frac{1}{2} \sum_{ij} \langle ij || ij \rangle + \sum_i \langle i | \hat{g} | i \rangle \quad (8.94)$$

and represents the vacuum expectation value $\langle 0 | \hat{V} | 0 \rangle$ of the unmodified perturbation (which is different for each model state). The remaining part of the first-order level-shift operator is the modified operator $\hat{W}'^{(1)}$ of Section 8.3; it has no diagonal contribution here because $\langle 0 | \hat{W}'^{(1)} | 0 \rangle = 0$.

The off-diagonal part of the first-order level-shift operator is represented by the two diagrams

$$\text{diagram 1} = \langle x | \hat{g} | u \rangle \{ \hat{x}^\dagger \hat{u} \}, \quad (8.95)$$

$$\text{diagram 2} = \langle xy || uv \rangle \{ \hat{x}^\dagger \hat{y}^\dagger \hat{v} \hat{u} \}. \quad (8.96)$$

with the creation or annihilation operators acting on the respective initial state. The first diagram represents a single replacement for the final (bra) state relative to the initial (ket) state, with matrix element

$$\langle \Phi_u^x | \hat{W}^{(1)} | 0 \rangle = \langle x | \hat{g} | u \rangle. \quad (8.97)$$

The second diagram represents a double replacement, with matrix element

$$\langle \Phi_{uv}^{xy} | \hat{W}^{(1)} | 0 \rangle = \langle xy || uv \rangle. \quad (8.98)$$

In both these equations $|0\rangle$ represents the ket state for the respective matrix element, and $|\Phi_u^x\rangle$ and $|\Phi_{uv}^{xy}\rangle$ are defined relative to this particular ket state. There are no first-order contributions for more than two replacements. When an incomplete model space is used, the label values for the open lines are restricted to exclude states that are not part of the model space.

The first-order wave operator is represented by the same diagrams as the first-order wave function in the nondegenerate case, (5.15), (5.16), but with

a modified one-electron interaction:

$$(a) \begin{array}{c} \diagup \quad \diagdown \\ \text{---} \otimes \end{array} (i) = \sum_{ai} \frac{\langle a | \hat{g} | i \rangle}{\varepsilon_i^a} \{ \hat{a}^\dagger \hat{i} \}, \quad (8.99)$$

$$(a) \begin{array}{c} \diagup \quad \diagdown \\ \text{---} \end{array} (i) \text{---} \text{---} \begin{array}{c} \diagup \quad \diagdown \\ \text{---} \end{array} (j) \begin{array}{c} \diagup \quad \diagdown \\ \text{---} \otimes \end{array} (b) = \frac{1}{4} \sum_{abij} \frac{\langle ab || ij \rangle}{\varepsilon_{ij}^{ab}} \{ \hat{a}^\dagger \hat{b}^\dagger \hat{j} \hat{i} \}. \quad (8.100)$$

These diagrams are similar to those for the off-diagonal elements of the first-order level-shift operator, (8.95), (8.96), but with single arrows instead of double arrows and with an implied resolvent line above the vertex. Again, it should be remembered that the particle or hole classification and the modified one-electron interaction are specific to each column of the wave operator matrix, being determined by the corresponding ket state as the Fermi vacuum, and that model states must be excluded from the sum over final states in wave-operator diagrams. In the case of a complete model space this last restriction means that at least one open-line label in each term in these sums must not take on a valence state value.

8.7.4 Second-order diagrams

Skeletons for the second-order level-shift operator are shown in Fig. 8.9. Skeletons 1, 2 are for diagonal elements, 3–6 represent single replacements, 7–10 represent double replacements, 11–13 represent triple replacements and 14 represents quadruple replacements. (However, the number of replacements cannot exceed the number of valence hole states or the number of valence particle states.) Skeletons 1, 2, 4, 5, 10, 12–14 generate one diagram each, skeletons 3, 6, 8, 9, 11 generate two diagrams each and skeleton 7 generates three diagrams, giving a total of 21 diagrams. The summations over intermediate states must exclude model states. Note that no resolvent line is present above the top vertex for any level-shift operator diagram.

The definition of linked and unlinked diagrams is the same in the HK formalism as in the QDPT formalism for the complete model spaces described in Sections 8.2–8.6, i.e. diagrams are considered unlinked if they have at least one disconnected part in which all open lines are valence lines. All the disconnected skeletons in Fig. 8.9 (skeletons 10 and 12–14) are unlinked, and they are excluded when a complete model space is used because they involve intermediate model states. However, for an incomplete model space it is necessary to retain those contributions to the corresponding unlinked

diagrams in which the intermediate state is not in the model space but the final state *is* in the model space.

As an example for the interpretation of the second-order level-shift diagrams, we take one of the diagrams generated from skeleton 8 of Fig. 8.9:

$$\begin{array}{c} \text{Diagram 1} \end{array} \quad \begin{array}{c} \text{Diagram 2} \end{array} \quad \begin{array}{c} \text{Diagram 3} \end{array} \quad \begin{array}{c} \text{Diagram 4} \end{array} = \sum_a \frac{\langle y|\hat{g}|a\rangle\langle xa||uv\rangle}{\varepsilon_{uv}^{xa}} \{\hat{x}^\dagger \hat{u} \hat{y}^\dagger \hat{v}\}. \quad (8.101)$$

The final state $|\Phi_{uv}^{xy}\rangle$, represented by the action of $\{\hat{x}^\dagger \hat{u} \hat{y}^\dagger \hat{v}\}$ on the initial state, must be a model state, while the summation over a is restricted to exclude intermediate model states. In a complete model space this exclusion implies that a is restricted to virtual states, but in an incomplete model space a may take on a valence index value provided that the resultant intermediate state $|\Phi_{uv}^{xa}\rangle$ is not part of the model space.

The second-order wave operator is given by (8.42), in which \hat{V} represents the modified (normal-ordered) operator \hat{V}_N of (8.49). The diagrams representing the principal term of this operator are the same in the HK formalism as in nondegenerate MBPT, Figs. 5.3 and 5.4, and are shown in skeleton form in Fig. 8.10. They are seen to be similar to the skeletons for the off-diagonal part of the second-order level-shift operator, Fig. 8.9, except that no bars are present on any of the lines and a resolvent line is implied above the top vertex. In this case the final states, as well as all intermediate states, must exclude model states. The disconnected diagrams are not unlinked and are included even in the complete model space case. However, we shall find that

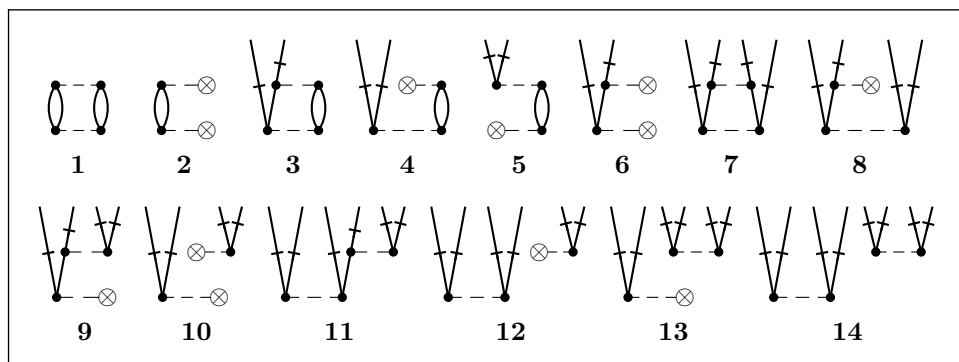


Fig. 8.9. Skeletons for the second-order level-shift operator in the Hose-Kaldor formalism. (A short bar across a line indicates limitation to active orbitals.)

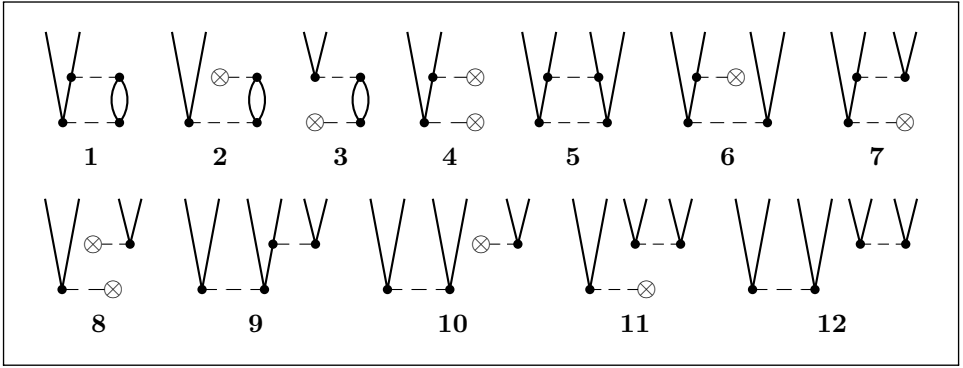


Fig. 8.10. Skeletons for the principal term of the second-order wave operator in the Hose–Kaldor formalism.

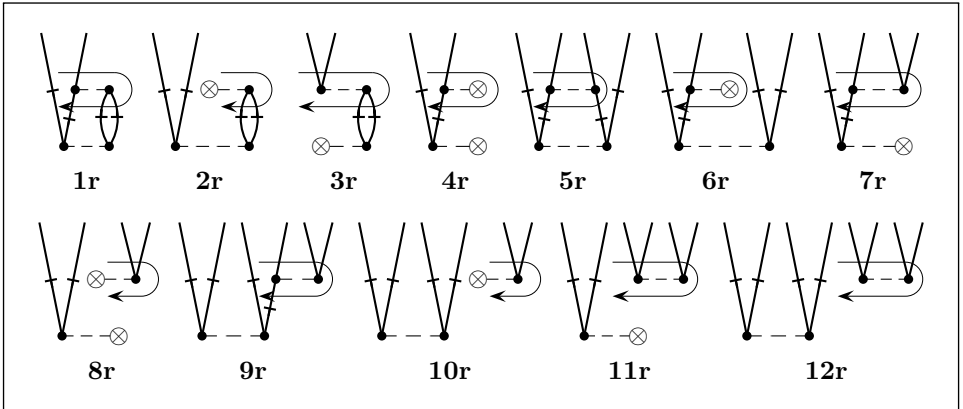
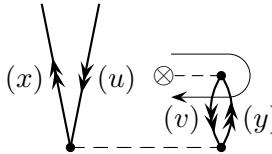


Fig. 8.11. Skeletons for the renormalization term of the second-order wave operator in the Hose–Kaldor formalism. An additional unfolded resolvent line at the top of each diagram is implied.

certain contributions to the disconnected diagrams are canceled by unlinked renormalization diagrams.

In the renormalization term those contributions in which the intermediate state is the same as the initial state ($|\beta\rangle = |\alpha\rangle = |0\rangle$ in (8.42)) vanish because for the normal-ordered perturbation operator we have $V_{00} = 0$. The other contributions remain and are described by folded diagrams. The skeletons for these folded diagrams are shown in the folded-resolvent-line notation in Fig. 8.11. An additional (unfolded) resolvent line at the top of each of these diagrams is implied but not shown; this line can also be drawn in folded form, with the lower branch below the lowest vertex.

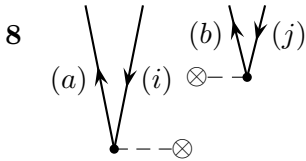
The intermediate state in these renormalization diagrams must be a model state, while the final state cannot be a model state. Therefore the diagram represented by skeleton 2r,



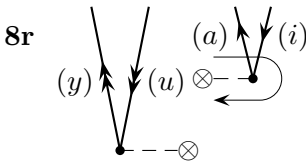
$$= \sum_{xyuv} \frac{\langle v|\hat{g}|y\rangle\langle xy||uv\rangle}{\varepsilon_u^x \varepsilon_{uv}^{xy}} \{\hat{x}^\dagger \hat{u}\}, \quad (8.102)$$

cannot contribute when the model space is complete, but with an incomplete model space those terms of this diagram in which the intermediate state $|\Phi_{uv}^{xy}\rangle$ is in the model space, while the final state $|\Phi_u^x\rangle$ is not, contribute to the second-order wave operator.

Unlike the disconnected diagrams among the principal term skeletons seen in Fig. 8.10, the disconnected folded diagrams in Fig. 8.11 are unlinked and cancel with certain contributions to the disconnected principal-term diagrams. We can illustrate this cancellation by considering diagrams 8 of Fig. 8.10 and 8r of Fig. 8.11:



$$= \sum_{abij} \frac{\langle b|\hat{g}|j\rangle\langle a|\hat{g}|i\rangle}{\varepsilon_{ij}^{ab} \varepsilon_i^a} \{\hat{a}^\dagger \hat{i} \hat{b}^\dagger \hat{j}\}, \quad (8.103)$$



$$= - \sum_{ayiu} \frac{\langle a|\hat{g}|i\rangle\langle y|\hat{g}|u\rangle}{\varepsilon_{iu}^{ay} \varepsilon_i^a} \{\hat{a}^\dagger \hat{i} \hat{y}^\dagger \hat{u}\} \quad (8.104)$$

(the minus sign for diagram 8r is due to the fold.) It is seen that the whole of diagram 8r cancels with those terms of diagram 8 in which b and j take on valence values (i.e. $b = y$ and $j = u$). The canceled terms are just those that cause diagram 8 to become unlinked.

In the case of an incomplete model space there are two complications. First, because Φ_u^y in diagram 8r must be in the model space, the cancellation includes only those terms of diagram 8 for which Φ_j^b is in the model space, leaving behind terms for which j and b take on valence label values but Φ_j^b is not in the model space. Second, those terms of diagram 8r for which Φ_i^a is in the model space, but Φ_{iu}^{ay} is not, are not canceled because they do not have corresponding contributions in diagram 8.

In a similar way, diagrams 10r, 11r and 12r cancel those terms of diagrams 11, 10 and 12, respectively, in which the upper disconnected part, taken separately, represents a model state. Since the lower disconnected part of the disconnected principal-term diagrams must not be a model state (because it determines the intermediate state), the only surviving terms are those in which neither disconnected part of a disconnected principal-term diagram, taken separately, represents a final model state. For the folded diagrams, no such unlinked diagrams remain for a complete model space but for an incomplete model space the only contributions of unlinked folded diagrams that remain are those for which both disconnected parts, taken separately, represent model states, while the entire final state is not in the model space.

8.7.5 Third-order level-shift diagrams

In order to identify all the distinct skeletons for the principal term of the third-order level-shift operator, we use a scheme similar to that used in subsection 8.6.6 and divide the skeletons into classes and sets. The notation (klm) will be used to describe a class of skeletons with k, l and m open lines connected to the first, second and third vertex, respectively (counting downwards from the top vertex). The various classes of linked skeletons are organized in sets. The different classes in a set all have the same number of skeletons and diagrams and can be obtained from each other by permutation of the three vertices. The numbers of ASG skeletons and diagrams in one representative class in each set and the total number of skeletons and diagrams are listed in Table 8.2, separately for linked and unlinked skeletons. The linked and unlinked Hugenholtz skeletons for the representative classes are shown in Figs. 8.12 and 8.13, respectively. For the unlinked skeletons, classes (200) and (400) are omitted because they involve vacuum gaps and classes (020) and (040) are used instead as representative classes.

The ASG diagrams for the principal term of the diagonal elements belong to class (000) and are the same as those for nondegenerate MBPT, Figs. 5.1 and 5.2. They are repeated in skeleton form in Fig. 8.14, in order to facilitate later discussion of the renormalization terms that can be derived from them. Again, a characteristic of the QDPT case is that intermediate model states are excluded from the summations for these diagrams. There are no unlinked diagonal-element diagrams but, unlike nondegenerate MBPT, there are diagonal renormalization contributions (as there are in the complete-model-space formalism described in Section 8.6).

The linked principal-term ASG skeletons for the off-diagonal elements of the third-order level-shift operator are shown in Figs. 8.15–8.17, organized by

Table 8.2. *Representative classes, numbers of distinct ASG skeletons and diagrams in each class and set and total number of principal-term skeletons and diagrams for the third-order level-shift operator (vacuum-gap skeletons are omitted)*

Number of replace- ments	Representative class	No. of classes in set	Number in class		Number in set	
			Skelets.	Diagrams	Skelets.	Diagrams
Linked						
0	(000)	1	8	14	8	14
1	(200)	3	4	6	12	18
	(110)	3	7	18	21	54
2	(310)	6	3	6	18	36
	(220)	3	2	7	6	21
	(211)	3	4	18	12	54
3	(330)	3	1	2	3	6
	(321)	6	2	8	12	48
	(222)	1	1	8	1	8
4	(332)	3	1	4	3	12
Total linked			34	91	96	271
Unlinked						
1	(020)	2	2	2	4	4
2	(040)	2	2	2	4	4
	(220)	3	2	2	6	6
	(211)	3	2	4	6	12
3	(420)	6	1	1	6	6
	(411)	3	2	4	6	12
	(321)	6	1	2	6	12
	(222)	1	4	10	4	10
4	(422)	3	2	4	6	12
	(431)	6	1	2	6	12
	(332)	3	1	2	3	6
5	(442)	3	1	1	3	3
	(433)	3	1	2	3	6
6	(444)	1	1	1	1	1
Total unlinked			23	39	64	106

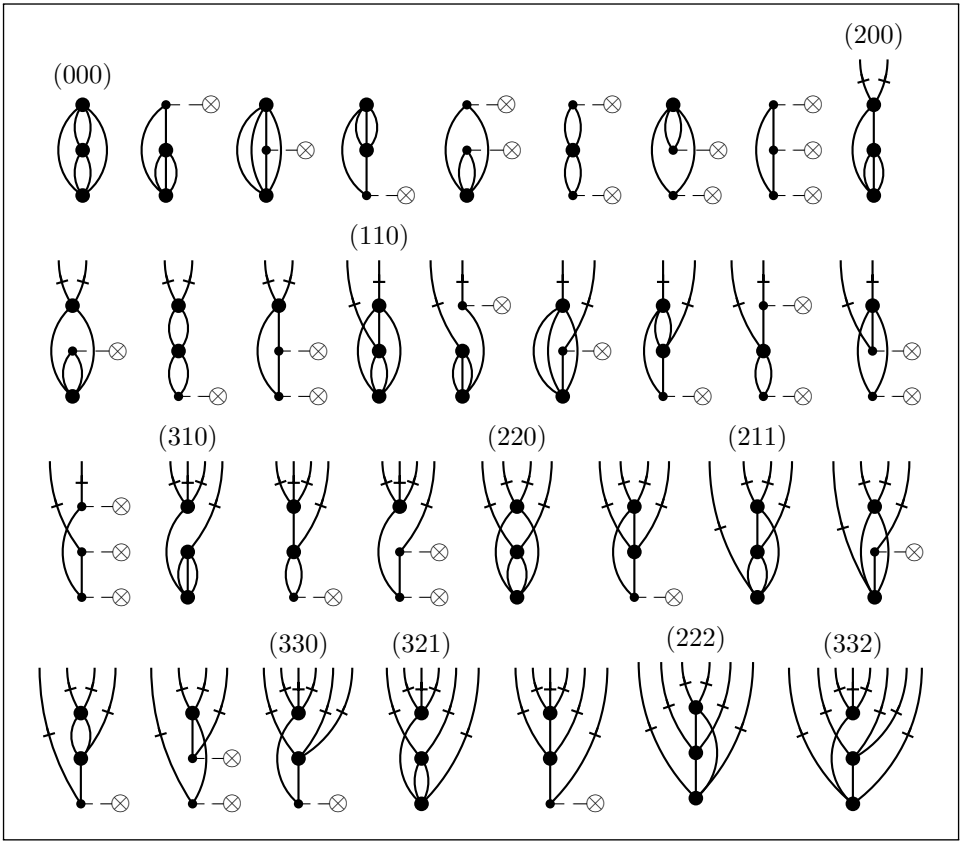


Fig. 8.12. Linked Hugenholtz skeletons for representative classes of the principal term of the third-order level-shift operator in the HK formalism.

the number of replacements for the final state relative to the initial (vacuum) state. The unlinked principal-term skeletons are shown, similarly organized, in Figs. 8.18–8.20. In order to be able to identify all non-contributing diagrams, and for convenience in our later consideration of renormalization skeletons, the principal-term ASG skeletons are shown for all classes, not just the representative classes.

In the conversion of Hugenholtz skeletons to ASG skeletons it is important to realize that some Hugenholtz skeletons may require more than one ASG skeleton to describe the full set of diagrams that can be generated from those skeletons. In the present case this situation occurs for the first skeleton of the (211) class in Fig. 8.12 as well as for the corresponding skeletons of the other two classes in that set, (121) and (112). This (211) Hugenholtz

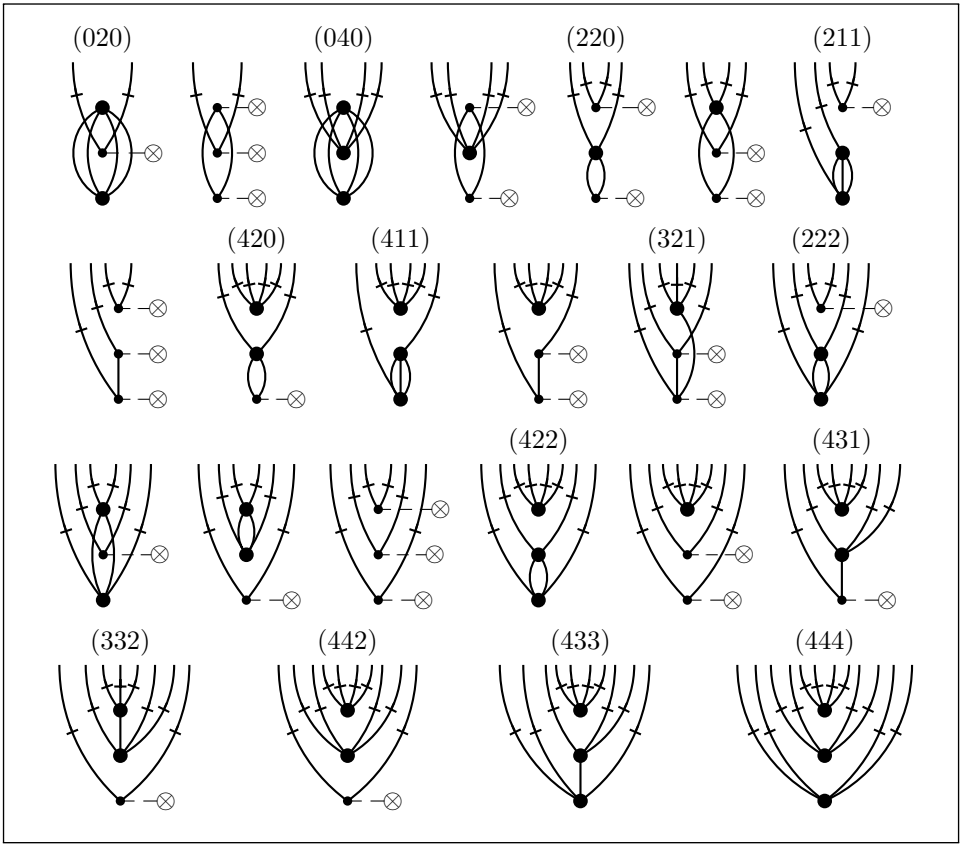


Fig. 8.13. Unlinked Hugenholtz skeletons for representative classes of the principal term of the third-order level-shift operator in the HK formalism.

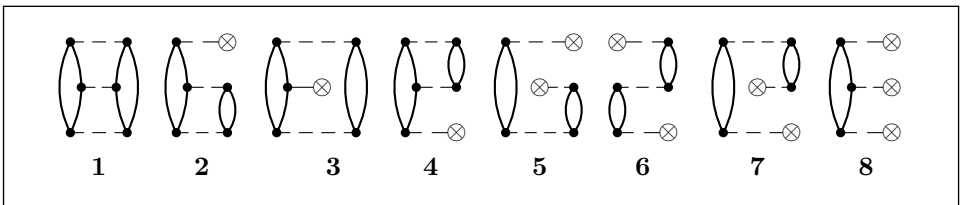
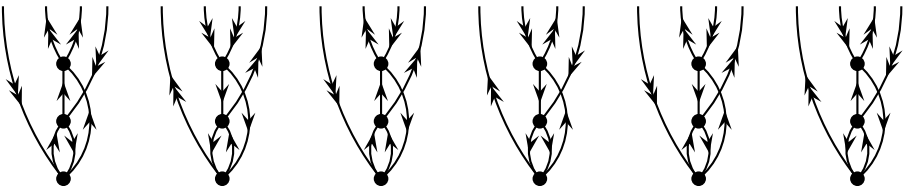


Fig. 8.14. Diagonal linked ASG skeletons for the principal term of the third-order level-shift operator in the Hose-Kaldor formalism.

skeleton generates six diagrams:



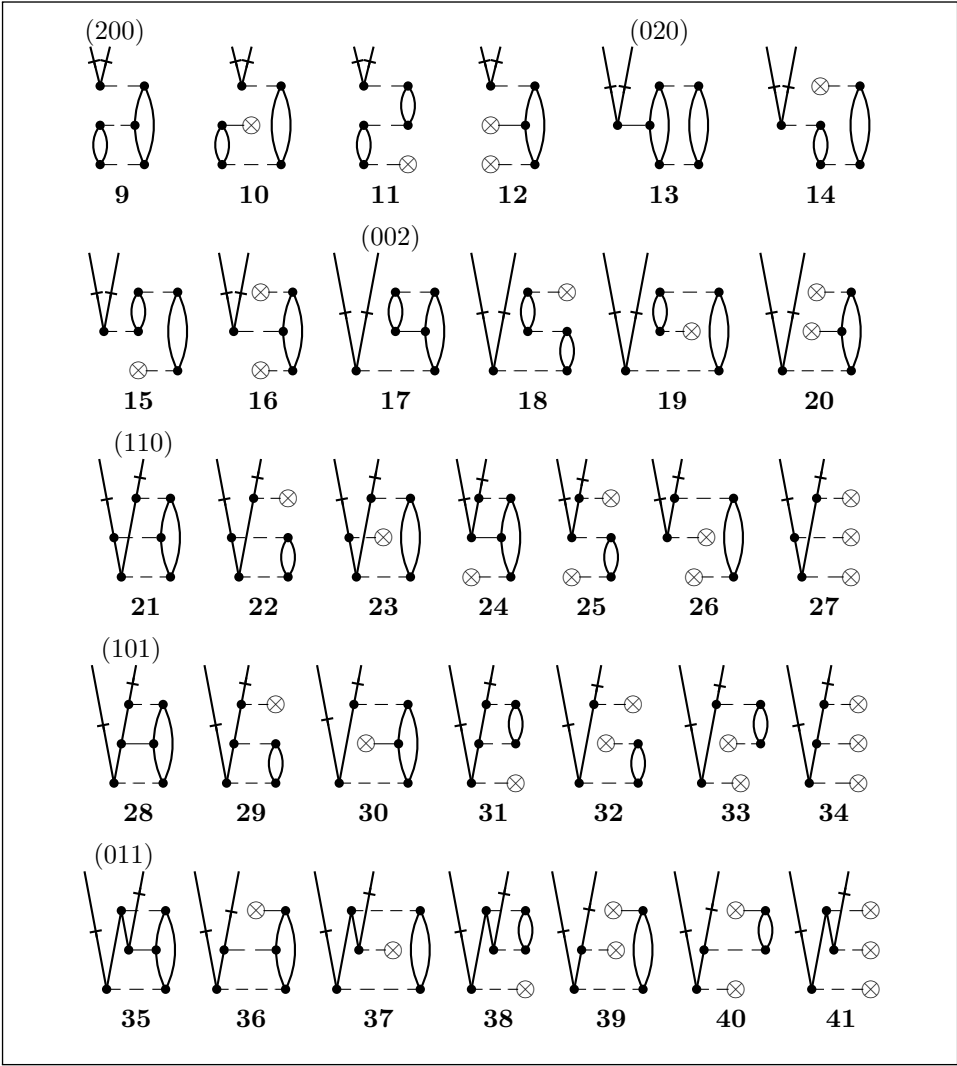
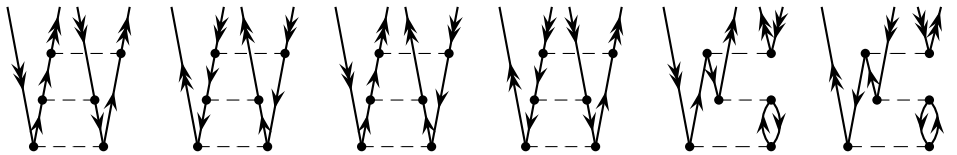


Fig. 8.15. Single-replacement linked ASG skeletons for the principal term of the third-order level-shift operator in the Hose-Kaldor formalism.

Two inequivalent ASG skeletons are needed to represent the same six diagrams:



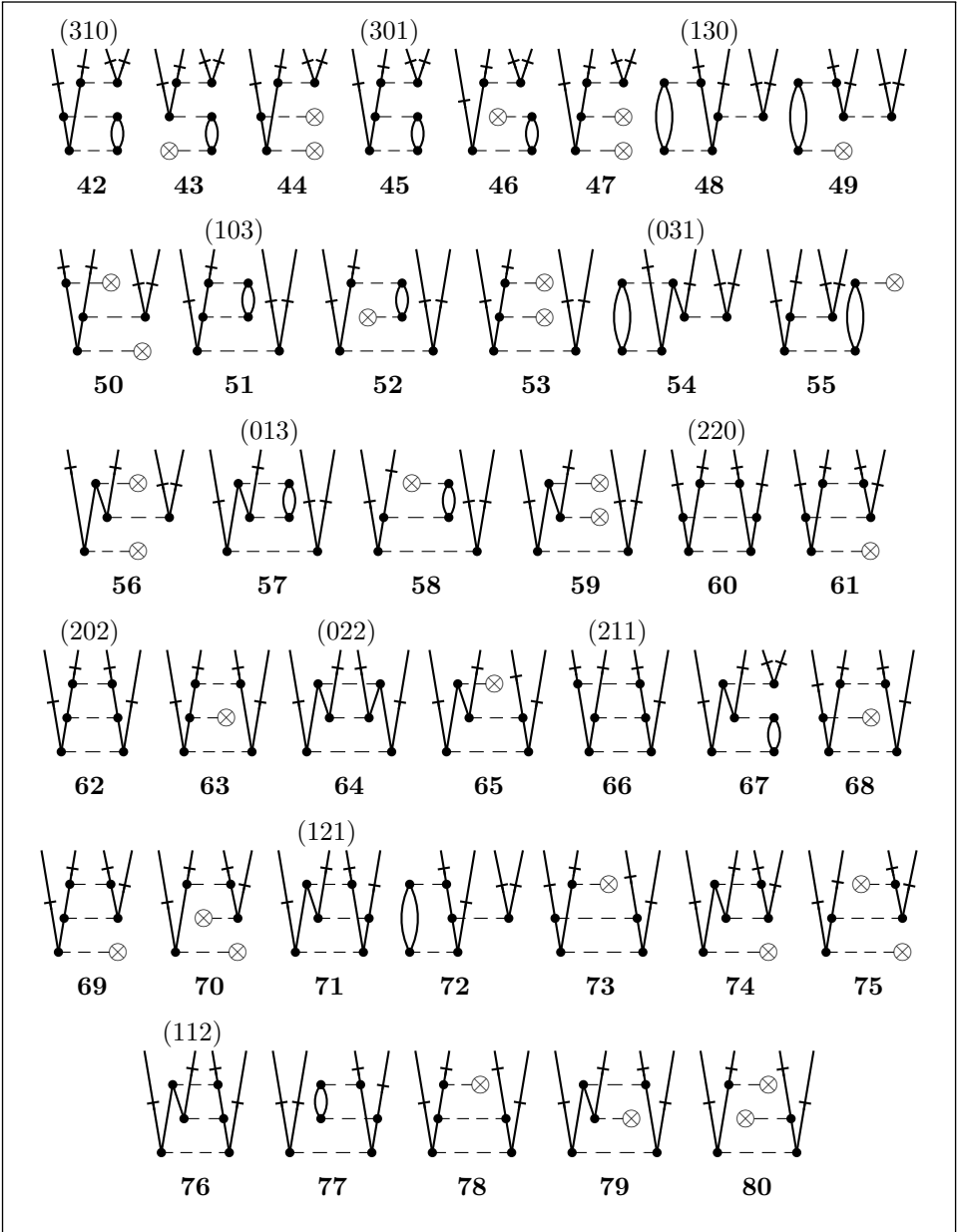


Fig. 8.16. Double-replacement linked ASG skeletons for the principal term of the third-order level-shift operator in the Hose-Kaldor formalism.

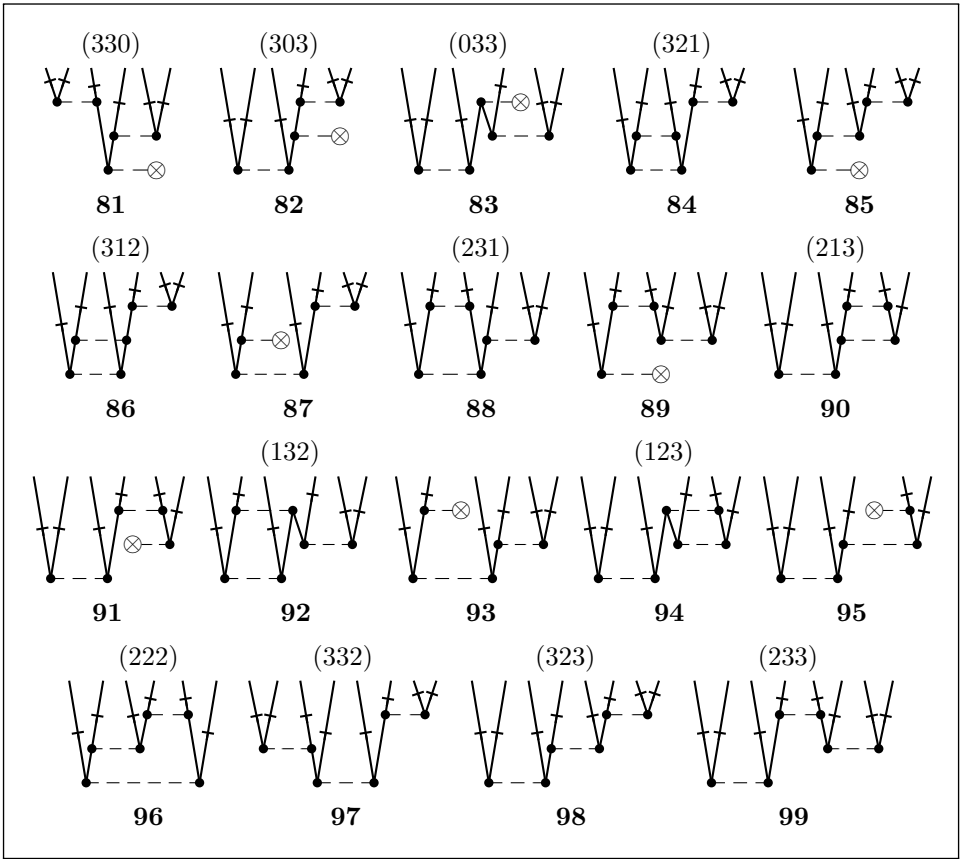


Fig. 8.17. Triple- and quadruple-replacement linked ASG skeletons for the principal term of the third-order level-shift operator in the Hose–Kaldor formalism.

Thus there are only four Hugenholtz (211) skeletons in Fig. 8.12, while five ASG skeletons are shown for each class in this set in Fig. 8.16; see Table 8.2.

Most skeletons in Figs. 8.14–8.20 generate one, two or four diagrams each. The exceptions are skeletons 1, 60, 62, 138–140, 142, 144, 146, which generate three diagrams each, and skeleton 96, which generates eight diagrams.

The unlinked diagrams represented by skeletons 102, 103, 106 and 107 of Fig. 8.18 can never contribute to the principal term of the third-order level-shift operator, because their lower intermediate state is the same as their final state and is thus a model state. These skeletons are included in the figure in order to facilitate the consideration of renormalization skeletons that can be derived from them. It will be shown later that skeletons 100, 102, 104, 105 always cancel fully with renormalization skeletons, so that none of the unlinked principal-term skeletons 100–107 remains, even when the model space is incomplete.

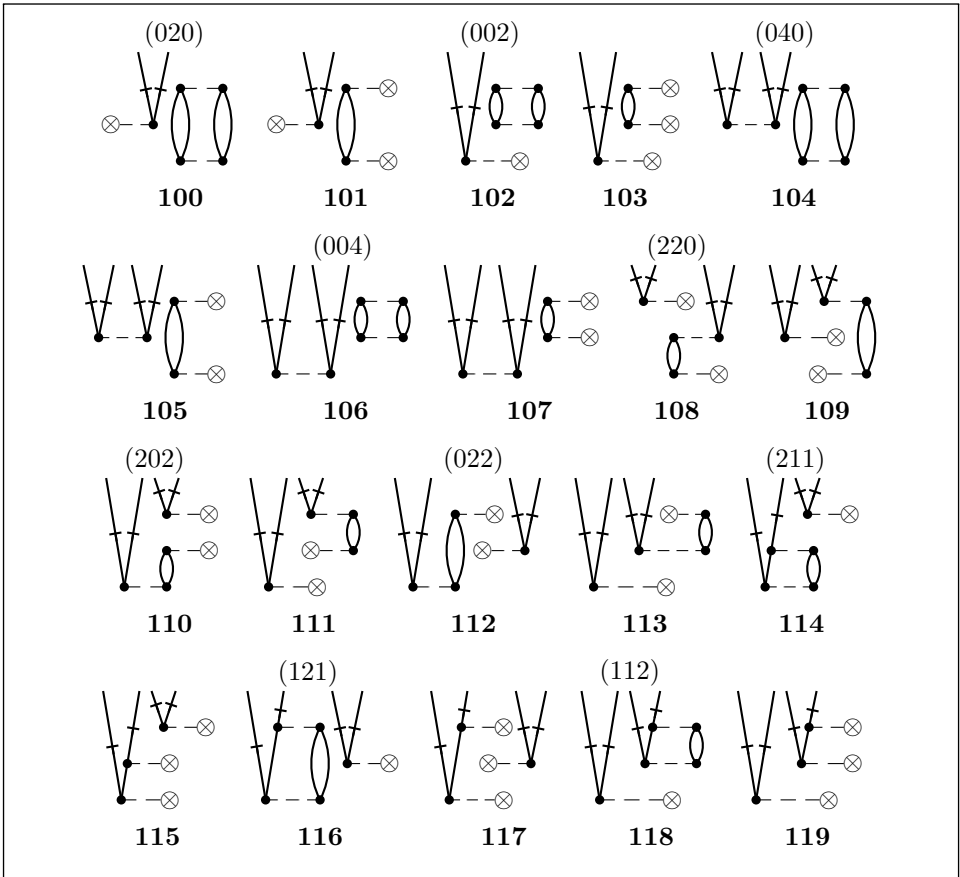


Fig. 8.18. Single- and double-replacement unlinked ASG skeletons for the principal term of the third-order level-shift operator in the Hose-Kaldor formalism.

When the model space is complete, any unlinked third-order skeleton that has no line directly connecting the top and bottom vertices to each other necessarily involves a model state either as the upper or lower intermediate state and cannot contribute to the principal term. (A classification of skeletons according to their contribution status is given in Table 8.3.) As examples we consider the diagrams derived from skeletons 108 and 111:

$$\begin{array}{c}
 \begin{array}{c}
 \text{Diagram 108: Top vertex connected to two intermediate vertices (dots) by solid lines labeled } x \text{ and } u. \text{ The first intermediate vertex is connected to a bottom vertex by a dashed line labeled } y. \text{ The second intermediate vertex is connected to the bottom vertex by a solid line labeled } v. \text{ The bottom vertex is connected to a final vertex (crossed circle) by a dashed line.} \\
 \text{Diagram 111: Top vertex connected to two intermediate vertices (dots) by solid lines labeled } x \text{ and } u. \text{ The first intermediate vertex is connected to a bottom vertex by a dashed line labeled } y. \text{ The second intermediate vertex is connected to the bottom vertex by a solid line labeled } v. \text{ The bottom vertex is connected to a final vertex (crossed circle) by a dashed line.}
 \end{array}
 \\
 = \sum_{ai} \frac{\langle x|\hat{g}|u\rangle\langle iy||av\rangle\langle a|\hat{g}|i\rangle}{\varepsilon_v^y \varepsilon_i^a} \{\hat{x}^\dagger \hat{y}^\dagger \hat{v} \hat{u}\}
 \end{array} \quad (8.105)$$

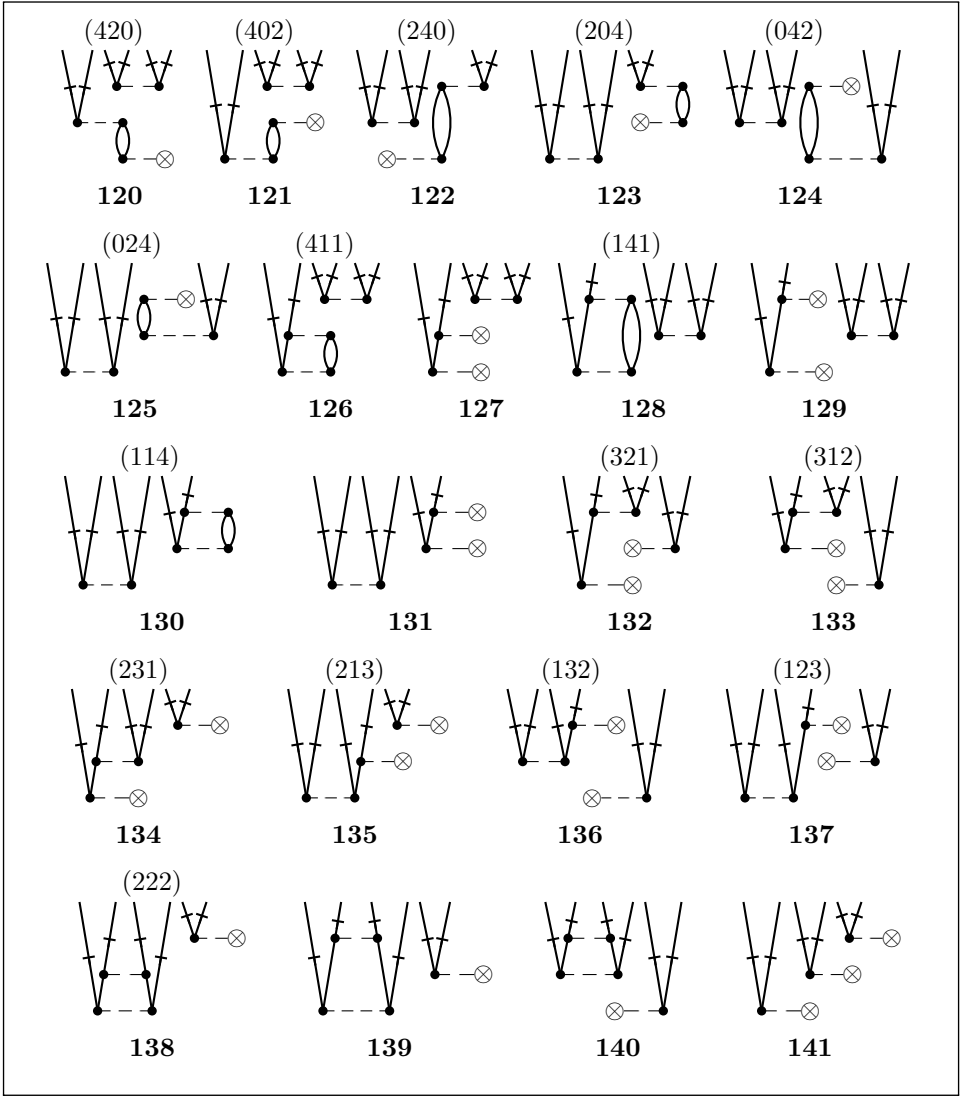


Fig. 8.19. Triple-replacement unlinked ASG skeletons for the principal term of the third-order level-shift operator in the Hose-Kaldor formalism.

and

$$(a) \begin{array}{c} \text{Diagram: A vertex } i \text{ with two incoming lines } x \text{ and } u, \text{ and one outgoing line } v. \text{ A dashed line connects } i \text{ to a cross-in-circle symbol.} \end{array} = \sum_{ai} \frac{\langle ix || au \rangle \langle a | \hat{g} | i \rangle \langle y | \hat{g} | v \rangle}{\varepsilon_{iv}^{ay} \varepsilon_v^y} \{ \hat{x}^\dagger \hat{y}^\dagger \hat{v} \hat{u} \}. \quad (8.106)$$

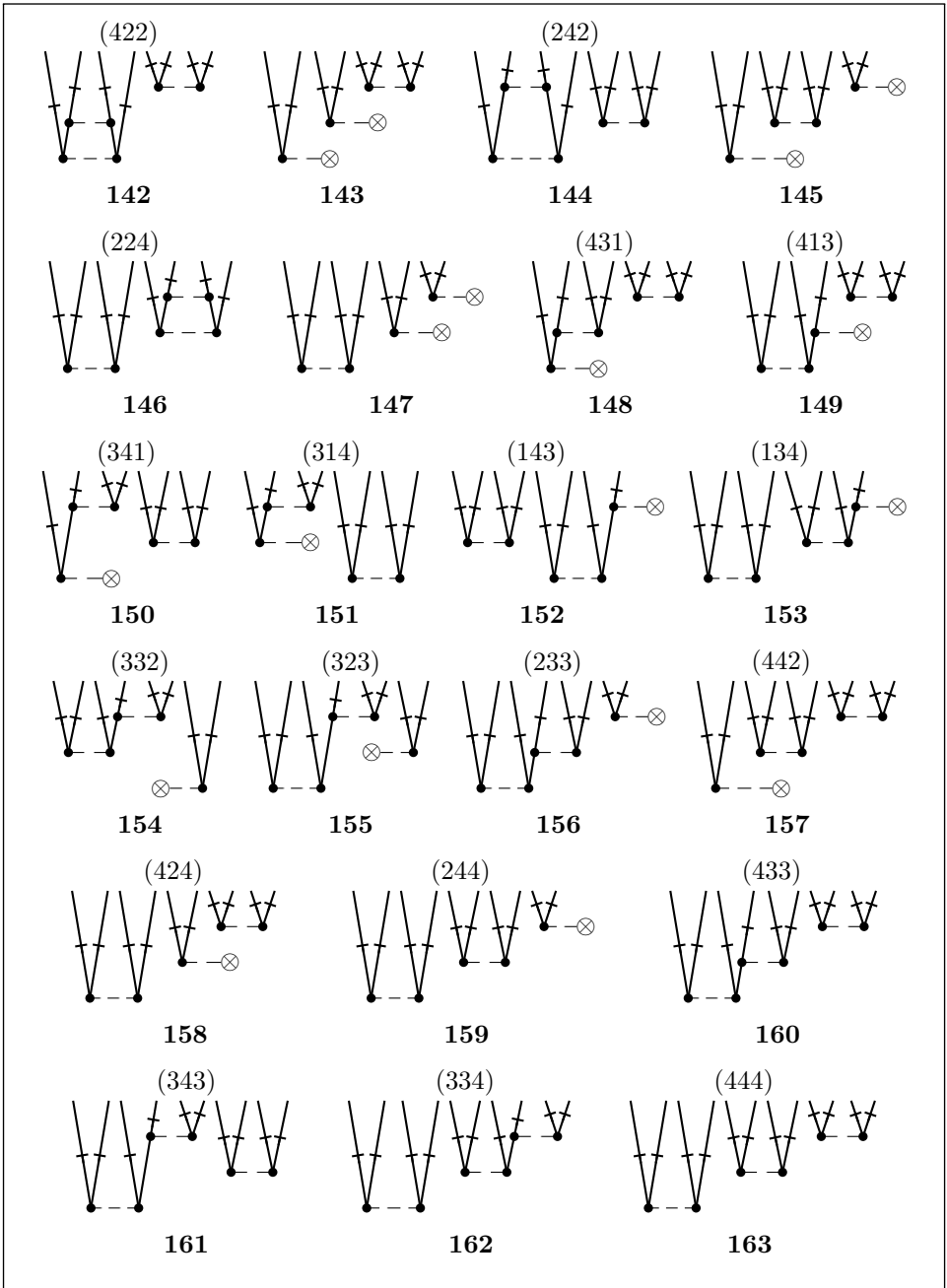


Fig. 8.20. Quadruple-, quintuple- and sextuple-replacement unlinked ASG skeletons for the principal term of the third-order level-shift operator in the Hose-Kaldor formalism.

Table 8.3. *Contribution status of third-order level-shift skeletons*

Unlinked principal-term skeletons that never contribute because their lower intermediate state is always a model state:

102, 103, 106, 107.

Unlinked principal-term skeletons that may have residual contributions when the model space is incomplete (skeletons that have no line connecting the top and bottom vertices to each other):

108, 110, 111, 113–115, 118–121, 123, 125–127, 130, 131, 133–136, 138, 140–143, 145–149, 151, 153, 154, 156–160, 162, 163.

Unlinked principal-term skeletons that cancel with renormalization skeletons but may have residual contributions when the model space is incomplete:

109, 112, 116, 117, 122, 124, 128, 129, 132, 137, 139, 144, 150, 152, 155, 161.

Renormalization skeletons (both linked and unlinked) that do not contribute when the model space is complete but may have residual contributions when the model space is incomplete (skeletons that have no line connecting the top two vertices to each other):

5r, 10r, 14r, 22r, 23r, 27r, 32r, 39r, 42r, 44r, 46r, 48r, 50r, 55r, 60r, 68r, 73r, 80r, 81r, 84r, 87r, 88r, 93r, 97r, 100r, 101r, 104r, 105r, 108r–110r, 112r, 114r–117r, 120r–122r, 124r, 126r–129r, 132r, 134r, 135r, 137r–139r, 141r–145r, 147r–150r, 152r, 155r–161r, 163r.

Skeletons pairs that cancel with each other but may have residual contributions when the model space is incomplete (asterisks indicate skeletons that have no residual contributions even in an incomplete model space):

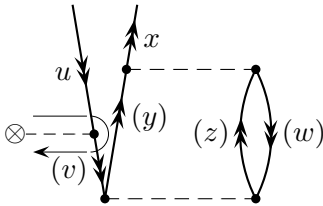
(100*, 102r), (101*, 103r), (104*, 106r), (105*, 107r), (109, 111r), (112, 113r), (116, 118r), (117, 119r), (122, 123r), (124, 125r), (128, 130r), (129, 131r), (132, 133r), (137, 136r), (139, 140r), (144, 146r), (150, 151r), (152, 153r), (155, 154r), (161, 162r).

These two diagrams can contribute only when the model space is incomplete and then only if the intermediate state Φ_v^y is not in the model space. In both cases the final state Φ_{uv}^{xy} must be in the model space, and terms in which the intermediate state Φ_i^a (in the first diagram) or Φ_{vi}^{ya} (in the second) is a model state are excluded from the sum.

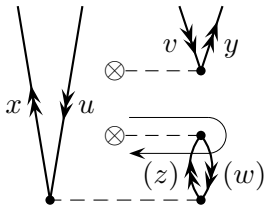
All the other unlinked skeletons cancel with unlinked renormalization skeletons, and no unlinked contributions of any kind remain when the model space is complete (see Table 8.3). With an incomplete model space the cancellations are incomplete, as will be shown in the following discussion of the renormalization terms.

Each principal-term third-order skeleton, whether linked or unlinked, has a corresponding renormalization skeleton, which is easily obtained from it by restricting the lower intermediate state to be a model state and replacing the lower resolvent line by a folded resolvent line surrounding the middle vertex. It is therefore unnecessary to show all the renormalization skeletons; these will be referred to using the numerical labels of the corresponding principal-term skeletons with an added 'r'.

Those renormalization skeletons, both linked and unlinked, that have no line directly connecting the top two vertices to each other cannot contribute when the model space is complete (Table 8.3). In these cases all lines are valence lines, some because they connect to the bottom vertex and the others because they are part of the final-state designation, making the upper intermediate state a model state. There are 24 linked and 44 unlinked renormalization skeletons of this type, including the diagonal skeleton 5r (see Fig. 8.14). As examples we shall consider one of the two diagrams generated by skeleton 23r and the diagram generated by skeleton 110r:



$$= \frac{1}{2} \sum_{yzvw} \frac{\langle xw \| yz \rangle \langle v | \hat{g} | u \rangle \langle yz \| vw \rangle}{\varepsilon_{uw}^{yz} \varepsilon_u^v} \{ \hat{x}^\dagger \hat{u} \}, \quad (8.107)$$



$$= -\langle y | \hat{g} | v \rangle \sum_{zw} \frac{\langle w | \hat{g} | z \rangle \langle xz \| uw \rangle}{\varepsilon_u^x \varepsilon_z^w} \{ \hat{x}^\dagger \hat{u} \hat{y}^\dagger \hat{v} \}. \quad (8.108)$$

The first diagram has one pair of equivalent lines, three hole lines and two loops (one of them a quasiloop). The resulting negative sign is canceled by the negative sign due to the fold. This diagram can only contribute in an incomplete model space, and then only from those terms in the sum for which Φ_{vw}^{yz} is in the model space while Φ_{uw}^{yz} is not. (In all cases, the final state Φ_u^x must be in the model space.) The second diagram has three hole lines, three loops and no equivalent lines. Again, the final state Φ_{uv}^{xy} must be in the model space, and the diagram can only contribute when Φ_u^x is not in the model space, and then only for those terms in the sum for which Φ_{uw}^{xz} is in the model space. Similar considerations apply to the other skeletons of this type.

As noted earlier, skeletons 100, 101, 104, 105 cancel completely with renormalization skeletons. This cancellation will be illustrated by skeletons 100 and 102r:

100

$$= \frac{1}{4} \sum_{abij} \frac{\langle ij || ab \rangle \langle y | \hat{g} | u \rangle \langle ab || ij \rangle}{\varepsilon_{iju}^{aby} \varepsilon_{ij}^{ab}} \{ \hat{y}^\dagger \hat{u} \}, \quad (8.109)$$

102r

$$= -\frac{1}{4} \sum_{abij} \frac{\langle ij || ab \rangle \langle ab || ij \rangle \langle y | \hat{g} | u \rangle}{\varepsilon_{iju}^{aby} \varepsilon_{ij}^{ab}} \{ \hat{y}^\dagger \hat{u} \}. \quad (8.110)$$

In both diagrams, Φ_u^y must be in the model space (since it is the final state), and terms in which Φ_{iju}^{aby} is in the model space are excluded. Thus the whole of diagram 100 is always canceled by corresponding terms in diagram 102r, but any terms in diagram 102r for which Φ_{ij}^{ab} is in the model space (while Φ_{iju}^{aby} is not) remain, because such terms are excluded from diagram 100. When the model space is complete, Φ_{ij}^{ab} cannot be in the model space when Φ_{iju}^{aby} is not; in this case the cancellation of the two diagrams is complete.

Similar behavior is obtained for the unlinked skeleton pairs 101 and 103r, 104 and 106r and 105 and 107r. Combined with the fact that principal-term skeletons 102, 103, 106 and 107 can never contribute, we find that none of the unlinked principal-term skeletons 100–107 survive for any model space.

All remaining unlinked principal-term and renormalization skeletons cancel in pairs, as listed in Table 8.3, but may have residual terms surviving the cancellation when the model space is incomplete. As examples we shall consider diagrams derived from the skeleton pairs (109, 111r) and (132, 133r):

109

$$= \sum_{ai} \frac{\langle yi || va \rangle \langle x | \hat{g} | u \rangle \langle a | \hat{g} | i \rangle}{\varepsilon_{ui}^{xa} \varepsilon_i^a} \{ \hat{x}^\dagger \hat{g}^\dagger \hat{v} \hat{u} \}, \quad (8.111)$$

111r

$$(i) \quad (a) = - \sum_{ai} \frac{\langle yi || va \rangle \langle a | \hat{g} | i \rangle \langle x | \hat{g} | u \rangle}{\varepsilon_{ui}^{xa} \varepsilon_i^a} \{ \hat{x}^\dagger \hat{y}^\dagger \hat{v} \hat{u} \} . \quad (8.112)$$

In both diagrams Φ_{uv}^{xy} must be in the model space, and the sums are restricted to terms in which Φ_{ui}^{xa} is not in the model space. However, cases in which Φ_u^x is not a model state are excluded from diagram 111r and thus remain uncanceled in diagram 109. Similarly, terms in the sum in which Φ_i^a is a model function (but Φ_{ui}^{xa} is not) are excluded from diagram 109 and thus remain uncanceled in diagram 111r. No uncanceled terms of these types remain when the model space is complete.

132

$$(i) \quad \otimes \quad \otimes = - \frac{1}{2} \sum_i \frac{\langle iy || uv \rangle \langle z | \hat{g} | w \rangle \langle x | \hat{g} | i \rangle}{\varepsilon_{iw}^{xz} \varepsilon_i^x} \{ \hat{x}^\dagger \hat{y}^\dagger \hat{z}^\dagger \hat{w} \hat{v} \hat{u} \} , \quad (8.113)$$

133r

$$(i) \quad \otimes \quad \otimes = \frac{1}{2} \sum_i \frac{\langle iy || uv \rangle \langle x | \hat{g} | i \rangle \langle z | \hat{g} | w \rangle}{\varepsilon_{iw}^{xz} \varepsilon_i^x} \{ \hat{x}^\dagger \hat{y}^\dagger \hat{z}^\dagger \hat{w} \hat{v} \hat{u} \} , \quad (8.114)$$

In both these diagrams Φ_{uvw}^{xyz} must be in the model space, and the sums are restricted to terms in which Φ_{iw}^{xz} is not in the model space. However, cases in which Φ_w^z is not a model state are excluded from diagram 133r and thus remain uncanceled in diagram 132. Similarly, terms in the sum in which Φ_i^x is a model function (but Φ_{iw}^{xz} is not) are excluded from diagram 132 and thus remain uncanceled in diagram 133r. No uncanceled terms of these types remain when the model space is complete.

The denominator factors in some residual terms for incomplete model spaces, as in (8.107), (8.108), involve differences in valence-orbital energies only and are thus likely to be relatively small. Nevertheless, in those terms that contribute to the sum, each factor represents a zero-order energy difference between a model state and an external state. As long as the choice

of model space maintains significant zero-order energy differences between all model states on the one hand and all external states on the other, convergence of the perturbation series need not be seriously impaired.

As in the case of the complete-model-space approach described in Sections 8.2–8.6, the number of diagrams generated in the HK approach is also quite large and increases very rapidly with the order of the calculation. Coupled with the summation restrictions, this situation makes QDPT calculations difficult, and they are rarely practicable beyond the third order of the energy.

9

Foundations of coupled-cluster theory

9.1 Coupled-cluster theory for noninteracting He atoms

Before beginning the formal development of coupled-cluster (CC) theory and its diagrammatic tools, we will introduce some essential elements of coupled-cluster theory in a conceptual form. For this purpose, we look again at the model problem of N noninteracting He atoms, which we examined in Section 1.7 in the context of CI and in Section 2.4 for BWPT and RSPT.

We shall use the notation and basis set of Section 1.7. In this basis we have two orthonormal two-electron functions for each atom, $\{\phi_0(i), \chi(i), i = 1, 2, \dots, N\}$, where $\phi_0(i)$ is the zero-order function for atom i and $\chi(i)$ represents a two-electron excitation from $\phi_0(i)$. Since the atoms are noninteracting, the functions on one atom are orthogonal to those on any other atom. We define a single-atom two-electron excitation operator \hat{t}_i for the i th atom in the space spanned by $\{\phi_0(i), \chi(i)\}$ by

$$\hat{t}_i \phi_0(i) = \tau \chi(i), \quad \hat{t}_i \chi(i) = 0, \quad (9.1)$$

where τ is a constant to be determined. The \hat{t}_i operator has no effect on the basis functions for the other atoms,

$$\hat{t}_i \phi_0(j) = \phi_0(j), \quad \hat{t}_i \chi(j) = \chi(j) \quad (i \neq j). \quad (9.2)$$

For the N -atom wave function we define the operator

$$\hat{T}_2 = \sum_i \hat{t}_i \quad (9.3)$$

(the subscript 2 on \hat{T}_2 indicates that it is a sum of operators that excite two electrons at a time). The effect of \hat{T}_2 on the N -atom functions Φ_0 , Φ_i , Φ_{ij} ,

etc. (Section 1.7) is easily found:

$$\begin{aligned}
 \hat{T}_2\Phi_0 &= \sum_i \hat{t}_i\Phi_0 = \tau \sum_i \Phi_i, \\
 \hat{T}_2\Phi_i &= \sum_j \hat{t}_j\Phi_i = \tau \sum_{j \ (j \neq i)} \Phi_{ij} = \tau \sum_j \Phi_{ij} \quad (\text{since } \Phi_{ii} = 0), \\
 \hat{T}_2^2\Phi_0 &= \tau \sum_i \hat{T}_2\Phi_i = \tau^2 \sum_{ij} \Phi_{ij}, \\
 \hat{T}_2^3\Phi_0 &= \tau^2 \sum_{ij} \hat{T}_2\Phi_{ij} = \tau^3 \sum_{ijk} \Phi_{ijk}, \quad \text{etc.}
 \end{aligned} \tag{9.4}$$

We know that the exact solution for N noninteracting He atoms can be written in the form

$$\Psi = \Phi_0 + \sum_i \tau \Phi_i + \frac{1}{2!} \sum_{ij} \tau^2 \Phi_{ij} + \frac{1}{3!} \sum_{ijk} \tau^3 \Phi_{ijk} + \dots \tag{9.5}$$

(compare (1.32)). Therefore (compare (1.34)),

$$\Psi = \Phi_0 + \hat{T}_2\Phi_0 + \frac{1}{2!}\hat{T}_2^2\Phi_0 + \frac{1}{3!}\hat{T}_2^3\Phi_0 + \dots = e^{\hat{T}_2}\Phi_0. \tag{9.6}$$

The exponential *Ansatz* $\Psi = e^{\hat{T}_2}\Phi_0$, which is a characteristic of the coupled-cluster approach, automatically accounts for the correct relationship between the coefficients τ, τ^2, \dots of the various excitation levels. In the CC approach we write the wave function in this exponential form and derive equations for the determination of the cluster operators (\hat{T}_2 in this case) and the corresponding energy.

The only unknown in \hat{T}_2 in this example is the coefficient τ , and to obtain equations for τ and the corresponding energy E we project the Schrödinger equation, in the form

$$(\hat{H} - E)e^{\hat{T}_2}\Phi_0 = 0, \tag{9.7}$$

onto $\langle \Phi_0 |$ and $\langle \Phi_i |$ (the different values of i all lead to the same final equation):

$$\begin{aligned}
 \langle \Phi_0 | (\hat{H} - E) e^{\hat{T}_2} | \Phi_0 \rangle &= 0, \\
 \langle \Phi_i | (\hat{H} - E) e^{\hat{T}_2} | \Phi_0 \rangle &= 0.
 \end{aligned} \tag{9.8}$$

Using (9.4) and (1.23) we obtain the following matrix elements:

$$\langle \Phi_0 | E e^{\hat{T}_2} | \Phi_0 \rangle = E \langle \Phi_0 | \Phi_0 \rangle + E \langle \Phi_0 | \hat{T}_2 | \Phi_0 \rangle + \cdots = E, \quad (9.9)$$

$$\begin{aligned} \langle \Phi_i | E e^{\hat{T}_2} | \Phi_0 \rangle &= E \langle \Phi_i | \Phi_0 \rangle + E \langle \Phi_i | \hat{T}_2 | \Phi_0 \rangle + \frac{1}{2} E \sum_{jk} \langle \Phi_i | \hat{T}_2^2 | \Phi_{jk} \rangle + \cdots \\ &= 0 + E \tau \sum_j \langle \Phi_i | \Phi_j \rangle + 0 + \cdots = E \tau, \end{aligned} \quad (9.10)$$

$$\begin{aligned} \langle \Phi_0 | \hat{H} e^{\hat{T}_2} | \Phi_0 \rangle &= \langle \Phi_0 | \hat{H} | \Phi_0 \rangle + \langle \Phi_0 | \hat{H} \hat{T}_2 | \Phi_0 \rangle + \frac{1}{2} \langle \Phi_0 | \hat{H} \hat{T}_2^2 | \Phi_0 \rangle + \cdots \\ &= E_0 + \tau \sum_i \langle \Phi_0 | \hat{H} | \Phi_i \rangle + 0 + \cdots = N \varepsilon_0 + N \tau \beta, \end{aligned} \quad (9.11)$$

$$\begin{aligned} \langle \Phi_i | \hat{H} e^{\hat{T}_2} | \Phi_0 \rangle &= \langle \Phi_i | \hat{H} | \Phi_0 \rangle + \langle \Phi_i | \hat{H} \hat{T}_2 | \Phi_0 \rangle + \frac{1}{2} \langle \Phi_i | \hat{H} \hat{T}_2^2 | \Phi_0 \rangle + \cdots \\ &= \beta^* + \tau \sum_j \langle \Phi_i | \hat{H} | \Phi_j \rangle + \frac{1}{2} \tau^2 \sum_{jk} \langle \Phi_i | \hat{H} | \Phi_{jk} \rangle + 0 + \cdots \\ &= \beta^* + \tau \langle \Phi_i | \hat{H} | \Phi_i \rangle + \frac{1}{2} \tau^2 \sum_j \langle \Phi_i | \hat{H} | (\Phi_{ij} + \Phi_{ji}) \rangle \\ &= \beta^* + \tau [(N-1) \varepsilon_0 + \alpha] + \tau^2 (N-1) \beta. \end{aligned} \quad (9.12)$$

Substituting in (9.8), we obtain a pair of simultaneous equations for τ and E :

$$N(\varepsilon_0 + \beta \tau) = E, \quad (9.13)$$

$$\beta^* + \tau[(N-1) \varepsilon_0 + \alpha] + \tau^2 (N-1) \beta = \tau E. \quad (9.14)$$

The second equation includes two terms, $\tau N \varepsilon_0$ and $\tau^2 N \beta$, containing N as a factor but, as we see from the first equation, their sum cancels against τE on the r.h.s., leaving a quadratic equation for τ that is independent of N :

$$\beta^* + (\alpha - \varepsilon_0) \tau - \beta \tau^2 = 0. \quad (9.15)$$

Since τ is independent of N , we see from the first equation that E is proportional to N , as required for extensivity. We can write

$$E = N \varepsilon, \quad \varepsilon = \varepsilon_0 + \Delta \varepsilon, \quad \Delta \varepsilon = \beta \tau. \quad (9.16)$$

In fact, it is easy to see that the equations obtained here for τ and $\Delta \varepsilon$ are equivalent to the equations (1.16), (1.17) for c and $\Delta \epsilon$ in the full-CI solution for a single He atom; thus $\tau = c$ and the CC solution is indeed the exact solution, (1.32), for the N -atom problem.

Thus, coupled-cluster theory (limited in this case to clusters of double excitations) gives the exact answer, in the form $e^{\hat{T}_2} \Phi_0$, for the noninteracting

He atoms. If we bring the atoms closer and allow them to interact, the correct wave function will have additional (but relatively smaller) terms.

The following characteristic features of the CC approach, in addition to the exponential *Ansatz* for the wave function and the resulting extensivity, should be noted.

- Instead of the eigenvalue equation of CI, we obtain a set of simultaneous algebraic equations by projecting the Schrödinger equation onto the zero-order function and onto the functions obtained by the operation of the cluster operators on the zero-order function.
- The first equation (called the *energy equation*) provides an expression for the energy in terms of the coefficients or amplitudes appearing in the cluster operators. The energy cancels in the other equations (the *amplitude equations*), allowing the amplitudes to be determined by the solution of these remaining simultaneous equations. After the amplitudes have been obtained, the energy can be calculated from the energy equation.
- The amplitude equations are nonlinear, containing powers and products of the various amplitudes. Iterative methods are generally required for their solution.

9.2 The coupled-cluster wave function

9.2.1 The exponential *Ansatz* and extensivity

In Section 2.5 we introduced the wave operator Ω , which converts a zero-order wave function Φ_0 into the exact wave function Ψ :

$$\Omega\Phi_0 = \Psi. \quad (9.17)$$

One form for Ω is given by a linked-diagram expansion,

$$\Omega|\Phi_0\rangle = |\Phi_0\rangle + \sum_{k=1}^{\infty} ((\hat{R}_0\hat{W})^k|\Phi_0\rangle)_L. \quad (9.18)$$

We will see shortly that Ω may also be written quite generally as

$$\Omega = e^{\hat{T}}, \quad \Psi = e^{\hat{T}}\Phi_0, \quad (9.19)$$

where \hat{T} is an excitation operator. This form, which is the coupled-cluster choice, is arguably the most convenient and powerful form of Ω . Before a formal derivation, however, let us consider some of the consequences of this choice.

The exponential *Ansatz* for the wave operator immediately manifests the extensivity property. Consider a system $A \cdots B$ composed of two noninteracting subsystems A and B and expressed in terms of orbitals localized on the two subsystems. If the zero-order wave function for the system is separable,

$$\Phi_0(A \cdots B) = \Phi_0(A)\Phi_0(B) \quad (9.20)$$

(overall antisymmetrization of the wave function is unnecessary since the systems are noninteracting), and if \hat{T} for the system is additive,

$$\hat{T}(A \cdots B) = \hat{T}(A) + \hat{T}(B), \quad (9.21)$$

then the total wave function is multiplicatively separable,

$$\begin{aligned} \Psi(A \cdots B) &= e^{\hat{T}(A \cdots B)} \Phi_0(A \cdots B) = e^{\hat{T}(A) + \hat{T}(B)} \Phi_0(A) \Phi_0(B) \\ &= e^{\hat{T}(A)} \Phi_0(A) e^{\hat{T}(B)} \Phi_0(B) = \Psi(A) \Psi(B) \end{aligned} \quad (9.22)$$

(operators on the A and B subsystems commute with each other). This separability of the wave function ensures additivity of the energy,

$$\begin{aligned} \hat{H}(A \cdots B) \Psi(A \cdots B) &= [\hat{H}(A) + \hat{H}(B)] \Psi(A) \Psi(B) \\ &= [\hat{H}(A) \Psi(A)] \Psi(B) + \Psi(A) [\hat{H}(B) \Psi(B)] \\ &= [E(A) + E(B)] \Psi(A \cdots B), \end{aligned} \quad (9.23)$$

as required for extensivity. Equation (9.23) is a weaker condition than (9.22) and is the preferred definition of extensivity. Unlike CC, finite-order MBPT (i.e. RSPT) does not satisfy the wave-function multiplicative separability condition (9.22), but it always gives extensive results for the energy.

9.2.2 The cluster operators

The coupled-cluster wave function is written in the form

$$\Psi = e^{\hat{T}} \Phi_0, \quad (9.24)$$

where $\Phi_0 = |0\rangle$ is the reference function and

$$\hat{T} = \hat{T}_1 + \hat{T}_2 + \hat{T}_3 + \cdots. \quad (9.25)$$

The one-body (\hat{T}_1) two-body (\hat{T}_2) etc. *cluster operators* are given by

$$\hat{T}_1 = \sum_{ia} t_i^a \hat{a}^\dagger \hat{i} = \sum_{ia} t_i^a \{\hat{a}^\dagger \hat{i}\} \quad (9.26)$$

$$\hat{T}_2 = \frac{1}{(2!)^2} \sum_{ijab} t_{ij}^{ab} \hat{a}^\dagger \hat{b}^\dagger \hat{j} \hat{i} = \frac{1}{4} \sum_{ijab} t_{ij}^{ab} \{\hat{a}^\dagger \hat{i} \hat{b}^\dagger \hat{j}\} \quad (9.27)$$

$$\hat{T}_3 = \frac{1}{(3!)^2} \sum_{ijkabc} t_{ijk}^{abc} \hat{a}^\dagger \hat{i} \hat{b}^\dagger \hat{j} \hat{c}^\dagger \hat{k} = \frac{1}{36} \sum_{ijkabc} t_{ijk}^{abc} \{\hat{a}^\dagger \hat{i} \hat{b}^\dagger \hat{j} \hat{c}^\dagger \hat{k}\} \quad (9.28)$$

etc., where $t_{ij\dots}^{ab\dots}$ are coefficients to be determined, usually referred to as the *amplitudes* for the corresponding operators, and the strings of creation and annihilation operators are automatically in normal-ordered form (as before, the braces $\{ \}$ indicate normal ordering). In general,

$$\hat{T}_m = \frac{1}{(m!)^2} \sum_{\substack{ij\dots \\ ab\dots}} t_{ij\dots}^{ab\dots} \{\hat{a}^\dagger \hat{i} \hat{b}^\dagger \hat{j} \dots\} \quad (9.29)$$

comprises m pairs of creation and annihilation operators, producing m -fold excitations, where $m \leq N$, the number of electrons. The $1/(m!)^2$ factor accounts for the redundancy created by the unrestricted summations, since any permutation of the m hole indices or of the m particle indices does not produce a distinct contribution. Furthermore, since for example

$$\hat{a}^\dagger \hat{i} \hat{b}^\dagger \hat{j} = -\hat{a}^\dagger \hat{j} \hat{b}^\dagger \hat{i} = -\hat{b}^\dagger \hat{i} \hat{a}^\dagger \hat{j} = \hat{b}^\dagger \hat{j} \hat{a}^\dagger \hat{i}, \quad (9.30)$$

we also require that

$$t_{ij}^{ab} = -t_{ji}^{ab} = -t_{ij}^{ba} = t_{ji}^{ba}, \quad (9.31)$$

so that the $(2!)^2 = 4$ contributions from permutations of the i, j and a, b indices will produce four equal terms, this repetition being offset by the factor $\frac{1}{4}$. More generally, all $t_{ij\dots}^{ab\dots}$ are defined to be antisymmetric in the hole indices and (separately) in the particle indices,

$$t_{\hat{P}(ij\dots)}^{\hat{P}'(ab\dots)} = (-1)^{\sigma(\hat{P})+\sigma(\hat{P}')} t_{ij\dots}^{ab\dots}, \quad (9.32)$$

where \hat{P} and \hat{P}' are permutation operators and $\sigma(\hat{P})$, $\sigma(\hat{P}')$ are their parities.

The \hat{T} operator for an N -electron system, (9.25), terminates with the N -fold cluster operator \hat{T}_N but in actual applications \hat{T} has to be truncated, usually at the \hat{T}_2 or \hat{T}_3 level, as discussed further below.

If the exponential wave operator is expanded in a Taylor series,

$$e^{\hat{T}} = 1 + \hat{T} + \frac{1}{2} \hat{T}^2 + \frac{1}{3!} \hat{T}^3 + \dots, \quad (9.33)$$

and \hat{T} is expanded as in (9.25), we obtain

$$\begin{aligned}\Psi &= \Phi_0 + \hat{T}_1\Phi_0 + \hat{T}_2\Phi_0 + \cdots \\ &\quad + \frac{1}{2}\hat{T}_1^2\Phi_0 + \hat{T}_1\hat{T}_2\Phi_0 + \frac{1}{2}\hat{T}_2^2\Phi_0 + \cdots \\ &\quad + \frac{1}{3!}\hat{T}_1^3\Phi_0 + \frac{1}{2}\hat{T}_1^2\hat{T}_2\Phi_0 + \frac{1}{2}\hat{T}_1\hat{T}_2^2\Phi_0 + \frac{1}{3!}\hat{T}_2^3\Phi_0 + \cdots \\ &\quad + \cdots\end{aligned}\tag{9.34}$$

(note that the different \hat{T}_m operators commute). Contributions to the wave function of the form $\hat{T}_m\Phi_0$ are called *connected-cluster* contributions while those involving products of cluster operators, such as $\frac{1}{2}\hat{T}_2^2\Phi_0$ or $\hat{T}_1\hat{T}_2\Phi_0$, are *disconnected-cluster* contributions. These disconnected-cluster terms, which are a direct consequence of the exponential form of the wave operator, are responsible for the extensivity of the CC wave function.

Because of the two-electron nature of the Hamiltonian, the most important connected-cluster contribution to the wave function is $\hat{T}_2\Phi_0$. If Φ_0 is a Hartree–Fock wave function (canonical or otherwise) for the state of interest, the contribution of $\hat{T}_1\Phi_0$ is quite small, as a consequence of the Brillouin theorem (Section 1.5). This theorem, which is valid for UHF and closed-shell RHF wave functions, states that matrix elements of the Hamiltonian between the Hartree–Fock function and singly excited determinants vanish:

$$\langle\Phi_i^a|\hat{H}|\Phi_0\rangle = 0 \quad (\text{HF case}).\tag{9.35}$$

In other cases, including ROHF, $\hat{T}_1\Phi_0$ may be important.

Compared with other correlation methods, CC treatments that include \hat{T}_1 and its products are relatively insensitive to the choices of Φ_0 and the orbitals (within a given basis set). This insensitivity is due to the fact that the effect of the operator $e^{\hat{T}_1}$ is to transform Φ_0 to another Slater determinant (Thouless, 1960), and it is thus equivalent to a transformation of the orbital basis (see subsection 3.2.4). This property of $e^{\hat{T}_1}$ is known as the Thouless theorem.

The most important *disconnected-cluster* contribution, at least in the Hartree–Fock case, is $\frac{1}{2}\hat{T}_2^2\Phi_0$ (though higher powers of \hat{T}_2 can become more important as the size of the system increases). The connected $\hat{T}_3\Phi_0$ contribution is important particularly in systems with high electron densities, including molecules containing multiple bonds. Higher-order connected contributions ($\hat{T}_4\Phi_0$, $\hat{T}_5\Phi_0$, $\hat{T}_6\Phi_0$ etc.) are of much less importance in general, though they can be important in special situations.

The simplest CC approach is that of *coupled-cluster doubles* (CCD), in which \hat{T} is truncated to

$$\hat{T}_{\text{CCD}} = \hat{T}_2. \quad (9.36)$$

The CCD wave function includes all connected and disconnected clusters involving \hat{T}_2 only,

$$\Psi_{\text{CCD}} = e^{\hat{T}_2} \Phi_0 = \Phi_0 + \hat{T}_2 \Phi_0 + \frac{1}{2} \hat{T}_2^2 \Phi_0 + \frac{1}{3!} \hat{T}_2^3 \Phi_0 + \cdots. \quad (9.37)$$

The most common extension of this model is *coupled-cluster singles and doubles* (CCSD), defined by

$$\hat{T}_{\text{CCSD}} = \hat{T}_1 + \hat{T}_2. \quad (9.38)$$

An excellent approximation to the exact wave function is usually provided by the CCSDT model, which adds the triple-excitation clusters:

$$\hat{T}_{\text{CCSDT}} = \hat{T}_1 + \hat{T}_2 + \hat{T}_3. \quad (9.39)$$

Owing to the high computational cost of including \hat{T}_3 , however, this model is often approximated in a number of ways.

9.3 The coupled-cluster doubles (CCD) equations

We shall derive the equations for the coupled-cluster doubles model in several ways, in order to clarify the correspondence between the various approaches and to demonstrate the advantages of the diagrammatic procedures. First, in subsection 9.3.1, we use configuration-space techniques, including the Slater–Condon rules for matrix elements of the Hamiltonian between Slater determinants, as commonly employed in the configuration-interaction formalism. Next, in subsection 9.3.2, we use an algebraic derivation, employing second quantization and the generalized Wick’s theorem. Following a section that introduces the diagrammatic representation of the cluster operators and demonstrates the connection between the exponential *Ansatz* of coupled-cluster theory and the linked-diagram theorem of MBPT, we derive the CCD equations diagrammatically in Section 9.5.

9.3.1 Coupled-cluster doubles equations: configuration-space derivation

Equation (9.37) provides the simplest coupled-cluster approximation, the coupled-cluster doubles model. We can derive the CCD equations for the \hat{T}_2

amplitudes and energy by applying the Slater–Condon rules in a configuration-space formalism.

Inserting Ψ_{CCD} into the Schrödinger equation, we obtain

$$\hat{H}\Psi_{\text{CCD}} = E_{\text{CCD}}\Psi_{\text{CCD}}, \quad (9.40)$$

Now projecting from the left with the reference function $\langle\Phi_0|$ we obtain the energy,

$$E_{\text{CCD}} = \langle\Phi_0|\hat{H}|\Psi_{\text{CCD}}\rangle, \quad (9.41)$$

since $\langle\Phi_0|\Psi_{\text{CCD}}\rangle = 1$ by the choice of intermediate normalization. Using the expansions in (9.27) and (9.37), the energy expression becomes

$$E_{\text{CCD}} = \langle\Phi_0|\hat{H}(1+\hat{T}_2)|\Phi_0\rangle = E_{\text{ref}} + \sum_{\substack{i>j \\ a>b}} \langle\Phi_0|\hat{H}|\Phi_{ij}^{ab}\rangle t_{ij}^{ab} = E_{\text{ref}} + \sum_{\substack{i>j \\ a>b}} \langle ij||ab\rangle t_{ij}^{ab} \quad (9.42)$$

(no other powers of \hat{T}_2 can contribute, as is easily seen from the Slater–Condon rules).

At this point it is convenient to subtract E_{ref} from both sides of the Schrödinger equation, to give

$$\hat{H}_{\text{N}}\Psi_{\text{CCD}} = \Delta E_{\text{CCD}}\Psi_{\text{CCD}}, \quad (9.43)$$

where $\hat{H}_{\text{N}} = \hat{H} - E_{\text{ref}}$. To bring out the correspondence with perturbation theory clearly, we write out the full Hamiltonian in first-quantization form, using the analysis in Section 3.5 and subsection 3.6.3. We have

$$\begin{aligned} \hat{H}_{\text{N}} &= \hat{F} - \hat{U} + \hat{H}_2 - E_{\text{ref}} \\ &= \hat{H}_0 + \hat{F}^{\text{o}} - \hat{U} + \hat{H}_2 - E_{\text{ref}}, \end{aligned} \quad (9.44)$$

where

$$\begin{aligned} \hat{H}_0 &= \hat{F}^{\text{d}} = \sum_{\mu} \hat{f}_{\mu}^{\text{d}}, & \langle p|\hat{f}^{\text{d}}|q\rangle &= \varepsilon_p \delta_{pq}, \\ \hat{F}^{\text{o}} &= \sum_{\mu} \hat{f}_{\mu}^{\text{o}}, & \langle p|\hat{f}^{\text{o}}|q\rangle &= (1 - \delta_{pq})\langle p|\hat{f}|q\rangle, \\ \hat{U} &= \sum_{\mu} \hat{u}_{\mu}, & \langle p|\hat{u}|q\rangle &= \sum_i \langle pi||qi\rangle, \\ \hat{H}_2 &= \sum_{\mu>\nu} \frac{1}{r_{\mu\nu}}, \\ E_{\text{ref}} &= E_0 + E^{(1)}, & E_0 &= \sum_i \varepsilon_i, & E^{(1)} &= -\frac{1}{2} \sum_{ij} \langle ij||ij\rangle. \end{aligned}$$

Note that, in the canonical HF case, $\hat{F}^{\text{o}} = 0$ and $\hat{F}^{\text{d}} = \hat{F}$.

To calculate the energy we need the amplitudes t_{ij}^{ab} , and we can obtain equations for these amplitudes by projecting (9.43) onto all double excitations. The number of resulting equations is exactly the same as the number of amplitudes t_{ij}^{ab} to be determined. For a given set of indices i, j, a, b we have

$$\langle \Phi_{ij}^{ab} | \hat{H}_N e^{\hat{T}_2} | \Phi_0 \rangle = \Delta E_{\text{CCD}} \langle \Phi_{ij}^{ab} | e^{\hat{T}_2} | \Phi_0 \rangle \quad (9.45)$$

or

$$\langle \Phi_{ij}^{ab} | \hat{H}_N (1 + \hat{T}_2 + \frac{1}{2} \hat{T}_2^2) | \Phi_0 \rangle = \Delta E_{\text{CCD}} t_{ij}^{ab}. \quad (9.46)$$

This equation contains a quadratic term, $\frac{1}{2} \hat{T}_2^2$, in addition to the linear term \hat{T}_2 , but note that there has been no truncation of the exponential operator since higher powers of \hat{T}_2 produce six-fold and higher excitations, which cannot interact with the double excitations in the bra part of the matrix element.

We next apply the Slater–Condon rules to the individual terms in the parentheses in (9.46). Only the two-electron part \hat{H}_2 of \hat{H}_N contributes to the first term, giving

$$\langle \Phi_{ij}^{ab} | \hat{H}_N | \Phi_0 \rangle = \langle ab || ij \rangle. \quad (9.47)$$

The second (linear) term is

$$\begin{aligned} \langle \Phi_{ij}^{ab} | \hat{H}_N \hat{T}_2 | \Phi_0 \rangle &= \sum_{\substack{k>l \\ c>d}} \langle \Phi_{ij}^{ab} | \hat{H}_N | \Phi_{kl}^{cd} \rangle t_{kl}^{cd} \\ &= \langle \Phi_{ij}^{ab} | \hat{H}_0 - E_{\text{ref}} | \Phi_{ij}^{ab} \rangle t_{ij}^{ab} + \sum_{\substack{k>l \\ c>d}} \langle \Phi_{ij}^{ab} | \hat{F}^o - \hat{U} | \Phi_{kl}^{cd} \rangle t_{kl}^{cd} \\ &\quad + \sum_{\substack{k>l \\ c>d}} \langle \Phi_{ij}^{ab} | \hat{H}_2 | \Phi_{kl}^{cd} \rangle t_{kl}^{cd} \\ &= L_0 + L_1 + L_2. \end{aligned} \quad (9.48)$$

From (3.154) we get

$$(\hat{H}_0 - E_0) | \Phi_{ij}^{ab} \rangle = (\varepsilon_a + \varepsilon_b - \varepsilon_i - \varepsilon_j) | \Phi_{ij}^{ab} \rangle = -\varepsilon_{ij}^{ab} | \Phi_{ij}^{ab} \rangle, \quad (9.49)$$

where $\varepsilon_{ij}^{ab} = \varepsilon_i + \varepsilon_j - \varepsilon_a - \varepsilon_b$, so that for the first term in (9.48) we have

$$L_0 = \left(-\varepsilon_{ij}^{ab} + \frac{1}{2} \sum_{kl} \langle kl || kl \rangle \right) t_{ij}^{ab}. \quad (9.50)$$

The second (one-electron) term in (9.48) contributes only if at least three of the indices k, l, c, d are equal to the same number of the indices i, j, a, b . Application of the Slater–Condon rules to this term gives:

$$\begin{aligned} L_1 = & - \sum_k u_{kk} t_{ij}^{ab} - \sum_k [(f_{jk}^o - u_{jk}) t_{ik}^{ab} - (f_{ik}^o - u_{ik}) t_{jk}^{ab}] \\ & + \sum_c [(f_{bc}^o - u_{bc}) t_{ij}^{ac} - (f_{ac}^o - u_{ac}) t_{ij}^{bc}]. \end{aligned} \quad (9.51)$$

Next we turn to the two-electron term L_2 in (9.48). For this term to be nonzero, at least two of the k, l, c, d indices must equal the same number of i, j, a, b . For $cd = ab$ we get

$$\sum_{k>l} \langle ij || kl \rangle t_{kl}^{ab},$$

and for $kl = ij$ we get

$$\sum_{c>d} \langle ab || cd \rangle t_{ij}^{cd}.$$

If we have one coincidence between the hole indices and another between the particle indices, we get

$$- \sum_{kc} (\langle bk || cj \rangle t_{ik}^{ac} - \langle bk || ci \rangle t_{jk}^{ac} - \langle ak || cj \rangle t_{ik}^{bc} + \langle ak || ci \rangle t_{jk}^{bc})$$

(the signs arise from the maximum-coincidence permutations required in the application of the Slater–Condon rules). Careful analysis shows that the above terms also account for most terms arising from the cases in which three or four of the indices k, l, c, d are equal to three or four, respectively, of i, j, a, b , except for the additional contributions

$$- \sum_{kl} (\langle jl || kl \rangle t_{ik}^{ab} - \langle il || kl \rangle t_{jk}^{ab}) + \sum_{cl} (\langle bl || cl \rangle t_{ij}^{ac} - \langle al || cl \rangle t_{ij}^{bc}),$$

arising from the three-coincidences case, and

$$\sum_{k>l} \langle kl || kl \rangle t_{ij}^{ab} = \frac{1}{2} \sum_{kl} \langle kl || kl \rangle t_{ij}^{ab},$$

arising from the four-coincidences case. These additional contributions are expressible in terms of matrix elements of \hat{u} and, together with the last term in L_0 , (9.50), cancel all the \hat{u} contributions to L_1 in (9.51).

The total result, $L_0 + L_1 + L_2 = L$, for the linear term is

$$\begin{aligned}
 L = & -\varepsilon_{ij}^{ab} t_{ij}^{ab} - \sum_k f_{jk}^o t_{ik}^{ab} + \sum_k f_{ik}^o t_{jk}^{ab} + \sum_c f_{bc}^o t_{ij}^{ac} - \sum_c f_{ac}^o t_{ij}^{bc} \\
 & + \sum_{k>l} \langle ij || kl \rangle t_{kl}^{ab} + \sum_{c>d} \langle ab || cd \rangle t_{ij}^{cd} \\
 & - \sum_{kc} (\langle bk || cj \rangle t_{ik}^{ac} - \langle bk || ci \rangle t_{jk}^{ac} - \langle ak || cj \rangle t_{ik}^{bc} + \langle ak || ci \rangle t_{jk}^{bc}) . \quad (9.52)
 \end{aligned}$$

In the canonical HF case $\hat{f}^o = 0$ and the last four terms in the first line of (9.52) vanish.

All the terms considered so far (i.e. through terms linear in \hat{T}_2) are the same terms that occur in a CID calculation. Coupled-cluster theory differs from CID primarily because of the quadratic term in (9.46),

$$Q = \frac{1}{2} \langle \Phi_{ij}^{ab} | H_N T_2^2 | \Phi_0 \rangle = \frac{1}{2} \sum_{\substack{k>l \\ c>d}} \sum_{\substack{m>n \\ e>f}} \langle \Phi_{ij}^{ab} | \hat{H}_N | \Phi_{klmn}^{cdef} \rangle t_{kl}^{cd} t_{mn}^{ef} . \quad (9.53)$$

This term introduces quadruple excitations into the wave function but with coefficients that are sums of products of the coefficients of double excitations. Nonzero contributions to Q are obtained only when four of the indices k, l, m, n, c, d, e, f in (9.53) are equal to i, j, a, b , and it is obvious that only \hat{H}_2 , the two-electron part of the Hamiltonian, can contribute. There are many possibilities for the required four coincidences, and it is left as an exercise for the reader to prove that

$$\begin{aligned}
 Q = \sum_{\substack{k>l \\ c>d}} \langle kl || cd \rangle [(t_{ij}^{ab} t_{kl}^{cd} + t_{ij}^{cd} t_{kl}^{ab}) - 2(t_{ij}^{ac} t_{kl}^{bd} + t_{ij}^{bd} t_{kl}^{ac}) \\
 - 2(t_{ik}^{ab} t_{jl}^{cd} + t_{ik}^{cd} t_{jl}^{ab}) + 4(t_{ik}^{ac} t_{jl}^{bd} + t_{ik}^{bd} t_{jl}^{ac})] . \quad (9.54)
 \end{aligned}$$

A very important observation pertains to the right-hand side of the amplitude equation (9.46). From (9.42) we see that

$$\Delta E_{\text{CCD}} = \sum_{\substack{i>j \\ a>b}} \langle ij || ab \rangle t_{ij}^{ab} \quad (9.55)$$

and, since the summation labels are dummy variables, the first term in Q , (9.54), is equal to $\Delta E_{\text{CCD}} t_{ij}^{ab}$. Consequently, this term cancels against the r.h.s. of (9.46), eliminating the unknown energy from the amplitude

equations. Rearranging terms and converting to unrestricted summations, the CCD amplitude equations can then be written as

$$\begin{aligned}
 \varepsilon_{ij}^{ab} t_{ij}^{ab} = & \langle ab || ij \rangle + \frac{1}{2} \sum_{cd} \langle ab || cd \rangle t_{ij}^{cd} + \frac{1}{2} \sum_{kl} \langle ij || kl \rangle t_{kl}^{ab} \\
 & - \sum_{kc} (\langle bk || cj \rangle t_{ik}^{ac} - \langle bk || ci \rangle t_{jk}^{ac} - \langle ak || cj \rangle t_{ik}^{bc} + \langle ak || ci \rangle t_{jk}^{bc}) \\
 & - \sum_k f_{jk}^o t_{ik}^{ab} + \sum_k f_{ik}^o t_{jk}^{ab} + \sum_c f_{bc}^o t_{ij}^{ac} - \sum_c f_{ac}^o t_{ij}^{bc} \\
 & + \sum_{klcd} \langle kl || cd \rangle \left[\frac{1}{4} t_{ij}^{cd} t_{kl}^{ab} - \frac{1}{2} (t_{ij}^{ac} t_{kl}^{bd} + t_{ij}^{bd} t_{kl}^{ac}) \right. \\
 & \quad \left. - \frac{1}{2} (t_{ik}^{ab} t_{jl}^{cd} + t_{ik}^{cd} t_{jl}^{ab}) + (t_{ik}^{ac} t_{jl}^{bd} + t_{ik}^{bd} t_{jl}^{ac}) \right]. \quad (9.56)
 \end{aligned}$$

Once again we see the emergence of simultaneous algebraic equations (instead of the eigenvalue problem of CI), which characterizes the CC methods. Since the equations are quadratic they are solved iteratively, substituting the amplitudes t_{ij}^{ab} obtained in each iteration into the quadratic terms for the next iteration.

As we shall see in the diagrammatic derivation in Section 9.5, the quantity $\Delta E_{\text{CCD}} t_{ij}^{ab}$ corresponds to an unlinked diagram and therefore must cancel in the final equations. Because of the absence of the $\frac{1}{2} \hat{T}_2^2$ term in the CID equations, $\Delta E_{\text{CID}} t_{ij}^{ab}$ is not canceled there and therefore the CI procedure retains contributions arising from unlinked diagrams. A CI-like model that corrects for this deficiency and restores extensivity is provided by the *linearized CCD (LCCD)* approach. In this approach, *after* cancellation of the unlinked terms the remaining quadratic contributions in (9.56) are neglected (Čížek 1966). The energy in this approximation corresponds to an infinite sum of double-excitation diagrams (Bartlett and Shavitt, 1977b) and is correct through third order in MBPT. This model has also been called D-MBPT(∞) (Bartlett, Shavitt and Purvis, 1979), CEPA(0) and LCPMET (Čížek 1966, Adams, Jankowski and Paldus 1979).

9.3.2 Coupled-cluster doubles equations: algebraic derivation

For an algebraic derivation of the coupled-cluster doubles equations we use second quantization and the generalized Wick's theorem for products of normal-ordered products of operators and write the Hamiltonian in

normal-ordered form according to subsection 3.6.3:

$$\begin{aligned}\hat{H}_N &= (\hat{H}_0)_N + \hat{F}_N^o + \hat{W} \\ &= \sum_p \varepsilon_p \{\hat{p}^\dagger \hat{p}\} + \sum_{p \neq q} f_{pq} \{\hat{p}^\dagger \hat{q}\} + \frac{1}{4} \sum_{pqrs} \langle pq || rs \rangle \{\hat{p}^\dagger \hat{q}^\dagger \hat{s} \hat{r}\}.\end{aligned}\quad (9.57)$$

To save work it will be convenient to combine the first two terms, using $\varepsilon_p = f_{pp}$, so that we have

$$\hat{H}_N = \hat{F}_N + \hat{W} = \sum_{pq} f_{pq} \{\hat{p}^\dagger \hat{q}\} + \frac{1}{4} \sum_{pqrs} \langle pq || rs \rangle \{\hat{p}^\dagger \hat{q}^\dagger \hat{s} \hat{r}\}.\quad (9.58)$$

Proceeding as in subsection 9.3.1, equations (9.40)–(9.43), we get

$$\begin{aligned}\Delta E_{\text{CCD}} &= \langle 0 | \hat{H}_N (1 + \hat{T}_2) | 0 \rangle = \langle 0 | \hat{H}_N \hat{T}_2 | 0 \rangle \\ &= \sum_{\substack{i>j \\ a>b}} \left\langle 0 \left| \left[\sum_{pq} f_{pq} \{\hat{p}^\dagger \hat{q}\} + \frac{1}{4} \sum_{pqrs} \langle pq || rs \rangle \{\hat{p}^\dagger \hat{q}^\dagger \hat{s} \hat{r}\} \right] \{\hat{a}^\dagger \hat{b}^\dagger \hat{j} \hat{i}\} \right| 0 \right\rangle t_{ij}^{ab},\end{aligned}\quad (9.59)$$

recalling that the vacuum expectation value of a normal-product operator is zero. The contribution of the one-electron part of \hat{H}_N in (9.59) vanishes, since there is no way of contracting all the operators in this term without using an internal contraction in one normal product. Converting to unrestricted summations, we then have

$$\Delta E_{\text{CCD}} = \frac{1}{16} \sum_{ijab} \sum_{pqrs} \langle pq || rs \rangle \langle 0 | \{\hat{p}^\dagger \hat{q}^\dagger \hat{s} \hat{r}\} \{\hat{a}^\dagger \hat{b}^\dagger \hat{j} \hat{i}\} | 0 \rangle t_{ij}^{ab}.\quad (9.60)$$

There are four ways of contracting all the operators between the normal products in the vacuum expectation value in (9.60), as follows:

$$\begin{aligned}& \left\langle 0 \left| \{\hat{p}^\dagger \hat{q}^\dagger \hat{s} \hat{r}\} \{\hat{a}^\dagger \hat{b}^\dagger \hat{j} \hat{i}\} + \{\hat{p}^\dagger \hat{q}^\dagger \hat{s} \hat{r}\} \{\hat{a}^\dagger \hat{b}^\dagger \hat{j} \hat{i}\} \right. \right. \\ & \quad \left. \left. + \{\hat{p}^\dagger \hat{q}^\dagger \hat{s} \hat{r}\} \{\hat{a}^\dagger \hat{b}^\dagger \hat{j} \hat{i}\} + \{\hat{p}^\dagger \hat{q}^\dagger \hat{s} \hat{r}\} \{\hat{a}^\dagger \hat{b}^\dagger \hat{j} \hat{i}\} \right| 0 \right\rangle \\ &= \delta_{pi} \delta_{qj} \delta_{sb} \delta_{ra} - \delta_{pi} \delta_{qj} \delta_{sa} \delta_{rb} - \delta_{pj} \delta_{qi} \delta_{sb} \delta_{ra} + \delta_{pj} \delta_{qi} \delta_{sa} \delta_{rb}.\end{aligned}$$

This results in four equal contributions to the sums, removing one factor $\frac{1}{4}$:

$$\Delta E_{\text{CCD}} = \frac{1}{4} \sum_{ijab} \langle ij || ab \rangle t_{ij}^{ab}.\quad (9.61)$$

This type of redundancy, in which multiple versions of the same term are generated, occurs often in the algebraic derivation but is removed automatically in the diagrammatic derivation.

Next we turn to the amplitude equation (9.46). The first term is the same as (9.60) without the $\frac{1}{4} \sum_{ijab}$ sum and without the amplitude factor, giving the same result as (9.47). The linear term is given by (9.48) and, with the normal-product Hamiltonian given by (9.58), we obtain

$$\begin{aligned} L &= \sum_{\substack{k>l \\ c>d}} \langle \Phi_{ij}^{ab} | \hat{H}_N | \Phi_{kl}^{cd} \rangle t_{kl}^{cd} = \frac{1}{4} \sum_{klcd} \langle \Phi_{ij}^{ab} | \hat{F}_N + \hat{W} | \Phi_{kl}^{cd} \rangle t_{kl}^{cd} \\ &= L_1 + L_2. \end{aligned} \quad (9.62)$$

The decomposition of L in (9.62) is not the same as in the configuration-space derivation (9.48), not only because of the incorporation of L_0 into L_1 but also because the cancellations between contributions to different components of L in (9.48) are incorporated at the outset by the use of normal-product operators in (9.62).

The one-particle part of L is

$$L_1 = \frac{1}{4} \sum_{klcd} \sum_{pq} f_{pq} \langle 0 | \{ \hat{i}^\dagger \hat{j}^\dagger \hat{b} \hat{a} \} \{ \hat{p}^\dagger \hat{q} \} \{ \hat{c}^\dagger \hat{d}^\dagger \hat{l} \hat{k} \} | 0 \rangle t_{kl}^{cd}. \quad (9.63)$$

To contract all operators between the different normal products in the vacuum expectation value, we must form three contractions between the first and third normal products and one contraction each between the first and second and between the second and third. There are 16 valid ways of accomplishing these contractions, four of which are

$$\begin{aligned} &\langle 0 | \{ \hat{i}^\dagger \hat{j}^\dagger \hat{b} \hat{a} \} \{ \hat{p}^\dagger \hat{q} \} \{ \hat{c}^\dagger \hat{d}^\dagger \hat{l} \hat{k} \} + \{ \hat{i}^\dagger \hat{j}^\dagger \hat{b} \hat{a} \} \{ \hat{p}^\dagger \hat{q} \} \{ \hat{c}^\dagger \hat{d}^\dagger \hat{l} \hat{k} \} \\ &+ \{ \hat{i}^\dagger \hat{j}^\dagger \hat{b} \hat{a} \} \{ \hat{p}^\dagger \hat{q} \} \{ \hat{c}^\dagger \hat{d}^\dagger \hat{l} \hat{k} \} + \{ \hat{i}^\dagger \hat{j}^\dagger \hat{b} \hat{a} \} \{ \hat{p}^\dagger \hat{q} \} \{ \hat{c}^\dagger \hat{d}^\dagger \hat{l} \hat{k} \} | 0 \rangle \\ &= \delta_{ik} \delta_{jl} \delta_{bd} \delta_{ap} \delta_{cq} + \delta_{ik} \delta_{jl} \delta_{ac} \delta_{bp} \delta_{dq} - \delta_{ik} \delta_{jq} \delta_{lp} \delta_{ac} \delta_{bd} - \delta_{iq} \delta_{kp} \delta_{jl} \delta_{ac} \delta_{bd}. \end{aligned}$$

Substituting this result into the sums in (9.63) gives

$$\sum_c f_{ac} t_{ij}^{cb} + \sum_d f_{bd} t_{ij}^{ad} - \sum_l f_{lj} t_{il}^{ab} - \sum_k f_{ki} t_{kj}^{ab}.$$

The other 12 terms are obtained by interchanging the termination points of the contractions connecting to the particle creation operators \hat{c}^\dagger and \hat{d}^\dagger and/or to the hole annihilation operators \hat{k} and \hat{l} . In each case we obtain

contributions that are equal to the above four terms, canceling the factor $\frac{1}{4}$ in (9.63). Changing the dummy summation indices in some terms and permuting some indices gives the final result,

$$\begin{aligned} L_1 &= - \sum_c (f_{ac} t_{ij}^{bc} - f_{bc} t_{ij}^{ac}) - \sum_k (f_{jk} t_{ik}^{ab} - f_{ik} t_{jk}^{ab}) \\ &= (\varepsilon_a + \varepsilon_b - \varepsilon_i - \varepsilon_j) t_{ij}^{ab} + \sum_c (f_{bc}^o t_{ij}^{ac} - f_{ac}^o t_{ij}^{bc}) + \sum_k (f_{ik}^o t_{jk}^{ab} - f_{jk}^o t_{ik}^{ab}). \end{aligned} \quad (9.64)$$

For the two-particle part of the linear term we have to evaluate

$$L_2 = \frac{1}{16} \sum_{pqrs} \sum_{klcd} \langle pq || rs \rangle \langle 0 | \{ \hat{j}^\dagger \hat{b} \hat{i}^\dagger \hat{a} \} \{ \hat{p}^\dagger \hat{q}^\dagger \hat{s} \hat{r} \} \{ \hat{c}^\dagger \hat{k} \hat{d} \hat{l} \} | 0 \rangle t_{kl}^{cd}. \quad (9.65)$$

To obtain valid contractions in this case we must form two contractions each between the first and second, the first and third and the second and third normal products. The contractions between the first and third normal products force identities between two of the ket indices k, l, c, d on the one hand and two of the bra indices i, j, a, b on the other; they can be used to classify the terms into three cases, according to whether we contract (a) two pairs of hole-index operators, (b) two pairs of particle-index operators or (c) one pair of each type. These contractions in turn determine the types of remaining contractions involving the second product.

The first and second of these cases can be accomplished in two ways (for example, contracting \hat{i}^\dagger with \hat{k} and \hat{j}^\dagger with \hat{l} , or \hat{i}^\dagger with \hat{l} and \hat{j}^\dagger with \hat{k} in the first term), giving rise to equal sums, while the third case can be accomplished in four equivalent ways (depending on which two ket operators $\hat{k}, \hat{l}, \hat{c}, \hat{d}$ are contracted). Combining the equal sums in each case, we can write the three types of terms as

$$\begin{aligned} L_{2a} &= \frac{1}{8} \sum_{pqrs} \sum_{klcd} \langle pq || rs \rangle \langle 0 | \overbrace{\{ \hat{i}^\dagger \hat{j}^\dagger \hat{b} \hat{a} \} \{ \hat{p}^\dagger \hat{q}^\dagger \hat{s} \hat{r} \} \{ \hat{c}^\dagger \hat{d} \hat{k} \hat{l} \}} | 0 \rangle t_{kl}^{cd} \\ &= \frac{1}{8} \sum_{pqrs} \sum_{cd} \langle pq || rs \rangle \langle 0 | \{ \hat{b} \hat{a} \} \{ \hat{p}^\dagger \hat{q}^\dagger \hat{s} \hat{r} \} \{ \hat{c}^\dagger \hat{d} \} | 0 \rangle t_{ij}^{cd}, \end{aligned} \quad (9.66)$$

$$\begin{aligned} L_{2b} &= \frac{1}{8} \sum_{pqrs} \sum_{klcd} \langle pq || rs \rangle \langle 0 | \overbrace{\{ \hat{i}^\dagger \hat{j}^\dagger \hat{b} \hat{a} \} \{ \hat{p}^\dagger \hat{q}^\dagger \hat{s} \hat{r} \} \{ \hat{c}^\dagger \hat{d} \hat{l} \hat{k} \}} | 0 \rangle t_{kl}^{cd}, \\ &= \frac{1}{8} \sum_{pqrs} \sum_{kl} \langle pq || rs \rangle \langle 0 | \{ \hat{i}^\dagger \hat{j}^\dagger \} \{ \hat{p}^\dagger \hat{q}^\dagger \hat{s} \hat{r} \} \{ \hat{l} \hat{k} \} | 0 \rangle t_{kl}^{ab}, \end{aligned} \quad (9.67)$$

$$\begin{aligned}
L_{2c} &= \frac{1}{4} \sum_{pqrs} \sum_{klcd} \langle pq || rs \rangle \left\langle 0 \left| \overbrace{\{\hat{i}^\dagger \hat{j}^\dagger \hat{b} \hat{a}\} \{\hat{p}^\dagger \hat{q}^\dagger \hat{s} \hat{r}\} \{\hat{c}^\dagger \hat{d}^\dagger \hat{l} \hat{k}\}} + \overbrace{\{\hat{i}^\dagger \hat{j}^\dagger \hat{b} \hat{a}\} \{\hat{p}^\dagger \hat{q}^\dagger \hat{s} \hat{r}\} \{\hat{c}^\dagger \hat{d}^\dagger \hat{l} \hat{k}\}} \right. \right. \\
&\quad + \overbrace{\{\hat{i}^\dagger \hat{j}^\dagger \hat{b} \hat{a}\} \{\hat{p}^\dagger \hat{q}^\dagger \hat{s} \hat{r}\} \{\hat{c}^\dagger \hat{d}^\dagger \hat{l} \hat{k}\}} + \overbrace{\{\hat{i}^\dagger \hat{j}^\dagger \hat{b} \hat{a}\} \{\hat{p}^\dagger \hat{q}^\dagger \hat{s} \hat{r}\} \{\hat{c}^\dagger \hat{d}^\dagger \hat{l} \hat{k}\}} \left. \right| 0 \rangle t_{kl}^{cd} \\
&= \frac{1}{4} \sum_{pqrs} \sum_{kc} \langle pq || rs \rangle [\langle 0 | \{\hat{j}^\dagger \hat{b}\} \{\hat{p}^\dagger \hat{q}^\dagger \hat{s} \hat{r}\} \{\hat{c}^\dagger \hat{k}\} | 0 \rangle t_{ik}^{ac} \\
&\quad - \langle 0 | \{\hat{i}^\dagger \hat{b}\} \{\hat{p}^\dagger \hat{q}^\dagger \hat{s} \hat{r}\} \{\hat{c}^\dagger \hat{k}\} | 0 \rangle t_{jk}^{ac} \\
&\quad - \{\hat{j}^\dagger \hat{a}\} \{\hat{p}^\dagger \hat{q}^\dagger \hat{s} \hat{r}\} \{\hat{c}^\dagger \hat{k}\} | 0 \rangle t_{ik}^{bc} \\
&\quad + \langle 0 | \{\hat{i}^\dagger \hat{a}\} \{\hat{p}^\dagger \hat{q}^\dagger \hat{s} \hat{r}\} \{\hat{c}^\dagger \hat{k}\} | 0 \rangle t_{jk}^{bc}] . \quad (9.68)
\end{aligned}$$

The signs for all these terms can be determined by the number of interchanges needed to bring the contracted operators out in front of the remaining normal products.

The vacuum expectation value in L_{2a} can be evaluated as

$$\begin{aligned}
&\langle 0 | \overbrace{\{\hat{b} \hat{a}\} \{\hat{p}^\dagger \hat{q}^\dagger \hat{s} \hat{r}\} \{\hat{c}^\dagger \hat{d}^\dagger\}} + \overbrace{\{\hat{b} \hat{a}\} \{\hat{p}^\dagger \hat{q}^\dagger \hat{s} \hat{r}\} \{\hat{c}^\dagger \hat{d}^\dagger\}} \\
&\quad + \overbrace{\{\hat{b} \hat{a}\} \{\hat{p}^\dagger \hat{q}^\dagger \hat{s} \hat{r}\} \{\hat{c}^\dagger \hat{d}^\dagger\}} + \overbrace{\{\hat{b} \hat{a}\} \{\hat{p}^\dagger \hat{q}^\dagger \hat{s} \hat{r}\} \{\hat{c}^\dagger \hat{d}^\dagger\}} | 0 \rangle \\
&= \delta_{bq} \delta_{ap} \delta_{ds} \delta_{cr} - \delta_{bq} \delta_{ap} \delta_{cs} \delta_{dr} - \delta_{bp} \delta_{aq} \delta_{ds} \delta_{cr} + \delta_{bp} \delta_{aq} \delta_{cs} \delta_{dr} ,
\end{aligned}$$

where the parity of the number of intersections between the contraction lines determines the sign of each term. Substituting this result into the summations and rearranging the indices in each case to obtain the same order, $\langle ab || cd \rangle$, we get four equal terms, so that

$$L_{2a} = \frac{1}{2} \sum_{cd} \langle ab || cd \rangle t_{ij}^{cd} . \quad (9.69)$$

A similar procedure for the second component of L_2 results in

$$L_{2b} = \frac{1}{2} \sum_{kl} \langle kl || ij \rangle t_{kl}^{ab}. \quad (9.70)$$

For the third component of L_2 , each of the four terms in (9.68) can be fully contracted in four ways. Taking the first term as an example, the vacuum expectation value for this term becomes

$$\begin{aligned} & \left\langle 0 \left| \overbrace{\{\hat{j}^\dagger \hat{b}\} \{\hat{p}^\dagger \hat{q}^\dagger \hat{s} \hat{r}\} \{\hat{c}^\dagger \hat{k}\}} + \overbrace{\{\hat{j}^\dagger \hat{b}\} \{\hat{p}^\dagger \hat{q}^\dagger \hat{s} \hat{r}\} \{\hat{c}^\dagger \hat{k}\}} \right. \right. \\ & \quad \left. \left. + \overbrace{\{\hat{j}^\dagger \hat{b}\} \{\hat{p}^\dagger \hat{q}^\dagger \hat{s} \hat{r}\} \{\hat{c}^\dagger \hat{k}\}} + \overbrace{\{\hat{j}^\dagger \hat{b}\} \{\hat{p}^\dagger \hat{q}^\dagger \hat{s} \hat{r}\} \{\hat{c}^\dagger \hat{k}\}} \right| 0 \right\rangle \\ & = \delta_{bp} \delta_{cs} \delta_{jr} \delta_{kq} - \delta_{bp} \delta_{cr} \delta_{js} \delta_{kq} - \delta_{bq} \delta_{cs} \delta_{jr} \delta_{kp} + \delta_{bq} \delta_{cr} \delta_{js} \delta_{kp}. \end{aligned}$$

Again substituting this result into the summations and rearranging the indices in each case to obtain the same order, in this case $\langle bk || cj \rangle$, we get four equal terms, giving $-\langle bk || cj \rangle t_{ik}^{ac}$. Applying the same procedure to the other three terms results in

$$L_{2c} = - \sum_{kc} \left(\langle bk || cj \rangle t_{ik}^{ac} - \langle bk || ci \rangle t_{jk}^{ac} - \langle ak || cj \rangle t_{ik}^{bc} + \langle ak || ci \rangle t_{jk}^{bc} \right). \quad (9.71)$$

Adding up all the components of $L = L_1 + L_{2a} + L_{2b} + L_{2c}$, we get the same result as in the configuration-space derivation, (9.52).

Turning to the quadratic term, only the two-electron part of \hat{H}_N will enable the eight creation or annihilation operators of the ket quadruple-excitation configuration to be fully contracted. Thus we need to evaluate

$$Q = \frac{1}{8} \sum_{pqrs} \sum_{\substack{k>l \\ c>d}} \sum_{\substack{m>n \\ e>f}} \langle pq || rs \rangle \langle 0 | \{\hat{i}^\dagger \hat{j}^\dagger \hat{b} \hat{a}\} \{\hat{p}^\dagger \hat{q}^\dagger \hat{s} \hat{r}\} \{\hat{c}^\dagger \hat{d}^\dagger \hat{l} \hat{k}\} \{\hat{e}^\dagger \hat{f}^\dagger \hat{n} \hat{m}\} | 0 \rangle t_{kl}^{cd} t_{mn}^{ef}. \quad (9.72)$$

No nonzero contractions are possible between the third and fourth normal products in (9.72) and thus, to obtain nonzero contributions, four of the eight operators in the third and fourth normal products have to be contracted with the first product, and the remaining four with the second product.

We shall first consider the case in which the four operators of the first product are contracted with the four operators of the fourth. This term, and the similar one in which the four contractions are between the first and third normal products, represent unlinked contributions since the set of contractions involving the first normal product is decoupled from the set

involving the second. Considering the inequalities in the restricted summations over m, n, e, f and the restriction $i > j, a > b$, the contractions between the first and fourth products can be accomplished in only one way:

$$\begin{aligned} \frac{1}{8} \sum_{pqrs} \sum_{\substack{k>l \\ c>d}} \sum_{\substack{m>n \\ e>f}} \langle pq||rs \rangle \left\langle 0 \left| \overbrace{\hat{i}^\dagger \hat{j}^\dagger \hat{b} \hat{a}}^{\text{contraction}} \{ \hat{p}^\dagger \hat{q}^\dagger \hat{s} \hat{r} \} \{ \hat{c}^\dagger \hat{d}^\dagger \hat{l} \hat{k} \} \{ \hat{e}^\dagger \hat{f}^\dagger \hat{n} \hat{m} \} \right| 0 \right\rangle t_{kl}^{cd} t_{mn}^{ef} \\ = \frac{1}{8} \sum_{pqrs} \sum_{\substack{k>l \\ c>d}} \langle pq||rs \rangle \langle 0 | \{ \hat{p}^\dagger \hat{q}^\dagger \hat{s} \hat{r} \} \{ \hat{c}^\dagger \hat{d}^\dagger \hat{l} \hat{k} \} | 0 \rangle t_{kl}^{cd} t_{ij}^{ab}. \end{aligned}$$

Contracting the remaining operators in the four ways that are possible gives four equal contributions, and results in

$$\frac{1}{2} \sum_{\substack{k>l \\ c>d}} \langle kl||cd \rangle t_{kl}^{cd} t_{ij}^{ab}.$$

The same result is obtained (after renaming the summation indices) for the case in which the four operators of the first product are contracted with those in the third product, thus canceling the factor $\frac{1}{2}$ for the total unlinked contribution. Comparing this result with (9.61), we see that it is equal to $\Delta E_{\text{CCD}} t_{ij}^{ab}$, and so cancels with the r.h.s. of the amplitude equations, (9.46), as we have already seen in the configuration-space derivation.

The remaining terms in the quadratic contribution fall into four classes, depending on the pattern of contractions of the first normal product. In class (a) the two hole operators of the first product are contracted with either the third or the fourth product (i.e. \hat{i}^\dagger and \hat{j}^\dagger are contracted with \hat{k} and \hat{l} , respectively, or with \hat{m} and \hat{n} , respectively, using ordered sums) while the two particle operators are contracted with the fourth or third product, respectively. These two types of contraction produce equal results, canceling a factor $\frac{1}{2}$. Then converting to unrestricted summations adds a factor $\frac{1}{4}$, which is later canceled by the four equivalent ways of contracting the remaining operators, giving

$$\begin{aligned} Q_a &= \frac{1}{16} \sum_{pqrs} \sum_{klcd} \langle pq||rs \rangle \langle 0 | \{ \hat{p}^\dagger \hat{q}^\dagger \hat{s} \hat{r} \} \{ \hat{l} \hat{k} \} \{ \hat{c}^\dagger \hat{d}^\dagger \} | 0 \rangle t_{ij}^{cd} t_{kl}^{ab} \\ &= \frac{1}{4} \sum_{klcd} \langle kl||cd \rangle t_{ij}^{cd} t_{kl}^{ab}. \end{aligned} \quad (9.73)$$

In class (b) one hole and one particle operator of the first normal product are contracted with operators in the third product, while the remaining two operators are contracted with operators in the fourth. Converting to

unrestricted summations, which introduces an additional factor $\frac{1}{16}$, we find that there are 64 choices for these contractions. Specifically, there are four ways for \hat{i}^\dagger and \hat{a} to be contracted with operators in the third product while \hat{j}^\dagger and \hat{b} can be contracted with operators in the fourth product in four ways, giving 16 equal terms; contracting \hat{i}^\dagger and \hat{a} with operators in the fourth product while \hat{j}^\dagger and \hat{b} are contracted with operators in the third product give 16 more terms equal to the above, for a total of 32 equal terms. Another set of 32 equal terms is obtained by contracting \hat{i}^\dagger and \hat{b} with operators in the third product while \hat{j}^\dagger and \hat{a} are contracted with operators in the fourth product, or vice versa. In total, after renaming the summation indices and performing the remaining contractions we get

$$\begin{aligned} Q_b &= \frac{1}{4} \sum_{pqrs} \sum_{klcd} \langle pq || rs \rangle \langle 0 | \{ \hat{p}^\dagger \hat{q}^\dagger \hat{s} \hat{r} \} \{ \hat{c}^\dagger \hat{k} \} \{ \hat{d}^\dagger \hat{l} \} | 0 \rangle (t_{ik}^{ac} t_{jl}^{bd} - t_{ik}^{bc} t_{jl}^{ad}) \\ &= \sum_{klcd} \langle kl || cd \rangle (t_{ik}^{ac} t_{jl}^{bd} - t_{ik}^{bc} t_{jl}^{ad}) = \sum_{klcd} \langle kl || cd \rangle (t_{ik}^{ac} t_{jl}^{bd} + t_{ik}^{bd} t_{jl}^{ac}), \quad (9.74) \end{aligned}$$

where in the final expression we have interchanged the summation indices c, d in the second term, necessitating a change of sign to restore them to their original order in the antisymmetric integral.

In classes (c) and (d) three operators of the first normal product are contracted with operators in the third product and one with an operator in the fourth, or vice versa. In class (c) the set of three operators in the first product consists of two particle operators and one hole operator while in class (d) it consists of one particle operator and two hole operators. Furthermore, each case can be generated in two distinct ways, depending on whether the set of three operators is $\hat{i}^\dagger \hat{a} \hat{b}$ or $\hat{j}^\dagger \hat{a} \hat{b}$ for (c) and $\hat{i}^\dagger \hat{j}^\dagger \hat{a}$ or $\hat{i}^\dagger \hat{j}^\dagger \hat{b}$ for (d). There are 16 possibilities in each case: the set of three operators in the first product can be contracted with operators in the third or the fourth product, and in each case these three contractions can be done in four ways, while the remaining single contraction can be chosen in two ways. The 16 possibilities lead to equivalent results, canceling the factor $\frac{1}{16}$ obtained by converting to unrestricted summations. As an example, the first Q_c term can be written in the form

$$\begin{aligned} & \frac{1}{8} \sum_{pqrs} \sum_{klcd} \sum_{mnef} \langle pq || rs \rangle \langle 0 | \{ \hat{i}^\dagger \hat{j}^\dagger \hat{b} \hat{a} \} \{ \hat{p}^\dagger \hat{q}^\dagger \hat{s} \hat{r} \} \{ \hat{c}^\dagger \hat{d}^\dagger \hat{l} \hat{k} \} \{ \hat{e}^\dagger \hat{f}^\dagger \hat{n} \hat{m} \} | 0 \rangle t_{kl}^{cd} t_{mn}^{ef} \\ &= -\frac{1}{8} \sum_{pqrs} \sum_{klcd} \langle pq || rs \rangle \langle 0 | \{ \hat{p}^\dagger \hat{q}^\dagger \hat{s} \hat{r} \} \{ \hat{c}^\dagger \hat{d}^\dagger \hat{k} \} \{ \hat{l} \} | 0 \rangle t_{kj}^{cd} t_{li}^{ab}. \end{aligned}$$

The sign reflects the odd number of interchanges needed to move all the contracted operators to the front in pairs (note that the summation index m is changed to l after the contraction). The remaining operators can be contracted in four ways:

$$\begin{aligned}
 & \left\langle 0 \left| \overbrace{\{\hat{p}^\dagger \hat{q}^\dagger \hat{s} \hat{r}\} \{\hat{c}^\dagger \hat{d}^\dagger \hat{k}\} \{\hat{l}\}} + \overbrace{\{\hat{p}^\dagger \hat{q}^\dagger \hat{s} \hat{r}\} \{\hat{c}^\dagger \hat{d}^\dagger \hat{k}\} \{\hat{l}\}} \right. \right. \\
 & \quad \left. \left. + \overbrace{\{\hat{p}^\dagger \hat{q}^\dagger \hat{s} \hat{r}\} \{\hat{c}^\dagger \hat{d}^\dagger \hat{k}\} \{\hat{l}\}} + \overbrace{\{\hat{p}^\dagger \hat{q}^\dagger \hat{s} \hat{r}\} \{\hat{c}^\dagger \hat{d}^\dagger \hat{k}\} \{\hat{l}\}} \right| 0 \right\rangle \\
 & = \delta_{pl} \delta_{qk} \delta_{rd} \delta_{sc} - \delta_{pk} \delta_{ql} \delta_{rd} \delta_{sc} - \delta_{pl} \delta_{qk} \delta_{rc} \delta_{sd} + \delta_{pk} \delta_{ql} \delta_{rc} \delta_{sd}.
 \end{aligned}$$

All four terms produce the same value for the sum, and after exchanging and rearranging some of the indices we get

$$-\frac{1}{2} \sum_{klcd} \langle kl || cd \rangle t_{ik}^{ab} t_{jl}^{cd}.$$

Similarly, for the second term of Q_c we have

$$-\frac{1}{2} \sum_{klcd} \langle kl || cd \rangle t_{ik}^{cd} t_{jl}^{ab}$$

and these two terms add up to

$$Q_c = -\frac{1}{2} \sum_{klcd} \langle kl || cd \rangle (t_{ik}^{ab} t_{jl}^{cd} + t_{ik}^{cd} t_{jl}^{ab}). \quad (9.75)$$

Similar treatment of case (d) gives

$$Q_d = -\frac{1}{2} \sum_{klcd} \langle kl || cd \rangle (t_{ij}^{ac} t_{kl}^{bd} + t_{ij}^{bd} t_{kl}^{ac}). \quad (9.76)$$

When all the different parts of Q are put together, we get the result (9.54).

The algebraic derivation just presented is fairly laborious, but it serves to demonstrate many potential simplifications that are incorporated naturally in the diagrammatic derivation. In Section 9.4 below we will introduce diagrams for the general cluster operators as part of the formal introduction of the exponential *Ansatz* and will show their relationship to the diagrams of MBPT. In subsequent developments we will derive all expressions diagrammatically. In particular, the CCD equations are rederived diagrammatically in Section 9.5. Comparisons with the configuration-space derivation (subsection 9.3.1) and algebraic derivation (subsection 9.3.2) can then be readily made.

9.4 Exponential *Ansatz* and the linked-diagram theorem of MBPT

In this section we explore the relationship between the CC and MBPT wave-function expansions and show that the CC form of the wave function can actually be derived from the infinite-order MBPT expansion. This relationship demonstrates that the various CC models can be viewed as infinite-order summations of selected classes of MBPT diagrams.

The linked-diagram form of the MBPT wave function, (6.10), is

$$\Psi_{\text{MBPT}} = \sum_{n=0}^{\infty} (\hat{R}_0 \hat{V}_N)^n |0\rangle_L = \Phi_0 + \Psi^{(1)} + \Psi^{(2)} + \cdots, \quad (9.77)$$

where the superscripts indicate the order in \hat{V}_N and where $\hat{V}_N = \hat{F}_N^o + \hat{W}$ (noting that $\hat{H}_N = (\hat{H}_0)_N + \hat{V}_N$).

The individual orders of Ψ can be written in terms of the antisymmetrized wave-function diagrams in the form (omitting arrows except where they are needed to avoid ambiguity)

$$\begin{aligned} \Psi^{(1)} &= \text{Diagram 1} + \text{Diagram 2}, \quad (9.78) \\ \Psi^{(2)} &= \text{Diagram 3} + \text{Diagram 4} + \text{Diagram 5} + \text{Diagram 6} + \text{Diagram 7} \\ &+ \text{Diagram 8} + \text{Diagram 9} + \text{Diagram 10} + \text{Diagram 11} + \text{Diagram 12} + \text{Diagram 13} + \text{Diagram 14} \\ &+ \text{Diagram 15} + \text{Diagram 16} + \text{Diagram 17} + \text{Diagram 18} + \text{Diagram 19} \end{aligned} \quad (9.79)$$

etc. Only linked diagrams have been included, as required. Diagrams 8, 17, 18 and 19 above are disconnected but, since they have no closed disconnected parts, they are linked, by definition.

We can gather together classes of linked diagrams by the number r of disconnected parts that they contain. Thus $r = 1$ includes all possible

connected wave-function diagrams. We can represent this class formally by a connected operator \hat{T} ,

$$\hat{T}|0\rangle = \sum_{n=1}^{\infty} (\hat{R}_0 \hat{V}_N)^n |0\rangle_C. \quad (9.80)$$

The sum extends over all connected wave function diagrams in all orders. We may further classify the connected diagrams belonging to the operator \hat{T} by the number m of *pairs* of external lines they contain, up to N (the number of electrons),

$$\hat{T} = \sum_{m=1}^N \hat{T}_m. \quad (9.81)$$

Here \hat{T}_m is an operator that creates m pairs of hole-particle lines,

$$\begin{aligned} \hat{T}_m &= \frac{1}{(m!)^2} \sum_{\substack{i_1 i_2 \dots i_m \\ a_1 a_2 \dots a_m}} \langle a_1 a_2 \dots a_m | \hat{t}_m | i_1 i_2 \dots i_m \rangle_A \{ \hat{a}_1^\dagger \hat{a}_2^\dagger \dots \hat{a}_m^\dagger i_m \dots i_2 i_1 \} \\ &= \frac{1}{(m!)^2} \sum_{\substack{i_1 i_2 \dots i_m \\ a_1 a_2 \dots a_m}} t_{i_1 i_2 \dots i_m}^{a_1 a_2 \dots a_m} \{ \hat{a}_1^\dagger i_1 \hat{a}_2^\dagger i_2 \dots \hat{a}_m^\dagger i_m \dots \}, \end{aligned} \quad (9.82)$$

with antisymmetrized amplitudes $\langle a_1 a_2 \dots a_m | \hat{t}_m | i_1 i_2 \dots i_m \rangle_A = t_{i_1 i_2 \dots i_m}^{a_1 a_2 \dots a_m} = -t_{i_2 i_1 \dots i_m}^{a_1 a_2 \dots a_m} = \dots$. In particular,

$$\hat{T}_2 = \frac{1}{4} \sum_{ijab} t_{ij}^{ab} \{ \hat{a}^\dagger \hat{b}^\dagger \hat{j} \hat{i} \}, \quad (9.83)$$

where $t_{ij}^{ab} = -t_{ji}^{ab} = -t_{ij}^{ba} = t_{ji}^{ba}$. We represent the \hat{T}_m operators diagrammatically by

$$\hat{T}_1 = \begin{array}{c} \diagup \quad \diagdown \\ \downarrow \end{array}, \quad (9.84)$$

$$\hat{T}_2 = \begin{array}{c} \diagup \quad \diagdown \quad \diagup \quad \diagdown \\ \downarrow \quad \downarrow \end{array}, \quad (9.85)$$

$$\hat{T}_3 = \begin{array}{c} \diagup \quad \diagdown \quad \diagup \quad \diagdown \quad \diagup \quad \diagdown \\ \diagdown \quad \diagup \quad \diagdown \quad \diagup \quad \diagdown \quad \diagup \\ \hline \end{array} = \begin{array}{c} \diagup \quad \diagdown \quad \diagup \quad \diagdown \quad \diagup \\ \diagdown \quad \diagup \quad \diagdown \quad \diagup \quad \diagdown \\ \circ \end{array}, \quad (9.86)$$

$$\hat{T}_4 = \begin{array}{c} \diagup \quad \diagdown \quad \diagup \quad \diagdown \quad \diagup \quad \diagdown \quad \diagup \quad \diagdown \\ \diagdown \quad \diagup \quad \diagdown \quad \diagup \quad \diagdown \quad \diagup \quad \diagdown \quad \diagup \\ \hline \end{array} = \begin{array}{c} \diagup \quad \diagdown \quad \diagup \quad \diagdown \quad \diagup \quad \diagdown \quad \diagup \\ \diagdown \quad \diagup \quad \diagdown \quad \diagup \quad \diagdown \quad \diagup \quad \diagdown \\ \circ \end{array}, \quad (9.87)$$

etc. (Strictly speaking, these diagrams represent $\hat{T}_m|0\rangle$.) Note the use of solid horizontal lines to represent the \hat{T}_m operators, instead of the broken lines used for interaction vertices. The second designation for \hat{T}_3 and \hat{T}_4 emphasizes that all particle-hole pairs are equivalent, a fact which is not obvious in the first form since the middle pairs appear to be diagrammatically different. We shall use the first designation, with the understanding that all pairs are equivalent. Other variations of these forms have been used, including

$$\begin{array}{c} \diagup \quad \diagdown \\ \diagdown \quad \diagup \\ \hline \end{array}, \quad \begin{array}{c} \diagup \quad \diagdown \\ \diagdown \quad \diagup \\ \hline \end{array} \quad \text{and} \quad \begin{array}{c} \diagup \quad \diagdown \\ \diagdown \quad \diagup \\ \hline \end{array}.$$

A product of these cluster operators is represented simply by putting the corresponding \hat{T}_m diagrams side by side, as in the following example (the left-right order is immaterial):

$$\hat{T}_1\hat{T}_2 = \hat{T}_2\hat{T}_1 = \begin{array}{c} \diagup \quad \diagdown \\ \diagdown \quad \diagup \\ \hline \end{array} \begin{array}{c} \diagup \quad \diagdown \quad \diagup \quad \diagdown \\ \diagdown \quad \diagup \quad \diagdown \quad \diagup \\ \hline \end{array}. \quad (9.88)$$

Each \hat{T}_m diagram represents a sum of perturbation theory connected wave function diagrams, such as the connected diagrams in (9.78) and (9.79) but extending to all orders. We classify these contributions to each \hat{T}_m in terms of the order of perturbation theory in which they occur, i.e. in terms of the number of interaction lines (vertices) they contain,

$$\hat{T}_m = \sum_{n=1}^{\infty} \hat{T}_m^{(n)}, \quad (9.89)$$

$$\hat{T}_m^{(n)}|0\rangle = \{(\hat{R}_0\hat{V}_N)^n|0\rangle\}_{C,m},$$

where the subscripts in the last form indicate a restriction to n th-order connected diagrams with m external hole-particle line pairs. The order-by-order expansion of the \hat{T}_m operator implies a corresponding expansion for the amplitudes,

$$t_{i_1 i_2 \dots i_m}^{a_1 a_2 \dots a_m} = \sum_{n=1}^{\infty} t_{i_1 i_2 \dots i_m}^{a_1 a_2 \dots a_m (n)}. \quad (9.90)$$

The operator $\hat{T}_m^{(n)}$ can be represented by a \hat{T}_m diagram with subscript n , as in

$$\text{Diagram 1} = \text{Diagram 2} \quad (9.91)$$

for $\hat{T}_2^{(1)}$; this diagram implies that

$$\hat{t}_{ij}^{ab(1)} = \frac{\langle ab || ij \rangle}{\varepsilon_{ij}^{ab}} \quad (9.92)$$

(compare (5.15) and (9.83)).

The initial few terms, including the first- and second-order contributions, in the expansion of \hat{T}_1 , \hat{T}_2 and \hat{T}_3 in terms of MBPT diagrams are given in the following equations (as before, arrows are omitted except as needed to avoid ambiguity):

$$\begin{aligned} \hat{T}_1|0\rangle &= \text{Diagram 1} = (\hat{T}_1^{(1)} + \hat{T}_1^{(2)} + \hat{T}_1^{(3)} + \dots)|0\rangle \\ &= \text{Diagram 2} + \text{Diagram 3} + \text{Diagram 4} + \text{Diagram 5} \\ &\quad + \text{Diagram 6} + \text{Diagram 7} + \text{Diagram 8} + \dots, \end{aligned} \quad (9.93)$$

$$\begin{aligned} \hat{T}_2|0\rangle &= \text{Diagram 9} = (\hat{T}_2^{(1)} + \hat{T}_2^{(2)} + \hat{T}_2^{(3)} + \dots)|0\rangle \\ &= \text{Diagram 10} + \text{Diagram 11} + \text{Diagram 12} + \text{Diagram 13} \\ &\quad + \text{Diagram 14} + \text{Diagram 15} + \text{Diagram 16} + \text{Diagram 17} + \dots, \end{aligned} \quad (9.94)$$

$$\begin{aligned} \hat{T}_3|0\rangle &= \text{Diagram 18} = (\hat{T}_3^{(2)} + \hat{T}_3^{(3)} + \dots)|0\rangle \\ &= \text{Diagram 19} + \text{Diagram 20} + \dots. \end{aligned} \quad (9.95)$$

The first class of disconnected diagrams has $r = 2$ and consists of diagrams with two disconnected parts. Four such diagrams, 8, 17, 18, 19, are seen in (9.79). Using the factorization theorem (see Section 6.1) we can show

that the sum of all $r = 2$ diagrams can be expressed as the square of the \hat{T} operator:

$$\frac{1}{2}\hat{T}^2 = \frac{1}{2}\left(\sum_m \hat{T}_m\right)^2 = \frac{1}{2}\sum_m (\hat{T}_m)^2 + \sum_{m>n} \hat{T}_m \hat{T}_n. \quad (9.96)$$

To illustrate this, for $m = 2, r = 2$ in first order we have

$$\begin{aligned} \text{Diagram 1} - \text{Diagram 2} &= \frac{1}{2} \left(\text{Diagram 3} - \text{Diagram 4} + \text{Diagram 5} - \text{Diagram 6} \right), \\ &= \frac{1}{2} \left(\text{Diagram 7} - \text{Diagram 8} \right)^2 = \frac{1}{2} (\hat{T}_2^{(1)})^2. \end{aligned} \quad (9.97)$$

The first equality in (9.97) is due to the fact that the left-right order in the diagram is immaterial, and the second can be shown algebraically by inserting summation labels and bringing the resulting expressions to a common denominator, as in the proof of the factorization theorem:

$$\begin{aligned} & \text{(i)} \text{Diagram 9} \text{(a)} \text{Diagram 10} \text{(j)} \quad \text{(k)} \text{Diagram 11} \text{(c)} \text{(d)} \text{Diagram 12} \text{(l)} \\ &= \frac{1}{16} \sum \frac{\langle ab || ij \rangle \langle cd || kl \rangle}{\varepsilon_{ij}^{ab} \varepsilon_{ijkl}^{abcd}} \{ \hat{a}^\dagger \hat{i} \hat{b}^\dagger \hat{j} \} \{ \hat{c}^\dagger \hat{k} \hat{d}^\dagger \hat{l} \}, \\ & \text{(i)} \text{Diagram 13} \text{(a)} \text{(b)} \text{Diagram 14} \text{(j)} \quad \text{(k)} \text{Diagram 15} \text{(c)} \text{(d)} \text{Diagram 16} \text{(l)} \\ &= \frac{1}{16} \sum \frac{\langle ab || ij \rangle \langle cd || kl \rangle}{\varepsilon_{ijkl}^{abcd} \varepsilon_{kl}^{cd}} \{ \hat{a}^\dagger \hat{i} \hat{b}^\dagger \hat{j} \} \{ \hat{c}^\dagger \hat{k} \hat{d}^\dagger \hat{l} \}. \end{aligned}$$

Bringing these two expressions to a common denominator, adding them and then noting that $\varepsilon_{ij}^{ab} + \varepsilon_{kl}^{cd} = \varepsilon_{ijkl}^{abcd}$ gives the desired result,

$$\begin{aligned} & \text{Diagram 17} - \text{Diagram 18} + \text{Diagram 19} - \text{Diagram 20} \\ &= \frac{1}{16} \sum \frac{\langle ab || ij \rangle \langle cd || kl \rangle}{\varepsilon_{ij}^{ab} \varepsilon_{kl}^{cd}} \{ \hat{a}^\dagger \hat{i} \hat{b}^\dagger \hat{j} \} \{ \hat{c}^\dagger \hat{k} \hat{d}^\dagger \hat{l} \} \\ &= \frac{1}{16} \sum t_{ij}^{ab(1)} t_{kl}^{cd(1)} \{ \hat{a}^\dagger \hat{i} \hat{b}^\dagger \hat{j} \} \{ \hat{c}^\dagger \hat{k} \hat{d}^\dagger \hat{l} \} \\ &= (\hat{T}_2^{(1)})^2. \end{aligned}$$

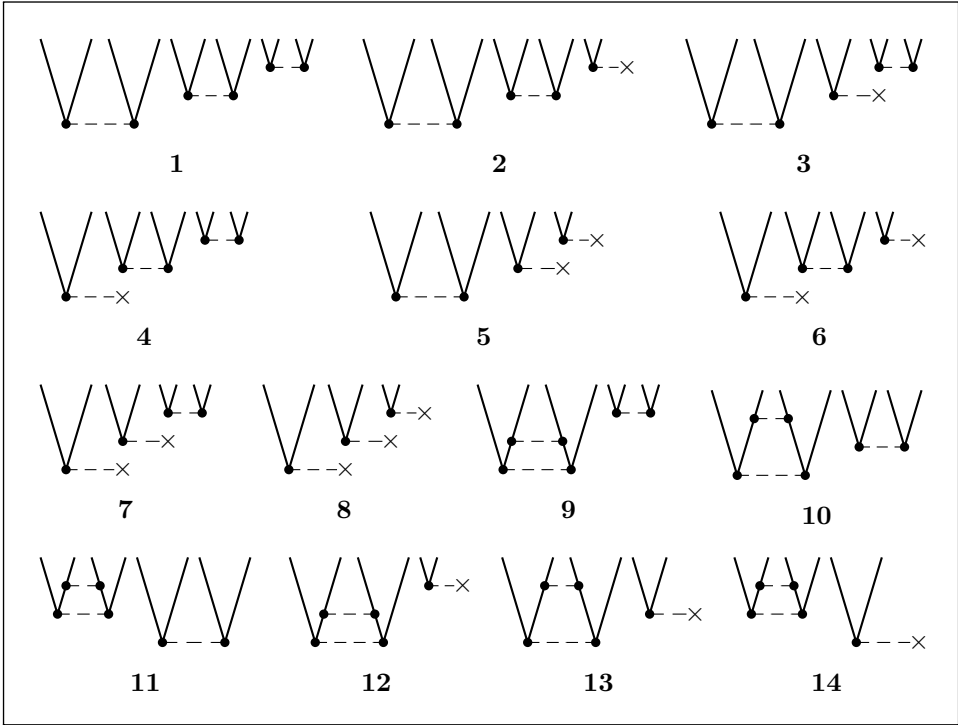


Fig. 9.1. Third-order disconnected wave function skeletons.

This derivation provides a simple illustration of how the factorization theorem is manifested in the amplitudes of \hat{T} and of how it is related to the exponential *Ansatz* of coupled-cluster theory.

Next we proceed to consider third-order disconnected contributions. All third-order disconnected wave-function skeletons are shown in Fig. 9.1. Each of skeletons 1–8 represents a single diagram while skeletons 9–14 represent three diagrams each, with three distinct arrow orientations, corresponding to the particle–particle, hole–hole and particle–hole cases for the second vertex in the left-hand part of the diagram. For each arrow orientation the sum of the corresponding diagrams originating in skeletons 9, 10 and 11 can be written in the form

$$S_{9,10,11} = \sum_{\substack{ijklmn \\ abcdef}} \left\{ \frac{N}{\varepsilon_{ij}^{ab} \varepsilon_{kl}^{cd} \varepsilon_{lmn}^{cdef}} + \frac{N}{\varepsilon_{ij}^{ab} \varepsilon_{ijmn}^{abef} \varepsilon_{klmn}^{cdef}} + \frac{N}{\varepsilon_{mn}^{ef} \varepsilon_{ijmn}^{abef} \varepsilon_{klmn}^{cdef}} \right\}, \quad (9.98)$$

where N is the numerator containing the integrals and operators. This numerator is different for the different arrow orientations, (9.98) but in each case it is the same for the three terms in the sum. Introducing a common denominator, we get

$$\begin{aligned}
 S_{9,10,11} &= \sum N \left[\frac{1}{\varepsilon_{ij}^{ab} \varepsilon_{kl}^{cd} \varepsilon_{klmn}^{cdef}} + \frac{1}{\varepsilon_{ijmn}^{abef} \varepsilon_{klmn}^{cdef}} \left(\frac{1}{\varepsilon_{ij}^{ab} + \varepsilon_{mn}^{ef}} \right) \right] \\
 &= \sum N \left[\frac{1}{\varepsilon_{ij}^{ab} \varepsilon_{kl}^{cd} \varepsilon_{klmn}^{cdef}} + \frac{1}{\varepsilon_{ij}^{ab} \varepsilon_{mn}^{ef} \varepsilon_{klmn}^{cdef}} \right] \\
 &= \sum \frac{N}{\varepsilon_{ij}^{ab}} \left[\frac{1}{\varepsilon_{klmn}^{cdef}} \left(\frac{1}{\varepsilon_{kl}^{cd} + \varepsilon_{mn}^{ef}} \right) \right] = \sum \frac{N}{\varepsilon_{ij}^{ab} \varepsilon_{kl}^{cd} \varepsilon_{mn}^{ef}}. \quad (9.99)
 \end{aligned}$$

Adding up this result for the three arrow orientations gives the product $\hat{T}_2^{(2)} \hat{T}_2^{(1)}$ (the $\hat{T}_2^{(1)}$ factor is the same for all three orientations), which is a component of $\frac{1}{2}(\hat{T}_2)^2$.

For an $r = 3$ example we consider skeleton 1 in Fig. 9.1, which generates a single diagram with just one distinct time order. Using a procedure similar to that for the quadratic term in (9.97), this diagram can be factored by splitting it into six equal contributions and labeling its lines in six different ways:

$$\begin{aligned}
 S_1 &= \frac{1}{6} \sum_{\substack{ijklmn \\ abcdef}} \left\{ \frac{\langle ab||ij \rangle \langle kl||cd \rangle \langle mn||ef \rangle}{\varepsilon_{ij}^{ab} \varepsilon_{ijkl}^{abcd} \varepsilon_{ijklmn}^{abcdef}} + \frac{\langle ab||ij \rangle \langle mn||ef \rangle \langle kl||cd \rangle}{\varepsilon_{ij}^{ab} \varepsilon_{ijmn}^{abef} \varepsilon_{ijklmn}^{abcdef}} \right. \\
 &\quad + \frac{\langle kl||cd \rangle \langle ab||ij \rangle \langle mn||ef \rangle}{\varepsilon_{kl}^{cd} \varepsilon_{kl ij}^{abcd} \varepsilon_{ijklmn}^{abcdef}} + \frac{\langle kl||cd \rangle \langle mn||ef \rangle \langle ab||ij \rangle}{\varepsilon_{kl}^{cd} \varepsilon_{mnkl}^{efcd} \varepsilon_{ijklmn}^{abcdef}} \\
 &\quad \left. + \frac{\langle mn||ef \rangle \langle ab||ij \rangle \langle kl||cd \rangle}{\varepsilon_{mn}^{ef} \varepsilon_{ijmn}^{abef} \varepsilon_{ijklmn}^{abcdef}} + \frac{\langle mn||ef \rangle \langle kl||cd \rangle \langle ab||ij \rangle}{\varepsilon_{mn}^{ef} \varepsilon_{klmn}^{cdef} \varepsilon_{ijklmn}^{abcdef}} \right\} \hat{R}, \quad (9.100)
 \end{aligned}$$

where \hat{R} is a product of creation and annihilation operators. Again, the numerators are all equal. Bringing the six terms to a common denominator, this sum can be factored as

$$\begin{aligned}
S_1 &= \frac{1}{6} \sum \frac{N}{\varepsilon_{ijklmn}^{abcdef}} \left(\frac{1}{\varepsilon_{ij}^{ab} \varepsilon_{ijkl}^{abcd}} + \frac{1}{\varepsilon_{ij}^{ab} \varepsilon_{ijmn}^{abef}} + \frac{1}{\varepsilon_{kl}^{cd} \varepsilon_{kl ij}^{abcd}} \right. \\
&\quad \left. + \frac{1}{\varepsilon_{kl}^{cd} \varepsilon_{klmn}^{cdef}} + \frac{1}{\varepsilon_{mn}^{ef} \varepsilon_{ijmn}^{abef}} + \frac{1}{\varepsilon_{mn}^{ef} \varepsilon_{klmn}^{cdef}} \right) \\
&= \frac{1}{6} \sum \frac{N}{\varepsilon_{ijklmn}^{abcdef}} \left(\frac{1}{\varepsilon_{ij}^{ab} \varepsilon_{kl}^{cd}} + \frac{1}{\varepsilon_{ij}^{ab} \varepsilon_{mn}^{ef}} + \frac{1}{\varepsilon_{mn}^{ef} \varepsilon_{kl}^{cd}} \right) \\
&= \frac{1}{6} \sum \frac{N}{\varepsilon_{ijklmn}^{abcdef}} \left(\frac{\varepsilon_{mn}^{ef} + \varepsilon_{kl}^{cd} + \varepsilon_{ij}^{ab}}{\varepsilon_{ij}^{ab} \varepsilon_{kl}^{cd} \varepsilon_{mn}^{ef}} \right) = \frac{1}{3!} \sum \frac{N}{\varepsilon_{ij}^{ab} \varepsilon_{kl}^{cd} \varepsilon_{mn}^{ef}}. \quad (9.101)
\end{aligned}$$

The latter, of course, represents $\frac{1}{3!}(\hat{T}_2^{(1)})^3$.

All other disconnected terms in Ψ_{MBPT} are similarly obtained as products of \hat{T}_m operators. This observation leads us to the deduction that the sum of all linked wave-function diagrams of all orders containing r disconnected parts is given by $\frac{1}{r!}\hat{T}^r|0\rangle$. This result can be proved inductively by first showing that it is correct for $r = 2$ and then showing that if it is correct for some value of r it is also correct for $r + 1$. The details are left as an exercise for the reader.

Since the Taylor series expansion of the exponential of the connected part is $e^{\hat{T}}|0\rangle = (1 + \hat{T} + \frac{1}{2}\hat{T}^2 + \frac{1}{3!}\hat{T}^3 + \dots)|0\rangle$, we can deduce that, in the infinite-order limit,

$$\Psi_{\text{MBPT}} = e^{\hat{T}}|0\rangle. \quad (9.102)$$

An important point to note is that while MBPT diagrams carry energy denominators, in CC diagrams at least some denominators are hidden in the amplitudes, as seen, for example in (9.92). Thus, in (9.101), the final expression corresponds to

$$\frac{1}{3!} \sum t_{ij}^{ab(1)} t_{kl}^{cd(1)} t_{mn}^{ef(1)} \{\hat{a}^\dagger \hat{i} \hat{b}^\dagger \hat{j}\} \{\hat{c}^\dagger \hat{k} \hat{d}^\dagger \hat{l}\} \{\hat{e}^\dagger \hat{m} \hat{f}^\dagger \hat{n}\}.$$

9.5 Diagrammatic derivation of the CCD equations

The diagrammatic derivation of the coupled-cluster equations makes use of the diagrammatic form of the Hamiltonian (Chapter 4) and of the cluster operators (Section 9.4). Underlying this development is the generalized Wick's theorem, which simplifies the evaluation of contractions of

normal-ordered operators. We use the normal-ordered Hamiltonian, as given in (9.57), (9.58), and the normal-product form of the Schrödinger equation,

$$\hat{H}_N \Psi = \Delta E \Psi, \quad (9.103)$$

where $\hat{H}_N = \hat{F}_N + \hat{W}$.

Following (4.16), the one-electron part of the Hamiltonian is represented diagrammatically as

$$\hat{F}_N = \sum_{ab} \begin{array}{c} a \uparrow \\ \bullet \\ b \uparrow \end{array} \text{---} \times + \sum_{ij} \begin{array}{c} j \downarrow \\ \bullet \\ i \downarrow \end{array} \text{---} \times + \sum_{ai} \begin{array}{c} i \downarrow \swarrow a \\ \bullet \end{array} \text{---} \times + \sum_{ia} \begin{array}{c} i \swarrow \downarrow a \\ \bullet \end{array} \text{---} \times \quad (9.104)$$

$$f_{ab}\{\hat{a}^\dagger \hat{b}\} \quad f_{ij}\{\hat{i}^\dagger \hat{j}\} \quad f_{ai}\{\hat{a}^\dagger \hat{i}\} \quad f_{ia}\{\hat{i}^\dagger \hat{a}\}$$

(the algebraic interpretation is given below each diagram). Note that in the HF case the last two sums in (9.104) vanish because of the block-diagonal nature of \hat{f} . Using the implicit summation convention for unlabeled lines, as in (4.19), and omitting nonessential arrows, this equation is written simply in the form

$$\hat{F}_N = \begin{array}{c} \uparrow \\ \bullet \\ \uparrow \end{array} \text{---} \times + \begin{array}{c} \downarrow \\ \bullet \\ \downarrow \end{array} \text{---} \times + \begin{array}{c} \swarrow \downarrow \\ \bullet \end{array} \text{---} \times + \begin{array}{c} \swarrow \downarrow \\ \bullet \end{array} \text{---} \times. \quad (9.105)$$

(0) (0) (+1) (-1)

The numbers below each diagram denote the excitation level represented by this diagram, i.e. the excess of particle-hole open-line pairs at the top over the number of such pairs at bottom. Note that here the vertex $\bullet \text{---} \times$ represents the full \hat{F}_N operator, unlike in perturbation theory where it represents just the off-diagonal part \hat{F}_N^o .

The two-electron operator (subsection 4.4.6) is similarly represented as

$$\hat{W} = \frac{1}{4} \sum_{abcd} \begin{array}{c} a \uparrow \quad b \uparrow \\ \bullet \quad \bullet \\ c \uparrow \quad d \uparrow \end{array} + \frac{1}{4} \sum_{ijkl} \begin{array}{c} k \downarrow \quad l \downarrow \\ \bullet \quad \bullet \\ i \downarrow \quad j \downarrow \end{array} + \sum_{ijab} \begin{array}{c} a \uparrow \quad b \uparrow \\ \bullet \quad \bullet \\ b \uparrow \quad i \uparrow \end{array}$$

$$\langle ab||cd\rangle\{\hat{a}^\dagger \hat{b}^\dagger \hat{d} \hat{c}\} \quad \langle ij||kl\rangle\{\hat{i}^\dagger \hat{j}^\dagger \hat{l} \hat{k}\} \quad \langle ai||bj\rangle\{\hat{a}^\dagger \hat{i}^\dagger \hat{j} \hat{b}\}$$

$$+ \frac{1}{2} \sum_{abci} \begin{array}{c} a \uparrow \quad i \downarrow \swarrow b \\ \bullet \quad \bullet \\ c \uparrow \end{array} + \frac{1}{2} \sum_{ijka} \begin{array}{c} j \downarrow \quad k \downarrow \swarrow a \\ \bullet \quad \bullet \\ i \downarrow \end{array} + \frac{1}{2} \sum_{abci} \begin{array}{c} a \uparrow \quad b \uparrow \\ \bullet \quad \bullet \\ b \uparrow \quad i \uparrow \end{array}$$

$$\langle ab||ci\rangle\{\hat{a}^\dagger \hat{b}^\dagger \hat{i} \hat{c}\} \quad \langle ia||jk\rangle\{\hat{i}^\dagger \hat{a}^\dagger \hat{k} \hat{j}\} \quad \langle ai||bc\rangle\{\hat{a}^\dagger \hat{i}^\dagger \hat{c} \hat{b}\}$$

$$\begin{aligned}
& + \frac{1}{2} \sum_{ijka} \begin{array}{c} k \\ \downarrow \\ i \end{array} \begin{array}{c} \downarrow \\ j \end{array} \begin{array}{c} \diagup \\ a \end{array} \begin{array}{c} \diagdown \\ b \end{array} + \frac{1}{4} \sum_{abij} \begin{array}{c} i \\ \downarrow \\ a \end{array} \begin{array}{c} \downarrow \\ j \end{array} \begin{array}{c} \diagup \\ a \end{array} \begin{array}{c} \diagdown \\ b \end{array} + \frac{1}{4} \sum_{ijab} \begin{array}{c} i \\ \downarrow \\ a \end{array} \begin{array}{c} \downarrow \\ j \end{array} \begin{array}{c} \diagup \\ a \end{array} \begin{array}{c} \diagdown \\ b \end{array}. \quad (9.106) \\
& \langle ij || ka \rangle \{ \hat{i}^\dagger \hat{j}^\dagger \hat{a} \hat{k} \} \quad \langle ab || ij \rangle \{ \hat{a}^\dagger \hat{b}^\dagger \hat{j} \hat{i} \} \quad \langle ij || ab \rangle \{ \hat{i}^\dagger \hat{j}^\dagger \hat{b} \hat{a} \}
\end{aligned}$$

In terms of unlabeled diagrams and with the usual rules for the assignment of weight factors, this operator takes the form

$$\begin{aligned}
\hat{W} = & \begin{array}{c} \uparrow \quad \uparrow \\ | \quad | \\ \bullet \quad \bullet \\ | \quad | \end{array} + \begin{array}{c} \downarrow \quad \downarrow \\ | \quad | \\ \bullet \quad \bullet \\ | \quad | \end{array} + \begin{array}{c} \uparrow \quad \downarrow \\ | \quad | \\ \bullet \quad \bullet \\ | \quad | \end{array} \\
& \quad (0) \quad \quad (0) \quad \quad (0) \\
& + \begin{array}{c} \uparrow \quad \downarrow \\ | \quad | \\ \bullet \quad \bullet \\ | \quad | \end{array} + \begin{array}{c} \downarrow \quad \downarrow \\ | \quad | \\ \bullet \quad \bullet \\ | \quad | \end{array} + \begin{array}{c} \uparrow \quad \downarrow \\ | \quad | \\ \bullet \quad \bullet \\ | \quad | \end{array} + \begin{array}{c} \downarrow \quad \downarrow \\ | \quad | \\ \bullet \quad \bullet \\ | \quad | \end{array} \\
& \quad (+1) \quad (+1) \quad (-1) \quad (-1) \\
& + \begin{array}{c} \downarrow \quad \downarrow \\ | \quad | \\ \bullet \quad \bullet \\ | \quad | \end{array} + \begin{array}{c} \downarrow \quad \downarrow \\ | \quad | \\ \bullet \quad \bullet \\ | \quad | \end{array} ; \quad (9.107) \\
& \quad (+2) \quad (-2)
\end{aligned}$$

the excitation level is indicated below each diagram.

To complete the representation of the CCD equations, we need to combine the Hamiltonian diagrams with the diagrams that represent the \hat{T}_2 operator,

$$\hat{T}_2 = \begin{array}{c} \diagup \quad \diagdown \\ | \quad | \\ \bullet \quad \bullet \\ | \quad | \end{array} = \frac{1}{(2!)^2} \sum_{ijab} t_{ij}^{ab} \{ \hat{a}^\dagger \hat{i} \hat{b}^\dagger \hat{j} \}. \quad (9.108)$$

The CCD energy (see (9.59)) is given by

$$\Delta E_{\text{CCD}} = \langle 0 | \hat{H}_N \hat{T}_2 | 0 \rangle. \quad (9.109)$$

The diagrammatic representation of this equation must begin and end with the Fermi vacuum state, i.e. no open lines should remain after the contraction of the \hat{H}_N and \hat{T}_2 operators. Put another way, the net excitation level of the energy diagrams should be zero. With \hat{T}_2 represented by (9.108), which has excitation level +2, we should contract it only with those diagrams from the representation of the Hamiltonian, (9.105), (9.107), which have excitation level -2. The only such term is $\begin{array}{c} \downarrow \quad \downarrow \\ | \quad | \\ \bullet \quad \bullet \\ | \quad | \end{array}$. Therefore

$$\Delta E_{\text{CCD}} = \begin{array}{c} \downarrow \quad \downarrow \\ | \quad | \\ \bullet \quad \bullet \\ | \quad | \end{array}, \quad (9.110)$$

which is just like the expression for the MBPT(2) energy except that we have a solid line instead of a broken line at the bottom of the diagram. The rules for the interpretation of this closed diagram are effectively the same as in MBPT (but without a denominator), with the addition of the interpretation of the solid line according to (9.108), giving

$$\Delta E_{\text{CCD}} = \frac{1}{4} \sum_{ijab} \langle ij || ab \rangle t_{ij}^{ab}. \quad (9.111)$$

Apart from the absence of a denominator, the usual interpretation rules apply to this diagram. The ascending and descending lines are assigned arbitrary particle and hole labels, respectively. The matrix element $\langle ij || ab \rangle$ corresponds to the top vertex $i \begin{array}{c} \nearrow \\ \nwarrow \end{array} \bar{a} \begin{array}{c} \nwarrow \\ \nearrow \end{array} \bar{b} j$, in the order left-out, right-out, left-in, right-in, and the t_{ij}^{ab} amplitude corresponds to the bottom vertex, $i \begin{array}{c} \nwarrow \\ \nearrow \end{array} \underline{a} \begin{array}{c} \nwarrow \\ \nearrow \end{array} \underline{b} j$. The factor $\frac{1}{4}$ is due to the fact that the diagram has two sets of equivalent lines, and the positive sign arises from the factor $(-1)^{h+l}$, as there are two hole lines and two loops.

The numerical factors are automatically accounted for in the diagrammatic notation, avoiding redundant terms, while the second-quantized algebraic derivation usually retains the redundancy. Other than this redundancy and the corresponding numerical factors, there is a one-to-one correspondence between the diagrams and the contractions of the second-quantized operators as evaluated using the generalized Wick's theorem (see subsection 9.3.2). When in doubt about a diagram or its interpretation, it is recommended that it be derived algebraically as a check.

Now we turn to the CCD amplitude equation (9.46), which we rewrite in the form

$$\langle ij || \hat{H}_N (1 + \hat{T}_2 + \frac{1}{2} \hat{T}_2^2) | 0 \rangle = \Delta E_{\text{CCD}} t_{ij}^{ab}, \quad (9.112)$$

using the shorthand notation $\langle ij || \equiv \langle \Phi_{ij}^{ab} |$. Obviously, the left-hand side represents a net double excitation, and the Hamiltonian diagrams used in the contractions for each term must be chosen to match this requirement. The first term is simply $\langle ij || \hat{H}_N | 0 \rangle$, and the only matching \hat{H}_N term is the +2 diagram $\begin{array}{c} \nwarrow \\ \nearrow \end{array} _ \begin{array}{c} \nwarrow \\ \nearrow \end{array}$, giving the same result as (9.47),

$$\langle ij || \hat{H}_N | 0 \rangle = i \begin{array}{c} \nwarrow \\ \nearrow \end{array} \underline{a} \begin{array}{c} \nwarrow \\ \nearrow \end{array} \underline{b} j = \langle ab || ij \rangle. \quad (9.113)$$

In the linear term, $\langle ij || \hat{H}_N \hat{T}_2 | 0 \rangle$, the \hat{T}_2 operator provides a double excitation; thus, to get a net +2 excitation level the only \hat{H}_N terms that can be

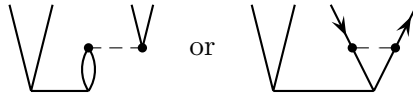
added above the \hat{T}_2 vertex should have excitation level zero. There are five such terms:

$$\begin{array}{ccc}
 \begin{array}{c} \text{Diagram 1: } L_{1a} \\ \text{Diagram 2: } L_{1b} \end{array} & \begin{array}{c} \text{Diagram 3: } L_{2a} \\ \text{Diagram 4: } L_{2b} \\ \text{Diagram 5: } L_{2c} \end{array}
 \end{array}$$

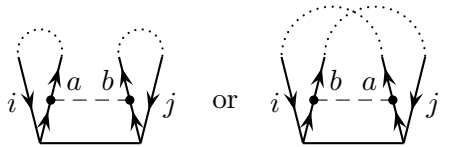
The diagrams are represented as follows:

- L_{1a} : A vertex with four external lines. Two lines enter from the left, labeled i and a . Two lines exit to the right, labeled j and b . A summation index (c) is indicated in parentheses.
- L_{1b} : Similar to L_{1a} , but with summation index (k) indicated in parentheses.
- L_{2a} : A vertex with four external lines. Two lines enter from the left, labeled i and a . Two lines exit to the right, labeled j and b . Summation indices (c) and (d) are indicated in parentheses.
- L_{2b} : A vertex with four external lines. Two lines enter from the left, labeled i and j . Two lines exit to the right, labeled a and b . Summation indices (k) and (l) are indicated in parentheses.
- L_{2c} : A vertex with four external lines. Two lines enter from the left, labeled i and a . Two lines exit to the right, labeled j and b . Summation indices (c) and (k) are indicated in parentheses.

where the labels in parentheses indicate summation indices. Note that diagram L_{2c} can equally well be drawn as



or their mirror images. The fixed labels i, j, a, b in these diagrams correspond to the “target” indices in the bra part of the matrix element in the amplitude equation. These target labels are paired in the diagram in correspondence with the vertical pairing in the bra function \langle_{ij}^{ab} , i with a and j with b . The pairing can be indicated by imaginary external connections of the correspondingly labeled lines, creating *quasi-loops*, as in



(These two diagrams are equivalent, as will become clear from the rules of interpretation.) Internal lines are summed over, so their labels are dummy labels and are usually omitted. When we include such dummy labels in the diagram to show a correspondence with the summation indices in the algebraic expression, as before we place them in parentheses.

The interpretation of these open diagrams introduces a new rule to ensure that all distinct terms are included. This rule requires the inclusion of all *distinct* permutations of the target indices, i, j, \dots and a, b, \dots , i.e. permutations of hole labels and of particle labels of *inequivalent* external lines. Two external lines are *quasi-equivalent* if closing the diagram by a two-particle interaction vertex would make them equivalent; otherwise they

are inequivalent. For example, in diagram L_{1a} the indices a and b are inequivalent while i and j are quasi-equivalent. Consequently, along with the diagram as given we have to include one in which a is permuted with b ; the total contribution is then expressed by means of the operator

$$\hat{P}(ab) = \hat{1} - \hat{P}_{ab}, \quad (9.114)$$

in which \hat{P}_{ab} permutes the labels a and b . This factor is included in the algebraic interpretation of the diagram,

$$L_{1a} = \hat{P}(ab) \sum_c f_{bc} t_{ij}^{ac} = \sum_c f_{bc} t_{ij}^{ac} - \sum_c f_{ac} t_{ij}^{bc}. \quad (9.115)$$

The overall sign is positive, because we have two quasiloops (which are treated as ordinary loops for the purpose of the sign rule) and two hole lines. Similarly, in diagram L_{1b} the indices a and b are quasi-equivalent while i and j are inequivalent. Forming the two external connections, we have two quasiloops and three hole lines, giving an overall minus sign, so we get

$$L_{1b} = -\hat{P}(ij) \sum_k f_{kj} t_{ik}^{ab} = -\sum_k f_{kj} t_{ik}^{ab} + \sum_k f_{ki} t_{jk}^{ab}. \quad (9.116)$$

The L_{1a} and L_{1b} terms together correspond to term L_1 , (9.64), of the algebraic derivation of subsection 9.3.2 (note that the \hat{f} operator is symmetric, $f_{ki} = f_{ik}$).

In the case of diagram L_{2a} , a and b are quasi-equivalent and so are i and j ; hence no permutation factor is needed and

$$L_{2a} = \frac{1}{2} \sum_{cd} \langle ab || cd \rangle t_{ij}^{cd}. \quad (9.117)$$

The factor $\frac{1}{2}$ arises from the fact that the diagram has one pair of equivalent internal lines, i.e. two lines that connect the same two vertices and go in the same direction. These factors can also be interpreted as a remnant of the $1/(m!)^2$ factor in the definition of the \hat{T}_m operator, (9.82), used there to compensate for the unrestricted summations. The remaining part of such factors disappears from the amplitude equations because the restriction to distinct diagrams and the fixed external-line labels in the amplitude equations eliminate redundant terms (except for the case of equivalent internal line pairs).

Returning to the interpretation of diagram L_{2a} , inserting imaginary external connections between i and a and between j and b , forming two quasiloops, and noting the two hole lines, we get a positive sign. If we had permuted the labels a and b then we would have had one quasiloop,

resulting in a minus sign, but this sign would have been compensated by a change of sign of the antisymmetric integral; so the result would have been the same and no additional distinct term would have been obtained.

The fourth diagram is similar, except that it has four hole lines including the two internal equivalent lines giving

$$L_{2b} = \frac{1}{2} \sum_{kl} \langle ij || kl \rangle t_{kl}^{ab}. \quad (9.118)$$

The fifth diagram is the most complicated, since the particle-hole interaction eliminates both the equivalence of internal lines and the quasi-equivalence of external lines, requiring the permutation factor

$$\hat{P}(ab|ij) = \hat{P}(ab)\hat{P}(ij) = (\hat{1} - \hat{P}_{ab})(\hat{1} - \hat{P}_{ij}) = \hat{1} - \hat{P}_{ab} - \hat{P}_{ij} + \hat{P}_{ab}\hat{P}_{ij}. \quad (9.119)$$

There are two quasiloops and three hole lines, so the overall sign is negative and the diagram is interpreted as

$$\begin{aligned} L_{2c} &= -\hat{P}(ij|ab) \sum_{kc} \langle ak || cj \rangle t_{ik}^{cb} \\ &= - \sum_{kc} (\langle ak || cj \rangle t_{ik}^{cb} - \langle bk || cj \rangle t_{ik}^{ca} - \langle ak || ci \rangle t_{jk}^{cb} + \langle bk || ci \rangle t_{jk}^{ca}). \end{aligned} \quad (9.120)$$

The terms L_{2a} , L_{2b} and L_{2c} correspond to the terms (9.69), (9.70) and (9.71) of the algebraic derivation.

Next we consider the quadratic term, $\frac{1}{2} \langle ab || \hat{H}_N \hat{T}_2^2 | 0 \rangle$. Since \hat{T}_2^2 corresponds to quadruple excitations while the target state is a double excitation, we must use a -2 de-excitation-level diagram from the representation of \hat{H}_N . There is only one such diagram, the last diagram in the representation of the two-particle part \hat{W} , (9.107). This diagram must be attached in all possible distinct ways to the representation of \hat{T}_2^2 .

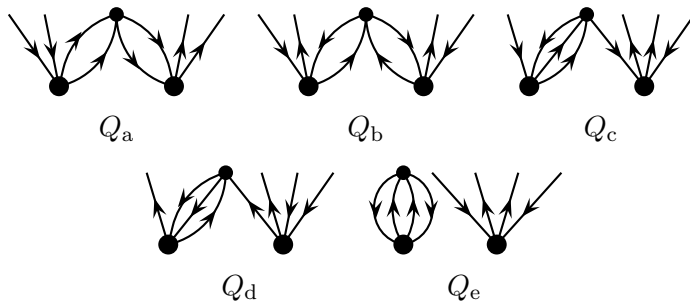
Identifying all the distinct ways in which such connections can be accomplished can be difficult, and a systematic way for dealing with this problem will be presented in Section 10.3. However, we can also use an extension of the Hugenholtz-diagram approach of MBPT to provide an unambiguous, easily applied procedure that generates all the combined diagrams and generates each distinct diagram only once. In this extension each two-particle vertex is collapsed into a medium dot (\bullet), as in the MBPT Hugenholtz diagrams, while each \hat{T} vertex is collapsed into a large dot (\bullet). Thus we need to combine the diagram elements



from \hat{W} and



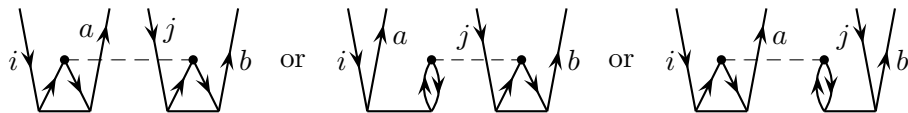
for \hat{T}_2^2 . This combination can be accomplished in five distinct ways:



Expanding these into antisymmetric Goldstone-like diagrams, we get

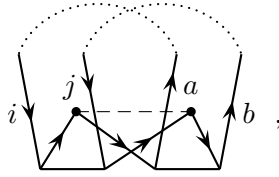
$$\begin{aligned}
 Q = & \text{diagram } Q_a + \text{diagram } Q_b + \text{diagram } Q_c \\
 & + \text{diagram } Q_d + \text{diagram } Q_e.
 \end{aligned} \tag{9.121}$$

As always, the detailed expansion of a Hugenholtz diagram is not unique but the result is the same for all valid expansions. For example, we could equally well have drawn diagram Q_b as



The fifth quadratic-term diagram, Q_e , is both disconnected and *unlinked* since it has a closed disconnected part. As such it should cancel against some other unlinked contribution. In fact, it is easy to see that $Q_e = \Delta E_{\text{CCD}} t_{ij}^{ab}$ and therefore that it cancels with the right-hand side of (9.112), removing the energy from the amplitude equations.

The sign factor for diagram Q_a is obtained by pairing i with a and j with b ,



resulting in two quasiloops. Combined with the four hole lines, we get a positive sign. Diagrams Q_c and Q_d each have two quasiloops plus one internal loop and four hole lines, resulting in a negative sign.

Diagram Q_b introduces our final interpretation rule: an extra factor $\frac{1}{2}$ is required for every pair of equivalent \hat{T}_m vertices in the diagram. Two such vertices are equivalent when they are of the same type (i.e. they have the same m value) and are connected to the interaction vertex with the same number (zero or more) of particle lines and the same number of hole lines. The equivalence of vertices is most easily judged in the Hugenholtz-like form of the diagram or in terms of the $+/-$ contraction-pattern notation to be introduced in Section 10.3. The need for this factor $\frac{1}{2}$ in diagram Q_b can also be understood from the observation that permuting i with j is equivalent in this diagram to permuting a with b , so for this case $\frac{1}{2}\hat{P}(ij|ab) = \hat{P}(ij) = \hat{P}(ab)$. The cancellation of the factor $\frac{1}{2}$ arising from a pair of equivalent vertices against a permutation of the labels of two open lines connected to these two vertices (going in the same direction) is quite general, as will be seen later in other examples. The factors $\frac{1}{2}$ introduced by this rule can be interpreted as remnants of the inverse factorial coefficients in the power series expansion of $e^{\hat{T}}$, the remainder of these coefficients having been accounted for by the restriction to distinct diagrams (see e.g. (9.96)).

Applying the rules of interpretation to the four uncanceled quadratic-term diagrams, we obtain

$$Q_a = \frac{1}{4} \sum_{klcd} \langle kl || cd \rangle t_{ij}^{cd} t_{kl}^{ab} \quad (9.122)$$

(two pairs of equivalent internal lines, four hole lines and two loops),

$$\begin{aligned} Q_b &= \frac{1}{2} \hat{P}(ij|ab) \sum_{klcd} \langle kl || cd \rangle t_{ik}^{ac} t_{lj}^{db} \\ &= \hat{P}(ij) \sum_{klcd} \langle kl || cd \rangle t_{ik}^{ac} t_{lj}^{db} = \hat{P}(ab) \sum_{klcd} \langle kl || cd \rangle t_{ik}^{ac} t_{lj}^{db} \end{aligned} \quad (9.123)$$

(a pair of equivalent vertices, four hole lines and four loops),

$$Q_c = -\frac{1}{2}\hat{P}(ij) \sum_{klcd} \langle kl||cd \rangle t_{ki}^{cd} t_{lj}^{ab} \quad (9.124)$$

(one pair of equivalent internal lines, four hole lines and three loops) and

$$Q_d = -\frac{1}{2}\hat{P}(ab) \sum_{klcd} \langle kl||cd \rangle t_{kl}^{ca} t_{ij}^{db}, \quad (9.125)$$

(one pair of equivalent internal lines, four hole lines and three loops), in agreement with the results obtained in the algebraic derivation, (9.73)–(9.76).

The diagrams for all three terms of the CCD amplitude equation (9.112) (incorporating cancellation of the disconnected diagram against the right-hand side) are collected in Fig. 9.2. The diagram numbering in this figure is part of a systematic scheme that will be followed in subsequent CC equations; the label D refers to the double-excitation amplitude equations. The final form of the algebraic amplitude equations for CCD is

$$\begin{aligned} & \langle ab||ij \rangle + \hat{P}(ab) \sum_c f_{bc} t_{ij}^{ac} - \hat{P}(ij) \sum_k f_{kj} t_{ik}^{ab} \\ & + \frac{1}{2} \sum_{cd} \langle ab||cd \rangle t_{ij}^{cd} + \frac{1}{2} \sum_{kl} \langle kl||ij \rangle t_{kl}^{ab} + \hat{P}(ij|ab) \sum_{kc} \langle kb||cj \rangle t_{ik}^{ac} \\ & + \frac{1}{4} \sum_{klcd} \langle kl||cd \rangle t_{ij}^{cd} t_{kl}^{ab} + \hat{P}(ij) \sum_{klcd} \langle kl||cd \rangle t_{ik}^{ac} t_{jl}^{bd} \\ & - \frac{1}{2} \hat{P}(ij) \sum_{klcd} \langle kl||cd \rangle t_{ik}^{dc} t_{lj}^{ab} - \frac{1}{2} \hat{P}(ab) \sum_{klcd} \langle kl||cd \rangle t_{lk}^{ac} t_{ij}^{db} \\ & = 0 \quad (\text{for all } i > j, a > b). \end{aligned} \quad (9.126)$$

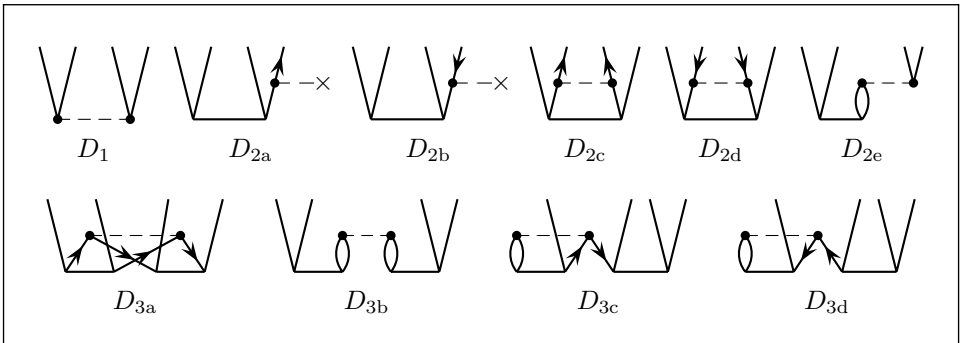


Fig. 9.2. Antisymmetrized Goldstone diagrams for the CCD amplitude equations.

Note that, in consistency with MBPT diagrammatic notation, a resolvent line and its corresponding denominator is implied above the top interaction line of each open diagram. However, in each CC amplitude equation these denominators would be the same in all terms, so they may be ignored. They resurface indirectly in the iterative form of the equations, as in (9.127), (9.128) below, and must be included in the interpretation of the amplitude iteration diagrams shown in Fig. 9.3.

In terms of perturbation theory, the diagonal elements of \hat{f} are chosen here as part of \hat{H}_0 while all other one- and two-electron matrix elements are part of the perturbation. We therefore set up an iterative scheme for the solution of the equations by separating the diagonal parts out of the second and third terms and moving them to the opposite side of the equation (the remaining off-diagonal parts vanish in the canonical HF case). Using $f_{ii} = \varepsilon_i$ etc. we then have, symbolically,

$$(\varepsilon_i + \varepsilon_j - \varepsilon_a - \varepsilon_b)t_{ij}^{ab} = \langle ab || ij \rangle + L(t) + Q(tt). \quad (9.127)$$

The first approximation is to neglect $L(t)$ and $Q(tt)$ and choose

$$t_{ij}^{ab(1)} = \frac{\langle ij || ab \rangle}{\varepsilon_i + \varepsilon_j - \varepsilon_a - \varepsilon_b} = \frac{\langle ij || ab \rangle}{\varepsilon_{ij}^{ab}}. \quad (9.128)$$

When inserted into the energy formula this gives the usual MBPT(2) energy. Inserting this approximation into $L(t)$ while neglecting $Q(tt)$ provides $t_{ij}^{ab(2)}$ and the MBPT(3) energy as the next-order contributions. Inserting $t_{ij}^{ab(1)}$ into $Q(tt)$ generates the quadruple-excitation MBPT(4) energy contributions, and inserting $t_{ij}^{ab(2)}$ into $L(t)$ provides the double-excitation MBPT(4) energy contributions.

Figure 9.3 illustrates this process diagrammatically, using the canonical Hartree–Fock case for simplicity. The correspondence of the energy contributions with the MBPT energy terms can be seen (compare Chapter 5). A systematic procedure for generating all the relevant diagrams will be presented later, in Section 10.3, but in the meantime we will briefly consider the generation of the fourth-order energy diagrams from the third-order wave-function diagrams in Fig. 9.3.

We obtain the fourth-order energy diagrams on closing each of the seven diagrams contributing to $\hat{T}_2^{(3)}$ by contracting it with a Hamiltonian vertex above it. As noted previously, the only Hamiltonian vertex that can be used in this case is the -2 vertex $\bigwedge^- \bigwedge$. When this vertex is contracted with each of the three diagrams containing second-order \hat{T}_2 vertices, and the $\hat{T}_2^{(2)}$ vertex is expanded in turn in terms of compatible second-order MBPT

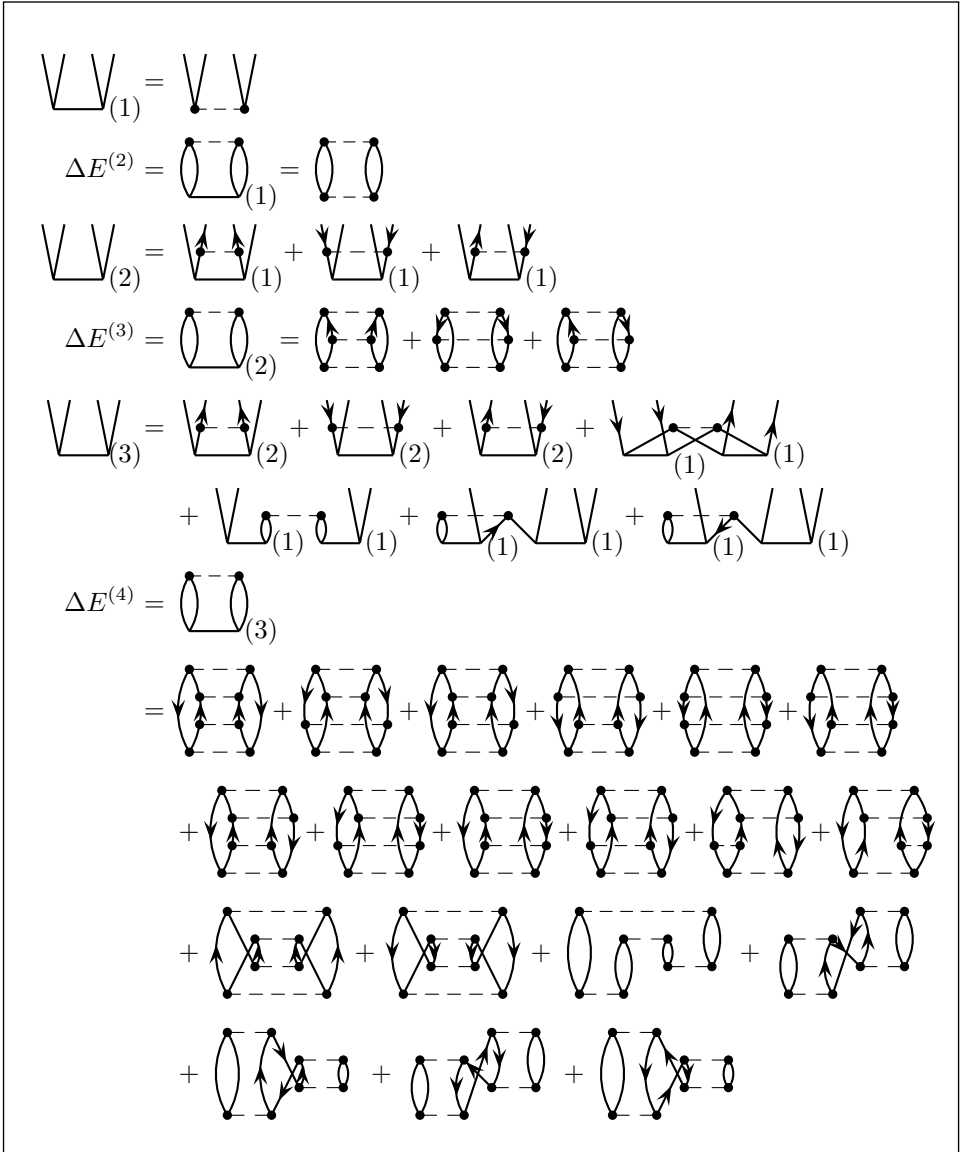


Fig. 9.3. Diagrammatic description of an iteration scheme for the solution of the CCD equations and its relationship to MBPT energies through the fourth-order energy (for the canonical Hartree-Fock case).

wave-function diagrams, we obtain in order the first three, the next three and the next six contributions to $\Delta E^{(4)}$ shown in Fig. 9.3, all of which are double-excitation fourth-order energy contributions. When we contract the Hamiltonian vertex with the four $(\hat{T}_2^{(1)})^2$ diagrams contributing to $\hat{T}_2^{(3)}$ we

obtain, in order, the next two, the next one, the next two and the last two fourth-order MBPT energy diagrams, all of which are quadruple-excitation contributions. Comparing with the MBPT results in Section 5.7, we see that all double-excitation and quadruple-excitation $\Delta E^{(4)}$ diagrams have been accounted for but that the single-excitation and triple-excitation contributions are missing. We can therefore state that in the Hartree–Fock case, in which the second- and third-order MBPT energies contain double-excitation contributions only, CCD is correct through third order in the energy and first order in the wave function.

In order to estimate the computational cost of solving the CCD equations, let n_h be the number of hole states (occupied spinorbitals) and n_p be the number of particle states. (Spin summations, as discussed in Chapter 7, can effectively reduce these numbers by up to a factor 2.) Normally $n_p \gg n_h$, so that the most expensive linear term arises from diagram L_{2a} , which contains four particle labels and two hole labels. The computational cost of this term is therefore proportional to $n_h^2 n_p^4$ per iteration, the same cost as for CISD and (without the iteration factor) for the third-order MBPT energy.

Although the quadratic terms have more indices, they can be summed in stages (analogously to the quadruple-excitation contributions to the fourth-order MBPT energy, as shown in Section 7.1), by considering one amplitude at a time. Taking diagram Q_b , (9.123), as an example, the procedure corresponds to evaluating

$$S_{il}^{ad} = \sum_{kc} \langle kl || cd \rangle t_{ik}^{ac}, \quad Q_b = \hat{P}(ij) \sum_{ld} S_{ik}^{ad} t_{lj}^{db}, \quad (9.129)$$

i.e. two $n_h^3 n_p^3$ processes. Thus the quadratic terms do not change the overall dependence of the computational cost on the number of spinorbitals. We refer to CCD as, roughly speaking, an n^6 process.

10

Systematic derivation of the coupled-cluster equations

10.1 The connected form of the CC equations

Before deriving additional coupled-cluster equations, such as the equations for the coupled-cluster singles and doubles (CCSD) model, we shall introduce an elegant and more convenient procedure than the heuristic approach that we have used to derive the CCD equations. While somewhat less transparent than the heuristic approach it is more powerful and compact, arrives at the cancellation of the energy in all the amplitude equations very easily at the outset and adds the connectedness condition for the CC amplitude equations.

The normal-product form of the Schrödinger equation for a general CC wave function can be written in the form

$$(\hat{H}_N - \Delta E)e^{\hat{T}}|0\rangle = 0. \quad (10.1)$$

We operate on this equation from the left with $e^{-\hat{T}}$ and obtain

$$(e^{-\hat{T}}\hat{H}_Ne^{\hat{T}} - \Delta E)|0\rangle = 0. \quad (10.2)$$

We have thus obtained a *non-Hermitian* similarity-transformed Hamiltonian,

$$\mathcal{H} = e^{-\hat{T}}\hat{H}_Ne^{\hat{T}}, \quad (10.3)$$

which has $|0\rangle$ as a right eigenfunction and ΔE as the corresponding eigenvalue. This operator is commonly referred to as the *CC effective Hamiltonian*, often using the symbol \overline{H} (“H-bar”), but it should not be confused with the effective Hamiltonian \hat{H}^{eff} of the Bloch equations, as used in QDPT (Chapter 8) and MRCC (Chapter 14).

Similarity transformations play an important role in PT and in CC theories, as is seen, for example, in the derivation of quasidegenerate

perturbation theory in Section 2.5. An important property of such transformations is that they do not change the eigenvalue spectrum of the operator.

For a more explicit form of \mathcal{H} we use the Baker–Campbell–Hausdorff expansion (Campbell 1897, Baker 1905, Hausdorff 1906),

$$\begin{aligned}
 e^{-\hat{B}}\hat{A}e^{\hat{B}} &= (1 - \hat{B} + \tfrac{1}{2}\hat{B}^2 - \tfrac{1}{3!}\hat{B}^3 + \cdots)\hat{A}(1 + \hat{B} + \tfrac{1}{2}\hat{B}^2 + \tfrac{1}{3!}\hat{B}^3 + \cdots) \\
 &= \hat{A} + (\hat{A}\hat{B} - \hat{B}\hat{A}) + \tfrac{1}{2}(\hat{A}\hat{B}^2 - 2\hat{B}\hat{A}\hat{B} + \hat{B}^2\hat{A}) \\
 &\quad + \tfrac{1}{3!}(\hat{A}\hat{B}^3 - 3\hat{B}\hat{A}\hat{B}^2 + 3\hat{B}^2\hat{A}\hat{B} - \hat{B}^3\hat{A}) + \cdots \\
 &= \hat{A} + [\hat{A}, \hat{B}] + \tfrac{1}{2}\{(\hat{A}\hat{B} - \hat{B}\hat{A})\hat{B} - \hat{B}(\hat{A}\hat{B} - \hat{B}\hat{A})\} \\
 &\quad + \tfrac{1}{3!}\{[(\hat{A}\hat{B} - \hat{B}\hat{A})\hat{B} - \hat{B}(\hat{A}\hat{B} - \hat{B}\hat{A})]\hat{B} \\
 &\quad - \hat{B}[(\hat{A}\hat{B} - \hat{B}\hat{A})\hat{B} - \hat{B}(\hat{A}\hat{B} - \hat{B}\hat{A})]\} + \cdots \\
 &= \hat{A} + [\hat{A}, \hat{B}] + \tfrac{1}{2}[[\hat{A}, \hat{B}], \hat{B}] + \tfrac{1}{3!}[[[\hat{A}, \hat{B}], \hat{B}], \hat{B}] + \cdots \quad (10.4)
 \end{aligned}$$

Applying this expansion to \mathcal{H} , we obtain

$$\begin{aligned}
 \mathcal{H} &= \hat{H}_N + [\hat{H}_N, \hat{T}] + \tfrac{1}{2}[[\hat{H}_N, \hat{T}], \hat{T}] + \tfrac{1}{3!}[[[\hat{H}_N, \hat{T}], \hat{T}], \hat{T}] \\
 &\quad + \tfrac{1}{4!}[[[[\hat{H}_N, \hat{T}], \hat{T}], \hat{T}], \hat{T}]. \quad (10.5)
 \end{aligned}$$

For reasons that will become clear later (related to the fact that \hat{H}_N has at most two-particle interactions), this series terminates with the four-fold commutator.

The commutator expansion of \mathcal{H} can be simplified, taking advantage of the generalized Wick's theorem and its diagrammatic representation. At this point we shall consider only one aspect of the simplification. Let \hat{A} and \hat{B} be two normal-product operators, each consisting of a product of an even number of creation or annihilation operators (these conditions are satisfied by the components of \hat{H}_N and \hat{T}). Then the generalized Wick's theorem, applied to their commutator, gives

$$[\hat{A}, \hat{B}] = \hat{A}\hat{B} - \hat{B}\hat{A} = \{\hat{A}\hat{B}\} + \{\overline{\hat{A}\hat{B}}\} - \{\hat{B}\hat{A}\} - \{\overline{\hat{B}\hat{A}}\}, \quad (10.6)$$

where $\{\}$ indicates a normal product and $\{\overline{\hat{A}\hat{B}}\}$ represents the sum of all normal products in which there are one or more contractions between the creation or annihilation operators in \hat{A} and those in \hat{B} . Since \hat{A} and \hat{B} each

contain an even number of creation or annihilation operators, we have

$$\{\hat{A}\hat{B}\} = \{\hat{B}\hat{A}\}, \quad (10.7)$$

so that all terms without contraction cancel and

$$[\hat{A}, \hat{B}] = \{\overline{\hat{A}\hat{B}}\} - \{\overline{\hat{B}\hat{A}}\}. \quad (10.8)$$

The canceled uncontracted terms correspond to disconnected diagrams in the diagrammatic representation of the CC equations, and their cancellation simplifies the equations considerably.

The \hat{T}_m cluster operators contain only particle creation operators $\hat{a}^\dagger, \hat{b}^\dagger, \dots$ and hole annihilation operators \hat{i}, \hat{j}, \dots . Since the only nonzero contractions are of the forms

$$\overline{\hat{a}\hat{b}^\dagger} = \delta_{ab} \quad \text{and} \quad \overline{\hat{i}^\dagger\hat{j}} = \delta_{ij},$$

no nonzero contractions can be obtained between different \hat{T}_m operators (and thus $[\hat{T}_m, \hat{T}_n] = 0$, i.e. the different \hat{T}_m operators commute, as might be expected). As a result, in the repeated commutators $[\dots, [\hat{H}_N, \hat{T}], \hat{T}], \dots, \hat{T}]$, the only surviving terms involve contractions between \hat{H}_N and one or more of the \hat{T}_m . Since each term in \hat{H}_N contains at most four creation or annihilation operators it can be contracted with at most four \hat{T}_m operators, thus accounting for the termination of the Baker–Campbell–Hausdorff expansion with the four-fold commutator.

Furthermore, since a particle creation operator, such as \hat{a}^\dagger , can only produce a nonzero contraction with a particle annihilation operator \hat{a} to its left and since a hole annihilation operator \hat{i} can only produce a nonzero contraction with a hole creation operator \hat{i}^\dagger to its left, the only surviving terms in the expansion (10.5) are those in which \hat{H}_N is the first operator on the left,

$$\begin{aligned} \mathcal{H} &= e^{-\hat{T}} \hat{H}_N e^{\hat{T}} \\ &= \hat{H}_N + \overline{\hat{H}_N \hat{T}} + \frac{1}{2} \overline{\hat{H}_N \hat{T} \hat{T}} + \frac{1}{3!} \overline{\hat{H}_N \hat{T} \hat{T} \hat{T}} + \frac{1}{4!} \overline{\hat{H}_N \hat{T} \hat{T} \hat{T} \hat{T}} \\ &= (\hat{H}_N e^{\hat{T}})_C. \end{aligned} \quad (10.9)$$

The contraction symbols of the form $\overline{}$ etc. indicate a sum over all terms in which \hat{H}_N is connected by at least one contraction with each of the following \hat{T} operators; the subscript C also indicates this restriction to connected terms. It is important to distinguish between disconnected clusters such as $\hat{T}_m \hat{T}_n \Phi_0$, which are present in the CC wave function, and disconnected terms (disconnected diagrams), which cancel in the expansion of $\mathcal{H} = (\hat{H}_N e^{\hat{T}} \Phi_0)_C$ and in the coupled-cluster equations.

When the connected-terms expansion of \mathcal{H} is substituted into the similarity-transformed form of the Schrödinger equation (10.2) we obtain the connected form of that equation,

$$(\hat{H}_N e^{\hat{T}} |0\rangle)_C = \Delta E |0\rangle. \quad (10.10)$$

This form of the Schrödinger equation will be used as the basis for the derivation of the various sets of CC equations. When it is projected onto the zero-order function we get the energy equation, which consists solely of linked (or closed, connected) diagrams,

$$\langle 0 | \hat{H}_N e^{\hat{T}} | 0 \rangle_C = \Delta E, \quad (10.11)$$

and when it is projected onto a set of excited functions we get the connected amplitude equation,

$$\langle \Phi_{ij\dots}^{ab\dots} | \hat{H}_N e^{\hat{T}} | 0 \rangle_C = 0. \quad (10.12)$$

With this derivation the energy has automatically disappeared from the amplitude equations; we do not have to work out its cancellation explicitly in each case.

It is sometimes convenient to write the CC equations (10.11), (10.12) in the form

$$\begin{aligned} \hat{P} \mathcal{H} \hat{P} &= \Delta E \hat{P}, \\ \hat{Q} \mathcal{H} \hat{P} &= 0, \end{aligned} \quad (10.13)$$

where \hat{P} and \hat{Q} are the familiar projection operators onto the reference space and its complement, respectively (Section 2.3). The appropriate general form (2.49) of the projection operators applies when nonorthonormal functions Φ_i are employed.

10.2 The general form of CC diagrams

Each term in the perturbation theory equations may contain multiple \hat{V} factors, and the corresponding diagrams may contain multiple interaction vertices $\blacktriangleright - \times$ and $\blacktriangleright - \blacktriangleleft$. In contrast, the terms appearing in coupled-cluster equations each contain only one operator derived from the normal-product Hamiltonian \hat{H}_N , as can be seen from (10.11) and (10.12). All other Hamiltonian-operator factors, as well as the associated denominators, have been absorbed into the \hat{T}_m cluster operators, as can be seen in Fig. 9.3, for example. Therefore the diagrams used to represent the various terms in coupled-cluster equations never have more than one interaction vertex each. Furthermore, that vertex is the top vertex in the diagram.

Interpretation rules for coupled-cluster diagrams

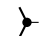
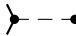
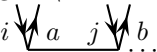
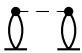


1. Label external (open) lines with the hole (i, j, \dots) and particle (a, b, \dots) target indices. (The target indices are those that occur in the bra part of the amplitude equation.) Label internal lines with hole and particle indices that are different from the target indices.
2. With any one-particle interaction vertex  $--\times$ associate a factor $f_{\text{out},\text{in}}$.
3. With any two-particle interaction vertex  $--\times$ associate an antisymmetric two-electron integral $\langle \text{left-out right-out} || \text{left-in right-in} \rangle$.
4. With every \hat{T}_m vertex  $i \underline{a} j \underline{b}$ associate an amplitude $t_{ij\dots}^{ab\dots}$.
5. Sum over all internal line labels.
6. Associate a factor $\frac{1}{2}$ with each pair of equivalent internal lines. (Two internal lines are considered equivalent if they connect the same two vertices, going in the same direction.)
7. Associate a factor $\frac{1}{2}$ also with each pair of equivalent \hat{T}_m vertices. (Two \hat{T} vertices are considered equivalent if they have the same number of line pairs and are connected in equivalent ways to the interaction vertex; examples are provided by the two \hat{T}_1 vertices in  and in , but not those in .)
8. Associate with each term a sign $-1^{(h-l)}$, where h is the number of hole lines and l is the number of loops. For the purpose of counting loops, paired external lines (lines with labels such as (i, a) or (j, b) that are paired vertically in the bra part of the amplitude equation) are considered connected externally through imaginary extensions, forming quasiloops.
9. Sum over all distinct permutations \hat{P} of labels of inequivalent external particle lines and of inequivalent external hole lines, including a parity factor $(-1)^{\sigma(\hat{P})}$. Lines that are quasi-equivalent (i.e. that would be equivalent if they became internal by the addition of an interaction vertex) are not considered inequivalent for this purpose. These sums over permutations are represented by operators of the form $\hat{P}(ij\dots|ab\dots)$; see (9.114), (9.119).
10. In open diagrams with equivalent vertices, cancel each factor $\frac{1}{2}$ arising from rule 7 above with a permutation of the labels of a pair of external lines connected to the equivalent vertices (going in the same direction).

Fig. 10.1. Summary of the rules of interpretation for coupled-cluster diagrams.

Because all terms in these equations must be connected, and because an interaction vertex has at most four lines and so can connect at most four \hat{T}_m vertices, there can be no more than four \hat{T}_m vertices in any connected diagram in the CC equations (demonstrating again the termination of the commutator expansion of \mathcal{H} , (10.5), with the four-fold commutator).

The coupled-cluster diagrams, like MBPT diagrams, fall into two classes: (a) closed diagrams, which occur in the energy equation (10.11); (b) open diagrams, which appear in the amplitude equations (10.12). There are only three distinct CC energy diagrams, shown here with their interpretations:

$$\begin{array}{ccc}
 \begin{array}{c} \text{Diagram 1: Two vertices connected by a dashed line. The left vertex has an incoming line from below labeled } i \text{ and an outgoing line to the right labeled } a. \text{ The right vertex has an incoming line from the left labeled } b \text{ and an outgoing line to the right labeled } j. \end{array} & \begin{array}{c} \text{Diagram 2: A single vertex with an incoming line from below labeled } i \text{ and an outgoing line to the right labeled } a. \end{array} & \begin{array}{c} \text{Diagram 3: Two vertices connected by a dashed line. The left vertex has an incoming line from below labeled } i \text{ and an outgoing line to the right labeled } a. \text{ The right vertex has an incoming line from the left labeled } b \text{ and an outgoing line to the right labeled } j. \end{array} \\
 \frac{1}{4} \sum_{ijab} \langle ij || ab \rangle t_{ij}^{ab} & \sum_{ia} f_{ia} t_i^a & \frac{1}{2} \sum_{ijab} \langle ij || ab \rangle t_i^a t_j^b
 \end{array}$$

These diagrams provide the energy expression at all levels of the coupled-cluster method. The differing energy results obtained at different CC levels are due to the differing amplitudes obtained for the cluster operators at those levels.

The rules of interpretation for CC diagrams are given in Fig. 10.1.

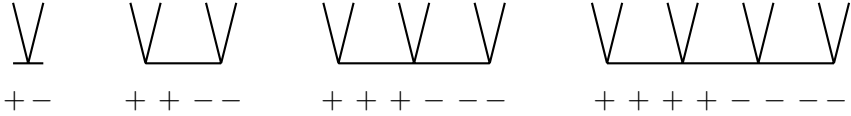
10.3 Systematic generation of CC diagrams

The process of constructing all the distinct diagrams that appear in the CC equations requires careful consideration of all the distinct ways in which Hamiltonian vertices can be added to cluster-operator diagrams. As we saw in the construction of the diagrams for the quadratic contribution to the CCD equations, (9.121), the use of Hugenholtz-like diagrams can be very helpful in this process. We now describe another method, using simple combinatorial elements, for generating distinct antisymmetrized CC diagrams.

This method is based on the assignment of a set of plus and minus labels to each Hamiltonian-operator (interaction) vertex and to each cluster-operator diagram. These labels describe the type and number of lines below the interaction vertex and above the cluster-operator vertex (or vertices) of the CC diagrams. A plus sign is included for each open particle line and a minus sign for each open hole line. A zero is used to indicate the absence of such lines. The Hamiltonian-operator vertices are thus assigned labels as follows:

$$\begin{array}{ccccccc}
 \begin{array}{c} \text{Diagram 1: A vertex with one line below and one line above, both ending in arrows pointing up.} \end{array} & \begin{array}{c} \text{Diagram 2: A vertex with one line below and one line above, both ending in arrows pointing down.} \end{array} & \begin{array}{c} \text{Diagram 3: A vertex with one line below and one line above, both ending in arrows pointing up and down.} \end{array} & \begin{array}{c} \text{Diagram 4: A vertex with one line below and one line above, both ending in arrows pointing up and down.} \end{array} & \begin{array}{c} \text{Diagram 5: A vertex with one line below and one line above, both ending in arrows pointing up and down.} \end{array} & \begin{array}{c} \text{Diagram 6: A vertex with one line below and one line above, both ending in arrows pointing up and down.} \end{array} & \begin{array}{c} \text{Diagram 7: A vertex with one line below and one line above, both ending in arrows pointing up and down.} \end{array} \\
 + & - & 0 & +- & ++ & -- & +- \\
 \\
 \begin{array}{c} \text{Diagram 8: A vertex with one line below and one line above, both ending in arrows pointing up and down.} \end{array} & \begin{array}{c} \text{Diagram 9: A vertex with one line below and one line above, both ending in arrows pointing up and down.} \end{array} & \begin{array}{c} \text{Diagram 10: A vertex with one line below and one line above, both ending in arrows pointing up and down.} \end{array} & \begin{array}{c} \text{Diagram 11: A vertex with one line below and one line above, both ending in arrows pointing up and down.} \end{array} & \begin{array}{c} \text{Diagram 12: A vertex with one line below and one line above, both ending in arrows pointing up and down.} \end{array} & \begin{array}{c} \text{Diagram 13: A vertex with one line below and one line above, both ending in arrows pointing up and down.} \end{array} & \begin{array}{c} \text{Diagram 14: A vertex with one line below and one line above, both ending in arrows pointing up and down.} \end{array} \\
 + & ++- & - & +- - & 0 & ++ -- &
 \end{array}$$

The cluster-operator vertices are given the following labels:



For repeated cluster operators the labels for the individual vertices are partitioned by vertical lines:



The key step in each stage of CC diagram construction is the addition of an interaction vertex above a set of \hat{T}_m vertices in all possible ways that generate distinct connected CC diagrams of the required excitation level. The interaction vertices must be selected to have the appropriate excitation level, see (9.105), (9.107), to produce final diagrams of the desired overall excitation level. Then, for each selected interaction vertex, all the particle or hole lines below it are contracted with (i.e. connected to) matching open lines of the CC diagram, using the + and - labels for guidance, in all possible non-redundant ways.

Note that neither the (+1) \hat{F}_N vertex (the third diagram in (9.105)) nor the (+2) \hat{W} vertex (the eighth diagram in (9.107)) can be used to generate connected CC diagrams. Furthermore, there are obvious limitations on the number of \hat{T}_m vertices that can be connected by each interaction vertex. Thus, (0)-excitation \hat{F}_N vertices (the first two diagrams in (9.105)) or the (+1) \hat{W} vertices (the fourth and fifth diagrams in (9.107)) can connect to only one \hat{T}_m vertex and thus cannot be used to generate connected CC diagrams from disconnected clusters of \hat{T}_m operators.

We will illustrate this process by applying it to the generation of the $Q(\hat{T}_2^2)$ diagrams of (9.121) (also seen in the $\hat{T}_2^{(3)}$ equation in Fig. 9.3). Since we are beginning with a quadruple excitation in \hat{T}_2^2 and the target diagram is a contribution to \hat{T}_2 , only double-de-excitation (-2) interaction vertices can be used and there is only one of those. Thus the

diagram parts that need to be connected, together with their + and - labels, are

$$\begin{array}{c}
 \begin{array}{cc} \bullet & \bullet \\ \diagdown & \diagup \\ \diagup & \diagdown \end{array} \quad \text{---} \quad \begin{array}{cc} \bullet & \bullet \\ \diagdown & \diagup \\ \diagup & \diagdown \end{array} \\
 + \quad + \quad - \quad - \\
 \\
 \begin{array}{cc} \diagdown & \diagup \\ \diagup & \diagdown \end{array} \quad \begin{array}{cc} \diagdown & \diagup \\ \diagup & \diagdown \end{array} \quad \begin{array}{cc} \diagdown & \diagup \\ \diagup & \diagdown \end{array} \quad \begin{array}{cc} \diagdown & \diagup \\ \diagup & \diagdown \end{array} \\
 + \quad + \quad - \quad - \quad | \quad + \quad + \quad - \quad -
 \end{array}$$

Four lines in the bottom part, corresponding to two + and two - labels, must be selected for contraction with the top part, giving rise to four distinct contraction patterns that connect *both* \hat{T}_2 vertices to the interaction vertex:

$$+ \quad + \quad | \quad - \quad - \qquad + \quad - \quad | \quad + \quad - \qquad + \quad + \quad - \quad | \quad - \qquad + \quad - \quad - \quad | \quad + \quad .$$

The order of the + and - labels in each partition is irrelevant. Furthermore, since the two \hat{T}_2 vertices are equivalent, the pattern - - | + + is equivalent to + + | - - and + + - | - is equivalent to - | + + -. The four distinct contraction patterns generate the four connected quadratic diagrams Q_a - Q_d of (9.121),

This procedure is equivalent to the approach described in Section 9.5 based on Hugenholtz-like diagrams, but it provides the sign determination directly. The use of antisymmetrized Goldstone diagrams together with the normal-ordered \hat{H}_N and \hat{T} operators and the above simple combinatorial scheme generates *all* amplitude diagrams unambiguously and without repetition.

10.4 The coupled-cluster singles and doubles (CCSD) equations

As can be seen from (9.78), the only first-order wave-function contribution to \hat{T}_1 is due to the one-electron operator \hat{f}^o ,

$$\underline{\bigvee}_{(1)} = \bigvee_{\bullet \text{---} \times} . \quad (10.14)$$

The second- and third-order contributions to the CC energy (see Fig. 9.3) are

$$\Delta E^{(2)} = \text{diagram (1)} + \text{diagram (1)}^{\text{---}\times}, \quad (10.15)$$

$$\Delta E^{(3)} = \text{diagram (2)} + \text{diagram (2)}^{\text{---}\times} + \text{diagram (1)} \text{diagram (1)}. \quad (10.16)$$

When a Hartree–Fock reference function (canonical or otherwise) is used, \hat{f} is block diagonal and any diagram containing a one-body particle–hole interaction ($\text{V}_{\text{---}\times}$ or $\text{A}^{\text{---}\times}$) vanishes. Thus there is no first-order wave function contribution to \hat{T}_1 , and the only nonzero contributions to the second- and third-order energy come from \hat{T}_2 . Thus we can say that in the HF case CCD is correct through first order in the wave function and third order in the energy, though it includes many higher-order contributions involving disconnected clusters such as disconnected quadruple excitations. The same conclusion can be reached by use of the Brillouin theorem, Section 1.5, which is just a manifestation of the block-diagonal nature of \hat{f} . Therefore CCD based on HF orbitals will frequently provide quite reasonable approximations. However, the addition of single-excitation contributions adds 35 diagrams but entails little computational effort and can be very useful in many situations.

A primary reason for the inclusion of single excitations in many cases is that it permits the use of non-HF reference functions, for which \hat{f} is not block diagonal and the Brillouin theorem does not hold. In such cases the matrix elements $\langle \Phi_i^a | \hat{H} | \Phi_0 \rangle = f_{ia}$ can be quite large, and single excitations can make substantial contributions to the first-order wave function and second-order energy. The same is true for restricted open-shell HF (ROHF) reference functions, which do not satisfy the usual Brillouin theorem either. Furthermore, including \hat{T}_1 and its disconnected cluster products in the wave function greatly reduces the sensitivity to orbital choice in CCSD and higher approximations, because the effect of $e^{\hat{T}_1}$ is to transform any single determinant into another single determinant. This property of $e^{\hat{T}_1}$ is known as the Thouless theorem (Thouless, 1960). However, including single excitations in truncated CI is not nearly as effective in reducing this sensitivity, because it leaves out most of the disconnected clusters involving \hat{T}_1 . Thus the inclusion of \hat{T}_1 introduces an important flexibility in CCSD and higher CC applications.

Another important reason for including single excitations, a reason that holds even for unrestricted and closed-shell restricted HF reference functions, has to do with the calculation of density matrices and associated properties. Such calculations involve matrix elements of various one-particle operators $\langle 0 | \hat{U} |_i^a \rangle$, which do not vanish in general even when HF orbitals are used. Single- and double-excitation contributions to such properties enter at the same order of perturbation theory, and should be treated on an equal footing.

To derive the CCSD equations, we substitute $\hat{T} = \hat{T}_1 + \hat{T}_2$ into (10.11) and (10.12). Arranging the resulting terms in approximate order of their importance, the equations take the form

$$\langle 0 | \hat{H}_N (\hat{T}_2 + \hat{T}_1 + \frac{1}{2} \hat{T}_1^2) | 0 \rangle_C = \Delta E, \quad (10.17)$$

$$\langle {}_i^a | \hat{H}_N (1 + \hat{T}_2 + \hat{T}_1 + \hat{T}_1 \hat{T}_2 + \frac{1}{2} \hat{T}_1^2 + \frac{1}{3!} \hat{T}_1^3) | 0 \rangle_C = 0, \quad (10.18)$$

$$\langle {}_{ij}^{ab} | \hat{H}_N (1 + \hat{T}_2 + \frac{1}{2} \hat{T}_2^2 + \hat{T}_1 + \hat{T}_1 \hat{T}_2 + \frac{1}{2} \hat{T}_1^2 + \frac{1}{2} \hat{T}_1^2 \hat{T}_2 + \frac{1}{3!} \hat{T}_1^3 + \frac{1}{4!} \hat{T}_1^4) | 0 \rangle_C = 0. \quad (10.19)$$

The energy equation (10.17) retains this form even in higher CC models, since clusters of more than two particles cannot contribute to the expectation value in this equation (because of the two-particle nature of \hat{H}_N). While the energy depends directly on the \hat{T}_1 and \hat{T}_2 amplitudes only, it is affected by the inclusion of connected triple, quadruple and higher excitations in higher CC models because these amplitudes are affected by the higher excitations through the coupled amplitude equations. The single-excitation equations (10.18) can include up to triple-excitation terms; however, in the CCSD model $\hat{T}_3 = 0$ so only *disconnected* triple-excitation clusters appear. Similarly, the double-excitation equations (10.19) contain disconnected triple- and quadruple-excitation terms but not \hat{T}_3 or \hat{T}_4 .

The “quadratic CI” analog of CCSD, the QCISD model of Pople, Head-Gordon and Raghavachari (1987), is an approximation to CCSD in which all terms containing \hat{T}_1 in (10.17)–(10.19), except the $\hat{T}_1 \hat{T}_2$ term in (10.18), are left out (Paldus, Čížek and Jeziorski 1989, 1990, Pople, Head-Gordon and Raghavachari 1989, Raghavachari, Head-Gordon and Pople 1990). However, the omission of these terms has negligible impact on the computational cost of the model and may, in some cases, adversely affect the quality of the results (Watts, Urban and Bartlett 1995).

Diagrammatically, the CCSD energy equation can be written

$$\Delta E = \text{diagram 1} + \text{diagram 2} + \text{diagram 3}. \quad (10.20)$$

As noted in the previous section, these three diagrams are *all* the distinct closed diagrams that can appear in any CC energy equation. The corresponding algebraic energy expression is

$$\Delta E = \frac{1}{4} \sum_{ijab} \langle ij || ab \rangle t_{ij}^{ab} + \sum_{ia} f_{ia} t_i^a + \frac{1}{2} \sum_{ijab} \langle ij || ab \rangle t_i^a t_j^b. \quad (10.21)$$

The last term can be combined with the first after splitting it into two terms and interchanging a and b in one of them, giving the antisymmetric form

$$\Delta E = \frac{1}{4} \sum_{ijab} \langle ij || ab \rangle (t_{ij}^{ab} + t_i^a t_j^b - t_i^b t_j^a) + \sum_{ia} f_{ia} t_i^a. \quad (10.22)$$

In the HF case $f_{ia} = 0$ and the last term in (10.22) vanishes.

The diagrams representing the single-excitation CCSD equations (10.18) are collected in Fig. 10.2. The numbering of the diagrams corresponds to the order of the terms in (10.18); the fixed labels i and a are understood for all open lines. The generation and interpretation of these diagrams is shown in Table 10.1, using the scheme introduced in Section 10.3 and the rules of interpretation (Fig. 10.1). The summations are over all the common indices

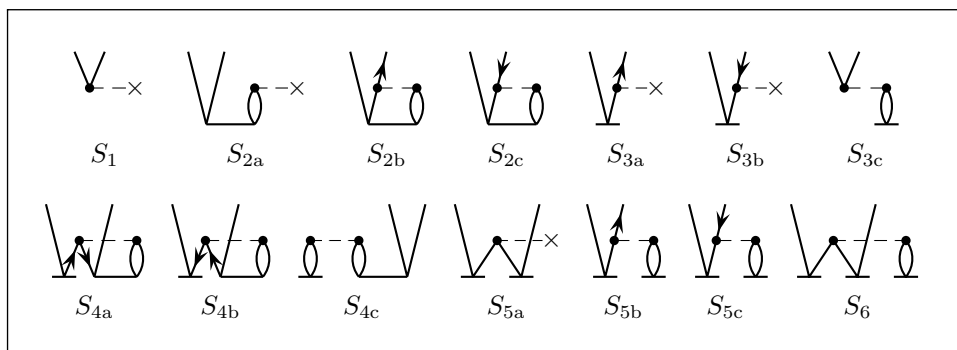


Fig. 10.2. Antisymmetrized Goldstone diagrams representing the CCSD \hat{T}_1 equations.

Table 10.1. *Generation and interpretation of diagrams for CCSD \hat{T}_1 amplitude equations (see (10.18))*

Interaction	Contractions	Diagram	Interpretation ^a
1 (no \hat{T} vertex, requires +1 interaction vertex)			
0	0	S_1	f_{ai}
\hat{T}_2 (vertex $++--$, requires -1 interaction vertex):			
$+-$	$+-$	S_{2a}	$\sum f_{kc} t_{ik}^{ac}$
$++--$	$++--$	S_{2b}	$\frac{1}{2} \sum \langle ak cd \rangle t_{ik}^{cd}$
$+- --$	$+- --$	S_{2c}	$-\frac{1}{2} \sum \langle kl ic \rangle t_{kl}^{ac}$
\hat{T}_1 (vertex $+-$, requires 0 interaction vertex):			
$+$	$+$	S_{3a}	$\sum f_{ac} t_i^c$
$-$	$-$	S_{3b}	$-\sum f_{ki} t_k^a$
$+-$	$+-$	S_{3c}	$\sum \langle ak ic \rangle t_k^c$
$\hat{T}_1 \hat{T}_2$ (vertices $+- ++--$, requires -2 interaction vertex):			
$++--$	$++--$	S_{4a}	$-\frac{1}{2} \sum \langle kl cd \rangle t_i^c t_{kl}^{ad}$
	$- ++--$	S_{4b}	$-\frac{1}{2} \sum \langle kl cd \rangle t_k^a t_{il}^{cd}$
	$+- ++--$	S_{4c}	$\sum \langle kl cd \rangle t_k^c t_{li}^{da}$
$\frac{1}{2} \hat{T}_1^2$ (vertices $+- +-$, requires -1 interaction vertex):			
$+-$	$+-$	S_{5a}	$-\sum f_{kc} t_i^c t_k^a$
$++--$	$++--$	S_{5b}	$\sum \langle ak cd \rangle t_i^c t_k^d$
$+- --$	$+- --$	S_{5c}	$-\sum \langle kl ic \rangle t_k^a t_l^c$
$\frac{1}{3!} \hat{T}_1^3$ (vertices $+- +- +-$, requires -2 interaction vertex):			
$++--$	$++--$	S_6	$-\sum \langle kl cd \rangle t_i^c t_k^a t_l^d$

^aIn this and all subsequent cases, the algebraic interpretation of the diagrams assumes that labels are assigned in alphabetical order, from left to right, within each class of lines (open particle lines, internal particle lines, open hole lines, internal hole lines), subject to the condition that a and i are on the same continuous path, so are b and j etc.

k, l, c, d that occur in each term. The single-excitation CCSD equations are then

$$\begin{aligned}
 & f_{ai} + \sum_{kc} f_{kc} t_{ik}^{ac} + \frac{1}{2} \sum_{kcd} \langle ak || cd \rangle t_{ik}^{cd} - \frac{1}{2} \sum_{klc} \langle kl || ic \rangle t_{kl}^{ac} + \sum_c f_{ac} t_i^c \\
 & - \sum_k f_{ki} t_k^a + \sum_{kc} \langle ak || ic \rangle t_k^c - \frac{1}{2} \sum_{klcd} \langle kl || cd \rangle t_i^c t_{kl}^{ad} - \frac{1}{2} \sum_{klcd} \langle kl || cd \rangle t_k^a t_{il}^{cd} \\
 & + \sum_{klcd} \langle kl || cd \rangle t_k^c t_{li}^{da} - \sum_{kc} f_{kc} t_i^c t_k^a + \sum_{kcd} \langle ak || cd \rangle t_i^c t_k^d \\
 & - \sum_{klc} \langle kl || ic \rangle t_k^a t_l^c - \sum_{klcd} \langle kl || cd \rangle t_i^c t_k^a t_l^d = 0 \quad (\text{for all } i, a). \quad (10.23)
 \end{aligned}$$

As in the CCD case, we separate the diagonal elements from the fifth and sixth terms in (10.23) (corresponding to diagrams S_{3a}, S_{3b}) and move them to the opposite side of the equation as $(f_{ii} - f_{aa})t_i^a = (\varepsilon_i - \varepsilon_a)t_i^a$, in order to set up an iterative solution. It is then obvious that the first approximation to t_i^a is

$$t_i^{a(1)} = \frac{f_{ai}}{\varepsilon_i - \varepsilon_a}, \quad (10.24)$$

and when this approximation is put into the energy expression it gives the second-order MBPT energy contribution from the single excitations,

$$\begin{array}{c} \text{---} \times \\ \text{---} \times \end{array} = \sum_{ia} \frac{|f_{ia}|^2}{\varepsilon_i - \varepsilon_a}. \quad (10.25)$$

In the Hartree–Fock case the first, second and eleventh terms of (10.23) (diagrams S_1, S_{2a}, S_{5a}) vanish, and so does the second-order energy contribution from the single excitations, (10.25). In the canonical HF case the off-diagonal parts of the fifth and sixth terms also vanish.

For the double-excitation part of the CCSD equations, we have already derived the contributions from the first three terms of (10.19), since those were present in CCD. The remaining terms are represented by the diagrams in Fig. 10.3. Diagrams D_{4a}, D_{4b} represent the linear \hat{T}_1 contributions to (10.19), while diagrams $D_{5a}–D_{5h}$ represent the quadratic $\hat{T}_1\hat{T}_2$ term. Another quadratic term, $\frac{1}{2}\hat{T}_1^2$, is represented by diagrams $D_{6a}–D_{6c}$. The two cubic terms, $\frac{1}{2}\hat{T}_1^2\hat{T}_2$ and $\frac{1}{3!}\hat{T}_1^3$, are represented by diagrams $D_{7a}–D_{7e}$ and D_{8a}, D_{8b} , respectively, while diagram D_9 represents the quartic term, $\frac{1}{4!}\hat{T}_1^4$.

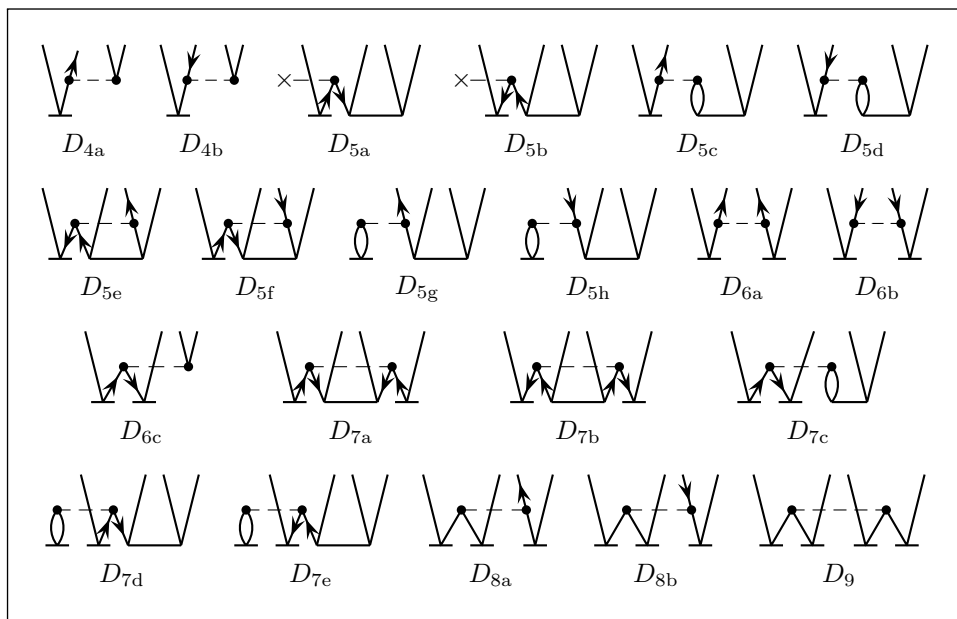
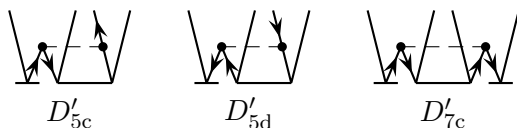


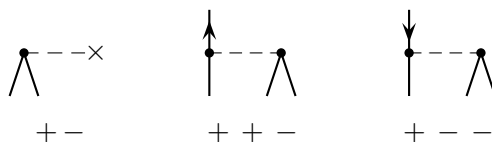
Fig. 10.3. Antisymmetrized Goldstone diagrams representing \hat{T}_1 contributions to the CCSD \hat{T}_2 equations.

Note that diagrams D_{5c} , D_{5d} and D_{7c} could also have been drawn in the equivalent forms



as can be verified by examining their $+$ and $-$ contraction patterns (or, equivalently, from the corresponding Hugenholtz-like forms).

The generation and interpretation of these diagrams is given in Table 10.2. As an illustration of the procedure we shall consider the $\hat{T}_1\hat{T}_2$ contribution. The cluster operators in this term provide a $+3$ excitation, and since we need a final $+2$ excitation for the \hat{T}_2 equations, we can only use the -1 components of the Hamiltonian. There are three such components,



from which the eight diagrams D_{5a} – D_{5h} are generated.

Table 10.2. *Generation and interpretation of diagrams for \hat{T}_1 contributions to CCSD \hat{T}_2 equations*

Interaction	Contractions	Diagram	Interpretation
\hat{T}_1 (vertex $+-$, requires $+1$ interaction vertex):			
$+$	$+$	D_{4a}	$\hat{P}(ij) \sum \langle ab cj \rangle t_i^c$
$-$	$-$	D_{4b}	$-\hat{P}(ab) \sum \langle kb ij \rangle t_k^a$
$\hat{T}_1 \hat{T}_2$ (vertices $+- ++ --$, requires -1 interaction vertex):			
$+-$	$+ -$	D_{5a}	$-\hat{P}(ij) \sum f_{kc} t_i^c t_{kj}^{ab}$
	$- +$	D_{5b}	$-\hat{P}(ab) \sum f_{kc} t_k^a t_{ij}^{cb}$
$++-$	$+ +-$	D_{5c}	$\hat{P}(ij ab) \sum \langle ak cd \rangle t_i^c t_{kj}^{db}$
	$- ++$	D_{5e}	$-\frac{1}{2} \hat{P}(ab) \sum \langle kb cd \rangle t_k^a t_{ij}^{cd}$
	$+ - +$	D_{5g}	$\hat{P}(ab) \sum \langle ka cd \rangle t_k^c t_{ij}^{db}$
$+- -$	$- +-$	D_{5d}	$-\hat{P}(ij ab) \sum \langle kl ic \rangle t_k^a t_{lj}^{cb}$
	$+ --$	D_{5f}	$\frac{1}{2} \hat{P}(ij) \sum \langle kl cj \rangle t_i^c t_{kl}^{ab}$
	$+ - -$	D_{5h}	$-\hat{P}(ij) \sum \langle kl ci \rangle t_k^c t_{lj}^{ab}$
$\frac{1}{2} \hat{T}_1^2$ (vertices $+- +-$, requires 0 interaction vertex):			
$++$	$+ +$	D_{6a}	$\frac{1}{2} \hat{P}(ij) \sum \langle ab cd \rangle t_i^c t_j^d = \sum \langle ab cd \rangle t_i^c t_j^d$
$--$	$- -$	D_{6b}	$\frac{1}{2} \hat{P}(ab) \sum \langle kl ij \rangle t_k^a t_l^b = \sum \langle kl ij \rangle t_k^a t_l^b$
$+-$	$+ -$	D_{6c}	$-\hat{P}(ij ab) \sum \langle kb cj \rangle t_i^c t_k^a$
$\frac{1}{2} \hat{T}_1^2 \hat{T}_2$ (vertices $+- +- +- --$, requires -2 interaction vertex):			
$++--$	$+ + -$	D_{7a}	$\frac{1}{4} \hat{P}(ij) \sum \langle kl cd \rangle t_i^c t_{kl}^{ab} t_j^d = \frac{1}{2} \sum \langle kl cd \rangle t_i^c t_{kl}^{ab} t_j^d$
	$- - ++$	D_{7b}	$\frac{1}{4} \hat{P}(ab) \sum \langle kl cd \rangle t_k^a t_{ij}^{cd} t_l^b = \frac{1}{2} \sum \langle kl cd \rangle t_k^a t_{ij}^{cd} t_l^b$
	$+ - +-$	D_{7c}	$-\hat{P}(ij ab) \sum \langle kl cd \rangle t_i^c t_k^a t_{lj}^{db}$
	$+ - + -$	D_{7d}	$-\hat{P}(ij) \sum \langle kl cd \rangle t_k^c t_i^a t_{lj}^{ab}$
	$+ - - +$	D_{7e}	$-\hat{P}(ab) \sum \langle kl cd \rangle t_k^c t_l^a t_{ij}^{db}$
$\frac{1}{3!} \hat{T}_1^3$ (vertices $+- +- +- -$, requires -1 interaction vertex):			
$++-$	$+ - +$	D_{8a}	$\frac{1}{2} \hat{P}(ij ab) \sum \langle kb cd \rangle t_i^c t_k^a t_j^d = \hat{P}(ab) \sum \langle kb cd \rangle t_i^c t_k^a t_j^d$
$+- -$	$+ - -$	D_{8b}	$\frac{1}{2} \hat{P}(ij ab) \sum \langle kl cj \rangle t_i^c t_k^a t_l^b = \hat{P}(ij) \sum \langle kl cj \rangle t_i^c t_k^a t_l^b$
$\frac{1}{4!} \hat{T}_1^4$ (vertices $+- +- +- +- -$, requires -2 interaction vertex):			
$++-$	$+ - +$	D_9	$\frac{1}{4} \hat{P}(ij ab) \sum \langle kl cd \rangle t_i^c t_j^d t_k^a t_l^b = \sum \langle kl cd \rangle t_i^c t_j^d t_k^a t_l^b$

The summations in the interpretation column of Table 10.2 are over the internal labels k, l, c, d present in each term. To clarify the interpretation rules further, it will be instructive to review some of the numerical coefficients and the permutation operators in the table in detail.

The factors $\frac{1}{2}$ in diagrams D_{5e} and D_{5f} result from the presence of a pair of equivalent internal lines. Diagrams D_{6a}, D_{6b} each have a pair of equivalent vertices (as shown by the contraction patterns) and a pair of external lines that are inequivalent (because they are connected to different vertices), resulting in a factor $\frac{1}{2}$ (rule 7, Fig. 10.1) and a permutation operator in each case. These two factors cancel with each other (rule 10), as shown in the table, since the permutation is equivalent to the relabeling of internal lines corresponding to dummy summation indices.

The factors $\frac{1}{4}$ in diagrams D_{7a}, D_{7b} arise because each diagram has one pair of equivalent internal lines and one pair of equivalent vertices (in diagram D_{7a} we use $+$ contractions for both \hat{T}_1 vertices while in D_{7b} we use $-$ contractions for both). One factor $\frac{1}{2}$ cancels with the permutation operator in each of these diagrams, as shown. In diagrams $D_{7c}-D_{7e}$ there are no equivalent lines and no equivalent vertices.

Diagrams D_{8a}, D_{8b} each have a pair of equivalent vertices, as can be seen from their contraction patterns, $++--$ and $+-+-$, respectively, and thus they acquire factors of $\frac{1}{2}$. These factors cancel with part of the $\hat{P}(ij|ab)$ permutation operator that results from the two pairs of inequivalent external lines. This cancellation is with the $\hat{P}(ij)$ operator in D_{8a} and with $\hat{P}(ab)$ in D_{8b} , as shown.

Diagram D_9 has two pairs of equivalent vertices (two vertices using a $+$ contraction and two using a $-$ contraction), resulting in a factor $\frac{1}{4}$ and two pairs of inequivalent external lines. Again, the $\hat{P}(ij|ab)$ permutation operator cancels with the factor $\frac{1}{4}$, since permuting a with b or i with j is equivalent to relabeling the internal lines.

Combining all the results in Table 10.2 together with those previously obtained for the CCD equations, the \hat{T}_2 amplitude equations for CCSD are obtained as

$$\begin{aligned}
 D_{\text{CCD}} + \hat{P}(ij) \sum_c \langle ab||cj \rangle t_i^c - \hat{P}(ab) \sum_k \langle kb||ij \rangle t_k^a - \hat{P}(ij) \sum_{kc} f_{kc} t_i^c t_{kj}^{ab} \\
 - \hat{P}(ab) \sum_{kc} f_{kc} t_k^a t_{ij}^{cb} + \hat{P}(ij|ab) \sum_{kcd} \langle ak||cd \rangle t_i^c t_{kj}^{db} \\
 - \hat{P}(ij|ab) \sum_{klc} \langle kl||ic \rangle t_k^a t_{lj}^{cb} - \frac{1}{2} \hat{P}(ab) \sum_{kcd} \langle kb||cd \rangle t_k^a t_{ij}^{cd}
 \end{aligned}$$

$$\begin{aligned}
& + \frac{1}{2} \hat{P}(ij) \sum_{klc} \langle kl || cj \rangle t_i^c t_{kl}^{ab} + \hat{P}(ab) \sum_{kcd} \langle ka || cd \rangle t_k^c t_{ij}^{db} \\
& - \hat{P}(ij) \sum_{klc} \langle kl || ci \rangle t_k^c t_{lj}^{ab} + \sum_{cd} \langle ab || cd \rangle t_i^c t_j^d + \sum_{kl} \langle kl || ij \rangle t_k^a t_l^b \\
& - \hat{P}(ij|ab) \sum_{kc} \langle kb || cj \rangle t_i^c t_k^a + \frac{1}{2} \sum_{klcd} \langle kl || cd \rangle t_i^c t_j^d t_{kl}^{ab} + \frac{1}{2} \sum_{klcd} \langle kl || cd \rangle t_k^a t_l^b t_{ij}^{cd} \\
& - \hat{P}(ij|ab) \sum_{klcd} \langle kl || cd \rangle t_i^c t_k^a t_{lj}^{db} - \hat{P}(ij) \sum_{klcd} \langle kl || cd \rangle t_k^c t_i^d t_{lj}^{ab} \\
& - \hat{P}(ab) \sum_{klcd} \langle kl || cd \rangle t_k^c t_l^a t_{ij}^{db} + \hat{P}(ab) \sum_{kcd} \langle kb || cd \rangle t_i^c t_k^d t_j^a \\
& + \hat{P}(ij) \sum_{klc} \langle kl || cj \rangle t_i^c t_k^a t_l^b + \sum_{klcd} \langle kl || cd \rangle t_i^c t_j^d t_k^a t_l^b \\
& = 0 \quad \text{for all } i > j, \ a > b,
\end{aligned} \tag{10.26}$$

where D_{CCD} stands for all the terms on the left-hand side of the CCD amplitude equations (9.126).

None of the terms in the CCSD equations raises the dependence of the computational cost on the number of spinorbitals over that of the CCD model. Thus the cost remains proportional to $n_h^2 n_p^4$ per iteration, or roughly an n^6 process.

10.5 Coupled-cluster singles, doubles and triples (CCSDT) equations

The importance of various cluster contributions to the wave function and to the energy is best judged in terms of the order of perturbation theory in which they first enter. As can be seen from Eqs. (9.78), (9.93), and (9.94), the only first-order contributions to the wave function come from single- and double-excitation configurations. Furthermore, the first-order single-excitation contribution vanishes in the HF case, in which the one-electron interaction operator \hat{f} is block diagonal. Therefore the lowest-order CC model is CCD, followed (particularly in non-HF cases) by CCSD. As previously discussed (see e.g. Section 10.4), these models include all the second- and third-order contributions to the energy.

The second-order wave function, (9.79), and the fourth-order energy add contributions from triple and quadruple excitations. In a CI expansion the most important second-order contribution to the wave function (at least in the HF case) comes from quadruple excitations and consists entirely of the disconnected-cluster $\frac{1}{2} \hat{T}_2^2$ term (diagram 8 in (9.79)), which is included in the

CCD and CCSD models. (The connected quadruple-excitation term \hat{T}_4 first enters in the third-order wave function and fifth-order energy.) However, the disconnected triple-excitation contribution to the second-order wave function (diagrams 18 and 19 in (9.79)) contains a one-electron interaction and vanishes in the HF case. Therefore the principal contribution to the CC wave function beyond the CCSD model is due to the connected triple-excitation cluster \hat{T}_3 (diagrams 6 and 7 in (9.79); see also (9.95)). This contribution enters the energy in fourth order, i.e. the same order as $\frac{1}{2}\hat{T}_2^2$. Thus the CCSDT model, which adds the terms containing \hat{T}_3 to CCSD, is the next level of improvement in CC methodology and is correct through the second-order wave function and fourth-order energy. Note also that \hat{T}_1 contributions that do not contain the one-electron interaction, and thus do not vanish even in the HF case, also enter the second-order wave function (diagrams 4 and 5 in (9.79), see also (9.93)) and the fourth-order energy.

The CCSDT wave function is

$$|\Psi_{\text{CCSDT}}\rangle = \exp(\hat{T}_1 + \hat{T}_2 + \hat{T}_3)|0\rangle. \quad (10.27)$$

The energy equation is the same as in the CCSD model, (10.17), though the \hat{T}_1 and \hat{T}_2 amplitudes that appear in the equation will be affected by the presence of the \hat{T}_3 operator in the amplitude equations. The CCSDT amplitude equations are

$$\langle_i^a|\hat{H}_N(1 + \hat{T}_2 + \hat{T}_1 + \hat{T}_1\hat{T}_2 + \frac{1}{2}\hat{T}_1^2 + \frac{1}{3!}\hat{T}_1^3 + \hat{T}_3)|0\rangle_C = 0, \quad (10.28)$$

$$\begin{aligned} \langle_{ij}^{ab}|\hat{H}_N(1 + \hat{T}_2 + \frac{1}{2}\hat{T}_2^2 + \hat{T}_1 + \hat{T}_1\hat{T}_2 + \frac{1}{2}\hat{T}_1^2 \\ + \frac{1}{2}\hat{T}_1^2\hat{T}_2 + \frac{1}{3!}\hat{T}_1^3 + \frac{1}{4!}\hat{T}_1^4 + \hat{T}_3 + \hat{T}_1\hat{T}_3)|0\rangle_C = 0, \end{aligned} \quad (10.29)$$

$$\begin{aligned} \langle_{ijk}^{abc}|\hat{H}_N(\hat{T}_2 + \hat{T}_3 + \frac{1}{2}\hat{T}_2^2 + \hat{T}_1\hat{T}_2 + \hat{T}_2\hat{T}_3 + \hat{T}_1\hat{T}_3 \\ + \frac{1}{2}\hat{T}_1^2\hat{T}_2 + \frac{1}{2}\hat{T}_1\hat{T}_2^2 + \frac{1}{2}\hat{T}_1^2\hat{T}_3 + \frac{1}{3!}\hat{T}_1^3\hat{T}_2)|0\rangle_C = 0. \end{aligned} \quad (10.30)$$

Note that \hat{T}_1 and its powers have been left out of (10.30) because they cannot produce connected triple-excitation diagrams with one interaction vertex.

The single-excitation equation has one new term added to the terms in the corresponding CCSD equation (10.18). This new term is represented by the diagram

$$\begin{array}{c} \diagup \\ \diagdown \\ \text{---} \end{array} \begin{array}{c} \bullet \\ \text{---} \end{array} \begin{array}{c} \bullet \\ \text{---} \end{array} \begin{array}{c} \diagup \\ \diagdown \\ \text{---} \end{array} = \frac{1}{4} \sum_{mnef} \langle mn || ef \rangle t_{imn}^{aef}. \quad (10.31)$$

S_7

The CCSDT singles equation can then be written as

$$S_{\text{CCSD}} + \frac{1}{4} \sum_{mnef} \langle mn || ef \rangle t_{imn}^{aef} = 0 \quad (\text{for all } i, a), \quad (10.32)$$

where S_{CCSD} stands for the entire left-hand side of the CCSD singles equation (10.23).

The doubles equation has two new terms, represented by the six diagrams in Fig. 10.4. The generation and interpretation of diagrams D_{10a} – D_{10c} , representing the term $\hat{H}_N \hat{T}_3$, is straightforward, giving the algebraic expressions

$$\sum_{me} f_{me} t_{ijm}^{abe} + \frac{1}{2} \hat{P}(ab) \sum_{mef} \langle bm || ef \rangle t_{ijm}^{aef} - \frac{1}{2} \hat{P}(ij) \sum_{mne} \langle mn || je \rangle t_{imn}^{abe}.$$

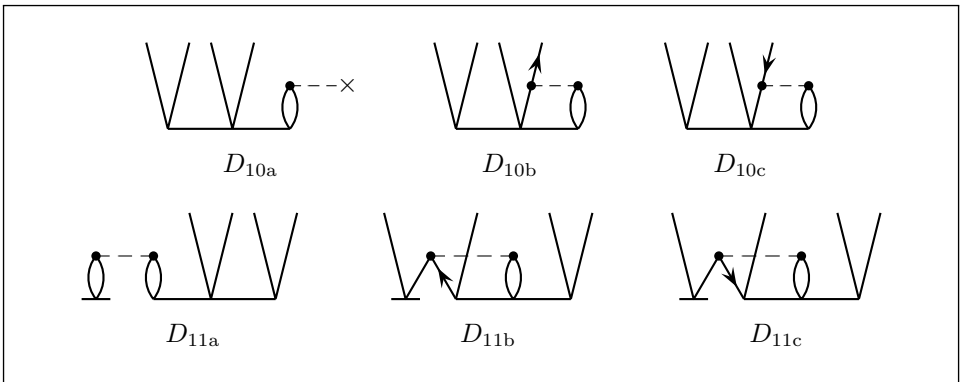


Fig. 10.4. Antisymmetrized Goldstone diagrams representing the \hat{T}_3 contributions to the CCSDT \hat{T}_2 equations.

For the diagrams representing $\hat{H}_N \hat{T}_1 \hat{T}_3$ we have

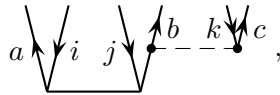
Vertices	Interaction	Contraction	Diagram
$+- ++++--$	$++--$	$+- +-$	$D_{11a} =$
		$- ++-$	$\sum \langle mn ef \rangle t_m^e t_{ni}^{fab}$
		$+ - - +$	$D_{11b} =$
			$-\hat{P}(ab) \sum \langle mn ef \rangle t_m^a t_{inj}^{efb}$
			$D_{11c} =$
			$-\hat{P}(ij) \sum \langle mn ef \rangle t_i^e t_{mnj}^{afb}$

The CCSDT doubles equation then takes the form

$$\begin{aligned}
 D_{\text{CCSD}} &+ \sum_{m,e} f_{me} t_{ijm}^{abe} + \frac{1}{2} \hat{P}(ab) \sum_{mef} \langle bm||ef \rangle t_{ijm}^{aef} \\
 &- \frac{1}{2} \hat{P}(ij) \sum_{mne} \langle mn||je \rangle t_{imn}^{abe} + \sum_{mnef} \langle mn||ef \rangle t_m^e t_{nij}^{fab} \\
 &- \hat{P}(ab) \sum_{mnef} \langle mn||ef \rangle t_m^a t_{inj}^{efb} - \hat{P}(ij) \sum_{mnef} \langle mn||ef \rangle t_i^e t_{mnj}^{afb} \\
 &= 0 \quad \text{for all } i > j, a > b,
 \end{aligned} \tag{10.33}$$

where D_{CCSD} stands for all the terms on the left-hand side of the CCSD doubles equation (10.26).

The triple-excitation CCSDT equation (10.30) has two linear, four quadratic and three cubic terms and one quartic term, which generate the 47 diagrams shown in Fig. 10.5. For the algebraic interpretation of these diagrams we introduce an extension of the notation for the permutation operators. Taking diagram T_{1a} as an example, and putting labels on the external lines,



we see that lines a and b are inequivalent, and so are a and c , but that b and c are quasi-equivalent. Thus we need to include the permutations \hat{P}_{ab} and \hat{P}_{ac} , but not \hat{P}_{bc} . We therefore define the permutation operator

$$\hat{P}(a/bc) = 1 - \hat{P}_{ab} - \hat{P}_{ac}. \tag{10.34}$$

Similarly, we need the operator $\hat{P}(k/ij) = 1 - \hat{P}_{ik} - \hat{P}_{jk}$; the total permutation operator for the diagram T_{1a} is $\hat{P}(a/bc|k/ij) = \hat{P}(a/bc)\hat{P}(k/ij)$. In contrast, in diagram T_{4c} all three open hole lines are inequivalent, requiring the permutation operator $\hat{P}(ijk|a/bc)$, in which all six permutations of i, j, k are included.

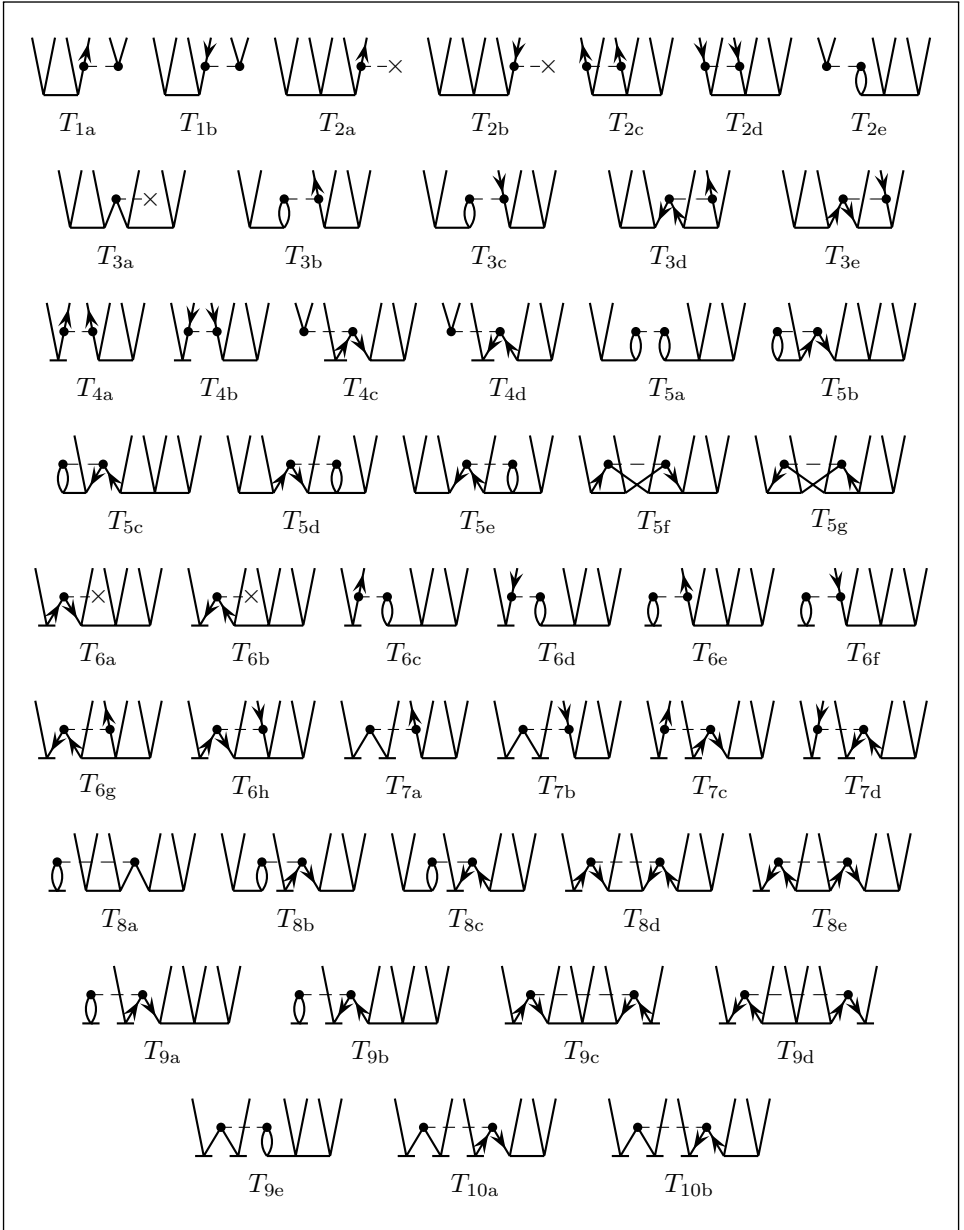


Fig. 10.5. Antisymmetrized Goldstone diagrams representing the CCSDT \hat{T}_3 equations.

The algebraic interpretation of the diagrams in Fig. 10.5, in corresponding order, is shown in Fig. 10.6, which gives the complete CCSDT triples equation. The summations are over those of the internal indices l, m, d, e that are present in each term. Note that diagrams T_{7c} , T_{7d} , T_{9c} , T_{9d} , T_{10a}

$$\begin{aligned}
& \hat{P}(k/ij|a/bc) \sum \langle bc \| dk \rangle t_{ij}^{ad} - \hat{P}(i/jk|c/ab) \sum \langle lc \| jk \rangle t_{il}^{ab} + \hat{P}(c/ab) \sum f_{cd} t_{ijk}^{abd} \\
& - \hat{P}(k/ij) \sum f_{lk} t_{ijl}^{abc} + \frac{1}{2} \hat{P}(c/ab) \sum \langle ab \| de \rangle t_{ijk}^{dec} + \frac{1}{2} \hat{P}(k/ij) \sum \langle lm \| ij \rangle t_{lmk}^{abc} \\
& + \hat{P}(i/jk|a/bc) \sum \langle al \| id \rangle t_{ijk}^{dbc} - \hat{P}(k/ij|a/bc) \sum f_{ld} t_{ijk}^{adl} \\
& + \hat{P}(i/jk|abc) \sum \langle lb \| de \rangle t_{il}^{ad} t_{jk}^{ec} - \hat{P}(ijk|a/bc) \sum \langle lm \| dj \rangle t_{il}^{ad} t_{mk}^{bc} \\
& - \frac{1}{2} \hat{P}(i/jk|c/ab) \sum \langle lc \| de \rangle t_{il}^{ab} t_{jk}^{de} + \frac{1}{2} \hat{P}(k/ij|a/bc) \sum \langle lm \| dk \rangle t_{ij}^{ad} t_{lm}^{bc} \\
& + \hat{P}(i/jk|c/ab) \sum \langle ab \| de \rangle t_i^{de} t_{jk}^{ec} + \hat{P}(k/ij|a/bc) \sum \langle lm \| ij \rangle t_i^{ab} t_{mk}^{bc} \\
& - \hat{P}(ijk|a/bc) \sum \langle al \| id \rangle t_j^{db} t_{lk}^{ec} - \hat{P}(i/jk|abc) \sum \langle al \| id \rangle t_l^{ba} t_{jk}^{dc} \\
& + \hat{P}(i/jk|a/bc) \sum \langle lm \| de \rangle t_{il}^{ad} t_{mjk}^{ebc} - \frac{1}{2} \hat{P}(i/jk) \sum \langle lm \| de \rangle t_l^{de} t_{mjk}^{abc} \\
& - \frac{1}{2} \hat{P}(a/bc) \sum \langle lm \| de \rangle t_{lm}^{da} t_{ijk}^{ebc} - \frac{1}{2} \hat{P}(k/ij|a/bc) \sum \langle lm \| de \rangle t_{ij}^{ad} t_{lmk}^{bec} \\
& - \frac{1}{2} \hat{P}(i/jk|c/ab) \sum \langle lm \| de \rangle t_{il}^{ab} t_{jmk}^{dec} + \frac{1}{4} \hat{P}(k/ij) \sum \langle lm \| de \rangle t_{ij}^{de} t_{lmk}^{abc} \\
& + \frac{1}{4} \hat{P}(c/ab) \sum \langle lm \| de \rangle t_{lm}^{ab} t_{ijk}^{dec} - \hat{P}(i/jk) \sum f_{ld} t_i^{ad} t_{jk}^{abc} - \hat{P}(a/bc) \sum f_{ld} t_l^{ad} t_{ijk}^{abc} \\
& + \hat{P}(i/jk|a/bc) \sum \langle al \| de \rangle t_i^{da} t_{jk}^{ebc} - \hat{P}(i/jk|a/bc) \sum \langle lm \| id \rangle t_l^{da} t_{mjk}^{ebc} \\
& + \hat{P}(a/bc) \sum \langle la \| de \rangle t_l^{da} t_{ijk}^{ebc} - \hat{P}(i/jk) \sum \langle lm \| di \rangle t_l^{da} t_{mjk}^{abc} \\
& - \frac{1}{2} \hat{P}(abc) \sum \langle lb \| de \rangle t_l^{da} t_{ijk}^{dec} + \frac{1}{2} \hat{P}(ijk) \sum \langle lm \| dj \rangle t_i^{da} t_{lmk}^{abc} \\
& - \hat{P}(i/jk|abc) \sum \langle lb \| de \rangle t_i^{da} t_{jk}^{ec} + \hat{P}(ijk|a/bc) \sum \langle lm \| dj \rangle t_i^{da} t_{lmk}^{abc} \\
& - \hat{P}(k/ij|a/bc) \sum \langle al \| de \rangle t_i^{da} t_{jk}^{ebc} + \hat{P}(i/jk|c/ab) \sum \langle lm \| id \rangle t_l^{da} t_{mjk}^{ebc} \\
& - \hat{P}(i/jk|c/ab) \sum \langle lm \| de \rangle t_{il}^{da} t_{im}^{ab} t_{jk}^{ec} - \hat{P}(ijk|a/bc) \sum \langle lm \| de \rangle t_{il}^{da} t_{jm}^{ebc} \\
& - \hat{P}(i/jk|abc) \sum \langle lm \| de \rangle t_{il}^{ad} t_m^{eb} t_{jk}^{ec} + \frac{1}{2} \hat{P}(i/jk|c/ab) \sum \langle lm \| de \rangle t_l^{da} t_{im}^{db} t_{jk}^{ec} \\
& + \frac{1}{2} \hat{P}(k/ij|a/bc) \sum \langle lm \| de \rangle t_l^{da} t_{ij}^{de} t_{mk}^{bc} - \hat{P}(i/jk) \sum \langle lm \| de \rangle t_l^{da} t_i^{eb} t_{mjk}^{abc} \\
& - \hat{P}(a/bc) \sum \langle lm \| de \rangle t_l^{da} t_m^{eb} t_{ijk}^{ec} + \frac{1}{2} \hat{P}(j/ik) \sum \langle lm \| de \rangle t_i^{da} t_{lm}^{ebc} t_k^e \\
& + \frac{1}{2} \hat{P}(b/ac) \sum \langle lm \| de \rangle t_l^{da} t_{ijk}^{dbe} t_m^{ec} - \hat{P}(i/jk|a/bc) \sum \langle lm \| de \rangle t_i^{da} t_l^{eb} t_{mjk}^{abc} \\
& + \hat{P}(k/ij|a/bc) \sum \langle lm \| de \rangle t_i^{da} t_l^{eb} t_{mjk}^{abc} + \hat{P}(i/jk|c/ab) \sum \langle lm \| de \rangle t_i^{da} t_l^{eb} t_m^{ec} t_{jk}^{ec} \\
& = 0 \quad (\text{for all } i > j > k, \ a > b > c)
\end{aligned}$$

Fig. 10.6. The CCSDT \hat{T}_3 equations.

Table 10.3. *Lowest wave-function orders at which triple-excitation CCSDT diagrams (Fig. 10.5) contribute*

Diagrams	Non-HF	Noncanonical HF	Canonical HF
T_{1a}, T_{1b}	2	2	2
T_{2a}, T_{2b} , diagonal	2	2	2
T_{2a}, T_{2b} , off-diag.	3	3	—
$T_{2c}-T_{2e}$	3	3	3
T_{3a}	3	—	—
$T_{3b}-T_{3e}$	3	3	3
$T_{4a}-T_{4d}$	3	4	4
$T_{5a}-T_{5g}$	4	4	4
T_{6a}, T_{6b}	4	—	—
$T_{6c}-T_{6h}$	4	5	5
$T_{7a}-T_{7d}$	4	6	6
$T_{8a}-T_{8e}$	4	5	5
$T_{9a}-T_{9e}$	5	7	7
T_{10a}, T_{10b}	5	8	8

and T_{10b} each have a pair of equivalent \hat{T}_1 vertices, and so the resulting factors $\frac{1}{2}$ cancel against part of the corresponding permutation operator. Specifically, the original factors for these diagrams, $-\frac{1}{2}\hat{P}(ijk|a/bc)$, $\frac{1}{2}\hat{P}(i/jk|abc)$, $\frac{1}{4}\hat{P}(ijk)$, $\frac{1}{4}\hat{P}(abc)$, $\frac{1}{2}\hat{P}(ijk|a/bc)$ and $\frac{1}{2}\hat{P}(i/jk|abc)$ (in order) become $-\hat{P}(k/ij|a/bc)$, $\hat{P}(i/jk|c/ab)$, $\frac{1}{2}\hat{P}(j/ik)$, $\frac{1}{2}\hat{P}(b/ac)$, $\hat{P}(k/ij|a/bc)$ and $\hat{P}(i/jk|c/ab)$, respectively.

The respective lowest wave-function orders at which the triple-excitation CCSDT diagrams contribute are listed in Table 10.3. Note that each \hat{T}_1 vertex is first order in the non-HF case but second order in the HF case (canonical or noncanonical), while the \hat{T}_2 and \hat{T}_3 vertices are first and second order, respectively. The diagonal part of the one-electron interaction vertex is zero order while the off-diagonal part is first order in general but does not contribute in the canonical HF case and contributes only for particle-particle and hole-hole vertices in the noncanonical HF case. The lowest energy order to which these diagrams contribute is two higher than

the wave-function order, since at least two interaction vertices are needed to close any of the triple-excitation diagrams.

The leading terms in the triple-excitation CCSDT equations (Fig. 10.5) are diagrams T_{1a}, T_{1b} and the diagonal parts of T_{2a}, T_{2b} , all of which are of second order. To set up an iterative sequence, following a similar procedure to that of previous cases we separate the diagonal part of each of diagrams T_{2a}, T_{2b} (the only nonzero part of these diagrams in the canonical HF case) and move it to the other side of the equation. Applying the permutation operators (see the third and fourth terms in Fig. 10.6), we get a total of six terms:

$$(\varepsilon_i + \varepsilon_j + \varepsilon_k - \varepsilon_a - \varepsilon_b - \varepsilon_c)t_{ijk}^{abc} = \varepsilon_{ijk}^{abc}t_{ijk}^{abc}.$$

The first attempt at including triple-excitation effects in the CC method used just the leading (second-order) terms in the CCSDT triples equations:

$$\varepsilon_{ijk}^{abc}t_{ijk}^{abc} = \hat{P}(a/bc|k/ij) \sum_d \langle bc||dk \rangle t_{ij}^{ad} - \hat{P}(c/ab|i/jk) \sum_l \langle lc||jk \rangle t_{il}^{ab}. \quad (10.35)$$

The t_{ijk}^{abc} amplitudes obtained from these equations were then substituted in the CCSDT singles and doubles equations (10.32), (10.33) but, because the \hat{T}_2 amplitudes enter in the right-hand side of (10.35), the solution required iteration of all three sets of equations. This model has been called CCSDT-1 (Lee and Bartlett 1984, Lee, Kucharski and Bartlett 1984) and has two variants, depending upon which diagrams involving a \hat{T}_3 vertex are included in the CCSDT doubles equations (Urban, Noga, Cole *et al.* 1985). The CCSDT-1a model includes the \hat{T}_3 contribution S_7 , (10.31), to the CCSDT singles equations, diagrams D_{10a} – D_{10c} (Fig. 10.4) in the CCSDT doubles equations, and diagrams T_{1a}, T_{1b} and T_{2a}, T_{2b} of the CCSDT triples equations. The CCSDT-1b model adds the remaining terms of the CCSDT doubles equations, diagrams D_{11a} – D_{11c} (Fig. 10.4). Diagram D_{10a} of the doubles equation vanishes in the HF case. The off-diagonal parts of diagrams T_{2a}, T_{2b} , which vanish in the canonical HF case, are included in other cases in order to maintain the invariance of the model to separate unitary transformations of the occupied and virtual orbitals. This invariance permits the removal of these off-diagonal parts by an orbital transformation to *semicanonical* orbitals, which diagonalizes the hole-hole and particle–

particle blocks of \hat{f} (without eliminating the off-diagonal blocks) (Handy, Pople, Head-Gordon *et al.* 1989, Watts, Gauss and Bartlett 1993).

The iterative process for the solution of the CCSDT-1 equations in the canonical HF case is shown diagrammatically in Fig. 10.7. Initially, the second-order approximation $t_{ijk}^{abc(2)}$ is obtained from the first-order approximations $t_{ij}^{ad(1)}$ and $t_{il}^{ab(1)}$, which, in turn, are just two-electron integrals divided by denominators, $\langle ad||ij \rangle / \varepsilon_{ij}^{ad}$ and $\langle ab||il \rangle / \varepsilon_{il}^{ab}$.

The evaluation of the \hat{T}_3 amplitudes from (10.35) in CCSDT-1 includes an $n_h^3 n_p^4$ step per iteration (diagram T_{1a} , the first term in Fig. 10.6), which may be compared with the $n_h^2 n_p^4$ process per iteration in CCD or CCSD. Except for the canonical HF case, there is another $n_h^3 n_p^4$ step per iteration for the off-diagonal part of T_{2a} . The insertion of the \hat{T}_3 amplitudes into diagrams D_{10b} and D_{10c} of the CCSDT doubles equations (10.33) includes yet another $n_h^3 n_p^4$ step per iteration. Besides the extra power of n_h , there also is the potential difficulty of having to store the $\sim n_h^3 n_p^3 t_{ijk}^{abc}$ amplitudes. Fortunately, it is possible to avoid this latter difficulty in the CCSDT-1 model (and also in the higher-order CCSDT-2 and CCSDT-3 models to be described later) by evaluating the contribution of each t_{ijk}^{abc} amplitude as soon as it is calculated from (10.35) to diagrams S_7 of the CCSDT singles equations and D_{10a} – D_{10c} (and, for CCSDT-1b, to D_{11a} – D_{11c}) of the CCSDT doubles equations (see Fig. 10.7).

In cases other than canonical HF (in this context these cases include restricted open-shell HF), the inclusion of the off-diagonal parts of diagrams T_{2a} , T_{2b} , besides adding another $n_h^3 n_p^4$ step, makes the triples amplitudes of each iteration dependent on the triples amplitudes of the previous iteration and thus requires the amplitudes to be stored. This difficulty can be eliminated by performing a semicanonical transformation, as already noted. The CCSDT-1 model is invariant under such a transformation provided that the full diagrams T_{2a} , T_{2b} are included. However, in the ROHF case this transformation destroys the equivalence of the spatial parts of the α -spin and β -spin orbitals, making the computational effort similar to that of a UHF-based calculation by precluding spin summations and essentially doubling the ranges of the various indices.

In all cases the full CCSDT method requires storage of the t_{ijk}^{abc} amplitudes. Moreover, the full CCSDT involves an $n_h^3 n_p^5$ step per iteration (diagram T_{2c} , the fifth term in Fig. 10.6). While the full CCSDT model has been implemented (Noga and Bartlett 1987, Trucks, Noga and Bartlett 1988), with inclusion of open-shell systems (Watts and Bartlett 1990), the CCSDT-1

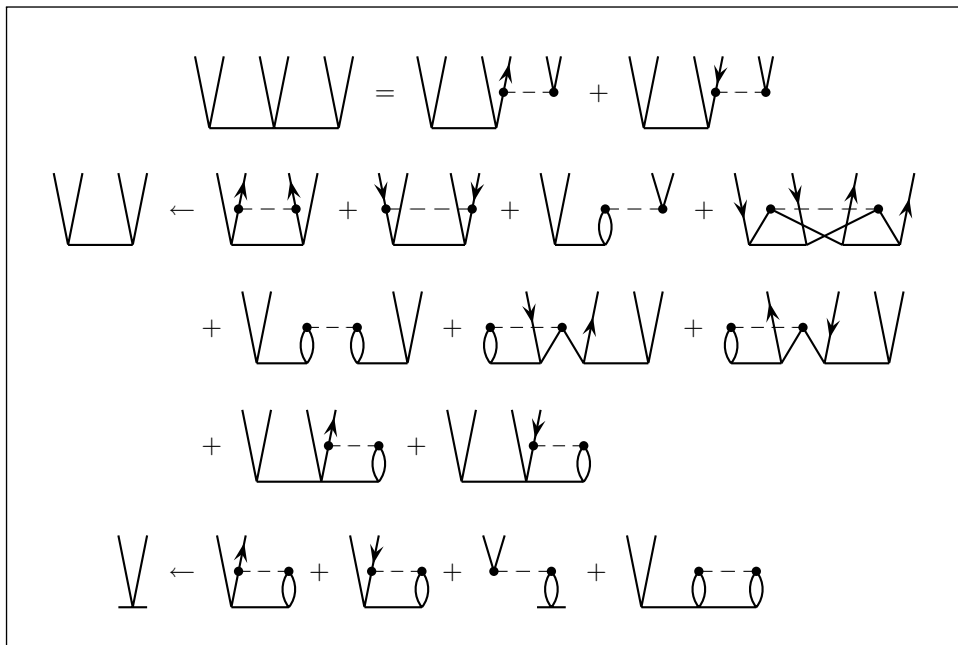


Fig. 10.7. One cycle in the CCSDT-1 iteration scheme (for the canonical Hartree–Fock case). The horizontal arrows indicate that the value of the expression on the r.h.s. is used as the next approximation for the l.h.s. in the iteration. As noted in the discussion following (9.126), a denominator corresponding to a resolvent line above each interaction vertex is to be understood for each diagram on the r.h.s. of the equations.

model and other CCSDT models have been developed in order to avoid the very high computational cost of the full CCSDT equations.

Typically, the number of iterations required to solve the CCSDT-1 equations is between 10 and 20, so a further approximation that eliminates the iterations in the evaluation and substitution of the t_{ijk}^{abc} amplitudes would result in a significant reduction in the computational cost. The simplest way to achieve this reduction would be to use the second-order $t_{ijk}^{abc(2)}$ amplitudes computed from the initial (first-order) $t_{ij}^{ad(1)}$ and $t_{il}^{ab(1)}$ amplitudes in all subsequent iterations of the CCSDT singles and doubles equations. As can be seen from the description of the iterative solution of the CCSDT-1 equations in Fig. 10.7, this procedure provides just the fourth-order triple-excitation contributions to the energy yet it requires two $n_h^3 n_p^4$ steps. However, the evaluation of triple-excitation contributions to the MBPT(4) energy requires only one $n_h^3 n_p^4$ step. This more economical MBPT evaluation is achieved, in effect, by “squaring” the $t_{ijk}^{abc(2)}$ quantity in the MBPT(4) procedure (see

Section 7.1); this is illustrated diagrammatically and algebraically by

$$E_T^{(4)} = \text{diagram} = \sum_{\substack{i>j>k \\ a>b>c}} t_{ijk}^{abc(2)*} t_{ijk}^{abc(2)} \varepsilon_{ijk}^{abc}. \quad (10.36)$$

This formula can be understood by writing the second-order \hat{T}_3 vertex as

$$\text{diagram} = \text{diagram}_1 + \text{diagram}_2 \quad (10.37)$$

and contracting it with its adjoint in all allowed ways, giving rise to the 16 MBPT triple-excitation antisymmetrized fourth-order energy diagrams (Fig. 5.9). The factor ε_{ijk}^{abc} is required to compensate for the fact that each $t_{ijk}^{abc(2)}$ carries one triple-excitation denominator.

Instead of using second-order \hat{T}_3 amplitudes in (10.36), we can employ \hat{T}_3 amplitudes obtained from (10.35) using *converged* CCSD \hat{T}_2 amplitudes. We designate these improved \hat{T}_3 amplitudes $t_{ijk}^{abc[2]}$, where the superscript [2] indicates a generalized order,

$$\text{diagram} = \text{diagram}_1 + \text{diagram}_2,$$

counting converged \hat{T}_2 amplitudes as first order since their initial appearance is in the first-order wave function. In the same sense we consider converged \hat{T}_1 amplitudes as second order in the HF case but first order otherwise, while \hat{T}_3 and \hat{T}_4 amplitudes are second and third order, respectively. Replacing just the bottom vertex in (10.36) by the improved $\hat{T}_3^{[2]}$ vertex provides the energy contributions of diagrams D_{10b} , D_{10c} subject to the use of (10.35) to define $\hat{T}_3^{[2]}$. This is exactly the contribution that would be obtained by adding these diagrams to the CCSD \hat{T}_2 amplitudes and including the added terms in the energy formula (10.21), as can be seen by using the adjoint of (10.37) for the top vertex. Also replacing the top vertex in (10.36) by the adjoint of the $\hat{T}_3^{[2]}$ vertex can be expected to provide additional higher-order corrections and may be justified in terms of an expectation-value form of the energy formula (Urban, Noga, Cole *et al.* 1985). The resulting expression can simply be added to the CCSD energy to provide an estimate of the CCSDT (or CCSDT-1) energy. This approximation leaves out energy contributions from diagrams S_7 and D_{10a} , and the effect of diagrams T_{2a} , T_{2b} on the \hat{T}_3 amplitudes, and is thus only suitable for the canonical HF case. It was first termed CCSD+T(CCSD), but is now known frequently as CCSD[T]

or, using a more complete terminology, CC4SD[T]. This notation implies infinite order in S and D and fourth order in T, the brackets in [T] being used to indicate the limitation to the HF case.

An extension of CC4SD[T] incorporating the energy contributions from diagram S_7 is known as CCSD(T) or CC4SD(T) (Raghavachari, Trucks, Pople *et al.* 1989) and can be generalized for non-HF cases by adding diagram D_{10a} (Watts, Gauss and Bartlett 1993), provided that a semicanonical transformation is first carried out to eliminate the off-diagonal parts of diagrams T_{2a} and T_{2b} (otherwise it would be necessary to iterate the evaluation of the triple-excitation amplitudes). This procedure includes all possible fourth-order contributions of single and double excitations subject to the simplified triples expression obtained from (10.35). Employing an approach similar to that used for the principal triples fourth-order energy contribution above in which lower-order singles and doubles amplitudes are replaced by their converged CCSD values, the resulting energy can be written as

$$E_{\text{CC4SD(T)}} = E_{\text{CCSD}} + E_{\text{T}}^{[4]} = E_{\text{CCSD}} + E_{\text{t}}^{[4]} + E_{\text{st}}^{[4]} + E_{\text{dt}}^{[4]}, \quad (10.38)$$

where

$$\begin{aligned} E_{\text{t}}^{[4]} &= \text{Diagram: A horizontal line with four vertical ovals (representing double excitations) connected in series.} \\ &= \frac{1}{36} \sum_{ijkabc} t_{ijk}^{abc[2]*} t_{ijk}^{abc[2]} \varepsilon_{ijk}^{abc} = \sum_{\substack{i>j>k \\ a>b>c}} t_{ijk}^{abc[2]*} t_{ijk}^{abc[2]} \varepsilon_{ijk}^{abc}, \end{aligned} \quad (10.39)$$

$$\begin{aligned} E_{\text{st}}^{[4]} &= \text{Diagram: A horizontal line with a large oval (double excitation) followed by two smaller ovals (single excitations) connected in series.} \\ &= \frac{1}{4} \sum_{ia} t_i^{a[1]*} \left\{ \sum_{jkb} \langle bc || jk \rangle t_{ijk}^{abc[2]} \right\} = \sum_{ia} t_i^{a[1]*} \left\{ \sum_{\substack{j>k \\ b>c}} \langle bc || jk \rangle t_{ijk}^{abc[2]} \right\}, \end{aligned} \quad (10.40)$$

$$\begin{aligned} E_{\text{dt}}^{[4]} &= \text{Diagram: A horizontal line with two large ovals (double excitations) connected in series, followed by a small oval (single excitation) and a cross symbol.} \\ &= \frac{1}{4} \sum_{ijab} t_{ij}^{ab[1]*} \left\{ \sum_{kc} f_{kc} t_{ijk}^{abc[2]} \right\} = \sum_{\substack{i>j \\ a>b}} t_{ij}^{ab[1]*} \left\{ \sum_{kc} f_{kc} t_{ijk}^{abc[2]} \right\}. \end{aligned} \quad (10.41)$$

The generalized orders (in superscript brackets) are for the non-HF case. In the HF case the order of the singles amplitudes becomes [2] instead of [1], and the E_{st} term is of order (5) while the E_{dt} term vanishes. In this case the

E_{st} term is small, and is the only difference between CCSD[T] and CCSD(T). While it is just one of many fifth-order terms that could contribute to the CCSDT energy, it is typically positive and serves to damp the sometimes excessive negative contribution of E_{T} in difficult cases. In our notation the (T) designation implies suitability to any type of reference function, in contrast with [T], which implies a restriction to the HF case. The CC4SD(T) model is common in quantum chemistry applications, since it is inexpensive enough to be usable for a large number of problems while providing results that are usually as accurate as can be obtained by any modern quantum chemistry method. All the approximations considered here for CCSDT are correct through fourth order in MBPT for both HF and non-HF cases, while containing many higher-order terms. Comparisons of numerical results for the different models will be presented later in Section 10.8.

The CCSDT-1 model, which led to the above noniterative approximations, includes all second-order terms in the triples equations. For higher accuracy we can consider the successive addition of further terms in these equations, see Figs. 10.5 and 10.6, culminating in the full CCSDT treatment. A systematic way to proceed would be to include all third-order terms in the triples equations (see Table 10.3). However, doing so requires the evaluation of diagrams $T_{2a}-T_{2e}$ (Fig. 10.5). Diagram T_{2a} introduces an $n_{\text{h}}^3 n_{\text{p}}^5$ step, which is one power of n_{p} higher than the costliest terms in CCSDT-1. The computational cost of this approach is, in fact, almost as high as that of full CCSDT, since it requires storage of the triple-excitation amplitudes and since the remaining terms in CCSDT are nonlinear and can be factored. Consequently, other strategies are recommended.

A characteristic of CC theory is that most linear terms, like diagrams T_{1a} , T_{1b} and $T_{2a}-T_{2e}$, tend to produce negative-energy contributions, while the contributions of the nonlinear terms tend to be positive. That is why LCCD, the linearized version of CCD, is usually lower in energy than CCD. Thus a sequence of linear approximations can often overestimate the correlation energy, as can happen for CCSDT-1. The CCSDT-2 model (Urban, Noga, Cole *et al.* 1985, Noga, Bartlett and Urban 1987) is an attempt to rectify this problem by adding the quadratic terms $T_{3a}-T_{3e}$ to the triples equations of CCSDT-1. Since these diagrams represent the $\frac{1}{2}\hat{T}_2^2$ term in (10.30), they should be the most important nonlinear terms. Furthermore, this model includes all purely \hat{T}_2 contributions to the \hat{T}_3 equations. The triples contributions to the \hat{T}_1 and \hat{T}_2 equation do not change, of course, as all such terms are already included in CCSDT-1b.

We can take this approach a step further by including all possible \hat{T}_1 and \hat{T}_2 contributions to the triples equation, adding diagrams $T_{4a}-T_{4d}$,

Table 10.4. *Approximations for $e^{\hat{T}}$ used in the equations in the CCSDT- n models (Urban, Noga, Cole et al. 1985).*

Equations	CCSDT-1a	CCSDT-1b	CCSDT-2	CCSDT-3
\hat{T}_1 , (10.28)	$e^{\hat{T}_1+\hat{T}_2+\hat{T}_3}$	$e^{\hat{T}_1+\hat{T}_2+\hat{T}_3}$	$e^{\hat{T}_1+\hat{T}_2+\hat{T}_3}$	$e^{\hat{T}_1+\hat{T}_2+\hat{T}_3}$
\hat{T}_2 , (10.29)	$e^{\hat{T}_1+\hat{T}_2} + \hat{T}_3$	$e^{\hat{T}_1+\hat{T}_2+\hat{T}_3}$	$e^{\hat{T}_1+\hat{T}_2+\hat{T}_3}$	$e^{\hat{T}_1+\hat{T}_2+\hat{T}_3}$
\hat{T}_3 , (10.30)	\hat{T}_2	\hat{T}_2	$e^{\hat{T}_2}$	$e^{\hat{T}_1+\hat{T}_2}$

T_{7a} – T_{7d} and T_{8a} – T_{8e} to those included in CCSDT-2. This choice defines the CCSDT-3 model (Urban, Noga, Cole *et al.* 1985, Noga, Bartlett and Urban 1987). Since the single excitations are instrumental in ensuring the insensitivity of CC theory to the choice of orbitals, the CCSDT-3 model benefits from the complete inclusion of their contributions by providing additional flexibility.

Because of the factorization of the nonlinear terms, the computational cost of both the CCSDT-2 and CCSDT-3 approximations is no worse than order $n_h^3 n_p^4$, and neither model requires the storage of the \hat{T}_3 amplitudes. All the iterative approximations to CCSDT can be characterized by the approximation to $e^{\hat{T}}$ implied by each model in each of the singles, doubles and triples equations, as shown in Table 10.4.

10.6 Coupled-cluster singles, doubles, triples and quadruples (CCSDTQ) equations

The state-of-the art in CC theory currently includes the CCSDTQ model (Kucharski and Bartlett 1992). Whereas CCSDT is correct through fourth order in the energy and second order in the wave function, CCSDTQ is correct through sixth order in the energy and third order in the wave function. This model introduces the connected \hat{T}_4 cluster, a third-order term contributing to the fifth-order energy. Compared with the CCSDT equations, new terms involving \hat{T}_4 appear in the doubles and triples CC amplitude equations, and a quadruples amplitude equation is added:

$$D_{\text{CCSDT}} + \langle_{ij}^{ab} | (\hat{H}_N \hat{T}_4)_C | 0 \rangle = 0, \quad (10.42)$$

$$T_{\text{CCSDT}} + \langle_{ijk}^{abc} | [\hat{H}_N (\hat{T}_4 + \hat{T}_1 \hat{T}_4)]_C | 0 \rangle = 0, \quad (10.43)$$

$$\langle ijkl | [\hat{H}_N(\hat{T}_3 + \hat{T}_4 + \hat{T}_1\hat{T}_3 + \hat{T}_1\hat{T}_4 + \frac{1}{2}\hat{T}_2^2 + \hat{T}_2\hat{T}_3 + \hat{T}_2\hat{T}_4 + \frac{1}{2}\hat{T}_3^2) + \frac{1}{3!}\hat{T}_2^3 + \frac{1}{2}\hat{T}_1^2\hat{T}_3 + \frac{1}{2}\hat{T}_1^2\hat{T}_4 + \frac{1}{2}\hat{T}_1\hat{T}_2^2 + \hat{T}_1\hat{T}_2\hat{T}_3 + \frac{1}{3!}\hat{T}_1^3\hat{T}_3 + \frac{1}{4}\hat{T}_1^2\hat{T}_2^2] | 0 \rangle_C = 0. \quad (10.44)$$

The new term in the doubles equation (10.42) is represented by

$$\underbrace{\text{Diagram}}_{D_{12}} = \frac{1}{4} \sum_{mnef} \langle mn || ef \rangle t_{ijmn}^{abef}. \quad (10.45)$$

The new terms in the triples equation (10.43) are represented by the diagrams in Fig. 10.8. Assigning labels in the diagrams from left to right in the order a, b, c and i, j, k to the open particle and hole lines, respectively, and e, f and m, n to internal particle and hole lines, respectively, the resulting triples equation takes the form

$$\begin{aligned} T_{\text{CCSDT}} &+ \sum_{me} f_{me} t_{ijkm}^{abce} + \frac{1}{2} P(c/ab) \sum_{mef} \langle cm || ef \rangle t_{ijkm}^{abef} \\ &- \frac{1}{2} P(k/ij) \sum_{mnf} \langle mn || kf \rangle t_{ijmn}^{abcf} + \sum_{mnef} \langle mn || ef \rangle t_m^e t_{nij}^{fabc} \\ &- \frac{1}{2} P(i/jk) \sum_{mnef} \langle mn || ef \rangle t_i^e t_{mnjk}^{afbc} \\ &- \frac{1}{2} P(a/bc) \sum_{mnef} \langle mn || ef \rangle t_m^a t_{injk}^{efbc} \\ &= 0 \quad \text{for all } i > j > k, a > b > c. \end{aligned} \quad (10.46)$$

The diagrams representing the \hat{T}_4 equation are shown in Fig. 10.9.

Analogously to the derivation of the CCSDT-1 model, we obtain the quadruples equation for the CCSDTQ-1 model (Kucharski and Bartlett 1989, 1998c) by taking the diagonal parts of diagrams Q_{2a} and Q_{2b} (Fig. 10.9)

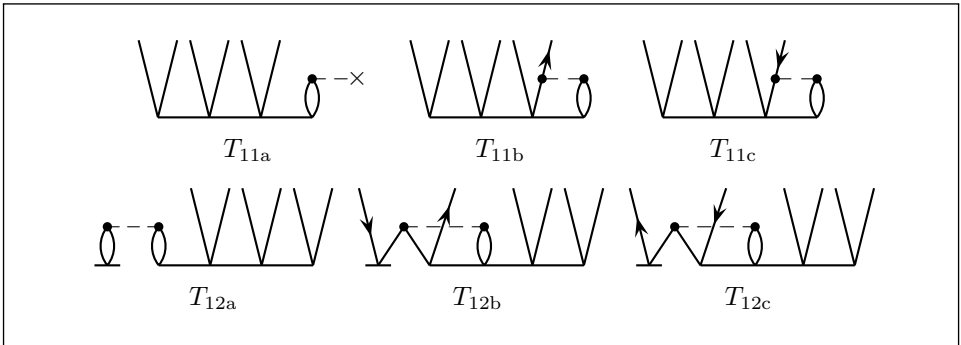


Fig. 10.8. Antisymmetrized Goldstone diagrams representing the \hat{T}_4 contributions to the CCSDTQ \hat{T}_3 equation



Fig. 10.9. Antisymmetrized Goldstone diagrams representing the CCSDTQ \hat{T}_4 equation.

to one side of the equation and retaining only the dominant terms, diagrams Q_{1a} , Q_{1b} and Q_{5a} – Q_{5c} , which are of third order, on the other side. The resulting equation is

$$\begin{aligned}
 \varepsilon_{ijkl}^{abcd} t_{ijkl}^{abcd} = & \hat{P}(ab/cd|ijk/l) \sum_e \langle cd||el \rangle t_{ijk}^{abe} \\
 & - \hat{P}(abc/d|ij/k/l) \sum_m \langle md||kl \rangle t_{ijm}^{abc} \\
 & + \frac{1}{2} \hat{P}(a/bc/d|ij/k/l) \sum_{ef} \langle bc||ef \rangle t_{ij}^{ae} t_{kl}^{fd} \\
 & + \frac{1}{2} \hat{P}(i/jk/l|ab/cd) \sum_{mn} \langle mn||jk \rangle t_{im}^{ab} t_{nl}^{cd} \\
 & - \hat{P}(ij/k/l|a/bc/d) \sum_{me} \langle md||el \rangle t_{ij}^{ae} t_{mk}^{bc}. \quad (10.47)
 \end{aligned}$$

In the permutation factors, the “/” notation separates groups of equivalent lines, so that permutations between the labels of these lines should be omitted. Thus, a permutation factor such as $\hat{P}(ab/cd|ijk/l)$ should be read as follows:

$$\begin{aligned}
 \hat{P}(ab/cd|ijk/l) &= \hat{P}(ab/cd) \hat{P}(ijk/l) \\
 &= (1 - \hat{P}_{ac} - \hat{P}_{ad} - \hat{P}_{bc} - \hat{P}_{bd} + \hat{P}_{ac} \hat{P}_{bd}) (1 - \hat{P}_{il} - \hat{P}_{jl} - \hat{P}_{kl}).
 \end{aligned}$$

Similarly, the factor $P(a/bc/d)$ implies all permutations of a, b, c, d except for any permutations that exchange the labels of equivalent lines (initially b and c),

$$\begin{aligned}
 \hat{P}(a/bc/d) &= 1 - \hat{P}_{ab} - \hat{P}_{ac} - \hat{P}_{ad} - \hat{P}_{bd} - \hat{P}_{cd} \\
 &\quad + \hat{P}_{ab} \hat{P}_{cd} + \hat{P}_{ac} \hat{P}_{bd} + \hat{P}_{bd} \hat{P}_{ad} + \hat{P}_{cd} \hat{P}_{ad} + \hat{P}_{ab} \hat{P}_{ad} + \hat{P}_{ac} \hat{P}_{ad}.
 \end{aligned}$$

In other words, we need to include all distinct assignments of target labels to the lines originally labeled a and d .

The factors $\frac{1}{2}$ in the third and fourth terms on the right-hand side of (10.47) (diagrams Q_{5a} and Q_{5b}) result from the fact that the two \hat{T}_2 vertices in each of these diagrams are equivalent (interpretation rule 7, Fig. 10.1). Using rule 10, these factors can be canceled with that arising from the permutation of labels a and d , resulting in the simplified form

$$\hat{P}(ad/bc|ij/k/l) \sum_{ef} \langle bc||ef \rangle t_{ij}^{ae} t_{kl}^{fd} + \hat{P}(il/jk|ab/cd) \sum_{mn} \langle mn||jk \rangle t_{im}^{ab} t_{nl}^{cd}$$

for these terms. However, to facilitate factorization of the sums, as discussed below, it is more convenient to use the form in (10.47).

It is clear from (10.47) that the \hat{T}_4 vertex arises in third order. To determine its initial contribution to the energy, we note that it affects the \hat{T}_2 amplitudes through diagram D_{12} , (10.45), and, since one interaction vertex is involved in this diagram, the effect here is of fourth order. When substituted in the energy equation (10.20), the result is a fifth-order contribution to the energy.

The CCSDTQ-1 model, as defined by (10.47) plus the inclusion of diagram D_{12} in the doubles equation, is correct through fifth order in the energy. It requires the evaluation of $\sim n_h^4 n_p^4$ amplitudes, each of which involves at most n_p terms (it is the first term on the r.h.s. of (10.47), corresponding to diagram Q_{1a}), resulting in an $\sim n_h^4 n_p^5$ procedure. As in other cases, the quadratic terms in (10.47) (diagrams Q_{5a} – Q_{5c}) can be factored and so do not raise the computational cost. Specifically, for the sum in the first quadratic term, diagram Q_{5a} , we can first sum over e ,

$$S_{ij}^{abcf} = \hat{P}(a/bc) \sum_e \langle bc || ef \rangle t_{ij}^{ae} \quad \text{for all } a > b > c, f, i > j,$$

and then evaluate

$$Q_{5a} = \frac{1}{2} \hat{P}(d/abc | ij/kl) \sum_f S_{ij}^{abcf} t_{kl}^{fd} \quad \text{for all } a > b > c > d, i > j > k > l,$$

an $\sim n_h^4 n_p^5$ procedure. In contrast, the complete CCSDTQ model results in an $\sim n_h^4 n_p^6$ procedure and requires the storage of $\sim n_h^4 n_p^4$ \hat{T}_4 amplitudes.

In non-HF cases we employ semicanonical orbitals to avoid the need to include the off-diagonal part of diagrams Q_{2a} and Q_{2b} and thus the need to store the \hat{T}_4 amplitudes, in analogy to CCSDT-1. In CCSDTQ-1 the \hat{T}_4 amplitudes can be calculated on the fly during the processing of the doubles equation, but the \hat{T}_3 amplitudes need to be stored. Note that the \hat{T}_4 contributions to the triples equation (10.43) (Fig. 10.8) result in energy contributions of sixth order for diagrams T_{11a} – T_{11c} and seventh order for diagrams T_{12a} – T_{12c} (eighth order in the HF case) and may thus be left out of CCSDTQ-1. A higher-level CCSDTQ-2 approximation, which is correct through sixth order in the energy, includes the $\hat{T}_2 \hat{T}_3$ and \hat{T}_2^3 terms in the quadruples equation (Kucharski and Bartlett 1993).

Analogously to the noniterative approximations for the triple-excitation contributions to CCSDT, we can also introduce a noniterative approximation for the quadruple-excitation contributions to CCSDTQ (Kucharski and Bartlett 1989, 1998c). We can obtain the fifth-order energy contribution of

the connected quadruple excitations by substituting diagram D_{12} , (10.45), into the energy equation (10.20); then, using the factorization techniques we get

$$\begin{aligned}
 \Delta E_Q^{(5)} &= \langle 0 | \hat{W} \hat{R}_0 \hat{W} \hat{T}_4^{(3)} | 0 \rangle_C = \text{diagram (3)} \\
 &= \frac{1}{2} \left\{ \text{diagram (3)} + \text{diagram (3)} \right\} \\
 &= \frac{1}{32} \sum_{abcd} \sum_{ijkl} \left\{ \frac{\langle ij || ab \rangle}{\varepsilon_{ij}^{ab}} \langle kl || cd \rangle + \frac{\langle kl || cd \rangle}{\varepsilon_{kl}^{cd}} \langle ij || ab \rangle \right\} t_{ijkl}^{abcd} \\
 &= \frac{1}{32} \sum_{abcd} \sum_{ijkl} \left\{ \frac{1}{\varepsilon_{ij}^{ab}} + \frac{1}{\varepsilon_{kl}^{cd}} \right\} \langle ij || ab \rangle \langle kl || cd \rangle t_{ijkl}^{abcd} \\
 &= \frac{1}{32} \sum_{abcd} \sum_{ijkl} \frac{\langle ij || ab \rangle}{\varepsilon_{ij}^{ab}} \frac{\langle kl || cd \rangle}{\varepsilon_{kl}^{cd}} \varepsilon_{ijkl}^{abcd} t_{ijkl}^{abcd}. \tag{10.48}
 \end{aligned}$$

Substituting for the last two factors from (10.47), we can write the result in the compact form

$$\Delta E_Q^{(5)} = \frac{1}{2} \langle 0 | (\hat{T}_2^{\dagger(1)})^2 [\hat{W}(\hat{T}_3 + \frac{1}{2}\hat{T}_2^2)] | 0 \rangle_C. \tag{10.49}$$

As in the CCSD(T) case, we can assume that closing the diagram with a final converged \hat{T}_2^{\dagger} vertex instead of its first-order approximation would provide a superior approximation. This is borne out by numerical studies (Kucharski and Bartlett 1998c) and alternative derivations based on the CC energy functional to be discussed in Section 12.7. The final estimate is the Q_f (factorized quadruples) correction,

$$\Delta E_{Q_f}^{[5]} = \frac{1}{2} \langle 0 | \hat{T}_2^{\dagger} \hat{T}_2^{\dagger(1)} [\hat{W}(\hat{T}_3 + \frac{1}{2}\hat{T}_2^2)] | 0 \rangle_C. \tag{10.50}$$

A very important feature of this approximation is that it requires only an $\sim n_h^3 n_p^4$ evaluation for the \hat{T}_3 part and roughly $\sim n^6$ for T_2^2 , instead of the $\sim n_h^4 n_p^5$ process of CCSDTQ-1. Since this approximation is used as a noniterative addition to a CCSDT calculation, the ultimate rate-determining step is in CCSDT itself, which is an $\sim n_h^3 n_p^5$ process. The method is termed CC5SDT(Q_f), indicating that it is fifth order in quadruples and infinite order in SDT. It does not change for non-HF cases, so it has the same

invariance properties as CC theory and the generalized CC4SD(T) of the previous section.

The type of factorization introduced here is not intrinsic to coupled-cluster theory, which does not have \hat{T}^\dagger terms in its defining equations. It derives from simplifications that are inherent in perturbation theory, related to Wigner's $2n + 1$ rule (subsection 2.2.6). To reduce the computational effort of the CC5SDT(Q_f) model further, we can couple (10.50) to one of the simpler CCSDT- n approximations.

Attempting to extend the Q_f approach from the noniterative CCSDT(Q_f) contribution to the iterative CCSDTQ-1 model, we soon encounter the problem that the factorization of the \hat{T}_4 energy diagram in (10.48) cannot be applied strictly to the corresponding wave-function diagram D_{12} , (10.45), of the \hat{T}_2 amplitude equation. Nevertheless, accepting the approximate nature of this factorization and replacing $[\hat{W}\hat{T}_4]_C|0\rangle$ in diagram D_{12} by $\{\frac{1}{2}\hat{T}_2^\dagger[\hat{W}(\hat{T}_3 + \frac{1}{2}\hat{T}_2^2)]\}_C|0\rangle$, as was done for $\Delta E_Q^{(5)}$ in (10.50), the \hat{T}_4 contribution to the double-excitation amplitude equation is replaced by $\frac{1}{2}\langle ab|\hat{T}_2^\dagger[\hat{W}(\hat{T}_3 + \frac{1}{2}\hat{T}_2^2)]|0\rangle_C$. The resulting model, labeled CCSDTQ_f-1 (Kucharski and Bartlett 1998c), incorporates the leading quadruple excitation effect in the amplitude equations without requiring any \hat{T}_4 diagrams or \hat{T}_4 equations. A lower-level approximation, CCSDQ_f, is obtained by adding $\frac{1}{4}\langle ab|\hat{T}_2^\dagger\hat{W}\hat{T}_2^2|0\rangle_C$ to the CCSD doubles equation, thus approximately incorporating a leading \hat{T}_4 contribution without including any \hat{T}_3 or \hat{T}_4 diagrams or equations.

The Q_f approximations involve a factorization of a connected-cluster diagram that is reminiscent of the factorization of linked quadruple-excitation diagrams in the fourth-order MBPT energy (Section 7.2). These approximations also indicate the potential for augmentation of the standard CC approach through alternative methods that involve the \hat{T}_4 operator, such as the unitary CC (UCC), the expectation value CC (XCC) and the extended CC *Ansätze* (Bartlett, Kucharski, Noga *et al.* 1989, Kutzelnigg 1977, Arponen and Bishop 1991, Van Voorhis and Head-Gordon 2000). Similar approaches could possibly be applied to \hat{T}_3 but, unlike \hat{T}_4 , the factorization of \hat{T}_3 would depend on \hat{T}_1 , which has a less important role in electron correlation than in orbital rotation (see Sections 12.2 and 12.3). However, the same approach can be applied to the \hat{T}_6 connected-cluster contributions to the \hat{T}_3 equation. At that level we would formally have a CCSDT procedure with implicit contributions from the connected \hat{T}_4 and \hat{T}_6 operators.

The iterative CCSDTQ_f-1 model and the noniterative CCSDT(Q_f) = CC5SDT(Q_f) and CCSD(TQ_f) = CC4SD(TQ_f) approximations have been applied to prototypical problems such as the vibrational frequencies of O₃

(Kucharski and Bartlett 1999) and the harmonic vibrational frequencies of N_2 and C_2 , for which an accuracy of 1 cm^{-1} relative to full CI was achieved after contributions from the fourth-order \hat{T}_5 operator had been included (Musiał, Kucharski and Bartlett 2000).

10.7 Coupled-cluster effective-Hamiltonian diagrams

A major reduction in the number of diagrams for the CC amplitude equations can be achieved by using diagrams representing the CC effective Hamiltonian $\mathcal{H} = (\hat{H}_{Ne}^{\hat{T}})_C$. These diagrams also provide valuable guidance for the efficient reuse of intermediates in the calculations.

The CC effective Hamiltonian can be expanded in terms of contributions with different numbers of creation and annihilation operators:

$$\begin{aligned} \mathcal{H} &= [H_N(1 + \hat{T}_1 + \hat{T}_2 + \dots + \frac{1}{2}\hat{T}_1^2 + \hat{T}_1\hat{T}_2 + \frac{1}{2}\hat{T}_2^2 + \dots)]_C \\ &= \chi_0 + \sum_{pq} \chi_{pq} \{\hat{p}^\dagger \hat{q}\} + \sum_{pqrs} \chi_{pqrs} \{\hat{p}^\dagger \hat{q}^\dagger \hat{s} \hat{r}\} \\ &\quad + \sum_{pqrst} \chi_{pqrst} \{\hat{p}^\dagger \hat{q}^\dagger \hat{r}^\dagger \hat{u} \hat{t} \hat{s}\} + \dots \end{aligned} \quad (10.51)$$

Here the constant term $\chi_0 = \Delta E$ corresponds to the $\hat{P}\mathcal{H}\hat{P}$ contribution, given diagrammatically in (10.20). This expansion separates \mathcal{H} into zero-body, one-body, two-body etc. terms. For an N -electron system the expansion terminates with the N -body term. Each term in (10.51) can be separated into parts involving different allocations of hole and particle indices. Thus, for the one-body term we have

$$\sum_{pq} \chi_{pq} \{\hat{p}^\dagger \hat{q}\} = \sum_{ab} \chi_{ab} \{\hat{a}^\dagger \hat{b}\} + \sum_{ai} \chi_{ai} \{\hat{a}^\dagger \hat{i}\} + \sum_{ai} \chi_{ia} \{\hat{i}^\dagger \hat{a}\} + \sum_{ij} \chi_{ij} \{\hat{i}^\dagger \hat{j}\}. \quad (10.52)$$

Using wavy lines to represent the \mathcal{H} vertices, we can diagram the various terms of the one-body contribution (10.52) as follows:

$$\chi_{ia} \{\hat{i}^\dagger \hat{a}\} \equiv \text{diagram} = \text{diagram}^{-\times} + \text{diagram}, \quad (10.53)$$

When we try to use intermediates from (10.53)–(10.55) in the expansion (10.56) we run into a complication: the third, fifth, tenth, eleventh and twelfth diagrams add up to

$$\text{Diagram 1} \quad (10.58)$$

The fourth, sixth, tenth, eleventh and thirteenth diagrams add up to

$$\text{Diagram 2} \quad (10.59)$$

If we used both these diagrams in the expansion we would be including twice the tenth and eleventh diagrams, which add up to

$$\text{Diagram 3}$$

To avoid this overcounting we define an intermediate,

$$\chi'_{ij} \{\hat{i}^\dagger \hat{j}\} \equiv \text{Diagram 4} = \text{Diagram 5} - \times + \text{Diagram 6} + j \text{Diagram 7} \quad (10.60)$$

Using this intermediate we can rewrite (10.55), (10.56) as

$$\chi_{ij} \{\hat{i}^\dagger \hat{j}\} \equiv \text{Diagram 8} = \text{Diagram 9} + j \text{Diagram 10} \quad (10.61)$$

$$\begin{aligned} \chi_{ai} \{\hat{a}^\dagger \hat{i}\} &\equiv \text{Diagram 11} \\ &= \text{Diagram 12} - \times + \text{Diagram 13} + a \text{Diagram 14} + i \text{Diagram 15} \\ &\quad + i \text{Diagram 16} + a \text{Diagram 17} + a \text{Diagram 18} + a \text{Diagram 19} \end{aligned} \quad (10.62)$$

In (10.62) the third diagram represents the sum of the third, fifth and twelfth diagrams of (10.56), the fourth represents the sum of the fourth, sixth, tenth, eleventh and thirteenth diagrams of (10.56) and the seventh represents the sum of the ninth and fourteenth diagrams of (10.56). This representation provides a compact pseudolinear form for the CC singles equation. The two-body matrix elements and intermediates are obtained in a similar manner:

$$\chi_{ijab} \{\hat{i}^\dagger \hat{j}^\dagger \hat{b} \hat{a}\} \equiv \text{Diagram 20} = \text{Diagram 21} \quad (10.63)$$

$$\chi'_{aibc} \{\hat{a}^\dagger \hat{i}^\dagger \hat{c} \hat{b}\} \equiv \text{diagram} = \text{diagram} + \frac{1}{2} \text{diagram}, \quad (10.64)$$

$$\chi_{aibc} \{\hat{a}^\dagger \hat{i}^\dagger \hat{c} \hat{b}\} \equiv \text{diagram} = \text{diagram} + \text{diagram}, \quad (10.65)$$

$$\chi'_{ikja} \{\hat{i}^\dagger \hat{k}^\dagger \hat{a} \hat{j}\} \equiv \text{diagram} = \text{diagram} + \frac{1}{2} \text{diagram}, \quad (10.66)$$

$$\chi_{ikja} \{\hat{i}^\dagger \hat{k}^\dagger \hat{a} \hat{j}\} \equiv \text{diagram} = \text{diagram} + \text{diagram}, \quad (10.67)$$

$$\begin{aligned} \chi'_{abcd} \{\hat{a}^\dagger \hat{b}^\dagger \hat{d} \hat{c}\} &\equiv \text{diagram} = \text{diagram} + \text{diagram} + \text{diagram} \\ &= \text{diagram} + \text{diagram}, \end{aligned} \quad (10.68)$$

$$\begin{aligned} \chi_{abcd} \{\hat{a}^\dagger \hat{b}^\dagger \hat{d} \hat{c}\} &\equiv \text{diagram} \\ &= \text{diagram} + \text{diagram} + \text{diagram} + \text{diagram} \\ &= \text{diagram} + \text{diagram}, \end{aligned} \quad (10.69)$$

$$\begin{aligned} \chi_{ijkl} \{\hat{i}^\dagger \hat{j}^\dagger \hat{l} \hat{k}\} &\equiv \text{diagram} \\ &= \text{diagram} + \text{diagram} + \text{diagram} + \text{diagram} \\ &= \text{diagram} + \text{diagram}, \end{aligned} \quad (10.70)$$

$$\begin{aligned}
\chi'_{ajib} \{\hat{a}^\dagger \hat{j}^\dagger \hat{b} \hat{i}\} &\equiv \text{diagram 1} \\
&= \text{diagram 2} + \frac{1}{2} \text{diagram 3} + \text{diagram 4} + \frac{1}{2} \text{diagram 5} \\
&= \text{diagram 6} + \frac{1}{2} \text{diagram 7} + \text{diagram 8},
\end{aligned} \tag{10.71}$$

$$\begin{aligned}
\chi''_{ajib} \{\hat{a}^\dagger \hat{j}^\dagger \hat{b} \hat{i}\} &\equiv \text{diagram 1} \\
&= \text{diagram 2} + \frac{1}{2} \text{diagram 3} + \frac{1}{2} \text{diagram 4} + \frac{1}{4} \text{diagram 5} \\
&= \text{diagram 6} + \frac{1}{2} \text{diagram 7} + \frac{1}{2} \text{diagram 8},
\end{aligned} \tag{10.72}$$

$$\begin{aligned}
\chi'''_{ajib} \{\hat{a}^\dagger \hat{j}^\dagger \hat{b} \hat{i}\} &\equiv \text{diagram 1} \\
&= \text{diagram 2} + \text{diagram 3} + \frac{1}{2} \text{diagram 4} + \frac{1}{2} \text{diagram 5} \\
&= \text{diagram 6} + \text{diagram 7} + \frac{1}{2} \text{diagram 8},
\end{aligned} \tag{10.73}$$

$$\begin{aligned}
\chi_{ajib} \{\hat{a}^\dagger \hat{j}^\dagger \hat{b} \hat{i}\} &\equiv \text{diagram 1} = \text{diagram 2} + \text{diagram 3} + \text{diagram 4} \\
&\quad + \text{diagram 5} + \text{diagram 6} \\
&= \text{diagram 7} + \frac{1}{2} \text{diagram 8} + \text{diagram 9},
\end{aligned} \tag{10.74}$$

$$\begin{aligned}
\chi''_{iajk} \{\hat{i}^\dagger \hat{a}^\dagger \hat{k} \hat{j}\} &\equiv \text{diagram 1} \\
&= \text{diagram 2} + \text{diagram 3} + \text{diagram 4} + \text{diagram 5} \\
&\quad + \text{diagram 6} + \text{diagram 7} + \text{diagram 8} + \text{diagram 9} \\
&\quad + \text{diagram 10} + \text{diagram 11} + \text{diagram 12} \\
&= \text{diagram 13} + \text{diagram 14} + \text{diagram 15} + \text{diagram 16} \\
&\quad + \text{diagram 17} + \text{diagram 18},
\end{aligned} \tag{10.78}$$

$$\begin{aligned}
\chi_{iajk} \{\hat{i}^\dagger \hat{a}^\dagger \hat{k} \hat{j}\} &\equiv \text{diagram 19} \\
&= \text{diagram 20} + \text{diagram 21} + \text{diagram 22} + \text{diagram 23} \\
&\quad + \text{diagram 24} + \text{diagram 25} + \text{diagram 26} + \text{diagram 27} \\
&\quad + \text{diagram 28} + \text{diagram 29} + \text{diagram 30} \\
&= \text{diagram 31} + \text{diagram 32}.
\end{aligned} \tag{10.79}$$

The interpretation rules for these diagrams are the same as those for the ordinary CC diagrams, Fig. 10.1, including the use of permutation

operators $\hat{P}(ij \cdots | ab \cdots)$ etc. for inequivalent open-line labels, according to rules 8 and 9, but labels on lines open at the top are never permuted with labels of lines open at the bottom. For example, the permutation operator $\hat{P}(ab) = 1 - \hat{P}_{ab}$ is applied to the second diagram for χ_{abcd} in the second line of (10.69), but in the third diagram the same operator cancels with the factor due to the pair of equivalent vertices. The intermediates χ'_{aibc} etc. are needed to avoid overcounting and to obtain the correct weights for diagrams with equivalent \hat{T} vertices. For example, if we had used the full expression for χ_{ikja} in the second diagram in the third line of (10.70), instead of the intermediate χ'_{ikja} , then the permutation operator $\hat{P}(kl)$ would have introduced the third diagram of the second line in two equivalent forms.

Like the case of the final one-body matrix element χ_{ai} , (10.56), the final two-body matrix element χ_{abij} expands to a sum of all the CC double-excitation diagrams, Figs. 9.2, 10.3, 10.4 and (10.45), and should add up to zero when the CC equations are satisfied. Using the various matrix elements and intermediates, it condenses to the pseudolinear form

$$\begin{aligned}
 \chi_{abij} \{\hat{a}^\dagger \hat{b}^\dagger \hat{j} \hat{i}\} &\equiv \text{diagram with vertices } a, i, j, b \text{ and wavy lines } i, j \\
 &= \text{diagram 1} + \text{diagram 2} + \text{diagram 3} \\
 &\quad + \text{diagram 4} + \text{diagram 5} + \text{diagram 6} \\
 &\quad + \text{diagram 7} + \text{diagram 8} + \text{diagram 9} \\
 &\quad + \text{diagram 10} + \text{diagram 11} + \text{diagram 12} .
 \end{aligned}
 \tag{10.80}$$

This form is untruncated, and no additional double-excitation diagrams would appear at any level of CC theory. Obviously, the last three diagrams would not be included in a CCSD calculation and the last diagram would be omitted in CCSDT. The corresponding untruncated three-body matrix element, which is equal to the sum of all the diagrams for the triple-excitation equations (Figs. 10.5 and 10.8 plus one diagram involving \hat{T}_5), can

$$\begin{aligned}
\chi'_{iabjkl} \{\hat{i}^\dagger \hat{a}^\dagger \hat{b}^\dagger \hat{l} \hat{k} \hat{j}\} &\equiv \text{diagram 1} \\
&= \frac{1}{2} \text{diagram 2} + \text{diagram 3} \\
&\quad + \text{diagram 4} + \text{diagram 5} \\
&\quad + \text{diagram 6}, \tag{10.83}
\end{aligned}$$

$$\chi'_{ibcajk} \{\hat{i}^\dagger \hat{b}^\dagger \hat{b}^\dagger \hat{k} \hat{j} \hat{a}\} \equiv \text{diagram 1} = \text{diagram 2}, \tag{10.84}$$

$$\chi'_{ijaklm} \{\hat{i}^\dagger \hat{j}^\dagger \hat{a}^\dagger \hat{k} \hat{l} \hat{m}\} \equiv \text{diagram 1} = \text{diagram 2}. \tag{10.85}$$

These intermediates are parts of the complete three-body matrix elements of \mathcal{H} , which are presented later in this section.

Using these intermediates, the untruncated four-body matrix element that defines the quadruple-excitation equation, representing all the diagrams in Fig. 10.9 plus diagrams containing \hat{T}_5 or \hat{T}_6 , is obtained as:

$$\begin{aligned}
\chi_{abcdijkl} \{\hat{a}^\dagger \hat{b}^\dagger \hat{c}^\dagger \hat{d}^\dagger \hat{l} \hat{k} \hat{j} \hat{i}\} &\equiv \text{diagram 1} \\
&= \text{diagram 2} + \text{diagram 3} \\
&\quad + \text{diagram 4} + \text{diagram 5} \\
&\quad + \text{diagram 6} + \text{diagram 7} \\
&\quad + \text{diagram 8} + \text{diagram 9} \\
&\quad + \text{diagram 10} + \text{diagram 11} \\
&\quad + \text{diagram 12} + \text{diagram 13}
\end{aligned}$$

$$\begin{aligned}
& + a \begin{array}{c} \swarrow i \searrow j \\ \swarrow b \searrow c \\ \swarrow k \searrow l \end{array} + i \begin{array}{c} \swarrow a \searrow b \\ \swarrow j \searrow k \\ \swarrow c \searrow d \end{array} \\
& + i \begin{array}{c} \swarrow a \searrow b \\ \swarrow j \searrow k \\ \swarrow c \searrow d \end{array} . \quad (10.86)
\end{aligned}$$

For later use in Chapters 11 and 13, we also present below the diagrams for the complete three-body and some four-body matrix elements of \mathcal{H} . Note that there can be no \mathcal{H} -matrix elements with four or more lines below the vertex, except for the single two-body element $\text{---}\text{---}\text{---}\text{---} = \text{---}\text{---}$, because \hat{T} -vertex lines can only be open at the top. The three-body elements are:

$$\chi_{ajbcdi} \{ \hat{a}^\dagger \hat{j}^\dagger \hat{b}^\dagger \hat{i} \hat{d} \hat{c} \} \equiv \begin{array}{c} a \swarrow \searrow i \\ \swarrow j \searrow d \\ \swarrow b \searrow c \end{array} = j \begin{array}{c} \swarrow a \searrow b \\ \swarrow \bar{d} \searrow \bar{c} \end{array} , \quad (10.87)$$

$$\chi_{ijakbl} \{ \hat{i}^\dagger \hat{j}^\dagger \hat{a}^\dagger \hat{l} \hat{b} \hat{k} \} \equiv \begin{array}{c} k \swarrow \searrow l \\ \swarrow j \searrow b \\ \swarrow i \searrow a \end{array} = b \begin{array}{c} \swarrow j \searrow \bar{i} \\ \swarrow k \searrow l \end{array} , \quad (10.88)$$

$$\begin{aligned}
\chi_{ibcajk} \{ \hat{i}^\dagger \hat{b}^\dagger \hat{c}^\dagger \hat{k} \hat{j} \hat{a} \} & \equiv \begin{array}{c} b \swarrow \searrow j \searrow c \\ \swarrow i \searrow a \end{array} \\
& = \begin{array}{c} j \swarrow \searrow b \searrow c \\ \swarrow i \searrow a \end{array} + \begin{array}{c} b \swarrow \searrow j \searrow c \\ \swarrow i \searrow a \end{array} \\
& + \begin{array}{c} b \swarrow \searrow j \searrow c \\ \swarrow i \searrow \bar{a} \end{array} , \quad (10.89)
\end{aligned}$$

$$\begin{aligned}
\chi_{abcdei} \{ \hat{a}^\dagger \hat{b}^\dagger \hat{c}^\dagger \hat{i} \hat{e} \hat{d} \} & \equiv \begin{array}{c} a \swarrow \searrow b \searrow c \searrow i \\ \swarrow d \searrow e \end{array} \\
& = \begin{array}{c} a \swarrow \searrow b \searrow c \searrow i \\ \swarrow d \searrow e \end{array} + \begin{array}{c} a \swarrow \searrow \bar{d} \searrow \bar{e} \searrow b \searrow c \searrow i \end{array} , \quad (10.90)
\end{aligned}$$

$$\begin{aligned}
\chi_{ijaklm} \{ \hat{i}^\dagger \hat{j}^\dagger \hat{a}^\dagger \hat{k} \hat{l} \hat{m} \} & \equiv \begin{array}{c} k \swarrow \searrow l \searrow m \searrow a \\ \swarrow i \searrow j \end{array} \\
& = \begin{array}{c} k \swarrow \searrow l \searrow m \searrow a \\ \swarrow i \searrow j \end{array} + \begin{array}{c} k \swarrow \searrow \bar{i} \searrow \bar{j} \searrow l \searrow m \searrow a \end{array} , \quad (10.91)
\end{aligned}$$

$$\begin{aligned}
\chi_{abcdij} \{\hat{a}^\dagger \hat{b}^\dagger \hat{c}^\dagger \hat{j} \hat{i} \hat{d}\} &\equiv \text{diagram 1} \\
&= \text{diagram 2} + \text{diagram 3} \\
&+ \text{diagram 4} + \text{diagram 5} \\
&+ \text{diagram 6} + \text{diagram 7},
\end{aligned} \tag{10.92}$$

$$\begin{aligned}
\chi_{iabjkl} \{\hat{i}^\dagger \hat{a}^\dagger \hat{b}^\dagger \hat{l} \hat{k} \hat{j}\} &\equiv \text{diagram 1} \\
&= \text{diagram 2} + \text{diagram 3} \\
&+ \text{diagram 4} + \text{diagram 5} \\
&+ \text{diagram 6} + \text{diagram 7}.
\end{aligned} \tag{10.93}$$

Only three four-body vertices will be needed. They are:

$$\chi_{akbcdeij} \{\hat{a}^\dagger \hat{k}^\dagger \hat{b}^\dagger \hat{c}^\dagger \hat{j} \hat{i} \hat{e} \hat{d}\} \equiv \text{diagram 1} = \text{diagram 2}, \tag{10.94}$$

$$\chi_{ijabkclm} \{\hat{i}^\dagger \hat{j}^\dagger \hat{a}^\dagger \hat{b}^\dagger \hat{m} \hat{l} \hat{c} \hat{k}\} \equiv \text{diagram 1} = \text{diagram 2}, \tag{10.95}$$

$$\begin{aligned}
\chi_{ibcda jkl} \{\hat{i}^\dagger \hat{b}^\dagger \hat{c}^\dagger \hat{d}^\dagger \hat{l} \hat{k} \hat{j} \hat{a}\} &\equiv \text{diagram 1} \\
&= \text{diagram 2} + \text{diagram 3} \\
&\quad + \text{diagram 4} + \text{diagram 5} .
\end{aligned}
\tag{10.96}$$

The diagrams are Feynman-like diagrams representing many-body terms. Diagram 1 is a wavy line with four vertices labeled b, j, k, c, d, l and a horizontal line with vertices i, a . Diagram 2 is a solid line with four vertices labeled j, b, c, k, l, d and a horizontal line with vertices i, a . Diagram 3 is a solid line with four vertices labeled b, j, k, c, d, l and a horizontal line with vertices i, a . Diagram 4 is a solid line with four vertices labeled b, j, k, c, d, l and a horizontal line with vertices i, a . Diagram 5 is a solid line with four vertices labeled b, j, k, c, d, l and a horizontal line with vertices i, a .

10.8 Results of various CC methods compared with full CI

It is very helpful to have some numerical data on the relative contributions of the various cluster operators and on the effects of the various approximations used in introducing correlation corrections. The most unambiguous assessment of the quality of the different models is provided by comparison with full-CI results using the same basis set, since full CI represents the exact results within the Hilbert space generated by the chosen basis set. The full-CI energy is a variational upper bound to the exact energy, is exactly extensive and is invariant under the choice of the molecular orbitals spanning the basis-set space. Thus the full-CI results are solely determined by the basis set.

Full-CI calculations require all possible excitations among any orbitals that are not frozen. For N electrons and n orbitals, the total number of determinants in a full-CI expansion is given asymptotically by $\sim n^N$. Consequently, only a comparatively few full-CI calculations are available for use as benchmarks and almost none of these use basis sets better than polarized double-zeta (DZP). Taking the example of H_2O with the inner-shell electrons on the oxygen atom frozen, a DZP basis contains a minimum of 23 functions for the eight valence electrons. While this type of basis is not sufficient for high-accuracy results, it is still expected to provide realistic indicators of the comparative merits of various approximations. In fact, comparisons with full CI are more useful for the assessment of the effectiveness of various correlation methods than comparisons with experimental data. Not only do such comparisons separate correlation-method contributions from basis-set effects, but they also avoid the questions of experimental uncertainties, corrections for zero-point vibrations, the Born–Oppenheimer approximation and relativistic effects.

In Table 10.5 results are given for CI, MBPT and CC for DZP (double-zeta + polarization) basis sets at various levels of correlation treatment for the FH and H₂O molecules at their equilibrium bond length R_e and at $1.5R_e$ and $2.0R_e$. The inner-shell pair of electrons on the heavier atom is frozen in these calculations, leaving the eight valence electrons to be correlated. The stretched geometries place great demands upon RHF-based single-reference treatments, since the restricted Hartree–Fock reference function does not separate correctly to neutral atoms, making the correlation error much greater at stretched geometries than at R_e .

As pointed out previously, the principal difference between CI methods on the one hand and MBPT and CC methods on the other is that the CI energy retains unlinked diagram contributions and, consequently, is not extensive until the full-CI limit is reached. Since the MBPT and CC theories are built upon the linked-diagram theorem, these methods benefit from the elimination of non-extensive terms at the outset. We can see the magnitude of this effect by comparing CID with CCD. Unlike MBPT, both these methods are of infinite order but the mean absolute error of CCD for the examples in Table 10.5 is a factor 2 better than that of CID. Furthermore, when single excitations are added the improvement in the mean absolute error of CCSD relative to CISD is a factor 3. When triple-excitations are added, we find that the mean absolute error for CCSDT is about 1 mE_h , while CISDT is still 22 mE_h above full CI on average. When we add quadruple excitations, the CISDTQ model achieves a dramatic reduction in the error compared to CISDT, since it now includes the disconnected quadruple excitation terms that serve to eliminate the most important unlinked term (see subsection 5.7.4). The part that remains is small for these small examples, but not quite negligible since CCSDTQ reduces the error by a factor 30 compared with CISDTQ, to 0.05 mE_h . For much larger molecules (or assemblies of molecules), the unlinked diagram error in CISDTQ would be much larger than in the examples presented here, eventually accounting for most of the correlation energy as the size of the system increases.

As confirmed by the presence of some negative-energy errors the MBPT and CC methods, unlike CI, are not variational, but this deficiency is a small price to pay for extensivity. While variational methods provide an upper bound to the total energy, there are no bounds on any energy differences of interest in chemistry and physics, and therefore the advantage of a variational method is of lesser consequence than the extensivity property of the many-body methods for most practical applications.

As seen from the diagrammatic expansions, MBPT models can be viewed as finite-order approximations to various levels of CC theory. The difference

Table 10.5. *Energy errors (in millihartrees), relative to full CI, for truncated CI calculations, many-body perturbation theory and coupled-cluster models for FH and H₂O in a DZP basis with frozen core at three bond lengths^a*

	FH			H ₂ O			Mean abs. error
	R_e	$1.5R_e$	$2.0R_e$	R_e	$1.5R_e$	$2.0R_e$	
Configuration interaction ^b							
CID	10.3	18.6	35.5	13.7	34.5	84.8	32.9
CISD	9.38	14.9	27.6	12.9	30.4	75.6	28.5
CISDT	7.01	11.1	19.2	10.6	23.5	60.3	22.0
CISDTQ	0.28	0.49	0.92	0.40	1.55	6.29	1.66
CISDTQP	0.08	0.16	0.28	0.16			
MBPT ^c							
MBPT(2)	7.80	10.6	24.0	13.0	23.3	53.7	22.1
MBPT(3)	5.44	11.9	27.0	7.22	26.4	74.6	25.4
MBPT(4)SDQ	2.75	5.39	12.5	4.40	13.3	34.2	12.1
MBPT(4)	−0.26	0.77	4.84	0.92	5.76	14.9	4.58
MBPT(5)	0.81	2.29	8.10	0.70	4.98	17.0	5.65
MBPT(6)	−0.23	−0.41	−1.13	0.08	1.82	4.06	1.29
Coupled cluster ^d							
CCD	3.76	8.13	21.9	5.01	15.9	40.2	15.8
CCSD	3.01	5.10	10.2	4.12	10.2	21.4	9.01
CCSD(T)	0.40	0.88	−0.26	0.72	2.09	4.63	1.50
CCSDT-1	0.17	0.49	0.22	0.60	1.99	−2.65	1.02
CCSDT	0.27	0.65	1.13	0.53	1.78	−2.47	1.14
CC5SDT[Q]	0.06	0.11	0.30	0.05	−0.02	−0.75	0.22
CC5SDTQ-1	0.06	0.11	0.35	0.05	−0.03	−1.58	0.36
CCSDTQ	0.02	0.04	0.06	0.02	0.14	−0.02	0.05
CCSDTQP	0.00	0.00	0.00	0.00	0.03	0.03	0.01

^aGeometries, basis sets and FCI energies are from Bauschlicher, Langhoff, Taylor *et al.* (1986) and Bauschlicher and Taylor (1986).

^bKállay and Surján (2000, 2001).

^cKucharski and Bartlett (1995).

^dKucharski and Bartlett (1992), Musiał, Kucharski and Bartlett (2002a).

between these approaches is that infinite order is used for selected terms in CC theory whereas a given finite order is used for all terms in MBPT. While MBPT rapidly improves with increasing order relative to CI because of the absence of unlinked diagrams, its errors are substantially greater than those for the comparable CC models. For pairs of methods that are accu-

Table 10.6. *Energy errors (in millihartrees), relative to full CI, for coupled-cluster calculations in a cc-pVDZ basis and frozen core for N₂ at several bond lengths, using RHF and UHF reference functions.^a*

Method	Bond length (in Å)					
	1.1208 ^b	1.2700	1.4288	1.5875	1.9050	2.2225
RHF reference function						
CCSD	14.469	21.481	31.807	45.188	72.223	40.698
CCSD(T)	1.866	3.087	5.182	7.700	−6.030	−165.014
CCSDT	1.839	3.631	6.834	10.310	−15.948	−113.131
CCSDT(Q _f)	0.295	0.349	0.038	−1.558	3.548	
CCSDTQ	0.229	0.572	1.368	2.396	0.5	
CCSDTQP	0.021					
CCSDTQPH	0.002					
UHF reference function						
CCSD	14.469	22.035	31.981	36.351	21.968	9.630
CCSD(T)	1.866	6.376	12.997	20.503	15.088	6.926
CCSDT	1.839	3.923	6.964	10.011	7.486	3.123
CCSDTQ	0.229	0.651	1.438	3.014	4.341	1.913
CCSDTQP	0.021	0.141	0.348	0.819	2.353	1.144
CCSDTQPH	0.002	0.073	0.134	0.202	0.744	0.827

^aRHF-based CCSD, CCSD(T) and CCSDT results, except for $R = 2.2225$ Å, from Krogh and Olsen (2001); all other results are from Chan, Kállay and Gauss (2004) and Musiał and Bartlett (2005).

^bEquilibrium bond length. The RHF and UHF wave functions are identical at this point.

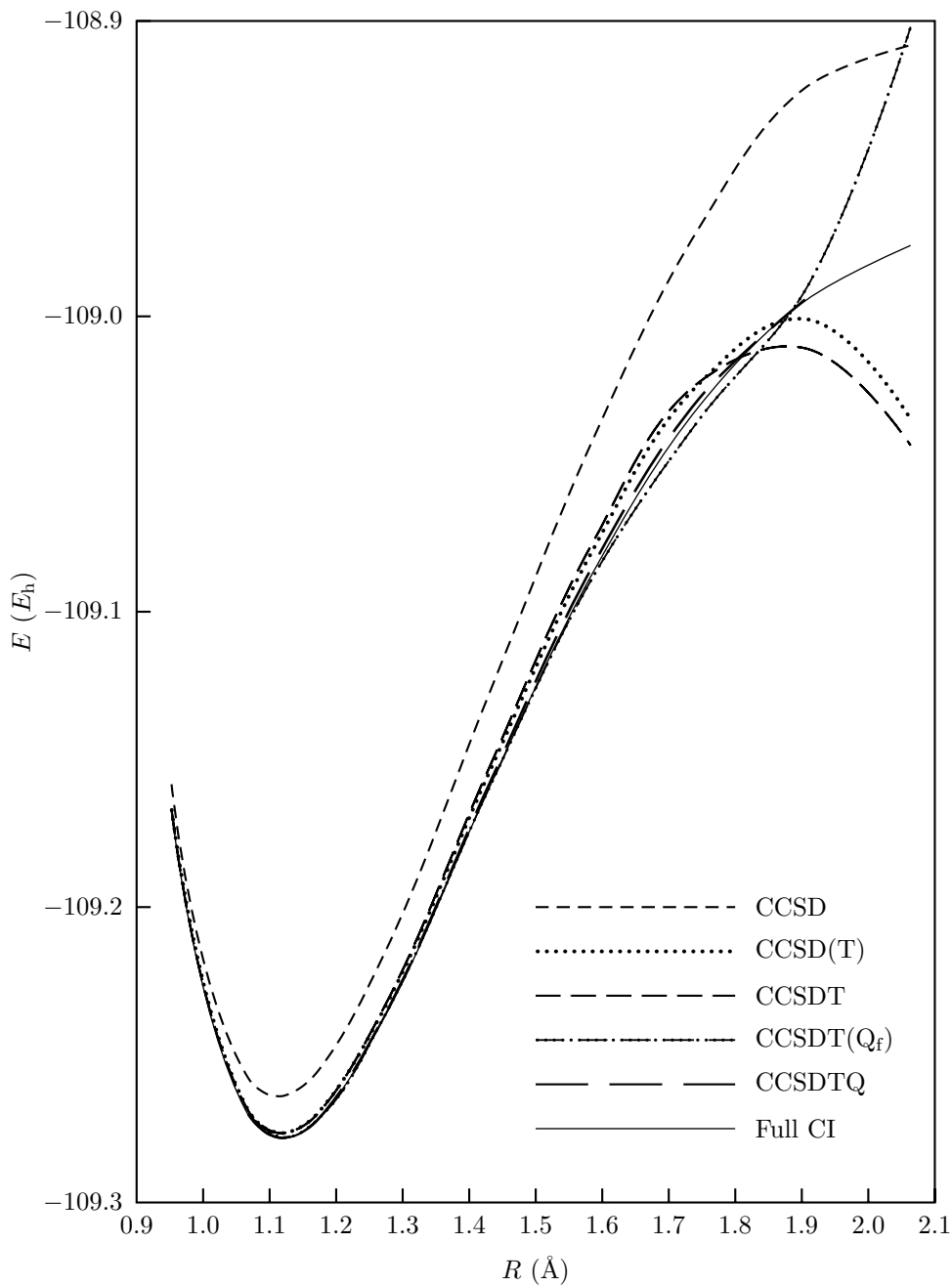
rate to the same order of perturbation theory, such as MBPT(3) and CCD, MBPT(4)SDQ and CCSD and MBPT(4) and CCSDT, the CC models give results that are several millihartrees better for the examples in Table 10.5. This difference holds also for the models that are correct through fifth order, as may be seen by comparing MBPT(5) with CCSDTQ-1. Only in sixth order does MBPT(6) narrow the gap with CCSDTQ. The comparative closeness of the results for these two models is the reason why non-iterative or perturbative corrections added to an underlying CC model are expected to be effective. In particular, CCSD(T) tends to retain the infinite-order advantages of CCSD versus MBPT(4)SDQ, while the perturbative triples estimate in CCSD(T) is consistent with the improvement of MBPT(4) relative to MBPT(4)SDQ. The iterative form of this approximation, CCSDT-1, is a little better for energies but can overcorrect in difficult cases

since it is fundamentally a linear approximation for the triple-excitations effect. The (T) approximation is no better but, because it is purely perturbative, i.e. triple-excitation amplitudes are not allowed to change the \hat{T}_1 and \hat{T}_2 amplitudes, the correction does not become excessive.

Although the energy results in Table 10.5 reflect the increased sophistication of the methods quite well, on their own they are an inadequate measure of the quality of an approximation. For example, potential-energy surfaces behave differently at large values of the internuclear distances and in the vicinity of the equilibrium geometry, and perturbation approximations fail for the stretched geometries if the reference function does not separate correctly. The infinite-order CC methods, even with approximations like CCSDT-1, do much better than MBPT at large R , though they still fail eventually as the bonds are stretched further since then the reference function becomes a very poor initial approximation. Several examples of this type of behavior are shown elsewhere (Bartlett 1989), along with results for other properties beside the energy that are pertinent to quantum-chemical applications.

A case that is particularly demanding for single-reference methods is the description of the stretching and breaking of a triple bond. The results of such calculations for the nitrogen molecule in a cc-pVDZ basis (Dunning 1989) at several bond lengths are shown in Table 10.6 (Krogh and Olsen 2001, Chan, Kállay and Gauss 2004, Musiał and Bartlett 2005). The first set of results in this table is based on an RHF reference function and deteriorates badly as the bond is stretched, producing energies far below the full-CI values. For CCSDTQ and higher levels the iterative procedures converge very slowly or fail to converge at all beyond the equilibrium bond length. Using a UHF reference function eliminates the long-range problems; however, it produces relatively poor results with high spin contamination at intermediate distances and a discontinuity in the energy derivatives at the point at which the RHF and UHF reference functions start to differ from each other, just beyond the equilibrium bond length, $2.118a_0$. Also included in this table are RHF-based CCSDT(Q_f) results (Musiał and Bartlett 2005), which show increasing deviations from the CCSDTQ values as the bond is stretched. Potential energy curves for some RHF-based CC results are shown in Fig. 10.10. It is seen in both the table and the potential energy plots that the CCSD(T) and CCSDT(Q_f) models are good approximations for CCSDT and CCSDTQ, respectively, at the shorter bond length but deteriorate as the bonds get longer.

The coupled-cluster techniques were extended to five-fold excitations by Musiał, Kucharski and Bartlett (2000, 2002a). Higher-order results were

Fig. 10.10. Potential energy curves for N_2 with RHF reference.

obtained by non-diagrammatic methods for some small examples for which the full-CI Hamiltonian matrix was available in a determinantal representation (Hirata and Bartlett, 2000). Methods for the automated generation of formulas and computer programs for high-order coupled cluster calculation have also been reported (Janssen and Schaefer 1991, Li and Paldus 1994, Kállay and Surján 2000, 2001, Hirata 2003, 2004, Auer, Baumgartner, Bernholdt *et al.* 2006). Some of these include automated optimization of the computational procedures, including a choice of intermediates.

Calculation of properties in coupled-cluster theory

11.1 Expectation value for a CC wave function

The exponential form of the coupled-cluster wave function requires an approach to the calculation of properties other than the energy that is different from that for more conventional wave functions, such as those in Hartree–Fock or CI. The expectation value \overline{O} (also written $\langle \hat{O} \rangle$) of an operator \hat{O} is given by

$$\overline{O} = \frac{\langle \Psi | \hat{O} | \Psi \rangle}{\langle \Psi | \Psi \rangle}. \quad (11.1)$$

When $|\Psi\rangle = e^{\hat{T}}|0\rangle$, this expression gives rise to series expansions in the numerator and denominator:

$$\begin{aligned} \overline{O} &= \frac{\langle 0 | e^{\hat{T}^\dagger} \hat{O} e^{\hat{T}} | 0 \rangle}{\langle 0 | e^{\hat{T}^\dagger} e^{\hat{T}} | 0 \rangle} \\ &= \frac{\langle 0 | [1 + T^\dagger + \frac{1}{2!}(T^\dagger)^2 + \frac{1}{3!}(T^\dagger)^3 + \dots] \hat{O} [1 + T + \frac{1}{2!}T^2 + \frac{1}{3!}T^3 + \dots] | 0 \rangle}{\langle 0 | [1 + \hat{T}^\dagger + \frac{1}{2!}(\hat{T}^\dagger)^2 + \frac{1}{3!}(\hat{T}^\dagger)^3 + \dots] [1 + \hat{T} + \frac{1}{2!}\hat{T}^2 + \frac{1}{3!}\hat{T}^3 + \dots] | 0 \rangle}. \end{aligned} \quad (11.2)$$

Individually, the expansions for $e^{\hat{T}^\dagger}$ and $e^{\hat{T}}$ in the numerator and denominator terminate when the total excitation level in the product of \hat{T} operators in any term exceeds the number of electrons in the CC wave function, in contrast with the behavior of the expansions in the CC amplitude equations, which always terminate after the product of four \hat{T} operators. Thus, even if we evaluated the numerator and denominator separately and then divide the results, the number of terms in each expansion and the computational effort required could be very high. Furthermore, the use of an expression involving a denominator can be inconvenient for some applications.

In fact, division by the denominator can be carried out formally, by factoring the numerator (Čížek 1969). For this purpose we examine each expansion diagrammatically, beginning with the denominator. The \hat{T} operator is a sum of connected terms $\hat{T}_1 + \hat{T}_2 + \dots$, but products of \hat{T} operators produce disconnected terms and thus the factor $e^{\hat{T}}|0\rangle$ contains both connected and disconnected (but not unlinked) diagrams. The products arising from the expansion of $\langle 0|e^{\hat{T}^\dagger}e^{\hat{T}}|0\rangle$ take the general form

$$\begin{aligned} & \frac{1}{m!n!} \langle 0|(\hat{T}^\dagger)^m \hat{T}^n |0\rangle \\ &= \sum_{\substack{0 < i_1 \neq i_2 \neq \dots \\ 0 < j_1 \neq j_2 \neq \dots \\ k_1 + k_2 + \dots = m \\ l_1 + l_2 + \dots = n \\ k_1 i_1 + k_2 i_2 + \dots \\ = l_1 j_1 + l_2 j_2 + \dots}} \frac{1}{k_1! k_2! \dots l_1! l_2! \dots} \langle 0|(\hat{T}_{i_1}^\dagger)^{k_1} (\hat{T}_{i_2}^\dagger)^{k_2} \dots (\hat{T}_{j_1})^{l_1} (\hat{T}_{j_2})^{l_2} \dots |0\rangle, \end{aligned} \quad (11.3)$$

resulting in closed diagrams in which the de-excitations in the \hat{T}^\dagger factors cancel the excitations in the \hat{T} factors.

To take several examples,

$$\langle 0|\hat{T}_2^\dagger \hat{T}_2|0\rangle = \langle \text{diagram} \rangle = \frac{1}{4} \sum_{ijab} t_{ij}^{ab*} t_{ij}^{ab}, \quad (11.4)$$

$$\langle 0|\hat{T}_2^\dagger \frac{1}{2!} (\hat{T}_1)^2 |0\rangle = \langle \text{diagram} \rangle = \frac{1}{2} \sum_{ijab} t_{ij}^{ab*} t_i^a t_j^b, \quad (11.5)$$

$$\langle 0|\hat{T}_2^\dagger \hat{T}_1^\dagger \hat{T}_3|0\rangle = \langle \text{diagram} \rangle = \frac{1}{4} \sum_{ijkabc} t_{ij}^{ab*} t_k^c t_{ijk}^{abc}, \quad (11.6)$$

$$\begin{aligned} \langle 0|\hat{T}_2^\dagger \hat{T}_1^\dagger \hat{T}_1 \hat{T}_2|0\rangle &= \langle \text{diagram 1} \rangle + \langle \text{diagram 2} \rangle + \langle \text{diagram 3} \rangle + \langle \text{diagram 4} \rangle \\ &= \frac{1}{4} \sum_{ijab} t_{ij}^{ab*} t_{ij}^{ab} \sum_{kc} t_k^{c*} t_k^c + \sum_{ijkabc} t_j^{b*} t_{ik}^{ac*} t_{ij}^{ab} t_k^c \\ &\quad - \frac{1}{2} \sum_{ijkabc} t_{ij}^{ac*} t_k^{b*} t_{ij}^{ab} t_k^c - \frac{1}{2} \sum_{ijkabc} t_{ik}^{ab*} t_j^{c*} t_{ij}^{ab} t_k^c. \end{aligned} \quad (11.7)$$

Analog of the above diagrams are obtained for the numerator. If

$$\begin{aligned}
 \hat{O} &= \sum_{pq} \langle p | \hat{o} | q \rangle \hat{p}^\dagger \hat{q} = \sum_{pq} o_{pq} \hat{p}^\dagger \hat{q} \\
 &= \sum_{pq} o_{pq} (\{ \hat{p}^\dagger \hat{q} \} + \overline{\hat{p}^\dagger \hat{q}}) \\
 &= \sum_{pq} o_{pq} \{ \hat{p}^\dagger \hat{q} \} + \sum_i o_{ii} = \hat{O}_N + \langle 0 | \hat{O} | 0 \rangle
 \end{aligned} \tag{11.8}$$

is a one-particle operator, its expectation value can be split into a *reference value* and a *correlation correction*,

$$\overline{O} = \langle 0 | \hat{O} | 0 \rangle + \overline{O}_N = O_{\text{ref}} + \Delta O. \tag{11.9}$$

With the normal-ordered part \hat{O}_N represented diagrammatically by

$$\hat{O}_N = \begin{array}{c} \uparrow \\ | \\ \uparrow \end{array} \text{---} \diamond + \begin{array}{c} \downarrow \\ | \\ \downarrow \end{array} \text{---} \diamond + \begin{array}{c} \vee \end{array} \text{---} \diamond + \begin{array}{c} \wedge \end{array} \text{---} \diamond, \tag{11.10}$$

the numerator of (11.2) will contain terms like

$$\begin{aligned}
 \langle 0 | \hat{T}_2^\dagger \hat{T}_1^\dagger \hat{O}_N \hat{T}_2 | 0 \rangle &= (a) \begin{array}{c} \text{Diagram 1: } \text{Upper loop } (i,j), \text{ lower loop } (b), \text{ vertex } (k) \text{ with } (c) \text{ line} \end{array} \text{---} \diamond + (j) \begin{array}{c} \text{Diagram 2: } \text{Upper loop } (b), \text{ lower loop } (a), \text{ vertex } (i) \text{ with } (k) \text{ line} \end{array} \text{---} \diamond \\
 &+ (a) \begin{array}{c} \text{Diagram 3: } \text{Upper loop } (i,j), \text{ lower loop } (b), \text{ vertex } (k) \text{ with } (c) \text{ line} \end{array} \text{---} \diamond + (i) \begin{array}{c} \text{Diagram 4: } \text{Upper loop } (a,b), \text{ lower loop } (j), \text{ vertex } (k) \text{ with } (c) \text{ line} \end{array} \text{---} \diamond \\
 &= \frac{1}{4} \sum_{ijab} t_{ij}^{ab*} t_{ij}^{ab} \sum_{kc} t_k^{c*} o_{ck} + \sum_{ijkabc} t_j^{b*} t_{ik}^{ac*} t_{ij}^{ab} o_{ck} \\
 &\quad - \frac{1}{2} \sum_{ijkabc} t_{ij}^{ac*} t_k^{b*} t_{ij}^{ab} o_{ck} - \frac{1}{2} \sum_{ijkabc} t_{ik}^{ab*} t_j^{c*} t_{ij}^{ab} o_{ck}. \tag{11.11}
 \end{aligned}$$

Factorization of the numerator requires independent summation over all indices, thus introducing exclusion-principle-violating (EPV) terms. There are two types of EPV contribution in these diagrams. Equal labels on lines connected to the same \hat{T}_i^\dagger or \hat{T}_i vertex produce zero contributions because of the antisymmetry of the $t_{ij\dots}^{ab\dots}$ amplitudes in the upper and lower indices, respectively, and thus such terms can be included freely in the summations. All other EPV terms can be shown to cancel. Taking (11.11) as an example, it is easily seen that terms with $k = j$ cancel between the first and fourth diagrams and between the second and third diagrams. Similarly, terms with $c = b$ cancel between the first and third and between the second and fourth

diagrams. The differences in the weights of these terms are accounted for by line equivalences in the respective diagrams; thus $k = i$ is equivalent to $k = j$ in the first diagram, providing two identical contributions with weight $\frac{1}{4}$ each to cancel a single contribution with weight $-\frac{1}{2}$ in the fourth term. Similarly, $k = i$ is also equivalent to $k = j$ in the third diagram, providing two identical contributions with weight $-\frac{1}{2}$ each to cancel a single contribution with weight 1 in the second diagram.

In the expansion of the numerator, terms in which the total excitation level $l_{1j_1} + l_{2j_2} + \dots$ (see (11.3)) in the product of \hat{T}_j factors exceeds the number of electrons N are necessarily EPV terms, since there are no more than N distinct hole states to excite. Such terms either vanish (because of the repetition of indices in any amplitude) or mutually cancel. Thus we can safely ignore the termination of the expansion by excitation level. The resulting nonterminating form of the expansion is necessary for complete factorization of the numerator.

The complete diagrammatic expansion of the numerator will contain both connected and disconnected closed diagrams, each of which has exactly one connected part containing the operator \hat{O}_N and any number (zero or more) of parts that do not contain this operator. Because of the inclusion of EPV terms and the related non-terminating form of the diagrammatic expansion, each disconnected diagram is simply equal to the product of the individual connected parts in it. Each part containing the \hat{O}_N operator will appear in the expansion of the numerator with all possible combinations of parts that do not contain this operator and thus it can be written as a product of the former part times the expansion of the denominator. Therefore the entire numerator can be written as the product of the sum of its connected terms multiplied by the denominator,

$$\langle 0 | e^{\hat{T}^\dagger} e^{\hat{T}} | 0 \rangle \langle 0 | e^{\hat{T}^\dagger} \hat{O}_N e^{\hat{T}} | 0 \rangle_C.$$

The first factor in this expression cancels the denominator, producing the result (first given in Čížek 1969)

$$\overline{O}_N = \frac{\langle 0 | e^{\hat{T}^\dagger} \hat{O}_N e^{\hat{T}} | 0 \rangle}{\langle 0 | e^{\hat{T}^\dagger} e^{\hat{T}} | 0 \rangle} = \langle 0 | e^{\hat{T}^\dagger} \hat{O}_N e^{\hat{T}} | 0 \rangle_C. \quad (11.12)$$

The final (connected) result retains EPV terms that, in the original numerator, canceled between connected and disconnected terms. These uncanceled EPV terms prevent the expansion (11.12) from terminating, since multiple excitations or de-excitations of the same hole state may now occur. As a result, evaluation of the expectation value in this form requires trunca-

tion at some level and prevents exact determination of the expectation value. On another level, the nonterminating nature of the result may be explained as due to the implicit series expansion of the inverse of the denominator, as in the expansion of $(1 + A)^{-1}$.

The result (11.12) is valid for all normal-ordered operators, not just for one-electron operators. When the operator \hat{O}_N is the normal-product Hamiltonian $\hat{H}_N = \hat{H} - \langle 0|\hat{H}|0\rangle$, (11.12) gives the correlation energy,

$$\Delta E = \frac{\langle 0|e^{\hat{T}^\dagger} \hat{H}_N e^{\hat{T}}|0\rangle}{\langle 0|e^{\hat{T}^\dagger} e^{\hat{T}}|0\rangle} = \langle 0|e^{\hat{T}^\dagger} \hat{H}_N e^{\hat{T}}|0\rangle_C. \quad (11.13)$$

Provided that the \hat{T} operator is the exact solution of the untruncated CC equations, this result is consistent with the normally used CC expression (10.11) for the correlation energy, $\Delta E = \langle 0|\hat{H}_N e^{\hat{T}}|0\rangle_C = \langle 0|e^{-\hat{T}} \hat{H}_N e^{\hat{T}}|0\rangle$. We can show the equivalence of these forms by inserting $e^{\hat{T}}(\hat{P} + \hat{Q})e^{-\hat{T}} = \hat{1}$ into the expectation-value form:

$$\begin{aligned} \Delta E &= \frac{\langle 0|e^{\hat{T}^\dagger} \hat{H}_N e^{\hat{T}}|0\rangle}{\langle 0|e^{\hat{T}^\dagger} e^{\hat{T}}|0\rangle} = \frac{\langle 0|e^{\hat{T}^\dagger} e^{\hat{T}}(\hat{P} + \hat{Q})e^{-\hat{T}} \hat{H}_N e^{\hat{T}}|0\rangle}{\langle 0|e^{\hat{T}^\dagger} e^{\hat{T}}|0\rangle} \\ &= \frac{\langle 0|e^{\hat{T}^\dagger} e^{\hat{T}}|0\rangle \langle 0|e^{-\hat{T}} \hat{H}_N e^{\hat{T}}|0\rangle}{\langle 0|e^{\hat{T}^\dagger} e^{\hat{T}}|0\rangle} = \langle 0|e^{-\hat{T}} \hat{H}_N e^{\hat{T}}|0\rangle = \langle 0|\mathcal{H}|0\rangle. \end{aligned} \quad (11.14)$$

This follows because the CC equations require that $\hat{Q}\mathcal{H}|0\rangle = 0$, (10.13). The equivalence is exact only when \hat{T} is the solution of the untruncated CC equations. If \hat{T} is truncated to a particular excitation level, say $\hat{T}_1 + \hat{T}_2$, the CC equations for higher cluster operators, such as \hat{T}_3 , are not satisfied and thus $\hat{Q}\mathcal{H}|0\rangle = 0$ is not strictly valid.

For properties represented by the expectation values of any operators for which the wave function is an eigenfunction, such as \hat{S}^2 or \hat{S}_z , we formally have the same equations as for \hat{H} , provided that a corresponding analog of the second equation in (10.13), such as $\hat{Q}e^{-\hat{T}}\hat{S}^2 e^{\hat{T}}|0\rangle = 0$, holds. Other than for a closed-shell system with doubly occupied orbitals, the CC equations do not always produce a spin eigenfunction, making it necessary to impose that condition when this aspect is important (Szalay and Gauss 1997, 2000). As an alternative, a spin-adapted formulation of CC theory based on the unitary group approach was given by Li and Paldus (1994, 1997). Other approaches to the at least approximate imposition of spin conditions have also been used (Neogrády, Urban and Hubáč 1992, 1994,

Jayatilaka and Lee 1993, Stanton and Gauss 1994, Bartlett 1995, Urban, Neogr  dy and Huba   1997). For expectation values of other operators, such as those representing dipole and quadrupole moments, electric field gradients or the kinetic energy, a general route toward their evaluation can be provided by introducing a *density matrix*, as will now be described in Section 11.2.

11.2 Reduced density matrices

The evaluation of the expectation values of one-electron operators is facilitated by the use of the one-body reduced density matrix

$$\begin{aligned}\gamma(x, x') &= \frac{N}{\langle \Psi | \Psi \rangle} \int \Psi(x, x_2, x_3, \dots, x_N) \Psi^*(x', x_2, x_3, \dots, x_N) dx_2 dx_3 \cdots dx_N \\ &= \sum_{pq} \phi_q(x) \gamma_{qp} \phi_p^*(x'),\end{aligned}\quad (11.15)$$

where each of x, x_2, \dots stands for the set of space and spin coordinates of an electron and, in the second line,

$$\gamma_{qp} = \frac{\langle \hat{p} \Psi | \hat{q} \Psi \rangle}{\langle \Psi | \Psi \rangle} = \frac{\langle \Psi | \hat{p}^\dagger \hat{q} | \Psi \rangle}{\langle \Psi | \Psi \rangle} \quad (11.16)$$

are the elements of the discrete matrix representation γ of the continuous matrix $\gamma(x, x')$ in the one-electron (spinorbital) basis. For the particular case of CC theory,

$$\gamma_{qp} = \frac{\langle 0 | e^{\hat{T}^\dagger} \hat{p}^\dagger \hat{q} e^{\hat{T}} | 0 \rangle}{\langle 0 | e^{\hat{T}^\dagger} e^{\hat{T}} | 0 \rangle} = \langle 0 | e^{\hat{T}^\dagger} \hat{p}^\dagger \hat{q} e^{\hat{T}} | 0 \rangle_C. \quad (11.17)$$

The expectation value of the one-electron operator (11.8) is given by

$$\overline{O} = \sum_{pq} o_{pq} \langle 0 | e^{\hat{T}^\dagger} \hat{p}^\dagger \hat{q} e^{\hat{T}} | 0 \rangle_C = \sum_{pq} o_{pq} \gamma_{qp}. \quad (11.18)$$

In terms of the continuous form of the density matrix this result can be obtained as

$$\begin{aligned}\overline{O} &= \text{tr } \hat{O} \gamma = \int \hat{o}(x) \gamma(x, x')|_{x'=x} dx \\ &= \sum_{pq} \int \hat{o}(x) \phi_q(x) \gamma_{qp} \phi_p^*(x')|_{x'=x} dx = \sum_{pq} o_{pq} \gamma_{qp},\end{aligned}\quad (11.19)$$

where it is understood that the substitution $x' = x$ is carried out *after* the operation of $\hat{\delta}(x)$ on $\gamma(x, x')$ and before the integration over x . In particular, the electron density at some space-spin point x'' is obtained as the expectation value of the Dirac δ -function operator $\delta(x'' - x)$. When inserted into (11.19) this operator gives

$$\begin{aligned}\gamma(x'') &\equiv \gamma(x'', x'') = \int \delta(x'' - x) \gamma(x, x')|_{x'=x} dx \\ &= \sum_{pq} \phi_q(x'') \gamma_{qp} \phi_p^*(x''),\end{aligned}\quad (11.20)$$

and the total electron population is obtained by integrating over x'' ,

$$\int \gamma(x'') dx'' = \sum_{pq} \langle \phi_p | \phi_q \rangle \gamma_{pq} = \sum_p \gamma_{pp} = N. \quad (11.21)$$

For the expectation value of two-electron operators (including the energy) we need the two-body density matrix,

$$\begin{aligned}\Gamma(x_1, x_2; x'_1, x'_2) &= \frac{N(N-1)}{2\langle \Psi | \Psi \rangle} \int \Psi(x_1, x_2, x_3, \dots, x_N) \Psi^*(x'_1, x'_2, x_3, \dots, x_N) dx_3 \cdots dx_N \\ &= \sum_{pqrs} \phi_r(x_1) \phi_s(x_2) \Gamma_{rspq} \phi_p^*(x'_1) \phi_q^*(x'_2),\end{aligned}\quad (11.22)$$

where

$$\Gamma_{rspq} = \frac{\langle \hat{q} \hat{p} \Psi | \hat{s} \hat{r} \Psi \rangle}{\langle \Psi | \Psi \rangle} = \frac{\langle \Psi | \hat{p}^\dagger \hat{q}^\dagger \hat{s} \hat{r} | \Psi \rangle}{\langle \Psi | \Psi \rangle} \quad (11.23)$$

are the elements of the discrete representation $\mathbf{\Gamma}$ of the continuous matrix $\Gamma(x_1, x_2; x'_1, x'_2)$ in the one-electron (spinorbital) basis. For a two-electron operator

$$\hat{G} = \frac{1}{4} \sum_{pqrs} \langle pq | \hat{g} | rs \rangle_A \hat{p}^\dagger \hat{q}^\dagger \hat{s} \hat{r} \quad (11.24)$$

(compare (3.53), (3.60)) we obtain the expectation value

$$\overline{G} = \frac{1}{4} \sum_{pqrs} \langle pq | \hat{g} | rs \rangle_A \Gamma_{rspq}. \quad (11.25)$$

As can be seen from (11.23), Γ_{rspq} has the same symmetry properties with respect to permutation of the indices as antisymmetrized two-electron integrals,

$$\Gamma_{rspq} = -\Gamma_{rsqp} = -\Gamma_{srpq} = \Gamma_{srqp} = \Gamma_{pqrs}^* = -\Gamma_{pqsr}^* = -\Gamma_{qprs}^* = \Gamma_{qpsr}^* \quad (11.26)$$

and $\Gamma_{rspp} = \Gamma_{rrpq} = \Gamma_{rrpp} = 0$.

For the purposes of the diagrammatic representation it is convenient to limit our attention to the correlation correction of the expectation value,

$$\bar{O}_N = \sum_{pq} o_{pq} \langle 0 | e^{\hat{T}^\dagger} \{ \hat{p}^\dagger \hat{q} \} e^{\hat{T}} | 0 \rangle_C = \sum_{pq} o_{pq} (\gamma_N)_{qp}, \quad (11.27)$$

where γ_N is the normal-ordered part of the one-body density matrix, with elements

$$(\gamma_N)_{qp} = \langle 0 | e^{\hat{T}^\dagger} \{ \hat{p}^\dagger \hat{q} \} e^{\hat{T}} | 0 \rangle_C. \quad (11.28)$$

The only difference between the elements of γ_N and γ is for the hole-hole elements,

$$(\gamma_N)_{ji} = \langle 0 | e^{\hat{T}^\dagger} (\hat{i}^\dagger \hat{j} - \overline{\hat{i}^\dagger \hat{j}}) e^{\hat{T}} | 0 \rangle_C = \gamma_{ji} - \delta_{ji}. \quad (11.29)$$

When used in the evaluation of the expectation value of a one-electron operator \hat{O} , this difference provides the vacuum-expectation-value part $\langle 0 | \hat{O} | 0 \rangle = \sum_i o_{ii}$ of the total expectation value (11.9).

For the two-body density matrix, using the generalized Wick's theorem we obtain

$$\begin{aligned} \Gamma_{rspq} = & (\Gamma_N)_{rspq} + \delta_{pi} \delta_{ri} (\gamma_N)_{sq} + \delta_{qi} \delta_{si} (\gamma_N)_{rp} - \delta_{pi} \delta_{si} (\gamma_N)_{rq} - \delta_{qi} \delta_{ri} (\gamma_N)_{sp} \\ & + \delta_{pi} \delta_{ri} \delta_{qj} \delta_{sj} - \delta_{pi} \delta_{si} \delta_{qj} \delta_{rj}, \end{aligned} \quad (11.30)$$

where i, j are any hole-state labels and

$$(\Gamma_N)_{rspq} = \langle 0 | e^{\hat{T}^\dagger} \{ \hat{p}^\dagger \hat{q}^\dagger \hat{s} \hat{r} \} e^{\hat{T}} | 0 \rangle_C. \quad (11.31)$$

Specifically, for different combinations of particles and holes,

$$\begin{aligned} \Gamma_{cdab} &= (\Gamma_N)_{cdab}, \\ \Gamma_{cdai} &= (\Gamma_N)_{cdai}, \\ \Gamma_{cdij} &= (\Gamma_N)_{cdij}, \\ \Gamma_{cjai} &= (\Gamma_N)_{cjai} + \delta_{ij} (\gamma_N)_{ca}, \\ \Gamma_{ckij} &= (\Gamma_N)_{ckij} + \delta_{kj} (\gamma_N)_{ci} - \delta_{ki} (\gamma_N)_{cj}, \\ \Gamma_{klij} &= (\Gamma_N)_{klij} + \delta_{ki} (\gamma_N)_{lj} + \delta_{lj} (\gamma_N)_{ki} \\ &\quad - \delta_{kj} (\gamma_N)_{li} - \delta_{li} (\gamma_N)_{kj} + \delta_{ki} \delta_{lj} - \delta_{kj} \delta_{li}. \end{aligned} \quad (11.32)$$

All other cases can be obtained by index permutations according to the rules in (11.26), which apply to Γ_N as well as to Γ .

The expectation value \overline{G} then becomes

$$\begin{aligned}\overline{G} &= \frac{1}{4} \sum_{pqrs} \langle pq | \hat{g} | rs \rangle_A (\Gamma_N)_{rspq} \\ &\quad + \frac{1}{4} \sum_{ipq} \left(\langle pi | \hat{g} | qi \rangle_A + \langle ip | \hat{g} | iq \rangle_A - \langle ip | \hat{g} | qi \rangle_A - \langle pi | \hat{g} | iq \rangle_A \right) (\gamma_N)_{qp} \\ &\quad + \frac{1}{2} \sum_{ij} \langle ij | \hat{g} | ij \rangle_A \\ &= \frac{1}{4} \sum_{pqrs} \langle pq | \hat{g} | rs \rangle_A (\Gamma_N)_{rspq} + \sum_{pq} g'_{pq} (\gamma_N)_{qp} + \frac{1}{2} \sum_{ij} \langle ij | \hat{g} | ij \rangle_A, \quad (11.33)\end{aligned}$$

where g'_{pq} is given by (3.174). The three sums in this equation correspond to the three terms \hat{G}_N , \hat{G}'_N and $\langle 0 | \hat{G} | 0 \rangle$ of (3.173), respectively.

In the diagrammatic representation of contributions to the one-body density matrix (11.28) we need a symbol for the operator $\{\hat{p}^\dagger \hat{q}\}$, which represents the generic (property-independent) part of the general one-electron operator expression (11.8). Here we will represent this operator by the markerless one-electron vertex \bullet —, which may be construed as a place-holder for the operator representing the actual property being calculated. Adding a marker, such as \diamond , corresponds to multiplication by the corresponding property integral o_{pq} and summation over p, q (but obviously the density matrix elements need to be calculated only once for any number of one-electron properties). In a common notation, a gap is left in place of this vertex; sometimes a dotted line is added across the gap or the vertex is marked with the label $1' \rightarrow 1$. It is to be understood that the two lines connected to the vertex carry fixed labels that identify the specific matrix element of γ and are not summed over. The indices on γ_{qp} correspond to the labels on the incoming and outgoing lines at the vertex, in that order.

In the evaluation of the expression (11.28) we need to contract the operators \hat{p}^\dagger and \hat{q} with operators in the expansions of $\langle 0 | e^{\hat{T}^\dagger}$ at the top and $e^{\hat{T}} | 0 \rangle$ at the bottom. Symbolically, we can represent this process by the schematic diagram

$$(\gamma_N)_{qp} = \begin{array}{c} \boxed{} \end{array} \begin{array}{c} \xrightarrow{q} \\ \xleftarrow{p} \end{array} \bullet \text{---} \quad (11.34)$$

where the box represents the $\langle 0|e^{\hat{T}^\dagger}$ and $e^{\hat{T}}|0\rangle$ parts and the slopes of the p and q lines have no significance in this case. In terms of the time sequence, the $\bullet \dashv \dashv$ vertex has to appear between the \hat{T}^\dagger operators at the top and the \hat{T} operators at the bottom. As for any one-electron quantity, the first index on γ_{qp} represents an outgoing line in the diagram relative to the respective box (incoming relative to the vertex) and the second index represents an incoming line relative to the box. More specifically, the density matrix elements $(\gamma_N)_{qp}$ fall into four types, depending on whether each of p and q represents a particle or hole label. Symbolically,

$$\gamma_{ba} = \begin{array}{c} \boxed{e^{\hat{T}^\dagger}} \\ \uparrow \text{a} \\ \uparrow \text{b} \\ \boxed{e^{\hat{T}}} \end{array}, \quad (\gamma_N)_{ji} = \begin{array}{c} \boxed{e^{\hat{T}^\dagger}} \\ \downarrow \text{j} \\ \downarrow \text{i} \\ \boxed{e^{\hat{T}}} \end{array}, \quad \gamma_{ia} = \begin{array}{c} \boxed{e^{\hat{T}^\dagger}} \\ \swarrow \text{a} \searrow \text{i} \\ \bullet \dashv \dashv \\ \boxed{e^{\hat{T}}} \end{array}, \quad \gamma_{ai} = \begin{array}{c} \boxed{e^{\hat{T}^\dagger}} \\ \swarrow \text{i} \searrow \text{a} \\ \bullet \dashv \dashv \\ \boxed{e^{\hat{T}}} \end{array}. \quad (11.35)$$

The $\{\hat{p}^\dagger \hat{q}^\dagger \hat{s} \hat{r}\}$ operator for the two-body density matrix will be represented by the double-dashed vertex $\bullet \dashv \dashv \bullet$. The corresponding schematic diagrams for the matrix elements of Γ_N take the forms

$$\begin{aligned} \Gamma_{cdab} &= \begin{array}{c} \boxed{e^{\hat{T}^\dagger}} \\ \uparrow \text{a} \uparrow \text{b} \\ \uparrow \text{c} \uparrow \text{d} \\ \boxed{e^{\hat{T}}} \end{array}, \quad (\Gamma_N)_{klji} = \begin{array}{c} \boxed{e^{\hat{T}^\dagger}} \\ \downarrow \text{k} \downarrow \text{l} \\ \downarrow \text{i} \downarrow \text{j} \\ \boxed{e^{\hat{T}}} \end{array}, \quad (\Gamma_N)_{ibaj} = \begin{array}{c} \boxed{e^{\hat{T}^\dagger}} \\ \swarrow \text{a} \searrow \text{i} \\ \bullet \dashv \dashv \bullet \\ \swarrow \text{j} \searrow \text{b} \\ \boxed{e^{\hat{T}}} \end{array}, \\ \Gamma_{idab} &= \begin{array}{c} \boxed{e^{\hat{T}^\dagger}} \\ \swarrow \text{a} \searrow \text{i} \\ \bullet \dashv \dashv \bullet \\ \uparrow \text{b} \uparrow \text{d} \\ \boxed{e^{\hat{T}}} \end{array}, \quad (\Gamma_N)_{akij} = \begin{array}{c} \boxed{e^{\hat{T}^\dagger}} \\ \swarrow \text{i} \searrow \text{a} \\ \bullet \dashv \dashv \bullet \\ \downarrow \text{k} \downarrow \text{j} \\ \boxed{e^{\hat{T}}} \end{array} \quad \text{etc.}, \quad (11.36) \end{aligned}$$

the indices on Γ_{rspq} corresponding to the labels on the lines at the vertex in the order left-in, right-in, left-out, right-out.

It is convenient to classify the various contributions to the density matrices according to the perturbation order in which they first arise. As shown in Section 9.4, the \hat{T}_m operators can be resolved into MBPT wave-function

components of different orders and each \hat{T}_m operator can be characterized by the lowest PT order in which it arises. The \hat{T}_2 operator is first order, \hat{T}_1 is second order in the HF case and first order otherwise, \hat{T}_3 is second order and so on.

Diagrams representing contributions from the various \hat{T}^\dagger and \hat{T} operators to the particle–hole and particle–particle elements of the one-body density matrix through fourth order in the general (non-HF) case are shown in Figs. 11.1 and 11.2, respectively. Arrows are shown explicitly only when different distinct arrow assignments are possible. Diagram 1 corresponds to the leading term (i.e. the number 1) in the series expansion of $e^{\hat{T}^\dagger}$. In the general case diagram 1 is first order, diagram 2 is second order, 3–7 are third order and 8–19 are fourth order. Looking at Fig. 11.2, diagrams 20 and 21 are second order, 22 and 23 are third order and 24–41 are fourth order. Since the density matrix is Hermitian, $\gamma_{pq} = \gamma_{qp}^*$, we need to calculate only one of every pair of complex-conjugate off-diagonal elements. Therefore the hole–particle diagrams, which are conjugate (Section 5.5) to the particle–hole diagrams, are not shown. The hole–hole diagrams are obtained from the particle–particle diagrams by the reversal of all arrows. It is important

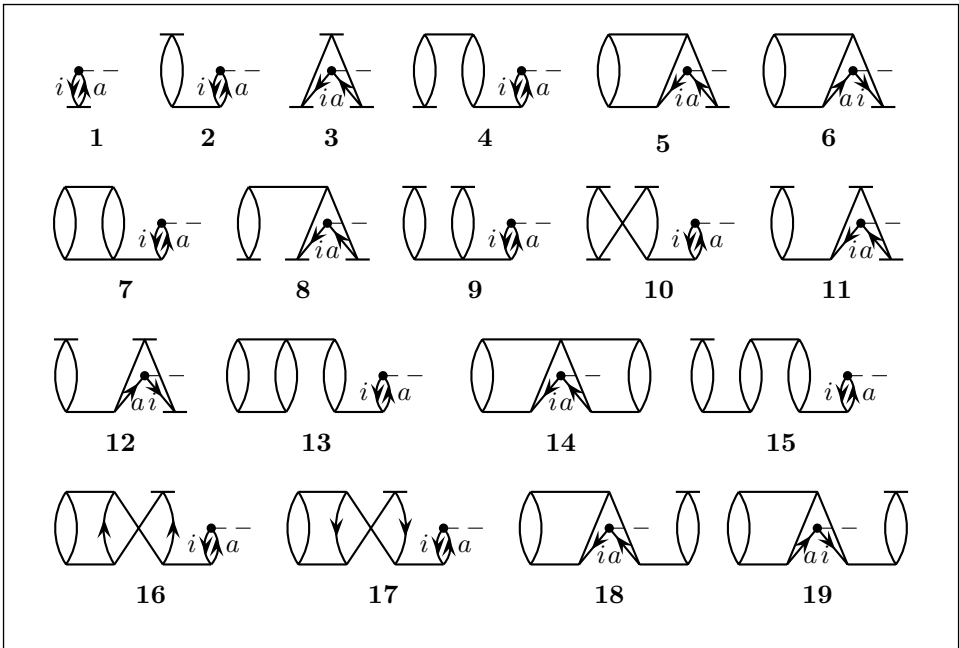


Fig. 11.1. Diagrams representing contributions to the particle–hole element γ_{ai} of the one-body reduced density matrix through fourth order.

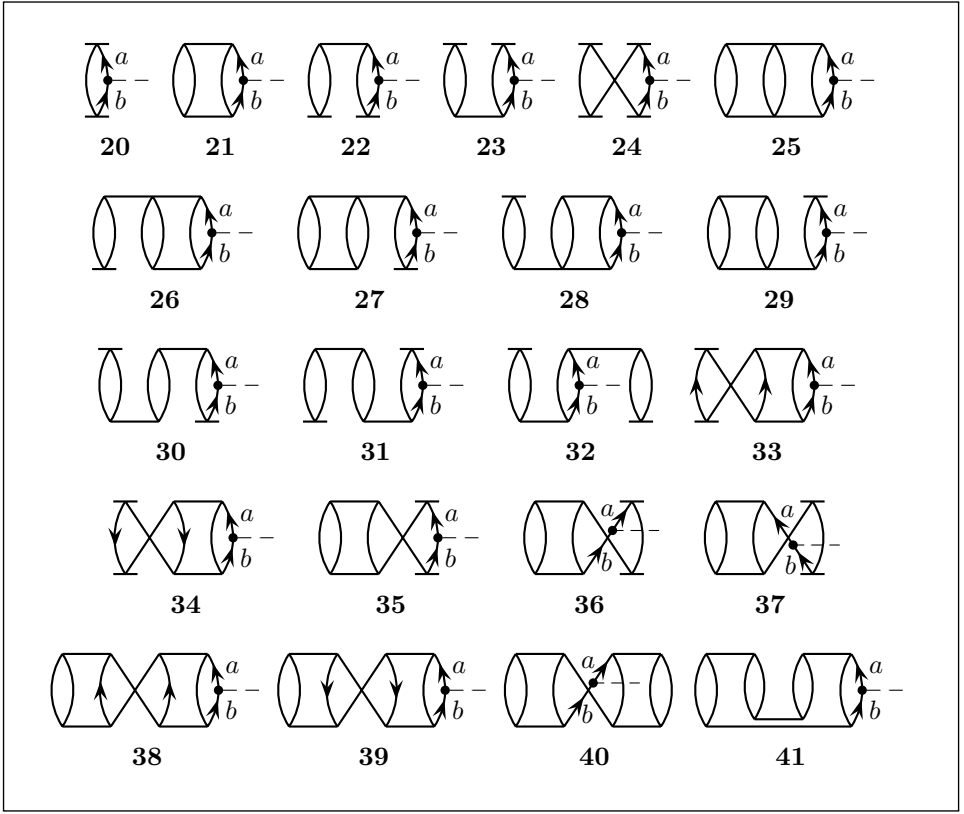


Fig. 11.2. Diagrams representing contributions to the particle-particle element γ_{ba} of the one-body reduced density matrix through fourth order.

to note that each of the particle-particle diagram pairs (22, 23), (26, 28), (27, 29) and (30, 31) in Fig. 11.2 are not conjugate to each other, because the fixed labels move with their lines in the conjugation process. Thus these diagram pairs represent different contributions to the same matrix element.

The first few terms in the algebraic expressions for the density matrix elements are easily obtained from Fig. 11.1 and 11.2 (the order of the terms in these expressions corresponds to the order of the diagrams in the figures):

$$\begin{aligned}
 \gamma_{ai} = & t_i^a + \sum_{jb} t_j^{b*} t_{ji}^{ba} - \sum_{jb} t_j^{b*} t_i^b t_j^a + \sum_{jkb} t_{kj}^{cb*} t_k^c t_{ji}^{ba} - \frac{1}{2} \sum_{jkb} t_{kj}^{cb*} t_{ki}^{cb} t_j^a \\
 & - \frac{1}{2} \sum_{jkb} t_{kj}^{cb*} t_{kj}^{ca} t_i^b + \frac{1}{4} \sum_{jkb} t_{kj}^{cb*} t_{kji}^{cba} - \sum_{jkb} t_{kj}^{cb*} t_k^c t_i^b t_j^a + \sum_{jkb} t_k^{c*} t_j^{b*} t_{kji}^{cba} \\
 & - \sum_{jkb} t_k^{c*} t_j^{b*} t_j^c t_{ki}^{ba} - \frac{1}{2} \sum_{jkb} t_k^{c*} t_j^{b*} t_{ki}^{cb} t_j^a - \frac{1}{2} \sum_{jkb} t_k^{c*} t_j^{b*} t_{kj}^{ca} t_i^b + \frac{1}{4} \sum_{jklbcd} t_{lkj}^{dcb*} t_{lk}^{dc} t_{ji}^{ba}
 \end{aligned}$$

$$\begin{aligned}
& -\frac{1}{4} \sum_{jklbcd} t_{kjl}^{cbd*} t_{ki}^{cb} t_{jl}^{ad} + \sum_{jklbcd} t_j^{d*} t_{kj}^{cb*} t_{lk}^{dc} t_{ji}^{ba} - \frac{1}{2} \sum_{jklbcd} t_{lk}^{dc*} t_j^{b*} t_{lj}^{dc} t_{ki}^{ba} \\
& -\frac{1}{2} \sum_{jklbcd} t_{lk}^{dc*} t_j^{b*} t_{lk}^{db} t_{ji}^{ca} - \frac{1}{2} \sum_{jklbcd} t_{kj}^{cb*} t_l^{d*} t_{ki}^{cb} t_{jl}^{ad} - \frac{1}{2} \sum_{jklbcd} t_{kj}^{cb*} t_l^{d*} t_{kj}^{ca} t_{il}^{bd} + \dots, \quad (11.37)
\end{aligned}$$

$$\begin{aligned}
\gamma_{ba} = & \sum_i t_i^{a*} t_i^b + \frac{1}{2} \sum_{ijc} t_{ji}^{ca*} t_{ji}^{cb} + \sum_{ijc} t_{ji}^{ca*} t_j^c t_i^b + \sum_{ijc} t_j^{c*} t_i^{a*} t_{ji}^{cb} - \sum_{ijc} t_j^{c*} t_i^{a*} t_i^c t_j^b \\
& + \frac{1}{24} \sum_{ijkcd} t_{kji}^{dca*} t_{kj}^{dcb} + \frac{1}{2} \sum_{ijkcd} t_{kji}^{dca*} t_k^d t_{ji}^{cb} + \frac{1}{4} \sum_{ijkcd} t_{kji}^{dca*} t_{kj}^{dc} t_i^b \\
& + \frac{1}{2} \sum_{ijkcd} t_k^{d*} t_{ji}^{ca*} t_{kj}^{dcb} + \frac{1}{4} \sum_{ijkcd} t_{kj}^{dc*} t_i^{a*} t_{kji}^{dcb} + \sum_{ijkcd} t_k^{d*} t_{ji}^{ca*} t_{kj}^{dc} t_i^b \\
& + \sum_{ijkcd} t_{kj}^{dc*} t_i^{a*} t_k^d t_{ji}^{cb} + \sum_{ijkcd} t_j^{c*} t_{ik}^{ad*} t_{ji}^{cb} t_k^d - \sum_{ijkcd} t_k^{d*} t_{ji}^{ca*} t_j^d t_{ki}^{cb} \\
& - \frac{1}{2} \sum_{ijkcd} t_k^{d*} t_{ji}^{ca*} t_k^c t_{ji}^{db} - \frac{1}{2} \sum_{ijkcd} t_{kj}^{dc*} t_i^{a*} t_{ki}^{dc} t_j^b - \frac{1}{2} \sum_{ijkcd} t_{kj}^{dc*} t_i^{a*} t_{kj}^{db} t_i^c \\
& - \frac{1}{2} \sum_{ijkcd} t_{kj}^{da*} t_i^{c*} t_{kj}^{dc} t_i^b - \frac{1}{2} \sum_{ijklde} t_{lk}^{ed*} t_{ji}^{ca*} t_{lj}^{ed} t_{ki}^{cb} - \frac{1}{4} \sum_{ijklde} t_{lk}^{ed*} t_{ji}^{ca*} t_{lk}^{ec} t_{ji}^{db} \\
& - \frac{1}{4} \sum_{ijklde} t_{kj}^{dc*} t_{il}^{ae*} t_{kj}^{db} t_{il}^{ce} + \sum_{ijklde} t_{lk}^{ed*} t_{ji}^{ca*} t_{li}^{eb} t_{kj}^{dc} + \dots, \quad (11.38)
\end{aligned}$$

$$\begin{aligned}
(\Gamma_N)_{ji} = & -\sum_a t_j^{a*} t_i^a - \frac{1}{2} \sum_{kab} t_{kj}^{ba*} t_{ki}^{ba} - \sum_{kab} t_{kj}^{ba*} t_k^b t_i^a - \sum_{kab} t_k^{b*} t_j^{a*} t_{ki}^{ba} \\
& + \sum_{kab} t_k^{b*} t_j^{a*} t_k^a t_i^b - \frac{1}{24} \sum_{klabc} t_{lkj}^{cba*} t_{lki}^{cba} - \frac{1}{2} \sum_{klabc} t_{lkj}^{cba*} t_l^c t_{ki}^{ba} \\
& - \frac{1}{4} \sum_{klabc} t_{lki}^{cba*} t_{lk}^{cb} t_i^b - \frac{1}{2} \sum_{klabc} t_l^{c*} t_{kj}^{ba*} t_{lki}^{cba} - \frac{1}{4} \sum_{klabc} t_{lk}^{cb*} t_j^{a*} t_{lki}^{cba} \\
& - \sum_{klabc} t_l^{c*} t_{kj}^{ba*} t_{lk}^{cb} t_i^a - \sum_{klabc} t_{lk}^{cb*} t_j^{a*} t_l^c t_{ki}^{ba} - \sum_{klabc} t_k^{b*} t_{jl}^{ac*} t_{ki}^{ba} t_l^c \\
& + \sum_{klabc} t_l^{c*} t_{kj}^{ba*} t_l^b t_{ki}^{ca} + \frac{1}{2} \sum_{klabc} t_l^{c*} t_{kj}^{ba*} t_k^c t_{li}^{ba} + \frac{1}{2} \sum_{klabc} t_{lk}^{cb*} t_j^{a*} t_{lk}^{ca} t_i^b \\
& + \frac{1}{2} \sum_{klabc} t_{lk}^{cb*} t_j^{a*} t_{li}^{cb} t_k^a + \frac{1}{2} \sum_{klabc} t_{lj}^{cb*} t_k^{a*} t_{lk}^{cb} t_i^a \\
& + \frac{1}{2} \sum_{klmabcd} t_{ml}^{dc*} t_{kj}^{ba*} t_{ml}^{db} t_{ki}^{ca} + \frac{1}{4} \sum_{klmabcd} t_{ml}^{dc*} t_{kj}^{ba*} t_{mk}^{dc} t_{li}^{ba} \\
& + \frac{1}{4} \sum_{klmabcd} t_{lk}^{cb*} t_{jm}^{ad*} t_{li}^{cb} t_{km}^{ad} - \sum_{klmabcd} t_{ml}^{dc*} t_{kj}^{ba*} t_{mi}^{da} t_{jk}^{cb} + \dots \quad (11.39)
\end{aligned}$$

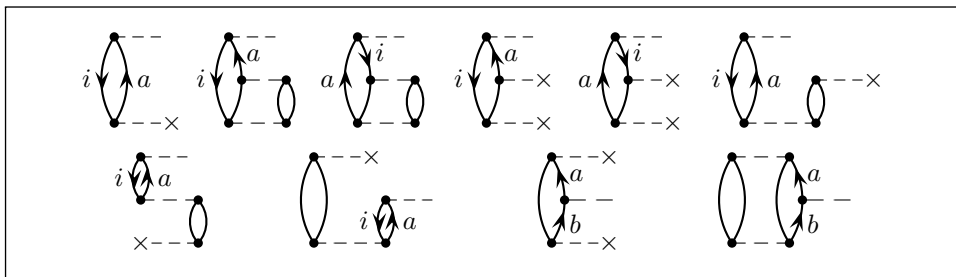


Fig. 11.3. The MBPT diagrams representing contributions to the particle-hole and particle-particle element of the one-body reduced density matrix through second order.

The coefficient $\frac{1}{24}$ for diagram 25 in the latter two equations derives from a factor $\frac{1}{(3!)}$ for a set of three equivalent lines times a factor $\frac{1}{2}$ for each of a pair of equivalent lines.

Using the MBPT expansions (9.93)–(9.95) etc. for the \hat{T}_m operators, we can generate the MBPT expansion for the density-matrix elements to any order. As an example, the diagrams for this expansion for the particle-hole and particle-particle elements to second order are shown in Fig. 11.3. The first eight diagrams in this figure represent γ_{ai} and the last two represent γ_{ba} . The first seven diagrams originate in the second-order MBPT expansion of diagram 1 of Fig. 11.1, the eighth originates from diagram 2 and the last two originate from diagrams 20 and 21, respectively, of Fig. 11.2.

The first diagram in Fig. 11.3 provides the only first-order contribution to the density matrix. When a Hartree–Fock reference function (canonical or otherwise) is used, this diagram vanishes since $f_{ia} = f_{ai} = 0$ in this case. Only the second, third and last diagrams survive in the HF case. All the diagrams in this figure originate in the \hat{T}_1 and \hat{T}_2 cluster operators (and their adjoints) in Figs. 11.1 and 11.2 and thus can be evaluated in a CCSD calculation. Hence the CCSD-derived density matrix is correct to second order, with many higher-order contributions included. The only other cluster operator in these figures is \hat{T}_3 , and therefore the CCSDT-derived density matrix is correct through fourth order. All the diagrams that contain a \hat{T}_3 vertex in Figs. 11.1 and 11.2 except diagram 7 require the second-order component only of the \hat{T}_3 operator to achieve fourth-order accuracy. Diagram 7 requires the third-order component of \hat{T}_3 for this purpose, and since this component is missing in the CCSDT-1 model (Section 10.5), this model produces a density matrix that is only accurate through third order. Similarly, the noniterative approximations to CCSDT-1, i.e. CCSD[T] and CCSD(T), also provide density matrices correct through third order.

A diagrammatic treatment of the two-body density matrix will be deferred to Section 11.7, pending the development of more effective tools for its evaluation. The CC wave function and the diagrammatic expansion of the density matrices can be used effectively to evaluate expectation values to any desired order of perturbation theory. This approach (Noga and Urban 1988) has only rarely been used but is sometimes a useful alternative to the definitive method discussed in the following sections. The nonterminating nature of the expansions and consequent lack of a closed-form expression and need for truncation are seen as serious disadvantages for the expectation-value approach from a formal viewpoint. The following sections describe the alternative, response, treatment for property evaluation, which is based on treating properties as responses to perturbations. The response treatment has become the standard approach to this problem.

11.3 The response treatment of properties

As an alternative to the use of expectation values, it is possible to evaluate properties in terms of the response of the molecular system to a suitable perturbation (Monkhorst 1977, Jørgensen and Simons 1983, Bartlett 1986). In fact, many molecular properties, such as derivatives of the energy with respect to displacements of the nuclei (energy gradients, Hessians etc.), cannot be represented simply by an expectation value but require a response treatment.

A Hamiltonian that depends on a parameter λ can be expanded in a Maclaurin series in λ :

$$\begin{aligned}\hat{H}(\lambda) &= \hat{H}(0) + \lambda \left. \frac{d\hat{H}}{d\lambda} \right|_{\lambda=0} + \frac{1}{2} \lambda^2 \left. \frac{d^2\hat{H}}{d\lambda^2} \right|_{\lambda=0} + \dots \\ &= \hat{H}^{(0)} + \lambda \hat{H}^{(1)} + \lambda^2 \hat{H}^{(2)} + \dots,\end{aligned}\tag{11.40}$$

where

$$\hat{H}^{(n)} = \left. \frac{1}{n!} \frac{d^n \hat{H}}{d\lambda^n} \right|_{\lambda=0}.\tag{11.41}$$

Here the unperturbed Hamiltonian $\hat{H}^{(0)} = \hat{H}(0)$ is the usual molecular Hamiltonian, including electron correlation, and the parameter λ represents the strength of a perturbation (such as an electric or magnetic field or the displacement of a nucleus). This expansion can be seen as a generalization of the usual perturbation expression $\hat{H} = \hat{H}_0 + \lambda \hat{V}$, in which the perturbation is linear in λ , with $\hat{H}^{(1)} = \hat{V}$, $\hat{H}^{(2)} = \hat{H}^{(3)} = \dots = 0$.

The energies corresponding to the Hamiltonian (11.40) can also be expanded in λ :

$$\begin{aligned} E(\lambda) &= E(0) + \lambda \left. \frac{dE}{d\lambda} \right|_{\lambda=0} + \frac{1}{2} \lambda^2 \left. \frac{d^2 E}{d\lambda^2} \right|_{\lambda=0} + \cdots \\ &= E^{(0)} + \lambda E^{(1)} + \lambda^2 E^{(2)} + \cdots, \end{aligned} \quad (11.42)$$

with a similar expansion for the wave function. When these expansions are substituted into the Schrödinger equation and terms of first order in λ are collected, we obtain the first-order equation

$$(\hat{H}^{(0)} - E^{(0)})|\Psi^{(1)}\rangle + (\hat{H}^{(1)} - E^{(1)})|\Psi^{(0)}\rangle = 0. \quad (11.43)$$

Projecting this equation onto $\langle\Psi^{(0)}|$ and noting that $\langle\Psi^{(0)}|\hat{H}^{(0)} = \langle\Psi^{(0)}|E^{(0)}$, we find

$$E^{(1)} = \left. \frac{dE(\lambda)}{d\lambda} \right|_{\lambda=0} = \frac{\langle\Psi^{(0)}|\hat{H}^{(1)}|\Psi^{(0)}\rangle}{\langle\Psi^{(0)}|\Psi^{(0)}\rangle}, \quad (11.44)$$

so that the expectation value of $\hat{H}^{(1)}$, which is the expectation value of the property operator \hat{O} when $\hat{H}(\lambda) = \hat{H}(0) + \lambda\hat{O}$, can be obtained as the derivative of the energy with respect to λ at $\lambda = 0$.

When the perturbation is due to an electric field $\vec{\mathcal{E}}$, the perturbation operator is given by the dot product $-\vec{\mathcal{E}} \cdot \sum_{\mu} q_{\mu} \vec{\mathbf{r}}_{\mu}$, where q_{μ} and $\vec{\mathbf{r}}_{\mu}$ are the charges and position vectors of the particles in the system. The first derivatives of the perturbed energy $E(\mathcal{E})$ with respect to the components of the field strength provide the components of the permanent dipole moment vector, $d_a^{(0)} = -\partial E(\mathcal{E})/\partial \mathcal{E}_a|_{\mathcal{E}=0}$ ($a = x, y, z$). This result is consistent with the expectation-value form $\vec{\mathbf{d}}^{(0)} = \langle\Psi|\sum_{\mu} q_{\mu} \vec{\mathbf{r}}_{\mu}|\Psi\rangle/\langle\Psi|\Psi\rangle$. The second derivatives provide the components of the dipole polarizability tensor, $\alpha_{ab} = -\partial^2 E(\mathcal{E})/\partial \mathcal{E}_a \partial \mathcal{E}_b|_{\mathcal{E}=0}$, and higher derivatives provide the respective hyperpolarizabilities. Properties obtained as n th derivatives of the perturbed energy are referred to as n th-order properties.

Equation (11.44), which is a manifestation of the Hellmann–Feynman theorem, is exact only for a variationally optimized $|\Psi^{(0)}\rangle$ and thus holds only for full (untruncated) CC. The numerical differences between the expectation value and the energy derivative at several levels of truncated CC were examined for the dipole moment of BH by Noga and Urban (1988).

The conceptual difference between an expectation value and the equivalent energy derivative is quite important in MBPT and CC theory, because the derivative form leads to closed-form expressions for properties. This form also allows the calculation of properties using energies that do not necessarily correspond to a wave function, such as those obtained in CCSD(T).

The derivatives can also be evaluated by finite difference methods, using CC calculations at small positive and negative values of λ , but analytical evaluation, as described in the following analysis, is more accurate and more efficient particularly when many perturbations have to be considered, as in the case of energy gradient calculations.

Splitting the perturbed correlated Hamiltonian into its normal-product part and its vacuum expectation value,

$$\hat{H}(\lambda) = \langle 0 | \hat{H}(\lambda) | 0 \rangle + \hat{H}_N(\lambda) = E_{\text{ref}}(\lambda) + \hat{H}_N(\lambda), \quad (11.45)$$

the corresponding perturbed correlated energy is given by

$$E(\lambda) = E_{\text{ref}}(\lambda) + \Delta E(\lambda). \quad (11.46)$$

When $\hat{H}(\lambda) = \hat{H}(0) + \lambda \hat{O}$, using (11.9) the components of the above equation can be written as

$$\begin{aligned} E_{\text{ref}}(\lambda) &= E_{\text{ref}}(0) + \lambda O_{\text{ref}}, \\ \Delta E(\lambda) &= \Delta E(0) + \lambda \Delta O. \end{aligned} \quad (11.47)$$

The evaluation of $E_{\text{ref}}(\lambda)$ is considered in Section 11.8; we shall concentrate here on the evaluation of $\Delta E(\lambda)$.

Using the CC effective Hamiltonian $\mathcal{H} = e^{-\hat{T}} \hat{H}_N e^{\hat{T}}$, the perturbed CC correlation energy, see (10.13), can be written in the form

$$\Delta E(\lambda) \hat{P} = \hat{P} \mathcal{H}(\lambda) \hat{P}. \quad (11.48)$$

The derivative of $\mathcal{H}(\lambda)$ with respect to λ can be obtained as

$$\begin{aligned} \frac{d\mathcal{H}}{d\lambda} &= \frac{d}{d\lambda} (e^{-\hat{T}} \hat{H}_N e^{\hat{T}}) \\ &= -\hat{T}^\lambda \mathcal{H} + e^{-\hat{T}} \hat{H}_N^\lambda e^{\hat{T}} + \mathcal{H} \hat{T}^\lambda = \mathcal{H}^{[\lambda]} + [\mathcal{H}, \hat{T}^\lambda], \end{aligned} \quad (11.49)$$

where

$$\mathcal{H}^{[\lambda]} \equiv e^{-\hat{T}} \hat{H}_N^\lambda e^{\hat{T}}. \quad (11.50)$$

The superscript λ indicates the derivative with respect to λ , and we have used the fact that the excitation operators in \hat{T}^λ and \hat{T} commute. For a linear perturbation, with $\hat{H}(\lambda) = \hat{H}(0) + \lambda \hat{O}$, we have $\mathcal{H}^{[\lambda]} = e^{-\hat{T}} \hat{O}_N e^{\hat{T}}$. The energy derivative is obtained as

$$\frac{d\Delta E}{d\lambda} \hat{P} \equiv \Delta E^\lambda \hat{P} = \hat{P} \mathcal{H}^{[\lambda]} \hat{P} + \hat{P} [\mathcal{H}, \hat{T}^\lambda] \hat{P}. \quad (11.51)$$

The derivatives \hat{T}^λ of the perturbed amplitudes can be eliminated from (11.51), leading to a much more convenient expression for the derivative

of the correlation energy. Inserting $\hat{P} + \hat{Q} = \hat{1}$ and using $\hat{P}\mathcal{H}\hat{P} = \Delta E \hat{P}$, $\hat{Q}\mathcal{H}\hat{P} = 0$, the second term of (11.51) becomes

$$\begin{aligned}\hat{P}[\mathcal{H}, \hat{T}^\lambda]\hat{P} &= \hat{P}\mathcal{H}(\hat{P} + \hat{Q})\hat{T}^\lambda\hat{P} - \hat{P}\hat{T}^\lambda(\hat{P} + \hat{Q})\mathcal{H}\hat{P} \\ &= \Delta E \hat{P}\hat{T}^\lambda\hat{P} + \hat{P}\mathcal{H}\hat{Q}\hat{T}^\lambda\hat{P} - \Delta E \hat{P}\hat{T}^\lambda\hat{P} - 0 = \hat{P}\mathcal{H}\hat{Q}\hat{T}^\lambda\hat{P},\end{aligned}\quad (11.52)$$

and the perturbed correlation energy takes the form

$$\Delta E^\lambda \hat{P} = \hat{P}\mathcal{H}^{[\lambda]}\hat{P} + \hat{P}\mathcal{H}\hat{Q}\hat{T}^\lambda\hat{P}. \quad (11.53)$$

Similarly, taking the derivative of the amplitude equations (10.13) gives

$$\hat{Q}\mathcal{H}^{[\lambda]}\hat{P} + \hat{Q}[\mathcal{H}, \hat{T}^\lambda]\hat{P} = 0. \quad (11.54)$$

Inserting $\hat{P} + \hat{Q} = \hat{1}$, the second term becomes

$$\begin{aligned}\hat{Q}[\mathcal{H}, \hat{T}^\lambda]\hat{P} &= \hat{Q}\mathcal{H}(\hat{P} + \hat{Q})\hat{T}^\lambda\hat{P} - \hat{Q}\hat{T}^\lambda(\hat{P} + \hat{Q})\mathcal{H}\hat{P} \\ &= \hat{Q}\mathcal{H}\hat{P}\hat{T}^\lambda\hat{P} + \hat{Q}\mathcal{H}\hat{Q}\hat{T}^\lambda\hat{P} - \hat{T}^\lambda\hat{P}\mathcal{H}\hat{P} - \hat{T}^\lambda\hat{Q}\mathcal{H}\hat{P} \\ &= \hat{Q}(\hat{Q}\mathcal{H}\hat{Q} - \Delta E_0)\hat{Q}\hat{T}^\lambda\hat{P}.\end{aligned}$$

The perturbed amplitudes are then obtained as

$$\hat{Q}\hat{T}^\lambda\hat{P} = \hat{Q}(\Delta E_0 - \hat{Q}\mathcal{H}\hat{Q})^{-1}\hat{Q}\mathcal{H}^{[\lambda]}\hat{P}. \quad (11.55)$$

Inserting this expression into the perturbed correlation energy (11.53), we have

$$\Delta E^\lambda \hat{P} = \hat{P}\mathcal{H}^{[\lambda]}\hat{P} + \hat{P}\mathcal{H}\hat{Q}(\Delta E_0 - \hat{Q}\mathcal{H}\hat{Q})^{-1}\hat{Q}\mathcal{H}^{[\lambda]}\hat{P}, \quad (11.56)$$

in which \hat{T}^λ has been eliminated.

Defining an effective resolvent operator $\mathcal{R}(\lambda)$ based on $\mathcal{H}(\lambda)$,

$$\mathcal{R}(\lambda) = \hat{Q}[\Delta E(\lambda) - \hat{Q}\mathcal{H}(\lambda)\hat{Q}]^{-1}\hat{Q} \equiv \frac{\hat{Q}}{\Delta E(\lambda) - \mathcal{H}(\lambda)}, \quad (11.57)$$

we have

$$\Delta E^{(\lambda)} \hat{P} = \hat{P}\mathcal{H}^{[\lambda]}\hat{P} + \hat{P}\mathcal{H}\mathcal{R}\mathcal{H}^{[\lambda]}\hat{P}. \quad (11.58)$$

When $\lambda = 0$ this equation provides the first-order energy,

$$\Delta E^{(1)} \hat{P} = \hat{P}\mathcal{H}^{[1]}(0)\hat{P} + \hat{P}\mathcal{H}(0)\mathcal{R}(0)\mathcal{H}^{[1]}(0)\hat{P}. \quad (11.59)$$

Finally, recognizing that $\hat{P}\mathcal{H}\mathcal{R}\hat{Q}$ contains no derivatives (and is thus independent of the perturbation at the point $\lambda = 0$), we introduce a new operator (Bartlett 1986, Salter, Trucks and Bartlett 1989),

$$\Lambda(\lambda) = \hat{P}\mathcal{H}(\lambda)\mathcal{R}(\lambda)\hat{Q}, \quad (11.60)$$

so that we can write

$$\Delta E^\lambda \hat{P} = \hat{P}(1 + \Lambda)\mathcal{H}^{[\lambda]}\hat{P}. \quad (11.61)$$

Integrating this expression over λ we obtain $\Delta E \hat{P} = \hat{P}(1 + \Lambda)\mathcal{H}\hat{P}$, which is the fundamental energy functional of CC theory (Section 11.4).

Inversion of the denominator in (11.57) will not be required, because it is to be replaced by a solution of a system of simultaneous linear equations for Λ , as described in Section 11.5 below. Because this system of equations is solved at $\lambda = 0$, it is independent of the perturbation and needs to be solved only once for any number of perturbations. Once Λ is known, the first-order properties can be obtained in closed form.

Unlike the equivalence shown between the transition and expectation-value forms for the energy, this derivation does not depend upon $\hat{Q}\mathcal{H}\hat{P} = 0$ for all possible excitations; rather, the derivation of (11.53), (11.55) remains correct for any truncation of \hat{T} as long as the same truncation is applied consistently in all equations (including the original calculation of the unperturbed energy and amplitudes). Thus this procedure is applicable for any of the CC models discussed in Chapter 10 and for any order of perturbation theory. Furthermore, since correspondence between a wave function and an energy is not required in this analysis, these equations can equally well be applied for methods such as CCSDT-1, but they need some modification for two-step methods such as CCSD(T) (Lee and Rendell 1991; Watts, Gauss and Bartlett 1992, 1993).

It should be emphasized that $\Lambda(0)$ needs to be computed once only; this is followed by the evaluation of its dot product with $\hat{Q}\mathcal{H}^{[\lambda]}\hat{P}$ for any number of properties. The significance of this aspect is obvious when there are many perturbations, as in the case of analytical gradients of potential-energy surfaces when about $3N$ independent atomic displacements for the N atoms in a molecule need to be considered. If one had to compute all $3N \hat{T}^\lambda$ perturbed amplitudes, rather than evaluating the dot products of a single Λ with the set of \mathcal{H}^λ derivatives, coupled-cluster theory would not have become the exceptional tool it now is for applications to molecular potential-energy surfaces. This procedure, a manifestation of the *interchange theorem* familiar from double perturbation theory (Sternheimer and Foley 1953, Dalgarno and Stewart 1958, Hirschfelder, Byers-Brown and Epstein 1964), is what makes analytical derivatives viable in the non-variational CC theory (Adamowicz, Laidig and Bartlett 1984, Bartlett 1986, Scheiner, Scuseria, Rice *et al.* 1987, Salter, Trucks and Bartlett 1989).

11.4 The CC energy functional

We shall now derive the results of the previous section in a different way, based on a stationarity requirement of a functional. Such an approach is convenient for the calculation of derivatives, including the extension to higher derivatives, because certain derivatives vanish when the functional is made stationary, so that a generalized Hellmann–Feynman theorem is applicable.

Consider a functional of Λ and \hat{T} defined by

$$\mathcal{E}(\Lambda, \hat{T}) = \hat{P}\mathcal{E}(\Lambda, \hat{T})\hat{P} = \hat{P}(1 + \Lambda)e^{-\hat{T}}\hat{H}_N e^{\hat{T}}\hat{P}. \quad (11.62)$$

At this point nothing is said about the nature of Λ and \hat{T} , except that they (and \hat{H}_N) depend on λ and that Λ is a de-excitation operator while \hat{T} is an excitation operator:

$$\Lambda\hat{P} = 0, \quad \Lambda = \Lambda\hat{Q}, \quad \hat{P}\hat{T} = 0, \quad \hat{T} = \hat{Q}\hat{T}. \quad (11.63)$$

Noting (11.63), the variation of the functional with respect to its arguments is given by

$$\begin{aligned} \hat{P}\delta\mathcal{E}\hat{P} &= \hat{P}\delta\Lambda\hat{Q}\mathcal{H}\hat{P} + \hat{P}(1 + \Lambda\hat{Q})\delta(e^{-\hat{T}}\hat{H}_N e^{\hat{T}})\hat{P} \\ &= \hat{P}\delta\Lambda\hat{Q}\mathcal{H}\hat{P} + \hat{P}(1 + \Lambda\hat{Q})[\mathcal{H}, \delta\hat{T}]\hat{P}, \end{aligned} \quad (11.64)$$

where $\mathcal{H} = e^{-\hat{T}}\hat{H}_N e^{\hat{T}}$. Requiring that this functional be stationary with respect to both Λ and \hat{T} , we set the coefficients of $\delta\Lambda$ and $\delta\hat{T}$ to zero. For the first term we find

$$\hat{Q}\mathcal{H}\hat{P} = 0, \quad (11.65)$$

so that requiring that \mathcal{E} be stationary with respect to Λ corresponds to satisfying the CC amplitude equations. With this result, and with $\Delta E\hat{P} = \hat{P}\mathcal{H}\hat{P}$, the second term of (11.64) can be transformed to

$$\hat{P}[\mathcal{H}, \delta\hat{T}]\hat{P} + \hat{P}\Lambda\hat{Q}[\mathcal{H}, \delta\hat{T}]\hat{P} = \hat{P}(\mathcal{H} + \Lambda\hat{Q}\mathcal{H} - \Delta E\Lambda)\hat{Q}\delta\hat{T}\hat{P}.$$

Setting the coefficient of $\hat{Q}\delta\hat{T}\hat{P}$ to zero yields

$$\hat{P}\mathcal{H}\hat{Q} + \hat{P}\Lambda\hat{Q}(\mathcal{H} - \Delta E)\hat{Q} = 0. \quad (11.66)$$

When the stationarity conditions are satisfied we have

$$\hat{P}\mathcal{E}\hat{P} = \hat{P}(1 + \Lambda)\mathcal{H}\hat{P} = \hat{P}\mathcal{H}\hat{P} = \Delta E\hat{P}, \quad (11.67)$$

since $\Lambda = \Lambda\hat{Q}$. Thus, when it is stationary the functional \mathcal{E} provides the perturbed correlation energy. These results are correct for all values of λ .

Furthermore, differentiation of the stationary functional with respect to λ yields

$$\Delta E^\lambda \hat{P} = \hat{P} \mathcal{E}^\lambda \hat{P} = \hat{P}(1 + \Lambda) \mathcal{H}^{[\lambda]} \hat{P}, \quad (11.68)$$

in agreement with (11.61). This result represents a generalized Hellmann–Feynman theorem, allowing the evaluation of derivatives of the energy in terms of derivatives of the Hamiltonian without differentiation of the wave function.

The functional \mathcal{E} (Arponen 1983, Salter, Trucks and Bartlett 1989, Szalay and Bartlett 1992, Bartlett 1995, Szalay, Nooijen and Bartlett 1995), often written simply as $\Delta E(\Lambda, \hat{T})$ (or $E(\Lambda, \hat{T})$ when the full Hamiltonian \hat{H} is used instead of \hat{H}_N), has been called the *fundamental energy functional* of CC theory. It can also be interpreted in terms of a constrained optimization process in which \mathcal{E} is made stationary subject to the satisfaction of the CC amplitude equations by adding the left-hand sides $\langle \Phi_{ij\dots}^{ab\dots} | \mathcal{H} | 0 \rangle$ of these equations, multiplied by Lagrange multipliers $\lambda_{ab\dots}^{ij\dots}$ (see Section 11.5), to the correlation energy (Koch and Jørgensen 1990). This functional plays the same role in CC theory as the expectation value of the Hamiltonian, treated as a functional of the CI excitation operator $\hat{C} = \hat{C}_1 + \hat{C}_2 + \dots$, plays in CI, where $|\Psi\rangle = (1 + \hat{C})|0\rangle$. In both cases making the functional stationary yields the corresponding wave function and energy. In the CC case the stationarity of \mathcal{E} also yields the de-excitation operator Λ .

11.5 The Λ equations

It has been shown in the previous two sections that property values can be expressed as derivatives of the perturbed energy with respect to a strength parameter λ at $\lambda = 0$ and that these derivatives can be evaluated in terms of the operator Λ and derivatives of the perturbed Hamiltonian \hat{H}_N . Thus the evaluation of Λ at the point $\lambda = 0$ is a key step in property calculations. Because $\Lambda(0)$ is independent of the perturbation it needs to be evaluated only once for any number of properties.

Straightforward evaluation of $\Lambda(0)$ from (11.60) would involve the non-diagonal resolvent $\mathcal{R}(0)$, which in turn requires inversion of the denominator $\hat{Q}(\mathcal{H} - \Delta E)\hat{Q}$, but a more efficient procedure is to solve the simultaneous equations (11.66) for Λ . This approach corresponds to the solution of the left eigenfunction equation for \mathcal{H} ,

$$\hat{P}(1 + \Lambda \hat{Q})(\mathcal{H} - \Delta E) = 0, \quad (11.69)$$

in which the eigenvalue ΔE and the operator $\mathcal{H} = (\hat{H}_N e^{\hat{T}})_C$ are known from the solution of the CC amplitude equations. Thus we have a set of *linear* simultaneous equations for the components of Λ . On the one hand these equations resemble the CC amplitude equations in that they are simultaneous equations rather than an eigenvalue problem, but on the other hand resemble the CI equations in that the unknown amplitudes appear linearly, the energy is not eliminated and they do not arise from the commutator expansion of an exponential and so are not limited to connected terms.

As in the treatment of \hat{T} , we expand Λ in single-, double- etc. de-excitation operators,

$$\Lambda = \Lambda_1 + \Lambda_2 + \Lambda_3 + \cdots, \quad (11.70)$$

where

$$\begin{aligned} \Lambda_1 &= \sum_{ia} \lambda_a^i \{i^\dagger a\}, \\ \Lambda_2 &= \frac{1}{4} \sum_{ijab} \lambda_{ab}^{ij} \{i^\dagger a j^\dagger b\}, \\ \Lambda_n &= \frac{1}{(n!)^2} \sum_{\substack{ij\dots \\ ab\dots}} \lambda_{ab\dots}^{ij\dots} \{i^\dagger a j^\dagger b \dots\}, \end{aligned} \quad (11.71)$$

in these expressions the de-excitation amplitudes $\lambda_a^i, \lambda_{ab}^{ij}, \lambda_{abc}^{ijk}, \dots$ are to be determined. These operators are represented diagrammatically by

$$\begin{array}{ccc} \begin{array}{c} \overline{\text{---}} \\ \diagup \quad \diagdown \\ i \quad a \\ \diagdown \quad \diagup \\ \lambda_a^i \{i^\dagger \hat{a}\} \end{array} & , & \begin{array}{c} \overline{\text{---}} \\ \diagup \quad \diagdown \quad \diagup \quad \diagdown \\ i \quad a \quad j \quad b \\ \diagdown \quad \diagup \quad \diagdown \quad \diagup \\ \lambda_{ab}^{ij} \{i^\dagger \hat{a} j^\dagger \hat{b}\} \end{array} & , & \begin{array}{c} \overline{\text{---}} \\ \diagup \quad \diagdown \quad \diagup \quad \diagdown \quad \diagup \quad \diagdown \\ i \quad a \quad j \quad b \quad k \quad c \\ \diagdown \quad \diagup \quad \diagdown \quad \diagup \quad \diagdown \quad \diagup \\ \lambda_{abc}^{ijk} \{i^\dagger \hat{a} j^\dagger \hat{b} k^\dagger \hat{c}\} \end{array} & , & \text{etc.} \end{array}$$

Projecting (11.69) onto \hat{P} merely reproduces the CC energy expression (11.67). Projecting it onto \hat{Q} produces the Λ amplitude equation

$$\hat{P}(1 + \Lambda \hat{Q})(\mathcal{H} - \Delta E)\hat{Q} = 0$$

or

$$\hat{P}\mathcal{H}\hat{Q} + \hat{P}\Lambda\mathcal{H}\hat{Q} - \Delta E\hat{P}\Lambda\hat{Q} = 0. \quad (11.72)$$

Because of the appearance of the energy in these equations the Λ amplitudes could be disconnected. The energy can be eliminated formally by introducing a commutator for the second term,

$$\begin{aligned} \hat{P}\Lambda\mathcal{H}\hat{Q} &= \hat{P}[\Lambda, \mathcal{H}]\hat{Q} + \hat{P}\mathcal{H}(\hat{P} + \hat{Q})\Lambda\hat{Q} \\ &= \hat{P}(\Lambda\mathcal{H})_C\hat{Q} + \Delta E\hat{P}\Lambda\hat{Q} + \hat{P}\mathcal{H}\hat{Q}\Lambda\hat{Q}, \end{aligned} \quad (11.73)$$

where the subscript C indicates a restriction to connected terms. For future reference we also note that

$$\hat{P}\Lambda\mathcal{H}\hat{P} = \hat{P}[\Lambda, \mathcal{H}]\hat{P} + \hat{P}\mathcal{H}\Lambda\hat{P} = \hat{P}(\Lambda\mathcal{H})_C\hat{P}, \quad (11.74)$$

because $\Lambda\hat{P} = 0$.

Substituting (11.73) into (11.72) cancels the energy-containing term, leaving

$$\hat{P}\mathcal{H}\hat{Q} + \hat{P}(\Lambda\mathcal{H})_C\hat{Q} + \hat{P}\mathcal{H}\hat{Q}\Lambda\hat{Q} = 0 \quad (11.75)$$

or

$$\hat{P}(\hat{H}_N e^{\hat{T}})_C\hat{Q} + \hat{P}(\Lambda(\hat{H}_N e^{\hat{T}})_C)_C\hat{Q} + \hat{P}(\hat{H}_N e^{\hat{T}})_C\hat{Q}\Lambda\hat{Q} = 0, \quad (11.76)$$

in which the last term is the only one that is not fully connected, consisting as it does of a product of two terms. Explicitly, this equation can be written in the form

$$\begin{aligned} & \langle 0 | \hat{H}_N e^{\hat{T}} | \Phi_{ij\dots}^{ab\dots} \rangle_C + \langle 0 | \Lambda(\hat{H}_N e^{\hat{T}})_C | \Phi_{ij\dots}^{ab\dots} \rangle_C \\ & + \sum_{\substack{k < l < \dots \\ c < d < \dots}} \langle 0 | \hat{H}_N e^{\hat{T}} | \Phi_{kl\dots}^{cd\dots} \rangle_C \langle \Phi_{kl\dots}^{cd\dots} | \Lambda | \Phi_{ij\dots}^{ab\dots} \rangle = 0. \end{aligned} \quad (11.77)$$

The intermediate state $|\Phi_{kl\dots}^{cd\dots}\rangle$ in the disconnected term must represent a de-excitation of the initial state $|\Phi_{ij\dots}^{ab\dots}\rangle$, and thus its indices must be a subset of the indices of that initial state.

Equation (11.77) has to be solved for the Λ_n amplitudes for all $i < j < \dots$ and $a < b < \dots$. When $|\Phi_{ij\dots}^{ab\dots}\rangle$ is a singly excited state $|\Phi_i^a\rangle$ the third term vanishes, since no \hat{Q} -state can be obtained by de-excitation of a singly excited state, and so the Λ_1 equations are fully connected,

$$\langle 0 | \hat{H}_N e^{\hat{T}} | \Phi_i^a \rangle_C + \langle 0 | \Lambda(\hat{H}_N e^{\hat{T}})_C | \Phi_i^a \rangle_C = 0 \quad (11.78)$$

for all i and a . These equations, truncated to the CCSDT case ($\hat{T} = \hat{T}_1 + \hat{T}_2 + \hat{T}_3$ and $\Lambda = \Lambda_1 + \Lambda_2 + \Lambda_3$), are represented by the diagrams in Fig. 11.4. Diagrams 1 and 2 in this figure represent the first term of (11.78), while diagrams 3–83 represent the second term. The latter diagrams all have a single Λ vertex and a single \hat{H}_N vertex but may have as many as three \hat{T} vertices. Specifically, diagrams 3–5 represent $\Lambda_1\hat{H}_N$ terms, 6–11 represent $\Lambda_1\hat{H}_N\hat{T}_1$, 12–14 represent $\Lambda_1\hat{H}_N\hat{T}_2$, 15–17 represent $\Lambda_1\hat{H}_N\frac{1}{2}\hat{T}_1^2$, 18 and 19 represent $\Lambda_2\hat{H}_N$, 20–23 represent $\Lambda_2\hat{H}_N\hat{T}_1$, 24–31 represent $\Lambda_2\hat{H}_N\hat{T}_2$, 32–35 represent $\Lambda_2\hat{H}_N\frac{1}{2}\hat{T}_1^2$, 36–43 represent $\Lambda_2\hat{H}_N\hat{T}_1\hat{T}_2$, and 44 and 45 represent $\Lambda_2\hat{H}_N\frac{1}{3!}\hat{T}_1^3$. The remaining diagrams contain \hat{T}_3 and/or Λ_3 vertices, and would not be included in a CCSD calculation. The open lines in all these

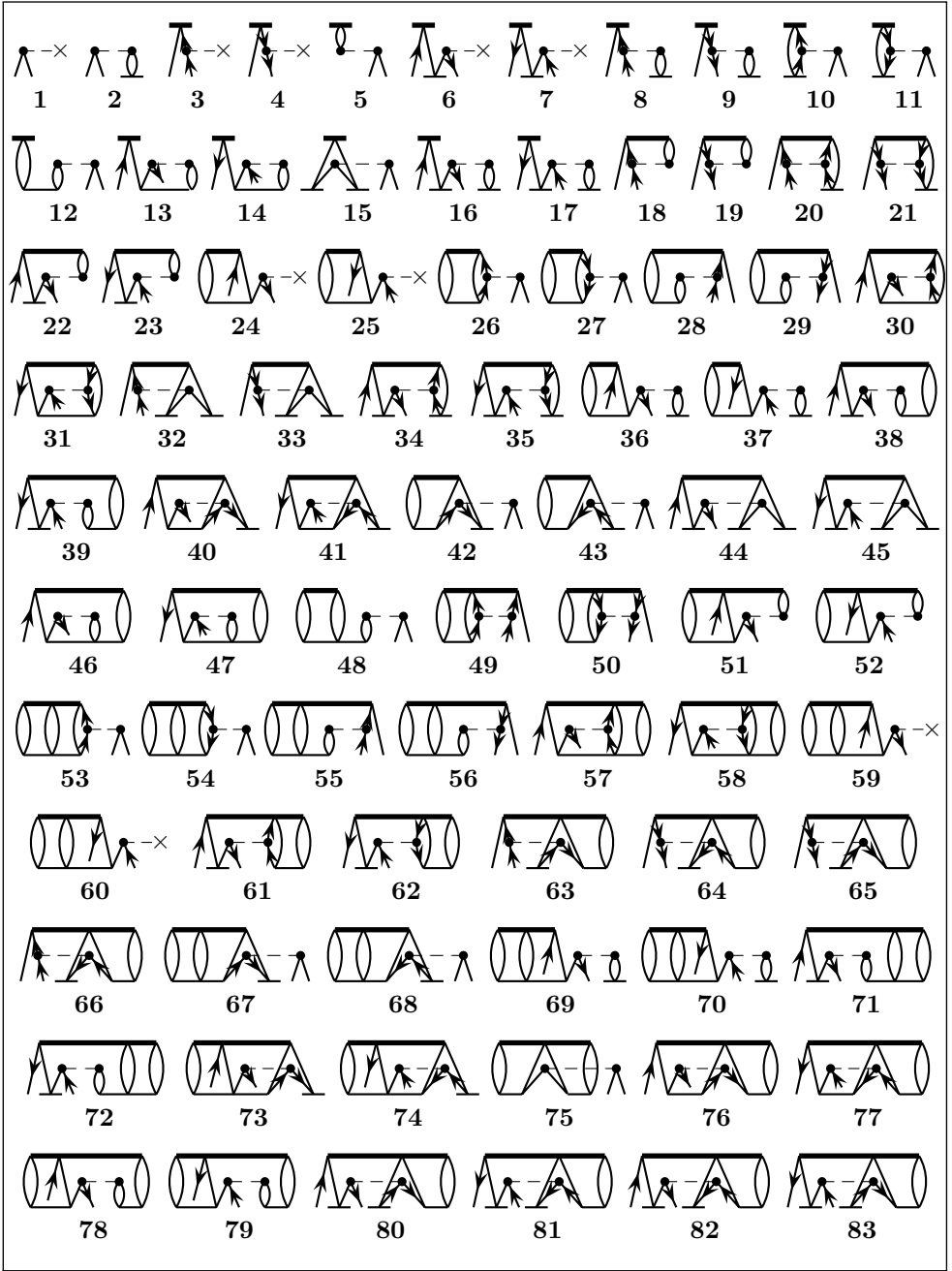


Fig. 11.4. Diagrams for the Λ_1 equations for CCSDT.

diagrams have the fixed labels a and i . Different values of a and i generate different equations in the set of simultaneous equations for Λ .

As indicated by the form of the second terms in (11.77) and (11.78), each \hat{T} vertex in the diagrams must have a direct connection to the interaction vertex. Diagrams that would become disconnected if the Λ vertex were removed, such as



do not contribute to the Λ equations. Furthermore, diagrams in which no open lines connect directly to the interaction vertex, such as



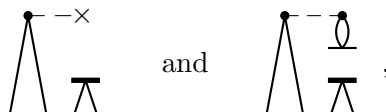
contain an embedded $\hat{Q}(\hat{H}_N e^{\hat{T}})_C |0\rangle$ component. While not individually vanishing, such diagrams add up to zero when the CC amplitude equations are satisfied and so have been left out of Fig. 11.4 and subsequent diagram sets for the Λ equations.

When $|\Phi_{ij\dots}^{ab\dots}\rangle$ in (11.77) is a doubly excited state we obtain the Λ_2 equations,

$$\langle 0 | \hat{H}_N e^{\hat{T}} | \Phi_{ij}^{ab} \rangle_C + \langle 0 | \Lambda \hat{H}_N e^{\hat{T}} | \Phi_{ij}^{ab} \rangle_C + \sum_{\substack{c=a,b \\ k=i,j}} \langle 0 | \hat{H}_N e^{\hat{T}} | \Phi_k^c \rangle_C \langle \Phi_k^c | \Lambda | \Phi_{ij}^{ab} \rangle = 0, \quad (11.79)$$

represented diagrammatically for the CCSDT case in Fig. 11.5. In this figure diagram 1 represents the first term in (11.79), the disconnected diagrams 2 and 3 represent the third term, and diagrams 4–71 represent the second term. Only diagrams 1–32 are needed in the CCSD case. The open lines in these diagrams carry the labels a, b, i, j and all permutations of a and b between inequivalent open particle lines and of i and j between inequivalent open hole lines must be included and also a weight factor $\frac{1}{2}$ for any pair of equivalent \hat{T} vertices, as in diagrams 31 and 32. As indicated in the rules of interpretation, Fig. 10.1, this factor can be canceled with one of the permutation operators.

The disconnected diagrams 2 and 3 represent $\hat{H}_N \Lambda_1$ and $\hat{H}_N \hat{T}_1 \Lambda_1$, respectively. Following the sequence of the operators in these terms, these diagrams should be drawn with the time sequences



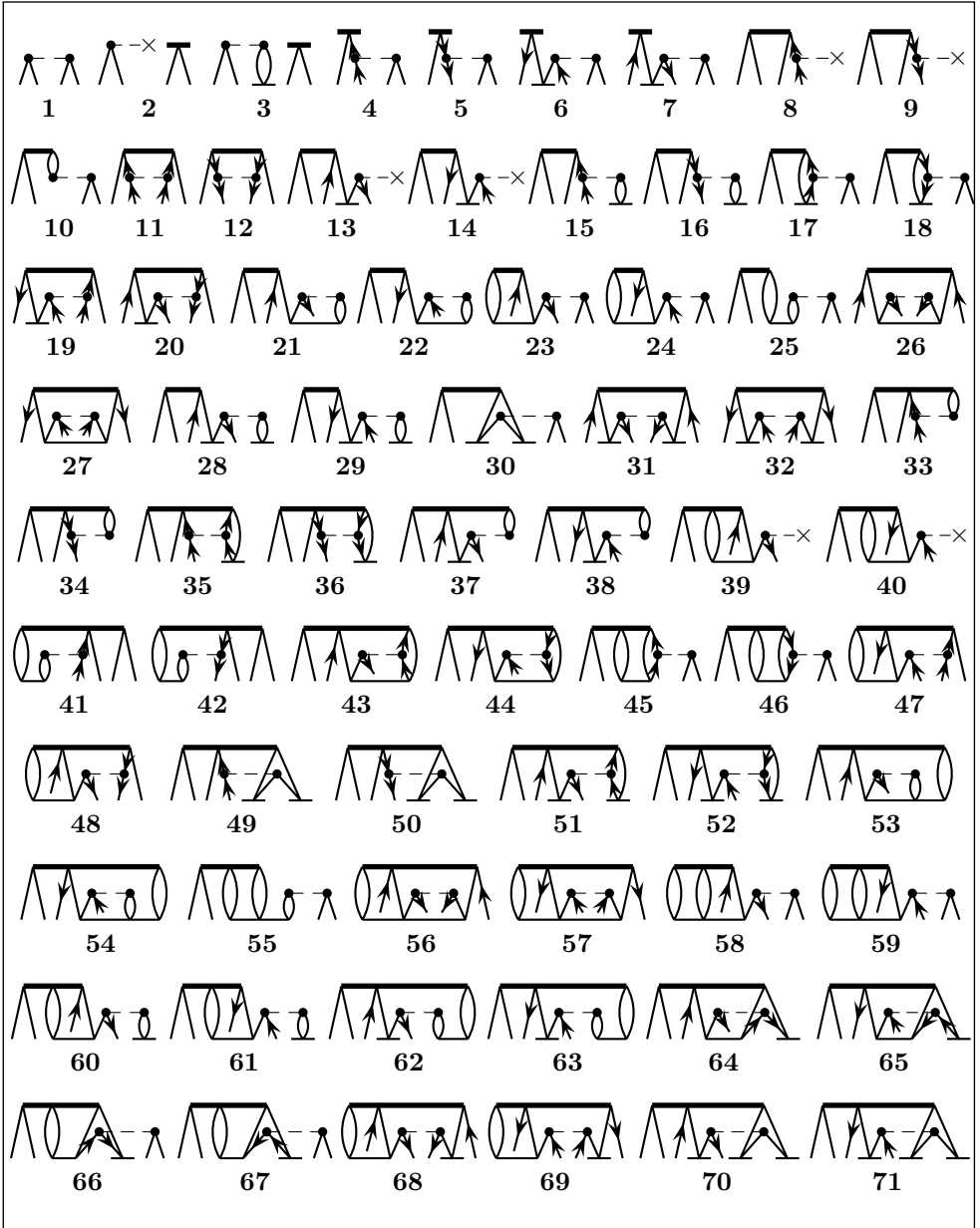


Fig. 11.5. Diagrams for the Λ_2 equations for CCSDT.

respectively, clearly showing the intermediate state. However, the sum over c and k in (11.77) can be expanded as follows,

$$\begin{aligned}
 \sum_{\substack{c=a,b \\ k=i,j}} \langle 0 | \hat{H}_N e^{\hat{T}} | \Phi_k^c \rangle_C \langle \Phi_k^c | \Lambda | \Phi_{ij}^{ab} \rangle \\
 &= \langle 0 | \hat{H}_N e^{\hat{T}} | \Phi_i^a \rangle_C \langle \Phi_i^a | \Lambda | \Phi_{ij}^{ab} \rangle + \langle 0 | \hat{H}_N e^{\hat{T}} | \Phi_i^b \rangle_C \langle \Phi_i^b | \Lambda | \Phi_{ij}^{ab} \rangle \\
 &\quad + \langle 0 | \hat{H}_N e^{\hat{T}} | \Phi_j^a \rangle_C \langle \Phi_j^a | \Lambda | \Phi_{ij}^{ab} \rangle + \langle 0 | \hat{H}_N e^{\hat{T}} | \Phi_j^b \rangle_C \langle \Phi_j^b | \Lambda | \Phi_{ij}^{ab} \rangle \\
 &= \langle 0 | \hat{H}_N e^{\hat{T}} | \Phi_i^a \rangle_C \langle 0 | \Lambda | \Phi_j^b \rangle - \langle 0 | \hat{H}_N e^{\hat{T}} | \Phi_i^b \rangle_C \langle 0 | \Lambda | \Phi_j^a \rangle \\
 &\quad - \langle 0 | \hat{H}_N e^{\hat{T}} | \Phi_j^a \rangle_C \langle 0 | \Lambda | \Phi_i^b \rangle + \langle 0 | \hat{H}_N e^{\hat{T}} | \Phi_j^b \rangle_C \langle 0 | \Lambda | \Phi_i^a \rangle \\
 &= \hat{P}(ij|ab) \langle 0 | \hat{H}_N e^{\hat{T}} | \Phi_i^a \rangle_C \langle 0 | \Lambda | \Phi_j^b \rangle. \tag{11.80}
 \end{aligned}$$

It is clear that this expression is represented by diagrams 2 and 3, interpreted as permutation sums of products of their disconnected parts, as drawn without regard for the time sequence in Fig. 11.5.

The diagrams for the Λ_3 equations for CCSDT are shown in Fig. 11.6. The disconnected diagrams 1–3 in this figure represent the third term of (11.77), which can be put into the form

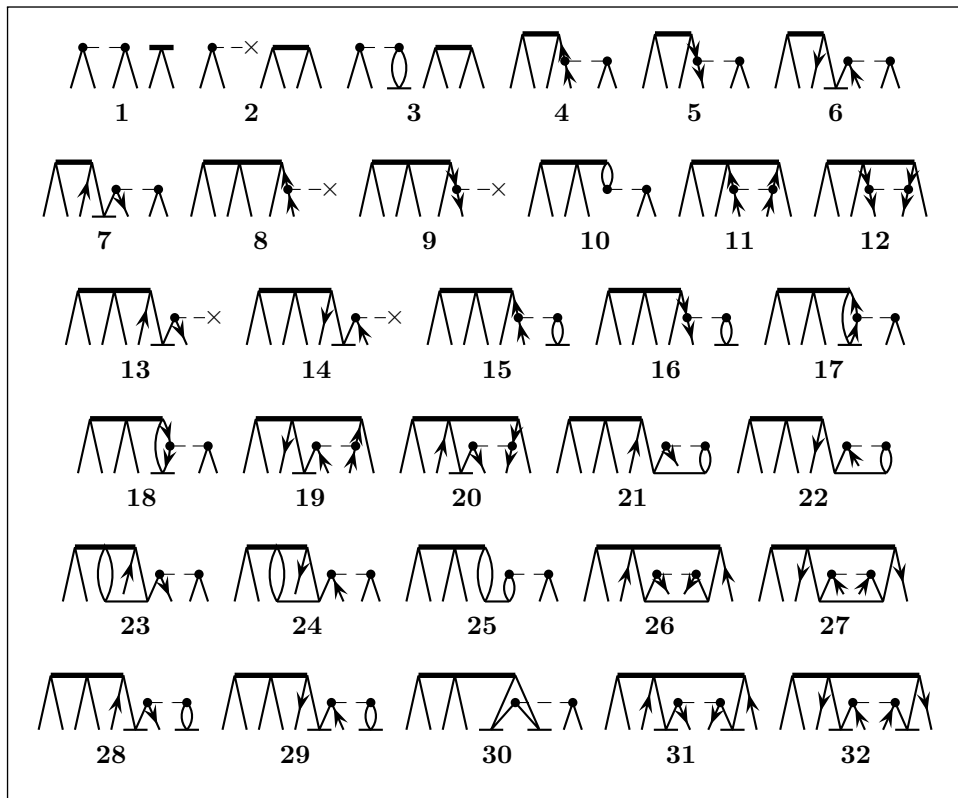
$$\sum_{\substack{d,e=a,b,c \\ l,m=i,j,k}} \langle 0 | \hat{H}_N e^{\hat{T}} | \Phi_{lm}^{de} \rangle_C \langle \Phi_{lm}^{de} | \Lambda | \Phi_{ijk}^{abc} \rangle + \sum_{\substack{d=a,b,c \\ k=i,j,k}} \langle 0 | \hat{H}_N e^{\hat{T}} | \Phi_l^d \rangle_C \langle \Phi_l^d | \Lambda | \Phi_{ijk}^{abc} \rangle,$$

involving both singly and doubly excited intermediate states. When drawn in the time sequence corresponding to the above expression, the disconnected diagrams take the forms



respectively, also represented as permutation sums of products, as drawn without regard to time sequence in Fig. 11.6.

While the Λ expansion includes disconnected terms, when the Λ diagrams are contracted with \mathcal{H} to form the diagrammatic representation of the CC energy functional (11.62) the resulting diagrams are fully connected. Thus all the CC energies and their derivatives are properly linked and connected, as required for extensivity.

Fig. 11.6. Diagrams for the Λ_3 equations for CCSDT.

Unlike the \hat{T} amplitude equations, which are nonlinear, the Λ amplitude equations are linear in Λ but are still solved iteratively because of their size. As in the treatment of the \hat{T} amplitude equations, the diagonal parts (involving f_{aa} and f_{ii}) of diagrams containing just the one-electron Hamiltonian operator and the Λ operator, i.e. diagrams 3 and 4 of Fig. 11.4 and diagrams 8 and 9 of Figs. 11.5 and 11.6, are moved to the opposite side of the equation, resulting in expressions for $\varepsilon_i^a \lambda_a^i$, $\varepsilon_{ij}^{ab} \lambda_{ab}^{ij}$ and $\varepsilon_{ijk}^{abc} \lambda_{abc}^{ijk}$, respectively, in terms of the other components of Λ .

Comparing the contributions of different perturbation-theory orders to the diagrams for the Λ equations with the corresponding contributions to the diagrams for the \hat{T} amplitude equations, it is easily seen that $\Lambda^{(1)} = \hat{T}^{(1)\dagger}$. Therefore \hat{T}^\dagger provides a suitable initial approximation to Λ in the iterative solution of the Λ equations. In second order we find a few differences between the diagrams contributing to the Λ equations and the adjoints of the diagrams contributing to the \hat{T} equations. For Λ_1 the difference is be-

tween diagram 2 of Fig. 11.4 and the adjoint of diagram S_{2a} of Fig. 10.2, so that

$$\begin{aligned} \varepsilon_i^a (\lambda_a^{i(2)} - t_i^{a(2)*}) &= \text{diagram 1} - \text{diagram 2}^{(1)} = \text{diagram 3} - \text{diagram 4} \\ &= \sum_{jb} \left(\frac{1}{\varepsilon_j^b} - \frac{1}{\varepsilon_{ij}^{ab}} \right) \langle ij \| ab \rangle f_{bj} = \varepsilon_i^a \sum_{jb} \frac{\langle ij \| ab \rangle f_{bj}}{\varepsilon_{ij}^{ab} \varepsilon_j^b}, \quad (11.81) \end{aligned}$$

where the thin horizontal lines indicate denominators. As a result we find that

$$\lambda_a^{i(2)} = t_i^{a(2)*} + \sum_{jb} t_{ij}^{ab(1)*} t_j^{b(1)}. \quad (11.82)$$

For Λ_2 we find

$$\lambda_{ab}^{ij(2)} = t_{ij}^{ab(2)*} + \hat{P}(ij) t_i^{a(1)*} t_j^{b(1)*}, \quad (11.83)$$

owing to the disconnected diagram 2 of Fig. 11.5, which has no counterpart in the \hat{T}_2 -equation diagrams of Figs. 9.2 and 10.3. Similarly,

$$\lambda_{abc}^{ijk(2)} = t_{ijk}^{abc(2)*} + \hat{P}(i/jk|a/bc) t_i^{a(1)*} t_{jk}^{bc(1)*}, \quad (11.84)$$

due to the disconnected diagrams 1 and 2 of Fig. 11.6. Equations (11.82)–(11.84) can be represented diagrammatically as

$$\overline{\Lambda}^{(2)} = \overline{\Lambda}^{(2)} + \overline{\Lambda}^{(1)} \text{diagram 1}, \quad (11.85)$$

$$\overline{\Lambda} \overline{\Lambda}^{(2)} = \overline{\Lambda} \overline{\Lambda}^{(2)} + \overline{\Lambda}^{(1)} \overline{\Lambda}^{(1)}, \quad (11.86)$$

$$\overline{\Lambda} \overline{\Lambda} \overline{\Lambda}^{(2)} = \overline{\Lambda} \overline{\Lambda} \overline{\Lambda}^{(2)} + \overline{\Lambda}^{(1)} \overline{\Lambda} \overline{\Lambda}^{(1)}. \quad (11.87)$$

All the second-order differences between Λ and \hat{T}^\dagger involve diagrams that vanish in the Hartree–Fock case, resulting in $\Lambda^{(2)} = \hat{T}^{(2)\dagger}$ and making \hat{T}^\dagger a particularly effective initial approximation to Λ in the HF case. The linearized CCSD approximation (LCCSD, analogous to the LCCD approximation of subsection 9.3.1) and MBPT through fourth order in the energy (which depends on the second-order wave function) involve linear terms only, so that in the HF case $\Lambda = \hat{T}^\dagger$ exactly and separate consideration of Λ is not required in these approximations.

11.6 Effective-Hamiltonian form of the Λ equations

Compact forms of the Λ equations can be obtained using the matrix elements of the effective Hamiltonian (10.51), given in Section 10.7. Expressing the Λ_1 equations for CCSDT in terms of effective-Hamiltonian matrix elements results in the 22 diagrams given in Fig. 11.7. The numbering of each diagram in this figure corresponds to the numbering of the leading term of its expansion in terms of the diagrams in Fig. 11.4. The diagrams of Fig. 11.4 accounted for by each diagram of Fig. 11.7 are listed in Table 11.1. Diagram 75 in this figure uses the three-body matrix element defined in (10.87). Its value does not change if all arrows are reversed; in either form, it expands into diagram 75 of Fig. 11.4.

All the diagrams in Fig. 11.7 are at most linear or pseudolinear in \hat{T} . However, pseudolinearity is less important in the Λ equations, because the \hat{T} amplitudes are known before these equations need to be solved.

Expressing the Λ_2 equations for CCSDT in terms of effective-Hamiltonian matrix elements results in the 22 diagrams given in Fig. 11.8. As in the case of the Λ_1 equations, the numbering of each diagram in this figure corresponds

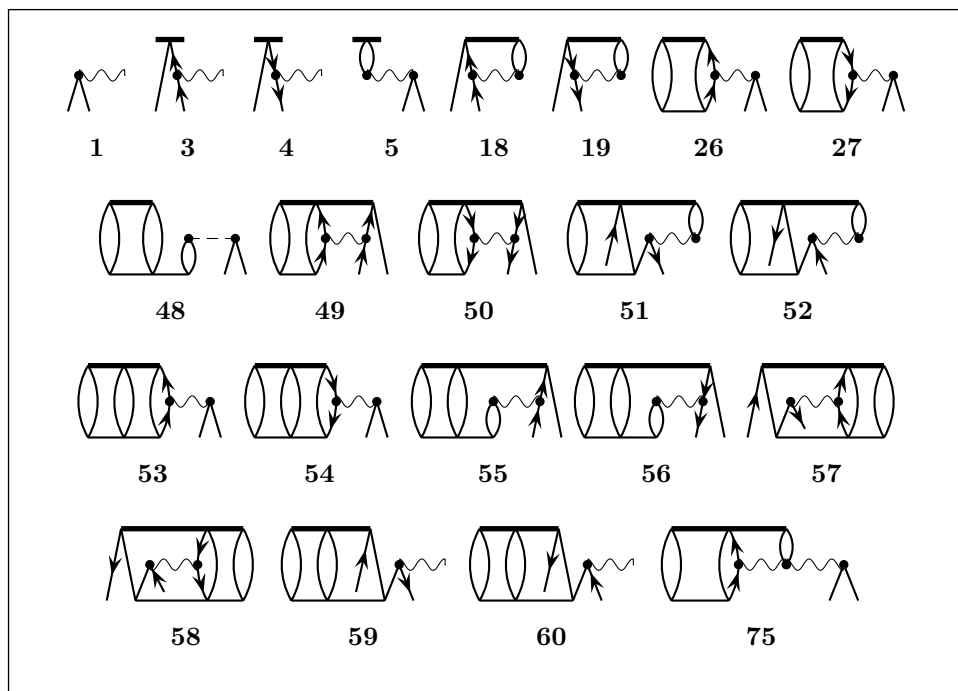


Fig. 11.7. Diagrams for the Λ_1 equations for CCSDT in terms of effective-Hamiltonian vertices.

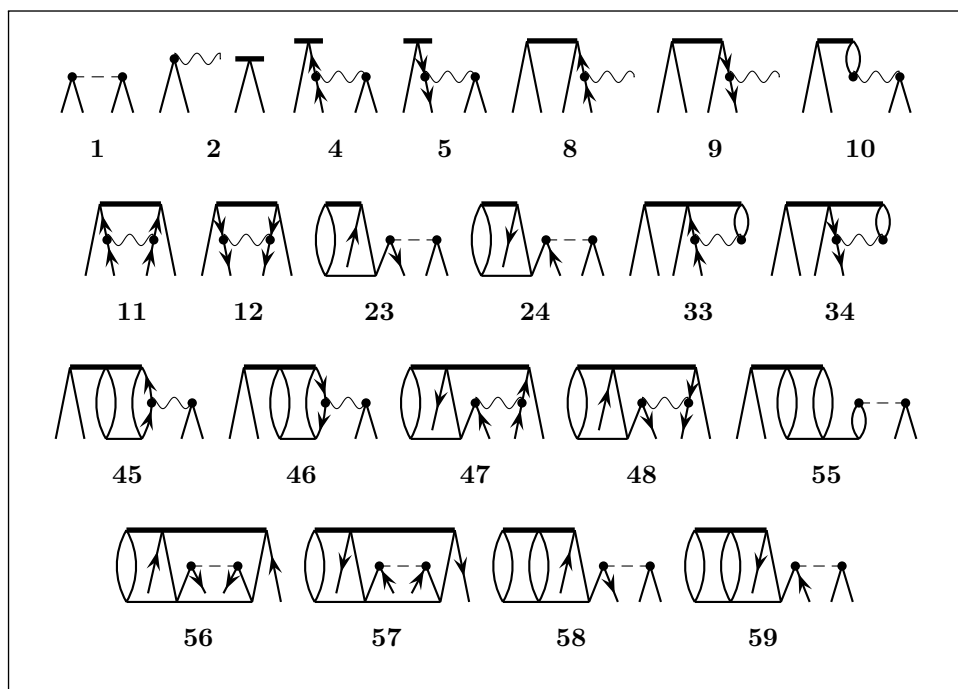


Fig. 11.8. Diagrams for the Λ_2 equations for CCSDT in terms of effective-Hamiltonian vertices.

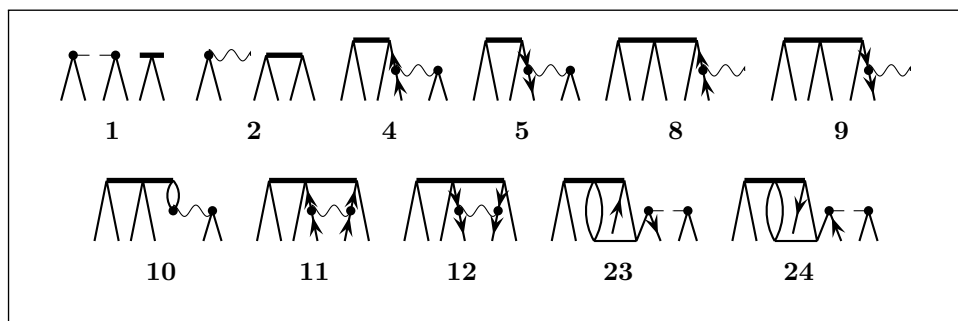


Fig. 11.9. Diagrams for the Λ_3 equations for CCSDT in terms of effective-Hamiltonian vertices.

to the numbering of the leading term of its expansion in terms of the diagrams in Fig. 11.5. The diagrams of Fig. 11.5 accounted for by each diagram of Fig. 11.8 are also listed in Table 11.1. Similar results for the Λ_3 equations are shown in Fig. 11.9 and Table 11.1.

The Λ -equation diagrams do not require the use of the various χ' , χ'' , etc. intermediates of Section 10.7. Permutation factors for labels of open lines

Table 11.1. Correspondence between the effective-Hamiltonian-based diagrams for the Λ equations and the original diagrams

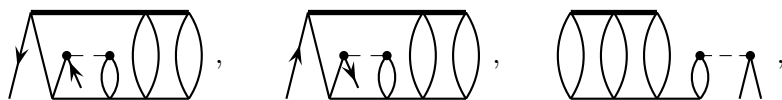
\mathcal{H} -based diagram	Original diagrams	\mathcal{H} -based diagram	Original diagrams
Λ_1 equations (Figs. 11.7 and 11.4)			
1	1, 2	50	50, 65, 76, 80
3	3, 7, 8, 14, 17	51	51, 61, 64, 78, 82
4	4, 6, 9, 13, 16	52	52, 62, 63, 79, 83
5	5, 10, 11, 12, 15	53	53, 67
18	18, 20, 23, 25, 28, 31, 32, 35, 37, 39, 41, 45, 47	54	54, 68
19	19, 21, 22, 24, 29, 30, 33, 34, 36, 38, 40, 44, 46	55	55, 72
26	26, 42	56	56, 71
27	27, 43	57	57, 73
48	48	58	58, 74
49	49, 66, 77, 81	59	59, 69
		60	60, 70
		75	75
Λ_2 equations (Figs. 11.8 and 11.5)			
1	1	33	33, 35, 38, 40, 41, 44, 49,
2	2, 3		52, 54, 61, 63, 65, 71
4	4, 6	34	34, 36, 37, 39, 42, 43, 50,
5	5, 7		51, 53, 60, 62, 64, 70
8	8, 14, 15, 22, 29	45	45, 66
9	9, 13, 16, 21, 28	46	46, 67
10	10, 17, 18, 25, 30	47	47, 69
11	11, 19, 27, 32	48	48, 68
12	12, 20, 26, 31	55	55
23	23	56	56
24	24	57	57
		58	58
		59	59
Λ_3 equations (Figs. 11.9 and 11.6)			
1	1	10	10, 17, 18, 25, 30
2	2, 3	11	11, 19, 27, 32
4	4, 6	12	12, 20, 26, 31
5	5, 7	23	23
8	8, 14, 15, 22, 29	24	24
9	9, 13, 16, 21, 28		

Table 11.2. Correspondence between the \hat{T} -free diagrams for the Λ equations in Fig. 11.10 and the diagrams in Figs. 11.7–11.9. Diagrams not listed, including all Λ_3 diagrams, are in one-to-one correspondence

Fig. 11.10	Figs. 11.7–11.9	Fig. 11.10	Figs. 11.7–11.9
Λ_1 equations		Λ_2 equations	
26	26, 27, 48	45	45, 46, 55
49	49, 52, 55, 58, 60 + one \hat{T}_4 diagram	47	47, 57
50	50, 51, 56, 57, 59 + one \hat{T}_4 diagram	48	48, 56
53	53, 54 + one \hat{T}_4 diagram		

that become closed lines when the diagrams expressing the \mathcal{H} vertices are embedded in the Λ -equation diagrams are automatically accounted for by the unrestricted summations over internal-line labels.

Using the three-body and four-body matrix elements of \mathcal{H} presented in Section 10.7, we can obtain even more compact representations of the Λ equations in terms of diagrams in which no \hat{T} vertices appear explicitly. These diagrams are given for CCSDT in Fig. 11.10, numbered according to their leading terms in Figs. 11.7–11.9. The correspondence between the two sets of diagrams is shown in Table 11.2. As indicated in that table, each of diagrams 49, 50 and 53 of the Λ_1 equation in Fig. 11.10 contains a \hat{T}_4 contribution that should be left out of a CCSDT calculation. These \hat{T}_4 contributions are described by the diagrams



in order.

The \hat{T} -free form of the Λ diagrams, as exemplified for CCSDT in Fig. 11.10, is the most direct representation of the Λ equation (11.75). The first term of that equation, $\hat{P}\mathcal{H}\hat{Q}$, is represented by the first diagram in each of the Λ_1 and Λ_2 diagram sets in Fig. 11.10. For the Λ_n equation, the second term, $\hat{P}(\Lambda\mathcal{H})_C\hat{Q}$, is represented by all connected diagrams that can be drawn containing a single \mathcal{H} vertex below a single Λ vertex, with n pairs of lines open at the bottom and no lines open at the top. (A pair of open lines consists of one particle line and one hole line.) Those connected diagrams in which the \mathcal{H} vertex has no open lines connecting directly to it contain an embedded $\hat{Q}\mathcal{H}\hat{P} = 0$ factor and may be left out. For the same equation,

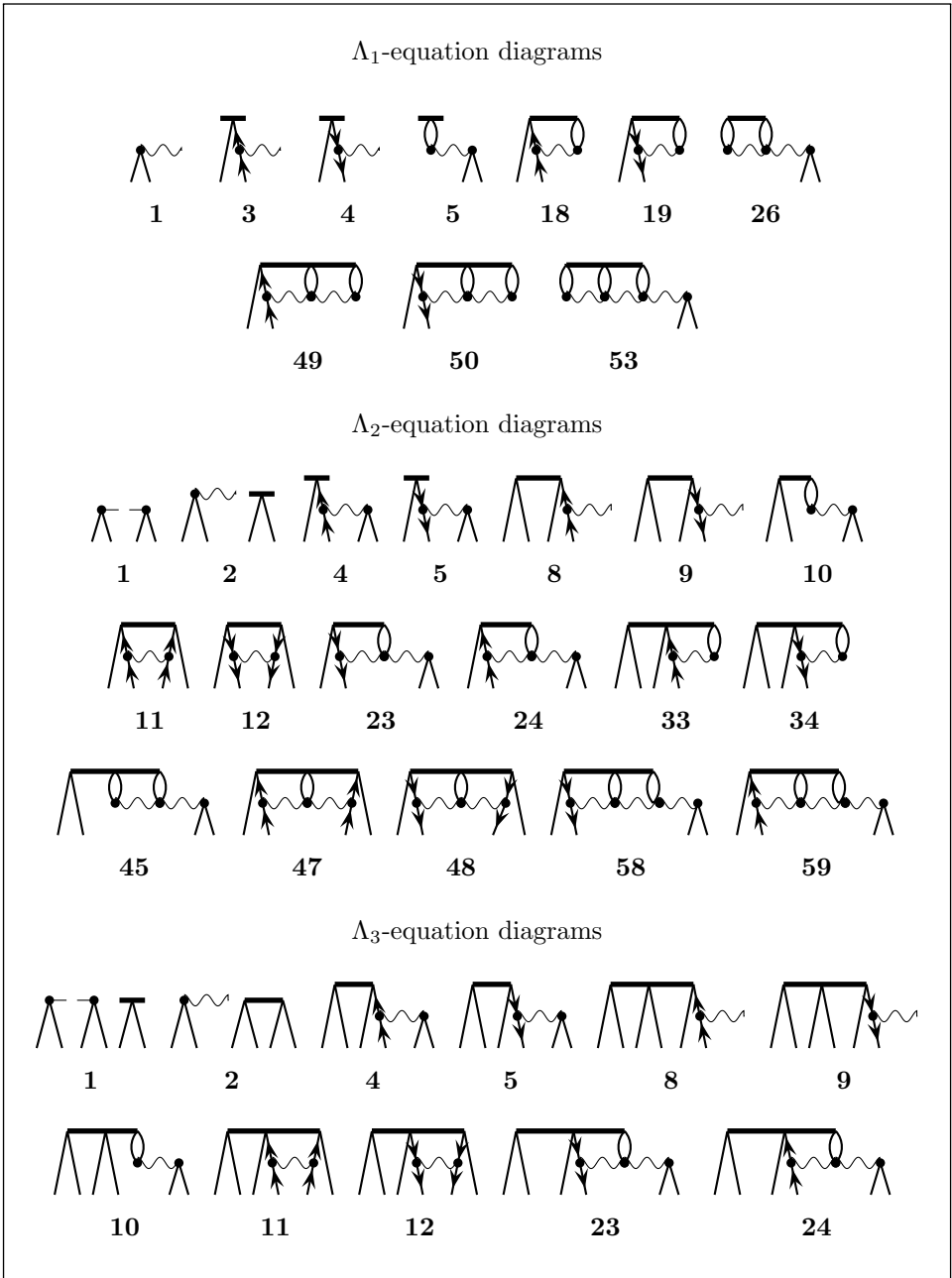


Fig. 11.10. The Λ -equation diagrams for CCSDT in terms of effective-Hamiltonian vertices without explicit \hat{T} vertices. The last three diagrams of the Λ_1 equation each contain a \hat{T}_4 contribution.

the third term, $\hat{P}\mathcal{H}\hat{Q}\Lambda\hat{Q}$, is represented by all diagrams containing one \mathcal{H} vertex and one Λ vertex disconnected from each other, with a total of n pairs of lines open at the bottom and no lines open at the top.

Using this analysis, the treatment can be extended to higher CC levels. Extension to CCSDTQ requires adding diagrams with Λ_4 vertices and possibly higher-order \mathcal{H} vertices to the Λ_1 – Λ_3 equations and generating the corresponding Λ_4 -equation diagrams. Additional intermediates would also need to be defined to facilitate efficient implementation of the calculations. In general, to generate diagrams describing the contributions of Λ_m vertices to the Λ_n equation, we need to use \mathcal{H} vertices with $n^\vee - n^\wedge = 2(m - n)$, where n^\vee and n^\wedge are the number of lines connecting to the \mathcal{H} vertex from above and from below, respectively. As noted previously, $n^\wedge < 4$ except for the two-body vertex, for which $n^\wedge = 4$ is also possible.

11.7 Response treatment of the density matrices

For coupled-cluster energy derivatives, and particularly for geometric derivatives of the potential-energy surface (gradients, Hessians etc.), it is important to maintain consistency between the energy calculations and the derivative calculations. Thus, for the correlation component of the energy derivatives we need the derivatives of the CC energy functional (11.62) rather than the derivatives of the correlation-energy expectation value (11.13). The density matrices appropriate for the determination of these derivatives are obtained by replacing the factor $e^{\hat{T}^\dagger}$ of (11.28), (11.31) by the factor $(1 + \Lambda)e^{-\hat{T}}$ of the CC energy functional, resulting in

$$(\gamma_N)_{qp} = \langle 0 | (1 + \Lambda) e^{-\hat{T}} \{ \hat{p}^\dagger \hat{q} \} e^{\hat{T}} | 0 \rangle = \langle 0 | (1 + \Lambda) \{ \{ \hat{p}^\dagger \hat{q} \} e^{\hat{T}} \}_C | 0 \rangle_C, \quad (11.88)$$

$$(\Gamma_N)_{rspq} = \langle 0 | (1 + \Lambda) \{ \{ \hat{p}^\dagger \hat{q}^\dagger \hat{s} \hat{r} \} e^{\hat{T}} \}_C | 0 \rangle_C, \quad (11.89)$$

noting (11.74). These matrices are referred to as *response density matrices*, to emphasize their origin in the CC energy derivatives treatment. Because of their linearity in Λ , they have the important benefit that they lead to finite expansions for any level of CC rather than the infinite expansions for the expectation-value forms seen in (11.37)–(11.39).

The diagrams for the hole–particle, particle–hole and particle–particle elements of the one-body response density matrix for the CCSDT case are shown in Fig. 11.11. Except for diagram 1', they are a subset of the diagrams in Figs. 11.1 and 11.2, with the top \hat{T}^\dagger vertex replaced by a Λ vertex, and are numbered correspondingly. Diagrams 14a and 14b have no counterparts in Fig. 11.1, because they are higher than fourth order in MBPT.

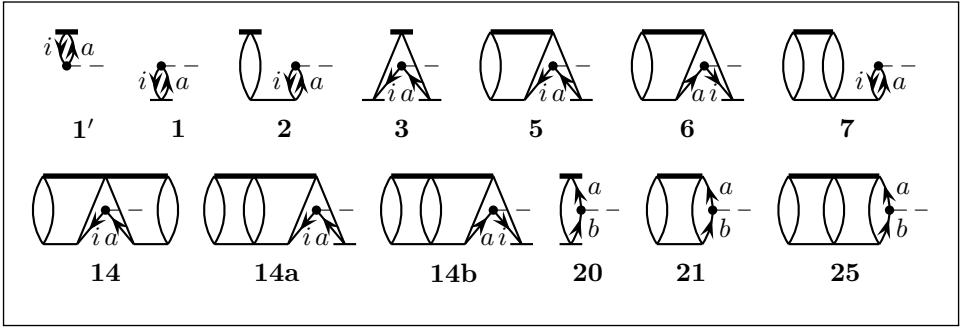


Fig. 11.11. Diagrams representing the hole-particle γ_{ia} (1'), the particle-hole γ_{ai} (1–14b) and the particle-particle γ_{ba} (20–25) elements of the one-body response density matrix for CCSDT.

Diagrams with more than one \hat{T}^\dagger vertex do not have a Λ counterpart, because of the linearity in Λ of the density matrix formula. Because of this linearity, the diagrams in Figs. 11.11 present untruncated expressions for the corresponding density-matrix elements for CCSDT. Also missing from the Λ -based diagrams are any diagrams that would become disconnected if the Λ vertex were removed, such as the counterparts of diagrams 4, 8 and 13 of Fig. 11.1, because of the connectedness restriction in (11.88). Diagram 1' represents the hole-particle element $\gamma_{ia} = \lambda_a^i$ and is the only surviving diagram arising from the adjoints of the diagrams of Fig. 11.1. Diagrams for the hole-hole matrix elements $(\gamma_N)_{ji}$ can be obtained by reversing all arrows in the particle-particle diagrams in Fig. 11.11 and replacing the particle labels a, b by hole labels j, i , respectively.

The asymmetry with respect to time inversion in the expansions obtained for the hole-particle (diagram 1') and particle-hole (diagrams 1–14b) elements is a manifestation of the non-Hermiticity of the CC energy functional and the corresponding Λ -based expressions for the density matrices, (11.88), (11.89). As a result, the response density matrices are not exactly Hermitian. Examination of the contributions of different MBPT orders to the hole-particle and particle-hole elements readily shows that $\gamma_{ia} = \gamma_{ai}^*$ in first order. At second order we find

$$\gamma_{ai}^{(2)} = \text{diagram 1' with two loops} + \text{diagram 1 with two loops} = t_i^{a(2)} + \sum_{jb} t_{ji}^{ba(1)} \lambda_b^{j(1)} = t_i^{a(2)} + \sum_{jb} t_{ji}^{ba(1)} t_j^{b(1)*}, \quad (11.90)$$

$$\gamma_{ia}^{(2)} = \text{diagram 1' with two loops} = \lambda_a^{i(2)} = t_i^{a(2)*} + \sum_{jb} t_{ji}^{ba(1)*} t_j^{b(1)}, \quad (11.91)$$

by (11.82), so that $\gamma_{ia}^{(2)} = \gamma_{ai}^{(2)*}$. As seen from diagrams 20 and 21 of Fig. 11.11, the particle–particle and hole–hole blocks of γ do not have first-order contributions, and they are Hermitian in second order because $\Lambda^{(1)} = \hat{T}^{(1)\dagger}$. Thus we see that γ is Hermitian at second order also.

For the two-body density matrix we find from (11.12) that some of the index-permutation relationships (11.26) still hold:

$$\Gamma_{rspq} = -\Gamma_{rsqp} = -\Gamma_{srpq} = \Gamma_{srqp}. \quad (11.92)$$

In general, $\Gamma_{rspq} \neq \Gamma_{pqrs}^*$. The diagrams for the two-body response density matrix for CCSDT are shown in Fig. 11.12 for the pppp, ppqh, phpp, pphh, hpph and hhpp elements, where p and h stand for particle and holes, respectively. Diagrams for hhph, hphh and hhhh can be obtained by reversing all arrows on the diagrams for ppph, phpp and pppp, respectively. The remaining matrix-element types can be obtained from matrix elements of the above diagrams using (11.92).

The pphh and hhpp blocks of Γ are the only blocks that have first-order contributions (from diagrams 21 and 66 of Fig. 11.12, respectively), and clearly are Hermitian conjugates of each other in that order. They also are Hermitian conjugates of each other in second order,

$$\Gamma_{abij}^{(2)} = a \text{---} \overbrace{\text{---} \text{---} \text{---} \text{---}}^{(2)} \text{---} b + a \text{---} \overbrace{\text{---} \text{---} \text{---} \text{---}}^{(1)} \text{---} b = t_{ij}^{ab(2)} + \hat{P}(ij)t_i^{a(1)}t_j^{b(1)}, \quad (11.93)$$

$$\Gamma_{ijab}^{(2)} = a \text{---} \overbrace{\text{---} \text{---} \text{---} \text{---}}^{(2)} \text{---} b = \lambda_{ab}^{ij(2)} = t_{ij}^{ab(2)*} + \hat{P}(ij)t_i^{a(1)*}t_j^{b(1)*}, \quad (11.94)$$

by (11.83), so that $\Gamma_{ijab}^{(2)} = \Gamma_{abij}^{(2)*}$. All other blocks involve only $\Lambda^{(1)}$ and $\hat{T}^{(1)}$ in second order and, because $\Lambda^{(1)} = \hat{T}^{(1)\dagger}$, the pppp, hhhh, phph and hphh blocks of Γ are clearly Hermitian at second order, and the hpph and phhp blocks are Hermitian conjugates of each other at second order. Only one diagram contributes at second order to each ppph and phpp block, and these blocks are also Hermitian conjugates of each other at second order. A similar result is obtained for the hhph and hphh blocks, the pphp and hhpp blocks, and the hhph and phhh blocks. Therefore Γ is Hermitian in second order.

The deviation from Hermiticity of the response density matrices is an artefact of the truncated CC treatment and disappears in full (untruncated) CC. As will be seen in Section 11.9, the anti-Hermitian components generate imaginary contributions to the CC energy derivatives used in property calculations. These contributions are mathematically correct components

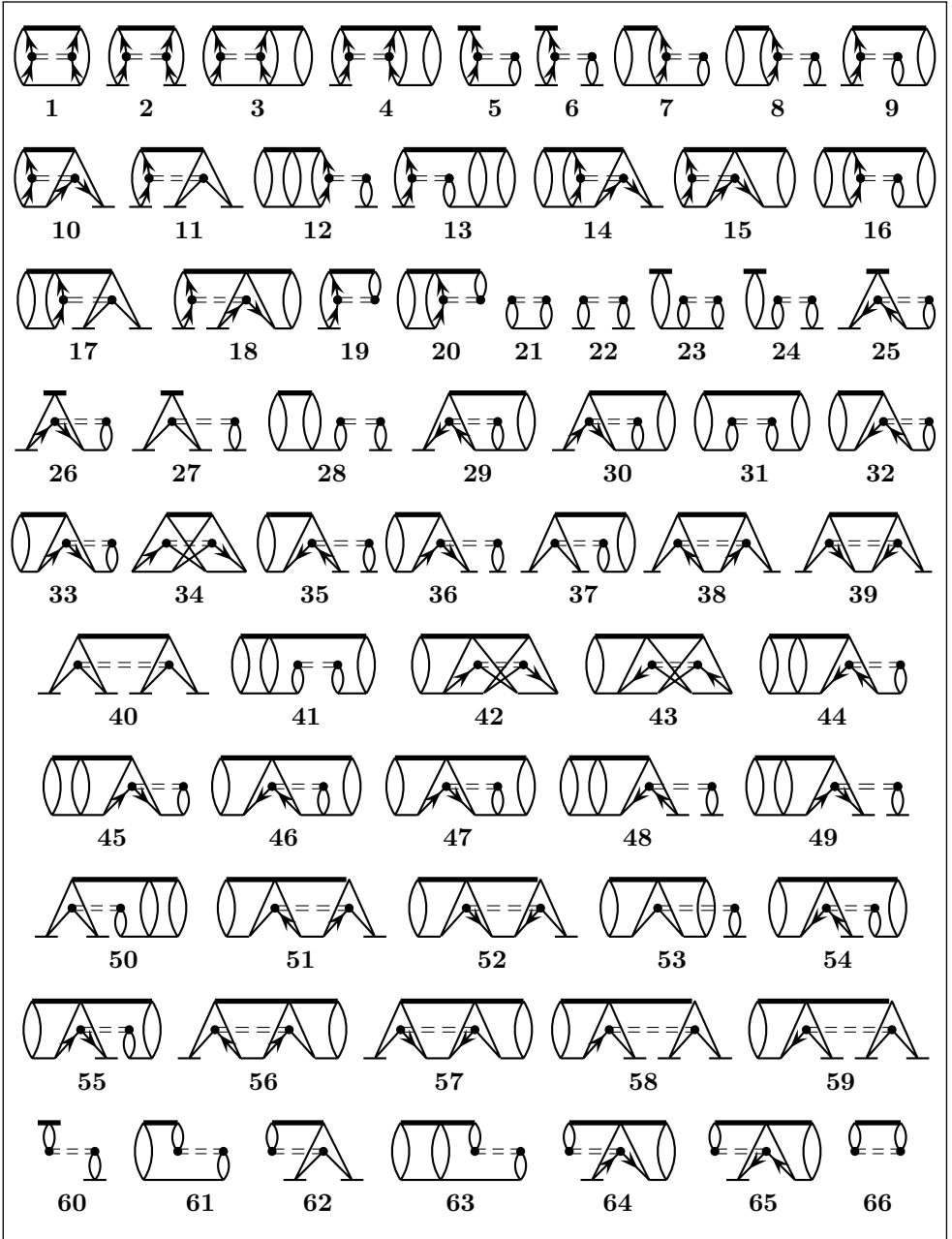


Fig. 11.12. Diagrams for the pppp (1–4), ppph (5–18), phpp (19, 20), pp hh (21–59), hpph (60–65) and hhpp (66) elements of the two-body response density matrix for CCSDT.

of the derivatives of the CC energy, consistent with the $\hat{Q}\hat{\mathcal{H}}\hat{P}$ energy expression, but they are clearly unphysical and are usually ignored. Because the response density matrix in CC property calculations appears only in dot products with sets of symmetric property integrals, lack of Hermiticity is not a problem. When the orbitals and matrices are real, as is the case in almost all calculations, the contributions from the anti-Hermitian components cancel.

The response density matrices can be defined for any system that offers an energy expression, even if there is no corresponding wave function. The need to solve the auxiliary Λ amplitude equations is the price paid for the failure of CC methods to produce a variational or stationary energy, but use of the CC energy functional redresses this defect. The calculation of properties in CI does not require knowledge of the λ -derivative of the CI coefficients, much less the solution of auxiliary equations. But for this small inconvenience in the CC methods we gain extensivity and the ability to generalize to any model that provides a well-defined energy expression. These advantages are shared by all MBPT approximations and by CC models such as CCSD(T) and are another reason why CC theory is the most frequently used high-level method in quantum chemistry today.

11.8 The perturbed reference function

When we are dealing with properties expressed in terms of expectation values of one-electron or two-electron operators, the above treatment, involving the solution of the Λ equations and evaluation of the corresponding response density matrices, is sufficient for the determination of the correlation contribution to the property values through (11.27) or (11.33). However, when the property also involves variation in the orbitals, additional factors accounting for orbital relaxation must be considered.

Within a given basis set, the electronic structure problem is fully specified by the set of one-electron and two-electron integrals over the basis functions (plus the internuclear-repulsion terms). On the one hand, in a full-CI calculation these integrals fully determine the results, regardless of how the basis functions are transformed into orbitals, since the wave function and energy are invariant under any linear transformation of the orbitals. On the other hand, in any truncated correlation treatment, such as truncated CI, finite-order perturbation theory or CC for any truncation of \hat{T} , the results are not invariant under arbitrary transformations of the orbitals, because these treatments depend critically on the choice of reference function (or reference space in the case of multireference treatments) and this function

depends, in turn, on the choice of the orbitals. The inclusion of \hat{T}_1 in a CC treatment reduces this dependence, because this operator has the effect of transforming the orbitals, but it does not eliminate it. In all these cases the results are fully determined by the one-electron and two-electron integrals over the *orbitals* and by the truncation scheme.

The dependence on the orbital integrals is obvious from the form of the second-quantized Hamiltonian. The creation and annihilation operators that appear in this Hamiltonian affect only the occupation numbers of the orbitals in the functions on which they operate. The orbitals must change smoothly under the effects of a perturbation, but their occupation numbers cannot be allowed to change if the wave function and energy are to vary smoothly. Therefore, while the creation and annihilation operators will create and annihilate the modified orbitals, the operators themselves remain formally unchanged and may be considered invariant under the perturbation as long as the orbital occupations do not change.

The orbitals, and thus the reference function, are usually chosen to satisfy some equation or condition that serves to provide a satisfactory zero-order function and, presumably, satisfactory convergence of the correlation treatment. Most commonly, this equation is the Hartree–Fock equation in any of its forms. For the consistency of the treatment for different values of the perturbation strength, and thus for obtaining meaningful values of the derivatives, we cannot ignore the impact of the perturbation on this equation or condition and its resulting effect on the reference function and orbitals. The resulting *orbital relaxation* leads to a perturbation of the response density matrix γ , to produce a *relaxed density matrix* as will be shown in Section 11.9.

In the present section we shall confine our analysis to the case in which the Hartree–Fock equation is used to determine the reference function. As throughout most of this book, the treatment will be in terms of the spin-orbitals, so that the relevant equation is the UHF equation. The common case of closed-shell restricted HF is easily accommodated by the spin-summation techniques described in Section 7.3. Other orbital choices can be treated by analogous methods, once we know the dependence of the orbitals on the perturbation. It will also be assumed here that the unperturbed HF function is in canonical form.

Under the effect of a one-electron perturbation, the usual UHF Fock operator

$$\hat{f} = \hat{h} + \hat{J} - \hat{K}, \quad (11.95)$$

with coulomb and exchange operators

$$\hat{J} = \sum_i \hat{J}_i, \quad \hat{K} = \sum_i \hat{K}_i \quad (11.96)$$

(Section 1.3), is modified not only by changes in the one-electron operator \hat{h} but also by changes induced in the Coulomb and exchange operators \hat{J} and \hat{K} by changes in the orbitals in terms of which they are defined. The perturbed Fock operator can be expanded in a strength parameter λ as

$$\begin{aligned} \hat{f}(\lambda) &= \hat{f}(0) + \lambda \left. \frac{d\hat{h}}{d\lambda} \right|_{\lambda=0} + \lambda \left. \frac{d(\hat{J} - \hat{K})}{d\lambda} \right|_{\lambda=0} \\ &\quad + \frac{1}{2} \lambda^2 \left. \frac{d^2 \hat{h}}{d\lambda^2} \right|_{\lambda=0} - \frac{1}{2} \lambda^2 \left. \frac{d^2 (\hat{J} - \hat{K})}{d\lambda^2} \right|_{\lambda=0} + \dots \\ &= \hat{f}^{(0)} + \lambda(\hat{h}^\lambda + \hat{J}^\lambda - \hat{K}^\lambda) + \dots = \hat{f}^{(0)} + \lambda \hat{f}^\lambda + \dots \end{aligned} \quad (11.97)$$

where

$$\hat{f}^\lambda = \hat{h}^\lambda + \hat{J}^\lambda - \hat{K}^\lambda. \quad (11.98)$$

In the common case in which the perturbation consists just of a one-electron operator $\lambda \hat{O} = \lambda \sum_{pq} \langle p | \hat{O} | q \rangle \{ \hat{p}^\dagger \hat{q} \}$ we simply have $\hat{h}^\lambda = \hat{O}$, without any higher-order terms in \hat{h} .

The basis functions used in the calculation may also be functions of λ . This dependence is absolutely essential when the property of interest is the analytical gradient, since atomic-orbital basis functions move with the atoms. In some other cases the basis functions can be made functions of an electric field (Pluta, Sadlej and Bartlett 1988) or magnetic field (London 1937, Ditchfield 1974, Gauss 1993). In the electric field case such a dependence is not common, but for a magnetic field the gauge dependence makes it a necessity. Of course, in a complete basis set or one that does not follow the atoms, such as a plane-wave basis, such variations should not arise.

The orbitals $\{\phi_p(\lambda)\}$ are expressed in terms of the basis functions $\{\chi_\nu(\lambda)\}$ by means of a transformation matrix $\mathbf{C}(\lambda)$:

$$\phi_p(\lambda) = \sum_\nu \chi_\nu(\lambda) C_{\nu p}(\lambda). \quad (11.99)$$

The elements $C_{\nu p}$ are known as the MO (molecular orbital) coefficients.

Without assuming that the perturbed HF orbitals are canonical, the HF equations can be written in the form

$$\hat{f}(\lambda)\phi_p(\lambda) = \sum_q \phi_q(\lambda)\varepsilon_{qp}(\lambda) \quad (\text{for all } p), \quad \langle \phi_p(\lambda) | \phi_q(\lambda) \rangle = \delta_{pq}, \quad (11.100)$$

with

$$\varepsilon_{ia}(\lambda) = \varepsilon_{ai}(\lambda) = 0 \quad (\text{for all } i, a). \quad (11.101)$$

Expanding $\phi_p(\lambda)$ according to (11.99) and operating from the left with $\langle \chi_\mu(\lambda) |$, we obtain the usual form of the HF equations in terms of the perturbed basis functions,

$$\mathbf{F}(\lambda)\mathbf{C}(\lambda) = \mathbf{S}(\lambda)\mathbf{C}(\lambda)\boldsymbol{\varepsilon}(\lambda), \quad \mathbf{C}^\dagger(\lambda)\mathbf{S}(\lambda)\mathbf{C}(\lambda) = \mathbf{1}, \quad (11.102)$$

where $F_{\mu\nu}(\lambda) = \langle \mu(\lambda) | \hat{f}(\lambda) | \nu(\lambda) \rangle$, $S_{\mu\nu}(\lambda) = \langle \mu(\lambda) | \nu(\lambda) \rangle$ and $\boldsymbol{\varepsilon}(\lambda)$ is the block-diagonal matrix of Lagrange multipliers $\varepsilon_{qp}(\lambda)$ satisfying (11.101).

We shall assume that the unperturbed HF function is canonical, so that the unperturbed equation is

$$\hat{f}^{(0)}\phi_p^{(0)} = \phi_p^{(0)}\varepsilon_p^{(0)} \quad (\text{for all } p), \quad (11.103)$$

or, in the unperturbed basis-function representation,

$$\mathbf{F}^{(0)}\mathbf{C}^{(0)} = \mathbf{S}^{(0)}\mathbf{C}^{(0)}\boldsymbol{\varepsilon}^{(0)} \quad (11.104)$$

where $\boldsymbol{\varepsilon}^{(0)}$ is the diagonal matrix of eigenvalues (orbital energies) $\{\varepsilon_p^{(0)}\}$.

We now expand the perturbed MO coefficients in terms of the unperturbed coefficients by means of a transformation matrix $\mathbf{U}(\lambda)$,

$$C_{\mu p}(\lambda) = \sum_q C_{\mu q}^{(0)} U_{qp}(\lambda), \quad \text{or} \quad \mathbf{C}(\lambda) = \mathbf{C}^{(0)}\mathbf{U}(\lambda). \quad (11.105)$$

Applying the transformation (11.105) to the perturbed HF equation (11.102) and multiplying on the left by $\mathbf{C}^{(0)\dagger}$, we obtain

$$\mathcal{F}(\lambda)\mathbf{U}(\lambda) = \mathcal{S}(\lambda)\mathbf{U}(\lambda)\boldsymbol{\varepsilon}(\lambda), \quad \mathbf{U}^\dagger(\lambda)\mathcal{S}(\lambda)\mathbf{U}(\lambda) = \mathbf{1}, \quad (11.106)$$

where

$$\mathcal{F}(\lambda) = \mathbf{C}^{(0)\dagger}\mathbf{F}(\lambda)\mathbf{C}^{(0)}, \quad \mathcal{S}(\lambda) = \mathbf{C}^{(0)\dagger}\mathbf{S}(\lambda)\mathbf{C}^{(0)}. \quad (11.107)$$

All matrices, orbitals and operators are expanded in powers of λ . For the zero-order matrices we have

$$\mathcal{F}^{(0)} = \boldsymbol{\varepsilon}^{(0)}, \quad \mathcal{S}^{(0)} = \mathbf{1}, \quad \mathbf{U}^{(0)} = \mathbf{1}. \quad (11.108)$$

The first-order perturbed HF equation is obtained from (11.106) as

$$\mathcal{F}^\lambda + \epsilon^{(0)} \mathbf{U}^\lambda = \mathcal{S}^\lambda \epsilon^{(0)} + \mathbf{U}^\lambda \epsilon^{(0)} + \epsilon^\lambda \quad (11.109)$$

or

$$[\mathbf{U}^\lambda, \epsilon^{(0)}] = \mathcal{F}^\lambda - \mathcal{S}^\lambda \epsilon^{(0)} - \epsilon^\lambda, \quad (11.110)$$

which corresponds to

$$(\epsilon_q^{(0)} - \epsilon_p^{(0)}) U_{pq}^\lambda = \mathcal{F}_{pq}^\lambda - \mathcal{S}_{pq}^\lambda \epsilon_q^{(0)} - \epsilon_{pq}^\lambda. \quad (11.111)$$

For $p = q$ the left-hand side of (11.111) vanishes, providing an equation for the diagonal elements of ϵ^λ ,

$$\epsilon_{pp}^\lambda = \mathcal{F}_{pp}^\lambda - \mathcal{S}_{pp}^\lambda \epsilon_p^{(0)}. \quad (11.112)$$

For the particle-hole block of \mathbf{U}^λ , for which $\epsilon_{ai}^\lambda = 0$, (11.111) becomes

$$(\epsilon_i^{(0)} - \epsilon_a^{(0)}) U_{ai}^\lambda = \mathcal{F}_{ai}^\lambda - \mathcal{S}_{ai}^\lambda \epsilon_i^{(0)}. \quad (11.113)$$

The equation for the hole-particle elements U_{ia}^λ is obtained by interchanging a and i in (11.113). For the hole-hole and particle-particle blocks of \mathbf{U}^λ we note that the off-diagonal Lagrange multipliers ϵ_{pq}^λ ($\{p, q\} = \{i, j\}$ or $\{a, b\}$) are at our disposal since they reflect separate unitary transformations among the perturbed hole orbitals and among the perturbed particle orbitals. Thus we choose a generalization of (11.112) in the form

$$\epsilon_{pq}^\lambda = \mathcal{F}_{pq}^\lambda - \frac{1}{2}(\epsilon_p^{(0)} + \epsilon_q^{(0)}) \mathcal{S}_{pq}^\lambda \quad (\{p, q\} = \{i, j\} \text{ or } \{a, b\}), \quad (11.114)$$

which satisfies the Hermiticity condition $\epsilon^{\lambda\dagger} = \epsilon^\lambda$. Substituting this choice into (11.111), we obtain

$$(\epsilon_q^{(0)} - \epsilon_p^{(0)}) U_{pq}^\lambda = \frac{1}{2}(\epsilon_p^{(0)} - \epsilon_q^{(0)}) \mathcal{S}_{pq}^\lambda$$

or

$$U_{pq}^\lambda = -\frac{1}{2} \mathcal{S}_{pq}^\lambda \quad (\{p, q\} = \{i, j\} \text{ or } \{a, b\}). \quad (11.115)$$

The diagonal elements U_{pp}^λ are not determined by (11.111) but can be obtained from the orthonormality condition in (11.106), which takes the first-order form

$$\mathbf{U}^{\lambda\dagger} + \mathcal{S}^\lambda + \mathbf{U}^\lambda = \mathbf{0}. \quad (11.116)$$

Because \mathcal{F}^λ and \mathcal{S}^λ are Hermitian, this condition is clearly satisfied by (11.113) and (11.115), so that the latter may also be used to determine the diagonal elements U_{pp}^λ .

Equations (11.111)–(11.115) provide expressions for all elements of \mathbf{U}^λ and $\boldsymbol{\varepsilon}^\lambda$, but equations (11.113) for the particle–hole block of \mathbf{U}^λ are not explicit because they are coupled by the dependence of \mathcal{F}^λ on \mathbf{U}^λ through the derivatives of the Coulomb and exchange integrals, (11.98). The equations (11.111) are known as the coupled-perturbed Hartree–Fock (CPHF) equations (Stevens, Pitzer and Lipscomb 1963, Gerratt and Mills 1968), and their solution will be derived in the following analysis.

The first-order perturbed orbitals are obtained from (11.99) and (11.105) as

$$\phi_p^\lambda = \sum_\nu (\chi_\nu^{(0)} C_{\nu p}^\lambda + \chi_\nu^\lambda C_{\nu p}^{(0)}) = \sum_q \phi_q^{(0)} U_{qp}^\lambda + \phi_p^{[\lambda]}, \quad (11.117)$$

where

$$\phi_p^{[\lambda]} = \sum_\nu \chi_\nu^\lambda C_{\nu p}^{(0)}. \quad (11.118)$$

For perturbations which do not involve changes in the basis functions the $\phi_p^{[\lambda]}$ part of (11.117) vanishes, and we need only consider the changes U_{qp}^λ in the orbital coefficients. For such perturbations, $\mathbf{S}(\lambda) = \mathbf{S}^{(0)}$, $\mathcal{S}(\lambda) = \mathbf{1}$ and $\boldsymbol{\mathcal{S}}^\lambda = \mathbf{0}$, resulting in the simplification of most of the preceding equations. Also, in such cases \mathbf{U}^λ is skew-Hermitian, i.e. $U_{ia}^\lambda = -U_{ai}^{\lambda*}$, and $U_{ij}^\lambda = U_{ab}^\lambda = 0$.

The matrix elements \mathcal{S}_{ai}^λ and \mathcal{F}_{ai}^λ , needed for the solution of the CPHF equations (11.113), are obtained as follows, where we set $|a\rangle = |\phi_a\rangle$, $|\mu\rangle = |\chi_\mu\rangle$ etc. and all (0) superscripts are omitted to simplify the notation:

$$\mathcal{S}_{ai}^\lambda = \sum_{\mu\nu} C_{\mu a}^* \langle \mu | \nu \rangle^\lambda C_{\nu i} = \langle a^{[\lambda]} | i \rangle + \langle a | i^{[\lambda]} \rangle = \langle a | i \rangle^{[\lambda]}, \quad (11.119)$$

$$\begin{aligned} \mathcal{F}_{ai}^\lambda &= \sum_{\mu\nu} C_{\mu a}^* \langle \mu(\lambda) | \hat{f}(\lambda) | \nu(\lambda) \rangle^\lambda C_{\nu i} \\ &= \langle a | \hat{f}^\lambda | i \rangle + \langle a^{[\lambda]} | \hat{f} | i \rangle + \langle a | \hat{f} | i^{[\lambda]} \rangle \\ &= \langle a | \hat{h}^\lambda | i \rangle + \langle a | \hat{J}^\lambda - \hat{K}^\lambda | i \rangle + \langle a^{[\lambda]} | \hat{J} - \hat{K} | i \rangle + \langle a | \hat{J} - \hat{K} | i^{[\lambda]} \rangle \\ &= \langle a | \hat{h}^\lambda | i \rangle + \sum_j (\langle a j^\lambda | i j \rangle + \langle a j | i j^\lambda \rangle + \langle a^{[\lambda]} j | i j \rangle + \langle a j | i^{[\lambda]} j \rangle) \\ &= \langle a | \hat{h}^\lambda | i \rangle + \sum_{jp} (U_{pj}^{\lambda*} \langle a p | i j \rangle + \langle a j | i p \rangle U_{pj}^\lambda) \end{aligned}$$

$$\begin{aligned}
& + \sum_j (\langle a j^{[\lambda]} \| i j \rangle + \langle a j \| i j^{[\lambda]} \rangle + \langle a^{[\lambda]} j \| i j \rangle + \langle a j \| i^{[\lambda]} j \rangle) \\
& = \langle a | \hat{h}^\lambda | i \rangle + \sum_{jb} (U_{bj}^{\lambda*} \langle ab \| i j \rangle + \langle a j \| i b \rangle U_{bj}^\lambda) \\
& + \sum_{jk} (U_{kj}^{\lambda*} \langle ak \| i j \rangle + \langle a j \| i k \rangle U_{kj}^\lambda) + \sum_j \langle a j \| i j \rangle^{[\lambda]}. \quad (11.120)
\end{aligned}$$

Since j and k are dummy summation indices in the first sum in the last line and may be interchanged, this sum may be written as

$$\sum_{jk} (U_{jk}^{\lambda*} + U_{kj}^\lambda) \langle a j \| i k \rangle = - \sum_{jk} \mathcal{S}_{kj}^\lambda \langle a j \| i k \rangle = - \sum_{jk} \langle a j \| i k \rangle \langle k | j \rangle^{[\lambda]},$$

using the orthogonality condition (11.116). Equation (11.120) then takes the form

$$\begin{aligned}
\mathcal{F}_{ai}^\lambda & = \langle a | \hat{h}^\lambda | i \rangle + \sum_{jb} (U_{bj}^{\lambda*} \langle ab \| i j \rangle + \langle a j \| i b \rangle U_{bj}^\lambda) \\
& - \sum_{jk} \langle a j \| i k \rangle \langle k | j \rangle^{[\lambda]} + \sum_j \langle a j \| i j \rangle^{[\lambda]}. \quad (11.121)
\end{aligned}$$

The CPHF equations (11.113) can now be written as

$$\begin{aligned}
(\varepsilon_i - \varepsilon_a) U_{ai}^\lambda & = \mathcal{F}_{ai}^\lambda - \mathcal{S}_{ai}^\lambda \varepsilon_i \\
& = \langle a | \hat{h}^\lambda | i \rangle + \sum_{jb} (U_{bj}^{\lambda*} \langle ab \| i j \rangle + \langle a j \| i b \rangle U_{bj}^\lambda) \\
& - \sum_{jk} \langle a j \| i k \rangle \langle k | j \rangle^{[\lambda]} + \sum_j \langle a j \| i j \rangle^{[\lambda]} - \langle a | i \rangle^{[\lambda]} \varepsilon_i. \quad (11.122)
\end{aligned}$$

The three terms in the last line of (11.122) are independent of the particle-hole block of \mathbf{U}^λ and vanish if the perturbation is not accompanied by a change in the basis functions. In other cases they can be computed from the basis-set derivative integrals; however, straightforward computation of the second term would require a four-index transformation of the basis-function derivative integrals to orbital derivative integrals, a relatively lengthy process that would have to be repeated for each perturbation. This transformation can be avoided by use of the reference-function density matrix in the basis-function representation,

$$P_{\nu\mu} = \sum_j C_{\mu j}^* C_{\nu j}, \quad (11.123)$$

or in matrix form

$$\mathbf{P} = \mathbf{C}_{\text{ref}} \mathbf{C}_{\text{ref}}^\dagger, \quad (11.124)$$

where it is understood that the matrix \mathbf{C}_{ref} contains only those columns of \mathbf{C} , (11.105), that correspond to the occupied (hole) orbitals. Using this density matrix (at zero order), the relevant term of (11.122) can be written as

$$\begin{aligned} \sum_j \langle aj || ij \rangle^{[\lambda]} &= \sum_{\mu\nu} C_{\mu a}^* C_{\nu i} \sum_{\sigma\tau} \langle \mu\sigma || \nu\tau \rangle^\lambda \sum_j C_{\sigma j}^* C_{\tau j} \\ &= \sum_{\mu\nu} C_{\mu a}^* C_{\nu i} \sum_{\sigma\tau} \langle \mu\sigma || \nu\tau \rangle^\lambda P_{\tau\sigma} \\ &= \sum_{\mu\nu} C_{\mu a}^* C_{\nu i} Y_{\mu\nu}^\lambda, \end{aligned} \quad (11.125)$$

where

$$Y_{\mu\nu}^\lambda = \sum_{\sigma\tau} \langle \mu\sigma || \nu\tau \rangle^\lambda P_{\tau\sigma} \quad (11.126)$$

represents a two-index contraction of the two-electron basis-set derivative integrals with the unperturbed reference-function density matrix.

Defining

$$X_{ai}^\lambda = \langle a | \hat{h}^\lambda | i \rangle - \langle a | i \rangle^{[\lambda]} \varepsilon_i - \sum_{jk} \langle aj || ik \rangle \langle k | j \rangle^{[\lambda]} + \sum_{\mu\nu} C_{\mu a}^* C_{\nu i} Y_{\mu\nu}^\lambda \quad (11.127)$$

and collecting the \mathbf{U}^λ -dependent terms on the left-hand side of the CPHF equation (11.113), we obtain

$$(\varepsilon_i - \varepsilon_a) U_{ai}^\lambda - \sum_{jb} (U_{bj}^{\lambda*} \langle ab || ij \rangle + \langle aj || ib \rangle U_{bj}^\lambda) = X_{ai}^\lambda. \quad (11.128)$$

If the perturbation is not accompanied by a change in the basis functions then (11.127) simplifies to

$$X_{ai}^\lambda = \langle a | \hat{h}^\lambda | i \rangle. \quad (11.129)$$

We next introduce the \mathbf{A} and \mathbf{B} matrices,

$$\begin{aligned} A_{ai,bj} &\equiv \langle \Phi_i^a | \hat{H} | \Phi_j^b \rangle = (\epsilon_a - \epsilon_i) \delta_{ij} \delta_{ab} - \langle aj || bi \rangle, \\ B_{ai,bj} &\equiv \langle \Phi_{ij}^{ab} | \hat{H} | 0 \rangle = \langle ab || ij \rangle, \end{aligned} \quad (11.130)$$

in which ai and bj are each treated as a single composite index. The CPHF equations (11.111) can then be rewritten as

$$\sum_{bj} (A_{ai,bj} U_{bj}^{\lambda} + B_{ai,bj} U_{bj}^{\lambda*}) = -X_{ai}^{\lambda} \quad (11.131)$$

or

$$\mathbf{A}\mathbf{U}^{\lambda} + \mathbf{B}\mathbf{U}^{\lambda*} = -\mathbf{X}^{\lambda}. \quad (11.132)$$

When \mathbf{A} , \mathbf{B} and \mathbf{X}^{λ} are real this equation simplifies to

$$(\mathbf{A} + \mathbf{B})\mathbf{U}^{\lambda} = -\mathbf{X}^{\lambda}, \quad (11.133)$$

which is the equation used in most applications.

In the complex case, (11.132) can be transformed into a set of coupled equations for the real and imaginary parts of \mathbf{U}^{λ} ,

$$\begin{pmatrix} \mathbf{A}_R + \mathbf{B}_R & -\mathbf{A}_I + \mathbf{B}_I \\ \mathbf{A}_I + \mathbf{B}_I & \mathbf{A}_R - \mathbf{B}_R \end{pmatrix} \begin{pmatrix} \mathbf{U}_R^{\lambda} \\ \mathbf{U}_I^{\lambda} \end{pmatrix} = - \begin{pmatrix} \mathbf{X}_R^{\lambda} \\ \mathbf{X}_I^{\lambda} \end{pmatrix}, \quad (11.134)$$

where the subscripts R and I indicate the real and imaginary parts, respectively, of the corresponding matrix or vector, with $\mathbf{A} = \mathbf{A}_R + i\mathbf{A}_I$ etc. The coefficients U_{ia}^{λ} describing the changes in the virtual orbitals are related to the coefficients U_{ai}^{λ} by the orthogonality relationship (11.116).

Actual evaluation of the U_{ai}^{λ} coefficients would require a separate solution of the CPHF equations for each perturbation, but this multiple solving can be avoided by use of the interchange theorem, as shown in detail in Section 11.9 below.

Before proceeding to discuss the correlation-energy derivatives in Section 11.9, we shall consider the derivatives of the reference energy. Practical procedures for evaluating these derivatives were first developed, primarily for the calculation of SCF energy gradients and force constants, by Gerratt and Mills (1968) and by Pulay (1969).

Leaving out the nuclear repulsion term, the derivative of which is easily calculated, and using (3.115), we write the perturbed reference energy in the form

$$E_{\text{ref}}(\lambda) = \sum_i \langle i(\lambda) | \hat{h}(\lambda) | i(\lambda) \rangle + \frac{1}{2} \sum_{ij} \langle i(\lambda) j(\lambda) | | i(\lambda) j(\lambda) \rangle. \quad (11.135)$$

The derivative of this expression is given by

$$\begin{aligned}
 E_{\text{ref}}^{\lambda} &= \sum_i (\langle i^{\lambda} | \hat{h} | i \rangle + \langle i | \hat{h}^{\lambda} | i \rangle + \langle i | \hat{h} | i^{\lambda} \rangle) \\
 &\quad + \frac{1}{2} \sum_{ij} (\langle i^{\lambda} j | i j \rangle + \langle i j^{\lambda} | i j \rangle + \langle i j | i^{\lambda} j \rangle + \langle i j | i j^{\lambda} \rangle) \\
 &= \sum_i (\langle i^{\lambda} | \hat{h} | i \rangle + \langle i | \hat{h}^{\lambda} | i \rangle + \langle i | \hat{h} | i^{\lambda} \rangle) + \sum_{ij} (\langle i^{\lambda} j | i j \rangle + \langle i j | i^{\lambda} j \rangle) \\
 &= \sum_i \left[\langle i | \hat{h}^{\lambda} | i \rangle + \left\langle i^{\lambda} \left| \hat{h} + \sum_j (\hat{J}_j - \hat{K}_j) \right| i \right\rangle + \left\langle i \left| \hat{h} + \sum_j (\hat{J}_j - \hat{K}_j) \right| i^{\lambda} \right\rangle \right] \\
 &= \sum_i (\langle i | \hat{h}^{\lambda} | i \rangle + \langle i^{\lambda} | \hat{f} | i \rangle + \langle i | \hat{f} | i^{\lambda} \rangle), \tag{11.136}
 \end{aligned}$$

where the Coulomb and exchange operators \hat{J} and \hat{K} are given by (11.96). Even though we are assuming that the reference function is canonical, it would be incorrect at this point to replace $\hat{f}|i\rangle$ by $\epsilon_i|i\rangle$ in the last form of (11.136), because the unperturbed HF equation is not valid in the space spanned by the perturbed orbitals. Instead, we expand the orbital derivatives in terms of the basis functions and their derivatives, (11.117), and obtain

$$\begin{aligned}
 E_{\text{ref}}^{\lambda} &= \sum_i \langle i | \hat{h}^{\lambda} | i \rangle + \sum_i (\langle i^{[\lambda]} | \hat{f} | i \rangle + \langle i | \hat{f} | i^{[\lambda]} \rangle) \\
 &\quad + \sum_i \left[\sum_p (U_{pi}^{\lambda*} \langle p | i \rangle + \langle i | p \rangle U_{pi}^{\lambda}) \right] \epsilon_i \\
 &= \sum_i \langle i | \hat{h}^{\lambda} | i \rangle + \sum_i (\langle i^{[\lambda]} | \hat{f} | i \rangle + \langle i | \hat{f} | i^{[\lambda]} \rangle) + \sum_i (U_{ii}^{\lambda*} + U_{ii}^{\lambda}) \epsilon_i. \tag{11.137}
 \end{aligned}$$

Using (11.115) this becomes

$$E_{\text{ref}}^{\lambda} = \sum_i \langle i | \hat{h}^{\lambda} | i \rangle + \sum_i (\langle i^{[\lambda]} | \hat{f} | i \rangle + \langle i | \hat{f} | i^{[\lambda]} \rangle) - \sum_i \mathcal{S}_{ii}^{\lambda*} \epsilon_i. \tag{11.138}$$

where the transformed overlap matrix $\mathcal{S}(\lambda)$ is given by (11.107) and its derivatives are computed from the derivatives of the basis-set orbital integrals.

The first sum in this expression is referred to as the Hellmann–Feynman term. The last sum can be expressed in terms of an energy-weighted density matrix $\mathbf{\Pi}$:

$$\sum_i \mathcal{S}_{ii}^{\lambda*} \epsilon_i = \sum_{\mu\nu} \left(\sum_i C_{\mu i}^* C_{\nu i} \epsilon_i \right) \langle \mu | \nu \rangle^{\lambda} = \sum_{\mu\nu} \Pi_{\nu\mu} \langle \mu | \nu \rangle^{\lambda}, \tag{11.139}$$

where

$$\mathbf{\Pi} = \mathbf{C}_{\text{ref}} \mathbf{\epsilon} \mathbf{C}_{\text{ref}}^\dagger \quad \text{or} \quad \Pi_{\nu\mu} = \sum_i C_{\mu i}^* C_{\nu i} \epsilon_i. \quad (11.140)$$

Expanding \hat{f} in the middle sum of (11.138) in terms of two-electron integrals, the energy derivative becomes

$$\begin{aligned} E_{\text{ref}}^\lambda &= \sum_i (\langle i | \hat{h}^\lambda | i \rangle + \langle i^{[\lambda]} | \hat{h} | i \rangle + \langle i | \hat{h} | i^{[\lambda]} \rangle) \\ &\quad + \sum_{ij} (\langle i^{[\lambda]} j | i j \rangle + \langle i j | i^{[\lambda]} j \rangle) - \sum_{\mu\nu} \Pi_{\nu\mu} \langle \mu | \nu \rangle^\lambda \\ &= \sum_i \langle i | \hat{h} | i \rangle^{[\lambda]} + \frac{1}{2} \sum_{ij} \langle i j | i j \rangle^{[\lambda]} - \sum_{\mu\nu} \Pi_{\nu\mu} \langle \mu | \nu \rangle^\lambda. \end{aligned} \quad (11.141)$$

In order to avoid a full transformation of the derivative two-electron integrals, E_{ref}^λ is usually calculated directly from the basis-set derivative integrals and the reference-function density matrix \mathbf{P} :

$$E_{\text{ref}}^\lambda = \sum_{\mu\nu} (P_{\nu\mu} \langle \mu | \hat{h} | \nu \rangle^\lambda - \Pi_{\nu\mu} \langle \mu | \nu \rangle^\lambda) + \frac{1}{2} \sum_{\mu\nu\sigma\tau} P_{\nu\mu} P_{\tau\sigma} \langle \mu\sigma | \nu\tau \rangle^\lambda. \quad (11.142)$$

This derivation assumes that the reference function has been variationally optimized, as is the case for SCF wave functions. In this case it may be seen from (11.142) that the solution of the CPHF equations is not needed for the determination of the reference-energy derivative. Furthermore, for perturbations that do not require changes in the basis functions, only the Hellmann–Feynman term, the first term in (11.138), survives. However, in more general cases in which the orbitals are not variationally optimized for the state in question (such as for quasi-HF, in which the orbitals are obtained from an SCF optimization for a different electronic state), there is an added term involving the derivative of the reference-function density matrix with respect to the perturbation,

$$\frac{dE_{\text{ref}}}{d\lambda} = \frac{\partial E_{\text{ref}}}{\partial \lambda} + \frac{\partial E_{\text{ref}}}{\partial \mathbf{P}} \frac{d\mathbf{P}}{d\lambda}. \quad (11.143)$$

The second term vanishes in the SCF case because the orbitals have been variationally optimized. In other cases we have an additional contribution to the reference-energy derivative,

$$\Delta_P E_{\text{ref}}^\lambda = \sum_{\mu\nu} \langle \mu | \hat{h} | \nu \rangle P_{\nu\mu}^\lambda + \frac{1}{2} \sum_{\mu\nu\sigma\tau} \langle \mu\sigma | \nu\tau \rangle (P_{\nu\mu}^\lambda P_{\tau\sigma} + P_{\nu\mu} P_{\tau\sigma}^\lambda). \quad (11.144)$$

Evaluation of the density-matrix derivatives requires the knowledge of \mathbf{U}^λ , as seen from (11.105), and thus requires the solution of the CPHF equations, but the interchange-theorem technique to be described in the next section can be used to avoid explicit evaluation of \mathbf{U}^λ for each perturbation (Gauss, Stanton and Bartlett 1991).

11.9 The CC correlation-energy derivative

The coupled-cluster correlation-energy derivative, see (11.68), can be written in the form

$$\begin{aligned}\Delta E^\lambda &= \langle 0 | (1 + \Lambda) e^{-\hat{T}} \hat{H}_N^\lambda e^{\hat{T}} | 0 \rangle \\ &= \langle 0 | (1 + \Lambda) e^{-\hat{T}} \left(\sum_{pq} f_{pq}^\lambda \{ \hat{p}^\dagger \hat{q} \} + \frac{1}{4} \sum_{pqrs} \langle pq || rs \rangle^\lambda \{ \hat{p}^\dagger \hat{q}^\dagger \hat{s} \hat{r} \} \right) e^{\hat{T}} | 0 \rangle.\end{aligned}\quad (11.145)$$

Substituting the response density matrices (11.88), (11.89) into (11.145), we obtain

$$\Delta E^\lambda = \sum_{pq} f_{pq}^\lambda (\gamma_N)_{qp} + \frac{1}{4} \sum_{pqrs} \langle pq || rs \rangle^\lambda (\Gamma_N)_{rspq} = \Delta E_1^\lambda + \Delta E_2^\lambda, \quad (11.146)$$

where

$$\begin{aligned}\Delta E_1^\lambda &= \sum_{pq} f_{pq}^\lambda \gamma_{qp} = \sum_{pq} (\langle p | \hat{f}^\lambda | q \rangle + \langle p^\lambda | \hat{f} | q \rangle + \langle p | \hat{f} | q^\lambda \rangle) \gamma_{qp} \\ &= \sum_{pq} \left[\langle p | \hat{h}^\lambda | q \rangle + \sum_k (\langle pk^\lambda || qk \rangle + \langle pk || qk^\lambda \rangle + \langle p^\lambda i || qk \rangle + \langle pk || q^\lambda k \rangle) \right] \gamma_{qp} \\ &= \sum_{pq} \left[\langle p | \hat{h}^\lambda | q \rangle + \sum_k \langle pk || qk \rangle^\lambda \right] \gamma_{qp},\end{aligned}\quad (11.147)$$

$$\Delta E_2^\lambda = \frac{1}{4} \sum_{pqrs} \langle pq || rs \rangle^\lambda \Gamma_{rspq}. \quad (11.148)$$

Here and in the rest of the chapter we omit the subscript N from the normal-ordered density matrices to simplify the notation.

The two-electron derivative integrals in (11.147), (11.148) can be separated into contributions from the two terms in the expression for the first-order perturbed orbitals $\{\phi_p^\lambda\}$, (11.117). Considering the two-electron inte-

gral in (11.147) first, we have

$$\begin{aligned}
 \sum_k \langle pk||qk \rangle^\lambda &= \sum_{kr} \left(\langle rk||qk \rangle U_{rp}^{\lambda*} + \langle pk||rk \rangle U_{rq}^\lambda + \langle pr||qk \rangle U_{rk}^{\lambda*} + \langle pk||qr \rangle U_{rk}^\lambda \right) \\
 &\quad + \sum_k \langle pk||qk \rangle^{[\lambda]} \\
 &= \sum_r (f_{rq} U_{rp}^{\lambda*} + f_{pr} U_{rq}^\lambda) + \sum_{kr} (\langle pr||qk \rangle U_{rk}^{\lambda*} + \langle pk||qr \rangle U_{rk}^\lambda) \\
 &\quad + \sum_k \langle pk||qk \rangle^{[\lambda]}. \tag{11.149}
 \end{aligned}$$

Taking the second term in the first sum on the r.h.s of (11.149) as an example, and separating it into contributions from the different blocks of \mathbf{U}^λ , we obtain

$$\sum_{pqr} f_{pr} U_{rq}^\lambda \gamma_{qp} = \sum_{pia} f_{pa} U_{ai}^\lambda \gamma_{ip} + \sum_{pai} f_{pi} U_{ia}^\lambda \gamma_{ap} + \sum_{pab} f_{pb} U_{ba}^\lambda \gamma_{ap} + \sum_{pij} f_{pj} U_{ji}^\lambda \gamma_{ip}. \tag{11.150}$$

We next use (11.115), (11.116) to eliminate all but the particle-hole block of \mathbf{U}^λ :

$$\begin{aligned}
 \sum_{pqr} f_{pr} U_{rq}^\lambda \gamma_{qp} &= \sum_{pia} f_{pa} U_{ai}^\lambda \gamma_{ip} - \sum_{pai} f_{pi} U_{ai}^{\lambda*} \gamma_{ap} - \sum_{pai} f_{pi} \mathcal{S}_{ia}^\lambda \gamma_{ap} \\
 &\quad - \frac{1}{2} \sum_{pab} f_{pb} \mathcal{S}_{ba}^\lambda \gamma_{ap} - \frac{1}{2} \sum_{pij} f_{pj} \mathcal{S}_{ji}^\lambda \gamma_{ip} \\
 &= \sum_{pia} (f_{pa} \gamma_{ip} U_{ai}^\lambda - f_{pi} \gamma_{ap} U_{ai}^{\lambda*}) - \sum_{pai} f_{pi} \langle i|a \rangle^{[\lambda]} \gamma_{ap} \\
 &\quad - \frac{1}{2} \sum_{pab} f_{pb} \langle b|a \rangle^{[\lambda]} \gamma_{ap} - \frac{1}{2} \sum_{pij} f_{pj} \langle j|i \rangle^{[\lambda]} \gamma_{ip}. \tag{11.151}
 \end{aligned}$$

Similar treatment for the first term in the first sum on the r.h.s of (11.149) produces

$$\begin{aligned}
 \sum_{pqr} f_{rq} U_{rp}^{\lambda*} \gamma_{qp} &= \sum_{qpr} f_{rp} U_{rq}^{\lambda*} \gamma_{pq} \\
 &= \sum_{ipa} (f_{ap} \gamma_{pi} U_{ai}^{\lambda*} - f_{ip} \gamma_{pa} U_{ai}^\lambda) - \sum_{pai} f_{ip} \langle a|i \rangle^{[\lambda]} \gamma_{pa} \\
 &\quad - \frac{1}{2} \sum_{pab} f_{bp} \langle a|b \rangle^{[\lambda]} \gamma_{pa} - \frac{1}{2} \sum_{pij} f_{jp} \langle i|j \rangle^{[\lambda]} \gamma_{pi}. \tag{11.152}
 \end{aligned}$$

The terms in the second sum of (11.149) result in

$$\begin{aligned} \sum_{pqrk} \langle pk \| qr \rangle U_{rk}^\lambda \gamma_{qp} &= \sum_{qpr i} \langle pi \| qr \rangle U_{ri}^\lambda \gamma_{qp} \\ &= \sum_{pqai} \langle pi \| qa \rangle \gamma_{qp} U_{ai}^\lambda - \frac{1}{2} \sum_{pqji} \langle pi \| qj \rangle \langle j | i \rangle^{[\lambda]} \gamma_{qp}, \quad (11.153) \end{aligned}$$

$$\begin{aligned} \sum_{pqrk} \langle pr \| qk \rangle U_{rk}^{\lambda*} \gamma_{qp} &= \sum_{pqr i} \langle qr \| pi \rangle U_{ri}^{\lambda*} \gamma_{pq} \\ &= \sum_{pqai} \langle qa \| pi \rangle \gamma_{pq} U_{ai}^{\lambda*} - \frac{1}{2} \sum_{pqji} \langle qj \| pi \rangle \langle i | j \rangle^{[\lambda]} \gamma_{pq}. \quad (11.154) \end{aligned}$$

Denoting the sum of the contributions to ΔE_1^λ , (11.147), that depend on the particle-hole block of \mathbf{U}^λ by ΔE_1^U , we collect all such terms in (11.151)–(11.154) and obtain

$$\begin{aligned} \Delta E_1^U &= \sum_{ia} \left\{ \left[\sum_p (f_{pa} \gamma_{ip} - f_{ip} \gamma_{pa}) + \sum_{pq} \langle pi \| qa \rangle \gamma_{qp} \right] U_{ai}^\lambda \right. \\ &\quad \left. + \left[\sum_p (f_{ap} \gamma_{pi} - f_{pi} \gamma_{ap}) + \sum_{pq} \langle qa \| pi \rangle \gamma_{pq} \right] U_{ai}^{\lambda*} \right\}. \quad (11.155) \end{aligned}$$

Equation (11.147) can now be written as

$$\Delta E_1^\lambda = \sum_{pq} \langle p | \hat{h}^\lambda | q \rangle \gamma_{qp} + \Delta E_1^U + \Delta E_1^{[\lambda]}, \quad (11.156)$$

where

$$\begin{aligned} \Delta E_1^{[\lambda]} &= - \sum_{ia} \left[\left(\sum_p f_{pi} \gamma_{ap} \right) \langle i | a \rangle^{[\lambda]} + \left(\sum_p f_{ip} \gamma_{pa} \right) \langle a | i \rangle^{[\lambda]} \right] \\ &\quad - \frac{1}{2} \sum_{ab} \left[\sum_p (f_{pa} \gamma_{bp} + f_{bp} \gamma_{pa}) \langle a | b \rangle^{[\lambda]} \right] \\ &\quad - \sum_{ij} \left[\frac{1}{2} \sum_p (f_{pi} \gamma_{jp} + f_{jp} \gamma_{pi}) + \sum_{pq} \langle pj \| qi \rangle \gamma_{qp} \right] \langle i | j \rangle^{[\lambda]} \\ &\quad + \sum_{pq} \left(\sum_i \langle pi \| qi \rangle^{[\lambda]} \right) \gamma_{qp}. \quad (11.157) \end{aligned}$$

The sums involving $\langle b | a \rangle^{[\lambda]}$ and $\langle j | i \rangle^{[\lambda]}$ were combined with those involving $\langle a | b \rangle^{[\lambda]}$ and $\langle i | j \rangle^{[\lambda]}$, respectively, by the interchange of dummy summation indices, including the interchange of p and q in (11.154). Both ΔE_1^U and $\Delta E_1^{[\lambda]}$ are simplified for canonical HF orbitals by the relation $f_{pq} = \varepsilon_p \delta_{pq}$.

A similar treatment of the two-electron contribution to ΔE^λ results in

$$\Delta E_2^\lambda = \Delta E_2^U + \Delta E_2^{[\lambda]}, \quad (11.158)$$

$$\begin{aligned} \Delta E_2^U = \frac{1}{2} \sum_{ai} \left[\left(\sum_{pqr} \langle pq || ra \rangle \Gamma_{ripq} - \langle ri || pq \rangle \Gamma_{pqra} \right) U_{ai}^\lambda \right. \\ \left. + \left(\sum_{pqr} \langle ra || pq \rangle \Gamma_{pqri} - \langle pq || ri \rangle \Gamma_{rapq} \right) U_{ai}^{\lambda*} \right], \end{aligned} \quad (11.159)$$

$$\begin{aligned} \Delta E_2^{[\lambda]} = -\frac{1}{2} \sum_{as} \left[\left(\sum_{pqr} \langle pq || rs \rangle \Gamma_{rapq} \right) \langle s | a \rangle^{[\lambda]} + \left(\sum_{pqr} \langle rs || pq \rangle \Gamma_{pqra} \right) \langle a | s \rangle^{[\lambda]} \right] \\ - \frac{1}{2} \sum_{pqrij} \left(\langle rj || pq \rangle \Gamma_{pqri} + \langle pq || ri \rangle \Gamma_{rjpq} \right) \langle i | j \rangle^{[\lambda]} + \sum_{pqrs} \langle pq || rs \rangle^{[\lambda]} \Gamma_{rspq}. \end{aligned} \quad (11.160)$$

For perturbations that are not accompanied by a change in the basis functions we have $\Delta E^{[\lambda]} = 0$, and then the entire first-order perturbed energy is given by $\Delta E^\lambda = \sum_{pq} \langle p | \hat{h}^\lambda | q \rangle + \Delta E_1^U + \Delta E_2^U$.

A common feature of almost all terms in the expansion of the first-order energy is that if we ignore the non-Hermiticity of the response density matrices then they come in complex-conjugate pairs. It is convenient to split the response density matrices into Hermitian and anti-Hermitian components:

$$\begin{aligned} \gamma_{pq} &= \gamma_{pq}^H + \gamma_{pq}^A = \gamma_{qp}^{H*} - \gamma_{qp}^{A*}, \\ \Gamma_{pqrs} &= \Gamma_{pqrs}^H + \Gamma_{pqrs}^A = \Gamma_{rspq}^{H*} - \Gamma_{rspq}^{A*}, \end{aligned} \quad (11.161)$$

where

$$\gamma_{pq}^H = \frac{1}{2}(\gamma_{pq} + \gamma_{qp}^*), \quad \Gamma_{pqrs}^H = \frac{1}{2}(\Gamma_{pqrs} + \Gamma_{rspq}^*), \quad (11.162)$$

$$\gamma_{pq}^A = \frac{1}{2}(\gamma_{pq} - \gamma_{qp}^*), \quad \Gamma_{pqrs}^A = \frac{1}{2}(\Gamma_{pqrs} - \Gamma_{rspq}^*). \quad (11.163)$$

Defining the perturbation-independent vectors \mathbf{M} and \mathbf{N} , with components

$$\begin{aligned} M_{ai} &= \sum_p \left(f_{pa} \gamma_{ip}^H - f_{ip} \gamma_{pa}^H + \sum_q \langle pi || qa \rangle \gamma_{qp}^H \right) \\ &+ \sum_{pqr} \left(\langle pq || ra \rangle \Gamma_{ripq}^H - \langle ri || pq \rangle \Gamma_{pqra}^H \right), \end{aligned} \quad (11.164)$$

$$\begin{aligned}
N_{ai} = & \sum_p \left(f_{pa} \gamma_{ip}^A - f_{ip} \gamma_{pa}^A + \sum_q \langle pi || qa \rangle \gamma_{qp}^A \right) \\
& + \sum_{pqr} \left(\langle pq || ra \rangle \Gamma_{ripq}^A - \langle ri || pq \rangle \Gamma_{pqra}^A \right)
\end{aligned} \tag{11.165}$$

(with ai treated as a single composite index), we can write the \mathbf{U}^λ -dependent part of the first-order energy as

$$\begin{aligned}
\Delta E^U &= \Delta E_1^U + \Delta E_2^U \\
&= \sum_{ai} [(M_{ai} + N_{ai})U_{ai}^\lambda + (M_{ai} - N_{ai})^*U_{ai}^{\lambda*}] \\
&= (\mathbf{M} + \mathbf{N})^T \mathbf{U}^\lambda + (\mathbf{M} - \mathbf{N})^\dagger \mathbf{U}^{\lambda*} \\
&= 2(\mathbf{M}_R^T \mathbf{U}_R^\lambda - \mathbf{M}_I^T \mathbf{U}_I^\lambda) + 2i(\mathbf{N}_R^T \mathbf{U}_I^\lambda + \mathbf{N}_I^T \mathbf{U}_R^\lambda),
\end{aligned} \tag{11.166}$$

where the superscript T indicates the transpose and subscripts R and I indicate the real and imaginary parts of the respective vectors; $\mathbf{M} = \mathbf{M}_R + i\mathbf{M}_I$ etc. When all quantities are real, this result simplifies to

$$\Delta E^U = 2 \sum_{ai} M_{ai} U_{ai}^\lambda = 2\mathbf{M}^T \mathbf{U}^\lambda, \tag{11.167}$$

and the vector \mathbf{N} and the anti-Hermitian components of the response density matrices are not needed for the calculation of ΔE^U .

As stated in Section 11.8, the explicit calculation of \mathbf{U}^λ , which would require repeated solution of the CPHF equations for different perturbations, can be avoided by use of the interchange theorem (Sternheimer and Foley 1953, Dalgarno and Stewart 1958, Hirschfelder, Byers-Brown and Epstein 1964, Handy and Schaefer 1984); this is sometimes referred to in the CPHF context as the Z -vector method. (A more general use of the interchange theorem for the correlation problem is represented by the introduction of the Λ equations in Section 11.5; see Adamowicz, Laidig and Bartlett (1984) and Salter, Trucks and Bartlett (1989)). Considering first the case in which all quantities are real, the quantity needed for the evaluation of ΔE^U is the contraction $2\mathbf{M}^T \mathbf{U}^\lambda$, (11.167). To obtain this result, instead of solving (11.133) for each perturbation we solve a single perturbation-independent equation,

$$(\mathbf{A} + \mathbf{B})^T \mathbf{Z} = 2\mathbf{M}. \tag{11.168}$$

Then the contractions of the solution vector \mathbf{Z} with the right-hand-side vectors $-\mathbf{X}^\lambda$ for the various perturbations,

$$-\mathbf{Z}^T \mathbf{X}^\lambda = -2\mathbf{M}^T (\mathbf{A} + \mathbf{B})^{-1} \mathbf{X}^\lambda = 2\mathbf{M}^T \mathbf{U}^\lambda, \tag{11.169}$$

provide the required answers.

As given in (11.129), when the perturbation does not involve changes in the basis functions we have $X_{ai} = \langle a | \hat{H}^\lambda | i \rangle = h_{ai}^\lambda$. For this case ΔE^λ is given completely by ΔE^U , and when all quantities are real we have

$$\Delta E^U = 2\mathbf{M}^T U^\lambda = -2\mathbf{M}^T (\mathbf{A} - \mathbf{B})^{-1} \mathbf{h}^\lambda, \quad (11.170)$$

where \mathbf{h}^λ is treated as a vector with components identified by the composite index ai . This form can be used to define a *relaxed density matrix* \mathbf{D} that incorporates the effects of orbital relaxation, for which

$$\begin{aligned} D_{ia} = -2 \sum_{bj} \left[\sum_p (f_{pb} \gamma_{jp} - f_{jp} \gamma_{pb}) + \sum_{pq} \langle pj || qb \rangle \gamma_{qp} \right. \\ \left. + \sum_{pqr} (\langle pq || rb \rangle \Gamma_{rjpq} - \langle rj || pq \rangle \Gamma_{pqrb}) \right] [(\mathbf{A} - \mathbf{B})^{-1}]_{bj, ai}, \end{aligned} \quad (11.171)$$

so that

$$\Delta E^U = \sum_{ai} D_{ia} h_{ai}^\lambda. \quad (11.172)$$

One-electron properties given by $\hat{H}^\lambda = \hat{O}$ can then be obtained as

$$\bar{O}_N = \sum_{ai} D_{ia} o_{ai}. \quad (11.173)$$

The relaxed density matrix is perturbation independent and needs to be computed once only for any number of perturbations. The same techniques involving the interchange theorem, described in connection with the treatment of the \mathbf{U}^λ equations, are used in its calculation to avoid the explicit inversion of $\mathbf{A} - \mathbf{B}$. Generalization of this treatment to the case of complex functions is straightforward.

As will be discussed in Section 12.8, the truncated-CC unperturbed energy, computed as $\hat{P} \mathcal{H} \hat{P}$, may be complex; such a result is not normally expected, however, at least when real orbitals are used for ground-state molecules near their equilibrium geometry. In any case, the imaginary component of any CC energy-derivative result is unphysical, being an artefact of the non-Hermiticity of the response density matrices, and it is reasonable to ignore it. Though the non-Hermitian forms can be used, replacing them by their Hermitian average is sometimes useful.

Even if the \mathbf{A} and \mathbf{B} matrices are real, the right-hand-side vector $-\mathbf{X}^\lambda$ of the CPHF equations (11.132) may still be complex, leading to complex \mathbf{U}^λ vectors. Such a situation can arise when the HF solution is unstable with respect to a lower-energy symmetry-broken HF solution (Čížek and Paldus 1967, Sekino and Bartlett 1986). Another example arises when *gauge-including atomic orbitals* (GIAOs, also referred to as *gauge invariant atomic orbitals*) are used as basis functions (London 1937, Ditchfield 1974, Gauss, Ruud and Helgaker 1996) in calculations involving some magnetic perturbations, such as those due to magnetic susceptibility or nuclear magnetic shielding (used in the evaluation of NMR chemical shifts). In such cases the basis-set-integral derivatives, and thus \mathbf{X}^λ and \mathbf{U}^λ , are pure imaginary but these properties are of second order, with zero first-order contributions, and the second-order (and all even-order) energy derivatives are real (Gauss 1993).

In calculations on atoms, linear molecules and molecules belonging to degenerate irreducible representations of axial point groups such as C_n , C_{nh} and S_{nh} ($n > 2$), the use of complex orbitals may be useful for spatial symmetry adaptation and may result in complex \mathbf{A} and \mathbf{B} matrices. For the sake of completeness an analysis of the complex case, represented by the CPHF equations (11.134), including the anti-Hermitian contributions, will now be given.

As seen in (11.166), in the complex case we need two contractions,

$$\mathbf{M}^T \mathbf{U}^\lambda + \mathbf{M}^{T*} \mathbf{U}^{\lambda*} = 2(\mathbf{M}_R^T \mathbf{U}_R^\lambda - \mathbf{M}_I^T \mathbf{U}_I^\lambda) \quad (11.174)$$

and

$$\mathbf{N}^T \mathbf{U}^\lambda - \mathbf{N}^{T*} \mathbf{U}^{\lambda*} = 2i(\mathbf{N}_I^T \mathbf{U}_R^\lambda + \mathbf{N}_R^T \mathbf{U}_I^\lambda). \quad (11.175)$$

These contributions to the correlation-energy derivative can be obtained by solving two sets of coupled equations,

$$\begin{pmatrix} \mathbf{A}_R + \mathbf{B}_R & -\mathbf{A}_I + \mathbf{B}_I \\ \mathbf{A}_I + \mathbf{B}_I & \mathbf{A}_R - \mathbf{B}_R \end{pmatrix}^T \begin{pmatrix} \mathbf{Z}_R \\ \mathbf{Z}_I \end{pmatrix} = \begin{pmatrix} \mathbf{M}_R \\ -\mathbf{M}_I \end{pmatrix} \quad (11.176)$$

and

$$\begin{pmatrix} \mathbf{A}_R + \mathbf{B}_R & -\mathbf{A}_I + \mathbf{B}_I \\ \mathbf{A}_I + \mathbf{B}_I & \mathbf{A}_R - \mathbf{B}_R \end{pmatrix}^T \begin{pmatrix} \mathbf{Z}'_R \\ \mathbf{Z}'_I \end{pmatrix} = \begin{pmatrix} \mathbf{N}_I \\ \mathbf{N}_R \end{pmatrix}. \quad (11.177)$$

Then

$$\begin{aligned} -2 \begin{pmatrix} \mathbf{Z}_R^T & \mathbf{Z}_I^T \end{pmatrix} \begin{pmatrix} \mathbf{X}_R^\lambda \\ \mathbf{X}_I^\lambda \end{pmatrix} &= -2 \begin{pmatrix} \mathbf{M}_R^T & -\mathbf{M}_I^T \end{pmatrix} \begin{pmatrix} \mathbf{A}_R + \mathbf{B}_R & -\mathbf{A}_I + \mathbf{B}_I \\ \mathbf{A}_I + \mathbf{B}_I & \mathbf{A}_R - \mathbf{B}_R \end{pmatrix}^{-1} \begin{pmatrix} \mathbf{X}_R^\lambda \\ \mathbf{X}_I^\lambda \end{pmatrix} \\ &= 2 \begin{pmatrix} \mathbf{M}_R^T & -\mathbf{M}_I^T \end{pmatrix} \begin{pmatrix} \mathbf{U}_R^\lambda \\ \mathbf{U}_I^\lambda \end{pmatrix} \end{aligned} \quad (11.178)$$

and

$$\begin{aligned} -2i \begin{pmatrix} \mathbf{Z}_R^T & \mathbf{Z}_I^T \end{pmatrix} \begin{pmatrix} \mathbf{X}_R^\lambda \\ \mathbf{X}_I^\lambda \end{pmatrix} &= -2i \begin{pmatrix} \mathbf{N}_I^T & \mathbf{N}_R^T \end{pmatrix} \begin{pmatrix} \mathbf{A}_R + \mathbf{B}_R & -\mathbf{A}_I + \mathbf{B}_I \\ \mathbf{A}_I + \mathbf{B}_I & \mathbf{A}_R - \mathbf{B}_R \end{pmatrix}^{-1} \begin{pmatrix} \mathbf{X}_R^\lambda \\ \mathbf{X}_I^\lambda \end{pmatrix} \\ &= 2i \begin{pmatrix} \mathbf{N}_I^T & \mathbf{N}_R^T \end{pmatrix} \begin{pmatrix} \mathbf{U}_R^\lambda \\ \mathbf{U}_I^\lambda \end{pmatrix} \end{aligned} \quad (11.179)$$

provide the required answer.

The anti-Hermitian part of the response density matrices is of at least third order in MBPT (Section 11.7) and would normally be very small. As previously stated, its contribution to ΔE^U is pure imaginary and, while mathematically it constitutes a correct part of the derivative of the CC energy, it is unphysical and therefore is usually ignored: the vector \mathbf{N} is not calculated and the corresponding equations (11.177) are not solved.

It is also instructive to look at the case in which all unperturbed quantities are real but the perturbed orbitals, and thus the \mathbf{X}^λ vector, are complex. In this case (11.176), (11.177) become

$$(\mathbf{A} + \mathbf{B})^T \mathbf{Z}_R = \mathbf{M} \quad (11.180)$$

and

$$(\mathbf{A} - \mathbf{B})^T \mathbf{Z}'_I = \mathbf{N}. \quad (11.181)$$

The contribution to the correlation-energy derivative is then given by

$$\begin{aligned} -2 \begin{pmatrix} \mathbf{Z}_R^T & i\mathbf{Z}'_I{}^T \end{pmatrix} \begin{pmatrix} \mathbf{X}_R^\lambda \\ \mathbf{X}_I^\lambda \end{pmatrix} &= -2 \begin{pmatrix} \mathbf{M}^T & i\mathbf{N}^T \end{pmatrix} \begin{pmatrix} (\mathbf{A} + \mathbf{B})^{-1} \mathbf{X}_R^\lambda \\ (\mathbf{A} - \mathbf{B})^{-1} \mathbf{X}_I^\lambda \end{pmatrix} \\ &= 2 \begin{pmatrix} \mathbf{M}^T & i\mathbf{N}^T \end{pmatrix} \begin{pmatrix} \mathbf{U}_R^\lambda \\ \mathbf{U}_I^\lambda \end{pmatrix}. \end{aligned} \quad (11.182)$$

If \mathbf{X}^λ is pure imaginary, as in the case of magnetic perturbations with GIAO orbitals, we would only have (11.181), and (11.182) then becomes

$$-2i\mathbf{Z}'_I{}^T \mathbf{X}_I^\lambda = -2i\mathbf{N}^T (\mathbf{A} - \mathbf{B})^{-1} \mathbf{X}_I^\lambda = 2i\mathbf{N}^T \mathbf{U}_I^\lambda. \quad (11.183)$$

Again, the resulting imaginary energy derivative is unphysical, the correct result for the first-order energy being zero, and the first true nonzero contribution is of second order. In this case we do not need to solve (11.181), so that \mathbf{N} is not needed, but \mathbf{U}^λ , which is pure imaginary, plays a role in the second-order calculation.

If the basis functions are modified by the perturbation, we have to determine the $\Delta E^{[\lambda]}$ contributions. Collecting the terms from (11.157) and (11.160), and defining the perturbation-independent contractions

$$\begin{aligned}\xi_{pq} &= \sum_r f_{pr} \gamma_{rq}, & \eta_{pq} &= \sum_r \gamma_{pr} f_{rq}, & \zeta_{ji} &= \sum_{rs} \langle rj \| si \rangle \gamma_{sr}, \\ \mu_{pq} &= \sum_{rst} \langle tp \| rs \rangle \Gamma_{rstq}, & \nu_{pq} &= \sum_{rst} \Gamma_{tprs} \langle rs \| tq \rangle,\end{aligned}\quad (11.184)$$

the $\Delta E^{[\lambda]}$ contribution is obtained as

$$\begin{aligned}\Delta E^{[\lambda]} &= - \sum_{ai} [(\xi_{ia} + \frac{1}{2}\mu_{ia}) \langle a|i \rangle^{[\lambda]} + (\eta_{ai} + \frac{1}{2}\nu_{ai}) \langle i|a \rangle^{[\lambda]}] \\ &\quad - \frac{1}{2} \sum_{ab} (\xi_{ba} + \eta_{ba} + \mu_{ba} + \nu_{ba}) \langle a|b \rangle^{[\lambda]} \\ &\quad - \frac{1}{2} \sum_{ij} (\xi_{ji} + \eta_{ji} + \mu_{ji} + \nu_{ji} + 2\zeta_{ji}) \langle i|j \rangle^{[\lambda]} \\ &\quad + \sum_{pq} \left(\sum_i \langle pi \| qi \rangle^{[\lambda]} \right) \gamma_{qp} + \sum_{pqrs} \langle pq \| rs \rangle^{[\lambda]} \Gamma_{rspq}.\end{aligned}\quad (11.185)$$

This expression can also be separated into contributions from the Hermitian and anti-Hermitian parts of the response density matrices. For this purpose it is useful to note that

$$\begin{aligned}\eta^H &= \xi^{H\dagger}, & \nu^H &= \mu^{H\dagger}, & \zeta^H &= \zeta^{H\dagger}, \\ \eta^A &= -\xi^{A\dagger}, & \nu^A &= -\mu^{A\dagger}, & \zeta^A &= -\zeta^{A\dagger}.\end{aligned}\quad (11.186)$$

As in the case of ΔE^U , the anti-Hermitian terms will generate imaginary contributions to $\Delta E^{[\lambda]}$ and would not normally be calculated. When all quantities are real the anti-Hermitian contributions cancel.

To avoid repeated four-index transformations of two-electron derivative integrals from basis-function to orbital representations in the last two sums of (11.185), the corresponding sums are best evaluated in the basis-function representation, by transforming the response density matrices from the orbital representation to the basis-set representation:

$$\tilde{\gamma}_{\nu\mu} = \sum_{pq} C_{\mu p}^* C_{\nu q} \gamma_{qp}, \quad (11.187)$$

$$\tilde{\Gamma}_{\sigma\tau\mu\nu} = \sum_{pqrs} C_{\mu p}^* C_{\nu q}^* C_{\sigma r} C_{\tau s} \Gamma_{rspq}, \quad (11.188)$$

where we should remember that, even though the subscript N has been omitted, the response density matrices γ and Γ are the normal-ordered matrices γ_N and Γ_N , respectively. Then

$$\begin{aligned} \sum_{pq} \langle pi || qi \rangle^{[\lambda]} \gamma_{qp} &= \sum_{\mu\nu\sigma\tau} \langle \mu\sigma || \nu\tau \rangle^\lambda \left(\sum_i C_{\sigma i}^* C_{\tau i} \right) \sum_{pq} C_{\mu p}^* C_{\nu q} \gamma_{qp} \\ &= \sum_{\mu\nu\sigma\tau} \langle \mu\sigma || \nu\tau \rangle^\lambda D_{\tau\sigma} \tilde{\gamma}_{\nu\mu} = \sum_{\mu\nu} Y_{\mu\nu}^\lambda \tilde{\gamma}_{\nu\mu}, \end{aligned} \quad (11.189)$$

where \mathbf{Y}^λ is given by (11.126) and

$$\begin{aligned} \sum_{pqrs} \langle pq || rs \rangle^{[\lambda]} \Gamma_{rspq} &= \sum_{\mu\nu\sigma\tau} \langle \mu\nu || \sigma\tau \rangle^\lambda \sum_{pqrs} C_{\mu p}^* C_{\nu q}^* C_{\sigma r}^* C_{\tau s} \Gamma_{rspq} \\ &= \sum_{\mu\nu\sigma\tau} \langle \mu\nu || \sigma\tau \rangle^\lambda \tilde{\Gamma}_{\sigma\tau\mu\nu}. \end{aligned} \quad (11.190)$$

This approach is particularly important in the calculation of energy gradients, for which many different perturbations (displacements of the different atoms, each in up to three directions) need to be considered.

Finally, the total correlation-energy derivative is made up of the different contributions:

$$\begin{aligned} \Delta E^\lambda &= \sum_{pq} \langle p | \hat{h}^\lambda | q \rangle \gamma_{qp} + \Delta E^U + \Delta E^{[\lambda]} \\ &= \sum_{\mu\nu} \langle \mu | \hat{h}^\lambda | \nu \rangle \tilde{\gamma}_{\nu\mu} + \Delta E^U + \Delta E^{[\lambda]}. \end{aligned} \quad (11.191)$$

The relaxed density matrix (11.171) can be used to compute the ΔE^U term (11.172).

Extensions of the treatment described here can be used to obtain higher-order properties, including second and higher derivatives. Such methods for CC higher-order properties involving external fields, using EOM-CC methodology, are described in Section 13.5.

Additional aspects of coupled-cluster theory

This chapter addresses several more subtle but nevertheless important aspects of coupled-cluster MBPT theory.

12.1 Spin summations and computational considerations

The formalism described in the previous sections was presented in terms of spinorbitals, without regard to integration over spin coordinates. Even in the case of unrestricted Hartree–Fock (UHF) reference functions, in which the spatial orbitals for α and β spin are different, integration over spin is absolutely necessary to eliminate many integrals and to allow the introduction of constraints over the summation indices, achieving a computational effort of no more than three times that of comparable RHF calculations. Furthermore, all amplitudes in which the number of α and β spinorbitals is different for the hole and particle indices vanish, preserving the M_S , but not the S , quantum number. In the restricted closed-shell Hartree–Fock (RHF) case, spin integration is used to combine contributions from α and β spinorbitals, deriving expressions in terms of spatial orbitals only and thus reducing the range of all indices by about a factor 2 (see Section 7.3). Restricted open-shell Hartree–Fock (ROHF) calculations are usually performed as UHF, despite double occupancy, because the most effective algorithms are still of the spin-integrated, spatial-orbital, form. The double occupancy cannot be exploited further without special effort.

The incorporation of spin integration can be done algebraically or, in some cases, diagrammatically. As an example of the diagrammatic treatment of spin summation in coupled-cluster calculations we shall consider the case of the CCD equation with an RHF reference function. The diagrammatic representation of this equation in a spinorbital basis was given in Fig. 9.2 in terms of antisymmetrized Goldstone diagrams. For spin summation we

expand these diagrams in terms of ordinary Goldstone diagrams representing spatial orbitals (Čížek 1969), as shown in Fig. 12.1 (Bartlett and Musiał 2007, Fig. 8). The labels in this figure reflect the origin of each diagram in terms of a diagram of Fig. 9.2; an x in the label indicates exchange. For example, diagrams $D_{3b} - D_{3bx5}$ all originate in the antisymmetrized Goldstone diagram D_{3b} . This correspondence can be verified by the fact that all six of these diagrams collapse to the same Hugenholtz diagram (labeled Q_b in Section 9.5, just before (9.121)) when each vertex is collapsed to a dot.

The particle and hole lines in the diagrams of Fig. 12.1 represent spatial orbitals, indicated by capital letters I, J, \dots for holes and A, B, \dots for particles. In the RHF case considered here, each spatial orbital reflects the existence of two spinorbitals having the same spatial part, e.g. $I\alpha$ and $I\beta$. The interpretation of these diagrams differs in some respects from that of the antisymmetrized diagrams. The sign rule is the same, but the numerical weight factors and the permutation factors are different. There is a weight factor 2 for each closed loop (reflecting summation over two spin assignments) and a weight factor $\frac{1}{2}$ for diagrams with left-right symmetry (i.e. symmetry with respect to reflection in a vertical line), as for MBPT Goldstone diagrams. For example, diagram D_{3b} has two closed loops and

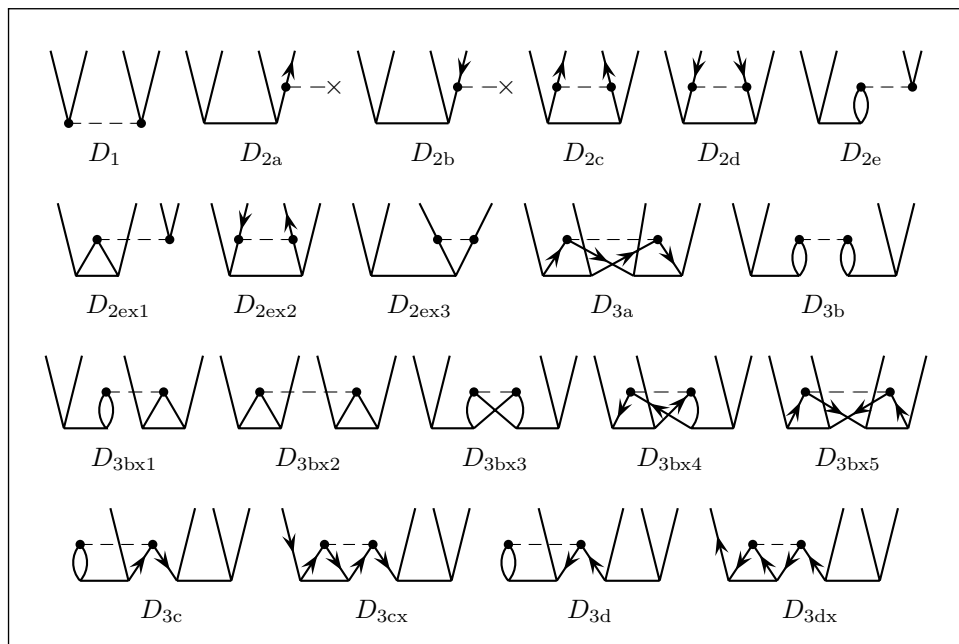
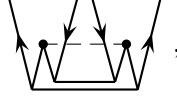


Fig. 12.1. Diagrams for the spin-summed CCD amplitude equations for an RHF reference function.

left-right symmetry, for a total weight equal to $2 \times 2 \times \frac{1}{2} = 2$, while diagram $D_{3\text{bx}3}$ has one closed loop and symmetry, giving a total weight 1. Special attention needs to be paid to diagram D_{3a} ; while as drawn in Fig. 12.1 this diagram does not show left-right symmetry, it can also be drawn in a symmetric form,



and therefore has weight $\frac{1}{2}$.

For the permutation factor (which does not appear in MBPT diagrams), we note that the spin-free amplitudes do not have the same antisymmetry property as in the spinorbital form,

$$t_{IJ}^{AB} = t_{JI}^{BA} \neq t_{IJ}^{BA} = t_{JI}^{AB}, \quad (12.1)$$

and so for the t_{IJ}^{AB} diagram I and A must remain on the same continuous path and so must J and B . Therefore we may only permute (IA) as a unit with (JB) , using the permutation factor

$$\hat{P}((IA)(JB)) = 1 + P_{IJ}P_{AB}. \quad (12.2)$$

The final form of the algebraic amplitude equations for CCD, with the terms ordered as in Fig. 12.1, is

$$\begin{aligned} & \langle AB|\hat{v}|IJ\rangle \\ & + \hat{P}((IA)(JB)) \left[\sum_C f_{BC} t_{IJ}^{AC} - \sum_K f_{KJ} t_{IK}^{AB} \right. \\ & \quad + \frac{1}{2} \sum_{CD} \langle AB|\hat{v}|CD\rangle t_{IJ}^{CD} + \frac{1}{2} \sum_{KL} \langle KL|\hat{v}|IJ\rangle t_{KL}^{AB} \\ & \quad + \sum_{KC} \left(2\langle KB|\hat{v}|CJ\rangle t_{IK}^{AC} - \langle KB|\hat{v}|CJ\rangle t_{KI}^{AC} \right. \\ & \quad \left. \left. - \langle KB|\hat{v}|IC\rangle t_{KJ}^{AC} - \langle KB|\hat{v}|JC\rangle t_{IK}^{AC} \right) \right] \end{aligned}$$

$$\begin{aligned}
& + \sum_{KLCD} \langle KL|\hat{v}|CD\rangle \left(\frac{1}{2}t_{IJ}^{CD}t_{KL}^{AB} + 2t_{IK}^{AC}t_{LJ}^{DB} - 2t_{IK}^{AC}t_{JL}^{DB} \right. \\
& \quad + \frac{1}{2}t_{IK}^{CA}t_{LJ}^{BD} - t_{IK}^{AD}t_{LJ}^{CB} + t_{KI}^{AD}t_{LJ}^{CB} \\
& \quad + \frac{1}{2}t_{IL}^{CB}t_{KJ}^{AD} - 2t_{KI}^{CD}t_{LJ}^{AB} + t_{IK}^{CD}t_{LJ}^{AB} \\
& \quad \left. - 2t_{KL}^{CA}t_{IJ}^{DB} + t_{KL}^{AC}t_{IJ}^{DB} \right) \Big] \\
& = 0 \quad (\text{for all } I \geq J \text{ and all } A, B). \tag{12.3}
\end{aligned}$$

The summations over internal lines are over spatial orbitals. For diagrams D_{2c} and D_{2d} the permutation factor can be canceled with the weight factor, because the permuted form is equal to the original.

Using the same interpretation rules, the CCD correlation energy is given by

$$\begin{aligned}
\Delta E_{\text{CCD}} &= \text{Diagram 1} + \text{Diagram 2} \\
&= \sum_{IJAB} (2\langle IJ|\hat{v}|AB\rangle - \langle IJ|\hat{v}|BA\rangle) t_{IJ}^{AB}. \tag{12.4}
\end{aligned}$$

Careful comparison of the spinorbital CCD equation (9.126) and the spin-free CCD equation (12.3) for the case in which the reference determinant is constructed solely from doubly occupied spatial orbitals shows the following relationships between the corresponding amplitudes:

$$t_{IJ}^{AB} = t_{I\alpha J\beta}^{A\alpha B\beta} = t_{I\beta J\alpha}^{A\beta B\alpha} = t_{JI}^{BA}, \tag{12.5}$$

$$t_{I\alpha J\alpha}^{A\alpha B\alpha} = t_{I\beta J\beta}^{A\beta B\beta} = t_{IJ}^{AB} - t_{IJ}^{BA}. \tag{12.6}$$

The two independent amplitudes t_{IJ}^{AB} and t_{IJ}^{BA} serve respectively as coefficients for two sums of four Slater determinants each,

$$\begin{aligned}
|\Phi_{IJ}^{AB}\rangle &\equiv \widehat{A\alpha}^\dagger \widehat{B\alpha}^\dagger \widehat{J\alpha} \widehat{I\alpha} |0\rangle + \widehat{A\alpha}^\dagger \widehat{B\beta}^\dagger \widehat{J\beta} \widehat{I\alpha} |0\rangle \\
&\quad + \widehat{A\beta}^\dagger \widehat{B\alpha}^\dagger \widehat{J\alpha} \widehat{I\beta} |0\rangle + \widehat{A\beta}^\dagger \widehat{B\beta}^\dagger \widehat{J\beta} \widehat{I\beta} |0\rangle, \tag{12.7}
\end{aligned}$$

$$\begin{aligned}
|\Phi_{IJ}^{BA}\rangle &\equiv \widehat{B\alpha}^\dagger \widehat{A\alpha}^\dagger \widehat{J\alpha} \widehat{I\alpha} |0\rangle + \widehat{B\alpha}^\dagger \widehat{A\beta}^\dagger \widehat{J\beta} \widehat{I\alpha} |0\rangle \\
&\quad + \widehat{B\beta}^\dagger \widehat{A\alpha}^\dagger \widehat{J\alpha} \widehat{I\beta} |0\rangle + \widehat{B\beta}^\dagger \widehat{A\beta}^\dagger \widehat{J\beta} \widehat{I\beta} |0\rangle, \tag{12.8}
\end{aligned}$$

where $|0\rangle$ is the reference determinant constructed from doubly occupied orbitals only. Each of these two linear combinations of Slater determinants

is a spin eigenfunction with $S = 0$. However, these two spin eigenfunctions are not orthogonal, because the first determinant in (12.8) is equal to the negative of the first determinant in (12.7), and the same is true of the last determinant in the two equations, resulting in an overlap

$$\langle \Phi_{IJ}^{AB} | \Phi_{IJ}^{BA} \rangle = -2 \quad (12.9)$$

(note that these functions are not normalized; $\langle \Phi_{IJ}^{AB} | \Phi_{IJ}^{AB} \rangle = \langle \Phi_{IJ}^{BA} | \Phi_{IJ}^{BA} \rangle = 4$). Any other doubly excited singlet-spin eigenfunction that can be constructed involving the same four orbitals would be linearly dependent on these two functions, which explains the exclusion of amplitudes such as $t_{I\alpha J\beta}^{AB\beta\alpha}$ and justifies the requirement that spin be conserved along each continuous path in the diagrams.

The cases $A = B$ and/or $I = J$ are simpler, resulting in one spin-free amplitude each and providing coefficients for the following singlet-spin eigenfunctions:

$$|\Phi_{IJ}^{AA}\rangle \equiv \widehat{A\alpha}^\dagger \widehat{A\beta}^\dagger \widehat{J\beta} \widehat{I\alpha} |0\rangle + \widehat{A\beta}^\dagger \widehat{A\alpha}^\dagger \widehat{J\alpha} \widehat{I\beta} |0\rangle, \quad (12.10)$$

$$|\Phi_{II}^{AB}\rangle \equiv \widehat{A\alpha}^\dagger \widehat{B\beta}^\dagger \widehat{I\beta} \widehat{I\alpha} |0\rangle + \widehat{A\beta}^\dagger \widehat{B\alpha}^\dagger \widehat{I\alpha} \widehat{I\beta} |0\rangle, \quad (12.11)$$

$$|\Phi_{II}^{AA}\rangle \equiv \widehat{A\alpha}^\dagger \widehat{A\beta}^\dagger \widehat{I\beta} \widehat{I\alpha} |0\rangle. \quad (12.12)$$

The situation is more complicated for higher excitations and for open-shell states. For ROHF cases the approach described here may lead to functions that are not spin eigenfunctions. A fully spin-adapted and orthogonal coupled-cluster formalism, including the treatment of open-shell systems, is provided by the *orthogonally spin-adapted coupled-cluster method* (Paldus 1977, Adams and Paldus 1979, Li and Paldus 1997).

Spin integration in UHF-based CCD calculations is described in terms of antisymmetrized diagrams by Bartlett and Musiał (2007, Fig. 9). For more general CC treatments using different orbitals for different spins, including open-shell UHF cases, only algebraic procedures are easily applicable; this is the approach used for all cases in the ACES program system (Stanton, Gauss, Watts *et al.* 1992, Bartlett and Watts 1998). This approach readily permits the treatment of high-spin open-shell molecules with either UHF or ROHF reference functions as well as the use of even more exotic reference functions, such as are found in quasi-restricted Hartree–Fock (QRHF) (Rittby and Bartlett 1988) or the Brueckner orbital representation to be described in Section 12.4. Low-spin open-shell states are not accessible in this way, because they require a multideterminantal zero-order function. These types of state require more sophisticated spin-adapted theories, such as the

orthogonally spin-adapted approach mentioned above. Open-shell singlets can be treated within a spinorbital context by a two-determinant-based CC theory (Balková and Bartlett 1992, Szalay and Bartlett 1994). Open-shell states can also be treated by the various EOM–CC techniques discussed in Chapter 13.

In all cases, careful organization of the calculations, the definition of appropriate intermediate sums and other summation techniques are important in keeping the computational work within reasonable bounds. Examples of the use of intermediates in CC calculations were presented by Noga and Bartlett (1987) for CCSDT and by Kucharski and Bartlett (1991a, 1992) for CCSDTQ. These techniques are discussed further in Section 10.7.

12.2 Coupled-cluster theory with an arbitrary single-determinant reference function

The maximum flexibility and range of applicability of the coupled-cluster method often derives from the use of reference functions that are not canonical Hartree–Fock determinants. Such reference functions may be noncanonical HF solutions, which require a block-diagonal Fock matrix, $f_{ai} = 0$, without requiring the individual hole–hole and particle–particle blocks to be diagonal, as would be the case for e.g. localized HF orbitals, or they can be more arbitrary non-HF single determinants, for which $f_{ai} \neq 0$. Because the use of a canonical HF reference function, with its computational simplifications, is so pervasive in CC and MBPT applications, generalizations to arbitrary reference functions often may not be given due consideration. In the discussions of MBPT and CC methods in this book we have always tried to include the general case. In this and the next sections we shall also show that using CC theory with an arbitrary reference function can lead to a generalized MBPT treatment (GMBPT) that provides the finite-order perturbation-theory approximations as well as the CC solution.

The normal-ordered Hamiltonian retains the same general form for any choice of orbitals,

$$\hat{H}_N = \sum_{pq} f_{pq} \{\hat{p}^\dagger \hat{q}\} + \frac{1}{4} \sum_{pqrs} \langle pq || rs \rangle \{\hat{p}^\dagger \hat{q}^\dagger \hat{s} \hat{r}\}. \quad (12.13)$$

In the general case we have to retain the f_{ai} elements, which reflect the non-HF nature of the reference function, as well as the off-diagonal f_{ij} and

f_{ab} elements; this leads to the detailed form

$$\begin{aligned} \hat{H}_N = & \sum_p f_{pp} \{\hat{p}^\dagger \hat{p}\} + \sum_{i \neq j} f_{ij} \{\hat{i}^\dagger \hat{j}\} + \sum_{a \neq b} f_{ab} \{\hat{a}^\dagger \hat{b}\} \\ & + \sum_{ai} (f_{ai} \{\hat{a}^\dagger \hat{i}\} + f_{ia} \{\hat{i}^\dagger \hat{a}\}) + \frac{1}{4} \sum_{pqrs} \langle pq || rs \rangle \{\hat{p}^\dagger \hat{q}^\dagger \hat{s} \hat{r}\}. \end{aligned} \quad (12.14)$$

We can separate this form into a zero-order part and a perturbation, in which the zero-order part includes the off-diagonal elements of the hole-hole and particle-particle blocks of the Fock matrix:

$$\hat{H}_N = (\hat{H}_0)_N + \hat{V}_N, \quad (12.15)$$

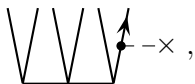
where

$$(\hat{H}_0)_N = \sum_p f_{pp} \{\hat{p}^\dagger \hat{p}\} + \sum_{i \neq j} f_{ij} \{\hat{i}^\dagger \hat{j}\} + \sum_{a \neq b} f_{ab} \{\hat{a}^\dagger \hat{b}\}, \quad (12.16)$$

$$\hat{V}_N = \sum_{ai} (f_{ai} \{\hat{a}^\dagger \hat{i}\} + f_{ia} \{\hat{i}^\dagger \hat{a}\}) + \frac{1}{4} \sum_{pqrs} \langle pq || rs \rangle \{\hat{p}^\dagger \hat{q}^\dagger \hat{s} \hat{r}\}. \quad (12.17)$$

In earlier descriptions of MBPT procedures and of the iterative solutions of the CC equations (see Chapters 9 and 10), only the diagonal part $(\hat{H}_0^d)_N$, i.e. the first term on the r.h.s. of (12.16), was used as the zero-order normal-product Hamiltonian; all other terms were treated as part of the perturbation. While this approach is practical and common, it has three weaknesses. First, in many-body theory we prefer the results to be invariant under linear transformations of the occupied orbitals or the unoccupied orbitals separately. This requirement is satisfied by the separation in (12.15)–(12.17) but not by a separation using $(\hat{H}_0^d)_N$. Second, using $(\hat{H}_0^d)_N$ increases the likelihood that large off-diagonal Fock-matrix elements will be included in the perturbation and will contribute to poor convergence of the iterative process.

Third, a diagram like



in the CCSDT equations (diagram T_{2a} of Fig. 10.5) can cause computational difficulties because, unlike the situation in the canonical HF case, the


off-diagonal  $-x$ interaction does not vanish. For non-HF and noncanonical HF orbitals the evaluation of this diagram would require an $\sim n_h^3 n_p^4$ procedure. In iterative CCSDT-1, CCSDT-3 or CCSDT calculations this

diagram is simply incorporated in the generalized intermediates without undue concern, but for a noniterative CCSD(T) calculation its off-diagonal part cannot be ignored and would become a serious limitation (Watts, Gauss and Bartlett 1993).

All three weaknesses can be readily removed by exploiting the invariance of CC theory under separate unitary transformations of the occupied orbitals and of the unoccupied orbitals. This objective is accomplished by a unitary transformation of the spinorbitals to *semicanonical form*, defined by the requirement that the Fock matrix takes the form

$$\begin{pmatrix} & \blacksquare \\ \blacksquare & \end{pmatrix}.$$

For the semicanonical orbitals, the hole-hole and particle-particle blocks of the Fock matrix are diagonal, $f_{ij} = f_{ii}\delta_{ij}$, $f_{ab} = f_{aa}\delta_{ab}$, and thus the difficulties of dealing with the corresponding off-diagonal elements are avoided. The hole-particle and particle-hole blocks are changed by the semicanonical transformation but do not vanish, $f_{ia} \neq 0$, $f_{ai} \neq 0$, and remain as a part of the perturbation \hat{V}_N , which has the effect of mixing the occupied and virtual spaces. With the semicanonical transformation, the only one-electron vertices that need to be included in the diagrams on the r.h.s. of the iterative CC equations are those that represent f_{ia} and f_{ai} interactions, which are easy to deal with in CC theory (unlike in MBPT) because they add very few diagrams. The iterations of the CC equations indirectly introduce *all* the noncanonical HF diagrams that would proliferate excessively in standard MBPT, and thereby the CC approach offers a far more effective evaluation of these contributions than individual MBPT diagrams. This is the basis for the GMBPT method to be discussed in the next section.

Because of the Thouless theorem (Thouless 1960), which states that any Slater determinant in a given Hilbert space can be generated from any other Slater determinant in that space by the application of an operator of the form $e^{\hat{T}_1}$, CC results at the CCSD level and beyond are much less sensitive than the corresponding CI results to the choice of reference determinant. This property of the CC method opens the door for the effective use of many convenient single-determinant choices as bases for CC expansions. One interesting possible choice is the Kohn-Sham determinant of density-functional theory (Kohn and Sham 1965), which is formulated to provide the exact electron density for the system. Another possible choice is a determinant composed of the N highest-occupancy natural spinorbitals (the so-called first natural configuration), for which the density matrix has maximum overlap with the exact one-particle density matrix (Löwdin 1955).

Yet another is a determinant composed of Brueckner orbitals (the reference determinant for which all single-excitation contributions to the exact wave function vanish), which has maximum overlap with the exact wave function.

A particular case of substantial interest is the use of a restricted open-shell Hartree–Fock (ROHF) reference function (Rittby and Bartlett 1988). Unlike unrestricted HF (UHF), this approach to open-shell problems employs an HF calculation that enforces all spin conditions, and often all or some point-group symmetry requirements, of the exact solution. In particular, the ROHF determinant has the maximum number of doubly occupied spatial orbitals consistent with the required multiplicity. The choice of an ROHF reference function can be beneficial in many cases, including treatments of the excited states of radicals by the EOM–CC method described in Chapter 13 (Hirata, Nooijen and Bartlett 2000a). Of course, as the full-CI level is approached, the dependence of the results on the choice of orbitals disappears.

For ROHF–CCSD(T) (Watts, Gauss and Bartlett 1993) and ROHF–MBPT (Lauderdale, Stanton, Gauss *et al.* 1991), as well as for ROHF–CCSD gradients (Gauss, Lauderdale, Stanton *et al.* 1991), the ROHF orbitals are used to construct the (noncanonical) spinorbital Fock matrix; this is followed by a semicanonical transformation to diagonalize the hole–hole and particle–particle blocks. As a result of this transformation, the spatial parts of the α and β spinorbitals are no longer equal in pairs and so the CC calculations are carried out in a spinorbital-based formalism in the same way as in a calculation based on a UHF reference function.

Another case of interest is the use of a so-called quasi-RHF (QRHF) reference function (Rittby and Bartlett 1988). In this approach, SCF orbitals from a related system are used to treat the system of interest. For example, the HF orbitals of CH_3^+ (a closed-shell system) can be used to study the CH_3^\bullet radical or the CH_3^- ion, or the HF orbitals of any of these systems can be used to study the others. If the orbitals of the radical are to be used then they would be taken from either the spin- α set or the spin- β set). This QRHF reference function is in no way variationally optimal for the problem addressed, but that deficiency is much less important in CCSD and higher CC levels than in CI and MBPT calculations, because of the Thouless theorem. In particular, QRHF orbitals are very useful when studying hole states of ions created by the excitation of an electron from an orbital other than the highest occupied. The HF orbitals of the neutral species can be used in the calculation, their occupancy in the reference determinant being adjusted to describe the desired hole state, thus avoiding the potential for variational

collapse that would be present if the reference function were to be optimized for the ion.

12.3 Generalized many-body perturbation theory

As discussed in Section 9.5 and in Chapter 10, iterations of the CC equations can easily be used to generate MBPT solutions for the usual case of an HF reference function with a diagonal zero-order Hamiltonian. Using the non-diagonal zero-order Hamiltonian (12.16) of the previous section and a semicanonical transformation, order-by-order generalized MBPT (GMBPT) solutions can be obtained for the non-diagonal case (subsection 2.4.5) from the corresponding CC iterations for arbitrary reference determinants. For example, the CC correlation energy,

$$\Delta E = \underbrace{\text{diagram}}_{D_1} + \underbrace{\text{diagram}}_{D_2} + \underbrace{\text{diagram}}_{D_3}, \quad (12.18)$$

can be expanded in orders of MBPT:

$$\Delta E = E^{(2)} + E^{(3)} + E^{(4)} + \dots, \quad (12.19)$$

where, for example,

$$E^{(2)} = \underbrace{\text{diagram}}_{D_1^{(2)}} + \underbrace{\text{diagram}}_{D_2^{(2)}}. \quad (12.20)$$

The first-order amplitudes are obtained explicitly from the first-order CCSD equations (noting that the diagonal f_{ii} and f_{aa} interactions are of zero order)

$$\underbrace{\text{diagram}}_{(1)} + \underbrace{\text{diagram}}_{(1)} + \underbrace{\text{diagram}}_{-\times} = 0, \quad (12.21)$$

$$\underbrace{\text{diagram}}_{(1)} + \underbrace{\text{diagram}}_{(1)} + \underbrace{\text{diagram}}_{--} = 0, \quad (12.22)$$

which, with the semicanonical transformation, simplify to

$$(f_{aa} - f_{ii})t_i^{a(1)} + f_{ai} = 0, \quad (12.23)$$

$$(f_{aa} + f_{bb} - f_{ii} - f_{jj})t_{ij}^{ab(1)} + \langle ab || ij \rangle = 0. \quad (12.24)$$

Noting that $f_{ii} = \varepsilon_i$, $f_{ii} - f_{aa} = \varepsilon_i^a$ etc., the insertion of these amplitudes into the second-order energy expression (12.20) provides the GMBPT(2) approximation,

$$E^{(2)} = \text{diagram 1} + \text{diagram 2}, \quad (12.25)$$

having the same components as the diagonal-case MBPT(2) energy, (5.9), (5.10).

Continuing to third order (compare with the diagonal CCD case in Fig. 9.3), we obtain

$$E^{(3)} = \underbrace{\text{diagram 1}}_{D_1^{(3)}} + \underbrace{\text{diagram 2}}_{D_2^{(3)}} + \underbrace{\text{diagram 3}}_{D_3^{(3)}}. \quad (12.26)$$

Knowing the first-order amplitudes, the second-order amplitudes in this equation are obtained explicitly from

$$\text{diagram 1} + \text{diagram 2} + \text{diagram 3} + \text{diagram 4} = 0, \quad (12.27)$$

$$\text{diagram 5} + \text{diagram 6} + \text{diagram 7} = 0, \quad (12.28)$$

where each skeleton represents the sum of the corresponding diagrams with all distinct arrow assignments. Substituting the resulting first-order and second-order amplitudes, the GMBPT(3) energy is obtained as

$$E^{(3)} = \text{diagram 1} + \text{diagram 2} + \text{diagram 3} + \text{diagram 4} + \text{diagram 5} + \text{diagram 6} + \text{diagram 7}. \quad (12.29)$$

Note the introduction of factorized-denominator MBPT diagrams,

$$\begin{aligned} \text{diagram 8} &= \frac{1}{2} \left(\text{diagram 9} + \text{diagram 10} \right) \\ &= \frac{1}{2} \frac{\langle ab || ij \rangle f_{ia} f_{jb}}{\varepsilon_{ij}^{ab}} \left(\frac{1}{\varepsilon_i^a} + \frac{1}{\varepsilon_j^b} \right) = \frac{1}{2} \frac{\langle ab || ij \rangle f_{ia} f_{jb}}{\varepsilon_i^a \varepsilon_j^b}, \end{aligned} \quad (12.30)$$

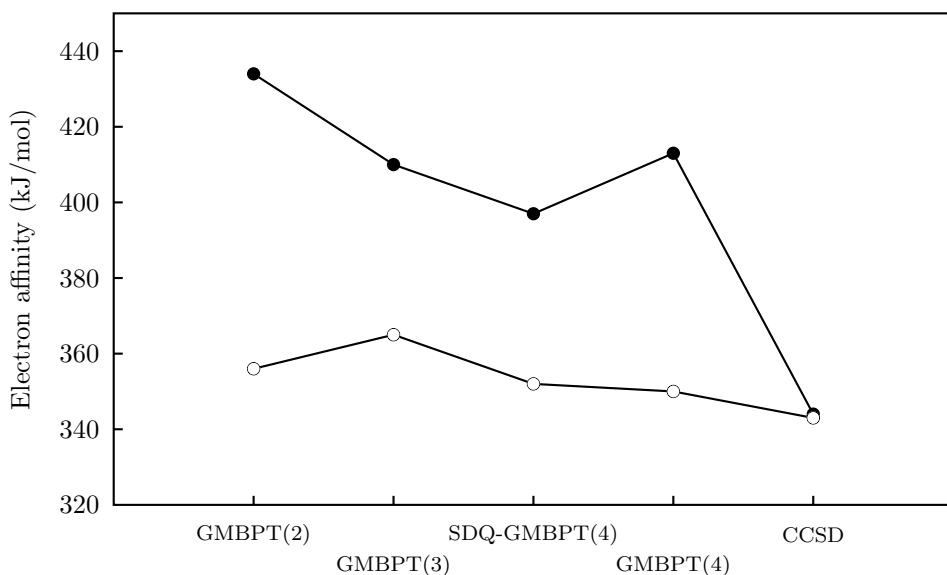


Fig. 12.2. GMBPT electron affinity of the CN radical. • UHF, ○ ROHF.

with a similar result for

$$\begin{array}{c} \text{---} \\ \text{---} \end{array} \begin{array}{c} \text{---} \\ \text{---} \end{array} = \frac{1}{2} \left(\begin{array}{c} \text{---} \\ \text{---} \end{array} \begin{array}{c} \text{---} \\ \text{---} \end{array} - \times + \times - \begin{array}{c} \text{---} \\ \text{---} \end{array} \begin{array}{c} \text{---} \\ \text{---} \end{array} \right). \quad (12.31)$$

The diagrams of (12.31) are conjugate (Section 5.5) to those of (12.30), and their values are complex conjugates of each other. Their sum is equal to twice the real part of either:

$$\begin{array}{c} \times - \\ \text{---} \end{array} \begin{array}{c} \text{---} \\ \text{---} \end{array} + \begin{array}{c} \text{---} \\ \text{---} \end{array} \begin{array}{c} \text{---} \\ \text{---} \end{array} = \text{Re} \left(\frac{\langle ab || ij \rangle f_{ia} f_{jb}}{\varepsilon_i^a \varepsilon_j^b} \right). \quad (12.32)$$

These denominator factorizations and summations are automatically incorporated in CC diagrams. As seen in (12.29), the GMBPT expansion for the energy is necessarily Hermitian, unlike the CC energy expression.

Extensions to higher orders of the explicit expression of the GMBPT energies in terms of MBPT diagrams can be made, but there is little reason to do so since the accumulated CC amplitudes naturally account for all higher-order diagrams including the proliferating non-HF (f_{ai} -dependent) terms. Obviously the latter terms do not appear when canonical HF orbitals are used and, since the semicanonical transformation also eliminates the off-diagonal f_{ij} and f_{ab} terms, the above procedure also regains the MBPT

diagrams for the canonical HF case. The result is a seamless treatment of MBPT for any choice of single-determinant reference functions and orbitals.

A comparison of ROHF-based and UHF-based GMBPT results for the electron affinity of the CN radical, computed as the energy difference between CN^\bullet and CN^- , is shown in Fig. 12.2 ((Lauderdale, Stanton, Gauss *et al.* 1991). In this example, excessive spin contamination in the UHF reference function causes very slow convergence of the corresponding GMBPT values in comparison with the ROHF case; ROHF-based GMBPT provides a satisfactory result even at second order, while the UHF-based calculation (which is the same as MBPT) does not approach the infinite-order CCSD result even at fourth order. As expected, because of the low sensitivity of CC theory to the choice of orbitals, the CCSD results for the two reference functions are almost identical.

12.4 Brueckner orbitals and alternative treatments of \hat{T}_1

The number of diagrams involving \hat{T}_1 can be quite large, making the expressions for the various CC approximations appear unnecessarily formidable. Most of this apparent complexity is removed in the pseudolinear form of the equations through the use of the intermediates (effective-Hamiltonian diagrams) introduced in Section 10.7. However, there are some advantages in removing \hat{T}_1 from the equations by a transformation to orbitals in terms of which $\hat{T}_1 = 0$. Such orbitals are known as *Brueckner orbitals* (Nesbet 1958, Löwdin 1962b). Another approach is to hide \hat{T}_1 in an effective Hamiltonian

$$\tilde{H} = e^{-\hat{T}_1} \hat{H}_N e^{\hat{T}_1}. \quad (12.33)$$

The second approach is more general, and we shall consider it first.

Because all \hat{T}_m operators commute with each other, we may rewrite the CC equations in the form

$$\hat{Q}(e^{-\hat{T}_2 - \hat{T}_3 - \dots} \tilde{H} e^{\hat{T}_2 + \hat{T}_3 + \dots}) \hat{P} = 0, \quad (12.34)$$

$$\Delta E = \langle 0 | \tilde{H} | 0 \rangle + \langle 0 | e^{-\hat{T}_2} \hat{W} e^{\hat{T}_2} | 0 \rangle = E_S + E_D, \quad (12.35)$$

$$E_S = \langle 0 | \hat{f}_N \hat{T}_1 | 0 \rangle_C + \frac{1}{2} \langle 0 | \hat{W} \hat{T}_1^2 | 0 \rangle_C, \quad (12.36)$$

separating the energy contributions of single-excitation amplitudes, E_S , from those of double-excitation amplitudes, E_D . Expanding the exponentials in

(12.33), we obtain

$$\begin{aligned}\tilde{H} = & \hat{H}_N + (\hat{f}_N \hat{T}_1)_C + \frac{1}{2}(\hat{f}_N \hat{T}_1^2)_C + (\hat{W} \hat{T}_1)_C \\ & + \frac{1}{2}(\hat{W} \hat{T}_1^2)_C + \frac{1}{3!}(\hat{W} \hat{T}_1^3)_C + \frac{1}{4!}(\hat{W} \hat{T}_1^4)_C.\end{aligned}\quad (12.37)$$

The one-electron part of this operator is represented diagrammatically by those one-electron components of the effective Hamiltonian \mathcal{H} , i.e. χ_{ia} , χ_{ab} , χ_{ij} and χ_{ai} , (10.53)–(10.56), that do not contain \hat{T} vertices other than \hat{T}_1 . Similarly, the two-electron part of \tilde{H} is represented by those terms of (10.63)–(10.80) that do not contain \hat{T} vertices other than \hat{T}_1 . Inspection of the three-electron and four-electron components of \mathcal{H} , (10.81)–(10.96), shows no terms with \hat{T}_1 vertices exclusively, so none of these contribute to \tilde{H} . Thus \tilde{H} is a normal-product two-electron operator, just like \hat{H}_N , and its evaluation is equivalent to a transformation of the original one-electron and two-electron integrals (the elements of \hat{H}_N) into the elements of \tilde{H} except that, unlike \hat{H}_N , \tilde{H} is not Hermitian.

A possible strategy for solving the CC equations is to build the \mathcal{H} operator first and then use it instead of \hat{H}_N in the CC equations, omitting \hat{T}_1 -containing terms. However, \hat{T}_1 and thus \tilde{H} depend on the solution of the CC equations and so an iterative procedure is required for the construction of \tilde{H} . Each iteration requires re-solving the CCD (and CCDT) equations using \tilde{H} instead of \hat{H}_N , recomputing the \hat{T}_1 amplitudes from the CCSD singles equation, Fig. 10.2, and transforming the elements of \tilde{H} to correspond to the updated \hat{T}_1 amplitudes. This transformation involves an n^5 computational process, which is less demanding than the $n_h^2 n_p^4$ algorithm needed for the solution of the CCD equations and much less than that for CC equations that retain triple and higher excitations. For algorithms that use the untransformed basis-set integrals directly, \tilde{H} can also be represented conveniently in terms of the basis functions (Koch, Christiansen, Kobayashi *et al.* 1994).

Brueckner orbitals can be defined, within a given one-electron Hilbert space, by either of two equivalent conditions on the orbitals occupied in the reference determinant: (a) the requirement that single-excitation contributions to the exact wave function vanish (Nesbet 1958) or (b) the requirement that the reference determinant has maximum overlap with the exact wave function (Löwdin 1962b). The equivalence of these conditions can be seen by considering the overlap between $|\Phi_B\rangle$, the Brueckner reference determinant, and the exact wave function $|\Psi\rangle$. Since any reference determinant can be converted to any other determinant constructed in the same one-electron

Hilbert space by a one-electron exponential operator of the form $e^{\hat{T}_1}$ (Thouless 1960), we can write the unnormalized Brueckner determinant in the form

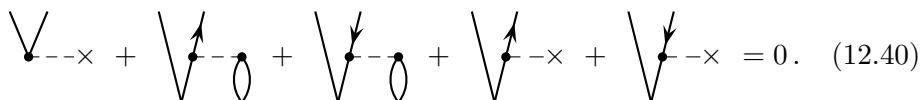
$$|\Phi_B\rangle = e^{\hat{T}_1}|0\rangle. \quad (12.38)$$

Requiring stationarity of the overlap with respect to the components of \hat{T}_1 leads to

$$0 = \frac{\partial}{\partial t_i^a} \langle \Psi | e^{\hat{T}_1} | 0 \rangle = \langle \Psi | \hat{a}^\dagger_i e^{\hat{T}_1} | 0 \rangle = \langle \Psi | (\Phi_B)_i^a \rangle, \quad (12.39)$$

showing that single excitations from the Brueckner determinant do not contribute to the exact wave function, so that $\hat{T}_1 = 0$; hence conditions (a) and (b) are equivalent.

Determining the Brueckner orbitals requires an iterative process. To determine a new set of \hat{T}_1 amplitudes from the current \hat{T}_2 amplitudes, the normal procedure uses the leading terms of the CCSD single-excitation equation, Fig. 10.2:



$$\text{Diagram 1} + \text{Diagram 2} + \text{Diagram 3} + \text{Diagram 4} + \text{Diagram 5} = 0. \quad (12.40)$$

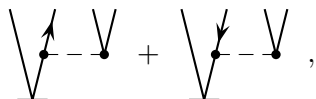
The higher-order terms involving \hat{T}_2 will be unimportant compared with the two \hat{T}_2 diagrams in (12.40). If explicit consideration of triples is of interest in the generation of Brueckner orbitals then the \hat{T}_3 diagram S_7 , (10.31), can be added. It should be recognized, however, that the first approximation of \hat{T}_3 can be deduced from \hat{T}_2 anyway, using the second-order \hat{T}_{1a} and \hat{T}_{1b} diagrams of the CCSDT triples equations, Fig. 10.5, and comparing them with the first-order \hat{S}_{2a} and \hat{S}_{2b} diagrams of the CCSD singles equation, Fig. 10.2.

Once a new set $\{t_i^a\}$ of \hat{T}_1 amplitudes has been obtained from (12.40), it is used to define a new set of orbitals by modifying the transformation matrix $\mathbf{C}^{(0)}$ defining the current orbitals $\{\phi_p^{(0)}\}$ in terms of the basis functions $\{\chi_\mu\}$, (11.99), according to

$$\begin{aligned} C_{\mu i} &= C_{\mu i}^{(0)} + \sum_a C_{\mu a}^{(0)} t_i^a, \\ C_{\mu a} &= C_{\mu a}^{(0)} - \sum_i C_{\mu i}^{(0)} t_i^a, \end{aligned} \quad (12.41)$$

where \mathbf{C} is a new transformation matrix (Chiles and Dykstra 1981). The transformed orbitals are orthonormalized, and the process is repeated by

re-solving the CCSD doubles equations for \hat{T}_2 using just the leading \hat{T}_1 contributions from Fig. 10.3,


(12.42)

plus all the \hat{T}_2 terms of the CCD equations, Fig. 9.2. Then (12.40) is solved again for new \hat{T}_1 amplitudes. As this process is iterated, the \hat{T}_1 amplitudes get progressively smaller, and the importance of the \hat{T}_1 contributions in CCSD (and higher) equations diminishes until they can be neglected altogether. At this point we have a set of Brueckner orbitals. With proper organization, this procedure can be made nearly as efficient as using pre-determined HF or other orbitals in CC calculations.

An advantage of Brueckner-orbital-based CC (B-CC) calculations is that, with $\hat{T}_1 = 0$, the effects of many nonlinear terms that are not included in CCSD, such as those due to $\hat{T}_1\hat{T}_3$ and $\hat{T}_1\hat{T}_4$ products, do not contribute in B-CC calculations and thus do not constrain the accuracy of the B-CCD or B-CCDT results. Furthermore, the exact vanishing of the \hat{T}_1 contributions in B-CC calculations of one-body reduced density matrices and electronic properties (Chapter 11), besides greatly reducing the number of diagrams that need to be included, may contribute to the accuracy of these density matrices, in which \hat{T}_1 terms often play a significant role (Bartlett, Grabowski, Hirata *et al.* 2005).

A comparative study of several difficult, potentially multireference, problems at the CCSDT level using B and HF orbitals was reported by Watts and Bartlett (1994). Extensive applications of B-CCD (referred to as BD) and B-CCD(T), including analytical gradients, were reported by Handy, Pople, Head-Gordon *et al.* (1989) and by Raghavachari, Pople, Replogle, *et al.* (1990).

Finally, for symmetry-broken cases, e.g. the comparative energy of the C_{2v} and D_{3h} forms of the open shell NO_3 molecule (Stanton, Gauss and Bartlett 1992), B-CC has been felt to have some advantages. Using B orbitals the two geometries can be described equivalently without the use of broken-symmetry orbitals, unlike the case for UHF or other choices of orbitals that may vary discontinuously as the symmetry of the molecular geometry changes. Obviously, all EOM-CC calculations (see Chapter 13) can be performed with B or any other orbitals, as can all property calculations.

12.5 Monitoring multiplicities in open-shell coupled-cluster calculations

The ability to use RHF, UHF, ROHF, QRHF, B (Brueckner), KS (Kohn–Sham), NO (natural orbitals) or any other single-determinant reference function, as discussed in Section 12.2 for example, provides a very useful flexibility in the application of CC methods to diverse problems. However, applications of these methods to open-shell states do not always result in pure-spin solutions. This deficiency is particularly evident for UHF reference functions, but even for ROHF the truncated CC wave function can deviate to some extent from being an \hat{S}^2 eigenfunction. Thus an indicator of the quality of an open-shell CC solution is provided by computing its \hat{S}^2 expectation value. For an accurate solution this value should equal $S(S+1)$, corresponding to the spin multiplicity $2S+1$ of the desired electronic state. The deviation of the computed expectation value from the correct eigenvalue is a useful diagnostic for the accuracy of the solution. Of course, all determinants contributing to the CC expansion are expected to be composed of pure spinorbitals and to be \hat{S}_z eigenfunctions having the same value of S_z .

Single-reference CC theory with an arbitrary single-determinant reference function treats spin passively, as opposed to most CI calculations, in which the spin-eigenstate requirement is enforced in every term (configuration state function) of the CI expansion. An untruncated, converged CC wave function is a spin eigenfunction, satisfying

$$\hat{H}\Psi = E\Psi, \quad (12.43)$$

$$\hat{S}^2\Psi = S(S+1)\Psi. \quad (12.44)$$

Approximate solutions Ψ_{approx} , such as in truncated CC, do not necessarily satisfy the spin eigenvalue equation (12.44). For such solutions we can derive an approximate value \bar{S} of the spin quantum number S using the *projected value* $\langle\hat{S}^2\rangle_{\text{proj}}$, defined by

$$\langle\hat{S}^2\rangle_{\text{proj}} \equiv \langle 0|\hat{S}^2|\Psi_{\text{approx}}\rangle = \bar{S}(\bar{S}+1). \quad (12.45)$$

Equation (12.45) constitutes a quadratic equation for \bar{S} in terms of $\langle\hat{S}^2\rangle_{\text{proj}}$, with the solution (Purvis, Sekino and Bartlett 1988)

$$2\bar{S}+1 = \sqrt{1+4\langle\hat{S}^2\rangle_{\text{proj}}}. \quad (12.46)$$

Satisfying the condition $\bar{S} = S$ does not generally guarantee an exact wave function, but for open-shell states the amount by which \bar{S} differs from the exact quantum number S is normally a useful measure of the quality of the solution.

A more appropriate measure of the spin property for CC wave functions (Stanton 1994) is provided by an expectation-value form based on the response treatment of properties (Chapter 11):

$$\langle \hat{S}^2 \rangle_{\text{resp}} = \langle 0 | (1 + \Lambda) e^{-\hat{T}} \hat{S}^2 e^{\hat{T}} | 0 \rangle. \quad (12.47)$$

This expectation value can be computed easily using the response density matrices (Section 11.7), as shown in the following analysis (Purvis, Sekino and Bartlett 1988, Stanton 1994). Of course, computation of the response density matrices requires the solution of the Λ equations, as would be required for any property calculation, including that of gradients and second derivatives.

To evaluate the matrix elements of \hat{S}^2 we use the well-known relationship

$$\hat{S}^2 = \hat{S}_- \hat{S}_+ + \hat{S}_z^2 + \hat{S}_z, \quad (12.48)$$

where \hat{S}_+ and \hat{S}_- are the spin raising and lowering operators, respectively. Here

$$\hat{S}_+ = \sum_{\mu} \hat{s}_{\mu+}, \quad \hat{S}_- = \sum_{\mu} \hat{s}_{\mu-}, \quad \hat{S}_z = \sum_{\mu} \hat{s}_{\mu z} \quad (12.49)$$

(the sums are over the electrons), with

$$\begin{aligned} \hat{s}_+ \alpha &= 0, & \hat{s}_+ \beta &= \alpha, \\ \hat{s}_- \alpha &= \beta, & \hat{s}_- \beta &= 0, \\ \hat{s}_z \alpha &= \frac{1}{2} \alpha, & \hat{s}_z \beta &= -\frac{1}{2} \beta. \end{aligned} \quad (12.50)$$

Using (12.50), the operators can be represented in second-quantized form as (Purvis, Sekino and Barlett 1988)

$$\hat{S}_- = \sum_{p\beta q\alpha} \Delta_{p\beta q\alpha} \hat{p}_{\beta}^{\dagger} \hat{q}_{\alpha}, \quad \hat{S}_+ = \sum_{r\alpha s\beta} \Delta_{r\alpha s\beta} \hat{r}_{\alpha}^{\dagger} \hat{s}_{\beta}, \quad (12.51)$$

$$\hat{S}_z = \sum_{pq} \langle p | \hat{s}_z | q \rangle \hat{p}^{\dagger} \hat{q} = \frac{1}{2} \sum_{p\alpha} \hat{p}_{\alpha}^{\dagger} \hat{p}_{\alpha} - \frac{1}{2} \sum_{r\beta} \hat{r}_{\beta}^{\dagger} \hat{r}_{\beta} = \frac{1}{2} \Delta \hat{n}, \quad (12.52)$$

where the sums over p_{α} and q_{β} are over spinorbitals with spin α and spin β , respectively, Δ_{pq} is the overlap integral between the spatial parts of the spinorbitals p and q , $\Delta \hat{n} = \hat{n}_{\alpha} - \hat{n}_{\beta}$ and \hat{n}_{α} and \hat{n}_{β} are the number operators for spinorbitals with spin α and spin β , respectively, returning the numbers n_{α} and n_{β} of the corresponding spinorbitals in the determinants on which they operate. In any wave function which is an eigenfunction of \hat{S}_z all determinants have the same values of n_{α} and of n_{β} . When \hat{S}_+ is applied

to a “high-spin” determinant (a determinant in which all singly occupied orbitals have spin α) the result is zero, so the first term in (12.48) can be ignored in such cases.

Using Wick’s theorem, we have

$$\begin{aligned}
 \hat{S}_- \hat{S}_+ &= \sum_{p\beta q\alpha r\alpha s\beta} \Delta_{p\beta q\alpha} \Delta_{r\alpha s\beta} \hat{p}_\beta^\dagger \hat{q}_\alpha \hat{r}_\alpha^\dagger \hat{s}_\beta \\
 &= \sum_{p\beta q\alpha r\alpha s\beta} \Delta_{p\beta q\alpha} \Delta_{r\alpha s\beta} \{\hat{p}_\beta^\dagger \hat{q}_\alpha \hat{r}_\alpha^\dagger \hat{s}_\beta\} + \sum_{a_\alpha p_\beta s_\beta} \Delta_{p_\beta a_\alpha} \Delta_{a_\alpha s_\beta} \{\hat{p}_\beta^\dagger \hat{s}_\beta\} \\
 &\quad - \sum_{i_\beta q_\alpha r_\alpha} \Delta_{i_\beta q_\alpha} \Delta_{r_\alpha i_\beta} \{\hat{r}_\alpha^\dagger \hat{q}_\alpha\} + \sum_{i_\beta a_\alpha} |\Delta_{i_\beta a_\alpha}|^2, \tag{12.53}
 \end{aligned}$$

where $\{\dots\}$ indicates the normal-ordered product, the second and third terms result from single contractions and the last term results from a double contraction. Similarly,

$$\begin{aligned}
 \hat{S}_z &= \frac{1}{2} \left(\sum_{p_\alpha} \hat{p}_\alpha^\dagger \hat{p}_\alpha - \sum_{p_\beta} \hat{p}_\beta^\dagger \hat{p}_\beta \right) \\
 &= \frac{1}{2} \left(\sum_{p_\alpha} \{\hat{p}_\alpha^\dagger \hat{p}_\alpha\} - \sum_{p_\beta} \{\hat{p}_\beta^\dagger \hat{p}_\beta\} \right) + \frac{1}{2} \left(\sum_{i_\alpha} 1 - \sum_{i_\beta} 1 \right) \\
 &= \frac{1}{2} \{\Delta \hat{n}\} + \frac{1}{2} \Delta n, \tag{12.54}
 \end{aligned}$$

$$\hat{S}_z^2 = \frac{1}{4} \left(\{\Delta \hat{n}\} + \Delta n \right)^2 = \frac{1}{4} \{\Delta \hat{n}\}^2 + \frac{1}{2} \{\Delta \hat{n}\} \Delta n + \frac{1}{4} (\Delta n)^2, \tag{12.55}$$

where $\{\Delta \hat{n}\} = \{\hat{n}_\alpha\} - \{\hat{n}_\beta\}$ and $\Delta n = n_\alpha - n_\beta$ (note the distinction between the operator $\Delta \hat{n}$ and the number Δn).

The vacuum expectation value of \hat{S}^2 is obtained by collecting the fully contracted terms of (12.53)–(12.55):

$$\langle 0 | \hat{S}^2 | 0 \rangle = \sum_{i_\beta a_\alpha} |\Delta_{i_\beta a_\alpha}|^2 + \frac{1}{2} \Delta n \left(\frac{1}{2} \Delta n + 1 \right). \tag{12.56}$$

In an ROHF-based high-spin calculation the overlap terms vanish and the last term clearly gives $S(S+1)$. The remaining terms constitute the normal-

product part of \hat{S}^2 ,

$$\begin{aligned}
 \hat{S}_N^2 &= \hat{S}^2 - \langle 0 | \hat{S}^2 | 0 \rangle \\
 &= \sum_{p\beta q\alpha r\alpha s\beta} \Delta_{p\beta q\alpha} \Delta_{r\alpha s\beta} \{ \hat{p}_\beta^\dagger \hat{q}_\alpha \hat{r}_\alpha^\dagger \hat{s}_\beta \} \\
 &\quad + \sum_{a_\alpha p\beta s\beta} \Delta_{p\beta a_\alpha} \Delta_{a_\alpha s\beta} \{ \hat{p}_\beta^\dagger \hat{s}_\beta \} - \sum_{i_\beta q\alpha r\alpha} \Delta_{i_\beta q\alpha} \Delta_{r\alpha i_\beta} \{ \hat{r}_\alpha^\dagger \hat{q}_\alpha \} \\
 &\quad + \frac{1}{4} \{ \Delta \hat{n} \}^2 + \frac{1}{2} \{ \Delta \hat{n} \} (\Delta n + 1) .
 \end{aligned} \tag{12.57}$$

The normal-product number operators $\{\hat{n}_\alpha\}$ and $\{\hat{n}_\beta\}$ provide the excess number of α and β spinorbitals, respectively, relative to the Fermi vacuum state, in the determinant on which they operate. In normal CC calculations this number is zero for all determinants with nonzero amplitudes, so that the terms in the last line of (12.57) may usually be left out. In EOM-CC (Chapter 13) or Fock-space MRCC (Chapter 14) these excess-occupancy numbers may be nonzero but are known numbers that are the same for all determinants in the computed wave function and can simply replace the corresponding operators in the last line of (12.57).

Substituting (12.57) (without the contributions from the last line) into (12.47) and comparing the result with the response density matrices (11.88) and (11.89), we see that the response expectation value of \hat{S}_N^2 can be computed easily from these density matrices and the overlaps between the spatial parts of the α and β spinorbitals,

$$\begin{aligned}
 \langle \hat{S}_N^2 \rangle_{\text{resp}} &= \sum_{p\beta q\alpha r\alpha s\beta} \Delta_{p\beta q\alpha} \Delta_{r\alpha s\beta} (\Gamma_N)_{q\alpha s\beta p\beta r\alpha} \\
 &\quad + \sum_{a_\alpha p\beta s\beta} \Delta_{p\beta a_\alpha} \Delta_{a_\alpha s\beta} (\gamma_N)_{s\beta p\beta} - \sum_{i_\beta q\alpha r\alpha} \Delta_{i_\beta q\alpha} \Delta_{r\alpha i_\beta} (\gamma_N)_{q\alpha r\alpha} .
 \end{aligned} \tag{12.58}$$

12.6 The A and B response matrices from the viewpoint of CCS

In the response treatment of properties in Section 11.8 we derived the CPHF equations for the determination of orbital changes due to a perturbation. An alternative way to view such orbital relaxation can be developed using the tools of CC theory (Paldus 1990).

Consider the (connected) expectation value for the CC-singles (CCS) wave function,

$$E = \langle 0 | e^{\hat{T}_1^\dagger} \hat{H} e^{\hat{T}_1} | 0 \rangle_C . \tag{12.59}$$

Expansion of the exponentials up to quadratic terms gives

$$E = \langle 0 | \hat{H} + \hat{T}_1^\dagger \hat{H} + \hat{H} \hat{T}_1 + \hat{T}_1^\dagger \hat{H} \hat{T}_1 + \frac{1}{2} \hat{T}_1^{\dagger 2} \hat{H} + \frac{1}{2} \hat{H} \hat{T}_1^2 | 0 \rangle_C + \dots \quad (12.60)$$

Optimization of this expression with respect to the \hat{T}_1^\dagger amplitudes, i.e. setting $\delta E / \delta t_a^{i*} = 0$, results in

$$\langle \Phi_i^a | \hat{H} + \hat{H} \hat{T}_1 + \hat{T}_1^\dagger \hat{H} | 0 \rangle = 0, \quad (12.61)$$

with a similar result for the complex conjugate. This equation is represented diagrammatically by

$$\text{Diagram 1} - \times + \text{Diagram 2} + \text{Diagram 3} = 0. \quad (12.62)$$

The coefficients of the \hat{T}_1 components in the first two diagrams constitute the elements of the singly excited CI matrix \mathbf{A} of (11.130), while the coefficients of the \hat{T}_1^\dagger components in the third diagram constitute the elements of the \mathbf{B} matrix in (11.130). Diagrammatic representations of these matrix elements can be obtained by stripping the \hat{T}_1 and \hat{T}_1^\dagger vertices from the diagrams. Using the non-standard notation introduced in Chapter 4, the matrix elements can be represented as

$$\begin{aligned} A_{ai,bj} &= \delta_{ij} \text{Diagram 1} + \delta_{ab} \text{Diagram 2} + \text{Diagram 3} \\ &= (\varepsilon_a - \varepsilon_i) \delta_{ij} \delta_{ab} + \langle a j || i b \rangle, \end{aligned} \quad (12.63)$$

$$B_{ai,bj} = \text{Diagram 4} = \langle ab || ij \rangle. \quad (12.64)$$

This analysis demonstrates that both matrices arise from orbital rotation, or \hat{T}_1 terms, which is contrary to some claims that the \mathbf{B} matrix represents a double-excitation, or correlation, contribution. It emphasizes the role of $e^{\hat{T}_1}$ in orbital relaxation and helps to explain why the inclusion of \hat{T}_1 in CCSD and higher CC levels results in a lowered sensitivity to orbital choices, allowing the use of QRHF and other reference functions that are not variationally optimum for the system being studied. It also shows that there is some overlap between the role of $e^{\hat{T}_1}$ in orbital rotation and explicit imposition of the CPHF conditions in the relaxed density matrix.

12.7 Noniterative approximations based on the CC energy functional

Following on from the introduction of the CC energy functional (11.62), it is useful to reconsider the noniterative triple- and quadruple-excitation corrections to CC on the basis of this functional (Kucharski and Bartlett 1998a,b, Crawford and Stanton 1998) as an alternative to the treatment in terms of the CC expectation value, given in Sections 10.5 and 10.6.

The CC energy functional (11.67) can be written as

$$\begin{aligned}\mathcal{E} &= \langle 0 | (1 + \Lambda) \mathcal{H} | 0 \rangle_C = \langle 0 | (1 + \Lambda) (\hat{H}_N e^{\hat{T}})_C | 0 \rangle_C \\ &= \langle 0 | (1 + \Lambda) [(\hat{F}_N + \hat{W})(1 + \hat{T} + \tfrac{1}{2}\hat{T}^2 + \cdots)]_C | 0 \rangle_C.\end{aligned}\quad (12.65)$$

Assuming that a CCSD solution for Λ and \hat{T} has been obtained, we focus on the terms in the CCSDT correlation-energy expression that depend upon \hat{T}_3 and/or Λ_3 and isolate those terms that can contribute to this energy in fourth order,

$$\begin{aligned}E_T^{[4]} &= \langle 0 | [\Lambda_3 (\hat{F}_N^d \hat{T}_3^{[2]})_C + \Lambda_3 (\hat{W} \hat{T}_2^{[2]})_C + \Lambda_2 (\hat{W} \hat{T}_3^{[2]})_C \\ &\quad + \Lambda_1 (\hat{W} \hat{T}_3^{[2]})_C + \Lambda_2 (\hat{F}_N^o \hat{T}_3^{[2]})_C] | 0 \rangle,\end{aligned}\quad (12.66)$$

where \hat{F}_N^d and \hat{F}_N^o stand for the diagonal and off-diagonal parts of \hat{F}_N , respectively.

The $\hat{T}_3^{[2]}$ amplitudes are obtained from the second-order diagrams in the CCSDT triple-excitation equation (diagrams T_{1a} , T_{1b} and the diagonal part of diagrams T_{2a} , T_{2b} of Fig. 10.5, see also Table 10.3):

$$(\hat{W} \hat{T}_2)_C | 0 \rangle + (\hat{F}_N^d \hat{T}_3^{[2]})_C | 0 \rangle = 0,\quad (12.67)$$

where \hat{T}_2 is taken from the CCSD solution. This condition means that the first two terms on the r.h.s. of (12.66) cancel through fourth order, and we are left with

$$E_T^{[4]} = \langle 0 | [\Lambda_2 (\hat{W} \hat{T}_3^{[2]})_C + \Lambda_1 (\hat{W} \hat{T}_3^{[2]})_C + \Lambda_2 (\hat{F}_N^o \hat{T}_3^{[2]})_C] | 0 \rangle,\quad (12.68)$$

which is represented diagrammatically as follows:

$$E_T^{[4]} = \text{Diagram 1}_{(2)} + \text{Diagram 2}_{(2)} + \text{Diagram 3}_{(2)}^{-\times};\quad (12.69)$$

the third diagram vanishes in the Hartree–Fock case.

Since $\Lambda = T^\dagger$ at first order (and at second order in the HF case), this approximation is very close to the original orbitally invariant CCSD(T) form

(10.39)–(10.41) except that, because of the time-inversion asymmetry between Λ and \hat{T} (Section 11.7), we cannot simplify further the first diagram as in (10.39).

This Λ -based ACCSD(T) model was shown to have the prospect of being a better approximation than the usual CCSD(T) (Kucharski and Bartlett 1998a, Crawford and Stanton 1998). Unlike the latter, however, it requires solutions for both Λ and \hat{T} . Nevertheless it is better for describing bond breaking, which recommends it for the treatment of transition states that do not differ too much from equilibrium geometry. No noniterative approximation can be fully satisfactory for large deviations from the equilibrium geometry since, depending upon the choice of reference function, the perturbation theory that underlies the noniterative correction can fail in such cases.

To apply the Λ -based approach to connected quadruple excitations, we start from the CCSDT solution and focus on the terms involving Λ_4 and $\hat{T}_4^{[3]}$ in the CCSDTQ equation. Proceeding in the same way as for the triples correction, and noting that $\hat{T}_4^{[3]}$ satisfies the third-order CCSDTQ equation

$$[(\hat{F}_N^d \hat{T}_4^{[3]})_C + \frac{1}{2}(\hat{W} \hat{T}_2^2)_C + (\hat{W} \hat{T}_3)_C] |0\rangle = 0, \quad (12.70)$$

where \hat{T}_2 and \hat{T}_3 are taken from the CCSDT solution, the \hat{T}_4 correction is obtained as

$$E_Q = \langle 0 | [\Lambda_3(\hat{W} \hat{T}_4^{[3]})_C + \Lambda_2(\hat{W} \hat{T}_4^{[3]})_C + \Lambda_3(\hat{F}_N^o \hat{T}_4^{[3]})_C] | 0 \rangle, \quad (12.71)$$

or, in diagrammatic form,

$$E_Q = \text{Diagram 1}_{(3)} + \text{Diagram 2}_{(3)} + \text{Diagram 3}_{(3)}^{-\times}; \quad (12.72)$$

this defines the ACCSDT(Q) model.

Unlike ACCSD(T), which contains only (generalized) fourth-order corrections, this model includes terms of both fifth order (the second diagram in (12.72)) and sixth order (the first and third diagrams). The computational effort for the first diagram, which is the rate-determining step in the calculation of this correction, is proportional to $n_h^4 n_p^5$, which may be compared with $n_h^3 n_p^4$ for the triples correction. If we limit ourselves to a fifth-order correction, as in (10.48), we obtain

$$E_Q^{[5]} = \text{Diagram 2}_{(3)}, \quad (12.73)$$

and the resulting computational effort is of order $n_h^4 n_p^4$. Furthermore, if we use a factorization similar to that used in Section 10.6, (10.49), (10.50),

though this factorization is not quite rigorous in this case because of the use of Λ , we obtain a $\Lambda\text{CCSDT}(\text{Q}_f)$ analog of the $\text{CCSDT}(\text{Q}_f)$ correction (Kucharski and Bartlett 1998a):

$$\Delta E_{\text{Q}_f}^{[5]} = \frac{1}{2} \langle 0 | \Lambda_2 \hat{T}_2^{\dagger(1)} [\hat{W}(\hat{T}_3 + \frac{1}{2} \hat{T}_2^2)]_C | 0 \rangle. \quad (12.74)$$

In this fifth-order approximation we avoid the need for computing $\hat{T}_4^{[3]}$, and the computational effort remains that of the underlying CCSDT , proportional to $n_h^3 n_p^5$. For (12.74) itself the computational scaling is of order $n_h n_p^5$ for the \hat{T}_2^2 term and $n_h^2 n_p^5$ for the \hat{T}_3 term. Odd-order contributions, however, tend to be less stable than those based on even orders of perturbation theory.

Several noniterative approximations for triple- and quadruple-excitation contributions to CCSD and their applications were described by Kucharski and Bartlett (1998a,b) and by Gwaltney and Head-Gordon (2001). Applications of the unfactorized fifth-order quadruples correction were given by Hirata, Fan, Auer *et al.* (2004), while applications of the sixth-order correction were considered by Bomble, Stanton, Kállay *et al.* (2005). A critical comparison of various quadruples corrections and their performance in studies of bond breaking was presented by Musiał and Bartlett (2005).

12.8 The nature of the solutions of CC equations

The CC amplitude equations are nonlinear, as are the Hartree–Fock equations, and therefore have multiple solutions (Kowalski and Jankowski 1998). The number and character of the solutions of the CC equations have been investigated by several researchers (Živković 1977, Živković and Monkhorst 1978, Paldus, Takahashi and Cho 1984, Jankowski and Kowalski 1999a–d, Jankowski, Kowalski, Grabowski *et al.* 1999, Piecuch and Kowalski 2000). These questions are of no practical concern for most CC applications but are of theoretical interest for the understanding of the CC method in all its aspects.

In practice, in single-reference CC we are usually interested in a specific electronic state (most often the ground state) and choose the reference function to be a reasonable approximation to the exact wave function for that state. As long as that reference function is a good approximation, and barring pathological cases such as near degeneracies, the usual iterative procedures for the solution of the CC equations converge to the one desired solution, the so-called *standard solution*. In almost all ground-state calculations at near-equilibrium geometries, at least when the orbitals are real the

standard solution is well behaved, with amplitudes that are small relative to unity, and results in a real energy. However, when the reference function is not the dominant component of the exact solution, which can happen in cases of near degeneracy or of many excited states, the standard solution may produce a complex energy even for real orbitals; this was demonstrated, for example, by Paldus, Takahashi and Cho (1984) in model calculations using semiempirical π -electron Hamiltonians for some cyclic aromatic hydrocarbons. (Paldus, Takahashi and Cho used complex orbitals, but their results should be invariant under a transformation to real orbitals.) The imaginary component of any CC energy result is unphysical, being an artefact of the non-Hermiticity of the CC effective Hamiltonian, and it is reasonable to ignore it. (Imaginary energy components are a proper result in some scattering calculations, where they determine the width of resonances, but are not proper components of stationary-state energies.)

Research on the number and nature of all the solutions of the CC amplitude equations, and particularly the work of Jankowski and Kowalski (1999a–d) and Jankowski, Kowalski, Grabowski *et al.* (1999), was summarized in the extensive review by Piecuch and Kowalski (2000). For the *full coupled-cluster (FCC)* model, in which the CC cluster operator \hat{T} is not truncated, the number of solutions is equal to the number of solutions of the full-CI (FCI) model that are not orthogonal to the reference function. (Solutions that are orthogonal to the reference function cannot be represented in intermediately normalized form.) Furthermore the wave functions obtained for the various solutions are orthogonal to each other, and all the corresponding energies (which are eigenvalues of their respective effective Hamiltonians, with $|0\rangle$ as the corresponding right eigenfunction) are necessarily real. However, when the CC cluster operator is *truncated*, as is necessary for practical reasons in virtually all CC calculations, the number of solutions increases substantially, the corresponding wave functions can no longer be orthogonal to each other and many solutions become complex. Analytic continuation methods connecting the solutions of truncated CC equations with those of the corresponding CI equations on one hand, and with those of the FCC (or equivalently, FCI) equations on the other hand, show many branch points and other singularities. Many of the solutions appear to lack physical meaning, and it is no longer possible to associate a specific nonstandard solution unambiguously with each FCC solution.

13

The equation-of-motion coupled-cluster method for excited, ionized and electron-attached states

13.1 Introduction

The conventional, single-reference, coupled-cluster method is very effective for electronic states dominated by a single determinant, such as most molecular ground states near their equilibrium geometry. Such states are predominantly closed-shell singlet states, and CC calculations on them produce pure singlet wave functions. But even these states become dominated by more than one determinant when one or more bonds are stretched close to breaking, so that single-reference CC based on RHF orbitals is then not usually appropriate for the calculation of entire potential-energy surfaces. While such problems can be partially treated by using UHF reference functions, which usually separate correctly, the UHF approach makes use of symmetry breaking and is poor in the spin-recoupling region.

Most excited, ionized and electron-attached states are open-shell states, and CC calculations on them using UHF or ROHF orbitals do not usually result in pure-spin wave functions. Furthermore, such states often involve large contributions from more than one determinant and thus do not respond well to conventional single-reference treatments.

One solution to these problems is to resort to multireference methods, such as those described in Chapters 8 and 14, but such treatments are still quite difficult to apply at a high enough level. An effective alternative in many cases is provided by the *equation-of-motion coupled-cluster (EOM-CC)* method (Emrich 1981, Sekino and Bartlett 1984, Comeau and Bartlett 1993, Stanton and Bartlett 1993a). A closely related approach is the coupled-cluster linear response (CCLR) method (Monkhorst 1977, Dalgaard and Monkhorst 1983, Koch and Jørgensen 1990). A third related approach is the symmetry-adapted cluster CI (SAC-CI) method (Nakatsuji 1979a,b,

Nakatsuji, Ohta and Hirao 1981), which is conceptually similar but, because of approximations made, is more like CI than CC.

The basic idea of EOM-CC is to start with a conventional CC calculation on some *initial state*, usually a conveniently chosen closed-shell state, and obtain the desired *target state* by application of a CI-like linear operator acting on the initial-state CC wave function. Most commonly, the initial state is the ground state, while the target state is an excited or ionic state. Although the calculations for the two states must use the same set of nuclei in the same geometrical arrangement and the same set of spinorbitals defining a common Fermi state $|0\rangle$, they need not have the same number of electrons, as shown by applications to ionization and electron-attachment processes. Thus we distinguish *excitation-energy EOM-CC (EE-EOM-CC)*, *ionization potential EOM-CC (IP-EOM-CC)* and *electron-attachment EOM-CC (EA-EOM-CC)*, as well as extensions to processes such as double ionization and double electron attachment.

13.2 The EOM-CC *Ansatz*

In the EOM-CC method we consider two Schrödinger-equation eigenstates simultaneously, an *initial state* Ψ_0 and a *target state* Ψ_k ,

$$\hat{H}\Psi_0 = E_0\Psi_0, \quad \hat{H}\Psi_k = E_k\Psi_k. \quad (13.1)$$

The initial state is often referred to as the *reference state*, but we shall not use this term in order to avoid confusion with the *reference determinant* $|0\rangle$. The aim of the method is to determine the energy difference

$$\omega_k = E_k - E_0 \quad (13.2)$$

and related properties of the target state efficiently by canceling common terms in the solutions for the two states *before* the actual calculation.

If we use the normal-product form of the Hamiltonian, equations (13.1) become

$$\hat{H}_N\Psi_0 = \Delta E_0\Psi_0, \quad (13.3)$$

$$\hat{H}_N\Psi_k = \Delta E_k\Psi_k, \quad (13.4)$$

where $\Delta E_0 = E_0 - E_{\text{ref}}$ and $\Delta E_k = E_k - E_{\text{ref}}$, with $E_{\text{ref}} = \langle 0|\hat{H}|0\rangle$. Then we have

$$\omega_k = \Delta E_k - \Delta E_0, \quad (13.5)$$

since the same reference energy has been subtracted from both E_0 and E_k .

The initial-state coupled-cluster wave function is represented by the action of an exponential wave operator $\Omega_0 = e^{\hat{T}}$ on a single-determinant reference function $|0\rangle$,

$$|\Psi_0\rangle = \Omega_0|0\rangle = e^{\hat{T}}|0\rangle. \quad (13.6)$$

The operator \hat{T} consists solely of connected terms, and its exponential $e^{\hat{T}}$ corresponds to a sum of linked diagrams arising from \hat{T} and its disconnected products. An operator \hat{R}_k is used to generate the target state from the initial state,

$$|\Psi_k\rangle = \hat{R}_k|\Psi_0\rangle, \quad (13.7)$$

so that, using (13.6), the target-state Schrödinger equation (13.4) can be written in the form

$$\hat{H}_N \hat{R}_k e^{\hat{T}}|0\rangle = \Delta E_k \hat{R}_k e^{\hat{T}}|0\rangle. \quad (13.8)$$

In the EE-EOM-CC case, if all possible excitations from the initial state are included we have

$$\hat{R}_k = r_0 + \sum_{i,a} r_i^a \{\hat{a}^\dagger \hat{i}\} + \sum_{i<j, a<b} r_{ij}^{ab} \{\hat{a}^\dagger \hat{i} \hat{b}^\dagger \hat{j}\} + \cdots. \quad (13.9)$$

The constant term r_0 is required for the description of states of the same symmetry as the initial state; if the two states are of different symmetry then $r_0 = 0$. The objective then is to determine the amplitudes in the \hat{R}_k operator. Since \hat{R}_k is an excitation operator, it commutes with the CC cluster operator \hat{T} and all its components. Clearly, if \hat{R}_k is not truncated then it will produce the full-CI result for the target state. Unlike the initial-state wave operator $\Omega_0 = e^{\hat{T}}$, this operator is linear and thus CI-like.

Multiplying (13.8) on the left with $e^{-\hat{T}}$ and using the commutation between \hat{R}_k and \hat{T} , we get

$$\mathcal{H} \hat{R}_k |0\rangle = \Delta E_k \hat{R}_k |0\rangle, \quad (13.10)$$

showing that $\hat{R}_k |0\rangle$ is a right eigenfunction of \mathcal{H} with eigenvalue ΔE_k . It is similar to the CI eigenvalue equation in normal-product form,

$$\hat{H}_N \hat{C}_k |0\rangle = \Delta E_k \hat{C}_k |0\rangle \quad (13.11)$$

where

$$\hat{C}_k = 1 + \sum_{i,a} c_i^a \{\hat{a}^\dagger \hat{i}\} + \sum_{i<j, a<b} c_{ij}^{ab} \{\hat{a}^\dagger \hat{i} \hat{b}^\dagger \hat{j}\} + \cdots, \quad (13.12)$$

except that the operator \mathcal{H} is non-Hermitian and therefore also has left eigenfunctions $\langle 0|\hat{L}_k$, with the same eigenvalues ΔE_k as the corresponding right eigenfunctions $\hat{R}_k|0\rangle$, satisfying

$$\langle 0|\hat{L}_k\mathcal{H} = \langle 0|\hat{L}_k\Delta E_k. \quad (13.13)$$

The operator \hat{L}_k is a de-excitation operator,

$$\hat{L}_k = l_0 + \sum_{i,a} l_a^i \{i^\dagger \hat{a}\} + \sum_{i<j, a<b} l_{ab}^{ij} \{i^\dagger \hat{a} j^\dagger \hat{b}\} + \dots \quad (13.14)$$

and therefore satisfies

$$\hat{L}_k \hat{P} = 0, \quad \hat{L}_k = \hat{L}_k \hat{Q}. \quad (13.15)$$

For the initial state ($k=0$) we have $\hat{R}_0 = \hat{1}$, but $\hat{L}_0 \neq \hat{1}$.

The two sets of eigenfunctions are biorthogonal and can be normalized to satisfy

$$\langle 0|\hat{L}_k \hat{R}_l|0\rangle = \delta_{kl}. \quad (13.16)$$

They provide a resolution of the identity,

$$\hat{1} = \sum_k \hat{R}_k|0\rangle \langle 0|\hat{L}_k, \quad (13.17)$$

as can be seen by placing this operator between any two left and right eigenfunctions,

$$\sum_k \langle 0|\hat{L}_l \hat{R}_k|0\rangle \langle 0|\hat{L}_k \hat{R}_m|0\rangle = \sum_k \delta_{lk} \delta_{km} = \delta_{lm} = \langle 0|\hat{L}_l \hat{R}_m|0\rangle.$$

Also, because $\hat{R}_0 = \hat{1}$ we have

$$\langle 0|\hat{L}_k|0\rangle = \delta_{k0}. \quad (13.18)$$

As mentioned above, the essence of the EOM-CC method is to eliminate common terms from the target-state and initial-state treatments *before* the actual calculations and thus obtain the energy difference directly. Since $\hat{R}_0 = 1$, the initial-state version of (13.10) is

$$\mathcal{H}|0\rangle = \Delta E_0|0\rangle. \quad (13.19)$$

Multiplying this equation on the left by \hat{R}_k and subtracting it from (13.10), we obtain the EOM-CC equation in the form

$$[\mathcal{H}, \hat{R}_k]|0\rangle = (\Delta E_k - \Delta E_0)\hat{R}_k|0\rangle$$

or

$$(\mathcal{H}\hat{R}_k|0\rangle)_C = \omega_k \hat{R}_k|0\rangle. \quad (13.20)$$

Comparing this equation with (13.10) we see that the restriction to connected terms eliminates the ground-state correlation energy ΔE_0 and the associated diagrams from the calculation and provides the excitation energy ω_k directly.

The EOM-CC equation can be separated into blocks by the \hat{P} and \hat{Q} projection operators,

$$\left[\begin{pmatrix} \hat{P}\mathcal{H}\hat{P} & \hat{P}\mathcal{H}\hat{Q} \\ \hat{Q}\mathcal{H}\hat{P} & \hat{Q}\mathcal{H}\hat{Q} \end{pmatrix} \begin{pmatrix} r_0\hat{P} \\ \hat{Q}\hat{R}_k\hat{P} \end{pmatrix} \right]_C = \omega_k \begin{pmatrix} r_0\hat{P} \\ \hat{Q}\hat{R}_k\hat{P} \end{pmatrix}. \quad (13.21)$$

The corresponding initial-state ($k=0$) equation, for which $r_0=1$, all other components of \hat{R}_0 vanish and $\omega_0=0$, is

$$\left[\begin{pmatrix} \hat{P}\mathcal{H}\hat{P} & \hat{P}\mathcal{H}\hat{Q} \\ \hat{Q}\mathcal{H}\hat{P} & \hat{Q}\mathcal{H}\hat{Q} \end{pmatrix} \begin{pmatrix} \hat{P} \\ 0 \end{pmatrix} \right]_C = \begin{pmatrix} 0 \\ 0 \end{pmatrix}, \quad (13.22)$$

giving

$$(\hat{P}\mathcal{H}\hat{P})_C = 0, \quad (\hat{Q}\mathcal{H}\hat{P})_C = 0, \quad (13.23)$$

the same as the initial-state CC equations (the initial-state correlation energy ΔE_0 has been eliminated from the first of these equations by the connectedness condition). Therefore we can eliminate the first column of (13.21), obtaining

$$(\hat{P}\mathcal{H}\hat{Q}\hat{R}_k\hat{P})_C = \omega_k r_0 \hat{P}, \quad (13.24)$$

$$(\hat{Q}\mathcal{H}\hat{Q}\hat{R}_k\hat{P})_C = \omega_k \hat{Q}\hat{R}_k\hat{P}. \quad (13.25)$$

Equation (13.25) is the key equation of the EOM-CC method. It is an eigenvalue equation for \hat{R}_k and ω_k and, once it has been solved, the constant term r_0 can be obtained from (13.24). As an eigenvalue equation, its solution benefits from the techniques, developed for the direct CI approach, based on the Davidson algorithm (Davidson 1975) or any of its variations. This iterative method avoids explicit evaluation of the matrix and requires instead direct calculation of the matrix–vector product, using the current estimate of the solution vector, in each iteration. Diagrammatic techniques are used in EOM-CC to calculate the elements of this product, i.e. the elements of $(\hat{Q}\mathcal{H}\hat{Q}\hat{R}_k\hat{P})_C$, using the current estimate of the amplitudes in \hat{R}_k .

Recognizing that the energy functional defined in the treatment of properties in Chapter 11 can be written in the form

$$\mathcal{E}_0 = \langle 0 | (1 + \Lambda) \mathcal{H} | 0 \rangle = \langle 0 | \hat{L}_0 \mathcal{H} \hat{R}_0 | 0 \rangle, \quad (13.26)$$

where

$$\hat{L}_0 = 1 + \Lambda, \quad \hat{R}_0 = 1, \quad (13.27)$$

we find that EOM-CC provides a natural generalization for excited states (Stanton and Bartlett 1993a). In particular, excited-state properties are usually obtained in EOM-CC using excited-state generalizations of the ground-state response density matrices,

$$(\gamma_N)_{qp}^k = \langle 0 | \hat{L}_k e^{-\hat{T}} \{ \hat{p}^\dagger \hat{q} \} e^{\hat{T}} \hat{R}_k | 0 \rangle. \quad (13.28)$$

The dipole strength for a transition between states k and l is proportional to the absolute square $|\langle \Psi_k | \vec{\mathbf{D}} | \Psi_l \rangle|^2$ of the matrix element of the dipole operator

$$\vec{\mathbf{D}} = \langle 0 | \vec{\mathbf{D}} | 0 \rangle + \vec{\mathbf{D}}_N = \langle 0 | \vec{\mathbf{D}} | 0 \rangle + \sum_{pq} \vec{\mathbf{d}}_{pq} \{ \hat{p}^\dagger \hat{q} \}, \quad (13.29)$$

where $\vec{\mathbf{d}} = \sum_{\mu} q_{\mu} \vec{\mathbf{r}}_{\mu}$ and q_{μ} and $\vec{\mathbf{r}}_{\mu}$ are the electric charges and position vectors of the particles in the system. Because of the orthogonality of Ψ_k and Ψ_l the vacuum-expectation-value term in (13.29) does not contribute to the matrix element $\langle \Psi_k | \vec{\mathbf{D}} | \Psi_l \rangle$, which can be obtained from the transition density matrix γ_N^{lk} , whose elements are

$$(\gamma_N)_{qp}^{lk} = \langle 0 | \hat{L}_k e^{-\hat{T}} \{ \hat{p}^\dagger \hat{q} \} e^{\hat{T}} \hat{R}_l | 0 \rangle, \quad (13.30)$$

as

$$\langle \Psi_k | \vec{\mathbf{D}} | \Psi_l \rangle = \langle \Psi_k | \vec{\mathbf{D}}_N | \Psi_l \rangle = \sum_{pq} (\gamma_N)_{qp}^{lk} \vec{\mathbf{d}}_{pq}. \quad (13.31)$$

The application of EOM-CC methods to the calculation of higher-order properties of the initial state is described below in Section 13.5. The application of these methods to a time-dependent perturbation theory treatment of excited states is discussed in Section 13.6.

In the following we shall drop the index k from the notation for \hat{R}_k and ω_k , and write

$$\hat{R} = r_0 + \hat{R}_1 + \hat{R}_2 + \cdots, \quad (13.32)$$

where \hat{R}_n collects the n -tuple excitation terms of (13.9), in analogy with the notation for $\hat{T} = \hat{T}_1 + \hat{T}_2 + \cdots$. In applications to excitation-energy calculations both \hat{R} and \hat{T} are truncated at the same excitation level. The truncation of \hat{T} manifests itself in the structure of the effective Hamiltonian \mathcal{H} .

13.3 Diagrammatic treatment of the EE-EOM-CC equations

The application of diagrammatic methods to the solution of the EE-EOM-CC equation benefits greatly from the diagrammatic representation of \mathcal{H} described in Section 10.7. The components of the operator \hat{R} are represented by diagrams similar to the corresponding \hat{T} diagrams but with a heavy horizontal line to distinguish them from the former, as in

$$\begin{array}{ccc} \begin{array}{c} a \swarrow \downarrow i \\ \hline \end{array} & , & \begin{array}{c} a \swarrow \downarrow i \quad b \swarrow \downarrow j \\ \hline \end{array} & , & \begin{array}{c} a \swarrow \downarrow i \quad b \swarrow \downarrow j \quad c \swarrow \downarrow k \\ \hline \end{array} & \text{etc.} \\ r_i^a \{\hat{a}^\dagger \hat{i}\} & & r_{ij}^{ab} \{\hat{a}^\dagger \hat{i} \hat{b}^\dagger \hat{j}\} & & r_{ijk}^{abc} \{\hat{a}^\dagger \hat{i} \hat{b}^\dagger \hat{j} \hat{c}^\dagger \hat{k}\} & \end{array}$$

The left-eigenstate operator \hat{L} is represented similarly,

$$\begin{array}{ccc} \begin{array}{c} i \swarrow \downarrow a \\ \hline \end{array} & , & \begin{array}{c} i \swarrow \downarrow a \quad j \swarrow \downarrow b \\ \hline \end{array} & , & \begin{array}{c} i \swarrow \downarrow a \quad j \swarrow \downarrow b \quad k \swarrow \downarrow c \\ \hline \end{array} & \text{etc.,} \\ l_a^i \{\hat{i}^\dagger \hat{l}\} & & l_{ab}^{ij} \{\hat{i}^\dagger \hat{a} \hat{j}^\dagger \hat{b}\} & & l_{abc}^{ijk} \{\hat{i}^\dagger \hat{a} \hat{j}^\dagger \hat{b} \hat{k}^\dagger \hat{c}\} & \end{array}$$

consistently with the representation of Λ in Chapter 11. However, it should be noted that this notation masks the fact that these two sets of operators are not adjoint to each other.

The single-excitation (\hat{R}_1 , particle-hole or ph) component of the eigenvalue equation (13.25) can be written in the form

$$\langle \Phi_i^a | \mathcal{H} \hat{Q} \hat{R} | 0 \rangle_C = \omega \langle \Phi_i^a | \hat{R} | 0 \rangle = \omega r_i^a. \quad (13.33)$$

This equation is represented diagrammatically for EE-EOM-CCSDT by the first equation in Fig. 13.1. The fixed labels a and i are understood to be associated with the open lines in these diagrams. The eigenvalue ω (the excitation energy) multiplies the left-hand-side diagram of the equation. For the last diagram we have taken advantage of (10.63). The diagrammatic representation of the double-excitation (\hat{R}_2 or pphh) and triple-excitation (\hat{R}_3 or ppphhh) equations for EE-EOM-CCSDT are also shown in Fig. 13.1. These diagrams are given in terms of effective-Hamiltonian vertices; actual calculations use intermediates and factorization techniques along the lines of Section 10.7 (Kucharski, Włoch, Musiał *et al.* 2001, Musiał, Kucharski and Bartlett 2003, Musiał and Bartlett 2003). Once the eigenvalue problem has been solved and the excitation energy ω is available, the constant term r_0 can be obtained from (13.24); this is represented diagrammatically as follows:

$$\omega r_0 = \begin{array}{c} \text{diagram 1} \end{array} + \begin{array}{c} \text{diagram 2} \end{array}. \quad (13.34)$$

The algebraic forms of the EE-EOM-CCSDT equations are shown in Fig. 13.2.

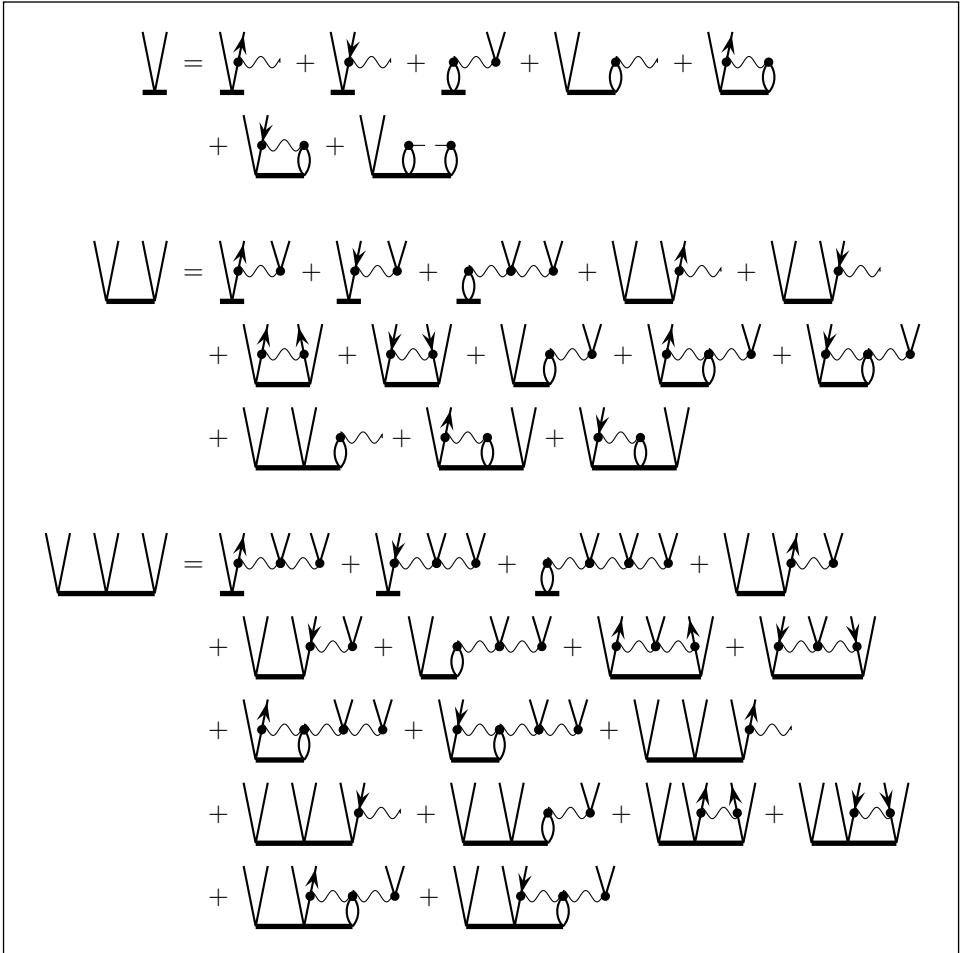


Fig. 13.1. Diagrammatic representation of the EE-EOM-CCSDT equations.

In analogy with the case of the Λ equations in Section 11.6, in order to generate diagrams describing the contributions of the \hat{R}_m vertices to the \hat{R}_n equation we need to use \mathcal{H} vertices with $n^\vee - n^\wedge = 2(n - m)$, where n^\vee and n^\wedge are the number of lines connecting to the \mathcal{H} vertex from above and from below, respectively.

The diagrams for the \hat{R} equations are not identical to the upside-down images of the Λ -equation diagrams seen in Fig. 11.10, because of the unsymmetrical nature of the \mathcal{H} vertices with respect to up-down reflection. This asymmetry, which reflects the non-Hermiticity of \mathcal{H} , is manifested by the limitation $n^\wedge < 4$ (except for the two-body vertex, for which $n^\wedge = 4$ is also possible), without such limitation for n^\vee .

$$\sum_d \chi_{ad} r_i^d - \sum_l \chi_{li} r_l^a + \sum_{dl} \chi_{ladi} r_l^d + \sum_{dl} \chi_{ld} r_{il}^{ad} + \frac{1}{2} \sum_{del} \chi_{alde} r_{il}^{de} - \frac{1}{2} \sum_{dlm} \chi_{lmid} r_{lm}^{ad} + \frac{1}{4} \sum_{delm} \langle lm || de \rangle r_{ilm}^{ade} = \omega r_i^a \quad (\text{for all } i, a),$$

$$\begin{aligned} & \hat{P}(ij) \sum_d \chi_{abej} r_i^d - \hat{P}(ab) \sum_l \chi_{lbij} r_l^a + \sum_{dl} \chi_{labdij} r_l^d + \hat{P}(ab) \sum_d \chi_{bd} r_{ij}^{ad} \\ & - \hat{P}(ij) \sum_l \chi_{lj} r_{il}^{ab} + \frac{1}{2} \sum_{de} \chi_{abde} r_{ij}^{de} + \frac{1}{2} \sum_{lm} \chi_{lmij} r_{lm}^{ab} \\ & + \hat{P}(ab|ij) \sum_{dl} \chi_{lbaj} r_{il}^{ad} + \frac{1}{2} \hat{P}(ij) \sum_{del} \chi_{albd ej} r_{il}^{de} - \frac{1}{2} \hat{P}(ab) \sum_{dlm} \chi_{lmbidj} r_{lm}^{ae} \\ & + \sum_{dl} \chi_{ld} r_{ijl}^{abd} + \frac{1}{2} \hat{P}(ab) \sum_{del} \chi_{alde} r_{ilj}^{deb} - \frac{1}{2} \hat{P}(ij) \sum_{dlm} \chi_{lmid} r_{lmj}^{adb} \\ & = \omega r_{ij}^{ab} \quad (\text{for all } i > j, a > b), \end{aligned}$$

$$\begin{aligned} & \hat{P}(i/jk) \sum_d \chi_{abcejk} r_i^d - \hat{P}(a/bc) \sum_l \chi_{lbcijk} r_l^a + \sum_{dl} \chi_{labcdijk} r_l^d \\ & + \hat{P}(a/bc|k/ij) \sum_d \chi_{bcdk} r_{ij}^{ad} - \hat{P}(i/jk|c/ab) \sum_l \chi_{lcjk} r_{il}^{ab} \\ & + \hat{P}(a/bc|i/jk) \sum_{dl} \chi_{lbcdjk} r_{il}^{ad} + \frac{1}{2} \hat{P}(j/ik) \sum_{de} \chi_{abcdje} r_{ik}^{de} \\ & + \frac{1}{2} \hat{P}(b/ac) \sum_{lm} \chi_{lbmijk} r_{lm}^{ac} + \frac{1}{2} \hat{P}(i/jk) \sum_{del} \chi_{albcd ejk} r_{il}^{de} \\ & - \frac{1}{2} \hat{P}(a/bc) \sum_{dlm} \chi_{lmbcidjk} r_{lm}^{ae} + \hat{P}(c/ab) \sum_d \chi_{cd} r_{ijk}^{abd} \\ & - \hat{P}(k/ij) \sum_l \chi_{lk} r_{ijl}^{abc} + \hat{P}(c/ab|k/ij) \sum_{dl} \chi_{lcdk} r_{ijl}^{abd} \\ & + \frac{1}{2} \hat{P}(a/bc) \sum_{de} \chi_{bcde} r_{ijk}^{ade} + \frac{1}{2} \hat{P}(i/jk) \sum_{lm} \chi_{lmjk} r_{ilm}^{abc} \\ & + \frac{1}{2} \hat{P}(a/bc|k/ij) \sum_{del} \chi_{blcd ek} r_{ijl}^{abe} - \frac{1}{2} \hat{P}(c/ab|i/jk) \sum_{dlm} \chi_{lmcdjk} r_{ilm}^{abe} \\ & = \omega r_{ijk}^{abc} \quad (\text{for all } i > j > k, a > b > c), \end{aligned}$$

$$\omega r_0 = \sum_{dl} \chi_{ld} r_l^d + \frac{1}{4} \sum_{delm} \langle lm || de \rangle r_{lm}^{de}.$$

Fig. 13.2. The EE-EOM-CCSDT eigenvalue equations, followed by the equation for the constant term r_0 .

The diagrams for the \hat{L} equations, representing the left eigenfunctions, are identical to those for the Λ equations in Fig. 11.10, including the disconnected diagrams, because there is no connectedness condition for the left-eigenfunction equation (13.13). The solutions for these equations are different for each target state and different from the initial-state Λ -equation solutions, because the energy differences ω , obtained from the solution of the \hat{R} eigenvalue problem, are different for each state.

A particularly important application of EE-EOM-CC is to a class comprising problems that are difficult to treat otherwise by single-reference methods: the low-spin open-shell states, particularly open-shell singlets obtained by a single excitation from a closed-shell state. Since most electronic states reached by dipole-allowed optical excitation from closed-shell ground states are open-shell singlets, such states have to be treatable in any reasonable theoretical approach for excited states.

The zero-order approximation for an open-shell singlet state is a two-determinant wave function,

$$\begin{aligned} \Phi_{OS} = & \frac{1}{\sqrt{2}} \mathcal{A}\{(\text{core})[\phi_A(N-1)\alpha(N-1)\phi_B(N)\beta(N) \\ & - \phi_A(N-1)\beta(N-1)\phi_B(N)\alpha(N)]\}, \quad (13.35) \end{aligned}$$

where “(core)” is a product of the spinorbitals occupied by the other $N-2$ electrons. For this wave function, the two spinorbital determinants, described symbolically as $a\bar{b}$ and $\bar{a}b$, appear with equal-magnitude weights. The $a\bar{b} - \bar{a}b$ combination describes the singlet, while $a\bar{b} + \bar{a}b$ describes the $M_S = 0$ component of the triplet. The triplet state can easily be handled in a single-reference treatment by using the $M_S = 1$ or $M_S = -1$ component, with the zero-order descriptions ab and $\bar{a}\bar{b}$, respectively, but no such alternative is available for the open-shell singlet.

A single-determinant-based CC description of the open-shell singlet state would require using one of the two determinants in (13.35) as the reference determinant, the other determinant being part of the external space (i.e. the Q space) in the CC expansion. At convergence both determinants should have coefficients of the same magnitude (but opposite sign). Since the reference determinant always has coefficient 1 because of intermediate normalization, the coefficient of the second determinant has to grow to that same magnitude, making the basic perturbative structure for solving the CC equations poorly convergent. Of course, if we simply anticipate this equivalence then we can accelerate the process but even so the

treatment would be unbalanced since the excitation levels included relative to the second determinant would be fewer than those relative to the first.

Clearly, the EOM-CC method provides an effective solution to this problem. As seen in Section 13.2, the excited states are obtained in EOM-CC from a matrix eigenvalue problem as eigenstates of \mathcal{H} , and therefore there are no restrictions on the coefficient magnitudes (the amplitudes of \hat{R}_k) in the solutions. In particular, if the EOM-CC treatment is based on a closed-shell initial state then all eigenstates are pure spin eigenfunctions. Even when the EOM-CC calculation is based on an open-shell initial state, such as a high-spin state, whether one is using ROHF (spin eigenfunctions) or UHF to define the spinorbitals and the Fermi state in the underlying CC calculation the initial-state CC wave function does not deviate greatly from a pure spin eigenfunction (Rittby and Bartlett 1988, Purvis, Sekino and Bartlett 1988, Stanton 1994); most EOM-CC eigenstates are found to be close to spin eigenfunctions, as measured by the value of $\langle 0 | \hat{L}_k e^{-\hat{T}} \hat{S}^2 e^{\hat{T}} \hat{R}_k | 0 \rangle$. Furthermore, the evaluation of \hat{S}^2 can be made a part of the EOM-CC calculation, and constraints on the amplitudes can be imposed to guarantee pure-spin eigenstates for open-shell-based calculations (Szalay and Gauss 1997, 2000).

In principle, the EE-EOM-CC method is just as effective for other low-spin open-shell states, which may require more than two determinants for their zero-order description. In practice higher excitations, like those due to \hat{R}_3 , should be included for the correct description of, for example, a low-spin doublet state. Often, the EOM-CC approach, in its various forms, can also provide an alternative to multireference methods for the treatment of other states that are not well described by a truncated single-reference expansion; this includes states involving bond breaking, in which several quasidegenerate determinants need to be treated equivalently. A generalization of EOM-CC, the spin-flip CC method (Krylov 2001), achieves even more flexibility for applications to open-shell states and bond breaking.

As an example, computed excitation energies at several levels of EE-EOM-CC for three states of the CH^+ ion (Hirata, Nooijen and Bartlett 2000a) are given, with full-CI values for comparison, in Table 13.1. The initial state in these calculations is the closed-shell ground $1^1\Sigma^+$ state. Since only the four valence electrons are correlated, CCSDTQ would be equivalent to full CI for this example. For a closed-shell HF reference function, EOM-CCS is equivalent to CIS because the contributions of single excitations to the ground state vanish in the absence of double excitations.

Table 13.1. *Excitation energies relative to the full CI results (in eV) at several levels of EOM-CC for three states of the CH^+ ion^a*

State	Full CI	CCS ^b	CCSD	CCSDT-3	CCSDT	Weights ^c
$1^1\Pi$	3.2087	0.282	0.028	—	0.002	94.7/3.1
$2^1\Sigma^+$	8.5304	—	0.544	0.231	0.073	0.23/95.6
$3^1\Sigma^+$	14.304	0.548	0.062	0.022	0.003	87.5/9.5

^aFrozen core, 6-31G** basis set, $R_{\text{CH}} = 1.131\text{\AA}$ (Hirata, Nooijen and Bartlett 2000a). The various CC results are given as differences from the full-CI values.

^bCCS is equivalent to CIS.

^cPercentage weights of single and double excitations in the excited-state wave function.

This simple example illustrates an important aspect of EOM-CC. When the target state is dominated by single excitations relative to the initial state, as measured by the weight of single excitations in the target-state wave function, we expect satisfactory excitation energies from EOM-CCSD, and this expectation is confirmed for the open-shell singlet states $1^1\Pi$ and $3^1\Sigma^+$ (Table 13.1). However, for states containing significant contributions of double excitations EOM-CCSD is less accurate, sometimes by one or more eV, because of an imbalance in the treatment of the initial and target states. While the initial-state CCSD wave function accounts for almost all the correlation energy for the initial state, this is not the case for an EOM-CCSD treatment of an excited state that contains a significant double-excitation component. Once the treatment is extended to EOM-CCSDT, most of this inaccuracy is resolved. At the same time, such an extension also improves the results for singly excited states, though not as dramatically.

The EOM-CCSDT-3 results included in Table 13.1 represent an approximation of full EOM-CCSDT that uses the CCSDT-3 wave function (Table 10.4) for the initial state but does not truncate the EOM-CCSDT \hat{R} equations. This approximation neglects the contribution of \hat{T}_3 to the \hat{T}_3 equations, reducing the scaling of the ground-state calculation from $n_h^3 n_p^5$ to $n_h^3 n_p^4$. The treatments of the initial and target states remains consistent, since the same approximate \hat{T} operators are used in both.

Another instructive example is provided by the methylene (CH_2) molecule (Hirata, Nooijen and Bartlett 2000a), when excitation energies for various states at several EOM-CC levels are compared with full CI results in a 6-31G* basis set (Table 13.2). Comparisons with full CI, which can usually

Table 13.2. *Energies for various states of CH₂, relative to the lowest singlet state, for several levels of EOM-CC (eV).^a*

State	CCS ^b	CCSD	CCSDT-3	CCSDT	CCSDTQ	CCSDTQP	full CI	Weights ^c
¹ B ₁	1.55	1.67	1.67	1.68	1.68	1.68	1.68	94.6/2.7
¹ A ₁	—	5.84	4.97	4.56	4.52	4.52	4.52	0.2/92.6
¹ A ₂	6.45	6.10	6.10	6.09	6.09	6.09	6.09	92.2/5.1
¹ B ₂	—	9.69	8.75	8.28	8.25	8.25	8.25	2.8/92.6
¹ A ₁	9.69	9.12	9.08	9.06	9.05	9.05	9.05	89.3/7.6
³ B ₁	-0.76	-0.344	-0.322	-0.312	-0.310	-0.310	-0.310	94.9/2.3
³ A ₂	5.28	5.30	5.31	5.31	5.32	5.32	5.32	93.0/4.3
³ B ₂	—	8.38	7.47	6.95	6.91	6.90	6.90	2.5/93.0
³ A ₁	8.59	8.39	8.35	8.33	8.33	8.33	8.33	90.1/6.6
³ B ₂	8.79	9.30	9.19	9.15	9.15	9.15	9.15	91.2/5.5

^aFrozen core, 6-31G* basis set, $R_{\text{CH}} = 1.102 \text{ \AA}$, $\alpha_{\text{HCH}} = 104.7 \text{ deg}$. The lowest singlet state, ¹A₁, is used as the initial state (Hirata, Nooljen and Bartlett 2000a).

^bCCS is equivalent to CIS.

^cPercentage weights of single and double excitations (relative to ¹A₁) in the wave function.

be done only with relatively small basis sets, are more instructive than those with experimental data, because the full-CI comparisons separate basis-set effects from correlation-treatment effects. Furthermore, comparisons with experiment can involve many uncertainties, including questions of interpretation, particularly when one is accounting for zero-level vibrational contributions or extracting accurate vertical excitation energies from high-resolution spectra. Several comparisons of EOM-CC results with experimental data can be found in the extensive review by Bartlett and Musiał (2007).

In this example the closed-shell lowest singlet (1A_1) state is the initial state, so that the ground state 3B_1 appears as a de-excitation. Nonetheless, an accurate description of a full spectrum of states is readily obtained. Had the open-shell ground state been used as the initial state, the results would have been very similar but would not have produced pure-spin eigenfunctions. Once again, large errors are encountered at the EOM-CCSD level for states with a high percentage of double excitations. The EOM-CCSDT-3 approximation corrects this deficiency to some extent, but full EOM-CCSDT is needed to obtain a satisfactory description of these states.

The use of different levels of excitation in \hat{T} and in \hat{R} has been explored but in such a case (13.23) would no longer hold, preventing the separation of the r_0 equation (13.24) from the rest of the EOM-CC eigenvalue problem. Such an unbalanced approach would also cause difficulties in derivative calculations for properties.

The CH^+ and CH_2 results quoted here could have been obtained by the diagrammatic methods normally used for larger basis sets and molecules (Kucharski, Włoch, Musiał *et al.* 2001) but, to allow very-high-order excitation levels as in EOM-CCSDTQP, an algorithm based on the availability of the full CI Hamiltonian matrix in a determinantal representation was used instead (Hirata, Nooijen and Bartlett 2000a); these calculations were similar to the high-order benchmark calculations for the coupled-cluster method quoted in Chapter 10 (Hirata and Bartlett 2000).

Other comparison of calculated EOM-CC (or CCLR) excitation energies with full-CI results can be found in Koch, Christiansen, Jørgensen *et al.* (1995), Christiansen, Koch, Jørgensen *et al.* (1996), Meissner (1998), Larsen, Hald, Olsen *et al.* (2001), Hirata (2004) and Musiał and Bartlett (2004).

The calculation of the first and second derivatives of EOM-CC potential-energy surfaces was described by Stanton (1993) and by Stanton and Gauss (1995), respectively.

13.4 EOM-CC treatment of ionization and electron attachment

Because second-quantized operators are Fock-space operators that are not restricted to a specific number of electrons, the formalisms described here can be used for processes involving changes in the number of electrons, such as ionization and electron attachment. These techniques are related to Green's function methods (Nooijen and Snijders 1992, 1993), but Green's functions are normally Hermitian while EOM-CC is not.

The ionization process can be treated by using an \hat{R} operator that reduces the number of electrons by one,

$$\hat{R} = \sum_i r_i \hat{i} + \sum_{b, j > i} r_{ji}^b \hat{b}^\dagger \hat{j} \hat{i} + \sum_{b > c, j > k > i} r_{jki}^{bc} \hat{b}^\dagger \hat{j} \hat{c}^\dagger \hat{k} \hat{i} + \dots \quad (13.36)$$

The eigenvalue equation for this operator, the IP-EOM-CC equation, is formally the same as the EE-EOM-CC equation except that $(\mathcal{H}\hat{R}|0\rangle)_C$ now reflects the altered structure of the \hat{R} operator. Instead of the ph (particle-hole), pphh, ppphhh etc. sectors of \hat{R} used in the EE-EOM-CC treatment, in IP-EOM-CC we use the h, phh, ppphhh etc. sectors. The IP-EOM-CCSD model uses the h and phh sectors of \hat{R} , while IP-EOM-CCSDT (Musiał, Kucharski and Bartlett 2003) adds the ppphhh sector. The IP-EOM-CCSDT equations are represented diagrammatically in Fig. 13.3.

Since all ionized states are preceded by a series of Rydberg excitations that approach the ionization continuum, the eigenvalues and eigenvectors of EE-EOM-CC smoothly approach those of IP-EOM-CC. In fact, simply zeroing out the appropriate matrix elements in the EE-EOM-CC equations, corresponding to the removal of an excited electron into the continuum, will provide the IP-EOM-CC solutions (Stanton and Gauss 1999), but this procedure does not translate into an optimal factorized CC program. The latter requires the use of the IP-EOM-CC structure from the outset (Musiał, Kucharski and Bartlett 2003).

The analogous treatment of electron attachment (EA-EOM-CC) is represented in EOM-CC by using the p, pph, ppphh etc. sectors of \hat{R} (Musiał and Bartlett 2003),

$$\hat{R} = \sum_a r^a \hat{a}^\dagger + \sum_{a > b, j} r_j^{ba} \hat{b}^\dagger \hat{j} \hat{a}^\dagger + \dots \quad (13.37)$$

The diagrammatic representation of these equations in terms of effective-Hamiltonian vertices is shown in Fig. 13.4. It is clear that this representation is identical to the corresponding representation for the IP-EOM-CC equations except that some line directions are reversed. However, this change in

direction introduces different intermediates because of the asymmetry with respect to time inversion of the diagrammatic expansion of \mathcal{H} (Section 10.7).

The dimensions of the matrices in the eigenvalue equations are of order $n_h^2 n_p$ for IP-EOM-CCSD, $n_h^3 n_p^2$ for IP-EOM-CCSDT, $n_h n_p^2$ for EA-EOM-CCSD and $n_h^2 n_p^3$ for EA-EOM-CCSDT.

Sample results, with full-CI results for comparison, for IP-EOM-CC calculations for two ionization potentials of C_2 and EA-EOM-CC calculations for two electron affinities of CH^+ are given in Tables 13.3 and 13.4, respectively (Hirata, Nooijen and Bartlett 2000b). Like the EE-EOM-CC examples described in Section 13.3, these results were obtained by utilizing the full-CI Hamiltonian matrix in a determinantal representation.

Analogous treatments can be applied to double-ionization (DIP-EOM-CC) and double-electron-attachment (DEA-EOM-PP) processes by natural extensions of the IP-EOM-CC and EA-EOM-CC methods. Double ionization has an obvious application to Auger experiments, but both

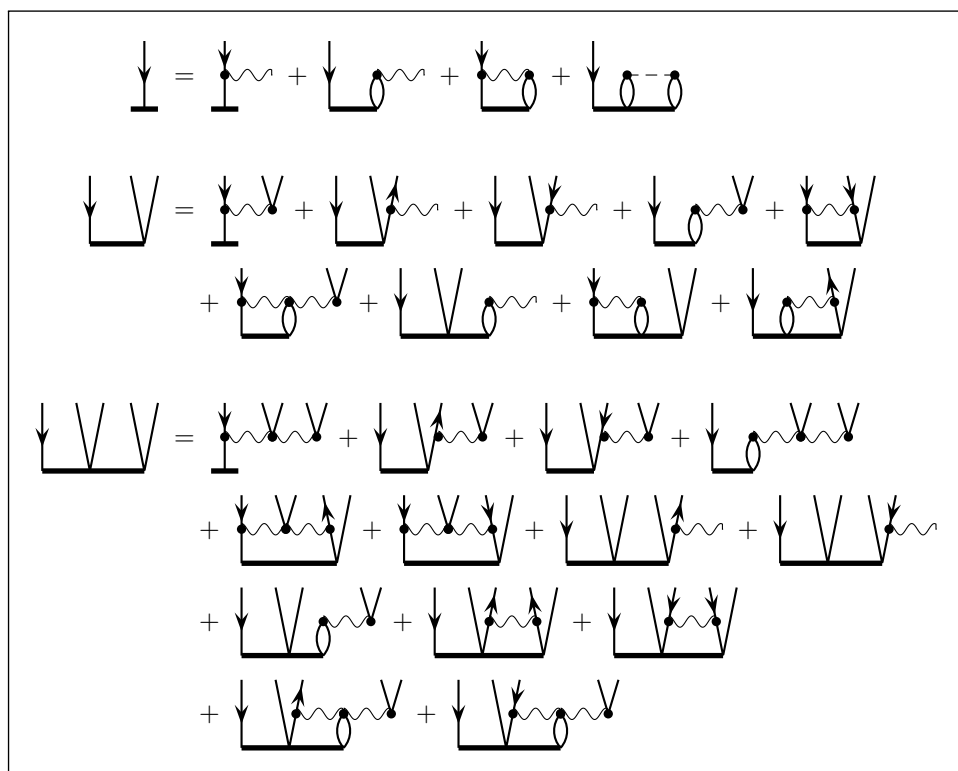


Fig. 13.3. Diagrammatic representation of the IP-EOM-CCSDT equations.

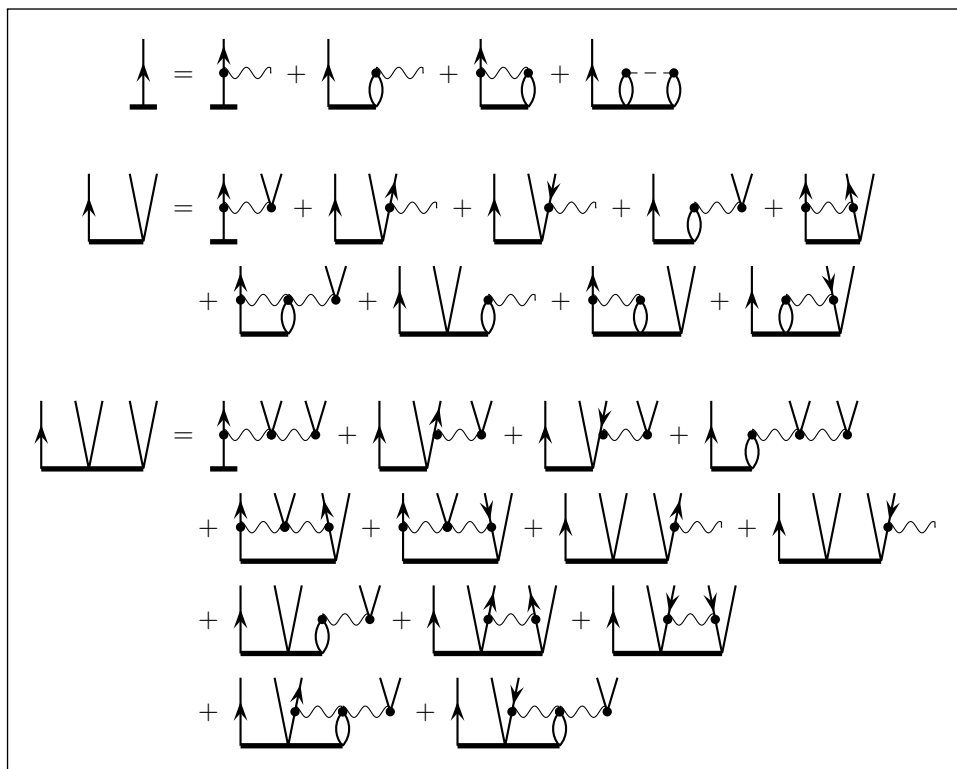


Fig. 13.4. Diagrammatic representation of the EA-EOM-CCSDT equations.

Table 13.3. Ionization potentials of C_2 at several levels of IP-EOM-CC with the full CI results (in eV) for comparison^a

State	CCS ^b	CCSD	CCSDT	CCSDTQ	CCSDTQP	Full CI
$1\pi_u \rightarrow \infty$	12.195	12.662	12.134	12.151	12.130	12.131
$2\sigma_u^- \rightarrow \infty$	13.942	15.180	14.803	14.749	14.724	14.721

^aFrozen core, 6-31G basis set, $R_{CC} = 1.262 \text{ \AA}$ (Hirata, Nooijen and Bartlett 2000b).

^bThe CCS approximation is equivalent to Koopmans' theorem.

double-ionization and double electron attachment can be useful in treating bond breaking and some other multireference problems.

Wave functions describing the stretching and breaking of bonds in molecules, such as required in calculations of potential-energy curves and surfaces, usually have more than one dominant configuration. In the simplest

Table 13.4. *Electron affinities of CH^+ at several levels of EA-EOM-CC, compared with full CI results (in eV)^a*

State	CCS ^b	CCSD	CCSDT	CCSDTQ	Full CI
$\infty \rightarrow 1\pi$	8.922	10.150	10.117	10.109	10.109
$\infty \rightarrow 3\sigma$	1.159	1.701	1.734	1.740	1.741

^aFrozen core, 6-31G* basis set, $R_{\text{CH}} = 1.120 \text{ \AA}$ (Hirata, Nooijen and Bartlett 2000b).

^bThe CCS approximation is equivalent to Koopmans' theorem.

example, the breaking of a single bond in a closed-shell molecule, two configurations, described symbolically as $(\text{core})a^2$ and $(\text{core})b^2$, where a and b describe the bonding and antibonding orbitals, respectively, approach degeneracy as the bond is stretched. Such situations can be treated by double-electron-attachment EOM-CC, using the doubly ionized “core” state as the initial state. Since the a and b orbitals are both in the Q -space in such a calculation, and are treated equivalently, a proper description of the dissociation process can be obtained. In addition to the $(\text{core})a^2$ and $(\text{core})b^2$ configurations, such a calculation would automatically include the $(\text{core})a\bar{b}$ and $(\text{core})\bar{a}b$ configurations (assuming that a and b have the same spatial symmetry). Alternatively, this problem can also be treated by double-ionization EOM-CC, using the $(\text{core})a^2b^2$ configuration as the initial state (Nooijen and Bartlett 1997b).

An important consideration in such applications is the suitability of the orbitals of the underlying initial-state calculation for the description of the target state. The initial-state CC calculation is relatively insensitive to the orbital choice because of the inclusion of the $e^{\hat{T}_1}$ operator, but EOM-CC uses a linear CI-like operator and is more sensitive. When the orbitals are far from optimal for the target state, the EOM results are bound to reflect this deficiency (Tobita, Perera, Musiał *et al.* 2003).

The IP-EOM-CC and EA-EOM-CC methods also occur as steps in the calculation of excitation energies by the similarity-transformed EOM-CC (STOEM-CC) approach (Nooijen and Bartlett 1997a,b). This approach produces results very close to those of Fock-space (multireference) CC, to be discussed in Chapter 14.

The calculation of derivatives of potential-energy surfaces in IP-EOM-CC has been described by Stanton and Gauss (1994). The automated generation

of computer programs for high-order EOM-CC calculations was described by Hirata (2003, 2004).

13.5 EOM-CC treatment of higher-order properties

The EOM-CC method generates energies and wave functions for a range of states up to a specified excitation level relative to a given *initial state*. As a result, it provides a path for the calculation of higher-order properties of the initial state by a closed-form equivalent of the usual perturbation theory that manifests a *sum-over-states (SOS)* form.

As shown in Section 13.2, the EOM-CC wave functions are obtained, in terms of two biorthogonal sets of eigenfunctions $\hat{R}_k|0\rangle$ and $\langle 0|\hat{L}_k$ of the CC effective Hamiltonian $\mathcal{H} = e^{-\hat{T}}\hat{H}_Ne^{\hat{T}}$, as $|\Psi_k\rangle = e^{\hat{T}}\hat{R}_k|0\rangle$ and $\langle\Psi_k| = \langle 0|\hat{L}_ke^{-\hat{T}}$. The corresponding eigenvalues are the energies $\Delta E_k = E_k - E_{\text{ref}}$ relative to the Fermi-vacuum reference energy $E_{\text{ref}} = \langle 0|\hat{H}|0\rangle$. In the perturbation treatment of properties it is convenient not to separate the reference energy from the total energy and therefore we define a modified CC effective Hamiltonian, which in this context we shall denote by \overline{H} (“H-bar”) to distinguish it from \mathcal{H} , by

$$\overline{H} = e^{-\hat{T}}\hat{H}e^{\hat{T}} = \mathcal{H} + \langle 0|\hat{H}|0\rangle. \quad (13.38)$$

This operator has the same biorthogonal sets of eigenfunctions as \mathcal{H} but its eigenvalues are the total energies E_k . The energy differences $\omega_k = E_k - E_0 = \Delta E_k - \Delta E_0$ are not affected. Using (13.10), (13.13) and (13.16), we find that

$$E_k = \langle 0|\hat{L}_k\overline{H}\hat{R}_k|0\rangle. \quad (13.39)$$

In particular, using (13.18) and (13.19), the initial-state energy is given by

$$E_0 = \langle 0|\overline{H}|0\rangle. \quad (13.40)$$

Now consider a perturbed Hamiltonian

$$\hat{H}(\lambda) = \hat{H}_0 + \lambda\Theta, \quad (13.41)$$

with perturbation-strength parameter λ . An example, first discussed in Section 11.3, is a perturbation due to an electric field $\lambda\vec{\mathcal{E}}$, for which the perturbation operator is given by the dot product $\Theta = -\vec{\mathcal{E}} \cdot \sum_{\mu} q_{\mu}\vec{\mathbf{r}}_{\mu}$, where q_{μ} and $\vec{\mathbf{r}}_{\mu}$ are the charges and position vectors of the particles in the system. The first-order perturbed energy can be used to obtain the static dipole

moment of the system, the second order will yield the static dipole polarizability and higher-order terms yield static hyperpolarizabilities (Sekino and Bartlett 1993).

The perturbed initial-state wave function is

$$|\Psi_0(\lambda)\rangle = e^{\hat{T}(\lambda)}|0\rangle. \quad (13.42)$$

As is common in most applications, we have assumed that the reference function $|0\rangle$ is not affected by the perturbation (but relaxed-orbital choices are possible; this aspect was used previously to distinguish the relaxed and response density matrices in Section 11.9).

The CC cluster operator $\hat{T}(\lambda)$ can be separated into an unperturbed part \hat{T}_0 and a perturbation (which commute with each other),

$$\hat{T}(\lambda) = \hat{T}_0 + \Delta\hat{T}(\lambda), \quad (13.43)$$

where

$$\Delta\hat{T}(\lambda) = \lambda\hat{T}^{(1)} + \lambda^2\hat{T}^{(2)} + \dots. \quad (13.44)$$

The perturbed wave function can then be written as

$$\begin{aligned} |\Psi_0(\lambda)\rangle &= e^{\hat{T}_0}e^{\Delta\hat{T}(\lambda)}|0\rangle \\ &= e^{\hat{T}_0}|\Upsilon(\lambda)\rangle \end{aligned} \quad (13.45)$$

where

$$|\Upsilon(\lambda)\rangle = e^{\Delta\hat{T}(\lambda)}|0\rangle = |0\rangle + \lambda|\Upsilon^{(1)}\rangle + \lambda^2|\Upsilon^{(2)}\rangle + \dots. \quad (13.46)$$

Each order of $|\Upsilon\rangle$ equals the corresponding order of $\hat{T}|0\rangle$ plus any products of $\hat{T}^{(n)}$ terms that combine to give the same order,

$$|\Upsilon^{(1)}\rangle = \hat{T}^{(1)}|0\rangle, \quad (13.47)$$

$$|\Upsilon^{(2)}\rangle = [\hat{T}^{(2)} + (\hat{T}^{(1)})^2]|0\rangle, \quad (13.48)$$

$$|\Upsilon^{(3)}\rangle = [\hat{T}^{(3)} + \hat{T}^{(1)}\hat{T}^{(2)} + (\hat{T}^{(1)})^3]|0\rangle \quad (13.49)$$

etc.

The Schrödinger equation for the perturbed initial state $\Psi_0(\lambda) = e^{\hat{T}(\lambda)}|0\rangle$ is

$$\hat{H}(\lambda)e^{\hat{T}(\lambda)}|0\rangle = E_0(\lambda)e^{\hat{T}(\lambda)}|0\rangle, \quad (13.50)$$

or, using (13.41) and (13.45),

$$(\hat{H}_0 + \lambda\Theta)e^{\hat{T}_0}|\Upsilon(\lambda)\rangle = E_0(\lambda)e^{\hat{T}_0}|\Upsilon(\lambda)\rangle; \quad (13.51)$$

multiplying on the left by $e^{-\hat{T}_0}$ results in

$$(\overline{H}_0 + \lambda \overline{\Theta})|\Upsilon(\lambda)\rangle = E_0(\lambda)|\Upsilon(\lambda)\rangle, \quad (13.52)$$

where

$$\overline{H}_0 = e^{-\hat{T}_0} \hat{H}_0 e^{\hat{T}_0}, \quad (13.53)$$

$$\overline{\Theta} = e^{-\hat{T}_0} \Theta e^{\hat{T}_0}. \quad (13.54)$$

Thus the separation of \hat{T} in (13.43) allowed us to absorb $e^{\hat{T}_0}$ into the operators and to incorporate $e^{\Delta\hat{T}}$ into Υ . Projecting (13.52) onto $\langle 0|(1+\Lambda)e^{-\Delta\hat{T}(\lambda)}$ and noting (13.46), we obtain the perturbed energy,

$$\langle 0|[1 + \Lambda(\lambda)]e^{-\Delta\hat{T}(\lambda)}(\overline{H}_0 + \lambda \overline{\Theta})e^{\Delta\hat{T}(\lambda)}|0\rangle = E_0(\lambda). \quad (13.55)$$

The l.h.s. of this equation defines a corresponding CC energy functional,

$$\mathcal{E}'(\Lambda, \hat{T}) = \langle 0|[1 + \Lambda(\lambda)]e^{-\Delta\hat{T}(\lambda)}(\overline{H}_0 + \lambda \overline{\Theta})e^{\Delta\hat{T}(\lambda)}|0\rangle, \quad (13.56)$$

which is equal to $E_0(\lambda)$ when the functional is stationary. The prime is intended to distinguish this functional from the CC energy functional $\mathcal{E}(\Lambda, \hat{T})$ of Section 11.4 which becomes equal to $\Delta E = E - \langle 0|\hat{H}|0\rangle$ when stationary, reflecting the use of \overline{H} instead of \mathcal{H} in the present context.

Applying standard Rayleigh–Schrödinger perturbation theory (Section 2.2) to (13.52) results in inhomogeneous equations for the various orders of Υ and E_0 , subject to intermediate normalization,

$$(E_0 - \overline{H}_0)|\Upsilon^{(1)}\rangle = (\overline{\Theta} - E^{(1)})|0\rangle, \quad (13.57)$$

$$(E_0 - \overline{H}_0)|\Upsilon^{(2)}\rangle = (\overline{\Theta} - E^{(1)})|\Upsilon^{(1)}\rangle - E^{(2)}|0\rangle, \quad (13.58)$$

etc. Extracting the energies requires left-multiplication by $\langle 0|L_0 = \langle 0|(1 + \Lambda)$, since $\langle 0|$ is not an eigenfunction of \overline{H}_0 ; we obtain

$$\begin{aligned} E^{(1)} &= \langle 0|(1 + \Lambda)\overline{\Theta}|0\rangle - \langle 0|(1 + \Lambda)(E_0 - \overline{H}_0)|\Upsilon^{(1)}\rangle \\ &= \langle 0|(1 + \Lambda)\overline{\Theta}|0\rangle - \langle 0|(1 + \Lambda)(E_0 - \overline{H}_0)|\hat{T}^{(1)}|0\rangle \\ &= \langle 0|(1 + \Lambda)\overline{\Theta}|0\rangle = \langle \overline{\Theta} \rangle, \end{aligned} \quad (13.59)$$

$$\begin{aligned} E^{(2)} &= \langle 0|(1 + \Lambda)(\overline{\Theta} - E^{(1)})|\Upsilon^{(1)}\rangle - \langle 0|(1 + \Lambda)(E_0 - \overline{H}_0)|\Upsilon^{(2)}\rangle \\ &= \langle 0|(1 + \Lambda)(\overline{\Theta} - E^{(1)})|\hat{T}^{(1)}|0\rangle - \langle 0|(1 + \Lambda)(E_0 - \overline{H}_0)[\hat{T}^{(2)} - (\hat{T}^{(1)})^2]|0\rangle \\ &= \langle 0|(1 + \Lambda)(\overline{\Theta} - E^{(1)})|\hat{T}^{(1)}|0\rangle - \langle 0|(1 + \Lambda)(E_0 - \overline{H}_0)(\hat{T}^{(1)})^2|0\rangle. \end{aligned} \quad (13.60)$$

The $\hat{T}^{(1)}$ term in (13.59) and the $\hat{T}^{(2)}$ part in the second term in (13.60) are eliminated by intermediate normalization. The quadratic term in (13.60) remains, as does $-E^{(1)}$.

As in all many-body applications, linked connected expressions are the most desirable, producing extensive and (when appropriate) intensive results, but the presence of $-E^{(1)}$ does not allow that. Using the diagrammatic techniques of Chapter 5, we find that all the expressions we have obtained for the energy and wave function can be written in a connected and linked form that eliminates all renormalization terms, though Λ itself is necessarily disconnected. In particular, the second-order energy (13.60) becomes

$$\begin{aligned} E^{(2)} &= \langle 0|(1+\Lambda)(\bar{\Theta}\hat{T}^{(1)}|0\rangle)_{\text{C}} - \langle 0|(1+\Lambda)(\bar{H}_0(\hat{T}^{(1)})^2|0\rangle)_{\text{C}} \\ &= \langle 0|(1+\Lambda)[\bar{\Theta}, \hat{T}^{(1)}]|0\rangle - \langle 0|(1+\Lambda)[[\bar{H}_0, \hat{T}^{(1)}], \hat{T}^{(1)}]|0\rangle. \end{aligned} \quad (13.61)$$

This fully connected form is the most satisfactory expression for the second-order energy but does not correspond to an SOS form. It is also more laborious to compute because of the quadratic term.

By providing a resolution of the identity, the biorthogonal sets of eigenfunctions of \bar{H} , which constitute the basis for the sum-over-states perturbation treatment, allow a separation of the Hilbert space into two complementary subspaces, defined by the projectors

$$\mathcal{P} = \hat{R}_0|0\rangle\langle 0|\hat{L}_0 = |0\rangle\langle 0|(1+\Lambda) \quad (13.62)$$

and

$$\mathcal{Q} = 1 - \mathcal{P} = \sum_{k \neq 0} \hat{R}_k|0\rangle\langle 0|\hat{L}_k, \quad (13.63)$$

and a related resolvent (similar, but not identical, to the resolvent (11.55))

$$\mathcal{R} = \mathcal{Q}(E_0 - \mathcal{Q}\bar{H}_0\mathcal{Q})^{-1}\mathcal{Q} = \sum_{k \neq 0} \frac{\hat{R}_k|0\rangle\langle 0|\hat{L}_k}{\omega_k}. \quad (13.64)$$

Using this resolvent (compare subsection 2.4.4) we find that

$$|\Upsilon^{(1)}\rangle = \mathcal{R}\bar{\Theta}|0\rangle = \sum_{k \neq 0} \frac{\hat{R}_k|0\rangle\langle 0|\hat{L}_k\bar{\Theta}|0\rangle}{\omega_k} \quad (13.65)$$

and the $E^{(1)}$ term is removed. This provides a linear approximation,

$$\begin{aligned} E_{\text{lin}}^{(2)} &= \langle 0|(1+\Lambda)\bar{\Theta}|\Upsilon^{(1)}\rangle = \langle 0|(1+\Lambda)\bar{\Theta}\mathcal{R}\bar{\Theta}|0\rangle \\ &= \sum_{k \neq 0} \frac{\langle 0|(1+\Lambda)\bar{\Theta}\hat{R}_k|0\rangle\langle 0|\hat{L}_k\bar{\Theta}|0\rangle}{\omega_k}. \end{aligned} \quad (13.66)$$

In practice, the preferred representation of the resolvent operator is by means of a set of excitations $|\mathbf{h}\rangle$ that are orthogonal to the reference function

$\langle 0|$ instead of to $\langle 0|(1 + \Lambda)$. Such a resolvent involves the usual projector $\hat{Q} = 1 - \hat{P} = 1 - |0\rangle\langle 0|$ and takes the form

$$\begin{aligned}\mathcal{R} &= \hat{Q}(E_0 - \bar{H}_0)^{-1}\hat{Q} \\ &= |\mathbf{h}\rangle\langle \mathbf{h}|E_0 - \bar{H}_0|\mathbf{h}\rangle^{-1}\langle \mathbf{h}|.\end{aligned}\quad (13.67)$$

(Here $\langle \mathbf{h}|$ and $|\mathbf{h}\rangle$ are column and row vectors, respectively.) The equations for the perturbed wave function and energy become

$$|\Upsilon^{(1)}\rangle = |\mathbf{h}\rangle\langle \mathbf{h}|E_0 - \bar{H}_0|\mathbf{h}\rangle^{-1}\langle \mathbf{h}|\bar{\Theta}|0\rangle, \quad (13.68)$$

providing a CI-like approximation,

$$E_{\text{CI}}^{(2)} = \langle 0|(1 + \Lambda)(\bar{\Theta} - \langle \bar{\Theta} \rangle)\mathbf{h}\rangle\langle \mathbf{h}|E_0 - \bar{H}_0|\mathbf{h}\rangle^{-1}\langle \mathbf{h}|\bar{\Theta}|0\rangle. \quad (13.69)$$

Note the appearance of $\langle \bar{\Theta} \rangle = E^{(1)}$ in the $E_{\text{CI}}^{(2)}$ equation; this term was left out of (13.60) and (13.61) because of the intermediate normalization condition, $\langle 0|(1 + \Lambda)|\Upsilon\rangle = 0$, but must be included here because of the change in orthogonality, $\langle 0|(1 + \Lambda)|\mathbf{h}\rangle \neq 0$. A connected form of (13.69) can be recovered if the space \hat{Q} of $|\mathbf{h}\rangle$ spans fully the original \mathcal{Q} space of the EOM-CC excited states.

The form (13.69) (Stanton and Bartlett 1993b), referred to as the *effective Hamiltonian approximation*, when truncated retains the $\langle \bar{\Theta} \rangle$ term, causing this approximation to behave more like CI (Koch, Kobayashi, de Merás *et al.* 1994). The first-order function can be expressed as $|\Upsilon^{(1)}\rangle = |\mathbf{h}\rangle\mathbf{t}^{(1)}$, where $\mathbf{t}^{(1)}$ is the column vector of $\hat{T}^{(1)}$ amplitudes and is obtained as the solution to a set of linear equations

$$\langle \mathbf{h}|E_0 - \bar{H}_0|\mathbf{h}\rangle\mathbf{t}^{(1)} = \bar{\boldsymbol{\theta}}, \quad (13.70)$$

with $\bar{\boldsymbol{\theta}} = \langle \mathbf{h}|\bar{\Theta}|0\rangle$. These equations are solved using iterative strategies, as in CI, to avoid matrix inversion. Then the second-order energy is obtained in either of two forms:

$$E_{\text{CI}}^{(2)} = \langle 0|(1 + \Lambda)(\bar{\Theta} - E^{(1)})|\mathbf{h}\rangle\mathbf{t}^{(1)} \quad (13.71)$$

$$E_{\text{lin}}^{(2)} = \langle 0|(1 + \Lambda)\bar{\Theta}|\mathbf{h}\rangle\mathbf{t}^{(1)}. \quad (13.72)$$

The second, linear, form (13.72) is usually a very good approximation with reasonable choices of $|\mathbf{h}\rangle$ (Sekino and Bartlett 1999, Tam, Russ and Crawford 2004). Iterative solution of the linear equations (13.71) or (13.72) provides a closed-form evaluation of the first-order wave function that is equivalent to an SOS expression like (13.65). Including the quadratic correction adds a double-commutator term, which is still linear but cannot be expressed in SOS form. The various approximations, CI-like, linear and quadratic, have

been compared for nuclear magnetic resonance coupling constants (Perera, Nooijen and Bartlett 1996) and polarizabilities (Rozyczko, Perera, Nooijen *et al.* 1997) and little numerical difference observed, so the comparative ease of evaluation of the connected form of (13.72) recommends it for most routine calculations (Sekino and Bartlett 1999).

One other form has been suggested (Sekino and Bartlett 1999). The reason the linear form is not exactly extensive is that Λ itself has disconnected parts, though these are small for HF reference functions. Hence, a slightly modified Λ equation can be solved that removes the disconnected terms. This procedure (called Model III by Sekino and Bartlett) gives a fully linked extensive expression, now termed EOM-CC_L (Crawford and Sekino 2009). This model has been found to provide highly accurate approximations to the quadratic expression for circular dichroism, at a saving of $\approx 30\%$ in computation.

13.6 EOM-CC treatment of frequency-dependent properties

The EOM-CC approach is a time-independent method built upon stationary states, aimed at determining the energy difference between two such states, including states with different numbers of electrons, and their associated wave functions. Properties of the stationary states can then be obtained using the corresponding EOM-CC left and right eigenfunctions. Alternatively, we can consider the time-dependent Schrödinger equation and ask how a molecule responds to the imposition of a perturbing oscillating electric field, as would be used in a spectroscopy experiment. The molecule will undergo an excitation when the imposed frequency is in resonance with the transition frequency to another stationary state of the molecule. Instead of a purely stationary-state description, this approach follows time-dependent perturbation theory to obtain dynamic (frequency-dependent) properties, such as frequency-dependent polarizabilities (Monkhorst 1977, Dalgaard and Monkhorst 1983).

Consider the time-dependent Schrödinger equation,

$$\hat{H}(t)\Psi(t) = i\frac{\partial}{\partial t}\Psi(t), \quad (13.73)$$

with the perturbed Hamiltonian

$$\begin{aligned} \hat{H}(t, \lambda) &= \hat{H}_0 + \lambda\Theta(e^{i\omega t} + e^{-i\omega t}) \\ &= \hat{H}_0 + \lambda\hat{V}(t). \end{aligned} \quad (13.74)$$

The periodicity of the perturbation is given by

$$\hat{V}(t) = \hat{V}(t + m\tau) \quad (m = 0, \pm 1, \pm 2, \dots), \quad (13.75)$$

where $\tau = 2\pi/\omega$ is the period. Static properties emerge in the limit $\omega \rightarrow 0$. The unperturbed solution is $|\Psi_0\rangle = e^{\hat{T}_0}|0\rangle$, where $|0\rangle$ is the time-independent Fermi-vacuum reference function. Thus, for the unperturbed state, we have

$$\hat{H}_0 e^{\hat{T}_0}|0\rangle = E_0 e^{\hat{T}_0}|0\rangle, \quad (13.76)$$

and projection onto $\langle 0|(1 + \Lambda)e^{-\hat{T}_0}$ results in

$$E_0 = \langle 0|(1 + \Lambda)e^{-\hat{T}_0}\hat{H}_0e^{\hat{T}_0}|0\rangle = \langle 0|(1 + \Lambda)|\bar{H}_0|0\rangle, \quad (13.77)$$

where $\bar{H}_0 = e^{-\hat{T}_0}\hat{H}_0e^{\hat{T}_0}$ is the form of the CC effective Hamiltonian used in Section 13.5, satisfying

$$\bar{H}_0|0\rangle = E_0|0\rangle. \quad (13.78)$$

Under the effect of a periodic perturbation, the time-dependent wave function undergoes periodic oscillations,

$$\Psi(\mathbf{x}, t, \lambda) = \psi(\mathbf{x}, t, \lambda)e^{-i\mathcal{E}(\lambda, t)t} = e^{\hat{T}(t, \lambda)}|0\rangle e^{-i\mathcal{E}(\lambda, t)t}. \quad (13.79)$$

where \mathbf{x} represents all the spatial and spin coordinates of the particles. This wave function and its components, including the phase factor $e^{-i\mathcal{E}(\lambda, t)t}$, are periodic in t . The time average of $\mathcal{E}(\lambda, t)$ over one period,

$$\mathcal{E}(\lambda) = \frac{1}{\tau} \int_0^\tau \mathcal{E}(\lambda, t) dt, \quad (13.80)$$

is called the *quasienergy*; thus (13.79) becomes analogous to the time-dependent wave function for a stationary state of energy E ,

$$\Psi(\mathbf{x}, t) = \psi(\mathbf{x})e^{-iEt}, \quad (13.81)$$

where $\hat{H}\psi(\mathbf{x}) = E\psi(\mathbf{x})$.

Since all quantities are periodic in t , i.e. $\psi(\mathbf{x}, t, \lambda) = \psi(\mathbf{x}, t + m\tau, \lambda)$, $T(\lambda, t) = T(\lambda, t + m\tau)$ etc., the analysis can be limited to the first period, which is analogous to a Brillouin zone for a solid. The functions $\psi(\mathbf{x}, t)$ are defined in an extended Hilbert space $\mathbf{x} \oplus t$ with scalar product

$$\langle\langle a(\mathbf{x}, t)|b(\mathbf{x}, t)\rangle\rangle = \frac{1}{\tau} \int_0^\tau \langle a(\mathbf{x}, t)|b(\mathbf{x}, t)\rangle dt = \frac{1}{\tau} \int_0^\tau dt \int d\mathbf{x} a^*(\mathbf{x}, t)b(\mathbf{x}, t). \quad (13.82)$$

Also, $\psi_0(\mathbf{x}, t) = \psi_0(\mathbf{x})e^{-E_0t}$, in which $\psi_0(\mathbf{x}) = e^{\hat{T}_0}|0\rangle$ is the stationary ground state.

Various approaches can be used for time-dependent perturbation theory (Langhoff, Epstein and Karplus 1972, Sambe 1973, Christiansen, Jørgensen and Hättig 1998). Perhaps the simplest approach is to recognize that all relevant quantities have an oscillatory behavior, which enables them to be described by a finite Fourier series, the terms of which can simply be collected in multiples of $e^{ik\omega t}$ and in which the phase factor can then be eliminated to provide equations largely analogous to those of time-independent perturbation theory for each order.

The time derivative of the time-dependent wave function (13.79) is

$$i \frac{\partial}{\partial t} \Psi(\mathbf{x}, t, \lambda) = e^{-i\mathcal{E}(\lambda, t)t} \left\{ \frac{\partial}{\partial t} [\mathcal{E}(\lambda, t)t] + i \frac{\partial}{\partial t} \right\} \psi(\mathbf{x}, t, \lambda). \quad (13.83)$$

Substituting in the time-dependent Schrödinger equation (13.73) with the perturbed Hamiltonian (13.74) results in

$$[\hat{H}_0 + \lambda \hat{V}(t)] \psi(\mathbf{x}, t, \lambda) e^{-i\mathcal{E}(\lambda, t)t} = e^{-i\mathcal{E}(\lambda, t)t} \left\{ \frac{\partial}{\partial t} [\mathcal{E}(\lambda, t)t] + i \frac{\partial}{\partial t} \right\} \psi(\mathbf{x}, t, \lambda), \quad (13.84)$$

which, after elimination of the phase factor, leads to

$$[\mathfrak{H}_0 + \lambda V(t)] \psi(\mathbf{x}, t, \lambda) = [\mathcal{D}\mathcal{E}(\lambda, t)] \psi(\mathbf{x}, t, \lambda), \quad (13.85)$$

where

$$\mathcal{D} = 1 + t \frac{\partial}{\partial t} \quad (13.86)$$

and

$$\mathfrak{H}_0 = \hat{H}_0 - i \frac{\partial}{\partial t}. \quad (13.87)$$

The energy and wave function are expanded in orders of the external perturbation,

$$\mathcal{E}(\lambda, t) = E_0 + \lambda \mathcal{E}^{(1)}(t) + \lambda^2 \mathcal{E}^{(2)}(t) + \dots, \quad (13.88)$$

$$\psi(\mathbf{x}, t, \lambda) = \psi^{(0)}(\mathbf{x}) + \lambda \psi^{(1)}(\mathbf{x}, t) + \lambda^2 \psi^{(2)}(\mathbf{x}, t) + \dots, \quad (13.89)$$

where $\psi^{(0)}(\mathbf{x}) = e^{\hat{T}_0}|0\rangle$. To separate the time dependence from the spatial dependence, we invoke a Fourier expansion in the former,

$$\psi^{(n)}(\mathbf{x}, t) = \sum_k \psi_k^{(n)}(\mathbf{x}) e^{ik\omega t} \quad (k = -n, -n+2, \dots, n). \quad (13.90)$$

The spacing of k by 2 reflects a cosine choice for the Fourier expansion. The limits $-n \leq k \leq n$ are a consequence of the fact that no terms higher than

order n contribute to the n th order wave function. In particular, for the first and second orders,

$$\psi^{(1)}(\mathbf{x}, t) = \psi_{+1}^{(1)}(\mathbf{x})e^{i\omega t} + \psi_{-1}^{(1)}(\mathbf{x})e^{-i\omega t}, \quad (13.91)$$

$$\psi^{(2)}(\mathbf{x}, t) = \psi_0^{(2)}(\mathbf{x}) + \psi_{+2}^{(2)}(\mathbf{x})e^{2i\omega t} + \psi_{-2}^{(2)}(\mathbf{x})e^{-2i\omega t} \quad (13.92)$$

etc.

Application of the standard perturbation-theory methods leads to inhomogeneous equations analogous to those of the time-independent case,

$$(E_0 - \hat{H}_0)\psi^{(0)}(\mathbf{x}) = 0, \quad (13.93)$$

$$(E_0 - \mathfrak{H}_0)\psi^{(1)}(\mathbf{x}, t) = [\hat{V}(\mathbf{x}, t) - \mathcal{D}\mathcal{E}^{(1)}(t)]\psi^{(0)}(\mathbf{x}), \quad (13.94)$$

$$(E_0 - \mathfrak{H}_0)\psi^{(2)}(\mathbf{x}, t) = [\hat{V}(\mathbf{x}, t) - \mathcal{D}\mathcal{E}^{(1)}(t)]\psi^{(1)}(\mathbf{x}, t) - [\mathcal{D}\mathcal{E}^{(2)}(t)]\psi^{(0)}(\mathbf{x}) \quad (13.95)$$

etc. Inserting the Fourier expansion of the first-order wave function into the first-order equation results in

$$\begin{aligned} (E_0 - \hat{H}_0 - \omega)|\psi_{+1}^{(1)}(\mathbf{x})\rangle e^{+i\omega t} + (E_0 - \hat{H}_0 + \omega)|\psi_{-1}^{(1)}(\mathbf{x})\rangle e^{-i\omega t} \\ = [\Theta(e^{i\omega t} + e^{-i\omega t}) - \mathcal{D}\mathcal{E}^{(1)}(t)]e^{\hat{T}_0}|0\rangle. \end{aligned} \quad (13.96)$$

Left-multiplying by $\langle\psi_0(\mathbf{x})| = \langle 0|(1 + \Lambda)e^{-\hat{T}_0}$ eliminates the l.h.s. (because of intermediate normalization) and results in

$$\begin{aligned} \mathcal{D}\mathcal{E}^{(1)}(t) &= \langle\psi^{(0)}|\Theta|\psi^{(0)}\rangle(e^{i\omega t} + e^{-i\omega t}) \\ &= \langle 0|(1 + \Lambda)\bar{\Theta}|0\rangle(e^{i\omega t} + e^{-i\omega t}) = E^{(1)}(e^{i\omega t} + e^{-i\omega t}), \end{aligned} \quad (13.97)$$

where $\bar{\Theta} = e^{\hat{T}_0}\Theta e^{\hat{T}_0}$. Here $E^{(1)}$ is the usual static first-order term. The time average of (13.97) over one period is zero,

$$\langle\mathcal{D}\mathcal{E}^{(1)}(t)\rangle = \frac{1}{\tau} \int_0^\tau E^{(1)}(e^{i\omega t} + e^{-i\omega t})dt = 0. \quad (13.98)$$

Inserting (13.97) into the first-order equation (13.94) results in

$$(E_0 - \mathfrak{H}_0)\psi^{(1)}(\mathbf{x}, t) = [\hat{V}(\mathbf{x}, t) - E^{(1)}(e^{i\omega t} + e^{-i\omega t})]\psi^{(0)}(\mathbf{x}). \quad (13.99)$$

Just as in the time-independent case, the perturbed CC solutions are

$$|\psi^{(1)}(\mathbf{x}, t)\rangle = \hat{T}^{(1)}(t)e^{\hat{T}_0}|0\rangle, \quad (13.100)$$

$$|\psi^{(2)}(\mathbf{x}, t)\rangle = \left\{ \hat{T}^{(2)}(t) + [\hat{T}^{(1)}(t)]^2 \right\} e^{\hat{T}_0}|0\rangle \quad (13.101)$$

etc. and their Fourier components are given by

$$\hat{T}^{(1)}(t)|0\rangle = (\hat{T}_{+1}^{(1)}e^{i\omega t} + \hat{T}_{-1}^{(1)}e^{-i\omega t})|0\rangle \quad (13.102)$$

$$\hat{T}^{(2)}(t)|0\rangle = (\hat{T}_0^{(2)} + \hat{T}_{+2}^{(2)}e^{2i\omega t} + \hat{T}_{-2}^{(2)}e^{-2i\omega t})|0\rangle \quad (13.103)$$

etc. Left-multiplication by $e^{-\hat{T}_0}$, using $\bar{H}_0 = e^{-\hat{T}_0}\hat{H}_0e^{\hat{T}_0}$ and

$$\bar{V}(t) = e^{-\hat{T}_0}\hat{V}(t)e^{\hat{T}_0} = \bar{\Theta}(e^{i\omega t} + e^{-i\omega t}), \quad (13.104)$$

puts the first-order perturbed equations (13.99) into the form

$$(E_0 - \bar{H}_0 \mp \omega)\hat{T}_{\pm}^{(1)}|0\rangle e^{\pm i\omega t} = (\bar{\Theta} - \langle\bar{\Theta}\rangle)|0\rangle e^{\pm i\omega t}, \quad (13.105)$$

where the designation \pm indicates the sign of ω . Since this equation is true for all values of ω the factor $e^{\pm i\omega t}$ can be eliminated, providing the analogs of the time-independent equations, which are modified only by the presence of ω :

$$(E_0 - \bar{H}_0 \mp \omega)\hat{T}_{\pm}^{(1)}|0\rangle = (\bar{\Theta} - \langle\bar{\Theta}\rangle)|0\rangle. \quad (13.106)$$

Finally, projection by a set of determinants $\langle\mathbf{h}|$ sufficient to determine the vector of coefficients in $\hat{T}_{\pm}^{(1)}$, i.e. $\mathbf{t}_+^{(1)}(\omega) = \mathbf{t}_-^{(1)}(-\omega) = \mathbf{t}^{(1)} = \langle\mathbf{h}|\hat{T}_+^{(1)}|0\rangle$ (note that these are the same for positive and negative frequencies), gives

$$(E_0\mathbf{1} - \bar{\mathbf{H}}_0 + \omega\mathbf{1})\mathbf{t}^{(1)} = \bar{\boldsymbol{\theta}}, \quad (13.107)$$

with $\bar{\mathbf{H}}_0 = \langle\mathbf{h}|\bar{H}_0|\mathbf{h}\rangle$ and $\bar{\boldsymbol{\theta}} = \langle\mathbf{h}|\bar{\Theta}|0\rangle$. The homogeneous part of this linear equation provides the poles. Using ω_k to specify the position of the k th pole relative to E_0 , we have

$$\bar{\mathbf{H}}_0\mathbf{t}_k^{(1)} = \omega_k\mathbf{t}_k^{(1)} \quad (13.108)$$

for each transition with which the radiation can be in resonance. This result is equivalent to the EOM-CC expression (13.20), $\bar{\mathbf{H}}_0$ and \mathbf{t}_k representing \mathcal{H} and $\hat{R}_k|0\rangle$, respectively.

For the perturbed first-order wave function we find

$$T_{\pm 1}^{(1)}|0\rangle = \mathcal{R}(\pm\omega)\bar{\Theta}|0\rangle \quad (13.109)$$

where $\mathcal{R}(\pm\omega) = \hat{Q}(E_0 - \bar{H}_0 \pm \omega)^{-1}\hat{Q}$, with $\hat{Q} = 1 - \hat{P} = 1 - |0\rangle\langle 0|$. This resolvent is nonsingular provided that the reference function is nondegenerate and $\omega \neq 0$.

Continuing to the next order of perturbation theory, we can define the frequency-dependent (dynamic) polarizability. In second order we need to

consider all three Fourier components leading to $\hat{T}_0^{(2)}$, $\hat{T}_{+2}^{(2)}$, and $\hat{T}_{-2}^{(2)}$. For this purpose it is convenient to express the $\hat{V}(t)$ operator as

$$\hat{V}(t) = \Theta_+ e^{i\omega t} + \Theta_- e^{-i\omega t}, \quad (13.110)$$

even though $\Theta_+ = \Theta_-$. (More general situations can be accommodated by keeping these two terms separate from the outset.) Hence, after collecting factors of $e^{\pm 2i\omega t}$ and $e^0 = 1$,

$$\begin{aligned} (E_0 - \bar{H}_0 - 2\omega) \left[\hat{T}_{+2}^{(2)} + (\hat{T}_{+1}^{(1)})^2 \right] |0\rangle e^{+2i\omega t} - (\bar{\Theta}_+ - \langle \bar{\Theta}_+ \rangle) \hat{T}_{+1}^{(1)} |0\rangle e^{+2i\omega t} \\ = -\mathcal{DE}^{(2)}(t) |0\rangle, \end{aligned} \quad (13.111)$$

$$\begin{aligned} (E_0 - \bar{H}_0 + 2\omega) \left[\hat{T}_{-2}^{(2)} + (\hat{T}_{-1}^{(1)})^2 \right] |0\rangle e^{-2i\omega t} - (\bar{\Theta}_- - \langle \bar{\Theta}_- \rangle) \hat{T}_{-1}^{(1)} |0\rangle e^{-2i\omega t} \\ = -\mathcal{DE}^{(2)}(t) |0\rangle, \end{aligned} \quad (13.112)$$

$$\begin{aligned} (E_0 - \bar{H}_0) (\hat{T}_0^{(2)} + 2\hat{T}_{+1}^{(1)} \hat{T}_{-1}^{(1)}) |0\rangle - (\bar{\Theta}_+ - \langle \bar{\Theta}_+ \rangle) \hat{T}_{-1}^{(1)} |0\rangle - (\bar{\Theta}_- - \langle \bar{\Theta}_- \rangle) \hat{T}_{+1}^{(1)} |0\rangle \\ = -\mathcal{DE}^{(2)}(t) |0\rangle. \end{aligned} \quad (13.113)$$

Left-multiplication by $\langle 0 | (1 + \Lambda) = \langle 0 | \hat{L}_0$ eliminates the $\hat{T}^{(2)}$ operators because of the biorthogonality of the EOM-CC eigenfunctions, but it does not eliminate the $\hat{T}^{(1)} \hat{T}^{(1)}$ terms, as previously discussed for the static case. While $\langle 0 | \hat{L}_0$ is a left eigenfunction of \bar{H}_0 , if $\langle 0 | \Lambda$ is limited to categories of excitations in $\langle \mathbf{h} |$ such as singles and doubles then the products $\hat{T}^{(1)} \hat{T}^{(1)}$ can introduce triple and quadruple excitations that are not involved in the determination of Λ . Therefore the quadratic term should be retained in the expression for the energy derivative,

$$\begin{aligned} \mathcal{DE}^{(2)}(t) = \langle 0 | \hat{L}_0 (\bar{\Theta}_+ - \langle \bar{\Theta}_+ \rangle) \hat{T}_{-1}^{(1)} |0\rangle + \langle 0 | \hat{L}_0 (\bar{\Theta}_- - \langle \bar{\Theta}_- \rangle) \hat{T}_{+1}^{(1)} |0\rangle \\ - 2\langle 0 | \hat{L}_0 (E_0 - \bar{H}_0) \hat{T}_{+1}^{(1)} \hat{T}_{-1}^{(1)} |0\rangle. \end{aligned} \quad (13.114)$$

The second-order frequency-dependent energy can be obtained by time-averaging the energy derivative over one period. The terms involving $e^{\pm 2i\omega t}$

integrate to zero and leave just the time-independent terms:

$$\begin{aligned}
E^{(2)}(\omega, -\omega) &= \langle \mathcal{D}\mathcal{E}^{(2)} \rangle \\
&= \langle 0 | \hat{L}_0 (\bar{\Theta}_+ - \langle \bar{\Theta}_+ \rangle) \hat{T}_{-1}^{(1)} | 0 \rangle + \langle 0 | \hat{L}_0 (\bar{\Theta}_- - \langle \bar{\Theta}_- \rangle) \hat{T}_{+1}^{(1)} | 0 \rangle \\
&\quad - 2 \langle 0 | \hat{L}_0 (E_0 - \bar{H}_0) \hat{T}_{+1}^{(1)} \hat{T}_{-1}^{(1)} | 0 \rangle \\
&= \langle 0 | \hat{L}_0 (\bar{\Theta}_+ - \langle \bar{\Theta}_+ \rangle) \mathcal{R}(-\omega) \bar{\Theta}_- | 0 \rangle + \langle 0 | \hat{L}_0 (\bar{\Theta}_- - \langle \bar{\Theta}_- \rangle) \mathcal{R}(+\omega) \bar{\Theta}_+ | 0 \rangle \\
&\quad - \langle 0 | \hat{L}_0 (E_0 - \bar{H}_0) \hat{T}_{+1}^{(1)} \mathcal{R}(-\omega) \bar{\Theta}_- | 0 \rangle \\
&\quad - \langle 0 | \hat{L}_0 (E_0 - \bar{H}_0) \hat{T}_{-1}^{(1)} \mathcal{R}(+\omega) \bar{\Theta}_+ | 0 \rangle.
\end{aligned} \tag{13.115}$$

The dynamic polarizability, $\alpha(\omega, -\omega) = -2E^{(2)}(\omega, -\omega)$, is obtained when $\Theta = \sum_{\mu} q_{\mu} \vec{r}_{\mu}$.

An alternative choice for the resolvent $\mathcal{R}'(\pm\omega)$ is in terms of the EOM-CC left and right eigenfunctions of the non-Hermitian Hamiltonian \bar{H}_0 . The spectral expansion of this resolvent is

$$\mathcal{R}'(\omega) + \mathcal{R}'(-\omega) = \sum_k \left(\frac{\hat{R}_k | 0 \rangle \langle 0 | \hat{L}_k}{\omega_k + \omega} + \frac{\hat{R}_k | 0 \rangle \langle 0 | \hat{L}_k}{\omega_k - \omega} \right). \tag{13.116}$$

Then

$$\begin{aligned}
\alpha(\omega, -\omega) &= 2 \langle \hat{L}_0 | \bar{\Theta} \mathcal{R}'(\omega) \bar{\Theta} | \hat{R}_0 \rangle + \langle \hat{L}_0 | \bar{\Theta} \mathcal{R}'(-\omega) \bar{\Theta} | \hat{R}_0 \rangle \\
&\quad - \langle \hat{L}_0 | (E_0 - \bar{H}_0) \hat{T}_{-1}^{(1)} \mathcal{R}'(+\omega) \bar{\Theta}_- | \hat{R}_0 \rangle \\
&\quad - \langle \hat{L}_0 | (E_0 - \bar{H}_0) \hat{T}_{+1}^{(1)} \mathcal{R}'(-\omega) \bar{\Theta}_+ | \hat{R}_0 \rangle.
\end{aligned} \tag{13.117}$$

If we neglect the last two terms in (13.115), we obtain the time-dependent analog of the EOM CI-like approximation (13.66) (Stanton and Bartlett 1993b, Rozyczko, Perera, Noijen *et al.* 1997) discussed in Section 13.5. This approximation treats \bar{H}_0 as completely defined by its left and right eigenvectors, instead of explicitly introducing the expansion of $e^{\hat{T}_0}$ into the second-order perturbed wave function, and leads to the textbook sum-over-states expression,

$$\alpha_{\vec{r}\vec{r}}(\omega, -\omega) = 2 \sum_{l=0,1} \sum_k \frac{\langle 0 | \hat{L}_0 \vec{r} \hat{R}_k | 0 \rangle \langle 0 | \hat{L}_k \vec{r} \hat{R}_0 | 0 \rangle}{\omega_k + (-1)^l \omega}. \tag{13.118}$$

The numerator in this expression contains the left and right transition moments, whose products (the dipole strengths) are the residues at the poles.

If instead we first use the fully connected form, analogous to (13.61), in which all terms correspond to connected diagrams and then make the same approximation as in the static case, we regain the linearized connected

approximation that retains the SOS form for the dynamic polarizability. As also discussed in Section 13.5, retaining the last two terms of (13.117) gives the benefit that the full exponential expansion can be used, but this is at the cost of a more difficult evaluation. The result is a time-dependent analog of the connected approximation (13.72) (Sekino and Bartlett 1999). The numerical differences between these approximations are very small for most applications, including the frequency-dependent polarizabilities (Rozyczko, Perera, Nooijen *et al.* 1997). When the quadratic terms are included there are also slight changes to the values of the dipole strengths (Koch, Kobayashi, de Merás *et al.* 1994, Sekino and Bartlett 1999), though the right-hand transition moment in this approximation is linked, extensive and intensive (Sekino and Bartlett 1999).

Multireference coupled-cluster methods

14.1 Introduction

As in the case of quasidegenerate perturbation theory (Chapter 8), multireference coupled-cluster (MRCC) theory is designed to deal with electronic states for which a zero-order description in terms of a single Slater determinant does not provide an adequate starting point for calculating the electron correlation effects. As already discussed in Chapters 8 and 13, these situations arise primarily for certain open-shell systems that are not adequately described by a high-spin single determinant (such as transition-metal atoms), for excited states in general and for studies of bond breaking on potential-energy surfaces; they arise usually because of the degeneracy or quasidegeneracy of the reference determinants. While single-reference coupled-cluster (SRCC) methods are very effective in treating dynamic electron correlation, the conditions discussed here involve nondynamic correlation effects that are not described well by truncated SRCC at practical levels of treatment.

As shown in Section 13.4, many open-shell and multireference states can be treated by EOM-CC methods, including a single excitation from a closed-shell state to an open-shell singlet state, which normally requires two equally weighted determinants in its zero-order description. Furthermore, double-ionization and double-electron-attachment EOM-CC, as well as spin-flip CC (Krylov 2001), allow the treatment of many inherently multireference target states. These methods have the advantage of being operationally of single-reference form, since then the only choices that need to be made are of the basis set and the level of correlation treatment. Although, they require an SRCC solution for an initial state (not necessarily the ground state) to initiate the procedure, once initiated multireference target states are available by the diagonalization of an effective Hamiltonian matrix in

a determinantal representation. As in the case of perturbation theory, the multireference approach is the most general and natural way to extend the reach of high-accuracy electronic-structure calculations.

The methods employed in MRCC are a combination of the techniques of QDPT (Chapter 8) and SRCC (Chapters 9 and 10). They fall into two main classes: *Hilbert-space MRCC* (*HS-CC*, usually in the form of *state-universal CC*, or *SU-CC*), and *Fock-space CC* (*FS-CC*, also called *valence-universal MRCC*, or *VU-CC*). Hilbert-space MRCC also has a *state-specific* (*SS-CC*) version designed so as to obtain a single solution based on a multireference zero-order function; this is analogous to multireference CI (MRCI) but includes proper factorization of the disconnected clusters and leads to extensive solutions. Fock-space MRCC also has an additional version, *intermediate-Hamiltonian MRCC* (*IH-CC*). The differences between these approaches will be discussed in the following sections. In each case, the methods can be based either on complete model spaces (which are often too large for practical applications and also suffer from intruder-state problems) or on incomplete model spaces (which introduce some complications and may result in some loss of extensivity).

All multireference methods, including QDPT and MRCC, are based on the generalized Bloch equation

$$[\Omega, \hat{H}_0]\hat{P} = \hat{V}\Omega\hat{P} - \Omega\hat{P}\hat{V}\Omega\hat{P}. \quad (14.1)$$

As in QDPT, the projection operator \hat{P} projects onto a model space spanned by a set of model functions Φ_α ,

$$\hat{P} = \sum_{\alpha} |\Phi_\alpha\rangle\langle\Phi_\alpha| = \sum_{\alpha} \hat{P}_\alpha, \quad \hat{P}_\alpha = |\Phi_\alpha\rangle\langle\Phi_\alpha|, \quad (14.2)$$

and $\Omega = \Omega\hat{P}$ is the wave operator, which, when operating on the model space, produces the space spanned by the perturbed wave functions,

$$\Psi_\alpha = \Omega\Phi_\alpha = \Omega\hat{P}\Phi_\alpha. \quad (14.3)$$

With intermediate normalization, Ω is split into two components:

$$\Omega = \hat{P} + \hat{Q}\Omega, \quad (14.4)$$

where

$$\hat{Q} = \hat{1} - \hat{P} = \sum_I |\Phi_I\rangle\langle\Phi_I| = \sum_I \hat{Q}_I, \quad \hat{Q}_I = |\Phi_I\rangle\langle\Phi_I|, \quad (14.5)$$

is the projector onto the orthogonal (or complementary) space, i.e. the space

spanned by all the functions Φ_I that are not in the model space. From (14.3) and (14.4) it follows that

$$\hat{P}\Psi_\alpha = \Phi_\alpha. \quad (14.6)$$

Another common form of the generalized Bloch equation can be obtained by rearranging the terms in (14.1) and using $\hat{H}_0 + \hat{V} = \hat{H}$, at the same time noting that $\hat{P}\Omega = \hat{P}$ as can be seen from (14.4). The result is

$$\hat{H}\Omega = \Omega(\hat{H}_0\hat{P} + \hat{V}\Omega) = \Omega(\hat{H}_0 + \hat{V})\Omega$$

or

$$\hat{H}\Omega = \Omega\hat{H}\Omega. \quad (14.7)$$

This form is more convenient for MRCC because, unlike QDPT, it does not involve an order-by-order expansion but is generally formulated in terms of the full Hamiltonian. As in all coupled-cluster methods, instead of an order-by-order expansion of the wave operator Ω we express it in exponential form,

$$\Omega = e^{\hat{T}}, \quad (14.8)$$

and expand \hat{T} into different excitation levels. The details of this expansion and of the treatment of the model space will differ between the two classes of MRCC methods, HS-CC and FS-CC.

As discussed in Section 8.1, the functions Ψ_α , (14.3), are not individually eigenfunctions of \hat{H} but span the space of eigenfunctions $\tilde{\Psi}_\alpha$ for which the model space forms a zero-order approximation, i.e.

$$\begin{aligned} \tilde{\Psi}_\alpha &= \sum_{\beta} \Psi_{\beta} C_{\beta\alpha} \\ &= \sum_{\beta} \Omega \Phi_{\beta} C_{\beta\alpha} = \Omega \tilde{\Phi}_\alpha, \end{aligned} \quad (14.9)$$

where

$$\tilde{\Phi}_\alpha = \sum_{\beta} \Phi_{\beta} C_{\beta\alpha} \quad (14.10)$$

are the *bonnes fonctions* (Bloch 1958) already discussed in Section 8.1. In analogy with the case of QDPT, the weights (transformation coefficients) $C_{\beta\alpha}$ are obtained by diagonalization of an effective Hamiltonian, as shown by substituting these expansions into the Schrödinger equation

$$\hat{H}\tilde{\Psi}_\alpha = E_\alpha\tilde{\Psi}_\alpha. \quad (14.11)$$

Applying \hat{P} from the left, we get the matrix eigenvalue equation

$$\hat{P}\hat{H}\Omega\tilde{\Phi}_\alpha = E_\alpha\tilde{\Phi}_\alpha, \quad (14.12)$$

from which the transformation matrix \mathbf{C} can be determined.

The operator

$$\hat{H}^{\text{eff}} = \hat{P}\hat{H}\Omega, \quad (14.13)$$

which operates entirely in \hat{P} -space and whose eigenfunctions and eigenvalues are $\tilde{\Phi}_\alpha$ and E_α , respectively, is called the *effective Hamiltonian operator*. The notation \hat{H}^{eff} is used here, as in Chapter 8, to distinguish it from the coupled-cluster effective Hamiltonian \mathcal{H} of Chapters 10–13. With this notation, the generalized Bloch equation (14.7) can be written in the form

$$\hat{H}\Omega = \Omega\hat{H}^{\text{eff}}. \quad (14.14)$$

Once the Bloch equation is satisfied, we can obtain another expression for \hat{H}^{eff} by operating with Ω^{-1} on (14.14),

$$\hat{H}^{\text{eff}} = \Omega^{-1}\hat{H}\Omega. \quad (14.15)$$

14.2 Hilbert-space state-universal MRCC

The Hilbert-space approach to multireference coupled-cluster (MRCC) theory assumes a separate Fermi-vacuum definition, and thus a separate partition of the spinorbitals into hole and particle states, for each model-space determinant (Jeziorski and Monkhorst 1981). In this respect it resembles the Hose–Kaldor approach to incomplete-model-space QDPT (Section 8.7 and Fig. 8.8) but can be applied to both complete and incomplete model spaces.

Following the *Ansatz* of Jeziorski and Monkhorst, the wave operator is separated into individual wave operators for the different model states,

$$\Omega = \sum_{\alpha} \Omega_{\alpha} = \sum_{\alpha} e^{\hat{T}^{\alpha}} \hat{P}_{\alpha}, \quad (14.16)$$

where

$$\begin{aligned} \hat{T}^{\alpha} &= \hat{T}_1^{\alpha} + \hat{T}_2^{\alpha} + \dots \\ &= \sum'_{ia} t_i^a(\alpha) \hat{a}^{\dagger}_i \hat{i} + \sum'_{ijab} t_{ij}^{ab}(\alpha) \hat{a}^{\dagger}_i \hat{b}^{\dagger}_j \hat{j} \hat{i} + \dots \end{aligned} \quad (14.17)$$

In the last expression the primes on the summation signs indicate the exclusion of *internal excitations* (excitations that result in model-space

determinants), and $t_i^a(\alpha)$, $t_{ij}^{ab}(\alpha)$ etc. are amplitudes; it is to be remembered that the definitions of particle and hole states are different for each model state.

The exclusion of internal excitations in (14.17) is not an approximation, provided that the model space is complete. However, as discussed in Chapter 8, complete model spaces are usually impractical because of their size and because of intruder-state problems and so treatments using incomplete model spaces (IMS), also called *general model spaces (GMSs)*, are much more desirable. As shown by Li and Paldus (2003a), the exclusion of internal excitations from the cluster operators \hat{T}^α is not valid for incomplete model spaces. If we expand the wave operator Ω_α in a CI-like series (compare (1.8)),

$$\Omega_\alpha = (1 + \hat{C}_1^\alpha + \hat{C}_2^\alpha + \cdots) \hat{P}_\alpha \quad (14.18)$$

where \hat{C}_n^α is a linear combination of n -fold excitation operators on Φ_α , then (14.2) and $\Omega = \Omega \hat{P}$ require the exclusion of internal excitations from each \hat{C}_n^α . But this exclusion is not equivalent to the exclusion of such excitations from \hat{T}_n^α because, expanding $e^{\hat{T}^\alpha}$ in its power series, we find that the exact (full CI) expansion must satisfy

$$\begin{aligned} \hat{C}_2^\alpha &= \frac{1}{2}(\hat{T}_1^\alpha)^2 + \hat{T}_2^\alpha, \\ \hat{C}_3^\alpha &= \frac{1}{3!}(\hat{T}_1^\alpha)^3 + \hat{T}_1^\alpha \hat{T}_2^\alpha + \hat{T}_3^\alpha \quad \text{etc.} \end{aligned} \quad (14.19)$$

When the model space is complete, any term in \hat{T}_n^α that generates a model-space function is accompanied in (14.19) by disconnected-cluster terms generating the same model function, expressed as products of lower-order excitations each of which also generates a model-state function. In this case the exclusion of internal excitations from \hat{T}^α is equivalent to their exclusion from Ω_α . But when the model space is incomplete some lower excitations in the above disconnected-cluster terms can generate \hat{Q} -space functions, so that the relevant connected-cluster amplitudes cannot be set to zero without introducing approximations. Thus, instead of excluding all internal excitations from \hat{T}_n^α such operators must be retained, their amplitudes being determined by the requirement that the corresponding terms in \hat{C}_n^α have zero amplitude in (14.19). For example, if the operator $\hat{a}^\dagger \hat{b}^\dagger \hat{j} \hat{i}$ generates a model-space function when operating on Φ_α , the amplitude of the function is given by

$$t_{ij}^{ab}(\alpha) = -[t_i^a(\alpha)t_j^b(\alpha) - t_j^a(\alpha)t_i^b(\alpha)], \quad (14.20)$$

which would be nonzero if $\hat{a}^\dagger \hat{i}$ and $\hat{b}^\dagger \hat{j}$ and/or $\hat{a}^\dagger \hat{j}$ and $\hat{b}^\dagger \hat{i}$ are external excitations. These requirements, which were termed the *connectivity conditions*

(or *C-conditions*) by Li and Paldus, can be represented compactly in diagrammatic form. For an excitation from internal state Φ_α to an internal state Φ_β that differs from it by a single, double, triple, ... excitation, respectively, its amplitude must satisfy

$$\begin{array}{c} \boxed{\beta} \\ \text{---} \text{---} \\ \text{---} \end{array} = 0, \quad (14.21)$$

$$\begin{array}{c} \boxed{\beta} \\ \text{---} \text{---} \\ \text{---} \end{array} + \begin{array}{c} \boxed{\beta} \\ \text{---} \text{---} \\ \text{---} \end{array} = 0, \quad (14.22)$$

$$\begin{array}{c} \boxed{\beta} \\ \text{---} \text{---} \text{---} \\ \text{---} \end{array} + \begin{array}{c} \boxed{\beta} \\ \text{---} \text{---} \text{---} \\ \text{---} \end{array} + \begin{array}{c} \boxed{\beta} \\ \text{---} \text{---} \text{---} \\ \text{---} \end{array} = 0 \quad (14.23)$$

etc., where the diagrams are in the Φ_α representation and the box at the top indicates the final state Φ_β . The disconnected diagrams in these equations implicitly include all distinct permutations of their labels, e.g.

$$\begin{array}{c} \boxed{\beta} \\ \text{---} \text{---} \\ \text{---} \end{array} = u \begin{array}{c} \text{---} \text{---} \\ \text{---} \end{array} x \begin{array}{c} \text{---} \text{---} \\ \text{---} \end{array} y - u \begin{array}{c} \text{---} \text{---} \\ \text{---} \end{array} y \begin{array}{c} \text{---} \text{---} \\ \text{---} \end{array} x, \quad (14.24)$$

where $|\Phi_\beta\rangle = |\Phi_{uv}^{xy}(\alpha)\rangle = \hat{x}^\dagger \hat{u} \hat{y}^\dagger \hat{v} |\Phi_\alpha\rangle$. All these diagrams involve only the spinorbitals that are occupied in one, but not both, of the two internal states. Such spinorbitals were called *local active spinorbitals* by Li and Paldus, in analogy with the valence orbitals in a “local” version of the classification of the spinorbital space used in the incomplete-model-space perturbation theory, Section 8.7 (see Fig. 8.8); however, they are defined by just the two model states involved in the matrix element. The limitation on the spinorbital labels is indicated by the bars and double arrows in these diagrams, in analogy with the notation in Section 8.7.

The C-conditions indirectly introduce some disconnected-cluster contributions into the MRCC equations, in analogy with such contributions in incomplete-model-space MRPT (subsection 8.7.1). Most importantly, enforcing the C-conditions ensures the extensivity of the MRCC energy when the \hat{T} operators are truncated consistently at any excitation level.

Substituting the definition of the wave operator (14.16), the generalized Bloch equation (14.14) may be written in the form

$$\sum_{\beta} \hat{H} e^{\hat{T}^{\beta}} \hat{P}_{\beta} = \sum_{\beta} e^{\hat{T}^{\beta}} \hat{P}_{\beta} \hat{H}^{\text{eff}} \hat{P}. \quad (14.25)$$

Projecting on the left with $e^{-\hat{T}^{\alpha}}$ and on the right with \hat{P}_{α} we obtain

$$e^{-\hat{T}^{\alpha}} \hat{H} e^{\hat{T}^{\alpha}} \hat{P}_{\alpha} = \sum_{\beta} e^{-\hat{T}^{\alpha}} e^{\hat{T}^{\beta}} \hat{P}_{\beta} \hat{H}^{\text{eff}} \hat{P}_{\alpha}. \quad (14.26)$$

Applying an external-space determinant $\langle \Phi_{ij\dots}^{ab\dots}(\alpha) | = \langle \hat{a}^{\dagger} \hat{i} \hat{b}^{\dagger} \hat{j} \dots \Phi_{\alpha} |$ on the left and the model function $|\Phi_{\alpha}\rangle$ on the right, we obtain equations for the external-excitation amplitudes $t_{ij\dots}^{ab\dots}(\alpha)$ contained in the operators \hat{T}^{α} :

$$\langle \Phi_{ij\dots}^{ab\dots}(\alpha) | e^{-\hat{T}^{\alpha}} \hat{H} e^{\hat{T}^{\alpha}} | \Phi_{\alpha} \rangle = \sum_{\beta} \langle \Phi_{ij\dots}^{ab\dots}(\alpha) | e^{-\hat{T}^{\alpha}} e^{\hat{T}^{\beta}} | \Phi_{\beta} \rangle \langle \Phi_{\beta} | \hat{H}^{\text{eff}} | \Phi_{\alpha} \rangle. \quad (14.27)$$

The matrix elements of the effective Hamiltonian \hat{H}^{eff} appearing in this equation are obtained, using (14.13) and (14.16), as

$$H_{\beta\alpha}^{\text{eff}} = \langle \Phi_{\beta} | \hat{H}^{\text{eff}} | \Phi_{\alpha} \rangle = \langle \Phi_{\beta} | \hat{H} \Omega | \Phi_{\alpha} \rangle = \langle \Phi_{\beta} | \hat{H} e^{\hat{T}^{\alpha}} | \Phi_{\alpha} \rangle. \quad (14.28)$$

For the use of diagrammatic techniques, the Hamiltonian \hat{H} on the l.h.s. of (14.27) can be replaced by

$$\hat{H}_{\text{N}}^{\alpha} = \hat{H} - \langle \Phi_{\alpha} | \hat{H} | \Phi_{\alpha} \rangle, \quad (14.29)$$

where normal order is defined relative to Φ_{α} as the Fermi vacuum, since the the constant term does not contribute to the matrix element. We can then use the CC effective Hamiltonian (the similarity-transformed Hamiltonian) for model state Φ_{α} ,

$$\mathcal{H}^{\alpha} = e^{-\hat{T}^{\alpha}} \hat{H} e^{\hat{T}^{\alpha}} = (\hat{H} e^{\hat{T}^{\alpha}})_{\text{C}}. \quad (14.30)$$

The internal-excitation amplitudes in \hat{T}^{α} are determined by the C-conditions, while the equations for the external-excitation amplitudes take the form

$$\langle \Phi_{ij\dots}^{ab\dots}(\alpha) | \mathcal{H}^{\alpha} | \Phi_{\alpha} \rangle = \sum_{\beta} \langle \Phi_{ij\dots}^{ab\dots}(\alpha) | e^{-\hat{T}^{\alpha}} e^{\hat{T}^{\beta}} | \Phi_{\beta} \rangle H_{\beta\alpha}^{\text{eff}}. \quad (14.31)$$

The diagrammatic techniques of single-reference CC (Chapter 10) can be used for the left-hand side of these equations, but the equations differ from those of single-reference CC in two respects. A minor difference is the distinction between the treatment of internal and external excitations (relative to the model space). A major difference is the appearance

of the coupling term on the right-hand side. Because of this coupling the equations are solved iteratively, cycling through the different model-state equations using current approximate values for the amplitudes on the r.h.s. and updating these amplitudes with new values as they become available, until self-consistency is achieved between the input and output amplitudes.

We now consider in more detail the evaluation of the various matrix elements that appear in (14.28) and (14.31), following the analysis of Li and Paldus (2003a). For the diagonal elements of \hat{H}^{eff} we note that $\langle \Phi_\alpha | \hat{T}^\alpha = 0$, so that

$$\langle \Phi_\alpha | e^{-\hat{T}^\alpha} = \langle \Phi_\alpha | (1 - \hat{T}^\alpha + \dots) = \langle \Phi_\alpha | \quad (14.32)$$

and therefore

$$H_{\alpha\alpha}^{\text{eff}} = \langle \Phi_\alpha | e^{-\hat{T}^\alpha} \hat{H} e^{\hat{T}^\alpha} | \Phi_\alpha \rangle = \langle \Phi_\alpha | \mathcal{H}^\alpha | \Phi_\alpha \rangle. \quad (14.33)$$

Thus we can use the diagrammatic formulas of single-reference CC to calculate these elements, with the minor difference that the internal excitations are omitted from \hat{T}^α .

Considering now the off-diagonal elements of (14.28), $\langle \Phi_\beta | \hat{T}^\alpha$ does not necessarily vanish unless the model space is complete and therefore the insertion of $e^{-\hat{T}^\alpha}$ in (14.28) may not be justified for incomplete model spaces. Instead, we insert $e^{\hat{T}^\alpha} e^{-\hat{T}^\alpha} = 1$ and obtain

$$H_{\beta\alpha}^{\text{eff}} = \langle \Phi_\beta | e^{\hat{T}^\alpha} \mathcal{H}^\alpha | \Phi_\alpha \rangle. \quad (14.34)$$

The only excitations in \hat{T}^α that can contribute to $\langle \Phi_\beta | e^{\hat{T}^\alpha}$ involve local active spinorbitals. For typical incomplete model spaces the number of such excitations is quite small and a series expansion of $e^{\hat{T}^\alpha}$ will then include just a few contributing terms, allowing easy diagrammatic evaluation of a matrix element.

When the model state Φ_β represents a single excitation relative to Φ_α we obtain

$$H_{\beta\alpha}^{\text{eff}} = \text{diagram} + \text{diagram} \times H_{\alpha\alpha}^{\text{eff}}. \quad (14.35)$$

The second term, which is unlinked (since $H_{\alpha\alpha}^{\text{eff}}$ is a closed disconnected part), vanishes because it involves amplitudes for internal single excitations,

(14.21). For a double excitation we get

$$H_{\beta\alpha}^{\text{eff}} = \text{diagram 1} + \text{diagram 2} + \left(\text{diagram 3} + \text{diagram 4} \right) \times H_{\alpha\alpha}^{\text{eff}}. \quad (14.36)$$

The sum in the parentheses vanishes when the C-conditions are satisfied, (14.22), eliminating the unlinked term. The single-excitation amplitudes in the second and third term are not necessarily zero, except in the complete-model-space case, because they may correspond to external excitations individually and only lead to the internal state Φ_β in the indicated combinations.

Similarly, for a triple excitation we have

$$H_{\beta\alpha}^{\text{eff}} = \text{diagram 1} + \text{diagram 2} + \text{diagram 3} + \text{diagram 4} + \left(\text{diagram 5} + \text{diagram 6} + \text{diagram 7} \right) \times H_{\alpha\alpha}^{\text{eff}}, \quad (14.37)$$

where the unlinked terms vanish when the C-conditions are satisfied. As stated above, the labels on the lines in the diagrams for $\langle \Phi_\beta | \hat{H}^{\text{eff}} | \Phi_\alpha \rangle$ are restricted to local active spinorbitals. Furthermore, when the model space is complete all diagrams that include \hat{T} vertices vanish, leaving only the first diagram for each matrix element.

Next we consider the first factor in the sum on the r.h.s. of (14.31),

$$\begin{aligned} S_{ij\dots}^{ab\dots}(\alpha, \beta) &= \langle \Phi_{ij\dots}^{ab\dots}(\alpha) | e^{-\hat{T}^\alpha} e^{\hat{T}^\beta} | \Phi_\beta \rangle \\ &= \langle \Phi_{ij\dots}^{ab\dots}(\alpha) | e^{-\hat{T}^\alpha} e^{\hat{T}^\beta} | \Phi_{uv\dots}^{xy\dots}(\alpha) \rangle, \end{aligned} \quad (14.38)$$

where $|\Phi_\beta\rangle = |\Phi_{uv\dots}^{xy\dots}(\alpha)\rangle$. Inserting a resolution of the identity between the two exponentials, we obtain

$$S_{ij\dots}^{ab\dots}(\alpha, \beta) = \sum_I \langle \Phi_{ij\dots}^{ab\dots}(\alpha) | e^{-\hat{T}^\alpha} | \Phi_I \rangle \langle \Phi_I | e^{\hat{T}^\beta} | \Phi_{uv\dots}^{xy\dots}(\alpha) \rangle. \quad (14.39)$$

The series expansions of the exponentials in this equation result in expressions, involving CI-like amplitudes, corresponding to linear combinations of \hat{T} amplitudes and their products; these are analogous to the expressions (14.21)–(14.23) involving the C-conditions but they also contain excitations

Table 14.1. *State-universal MRCC excitation energies, in eV, for $^{1,3}A_1$ states of the water molecule^a*

State	Excitation	CI ^b	SU model-space dimension		
			3	6	10
1A_1	gd. state ^c	-0.241833	-0.238073	-0.238149	-0.238252
3A_1	$3a_1 \rightarrow 4a_1$	9.431	9.457	9.456	9.425
1A_1	$3a_1 \rightarrow 4a_1$	10.363	10.364	10.356	10.367
3A_1	$1b_1 \rightarrow 2b_1$	15.475		15.550	15.554
1A_1	$1b_1 \rightarrow 2b_1$	17.884		17.964	17.937
1A_1	$1b_2^2 \rightarrow 4a_1^2$	20.588		20.669	20.467
3A_1	$3a_1 \rightarrow 5a_1$	23.253			23.459
1A_1	$3a_1 \rightarrow 5a_1$	24.414			24.590
1A_1	$3a_1^2 \rightarrow 4a_1^2$	24.928			25.152
1A_1	$1b_2^2 \rightarrow 2b_1^2$	26.756			26.854

^aLi and Paldus (2004); SU-MRCCSD in a cc-pVDZ basis.

^bSingle-reference CISDTQP (single to five-fold excitations).

^cGround-state energies as $E + 76$ in E_h .

outside the model space. The diagrammatic representation and the evaluation of this expansion are described in detail by Paldus, Li and Petraco (2004); see also Kucharski and Bartlett (1991b) for the explicit equations, which will not be discussed further here.

Several applications of Hilbert-space SU-MRCCSD were discussed by Li and Paldus (2003c, 2004), who compared model spaces of different dimensions with high-excitation single-reference CI. As an example we show in Table 14.1 some of their results for several $^{1,3}A_1$ states of the water molecule. Additional results and comparisons with those obtained using various different methods can be found in the review by Bartlett and Musiał (2007).

14.3 Hilbert-space state-specific MRCC

The salient feature of the state-universal form of Hilbert-space MRCC is the simultaneous treatment of several electronic states (equal in number to the dimension of the model space) on an equal footing. This approach is most appropriate for cases of exact degeneracy of the model functions, as in the case of many open-shell states, and to some extent to cases of close quasidegeneracy. But, for most problems in electronic structure theory for which a multireference treatment is indicated, we are usually interested in just one electronic state, and the simultaneous computation of a number of states on an equal footing is an undesirable burden. An example of such a case is the

calculation of potential-energy surfaces (PESs), which often involve near degeneracy in some geometries but are far from quasidegenerate in most other geometries. A state-universal treatment of such potential-energy surfaces is bound to introduce intruder-state problems for some geometries, as the determinantal basis states (both model states and external states) change their relative energy positions and order in different regions of the PES.

Even when we are interested in a few electronic states at a time, their number may be smaller than the desired dimension of the model space. Li and Paldus (2003b) proposed a generalization of SU-CC for this type of situation. In this section we shall focus on state-specific MRCC, in which just one electronic state is computed using a multidimensional model space. We shall follow the general approach of Mukherjee and co-workers (Mahapatra, Datta and Mukherjee 1998, 1999, Chattopadhyay, Mahapatra and Mukherjee 1999).

State-specific MRCC is intended to provide a CC equivalent of multireference CI in generating a single electronic-state solution from a multideterminantal model space but, unlike MRCC, it benefits from the linked nature of the CC theory and, owing to the exponential nature of the wave operator, includes higher excitations obtained as disconnected clusters of lower excitations. The MRCI wave-function expansion is generated from a set of reference determinants (or spin-adapted linear combinations of determinants, called *configuration state functions*) similar to the model space in MRCC, to which are added all excitations of specified levels (usually just single and double excitations, MRCISD) from the reference determinants. The Hamiltonian matrix in the basis of all these determinants is constructed, usually implicitly (“direct CI”), and the desired eigenstate obtained. In CC theory, as usual, the eigenvalue problem is replaced by a set of simultaneous equations.

The desired SS-CC wave function $\tilde{\Psi}_\alpha$ for the electronic state α is obtained by the operation of a wave operator Ω on a linear combination $\tilde{\Phi}_\alpha$ of model functions Φ_α ,

$$|\tilde{\Psi}_\alpha\rangle = \Omega|\tilde{\Phi}_\alpha\rangle, \quad (14.40)$$

$$|\tilde{\Phi}_\alpha\rangle = \hat{P}|\tilde{\Psi}_\alpha\rangle, \quad (14.41)$$

where \hat{P} is the projector onto the model space. Typically, the reference \hat{P} -space will consist of several determinants $\{\Phi_\beta\}$ containing all the inactive core orbitals plus various sets of active orbitals, and the $\tilde{\Phi}_\alpha$ are linear combinations (the *bonnes fonctions*) of these model determinants, as in

(14.9), (14.10); the coefficients of the linear combination are obtained as the components $C_{\beta\alpha}$ of the appropriate eigenvector \mathbf{c}_α of the \mathbf{H}^{eff} matrix.

Inserting the Jeziorski–Monkhorst *Ansatz* (14.16) for Ω into (14.40), we obtain

$$|\tilde{\Psi}_\alpha\rangle = \Omega|\tilde{\Phi}_\alpha\rangle = \sum_{\beta} e^{\hat{T}^\beta} |\Phi_\beta\rangle \langle \Phi_\beta | \tilde{\Phi}_\alpha \rangle = \sum_{\beta} e^{\hat{T}^\beta} |\Phi_\beta\rangle C_{\beta\alpha}. \quad (14.42)$$

A complication arises in this procedure due to the fact that, unlike the case of SU-CC, the wave operator Ω operates directly on a linear combination of model determinants and may generate the same \hat{Q} -space functions from its operation on different model determinants, giving rise to redundancy and non-uniqueness in the formalism. It is therefore necessary to omit the redundant \hat{Q} -space functions from the expansions or to invoke a set of sufficiency conditions (Mahapatra, Datta and Mukherjee 1999).

When the wave function (14.42) is substituted into the Schrödinger equation we obtain

$$\sum_{\beta} [\hat{H} e^{\hat{T}^\beta} |\Phi_\beta\rangle C_{\beta\alpha} - E_\alpha e^{\hat{T}^\beta} |\Phi_\beta\rangle C_{\beta\alpha}] = 0. \quad (14.43)$$

In order to introduce the connected-cluster operator $e^{-\hat{T}^\beta} \hat{H} e^{\hat{T}^\beta} = \mathcal{H}^\beta$, we insert the identity $1 = e^{\hat{T}^\beta} e^{-\hat{T}^\beta} = e^{\hat{T}^\beta} (\hat{P} + \hat{Q}) e^{-\hat{T}^\beta}$, noting that $\hat{P} = \sum_{\gamma} |\Phi_\gamma\rangle \langle \Phi_\gamma|$, to obtain

$$\sum_{\beta\gamma} e^{\hat{T}^\beta} |\Phi_\gamma\rangle H_{\gamma\beta}^{\text{eff}} C_{\beta\alpha} + \sum_{\beta} e^{\hat{T}^\beta} \hat{Q} \mathcal{H}_\beta |\Phi_\beta\rangle C_{\beta\alpha} - E_\alpha \sum_{\beta} e^{\hat{T}^\beta} |\Phi_\beta\rangle C_{\beta\alpha} = 0, \quad (14.44)$$

where, in matrix form,

$$\mathbf{H}^{\text{eff}} = \langle \Phi | \hat{H} \Omega | \Phi \rangle = \left\langle \Phi \left| \hat{H} \sum_{\beta} e^{\hat{T}^\beta} \right| \Phi \right\rangle \quad (14.45)$$

and Φ is a vector composed of the model-space determinants $\{\Phi_\beta\}$. Exchanging the dummy summation variables β and γ in the first term of (14.44) leads to

$$\sum_{\beta} \left[\sum_{\gamma} e^{\hat{T}^\gamma} |\Phi_\beta\rangle H_{\beta\gamma}^{\text{eff}} C_{\gamma\alpha} + e^{\hat{T}^\beta} \mathcal{Q} \mathcal{H}^\beta |\Phi_\beta\rangle C_{\beta\alpha} - E_\alpha e^{\hat{T}^\beta} |\Phi_\beta\rangle C_{\beta\alpha} \right] = 0. \quad (14.46)$$

The redundancy in the determinants is taken into account for each β by setting the corresponding terms in the β -sum to zero.

To obtain the amplitudes we multiply this Schrödinger equation on the left by $e^{-\hat{T}^\beta}$ and project onto the \hat{Q} -space determinants, obtaining

$$\sum_{\gamma(\neq\beta)} \langle \Phi_{ij\cdots}^{ab\cdots}(\beta) | e^{-\hat{T}^\beta} e^{\hat{T}^\gamma} | \Phi_\beta \rangle \hat{H}_{\beta\gamma}^{\text{eff}} C_{\gamma\alpha} + \langle \Phi_{ij\cdots}^{ab\cdots}(\beta) | \mathcal{H}^\beta | \Phi_\beta \rangle C_{\beta\alpha} = 0 \quad (\text{for all } \beta). \quad (14.47)$$

Thus we obtain a single solution for state α . The coefficients $C_{\beta\alpha}$ are obtained as the components of the appropriate eigenvector \mathbf{c}_α of \mathbf{H}^{eff} , (14.45). Except for the \mathbf{c}_α vector, this equation is similar to a form of the SU-CC equation partitioned to separate one state from all the others.

Detailed discussions of extensivity considerations and the use of sufficiency conditions for dealing with the redundancies were given by Mahapatra, Datta and Mukherjee (1999), who also presented several applications demonstrating the efficacy of the approach.

Another version of SS-CC is based upon Brillouin–Wigner PT (subsection 2.4.2). As pointed out there, the main disadvantage of BWPT is that its energy is not extensive, because its equations retain a dependence on the exact energy E_α (as does a truncated-CI calculation). However, unlike RSPT, it does not have renormalization terms and one can derive therefore quite straightforwardly the relevant equations for BWCC. These equations for SS-CC were presented by Hubač, Pittner and Čárksy (2000) and by Pittner, Čárksy and Hubač (2002). The equations that determine the amplitudes have the form

$$E_\alpha \langle \Phi_{ij\cdots}^{ab\cdots}(\beta) | e^{\hat{T}^\beta} | \Phi_\beta \rangle - \langle \Phi_{ij\cdots}^{ab\cdots}(\beta) | \hat{H} | e^{\hat{T}^\beta} | \Phi_\beta \rangle = 0 \quad (\text{for all } \beta). \quad (14.48)$$

Hence, they are coupled only through E_α , making them virtually the same as the SRCC equations for each β once the contributions from the other active-orbital determinants are excluded from the β -equation. However, the lack of extensivity defeats the purpose of a CC theory. To account for this deficiency in an approximate manner, several *a posteriori* corrections for restoring the extensivity have been developed, as well as corrections to the iterative procedures. Nevertheless, this approach would appear to be inferior to the SS-CC approach of Mukherjee and co-workers.

Many of the currently applicable MRCC methods have been compared with high-level single-reference CC for several prototype multireference problems in a detailed paper by Evangelista, Allen and Schaefer (2006); also considered have been the insertion of Be into H_2 (Purvis, Shepard, Brown *et al.* 1983), the H_4 , P_4 and H_8 quasidegenerate systems (Jankowski and Paldus 1980) and cyclobutadiene and methylene (Balková and Bartlett 1994, 1995).

14.4 Fock-space valence-universal MRCC

14.4.1 The Fock-space approach

The Hilbert-space state-universal approach treats several states with the same number of electrons and can directly compute excitation energies (as shown in Table 14.1). A Fock space (Kutzelnigg 1982, 1984, Kutzelnigg and Koch 1983), which is the union of Hilbert spaces for a range of numbers of electrons, such as $n = 0, 1, 2, \dots, n_{\max}$, can deal with a set of electronic states with different numbers of valence electrons. This approach refers all equations to a *single Fermi vacuum* and uses a *single, valence-universal, wave operator* for all states. It finds its major applications in the determination of energy differences, such as ionization potentials and electron affinities as well as electronic-state excitation energies. Examples of the type of quasidegeneracy it can address include complicated open-shell atoms, for which many multiplets lie close in energy.

The Fock-space approach starts formally with the same Bloch equations as used in Hilbert-space methods, except that the meaning of the model functions and their projectors has to be extended to accommodate different numbers of electrons. The classification of the one-electron states is the same as in the Hose–Kaldor approach, Fig. 8.8, repeated here as Fig. 14.1 to introduce an extended notation. The model space is regarded as consisting of different sectors. The projector \hat{P} onto the model space is composed of

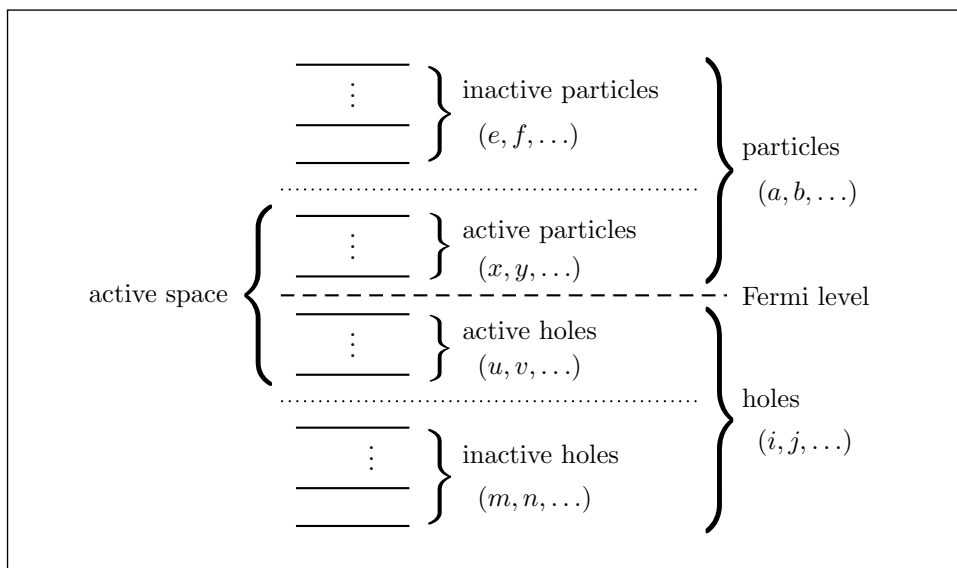


Fig. 14.1. Notation for the one-electron states in Fock-space MRCC.

different sector projectors $\hat{P}^{(p,h)}$ producing p active particles and h active holes in the common Fermi vacuum (see Fig. 14.1). The simplest sector projector is

$$\hat{P}^{(0,0)} = |0\rangle\langle 0|, \quad (14.49)$$

which projects onto the Fermi vacuum. The $\hat{P}^{(1,0)}$ projector produces model-space determinants $|\Phi^x\rangle = \hat{x}^\dagger|0\rangle$ for all active particle labels x , for $(n+1)$ -electron states:

$$\hat{P}^{(1,0)} = \sum_x \hat{x}^\dagger|0\rangle\langle 0|\hat{x} = \sum_x |\Phi^x\rangle\langle \Phi^x|. \quad (14.50)$$

Similarly, the $\hat{P}^{(0,1)}$ projector removes one active orbital (creates an active hole) to generate $(n-1)$ -electron states $|\Phi_u\rangle = \hat{u}|0\rangle$ for all active hole labels u , which is useful in the treatment of ionization potentials:

$$\hat{P}^{(0,1)} = \sum_u \hat{u}|0\rangle\langle 0|\hat{u}^\dagger = \sum_u |\Phi_u\rangle\langle \Phi_u|. \quad (14.51)$$

The $\hat{P}^{(1,1)}$ projector creates all possible single excitations from active holes to active particles,

$$\hat{P}^{(1,1)} = \sum_{xu} \hat{x}^\dagger \hat{u}|0\rangle\langle 0|\hat{u}^\dagger \hat{x} = \sum_{xu} |\Phi_u^x\rangle\langle \Phi_u^x|. \quad (14.52)$$

This sector projector is useful for the treatment of states dominated by single excitations from the Fermi vacuum. For states with strong double-excitation components we also need the $\hat{P}^{(2,2)}$ projector,

$$\hat{P}^{(2,2)} = \frac{1}{4} \sum_{xyuv} \hat{x}^\dagger \hat{u} \hat{y}^\dagger \hat{v}|0\rangle\langle 0|\hat{v}^\dagger \hat{y} \hat{u}^\dagger \hat{x} = \frac{1}{4} \sum_{xyuv} |\Phi_{uv}^{xy}\rangle\langle \Phi_{uv}^{xy}|. \quad (14.53)$$

In a similar manner, the $\hat{P}^{(1,2)}$ projector,

$$\hat{P}^{(1,2)} = \frac{1}{2} \sum_{xuv} \hat{x}^\dagger \hat{u} \hat{v}|0\rangle\langle 0|\hat{v}^\dagger \hat{u}^\dagger \hat{x} = \frac{1}{2} \sum_{xuv} |\Phi_{uv}^x\rangle\langle \Phi_{uv}^x|, \quad (14.54)$$

corresponds to shake-up effects in photoelectron spectroscopy. Other sectors have a role in Auger processes etc.

The total model-space projector \hat{P} is the sum of the sector projectors,

$$\hat{P} = \sum_{k=0}^{n_p} \sum_{l=0}^{n_h} \hat{P}^{(k,l)}, \quad (14.55)$$

where n_p and n_h are the numbers of particle and hole states, respectively, in the active space. For the projector onto the complementary space for each sector we have

$$\hat{Q}^{(p,h)} = 1 - \hat{P}^{(p,h)}, \quad (14.56)$$

which is restricted to terms with the same number of electrons as $\hat{P}^{(p,h)}$, including model determinants belonging to sectors other than $\hat{P}^{(p,h)}$ and including $|0\rangle$ for $\hat{Q}^{(k,k)}$ projectors. In complete-model-space (CMS) calculations, $|0\rangle$ cannot contribute because no connected diagrams can be constructed with it in the Bloch equations (Pal, Rittby, Bartlett *et al.* 1988). For incomplete model spaces (IMSSs), $|0\rangle$ may contribute to Ω and to \hat{H}^{eff} , so that intermediate normalization is no longer valid (Mukherjee 1986, Chaudhuri, Sinha and Mukherjee 1989). Unlike the $\hat{P}^{(p,h)}$ projectors, which consist of mutually exclusive sets, different $\hat{Q}^{(p,h)}$ projectors with the same number of electrons have most terms in common.

Partitioning the model-space determinants by their numbers of active particles and holes leads to a partitioning of the effective Hamiltonian:

$$\begin{aligned} \hat{P}\hat{H}^{\text{eff}}\hat{P} &= P^{(0,0)}\mathcal{H}P^{(0,0)} + \hat{P}^{(0,1)}\hat{H}^{\text{eff}}\hat{P}^{(0,1)} \\ &+ \hat{P}^{(1,0)}\hat{H}^{\text{eff}}\hat{P}^{(1,0)} + \hat{P}^{(1,1)}\hat{H}^{\text{eff}}\hat{P}^{(1,1)} + \dots \end{aligned} \quad (14.57)$$

The first term on the right describes the vacuum-sector contribution, corresponding to single-reference CC, and is obtained as

$$\begin{aligned} \hat{P}^{(0,0)}\hat{H}^{\text{eff}}\hat{P}^{(0,0)} &= \hat{P}^{(0,0)}\hat{H}e^{\hat{T}}\hat{P}^{(0,0)} \\ &= \hat{P}^{(0,0)}e^{\hat{T}}e^{-\hat{T}}\hat{H}e^{\hat{T}}\hat{P}^{(0,0)} = \hat{P}^{(0,0)}\mathcal{H}\hat{P}^{(0,0)}, \end{aligned} \quad (14.58)$$

because $\hat{P}^{(0,0)}e^{\hat{T}} = \hat{P}^{(0,0)}(1 + \hat{T} + \dots) = \hat{P}^{(0,0)}$, since \hat{T} is an excitation operator. Once the correlated wave function for the $(0,1)$ sector has been evaluated, the second term of (14.57) provides the ionization energies. The third term provides electron affinities, while the fourth term determines electronic excitation energies.

14.4.2 The valence-universal wave operator

The correlated wave function is also constructed in sectors, each based on the corresponding sector of the model space, through an exponential wave operator Ω :

$$\Psi^{(p,h)}\hat{P}^{(p,h)} = \Omega\hat{P}^{(p,h)}. \quad (14.59)$$

For the (0,0) sector this process simply reduces to the usual single-reference CC solution,

$$\Psi^{(0,0)} \hat{P}^{(0,0)} = e^{\hat{T}} \hat{P}^{(0,0)}, \quad (14.60)$$

but a more general treatment is needed for the other sectors. To proceed, we express the wave operator in terms of an auxiliary operator \tilde{S} (Lindgren 1978, Sinha, Mukhopadhyay and Mukherjee 1986):

$$\Omega = \{e^{\tilde{S}}\}, \quad (14.61)$$

where the braces indicate normal order. This operator is also partitioned by sectors of Fock space,

$$\tilde{S} = \hat{S}^{(0,0)} + \hat{S}^{(1,0)} + \hat{S}^{(0,1)} + \hat{S}^{(1,1)} + \dots + \hat{S}^{(n_p, n_h)}, \quad (14.62)$$

with

$$\hat{S}^{(0,0)} = \hat{T}. \quad (14.63)$$

We also define the partial sums

$$\tilde{S}^{(p,h)} = \sum_{k=0}^p \sum_{l=0}^h \hat{S}^{(k,l)} \quad (p \leq n_p, \quad h \leq n_h), \quad (14.64)$$

$$\Delta \tilde{S} = \tilde{S} - \hat{S}^{(0,0)}, \quad \Delta \tilde{S}^{(p,h)} = \tilde{S}^{(p,h)} - \hat{S}^{(0,0)}. \quad (14.65)$$

The components of \tilde{S} operate on model determinants. When operating on a determinant in the $\hat{P}^{(p,h)}$ sector they generate determinants belonging to $\hat{Q}^{(p,h)}$; thus the only nonvanishing matrix elements of \tilde{S} components are of the form $\langle \Phi_I^{*(p,h)} | \hat{S}^{(k,l)} | \Phi_\alpha^{(p,h)} \rangle$, with $k \leq p$, $l \leq h$, and furnish the s amplitudes. Here $\Phi_I^{*(p,h)}$ and $\Phi_\alpha^{(p,h)}$ are determinants belonging to $\hat{Q}^{(p,h)}$ and $\hat{P}^{(p,h)}$, respectively. Usually $\hat{S}^{(p,h)}$ operates on a model determinant in the $\hat{P}^{(p,h)}$ sector, although it can produce a nonvanishing result when operating on any model determinant that has at least p occupied active particle states and at least h unoccupied active hole states. The $\hat{S}^{(0,0)}$ operator operates on $|0\rangle$ and provides the usual definition of the t amplitudes of the single-reference \hat{T} operator. The objective of the valence-universal (VU) treatment is to add the excitation amplitudes that can arise with the multidimensional model space and that can be used to correlate the new states available with this model space.

Each model determinant in the $\hat{P}^{(1,0)}$ space has one more electron (active particle) than $|0\rangle$, and new terms are needed to provide correlation effects for this added electron. This task is accomplished by the new $\hat{S}^{(1,0)}$ operator,

which excites the active particle produced by $\hat{P}^{(1,0)}$ to an inactive particle state, possibly accompanied by additional excitations. Using the designation of Fig. 14.1,

$$\hat{S}_1^{(1,0)} \hat{P}^{(1,0)} = \sum_{ex} s_x^e \{ \hat{e}^\dagger \hat{x} \} \hat{P}^{(1,0)}, \quad (14.66)$$

$$\hat{S}_2^{(1,0)} \hat{P}^{(1,0)} = \frac{1}{2} \sum_{ixab} s_{xi}^{ab} \{ \hat{a}^\dagger \hat{b}^\dagger \hat{i} \hat{x} \} \hat{P}^{(1,0)} \quad (14.67)$$

etc. The excitation due to $\hat{S}_1^{(1,0)}$ has to be of the form $x \rightarrow e$ (active particle to inactive particle). An $x \rightarrow y$ excitation would result in a model determinant belonging to $\hat{P}^{(1,0)}$ and is excluded. For $\hat{S}_2^{(1,0)}$ the requirements are more relaxed: any $x \rightarrow a$ excitation may be accompanied by any $i \rightarrow b$ excitation. A diagrammatic representation of $\hat{S}^{(1,0)}$ and other \hat{S} operators is shown in Table 14.2. The thick bars in this figure represent the corresponding \hat{S} operators and have the value of the corresponding s amplitude. It is easy to see that $\hat{S}^{(0,1)}$ will be of the same form as $\hat{S}^{(1,0)}$, except that \hat{u}^\dagger will replace \hat{x} , because it can fill the vacant hole state created by $\hat{P}^{(0,1)}$ while \hat{m}, \hat{j} replace $\hat{e}^\dagger, \hat{b}^\dagger$:

$$\hat{S}_1^{(0,1)} \hat{P}^{(0,1)} = \sum_{mu} s_m^u \{ \hat{u}^\dagger \hat{m} \} \hat{P}^{(0,1)}, \quad (14.68)$$

$$\hat{S}_2^{(0,1)} \hat{P}^{(0,1)} = \frac{1}{2} \sum_{ijau} s_{ij}^{ua} \{ \hat{u}^\dagger \hat{a}^\dagger \hat{j} \hat{i} \} \hat{P}^{(0,1)} \quad (14.69)$$

etc. The $\hat{S}^{(1,1)}$ operator is given by

$$\hat{S}_1^{(1,1)} \hat{P}^{(1,1)} = \sum_{ux} s_x^u \{ \hat{u}^\dagger \hat{x} \} \hat{P}^{(1,1)}, \quad (14.70)$$

$$\hat{S}_2^{(1,1)} \hat{P}^{(1,1)} = \sum'_{aiux} s_{xi}^{au} \{ \hat{a}^\dagger \hat{u}^\dagger \hat{i} \hat{x} \} \hat{P}^{(1,1)}. \quad (14.71)$$

The prime on the summation sign in the expression involving the $\hat{S}_2^{(1,1)}$ operator indicates that the a and i labels cannot both refer to active orbitals at the same time (if they did then the resulting state would belong to $\hat{P}^{(1,1)}$). Operators for any other sector of Fock space can be diagrammed as in Fig. 14.2. Our notation for the s amplitudes does not specify the sector of \hat{S} to which they belong, because that information is evident from the type of subscripts and superscripts on the amplitude symbol.

The $\hat{S}_1^{(1,1)}$ operator contains only active lines and is a de-excitation operator taking the $|\Phi_x^u\rangle$ model function, generated by $\hat{P}^{(1,1)}$, back to the vacuum state $|0\rangle$. Such terms do not contribute at all for complete model spaces

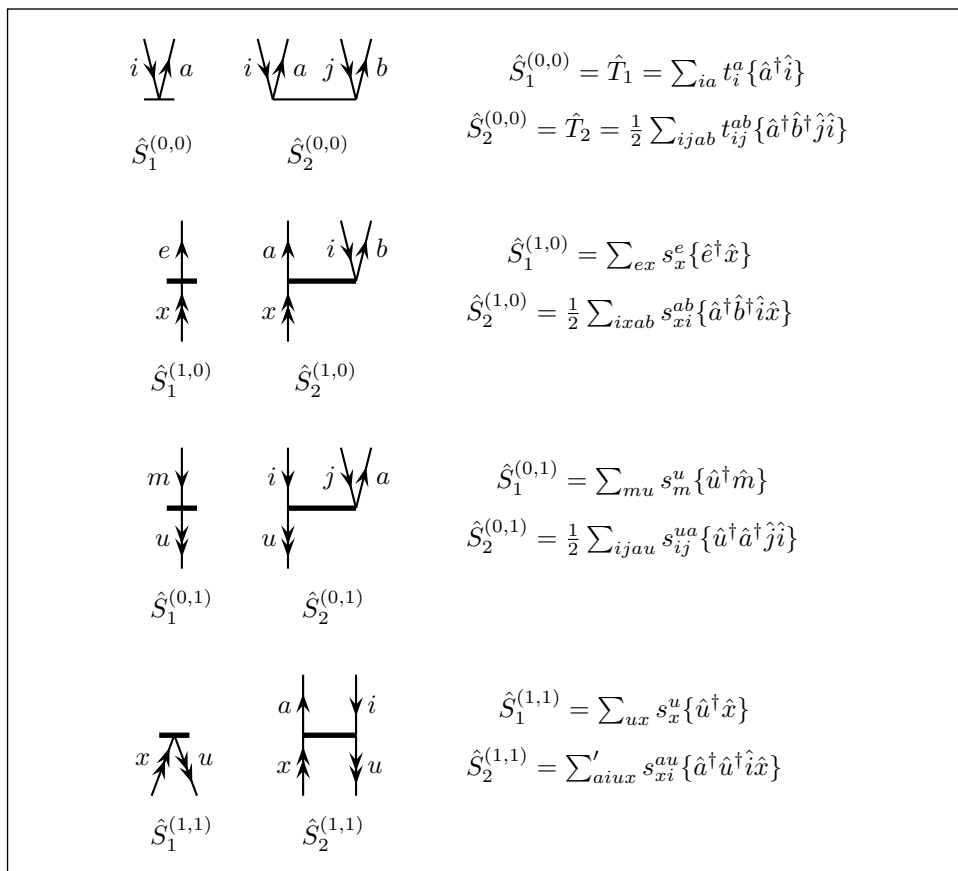


Fig. 14.2. Diagrammatic representation and algebraic expressions for the $\hat{S}^{(0,0)}$, $\hat{S}^{(1,0)}$, $\hat{S}^{(0,1)}$ and $\hat{S}^{(1,1)}$ operators at the CCSD level. The heavy bar represents the \hat{S} operator, and has the value of the corresponding s amplitude. In the definition of $\hat{S}_2^{(1,1)}$ the prime on the summation sign indicates exclusion of the case in which both upper labels (a and i) refer to active orbitals (see (14.68)–(14.71)).

(CMSs), and they do not contribute to the evaluation of excitation energies in important special cases of incomplete model spaces (IMSS) (Sinha, Mukhopadhyay and Mukherjee 1986, Meissner and Bartlett 1991), though they can contribute to the Fock-space wave function. This property applies, in particular, to MRCCSD calculations, in which $\hat{P}^{(1,1)}$ is the highest sector and defines the model space. Model spaces comprising complete sectors are called quasicomplete.

A critical feature of the VU approach is the need to insure normal ordering in products of \tilde{S} operators, such as those arising from the expansion of the exponential $e^{\tilde{S}}$, as indicated by the braces in the exponential *Ansatz*

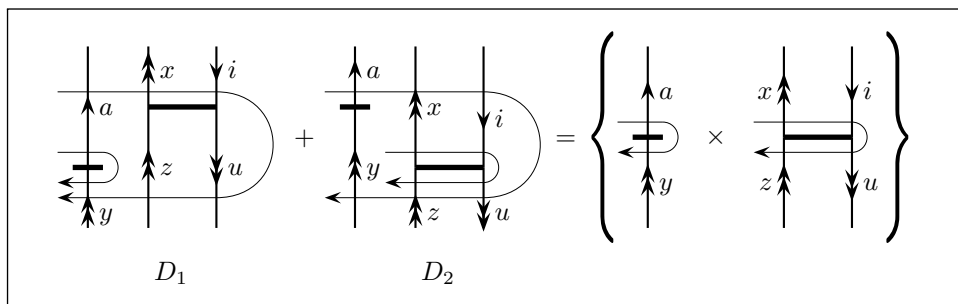


Fig. 14.3. Illustration of the factorization of disconnected diagrams in the open-shell case (Lindgren and Morrison 1986). The braces on the right-hand side of the equation denote normal order.

$\Omega\hat{P} = \{e^{\tilde{S}}\}\hat{P}$, (14.61). Normal ordering of the Hamiltonian and of the cluster operators $\hat{T}_1, \hat{T}_2, \dots$ and evaluation of their contractions via the generalized Wick's theorem have been used throughout this book. Normal ordering is easily imposed in the single-reference theory. In particular, the \hat{T} operators and their products are always in normal order because they consist of operators (for particle creation and hole annihilation) all of the same kind with respect to normal ordering, and therefore the exponential $e^{\hat{T}}$ is also in normal order. But the products of \tilde{S} operators in VU theory do not have this property and require explicit normal ordering of the exponential in (14.61).

A consequence of this situation is that the factorization of sums of different time orderings of disconnected diagrams, which is trivial in the single-reference theory, as shown for example in (9.97) and (9.101), requires explicit product normal ordering in VU theory (Lindgren 1978). As an example we examine the factorization shown in Fig. 14.3.

As is the case for \hat{T} operators, in first order the \tilde{S} operators can be represented by the one-body and two-body Hamiltonian operators of MBPT and QDPT theory. In fact, except for the reversed direction of two of the lines, the disconnected diagrams in Fig. 14.3 are equivalent, in first order, to diagrams 56 and 57 of Fig. 8.5. Such first-order approximations do not need explicit normal ordering, but going beyond first order introduces the requirement for product normal order.

The disconnected diagram D_1 , interpreted as a single diagram, has the value

$$D_1 = \frac{s_y^a s_{zi}^{xu}}{\varepsilon_y^a \varepsilon_{yzi}^{axu}} \{\hat{a}^\dagger \hat{x}^\dagger \hat{u}^\dagger \hat{i} \hat{z} \hat{y}\}. \quad (14.72)$$

(For the determination of the denominators see Section 8.5.) Reversing the time order gives diagram D_2 , with value

$$D_2 = \frac{s_y^a s_{zi}^{xu}}{\varepsilon_{zi}^{xu} \varepsilon_{yzi}^{axu}} \{\hat{a}^\dagger \hat{x}^\dagger \hat{u}^\dagger \hat{i} \hat{z} \hat{y}\}. \quad (14.73)$$

Using the factorization theorem and adding the two diagrams gives a factored denominator product, eliminating the six-index denominator factor:

$$D_1 + D_2 = \frac{s_y^a s_{zi}^{xu}}{\varepsilon_y^a \varepsilon_{zi}^{xu}} \{\hat{a}^\dagger \hat{x}^\dagger \hat{u}^\dagger \hat{i} \hat{z} \hat{y}\}. \quad (14.74)$$

However, the r.h.s. of the equation in Fig. 14.3 is a product of two diagrams and, disregarding the braces around it for now, its value is

$$\frac{s_y^a}{\varepsilon_y^a} \{\hat{a}^\dagger \hat{y}\} \times \frac{s_{zi}^{xu}}{\varepsilon_{zi}^{xu}} \{\hat{x}^\dagger \hat{u}^\dagger \hat{i} \hat{z}\} = \frac{s_y^a s_{zi}^{xu}}{\varepsilon_y^a \varepsilon_{zi}^{xu}} \{\hat{a}^\dagger \hat{y}\} \{\hat{x}^\dagger \hat{u}^\dagger \hat{i} \hat{z}\}. \quad (14.75)$$

The product of creation and annihilation operators in this equation is not in normal order, as seen by the fact that contraction is possible between \hat{y} and \hat{x}^\dagger . Only by imposing *product* normal order (indicated by the braces in Fig. 14.3),

$$\{\{\hat{a}^\dagger \hat{y}\} \{\hat{x}^\dagger \hat{u}^\dagger \hat{i} \hat{z}\}\} = \{\hat{a}^\dagger \hat{x}^\dagger \hat{u}^\dagger \hat{i} \hat{z} \hat{y}\}, \quad (14.76)$$

do we get the two sides of the equation in Fig. 14.3 to agree.

Such problems cannot arise in a closed-shell case involving products of \hat{T} operators, since all such products are automatically in normal order and all creation and annihilation operators anticommute. In the multireference case, however, the active orbital operators do not anticommute, and cannot simply be reordered, unless they are inside a single normal product. The correct result is restored by imposing normal order explicitly, as is done on the r.h.s. of Fig. 14.3. Lindgren (1978) offered this approach as a simple resolution of this problem, showing that the correct products will be obtained in a Fock-space theory once $\Omega = \{e^{\hat{S}}\}$ is *product* normal ordered.

A useful consequence of product normal ordering is that there can be no contractions among products of \tilde{S} operators, even though these operators may have open active hole lines that could have been contracted in the absence of normal ordering.

Several simplifications are possible in expressions containing the VU wave operator $\{e^{\hat{S}}\}\hat{P}$. First, consider the $(0, 1)$ sector, which involves a model space of determinants with one active hole vacant. While $\hat{S}^{(0,1)}\hat{P}^{(0,1)}$ is associated with s amplitudes, we have $(\hat{S}^{(0,1)})^2\hat{P}^{(0,1)} = 0$ since there is only one vacant active hole available for the two $\hat{S}^{(0,1)}$ operators. Similarly,

$(\hat{S}^{(1,1)})^2 \hat{P}^{(1,1)} = 0$ and in general $(\hat{S}^{(p,h)})^2 \hat{P}^{(p,h)} = 0$. However, a nonzero result can be obtained for products such as $\hat{S}^{(0,1)} \hat{S}^{(1,0)} \hat{P}^{(1,1)}$. Thus the VU wave operator, while formally an exponential, reduces to a linear form in the $(0, 1)$ and $(1, 0)$ sectors and only has nonlinear terms involving products of s amplitudes in higher sectors. As we shall see presently, the amplitudes in such a product derive from sectors below the sector of interest.

Another key simplification derives from the observation that terms like $\hat{S}^{(1,1)} \hat{P}^{(1,0)}$ and $\hat{S}^{(1,1)} \hat{P}^{(0,1)}$ vanish and, in general, $\hat{S}^{(k,l)} \hat{P}^{(i,j)} = 0$ if $k > i$ and/or $l > j$. A consequence of this property is that the expansion of the VU operator $\{e^{\Delta\tilde{S}}\} \hat{P}^{(p,h)}$ has to terminate. In particular, when operating on $\hat{P}^{(1,1)}$ there is no contribution from $\hat{S}^{(2,0)}$, $\hat{S}^{(2,1)}$, $\hat{S}^{(0,2)}$, $\hat{S}^{(1,2)}$ or $\hat{S}^{(2,2)}$. As a result,

$$\Delta\tilde{S} \hat{P}^{(1,1)} = (\hat{S}^{(1,0)} + \hat{S}^{(0,1)} + \hat{S}^{(1,1)}) \hat{P}^{(1,1)}, \quad (14.77)$$

and

$$\begin{aligned} \{e^{\Delta\tilde{S}}\} \hat{P}^{(1,1)} &= (\hat{S}^{(1,0)} + \hat{S}^{(0,1)} + \hat{S}^{(1,1)} \\ &\quad + \tfrac{1}{2}\{\hat{S}^{(0,1)} \hat{S}^{(1,0)}\} + \tfrac{1}{2}\{\hat{S}^{(1,0)} \hat{S}^{(0,1)}\}) \hat{P}^{(1,1)}. \end{aligned} \quad (14.78)$$

14.4.3 The Fock-space Bloch equations

Since $\hat{S}^{(0,0)} = \hat{T}$, the VU wave operator can be factored in the form

$$\Omega \hat{P} = e^{\hat{T}} \{e^{\Delta\tilde{S}}\} \hat{P}. \quad (14.79)$$

Our remaining objective is to derive the Fock-space VU equations, which will allow us to determine the amplitudes of $\Delta\tilde{S}$.

Substituting (14.79) in the Bloch equation (14.14) for the (p, h) sector, we get

$$\hat{H} e^{\hat{T}} \{e^{\Delta\tilde{S}}\} \hat{P}^{(p,h)} = e^{\hat{T}} \{e^{\Delta\tilde{S}}\} \hat{P}^{(p,h)} \hat{H}^{\text{eff}} \hat{P}^{(p,h)}. \quad (14.80)$$

Left-multiplying by $e^{-\hat{T}}$ gives

$$e^{-\hat{T}} \hat{H} e^{\hat{T}} \{e^{\Delta\tilde{S}}\} \hat{P}^{(p,h)} = \{e^{\Delta\tilde{S}}\} \hat{P}^{(p,h)} \hat{H}^{\text{eff}} \hat{P}^{(p,h)} \quad (14.81)$$

or

$$\mathcal{H} \{e^{\Delta\tilde{S}}\} \hat{P}^{(p,h)} = \{e^{\Delta\tilde{S}}\} \hat{P}^{(p,h)} \hat{H}^{\text{eff}} \hat{P}^{(p,h)}. \quad (14.82)$$

Now projecting by $\hat{P}^{(p,h)}$, and noting that $\hat{P}^{(p,h)}\{e^{\Delta\tilde{S}}\}\hat{P}^{(p,h)} = \hat{P}^{(p,h)}\{1 + \Delta\tilde{S} + \dots\}\hat{P}^{(p,h)} = \hat{P}^{(p,h)}$ because $\hat{P}^{(p,h)}\Delta\tilde{S} = 0$, we get an equation for the sectors of \hat{H}^{eff} :

$$\hat{H}^{\text{eff}(p,h)} = \hat{P}^{(p,h)}\hat{H}^{\text{eff}}\hat{P}^{(p,h)} = \hat{P}^{(p,h)}\mathcal{H}\{e^{\Delta\tilde{S}}\}\hat{P}^{(p,h)}. \quad (14.83)$$

Finally, projection of (14.82) by $\hat{Q}^{(p,h)}$ provides the amplitude equations,

$$\hat{Q}^{(p,h)}\mathcal{H}\{e^{\Delta\tilde{S}}\}\hat{P}^{(p,h)} = \hat{Q}^{(p,h)}\{e^{\Delta\tilde{S}}\}\hat{H}^{\text{eff}(p,h)}. \quad (14.84)$$

The simplest example is provided by the equations for the $(0, 1)$ sector,

$$\hat{H}^{\text{eff}(0,1)} = \hat{P}^{(0,1)}\mathcal{H}\{1 + \hat{S}^{(0,1)}\}\hat{P}^{(0,1)}, \quad (14.85)$$

$$\hat{Q}^{(0,1)}[\mathcal{H}\{1 + \hat{S}^{(0,1)}\}\hat{P}^{(0,1)} - \{1 + \hat{S}^{(0,1)}\}\hat{H}^{\text{eff}(0,1)}] = 0. \quad (14.86)$$

Using the standard diagram-generation techniques, the VU amplitude equations and the associated \hat{H}^{eff} can be diagrammed as shown in skeleton form in Figs. 14.4–14.6 for VU-CCSD. As in Chapter 8, short bars across a line indicate limitation to active orbitals. The main difference from the single-reference theory is the appearance of “folded” diagrams, from the r.h.s. of the equations, that depend upon \hat{H}^{eff} . Such diagrams are familiar from MR-MBPT, Chapter 8. The energies for each sector are obtained by diagonalizing the \mathbf{H}^{eff} matrix for the corresponding sector.

As can be seen from Figs. 14.5 and 14.6, solving the equations for $\hat{S}^{(1,1)}$ requires knowledge of the $\hat{S}^{(1,0)}$ and $\hat{S}^{(0,1)}$ amplitudes. This is a general feature of the VU equations: solution of the equations for $\hat{S}^{(p,h)}$ requires the prior solution of the equations for $\hat{S}^{(k,l)}$ for all $k \leq p$ and all $l \leq h$ (obviously not including $k = p$ and $l = h$ simultaneously). This requirement for the hierarchical solution for all sectors of Fock space lower than the sector of interest has been called the “subsystem embedding condition” (Haque and Mukherjee 1984, Chaudhuri, Mukhopadhyay and Mukherjee 1989).

An alternative demonstration of the subsystem embedding conditions can be obtained by comparing the number of amplitudes to be determined by the equations for each sector with the number of such equations. Considering first the $(0, 1)$ sector, which requires a model space of one-active-hole determinants, the number of such determinants is n_h , the number of active hole states. For an MRCCSD calculation we need to consider all single and double excitations from these model determinants, which requires $\hat{S}_1^{(0,1)}$ and $\hat{S}_2^{(0,1)}$. For $\hat{S}_1^{(0,1)}$ the single-excitation amplitudes are s_m^u (see Fig. 14.2), and their number is $n_h n'_h$, where n'_h is the number of inactive hole states. The various $\hat{S}_1^{(0,1)}$ equations (Fig. 14.4(A)) are distinguished by two labels,

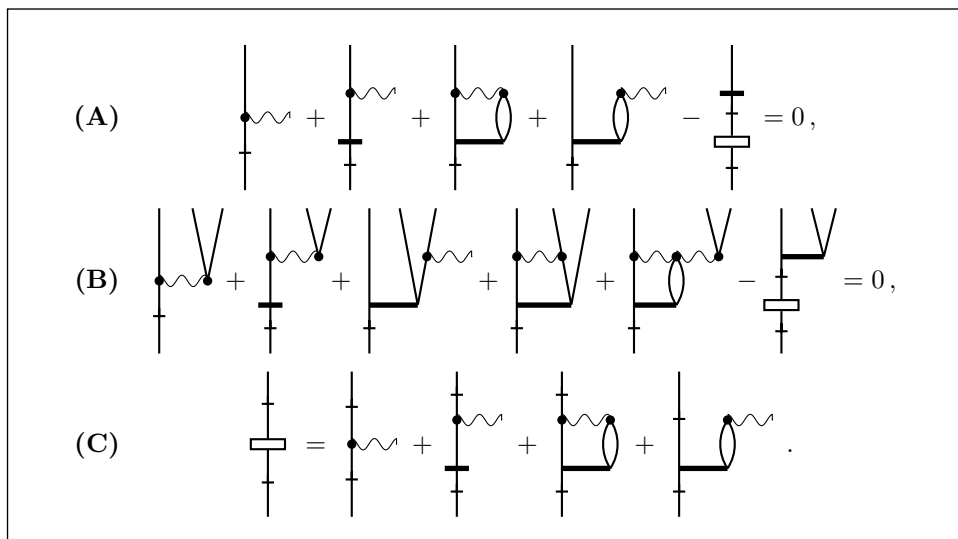


Fig. 14.4. Diagrammatic representation of the VU-CCSD equations for the (1, 0) and (0, 1) sectors in skeleton form; (A) is the equation for \hat{S}_1 , (B) is for \hat{S}_2 and (C) is for the one-electron part of \hat{H}^{eff} (represented by the rectangle).

those for the initial active hole line (e.g. u) and the final inactive hole line (m). (The internal lines are summed over and have dummy summation indices.) The number of these equations is thus $n_h n'_h$, the same as the number of amplitudes to be determined, allowing unique determination of all the amplitudes. Similarly, the number of possible amplitudes s_{ij}^{ub} for $\hat{S}_2^{(0,1)}$ is $\frac{1}{2} n_h n'_p (n'_h)^2$, equal to the number of $\hat{S}_2^{(0,1)}$ equations (Fig. 14.4(B)). Obviously, a similar result will be obtained for the $\hat{S}^{(1,0)}$ operator except that the corresponding numbers will be $n_p n'_p$ and $\frac{1}{2} n_p n'_h (n'_p)^2$, respectively.

This situation is to be contrasted with the case of $\hat{S}^{(1,1)}$. For VU-CCSD the relevant operators are $\hat{S}_1^{(1,1)}$ and $\hat{S}_2^{(1,1)}$ but, as can be seen from Fig. 14.2, $\hat{S}_1^{(1,1)}$ is not needed and we have enough equations to determine $\hat{S}_2^{(1,1)}$. However, we can see from Figs. 14.5 and 14.6 that we also need the amplitudes for $\hat{S}_1^{(1,0)}$ and $\hat{S}_1^{(0,1)}$ and therefore cannot solve the (1,1) sector independently without first solving the lower (1,0) and (0,1) sectors, as specified by the subsystem embedding condition.

The equations and diagrams given here are appropriate for the CMS case, but most also apply to a truncated MRCCSD calculation with (1,1) as the top-level sector. In this latter case the $\hat{S}_1^{(1,1)}$ operator contributes to Ω and thus to the wave function, where it introduces a $|0\rangle$ contribution, negating intermediate normalization. But there is no contribution to \hat{H}^{eff} and thus

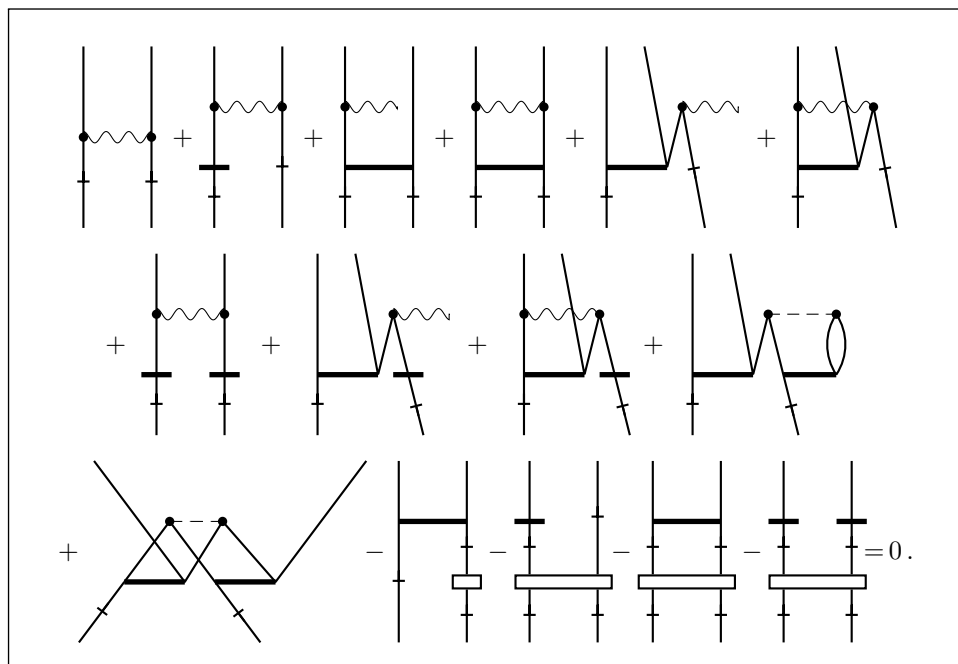


Fig. 14.5. Diagrammatic representation in skeletal form of the VU-CCSD equation for $\hat{S}_2^{(1,1)}$. The two-electron part of \hat{H}^{eff} is shown in Fig. 14.6.

to the energy. Therefore, for energy calculations only, the contribution of $\hat{S}_1^{(1,1)}$ and the lack of intermediate normalization can be ignored. If the wave function is also of interest, the $\hat{S}_1^{(1,1)}$ operator can be calculated from the corresponding Bloch equation, shown diagrammatically in Fig. 14.7. Its contribution to the wave function is given by

$$(x) \begin{array}{c} \uparrow \\ \downarrow \end{array} (u) = \sum_{ux} t_u^x s_x^u |0\rangle. \quad (14.87)$$

The IMS case imposes consistency requirements on the selection of the model states for the various sectors. Once the model states have been specified for the top sector, each lower sector must include all model states having as orbital indices all allowed subsets of the orbital indices of the selected model states of the sectors above it.

The $\hat{S}^{(1,1)}$ operator can be used to demonstrate another aspect of the VU formalism. It is possible to have the unusual situation in which, after an active hole state has become unoccupied by $\hat{P}^{(1,1)}$, it can be reoccupied by the next operator. Consider, for example, the following instance of the second and fourth diagrams of Fig. 14.5, in which the second diagram includes an

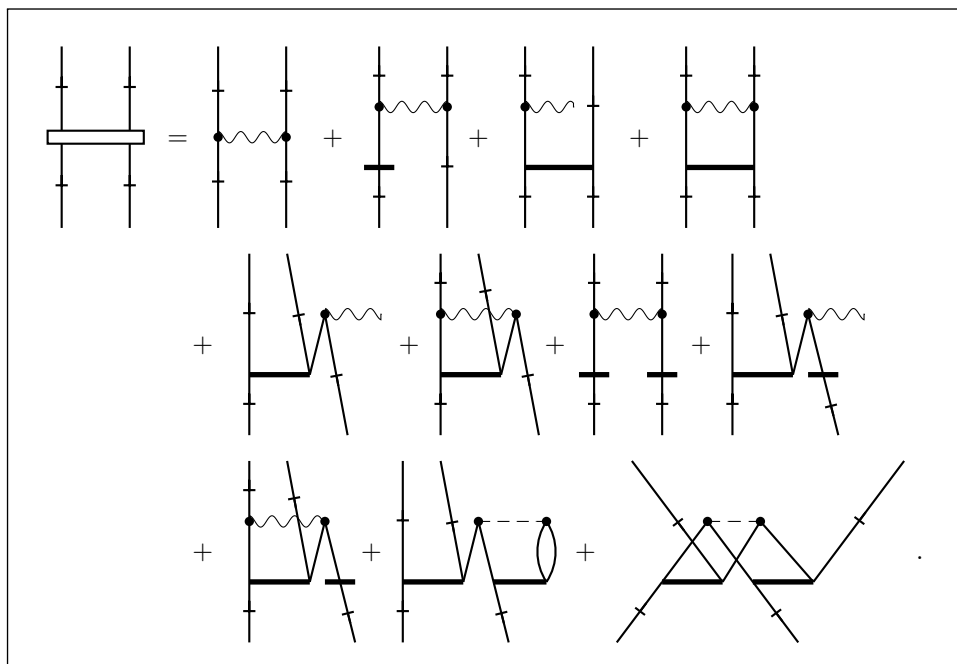


Fig. 14.6. Diagrammatic representation in skeletal form of the two-electron part of \hat{H}^{eff} .

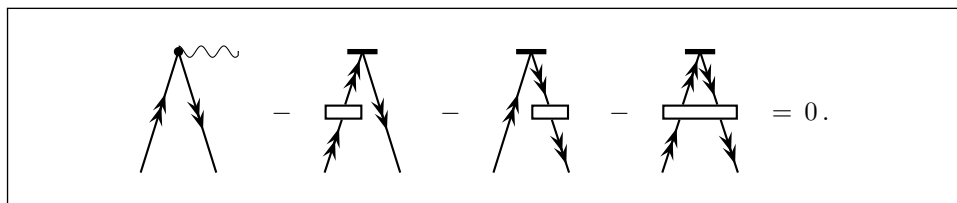
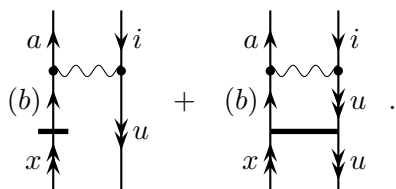


Fig. 14.7. Diagrammatic representation of the VU-CCSD equation for $\hat{S}_1^{(1,1)}$.

emptying and reoccupation of the active hole state u at the internal hole line (no other active hole label can replace the u on this line, although inactive hole lines would also produce valid contributions):



Both diagrams have the same initial and final state and have the matrix

element χ_{aubi} of \mathcal{H} (see Eq. 10.70) as a common factor. The lower parts of the two diagrams contribute the sum $s_x^u + s_{xu}^{bu}$. The second amplitude in this sum is called a *spectator amplitude*. If we were to go beyond VU-CCSD and include $\hat{S}_3^{(1,2)}$ we would also have s_{xuv}^{buu} as a spectator amplitude, with similar contributions at higher levels.

The required presence of these spectator terms in the VU theory limits the orbital relaxation found naturally in an FS calculation in comparison with a model that benefits fully from the presence of an exponential operator $e^{\hat{T}_1}$, because the full power of the exponential is not there. An illustration would be the poor accuracy of core-ionization states, where such effects are known to be quite important. To improve upon the accuracy, selective infinite summations of spectator terms have been recommended and, since they are fundamentally simple, such summations can in fact be accomplished (Jana, Bandyopadhyay and Mukherjee 1999).

14.4.4 Relationship to EOM-CC

Another interesting aspect is the similarity of VU-CC to EOM-CC (Chapter 13). Consider an ionized state dominated by the removal of an electron from hole state m . The IP-EOM-CC *Ansatz* for this state is

$$|\Psi_m\rangle = \hat{R}_m e^{\hat{T}} |0\rangle = e^{\hat{T}} \hat{R}_m |0\rangle, \quad (14.88)$$

$$\hat{R}_m = \sum_i r_i \hat{i} + \frac{1}{2} \sum_{ija} r_{ij}^a \{\hat{a}^\dagger \hat{j} \hat{i}\} + \cdots. \quad (14.89)$$

The dominant terms in (14.89) identify the hole state m as most strongly involved in the ionization. The second form in (14.88) takes advantage of the commutation of \hat{T} and \hat{R}_m . While operationally \hat{R}_m cannot be determined before \hat{T} , the two forms of the *Ansatz* in (14.88) allow two different interpretations of the result. In the first, $e^{\hat{T}}|0\rangle$ creates a correlated ground state and then \hat{R}_m removes an electron from this CC state and introduces the correlation changes due to ionization. In the second, \hat{R}_m removes an electron from the vacuum state and generates a CI-like expansion for the resulting ionized state and then $e^{\hat{T}}$ introduces ground-state correlation terms that, together with \hat{R}_m , result in the correct description of the ionized-state correlation.

In the VU-CC case, the *Ansatz* is

$$|\Psi_m\rangle = \{e^{\hat{S}^{(0,1)}}\} |\Phi_m\rangle = (1 + \hat{S}^{(0,1)}) |\Phi_m\rangle, \quad (14.90)$$

where $|\Phi_m\rangle = \hat{m}|0\rangle$ is a one-vacant-hole-state model-space determinant and the effective Hamiltonian matrix is

$$\mathbf{H}^{\text{eff}(0,1)} = \langle \Phi^{(0,1)} | \hat{H}^{\text{eff}} | \Phi^{(0,1)} \rangle = \langle \Phi^{(0,1)} | \mathcal{H}(1 + \hat{S}^{(0,1)}) | \Phi^{(0,1)} \rangle, \quad (14.91)$$

because $(\hat{S}^{(0,1)})^2 \hat{P}^{(0,1)} = 0$. Here $|\Phi^{(0,1)}\rangle$ is a row vector of the one-vacant-active-hole determinant and $\langle \Phi^{(0,1)} |$ is its adjoint column vector. The main difference between the matrix (14.91) and the IP-EOM-CCSD matrix implicit in (13.25) is that the latter has a dimension of one-hole single and double excitations while the former has the smaller dimension n_h of just the one-vacant-active-hole determinants. Thus we expect to have a matrix partitioning relating the two matrices.

Using (13.25) and noting that

$$\langle \Phi_i | r_i \hat{i} | 0 \rangle = r_i, \quad \langle \Phi_{ij}^a | r_{ij}^a \{ \hat{a}^\dagger \hat{j} \hat{i} \} | 0 \rangle = r_{ij}^a, \quad (14.92)$$

the IP-EOM-CCSD eigenvalue equation for hole state m can be written in partitioned form as

$$\begin{pmatrix} \langle \Phi^{(0,1)} | \mathcal{H} | \Phi^{(0,1)} \rangle & \langle \Phi^{(0,1)} | \mathcal{H} | \Phi^{(1,2)} \rangle \\ \langle \Phi^{(1,2)} | \mathcal{H} | \Phi^{(0,1)} \rangle & \langle \Phi^{(1,2)} | \mathcal{H} | \Phi^{(1,2)} \rangle \end{pmatrix}_C \begin{pmatrix} \mathbf{r}^{(0,1)} \\ \mathbf{r}^{(1,2)} \end{pmatrix} = \begin{pmatrix} \mathbf{r}^{(0,1)} \\ \mathbf{r}^{(1,2)} \end{pmatrix} \omega_m, \quad (14.93)$$

where ω_m is the ionization energy of hole state m . Normally, if we were to use sector designators such as $(0,1)$ and $(1,2)$ in EOM-CC then they would refer to all orbitals since there is no separation between active and inactive orbitals in this model. Specifically, $|\Phi^{(0,1)}\rangle$ and $|\Phi^{(1,2)}\rangle$ are row vectors consisting of all determinants of types Φ_i and Φ_{ij}^a , respectively; to bring out the analogy between EOM-CC and VU-CC, we may designate a subset of orbitals as active and restrict the sector definitions to this subset. Also, $\mathbf{r}^{(0,1)}$ and $\mathbf{r}^{(1,2)}$ are column vectors consisting of elements of types r_i and r_{ij}^a , respectively.

Separating the equation for r_m gives

$$\sum_n \langle \Phi_m | \mathcal{H} | \Phi_n \rangle r_n + \sum_{ija} \langle \Phi_m | \mathcal{H} | \Phi_{ij}^a \rangle r_{ij}^a = r_m \omega_m; \quad (14.94)$$

now multiplying on the right by r_m^{-1} we have

$$\langle \Phi_m | \mathcal{H} | \Phi_m \rangle + \sum_{n \neq m} \langle \Phi_m | \mathcal{H} | \Phi_n \rangle r_n r_m^{-1} + \sum_{ija} \langle \Phi_m | \mathcal{H} | \Phi_{ij}^a \rangle r_{ij}^a r_m^{-1} = \omega_m. \quad (14.95)$$

For the remaining equations we define the vectors

$$|\tilde{\Phi}\rangle = |\Phi^{(0,1)'} \quad \Phi^{(1,2)}\rangle, \quad (14.96)$$

$$\tilde{\mathbf{r}} = \begin{pmatrix} \mathbf{r}^{(0,1)'} \\ \mathbf{r}^{(1,2)} \end{pmatrix} \quad (14.97)$$

and the adjoint column vector $\langle \tilde{\Phi} |$. The prime on $(0, 1)$ indicates the omission of Φ_m and r_m . These equations now take the form

$$\langle \tilde{\Phi} | \mathcal{H} | \Phi_m \rangle + \langle \tilde{\Phi} | \mathcal{H} | \tilde{\Phi} \rangle \tilde{r}_m^{-1} = \tilde{r}_m \omega_m r_m^{-1}. \quad (14.98)$$

From (14.91), however,

$$\langle \Phi_m | \hat{H}^{\text{eff}} | \Phi_m \rangle = \langle \Phi_m | \mathcal{H} (1 + \hat{S}^{(0,1)}) | \Phi_m \rangle. \quad (14.99)$$

Identifying $\langle \Phi_m | \hat{H}^{\text{eff}} | \Phi_m \rangle$ with ω_m (which it equals when \mathbf{H}^{eff} is digonalized) and $\mathbf{S}^{(0,1)}$ with $\langle \tilde{\Phi} | \hat{S}^{(0,1)} | \Phi^{(0,1)} \rangle = \tilde{r}_m r_m^{-1}$, we regain the valence-universal \mathbf{H}^{eff} . Furthermore, the VU amplitude equation (14.98) becomes

$$\langle \tilde{\Phi} | \mathcal{H} | \Phi^{(0,1)} \rangle + \langle \tilde{\Phi} | \mathcal{H} | \tilde{\Phi} \rangle (\mathbf{S}^{(0,1)} - \mathbf{S}^{(0,1)} \mathbf{H}^{\text{eff}}) = \mathbf{0}. \quad (14.100)$$

With minor modifications we can identify any number of orbitals as active, treating active hole states similarly to state m . It does not matter which orbitals are actually active. Each principal ionization potential for any orbital in IP-EOM-CC can be obtained and, unlike a true multireference theory, expanding the number of active orbitals does not provide any better an approximation. In the event that all orbitals are active, we also have the simplification that there are no single excitation contributions to the amplitude equations for $\hat{S}_2^{(0,1)}$.

14.5 Intermediate-Hamiltonian Fock-space MRCC

The *intermediate Hamiltonian* (IH) approach was introduced by Malrieu, Durand and Daudey (1985) in order to overcome intruder-state problems in perturbative and other methods. Its original primary application was to quasidegenerate perturbation theory, but it was also used to provide “dressings” for extensivity-corrected multireference configuration interaction (Daudey, Heully and Malrieu 1993). Applications of this approach to Fock-space multireference coupled-cluster theory mostly use a similarity-transformation technique (Stolarczyk and Monkhorst 1985, Meissner and Nooijen 1995, Meissner 1998, Meissner and Malinowski 2000). Here we shall focus on the approach in Meissner (1998).

Intruder states are \hat{Q} -space states with energies close to or within the range of the energies of the model states. They are particularly common in complete-model-space treatments, because such spaces tend to include high-energy multiple-excitation model states that contribute little to the wave function but are included merely for completeness. The intruder states tend to be single (or very low) excitations into the lowest part of the inactive particle space or from the highest part of the inactive hole space. Because

they generate very small or negative energy denominators in perturbative or iterative solution procedures, they often result in divergence or severe convergence difficulties. Intruder states also tend to occur at regions of avoided crossings, where they often cause discontinuities in potential-energy curves and surfaces (Malrieu, Durand and Daudey 1985).

The intermediate-Hamiltonian approach overcomes intruder-state problems by interposing a buffer space between the model space and the rest of the \hat{Q} -space. The total space is divided into three subspaces (Fig. 14.8):

1. the main model space M , of dimension n , whose projector is \hat{P} (this is the original model space of the problem). Its complement has the projector \hat{Q} ;
2. the intermediate space M' , of dimension n' and projector \hat{P}' , usually consisting of a part of the original \hat{Q} -space closest in energy to M and including the states responsible for the intruder problems;
3. the rest of the \hat{Q} -space, with projector $\hat{Q}_I = \hat{Q} - \hat{P}'$.

The intermediate Hamiltonian \hat{H}^{int} operates in the augmented model space $M_I = M \cup M'$, the union of the main and intermediate spaces; M_I has dimension $n_I = n + n'$ and projector $\hat{P}_I = \hat{P} + \hat{P}'$, while the effective

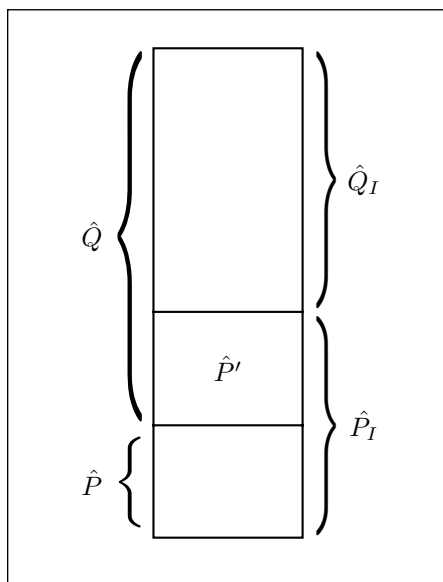


Fig. 14.8. Projectors for the various subspaces in the intermediate-Hamiltonian approach.

Hamiltonian \hat{H}^{eff} is defined in the main model space M . We have

$$\hat{P} + \hat{Q} = \hat{P}_I + \hat{Q}_I = \hat{1}. \quad (14.101)$$

In the usual Fock-space MRCC the solution of the amplitude equations provides an effective Hamiltonian \hat{H}^{eff} , of dimension n , which can be diagonalized to produce n eigensolutions that are equal to a subset of the eigensolutions of \hat{H} . The intermediate Hamiltonian \hat{H}^{int} , of dimension n_I , is defined on the \hat{P}_I -space, and n of its eigenvalues are required to be equal to the corresponding eigenvalues of \hat{H}^{eff} . The remaining $n_I - n$ eigenvalues are essentially arbitrary. They may (but need not) be rough approximations to the eigenvalues of \hat{H} . Because no requirements are imposed on this extra set of solutions, this procedure can be used to protect the main model space from intruder states in the low-lying part of the \hat{Q} -space.

Because of the arbitrariness of the extra solutions produced by \hat{H}^{int} , the intermediate Hamiltonian and the equations determining it are not unique. Different variants of the intermediate-Hamiltonian approach, using different auxiliary conditions to define a unique \hat{H}^{int} , have been proposed and applied. A particularly convenient and effective version of this approach when the objective is limited to obtaining energies, without wave functions, is the similarity-transformation method of Meissner (1998).

We first consider a general similarity-transformation treatment that is analogous to the Fock-space MRCC approach of the previous section. We note that the valence-universal wave operator is $\Omega = \{e^{\tilde{S}}\} = e^{\hat{T}}\{e^{\Delta\tilde{S}}\}$ and define a new operator \hat{X} , such that

$$\hat{X} = \{e^{\Delta\tilde{S}} - 1\}, \quad \hat{X} = \hat{Q}\hat{X}\hat{P}, \quad (14.102)$$

and for which

$$\hat{X}^2 = 0, \quad e^{\hat{X}} = 1 + \hat{X}, \quad e^{-\hat{X}} = 1 - \hat{X}. \quad (14.103)$$

Next we introduce a similarity transformation of the CC-transformed Hamiltonian $\mathcal{H} = e^{-\hat{T}}\hat{H}e^{\hat{T}}$ (Meissner 1998),

$$\tilde{H} = e^{-\hat{X}}\mathcal{H}e^{\hat{X}} = (1 - \hat{X})\mathcal{H}(1 + \hat{X}) \quad (14.104)$$

and require this transformation to satisfy the equation

$$\hat{Q}(1 - \hat{X})\mathcal{H}(1 + \hat{X})\hat{P} = 0 \quad (14.105)$$

in successive sectors of Fock space, according to the subsystem embedding condition. Writing this equation in the form

$$\hat{Q}\mathcal{H}(1 + \hat{X})\hat{P} - \hat{Q}\hat{X}\hat{P}\mathcal{H}(1 + \hat{X})\hat{P} = 0 \quad (14.106)$$

and noting that (14.83) for the FS effective Hamiltonian can be written as

$$\hat{P}\mathcal{H}(1 + \hat{X})\hat{P} = \hat{H}^{\text{eff}}, \quad (14.107)$$

we have

$$\hat{Q}\mathcal{H}(1 + \hat{X})\hat{P} - \hat{Q}\hat{X}\hat{P}\hat{H}^{\text{eff}}\hat{P} = 0, \quad (14.108)$$

which is equivalent to the Bloch equation (14.82).

Equation (14.105) is a quadratic equation in \hat{X} and thus has multiple solutions. Also, this procedure suffers from the intruder-state problem. To overcome these difficulties we introduce the intermediate-Hamiltonian approach by splitting the transformation (14.104) into two successive transformations, as follows:

$$\tilde{H} = e^{-\hat{Z}}e^{-\hat{Y}}\mathcal{H}e^{\hat{Y}}e^{\hat{Z}} = (1 - \hat{Z})(1 - \hat{Y})\mathcal{H}(1 + \hat{Y})(1 + \hat{Z}), \quad (14.109)$$

where

$$\hat{Y} = \hat{Q}_I\hat{X} = \hat{Q}_I\hat{Y}\hat{P}, \quad \hat{Z} = \hat{P}'\hat{X} = \hat{P}'\hat{Z}\hat{P} \quad (14.110)$$

and

$$\hat{X} = \hat{Y} + \hat{Z}, \quad (14.111)$$

$$1 + \hat{X} = (1 + \hat{Y})(1 + \hat{Z}), \quad 1 - \hat{X} = (1 - \hat{Z})(1 - \hat{Y}) \quad (14.112)$$

(the last line follows because $\hat{Y}\hat{Z} = \hat{Z}\hat{Y} = 0$).

For an IH-CCSD calculation the \hat{P}' subspace for the $(1, 1)$ sector consists of single excitations, while double excitations are put into the \hat{Q}_I -subspace. Explicitly, noting (14.102) and (14.111), the \hat{Z} and \hat{Y} operators are given by

$$\hat{Z} = \{\hat{S}_1^{(1,0)} + \hat{S}_1^{(0,1)} + \hat{S}_1^{(1,0)}\hat{S}_1^{(0,1)} + \hat{S}_2^{(1,1)}\}\hat{P}^{(1,1)}, \quad (14.113)$$

$$\hat{Y} = \{\hat{S}_2^{(1,0)} + \hat{S}_2^{(0,1)} + \hat{S}_1^{(1,0)}\hat{S}_2^{(0,1)} + \hat{S}_2^{(1,0)}\hat{S}_1^{(0,1)} + \hat{S}_2^{(1,0)}\hat{S}_2^{(0,1)}\}\hat{P}^{(1,1)} \quad (14.114)$$

(Bartlett and Musiał 2007).

The intermediate-Hamiltonian treatment starts with a conventional CC calculation for the Fermi-vacuum state (i.e. the $(0,0)$ sector) and construction of the CC transformed Hamiltonian \mathcal{H} . This step is followed by solution of the $(1,0)$ and $(0,1)$ sectors, either by VU-CC, as described in Section 14.4, or by EA-EOM and IP-EOM (Chapter 13). The principal eigenvalues obtained by these two methods should be the same, as discussed in subsection 14.4.4, while the eigenvectors would differ in their normalization. This procedure provides all the s amplitudes needed for the determination of \hat{Y} using (14.114).

Assuming that our objective is limited to obtaining energies, not wave functions, we do not need to evaluate \hat{Z} because $\hat{P}_I(1 - \hat{X})\mathcal{H}(1 + \hat{X})\hat{P}_I$ and $\hat{P}_I(1 - \hat{Y})\mathcal{H}(1 + \hat{Y})\hat{P}_I$ are related by a similarity transformation via $e^{\hat{Z}}$, as seen in (14.109), and thus have the same eigenvalues. As a result, we do not need to evaluate $\hat{S}_2^{(1,1)}$, the last term in (14.113), thus avoiding the need to solve the (1,1) sector. The next step is then the evaluation of the intermediate Hamiltonian

$$\hat{H}^{\text{int}} = \hat{P}_I \hat{H}^{\text{int}} \hat{P}_I = \hat{P}_I(1 - \hat{Y})\mathcal{H}(1 + \hat{Y})\hat{P}_I = \hat{P}_I\mathcal{H}(1 + \hat{Y})\hat{P}_I, \quad (14.115)$$

which is analogous to (14.107) for the effective Hamiltonian. The diagonalization of \hat{H}^{int} then provides the desired n eigenvalues, plus n' additional eigenvalues deriving from the contributions of the original buffer space \hat{P}' and likely to contain any intruder-state effects.

A diagrammatic representation of the intermediate Hamiltonian for IH-CCSD, derived from (14.114), (14.115), is shown in Fig. 14.9 (Bartlett and Musiał 2007). The representation includes disconnected diagrams but ex-

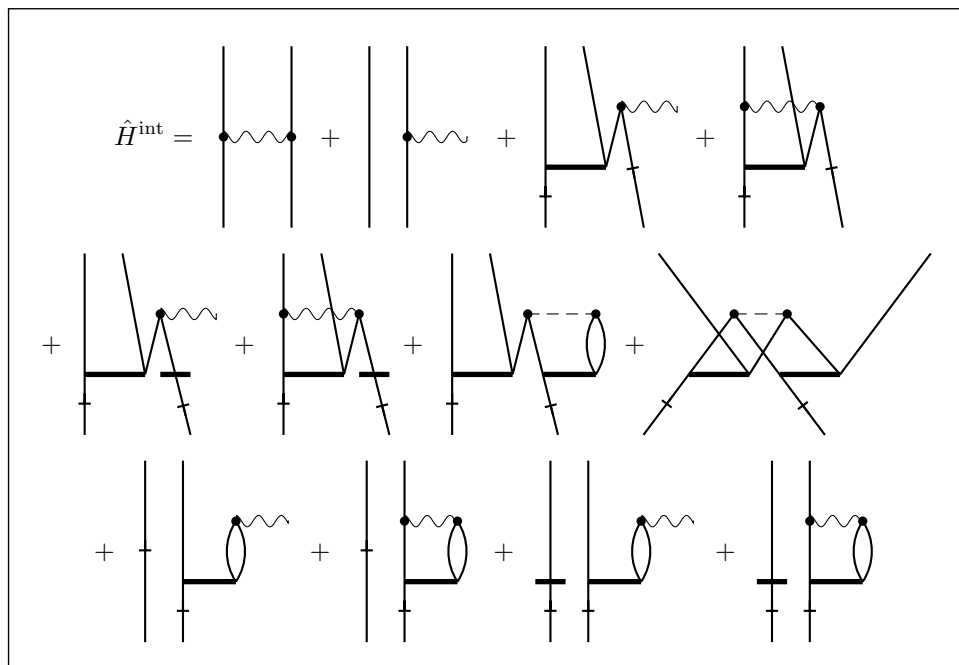


Fig. 14.9. Diagrammatic representation in skeletal form of the intermediate Hamiltonian for IH-FS-MRCCSD (Bartlett and Musiał 2007). The initial and final states in all diagrams are restricted to be in the \hat{P}_I -space.

Table 14.2. Vertical excitation energies, in eV, for the N_2 , C_2 and H_2O molecules and the neon atom calculated using the IH-CC and EOM-CC methods. The full-CI values are given for comparison^a

State	FCI ^b	IH-CC		EOM-CC	
		CCSD	CCSDT	CCSD	CCSDT
N ₂ (9, 4) ^c					
¹ Π _g	9.584	−0.333	0.028	0.081	0.009
¹ Σ _u [−]	10.329	−0.102	0.005	0.136	0.004
¹ Δ _u	10.718	−0.009	0.010	0.189	0.008
¹ Π _u	13.608	0.312	0.162	0.401	0.053
C ₂ (8, 3) ^c					
¹ Π _u	1.385	0.017	−0.005	0.089	0.034
¹ Σ _u ⁺	5.602	0.317	0.069	0.197	0.112
H ₂ O (4, 4) ^c					
¹ B ₁	7.447	0.095	−0.009	−0.072	−0.029
¹ A ₂	9.211	0.138	−0.015	−0.089	−0.033
¹ A ₁	9.874	0.111	−0.005	−0.068	−0.029
Ne (7, 4) ^c					
¹ P ⁰	16.398	−0.245	−0.022	−0.240	−0.026
¹ D	18.213	−0.206	−0.004	−0.250	−0.028
¹ P	18.256	−0.220	0.000	−0.251	−0.028
¹ S	18.485	−0.309	−0.047	−0.237	−0.035

^aMusiał and Bartlett (2008). The IH-CC and EOM-CC values are deviations from FCI (in eV). The inner-shell electrons are frozen.

^bThe calculations of Christiansen, Koch, Jørgensen *et al.* (1996) for N_2 , C_2 and H_2O , which include a description of the geometries and basis sets, and of Koch, Christiansen, Jørgensen *et al.* (1995) for Ne.

^cThe notation (m, n) indicates an active space of m spatial-orbital particles and n holes (which equals $2m$ spinorbital particles and $2n$ holes).

tensivity is preserved because the disconnected terms cancel in the diagonalization process.

An extension of the intermediate-Hamiltonian treatment to the IH-CCSDT case has been described by Musiał and Bartlett (2008). They provide a number of sample applications at both the MRCCSD and MRCCSDT levels and give comparisons with EOM-CC and the full-CI results. Their results are shown here in Table 14.2.

References

- Adams, B. G. and Paldus, J. (1979). Orthogonally-spin-adapted coupled-cluster theory for closed-shell systems including triexcited clusters, *Phys. Rev. A* **20**, 1–17.
- Adams, B. G., Jankowski, K. and Paldus, J. (1979). Quasi-degeneracy and coupled-pair theories, *Chem. Phys. Lett.* **67**, 144–8.
- Adamowicz, L., Laidig, W. D. and Bartlett, R. J. (1984). Analytical gradients for the coupled-cluster method, *Int. J. Quantum Chem., Quantum Chem. Symp.* **18**, 245–54.
- Ahlrichs, R., Lischka, H., Staemmler, V. and Kutzelnigg, W. (1975). PNO-CI (pair natural orbital configuration interaction) and CEPA-PNO (coupled electron pair approximation with pair natural orbitals) calculations of molecular systems. I. Outline of the method for closed-shell states, *J. Chem. Phys.* **62**, 1225–34.
- Arponen, J. (1983). Variational principles and linked-cluster exp S expansions for static and dynamic many-body problems, *Ann. Phys. (New York)* **151**, 311–82.
- Arponen, J. S. and Bishop, R. F. (1991). Independent-cluster parametrizations of wave functions in model field theories. I. Introduction to their holomorphic representations, *Ann. Phys. (New York)* **207**, 171–217.
- Auer, A. A., Baumgartner, G., Bernholdt D. E. *et al.* (2006). Automatic code generation for many-body electronic structure methods: the tensor contraction engine, *Mol. Phys.* **104**, 211–28.
- Baker, H. F. (1905). Alternants and continuous groups, *Proc. London Math. Soc., Ser. 2* **3**, 24–47.
- Balková, A. and Bartlett, R. J. (1992). Coupled-cluster method for open-shell singlet states, *Chem. Phys. Lett.* **193**, 364–72.

- Balková, A. and Bartlett, R. J. (1994). A multireference coupled-cluster study of the ground and lowest excited states of cyclobutadiene, *J. Chem. Phys.* **101**, 8972–87.
- Balková, A. and Bartlett, R. J. (1995). On the singlet–triplet separation in methylene. A critical comparison of single- versus two-determinant (generalized valence bond) coupled-cluster theory, *J. Chem. Phys.* **102**, 7116–23.
- Bartlett, R. J. (1981). Many-body perturbation theory and coupled cluster theory for electron correlation in molecules, *Ann. Rev. Phys. Chem.* **32**, 359–401.
- Bartlett, R. J. (1986). Analytical evaluation of gradients in coupled-cluster and many-body perturbation theory, in *Geometrical Derivatives of Energy Surfaces and Molecular Properties*, eds. P. Jørgensen and J. Simons (Reidel, Dordrecht), pp. 35–61.
- Bartlett, R. J. (1989). Coupled-cluster approach to molecular structure and spectra: a step toward predictive quantum chemistry, *J. Phys. Chem.* **93**, 1697–708.
- Bartlett, R. J. (1995). Coupled-cluster theory: an overview of recent developments, in *Modern Electronic Structure Theory, Part I*, ed. D. R. Yarkony (World Scientific, Singapore), pp. 1047–131.
- Bartlett, R. J. (2005). How and why coupled-cluster theory became the preeminent method in ab initio quantum chemistry, in *Theory and Applications of Computational Chemistry. The First Forty Years*, eds. C. Dykstra, G. Frenking, K. Kim and G. Scuseria (Elsevier, Amsterdam), pp. 1191–221.
- Bartlett, R. J. and Brändas, E. J. (1972). Reduced partitioning procedure in configuration interaction studies. I. Ground states, *J. Chem. Phys.* **56**, 5467–77.
- Bartlett, R. J., Cole, S. J., Purvis, G. D., Ermler, W. C., Hsieh, H. C. and Shavitt, I. (1987). The quartic force field of H₂O determined by many-body methods. II. Effects of triple excitations, *J. Chem. Phys.* **87**, 6579–91.
- Bartlett, R. J., Grabowski, I., Hirata, S. and Ivanov, S. (2005). The exchange-correlation potential in *ab initio* density functional theory, *J. Chem. Phys.* **122**, 034104-1–12.
- Bartlett, R. J., Kucharski, S. A., Noga, J., Watts, J. D. and Trucks, G. W. (1989). Some consideration of alternative ansätze in coupled-cluster theory, in *Many-Body Methods in Quantum Chemistry (Lecture Notes in Chemistry, No. 52)*, ed. U. Kaldor (Springer, Berlin), pp. 125–49.

- Bartlett, R. J. and Musiał, M. (2007). Coupled-cluster theory in quantum chemistry, *Rev. Mod. Phys.* **79**, 291–352.
- Bartlett, R. J. and Noga, J. (1988). The expectation value coupled-cluster method and analytical energy derivatives, *Chem. Phys. Lett.* **150**, 29–36.
- Bartlett, R. J. and Purvis III, G. D. (1978). Many-body perturbation theory, coupled-pair many-electron theory, and the importance of quadruple excitations for the correlation problem, *Int. J. Quantum Chem.* **14**, 561–81.
- Bartlett, R. J. and Purvis III, G. D. (1980). Molecular applications of coupled cluster and many-body perturbation methods, *Phys. Scripta* **21**, 255–65.
- Bartlett, R. J., Sekino, H. and Purvis III, G. D. (1983). Comparison of MBPT and coupled-cluster methods with full CI. Importance of triple excitations and infinite summations, *Chem. Phys. Lett.* **98**, 66–71.
- Bartlett, R. J. and Shavitt, I. (1977a). Determination of the size-consistency error in the single and double excitation configuration interaction model, *Int. J. Quantum Chem., Quantum Chem. Symp.* **11**, 165–73. Erratum (1978). *Int. J. Quantum Chem., Quantum Chem. Symp.* **12**, 543–4.
- Bartlett, R. J. and Shavitt, I. (1977b). Comparison of high-order many-body perturbation theory and configuration interaction for H₂O, *Chem. Phys. Lett.* **50**, 190–8. Erratum (1978). *Chem. Phys. Lett.* **57**, 157–8.
- Bartlett, R. J., Shavitt, I. and Purvis III, G. D. (1979). The quartic force field of H₂O determined by methods that include quadruple excitation effects, *J. Chem. Phys.* **71**, 281–91.
- Bartlett, R. J. and Silver, D. M. (1974a). Correlation energy in LiH, BH, and HF with many-body perturbation theory using Slater-type atomic orbitals, *Int. J. Quantum Chem., Quantum Chem. Symp.* **8**, 271–6. Erratum (1976). *Int. J. Quantum Chem.* **10**, 185–6.
- Bartlett, R. J. and Silver, D. M. (1974b). Many-body perturbation theory applied to hydrogen fluoride, *Chem. Phys. Lett.* **29**, 199–203. Erratum (1976). *Chem. Phys. Lett.* **37**, 198.
- Bartlett, R. J. and Stanton, J. F. (1994). Applications of post-Hartree–Fock methods: a tutorial, *Rev. Comput. Chem.* **5**, 65–169.
- Bartlett, R. J. and Watts, J. D. (1998). ACES II program system, in *Encyclopedia of Computational Chemistry*, eds. P. v. R. Schleyer,

- N. L. Allinger, T. Clark *et al.* (John Wiley & Sons, Chichester, UK), Vol. 1, pp. 1–7.
- Bartlett, R. J., Watts, J. D., Kucharski, S. A. and Noga, J. (1990). Non-iterative fifth-order triple and quadruple excitation energy corrections in correlated methods, *Chem. Phys. Lett.* **165**, 513–22.
- Bauschlicher Jr, C. W., Langhoff, S. R., Taylor, P. R., Handy, N. C. and Knowles P. J. (1986). Benchmark full configuration-interaction calculations on HF and NH₂, *J. Chem. Phys.* **85**, 1469–74.
- Bauschlicher Jr, C. W. and Taylor P. R. (1986). Benchmark full configuration-interaction calculations on H₂O, F, and F[−], *J. Chem. Phys.* **85**, 2779–83.
- Bethe, H. E. (1956). Nuclear many-body problem, *Phys. Rev.* **103**, 1353–90.
- Bethe H. E. and Goldstone, J. (1957). Effect of a repulsive core in the theory of complex nuclei, *Proc. R. Soc. (London) A* **238**, 551–67.
- Bethe H. E. and Salpeter, E. E. (1957). *Quantum Mechanics of One- and Two-Electron Atoms* (Springer, Berlin), pp. 122–3.
- Binkley, J. S. and Pople, J. A. (1975). Møller–Plesset theory for atomic ground state energies, *Int. J. Quantum Chem.* **9**, 229–36.
- Bloch, C. (1958). Sur la théorie des perturbations des états liés, *Nuc. Phys.* **6**, 329–47.
- Bloch, C. and Horowitz, J. (1958). Sur la détermination des premiers états d'un système de fermions dans le cas dégénéré, *Nuc. Phys.* **8**, 91–105.
- Bomble, Y. J., Stanton, J. F., Kállay, M. and Gauss, J. (2005). Coupled-cluster methods including noniterative corrections for quadruple excitations, *J. Chem. Phys.* **123**, 054101-1–8.
- Brändas, E. and Goscinski, O. (1970). Variation-perturbation expansions and Padé approximants to the energy, *Phys. Rev. A* **1**, 552–60.
- Brandow, B. (1966). Linked-cluster expansion for open-shell nuclei, in *Proceedings of the International School of Physics “Enrico Fermi”, Course 36*, ed C. Bloch (Academic Press, New York), pp. 496–512.
- Brandow, B. H. (1967). Linked-cluster expansions for the nuclear many-body problem, *Rev. Mod. Phys.* **39**, 771–828.
- Brandow, B. H. (1977). Linked-cluster perturbation theory for closed- and open-shell systems, *Adv. Quantum Chem.* **10**, 187–249.
- Brillouin, L. (1932). Les problèmes de perturbations et le champs self-consistents, *J. Phys. Radium, Ser. 7* **3**, 373–89.
- Brillouin, L. (1933a). Champs self-consistents et électron métalliques (III), *J. Phys. Radium, Ser. 7* **4**, 1–9.

- Brillouin, L. (1933b). La méthode du champ self-consistent, *Actual. Sci. Ind.*, No. 71.
- Brillouin, L. (1934). Les champs “self-consistents” de Hartree et de Fock, *Actual. Sci. Ind.*, No. 159.
- Brueckner, K. A. (1955). Many-body problem for strongly interacting particles. II. Linked cluster expansion, *Phys. Rev.* **100**, 36–45.
- Brueckner, K. A. and Levinson, C. A. (1955). Approximate reduction of the many-body problem for strongly interacting particles to a problem of self-consistent fields, *Phys. Rev.* **97**, 1344–52.
- Burton, P. G., Buenker, R. J., Bruna P. J. and Peyerimhoff, S. D. (1983). Comparison of perturbatively corrected MRD CI results with a full CI treatment of the BH ground state, *Chem. Phys. Lett.* **95**, 379–85.
- Campbell, J. E. (1897). On the law of combination of operators bearing on the theory of continuous transformation groups, *Proc. London Math. Soc.* **28**, 381–90.
- Chan, G. K.-L., Kállay, M. and Gauss, J. (2004). State-of-the-art density matrix renormalization group and coupled cluster theory studies of the nitrogen binding curve, *J. Chem. Phys.* **121**, 6110–6.
- Chattopadhyay, S., Mahapatra, U. S. and Mukherjee, D. (1999). Property calculations using perturbed orbitals via state-specific multireference coupled cluster and perturbation theories, *J. Chem. Phys.* **111**, 3820–31.
- Chaudhuri, R., Mukhopadhyay Jr, D. and Mukherjee, D. (1989). Applications of open-shell coupled cluster theory using an eigenvalue-independent partitioning technique: approximate inclusion of triples in IP calculations, *Chem. Phys. Lett.* **162**, 393–8.
- Chaudhuri, R., Sinha, D. and Mukherjee, D. (1989). On the extensivity of the roots of effective Hamiltonians in many-body formalisms employing incomplete model spaces, *Chem. Phys. Lett.* **163**, 165–70.
- Chiles, R. A. and Dykstra, C. E. (1981). An electron pair operator approach to coupled cluster wave functions. Application to He_2 , Be_2 , and Mg_2 and comparison with CEPA methods, *J. Chem. Phys.* **74**, 4544–56.
- Christiansen, O., Jørgensen, P. and Hättig, C. (1998). Response functions from Fourier component variational perturbation theory applied to a time-averaged quasienergy, *Int. J. Quantum Chem.* **68**, 1–52.
- Christiansen, O., Koch, H., Jørgensen, P. and Olsen, J. (1996). Excitation energies of H_2O , N_2 and C_2 in full configuration interaction and coupled cluster theory, *Chem. Phys. Lett.* **256**, 185–94.

- Čížek, J. (1966). On the correlation problem in atomic and molecular systems. Calculation of wavefunction components in Ursell-type expansion using quantum-field theoretical methods, *J. Chem. Phys.* **45**, 4256–66.
- Čížek, J. (1969). On the use of the cluster expansion and the technique of diagrams in calculations of correlation effects in atoms and molecules, *Adv. Chem. Phys.* **14**, 35–89.
- Čížek, J. and Paldus, J. (1967). Stability conditions for the solution of the Hartree–Fock equations for atomic and molecular systems. Application to the pi-electron model of cyclic polyenes, *J. Chem. Phys.* **47**, 3976–85.
- Čížek, J. and Paldus, J. (1971). Correlation problems in atomic and molecular systems III. Rederivation of the coupled-pair many-electron theory using the traditional quantum chemical methods, *Int. J. Quantum Chem.* **5**, 359–79.
- Coester, F. (1958). Bound states of a many-particle system, *Nucl. Phys.* **7**, 421–4.
- Coester, F. and Kümmel, H. (1960). Short-range correlation in nuclear wave functions, *Nucl. Phys.* **17**, 477–85.
- Comeau, D. C. and Bartlett, R. J. (1993). The equation-of-motion coupled-cluster method. Applications to open- and closed-shell reference states, *Chem. Phys. Lett.* **207**, 414–23.
- Crawford, T. D. and Sekino, H. (2009). On the performance of a size-extensive variant of equation-of-motion coupled cluster theory for optical rotation in chiral molecules, *Prog. Theor. Chem. Phys.*, in press.
- Crawford, T. D. and Stanton, J. F. (1998). Investigation of an asymmetric triple-excitation correction for coupled-cluster energies, *Int. J. Quantum Chem.* **70**, 601–11.
- Dalgaard, E. and Monkhorst, H. J. (1983). Some aspects of the time-dependent coupled-cluster approach to dynamic response functions, *Phys. Rev. A* **28**, 1217–22.
- Dalgarno, A. and Stewart, A. L. (1958). A perturbation calculation of properties of the helium iso-electronic sequence, *Proc. R. Soc. (London) A* **247**, 245–59.
- Daudey, J.-P., Heully, J.-L. and Malrieu, J.-P. (1993). Size-consistent self-consistent truncated or selected configuration interaction, *J. Chem. Phys.* **99**, 1240–54.

- Davidson, E. R. (1974). Configuration interaction description of electron correlation, in *The World of Quantum Chemistry*, eds. R. Daudel and B. Pullman (Reidel, Dordrecht), pp. 17–30.
- Davidson, E. R. (1975). The iterative calculation of a few of the lowest eigenvalues and corresponding eigenvectors of large real-symmetric matrices, *J. Comput. Phys.* **17**, 87–94.
- Davidson, E. R. and Silver, D. W. (1977). Size consistency in the dilute helium gas electronic structure, *Chem. Phys. Lett.* **52**, 403–6.
- Dirac, P. A. M. (1927). The quantum theory of the emission and absorption of radiation, *Proc. R. Soc. (London) A* **114**, 243–65.
- Ditchfield, R. (1974). Self-consistent perturbation theory of diamagnetism. I. A gauge-invariant LCAO method for N.M.R. chemical shifts, *Mol. Phys.* **27**, 789–807.
- Dunning Jr, T. H. (1989). Gaussian basis sets for use in correlated molecular calculations. I. The atoms boron through neon and hydrogen, *J. Chem. Phys.* **90**, 1007–23.
- Dyson, F. J. (1949a). The radiation theories of Tomonaga, Schwinger, and Feynman, *Phys. Rev.* **75**, 486–502.
- Dyson, F. J. (1949b). The *S* matrix in quantum electrodynamics, *Phys. Rev.* **75**, 1736–55.
- Emrich, K. (1981). An extension of the coupled cluster formalism to excited states, *Nucl. Phys. A* **351**, 379–96.
- Epstein, P. S. (1926). The Stark effect from the point of view of Schroedinger's quantum theory, *Phys. Rev.* **28**, 695–710.
- Evangelista, F. A., Allen, W. D. and Schaefer III, H. F. (2006). High-order excitations in state-universal and state-specific multireference coupled cluster theories: model systems, *J. Chem. Phys.* **125**, 154113-1–16.
- Feynman, R. P. (1949a). The theory of positrons, *Phys. Rev.* **76**, 749–59.
- Feynman, R. P. (1949b). Space-time approach to quantum electrodynamics, *Phys. Rev.* **76**, 769–89.
- Frantz, L. M. and Mills, R. L. (1960). Many-body basis for the optical model, *Nucl. Phys.* **15**, 16–32.
- Gauss, J. (1993). Effects of electron correlation in the calculation of nuclear magnetic resonance chemical shifts, *J. Chem. Phys.* **99**, 3629–43.
- Gauss, J., Lauderdale, W. J., Stanton, J. F., Watts, J. D. and Bartlett, R. J. (1991). Analytic energy gradients for open-shell coupled-cluster singles and doubles (CCSD) calculations using restricted open-shell Hartree-Fock (ROHF) reference functions, *Chem. Phys. Lett.* **182**, 207–15.

- Gauss, J., Ruud, K. and Helgaker, T. (1996). Perturbation-dependent atomic orbitals for the calculation of spin-rotation constants and rotational g tensors, *J. Chem. Phys.* **105**, 2804–12.
- Gauss, J. and Stanton, J. F. (1995). Gauge-invariant calculation of nuclear magnetic shielding constants at the coupled-cluster singles and doubles level, *J. Chem. Phys.* **102**, 251–3.
- Gauss, J. and Stanton, J. F. (2000). Analytic first and second derivatives for the CCSDT- n ($n = 1-3$) models: a first step toward the efficient calculation of CCSDT properties, *Phys. Chem. Chem. Phys.* **2**, 2047–60.
- Gauss, J., Stanton, J. F. and Bartlett, R. J. (1991). Analytic evaluation of energy gradients at the coupled-cluster singles and doubles level using quasi-restricted Hartree–Fock open-shell reference functions, *J. Chem. Phys.* **95**, 2639–45.
- Gerratt, J. and Mills, I. M. (1968). Force constants and dipole-moment derivatives of molecules from perturbed Hartree–Fock calculations. I, *J. Chem. Phys.* **49**, 1719–29.
- Goldstone, J. (1957). Derivation of the Brueckner many-body theory, *Proc. R. Soc. (London) A* **239**, 267–79.
- Goscinski, O. (1967). Continued fractions and upper and lower bounds in the Brillouin–Wigner perturbation scheme, *Int. J. Quantum Chem.* **1**, 769–80.
- Gwaltney, S. R. and Head-Gordon, M. (2001). A second-order perturbative correction to the coupled-cluster singles and doubles method: CCSD(2), *J. Chem. Phys.* **115**, 2014–21.
- Handy, N. C., Pople, J. A., Head-Gordon, M., Raghavachari, K. and Trucks, G. W. (1989). Size-consistent Brueckner theory limited to double substitutions, *Chem. Phys. Lett.* **164**, 185–92.
- Handy, N. C. and Schaefer III, H. F. (1984). On the evaluation of analytic energy derivatives for correlated wave functions, *J. Chem. Phys.* **81**, 5031–3.
- Haque, M. A. and Mukherjee, D. (1984). Application of cluster expansion techniques to open-shells: calculation of difference energies, *J. Chem. Phys.* **80**, 5058–69.
- Harris, F. E., Monkhorst, H. J. and Freeman, D. L. (1992). *Algebraic and Diagrammatic Methods in Many-Fermion Theory* (Oxford University Press, New York).
- Hausdorff, F. (1906). Die symbolische Exponentialformel in der Gruppentheorie, *Ber. Verhandl. Sächs. Akad. Wiss. Leipzig, Math.-Naturw. Kl.* **58**, 19–48.

- Hirao, K. and Nakatsuji, H. (1978a). Cluster expansion of the wave function. Structure of the closed-shell orbital theory, *J. Chem. Phys.* **69**, 4535–47.
- Hirao, K. and Nakatsuji, H. (1978b). Cluster expansion of the wave function. The open-shell orbital theory including electron correlation, *J. Chem. Phys.* **69**, 4548–63.
- Hirata, S. (2003). Tensor contraction engine: abstraction and automated parallel implementation of configuration-interaction, coupled-cluster, and many-body perturbation theory, *J. Phys. Chem. A* **107**, 9887–97.
- Hirata, S. (2004). Higher-order equation-of-motion coupled-cluster methods, *J. Chem. Phys.* **121**, 51–9.
- Hirata, S. and Bartlett, R. J. (2000). High-order coupled-cluster calculations through connected octuple excitations, *Chem. Phys. Lett.* **321**, 216–24.
- Hirata, S., Fan, P.-D., Auer, A. A., Nooijen, M. and Piecuch, P. (2004). Combined coupled-cluster and many-body perturbation theories, *J. Chem. Phys.* **121**, 12187–207.
- Hirata, S., Nooijen, M. and Bartlett, R. J. (2000a). High-order determinantal equation-of-motion coupled-cluster calculations for electronic excited states, *Chem. Phys. Lett.* **326**, 255–62.
- Hirata, S., Nooijen, M. and Bartlett, R. J. (2000b). High-order determinantal equation-of-motion coupled-cluster calculations for ionized and electron-attached states, *Chem. Phys. Lett.* **328**, 459–68.
- Hirschfelder, J. O., Byers-Brown, W. and Epstein, S. T. (1964). Recent developments in perturbation theory, *Adv. Quantum Chem.* **1**, 255–374.
- Hose, G. and Kaldor, U. (1979). Diagrammatic many-body perturbation theory for general model spaces, *J. Phys. B* **12**, 3827–55.
- Hose, G. and Kaldor, U. (1980). A general model space diagrammatic perturbation theory, *Phys. Scripta* **21**, 357–61.
- Hose, G. and Kaldor, U. (1982). Quasidegenerate perturbation theory, *J. Phys. Chem.* **86**, 2133–40.
- Hose, G. and Kaldor, U. (1984). General-model-space many-body perturbation theory: the $(2s\ 3p)^{1,3}P$ states in the Be isoelectronic sequence, *Phys. Rev. A* **30**, 2932–5.
- Hubač, I., Pittner, J. and Čársky, P. (2000). Size-extensivity correction for the state-specific multireference Brillouin–Wigner coupled-cluster theory, *J. Chem. Phys.* **112**, 8779–84.
- Hubbard, J. (1957). The description of collective motion in terms of many-body perturbation theory, *Proc. R. Soc. (London) A* **240**, 539–60.

- Hubbard, J. (1958a). The description of collective motion in terms of many-body perturbation theory. II. The correlation energy of a free-electron gas, *Proc. R. Soc. (London) A* **243**, 336–52.
- Hubbard, J. (1958b). The description of collective motion in terms of many-body perturbation theory. III. The extension of the theory to the non-uniform gas, *Proc. R. Soc. (London) A* **244**, 199–211.
- Huby, R. (1961). Formulae for non-degenerate Rayleigh–Schrödinger perturbation theory in any order, *Proc. Phys. Soc. (London)* **78**, 529–36.
- Hugenholtz, N. M. (1957). Perturbation theory of large quantum systems, *Physica* **23**, 481–532.
- Hylleraas, E. A. (1930). Über den Grundterm der Zweielektronenprobleme von H^- , He, Li^+ , Be^{++} usw. *Z. Phys.* **65**, 209–25.
- Jana, D., Bandyopadhyay, D. and Mukherjee, D. (1999). Development and applications of relaxation-inducing cluster expansion theory for treating strong relaxation and differential correlation effects, *Theor. Chem. Acc.* **102**, 317–27.
- Jankowski, K. and Kowalski, K. (1999a). Physical and mathematical content of coupled-cluster equations: correspondence between coupled-cluster and configuration-interaction solutions, *J. Chem. Phys.* **110**, 3714–29.
- Jankowski, K. and Kowalski, K. (1999b). Physical and mathematical content of coupled-cluster equations. II. On the origin of irregular solutions and their elimination via symmetry adaptations, *J. Chem. Phys.* **110**, 9345–52.
- Jankowski, K. and Kowalski, K. (1999c). Physical and mathematical content of coupled-cluster equations. III. Model studies of dissociation processes for various reference states, *J. Chem. Phys.* **111**, 2940–51.
- Jankowski, K. and Kowalski, K. (1999d). Physical and mathematical content of coupled-cluster equations. IV. Impact of approximations to the cluster operator on the structure of solutions, *J. Chem. Phys.* **111**, 2952–59.
- Jankowski, K., Kowalski, K., Grabowski, I. and Monkhorst, H. J. (1999). Correspondence between physical states and solutions to the coupled-cluster equations, *Int. J. Quantum Chem.* **75**, 483–96.
- Jankowski, K. and Paldus, J. (1980). Applicability of coupled-pair theories to quasi-degenerate electronic states: a model study, *Int. J. Quantum Chem.* **18**, 1243–69.
- Janssen, C. L. and Schaefer III, H. F. (1991). The automated solution of second quantization equations with application to the coupled cluster approach, *Theor. Chim. Acta* **79**, 1–42.

- Jayatilaka, D. and Lee, T. J. (1993). Open-shell coupled-cluster theory, *J. Chem. Phys.* **98**, 9734–47.
- Jeziorski, B. and Monkhorst, H. J. (1981). Coupled-cluster methods for multidimensional reference states, *Phys. Rev. A* **24**, 1668–81.
- Jordan, P. and Klein, O. (1927). Zum Mehrkörperproblem der Quantentheorie, *Z. Phys.* **45**, 751–65.
- Jordan, P. and Wigner, E. P. (1928). Über das Paulische Äquivalenzverbot, *Z. Phys.* **47**, 631–51.
- Jørgensen, P. and Simons, J. (1983). *Ab initio* analytical molecular gradients and Hessians, *J. Chem. Phys.* **79**, 334–57.
- Kaldor, U. (1973a). Many-body perturbation-theory calculations with finite, bound basis sets, *Phys. Rev. A* **7**, 427–34.
- Kaldor, U. (1973b). Many-body perturbation-theory calculations for excited molecular states, *Phys. Rev. Lett* **31**, 1338–40.
- Kaldor, U. (1984). General model space perturbation theory: excitation and ionization of N₂, *J. Chem. Phys.* **81**, 2406–10.
- Kállay, M. and Gauss, J. (2003). Analytic first derivatives for general coupled-cluster and configuration interaction models, *J. Chem. Phys.* **119**, 2991–3004.
- Kállay, M. and Gauss, J. (2004). Analytic second derivatives for general coupled-cluster and configuration interaction models, *J. Chem. Phys.* **120**, 6841–8.
- Kállay, M. and Surján P. R. (2000). Computing coupled-cluster wave functions with arbitrary excitations, *J. Chem. Phys.* **113**, 1359–65.
- Kállay, M. and Surján, P. R. (2001). Higher excitations in coupled-cluster theory, *J. Chem. Phys.* **115**, 2945–54.
- Kelly, H. P. (1963). Correlation effects in atoms, *Phys. Rev.* **131**, 684–99.
- Kelly, H. P. (1964a). Correlation effects in many fermion systems. II. Linked clusters, *Phys. Rev.* **134**, A1450–3.
- Kelly, H. P. (1964b). Many-body perturbation theory applied to atoms, *Phys. Rev.* **136**, B896–B912.
- Kelly, H. P. (1968). Correlation structure in atoms, *Adv. Theor. Phys.* **2**, 75–169.
- Kelly, H. P. (1969). Application of many-body diagram techniques in atomic physics, *Adv. Chem. Phys.* **14**, 129–90.
- Koch, H., Christiansen, O., Jørgensen, P. and Olsen, J. (1995). Excitation energies of BH, CH₂ and Ne in full configuration interaction and the hierarchy CCS, CC2, CCSD and CC3 of coupled cluster models, *Chem. Phys. Lett.* **244**, 75–82.

- Koch, H., Christiansen, O., Kobayashi, R., Jørgensen, P. and Helgaker, T. (1994). A direct atomic orbital driven implementation of the coupled cluster singles and doubles (CCSD) model, *Chem. Phys. Lett.* **228**, 233–8.
- Koch, H. and Jørgensen, P. (1990). Coupled cluster response functions, *J. Chem. Phys.* **93**, 3333–44.
- Koch, H., Kobayashi, R., de Merás, A. S. and Jørgensen, P. (1994). Calculation of size-intensive transition moments from the coupled cluster singles and doubles linear response function, *J. Chem. Phys.* **100**, 4393–400.
- Koch, S. and Kutzelnigg, W. (1981). Comparison of CEPA and CP-MET methods, *Theor. Chim. Acta* **59**, 387–411.
- Kohn, W. and Sham, L. J. (1965). Self-consistent equations including exchange and correlation effects, *Phys. Rev.* **140**, A1133–8.
- Kowalski, K. and Jankowski, K. (1998). Towards complete solutions to systems of nonlinear equations of many-electron theories, *Phys. Rev. Lett.* **81**, 1195–98.
- Krogh, J. W. and Olsen, J. (2001). A general coupled cluster study of the N₂ molecule, *Chem. Phys. Lett.* **344**, 578–86.
- Krylov, A. I. (2001). Size-consistent wave functions for bond-breaking: the equation-of-motion spin-flip model, *Chem. Phys. Lett.* **338**, 375–84.
- Kucharski, S. A. and Bartlett, R. J. (1988). Multireference many-body perturbation theory, *Int. J. Quantum Chem., Quantum Chem. Symp.* **22**, 383–405.
- Kucharski, S. A. and Bartlett, R. J. (1989). Coupled-cluster methods that include connected quadruple excitations, *T₄: CCSDTQ-1 and Q(CCSDT)*, *Chem. Phys. Lett.* **158**, 550–5.
- Kucharski, S. A. and Bartlett, R. J. (1991a). Recursive intermediate factorization and complete computational linearization of the coupled-cluster single, double, triple, and quadruple excitation equations, *Theor. Chim. Acta* **80**, 387–405.
- Kucharski, S. A. and Bartlett, R. J. (1991b). Hilbert space multireference coupled-cluster methods. I. The single and double excitation model, *J. Chem. Phys.* **95**, 8227–38.
- Kucharski, S. A. and Bartlett, R. J. (1992). The coupled-cluster single, double, triple, and quadruple excitation method, *J. Chem. Phys.* **97**, 4282–8.
- Kucharski, S. A. and Bartlett, R. J. (1993). Coupled-cluster methods correct through sixth order, *Chem. Phys. Lett.* **206**, 574–83.

- Kucharski, S. A. and Bartlett, R. J. (1995). Sixth-order many-body perturbation theory for molecular calculations, *Chem. Phys. Lett.* **237**, 264–72.
- Kucharski, S. A. and Bartlett, R. J. (1998a). Noniterative energy corrections through fifth-order to the coupled cluster singles and doubles method, *J. Chem. Phys.* **108**, 5243–54.
- Kucharski, S. A. and Bartlett, R. J. (1998b). Sixth-order energy corrections with converged coupled cluster singles and doubles amplitudes, *J. Chem. Phys.* **108**, 5255–64.
- Kucharski, S. A. and Bartlett, R. J. (1998c). An efficient way to include connected quadruple contributions into the coupled cluster method, *J. Chem. Phys.* **108**, 9221–6.
- Kucharski, S. A. and Bartlett, R. J. (1999). Connected quadruples for the frequencies of O₃, *J. Chem. Phys.* **110**, 8233–5.
- Kucharski, S. A., Włoch, M., Musiał, M. and Bartlett, R. J. (2001). Coupled-cluster theory for excited states: the full equation-of-motion coupled-cluster single, double and triple excitation method, *J. Chem. Phys.* **115**, 8263–6.
- Kutzelnigg, W. (1977). Pair correlation theories, in *Methods of Electronic Structure Theory*, ed. H. F. Schaefer III (Plenum, New York), pp. 129–88.
- Kutzelnigg, W. (1982). Quantum chemistry in Fock space. I. The universal wave and energy operators, *J. Chem. Phys.* **77**, 3081–97.
- Kutzelnigg, W. (1984). Quantum chemistry in Fock space. III. Particle–hole formalism, *J. Chem. Phys.* **80**, 822–30.
- Kutzelnigg, W. (2003). Theory of electron correlation, in *Explicitly Correlated Wave Functions in Chemistry and Physics. Theory and Applications*, ed. J. Rychlewski (Kluwer, Dordrecht), pp. 3–90.
- Kutzelnigg, W. and Koch, S. (1983). Quantum chemistry in Fock space. II. Effective Hamiltonians in Fock space, *J. Chem. Phys.* **79**, 4315–35.
- Kvasnička, V. (1974). Construction of model Hamiltonians in framework of Rayleigh–Schrödinger perturbation theory, *Czech. J. Phys. B* **24**, 605–15.
- Kvasnička, V. (1977a). A diagrammatic construction of formal E -independent model Hamiltonians, *Czech. J. Phys. B* **27**, 599–628.
- Kvasnička, V. (1977b). Application of diagrammatic quasidegenerate RSPT in quantum molecular physics, *Adv. Chem. Phys.* **36**, 345–412.
- Langhoff, P. W., Epstein, S. T. and Karplus, M. (1972). Aspects of time-dependent perturbation theory, *Rev. Mod. Phys.* **44**, 602–44.

- Langhoff, S. R. and Davidson, E. R. (1974). Configuration interaction calculations on the nitrogen molecule, *Int. J. Quantum Chem.* **8**, 61–72.
- Larsen, H., Hald, K., Olsen, J. and Jørgensen, P. (2001). Triplet excitation energies in full configuration interaction and coupled cluster theory, *J. Chem. Phys.* **115**, 3015–20.
- Lauderdale, W. J., Stanton, J. F., Gauss, J., Watts, J. D. and Bartlett, R. J. (1991). Many-body perturbation theory with a restricted open-shell Hartree–Fock reference, *Chem. Phys. Lett.* **187**, 21–8.
- Lee, T. J. and Rendell, A. P. (1991). Analytic gradients for coupled-cluster energies that include noniterative triple excitations: application to *cis*- and *trans*-HONO, *J. Chem. Phys.* **94**, 6229–36.
- Lee, Y. S. and Bartlett, R. J. (1984). A study of Be₂ with many-body perturbation theory and a coupled-cluster method including triple excitations, *J. Chem. Phys.* **80**, 4371–7.
- Lee, Y. S., Kucharski, S. A. and Bartlett, R. J. (1984). A coupled cluster approach with triple excitations, *J. Chem. Phys.* **81**, 5906–12. Erratum (1985). *J. Chem. Phys.* **82**, 5761.
- Li, X. and Paldus, J. (1994). Automation of the implementation of spin-adapted open-shell coupled cluster theories relying on the unitary group formalism, *J. Chem. Phys.* **101**, 8812–26.
- Li, X. and Paldus, J. (1997). Unitary group based coupled cluster methods and calculation of molecular properties, in *Recent Advances in Coupled-Cluster Methods*, ed. R. J. Bartlett (World Scientific, Singapore), pp. 183–219.
- Li, X. and Paldus, J. (2003a). General-model-space state-universal coupled-cluster theory: connectivity conditions and explicit equations, *J. Chem. Phys.* **119**, 5320–33.
- Li, X. and Paldus, J. (2003b). *N*-reference, *M*-state coupled-cluster method: merging the state-universal and reduced multireference coupled-cluster theories, *J. Chem. Phys.* **119**, 5334–45.
- Li, X. and Paldus, J. (2003c). The general-model-space state-universal coupled-cluster method exemplified by the LiH molecule, *J. Chem. Phys.* **119**, 5346–57.
- Li, X. and Paldus, J. (2004). Performance of the general-model-space state-universal coupled-cluster method, *J. Chem. Phys.* **120**, 5890–5902.
- Lindgren, I. (1974). The Rayleigh–Schrödinger perturbation and the linked-diagram theorem for a multiconfigurational model space, *J. Phys. B* **7**, 2441–70.

- Lindgren, I. (1978). A coupled-cluster approach to the many-body perturbation theory for open-shell systems, *Int. J. Quantum Chem., Quantum Chem. Symp.* **12**, 33–58.
- Lindgren, I. (1985a). Linked-diagram and coupled-cluster expansions for multi-configurational complete and incomplete model spaces, *Phys. Scripta* **32**, 291–302.
- Lindgren, I. (1985b). A note on the linked-diagram and coupled-cluster expansions for complete and incomplete model spaces, *Phys. Scripta* **32**, 611.
- Lindgren, I. (1998). Development of atomic many-body theory, in *Many-Body Atomic Physics*, eds. J. J. Boyle and M. S. Pindzola (Cambridge University Press, Cambridge), pp. 3–38.
- Lindgren, I. and Morrison, J. (1986). *Atomic Many-Body Theory*, second edition (Springer, Berlin).
- London, F. (1937). Théorie quantique des courants interatomiques dans les combinaisons aromatiques, *J. Phys. Radium*, Ser. 7, **8**, 397–409.
- Löwdin, P.-O. (1955). Quantum theory of many-particle systems. I. Physical interpretation by means of density matrices, natural spin-orbitals, and convergence problems in the method of configuration interaction, *Phys. Rev.* **97**, 1474–89.
- Löwdin, P.-O. (1959). Correlation problem in many-electron quantum mechanics. I. Review of different approaches and discussion of some current ideas, *Adv. Chem. Phys.* **2**, 207–322.
- Löwdin, P.-O. (1962a). Studies in perturbation theory. IV. Solution of eigenvalue problem by projection operator formalism, *J. Math. Phys.* **3**, 969–82.
- Löwdin, P.-O. (1962b). Studies in perturbation theory. V. Some aspects on the exact self-consistent field theory, *J. Math. Phys.* **3**, 1171–84.
- Löwdin, P.-O. (1965). Studies in perturbation theory. X. Lower bounds to energy eigenvalues in perturbation-theory ground state, *Phys. Rev. A* **139**, 357–72.
- Löwdin, P.-O. (1977). Quantum theory as a trace algebra, *Int. J. Quantum Chem.* **12**, Suppl. 1, 197–266.
- Mahapatra, U. S., Datta, B. and Mukherjee, D. (1998). A state-specific multi-reference coupled cluster formalism with molecular applications, *Mol. Phys.* **94**, 157–71.
- Mahapatra, U. S., Datta, B. and Mukherjee, D. (1999). A size-consistent state-specific multireference coupled cluster theory: formal developments and molecular applications, *J. Chem. Phys.* **110**, 6171–88.

- Malrieu, J. P., Durand, Ph. and Daudey, J. P. (1985). Intermediate Hamiltonian as a new class of effective Hamiltonians, *J. Phys. A Math. Gen.* **18**, 809–26.
- Manne, R. (1977). The linked-diagram expansion of the ground state of a many-electron system: a time-independent derivation, *Int. J. Quantum Chem., Quantum Chem. Symp.* **11**, 175–92.
- March, N. H., Young, W. H. and Sampanthar, S. (1967). *The Many-Body Problem in Quantum Mechanics* (Cambridge University Press, London).
- Martin, J. M. L., François, J. P. and Gijbels, R. (1990). On size-consistency corrections for limited configuration interaction calculations, *Chem. Phys. Lett.* **172**, 346–53.
- Meissner, L. (1988). Size-consistency corrections for configuration interaction calculations, *Chem. Phys. Lett.* **146**, 204–10.
- Meissner, L. (1998). Fock-space coupled-cluster method in the intermediate Hamiltonian formulation: model with singles and doubles, *J. Chem. Phys.* **108**, 9227–35.
- Meissner, L. and Bartlett, R. J. (1991). Transformation of the Hamiltonian in excitation energy calculations: comparison between Fock-space multireference coupled-cluster and equation-of-motion coupled-cluster methods, *J. Chem. Phys.* **94**, 6670–6.
- Meissner, L. and Malinowski, P. (2000). Intermediate Hamiltonian formulation of the valence-universal coupled-cluster method for atoms, *Phys. Rev. A* **61**, 062510-1–14.
- Meissner, L. and Nooijen, M. (1995). Effective and intermediate Hamiltonians obtained by similarity transformation, *J. Chem. Phys.* **102**, 9604–14.
- Meunier, A., Levy, B. and Berthier, G. (1976). The N^2 problem in molecular CI calculations, *Int. J. Quantum Chem.* **10**, 1061–70.
- Meyer, W. (1974). PNO-CI and CEPA studies of electron correlation effects. II. Potential curves and dipole moment functions of the OH radical, *Theor. Chim. Acta* **35**, 277–92.
- Møller, C. (1945). General properties of the characteristic matrix in the theory of elementary particles I, *K. Dan. Vidensk. Selsk. Mat.-Fys. Medd.* **23**, No. 1, 1–48.
- Møller, C. (1946). General properties of the characteristic matrix in the theory of elementary particles II, *K. Dan. Vidensk. Selsk. Mat.-Fys. Medd.* **22**, No. 19, 1–46.
- Møller, C. and M. S. Plesset (1934). Note on an approximation treatment for many-electron systems, *Phys. Rev.* **46**, 618–22.

- Monkhorst, H. J. (1977). Calculation of properties with the coupled-cluster method, *Int. J. Quantum Chem., Quantum Chem. Symp.* **11**, 421–32.
- Mukherjee, D. (1986). The linked-cluster theorem in the open-shell coupled-cluster theory for incomplete model spaces, *Chem. Phys. Lett.* **125**, 207–12.
- Mukhopadhyay Jr, D. and Mukherjee, D. (1989). Size-extensive effective Hamiltonian formalisms using quasi-Hilbert and quasi-Fock space strategies with incomplete model spaces, *Chem. Phys. Lett.* **163**, 171–7.
- Mukhopadhyay Jr, D. and Mukherjee, D. (1991). Molecular applications of size-extensive quasi-Hilbert- and quasi-Fock-space coupled-cluster formalisms using incomplete model spaces, *Chem. Phys. Lett.* **177**, 441–6.
- Musiał, M. and Bartlett, R. J. (2003). Equation-of-motion coupled cluster method with full inclusion of connected triple excitations for electron-attached states: EA-EOM-CCSDT, *J. Chem. Phys.* **119**, 1901–8.
- Musiał, M. and Bartlett, R. J. (2004). Fock-space multireference coupled cluster method with full inclusion of connected triples for excitation energies, *J. Chem. Phys.* **121**, 1670–5.
- Musiał, M. and Bartlett, R. J. (2005). Critical comparison of various connected quadruple excitation approximations in the coupled-cluster treatment of bond breaking, *J. Chem. Phys.* **122**, 224102-1–9.
- Musiał, M. and Bartlett, R. J. (2008). Benchmark calculations of the Fock-space coupled cluster single, double, and triple excitation method in the intermediate Hamiltonian formulation for electronic excitation energies, *Chem. Phys. Lett.* **457**, 267–70.
- Musiał, M., Kucharski, S. A. and Bartlett, R. J. (2000). T_5 operator in coupled-cluster calculations, *Chem. Phys. Lett.* **320**, 542–8.
- Musiał, M., Kucharski, S. A. and Bartlett, R. J. (2002a). Formulation and implementation of the full coupled-cluster method through pentuple excitations, *J. Chem. Phys.* **116**, 4382–8.
- Musiał, M., Kucharski, S. A. and Bartlett, R. J. (2002b). Diagrammatic structure of the general coupled-cluster equations, *Mol. Phys.* **100**, 1867–72.
- Musiał, M., Kucharski, S. A. and Bartlett, R. J. (2003). Equation-of-motion coupled cluster method with full inclusion of the connected

- triple excitations for ionized states: IP-EOM-CCSDT, *J. Chem. Phys.* **118**, 1128–36.
- Nakatsuji, H. (1979a). Cluster expansion of the wave function. Electron correlation in ground and excited states by SAC (symmetry-adapted-cluster) and SAC CI theories, *Chem. Phys. Lett.* **67**, 329–33.
- Nakatsuji, H. (1979b). Cluster expansion of the wave function. Calculation of electron correlations in ground and excited states by SAC and SAC CI theories, *Chem. Phys. Lett.* **67**, 334–42.
- Nakatsuji, H. and Hirao, K. (1978a). Cluster expansion of the wave function. Symmetry-adapted-cluster expansion, its variational determination, and extension of open-shell orbital theory, *J. Chem. Phys.* **68**, 2053–65.
- Nakatsuji, H. and Hirao, K. (1978b). Cluster expansion of the wave function. Pseudo-orbital theory based on the SAC expansion and its application to the spin density of open-shell systems, *J. Chem. Phys.* **68**, 4279–91.
- Nakatsuji, H., Ohta, K. and Hirao, K. (1981). Cluster expansion of the wave function. Electron correlation in ground state, valence and Rydberg excited states, ionized states and electron-attached states of formaldehyde by SAC and SAC-CI theories, *J. Chem. Phys.* **75**, 2952–8.
- Neogrady, P., Urban, M. and Hubac, I. (1992). Spin adapted restricted open shell coupled cluster theory. Linear version, *J. Chem. Phys.* **97**, 5074–80.
- Neogrady, P., Urban, M. and Hubac, I. (1994). Spin adapted restricted Hartree–Fock reference coupled cluster theory for open shell systems, *J. Chem. Phys.* **100**, 3706–16.
- Nesbet, R. K. (1955). Configuration interaction in orbital theories, *Proc. R. Soc. (London) A* **230**, 312–21.
- Nesbet, R. K. (1958). Brueckner’s theory and the method of superposition of configurations, *Phys. Rev.* **109**, 1632–8.
- Noga, J. and Bartlett, R. J. (1987). The full CCSDT model for molecular electronic structure, *J. Chem. Phys.* **86**, 7041–50. Erratum (1988). *J. Chem. Phys.* **89**, 3401.
- Noga, J., Bartlett, R. J. and Urban, M. (1987). Towards a full CCSDT model for electron correlation. CCSDT-*n* models, *Chem. Phys. Lett.* **134**, 126–32.
- Noga, J. and Urban, M. (1988). On expectation value calculations of one-electron properties using the coupled cluster wave function, *Theor. Chim. Acta* **73**, 291–306.

- Nooijen, M. and Bartlett, R. J. (1997a). A new method for excited states: Similarity transformed equation-of-motion coupled-cluster theory, *J. Chem. Phys.* **106**, 6441–8.
- Nooijen, M. and Bartlett, R. J. (1997b). Similarity transformed equation-of-motion coupled-cluster theory: Details, examples, and comparisons, *J. Chem. Phys.* **107**, 6812–30.
- Nooijen, M., Shamasundar, K. R. and Mukherjee, D. (2005). Reflections on size-extensivity, size-consistency and generalized extensivity in many-body theory, *Mol. Phys.* **103**, 2277–98.
- Nooijen, M. and Snijders, J. G. (1992). Coupled cluster approach to the single-particle Green's function, *Int. J. Quantum Chem., Quantum Chem. Symp.* **26**, 55–83.
- Nooijen, M. and Snijders, J. G. (1993). Coupled cluster Green's function method: working equations and applications, *Int. J. Quantum Chem.* **48**, 15–48.
- Pal, S., Rittby, M., Bartlett, R. J., Sinha, D. and Mukherjee, D. (1988). Molecular applications of multireference coupled-cluster methods using an incomplete model space: direct calculation of excitation energies, *J. Chem. Phys.* **88**, 4357–66.
- Paldus, J. (1977). Correlation problems in atomic and molecular systems. V. Spin-adapted coupled cluster many-electron theory, *J. Chem. Phys.* **67**, 303–18.
- Paldus, J. (1990). Hartree–Fock stability and symmetry breaking, in *Self-Consistent Field: Theory and Applications*, eds. R. Carbo and Klobukowski (Elsevier, Amsterdam), pp. 1–45.
- Paldus, J. (2005). The beginnings of coupled-cluster theory: an eyewitness account, in *Theory and Applications of Computational Chemistry. The First Forty Years*, eds. C. Dykstra, G. Frenking, K. Kim and G. Scuseria (Elsevier, Amsterdam), pp. 115–47.
- Paldus, J. and Čížek, J. (1974). Green's function approach to the direct perturbation calculation of the excitation energies of closed shell fermion systems, *J. Chem. Phys.* **60**, 149–63.
- Paldus, J. and Čížek, J. (1975). Time-independent diagrammatic approach to perturbation theory of fermion systems, *Adv. Quantum Chem.* **9**, 105–97.
- Paldus, J., Čížek, J. and Jeziorski, B. (1989). Coupled cluster approach or quadratic configuration interaction? *J. Chem. Phys.* **90**, 4356–62.
- Paldus, J., Čížek, J. and Jeziorski, B. (1990). Coupled cluster approach or quadratic configuration interaction?: Reply to comment by Pople, Head-Gordon and Raghavachari, *J. Chem. Phys.* **93**, 1485–6.

- Paldus, J., Čížek, J. and Shavitt, I. (1972). Correlation problems in atomic and molecular systems. IV. Extended coupled-pair many-electron theory and application to the BH_3 molecule, *Phys. Rev. A* **5**, 50–67.
- Paldus, J., Li, X. and Petraco, N. D. K. (2004). General-model-space state-universal coupled-cluster method: diagrammatic approach, *J. Math. Chem.* **35**, 215–51.
- Paldus, J., Takahashi, M. and Cho, R. W. H. (1984). Coupled-cluster approach to electron correlation in one dimension: cyclic polyene model in delocalized basis, *Phys. Rev. B* **30**, 4267–91.
- Perera, S. A., Nooijen and Bartlett, R. J. (1996). Electron correlation effects on the theoretical calculation of nuclear magnetic resonance spin–spin coupling constants, *J. Chem. Phys.* **104**, 3290–305.
- Piecuch, P. and Kowalski, K. (2000). In search of the relationship between multiple solutions characterizing coupled-cluster theories, in *Computational Chemistry: reviews of Current Trends*, Vol. 5, ed. J. Leszczynski (World Scientific Press, Singapore), pp. 1–105.
- Pittner, J., Čárský, P. and Hubač, I. (2002). Four- and 8-reference state-specific Brillouin–Wigner coupled-cluster method: study of the singlet oxygen, *Int. J. Quantum Chem.* **90**, 1031–7.
- Pluta, T., Sadlej, A. J. and Bartlett, R. J. (1988). Polarizability of OH^- , *Chem. Phys. Lett.* **143**, 91–6.
- Pople, J. A., Binkley, J. S. and Seeger, R. (1976). Theoretical models incorporating electron correlation, *Int. J. Quantum Chem., Quantum Chem. Symp.* **10**, 1–19.
- Pople, J. A., Head-Gordon, M. and Raghavachari, K. (1987). Quadratic configuration interaction. A general technique for determining electron correlation energies, *J. Chem. Phys.* **87**, 5968–75.
- Pople, J. A., Head-Gordon, M. and Raghavachari, K. (1989). Quadratic configuration interaction: reply to comment by Paldus, Čížek and Jeziorski, *J. Chem. Phys.* **90**, 4635–6.
- Pople, J. A., Seeger, R. and Krishnan, R. (1977). Variational configuration interaction methods and comparison with perturbation theory, *Int. J. Quantum Chem., Quantum Chem. Symp.* **11**, 149–63.
- Pulay, P. (1969). *Ab initio* calculation of force constants and equilibrium geometries in polyatomic molecules. I. Theory, *Mol. Phys.* **17**, 197–204.
- Purvis III, G. D. and Bartlett, R. J. (1982). A full coupled-cluster singles and doubles model: the inclusion of disconnected triples, *J. Chem. Phys.* **76**, 1910–8.

- Purvis III, G. D., Sekino, H. and Bartlett, R. J. (1988). Multiplicity of many-body wavefunctions using unrestricted Hartree-Fock reference functions, *Col. Czech. Chem. Comm.* **53**, 2203-13.
- Purvis III, G. D., Shepard, R., Brown, F. B. and Bartlett, R. J. (1983). C_{2v} insertion pathway for beryllium dihydride (BeH_2): a test for the coupled-cluster single and double excitation model, *Int. J. Quantum Chem.* **23**, 835-45.
- Raghavachari, K., Head-Gordon, M. and Pople, J. A. (1990). Reply to comment on: coupled cluster approach or quadratic configuration interaction?, *J. Chem. Phys.* **93**, 1486-7.
- Raghavachari, K., Pople, J. A., Replogle, E. S., Head-Gordon, M. and Handy, N. C. (1990). Size-consistent Brueckner theory limited to double and triple substitutions, *Chem. Phys. Lett.* **167**, 115-21.
- Raghavachari, K., Trucks, G. W., Pople, J. A. and Head-Gordon, M. (1989). A fifth-order perturbation comparison of electron correlation theories, *Chem. Phys. Lett.* **157**, 479-83.
- Raimes, S. (1972). *Many-Electron Theory* (North-Holland, Amsterdam).
- Rayleigh, J. W. Strutt, Baron (1894). *Theory of Sound*, second edition, Vol. 1 (Macmillan, London; reprinted, 1945, Dover, New York).
- Reid, C. E. (1967). Transformation of perturbation series into continued fractions, with application to an anharmonic oscillator, *Int. J. Quantum Chem., Quantum Chem. Symp.* **1**, 521-34.
- Rittby, M. and Bartlett, R. J. (1988). An open-shell spin-restricted coupled cluster method: application to ionization potentials in N_2 , *J. Phys. Chem.* **92**, 3033-6.
- Rosenberg, B. J., Ermler, W. C. and Shavitt, I. (1976). *Ab initio* SCF and CI studies of the ground state of the water molecule. II. Potential energy and property surfaces, *J. Chem. Phys.* **65**, 4072-80.
- Rosenberg, B. J. and Shavitt, I. (1975). *Ab initio* SCF and CI studies of the ground state of the water molecule. I. Comparison of CGTO and STO basis sets near the Hartree-Fock limit, *J. Chem. Phys.* **63**, 2162-74.
- Rozyczko, P. B., Perera, S. A., Nooijen, M. and Bartlett, R. J. (1997). Correlated calculations of molecular dynamic polarizabilities, *J. Chem. Phys.* **107**, 6736-47.
- Salter, E. A., Sekino, H. and Bartlett, R. J. (1987). Property evaluation and orbital relaxation in coupled cluster methods, *J. Chem. Phys.* **87**, 502-9.

- Salter, E. A., Trucks, G. W. and Bartlett, R. J. (1989). Analytic energy derivatives in many-body methods. I. First derivatives, *J. Chem. Phys.* **90**, 1752–66.
- Sambe, H. (1973). Steady states and quasienergies of a quantum-mechanical system in an oscillating field, *Phys. Rev. A* **7**, 2203–13.
- Sandars, P. G. H. (1969). A linked diagram treatment of configuration interaction in open-shell atoms, *Adv. Chem. Phys.* **14**, 365–419.
- Sasaki, F. (1977). Effectiveness of configuration interaction calculations for large molecules, *Int. J. Quantum Chem., Quantum Chem. Symp.* **11**, 125–30.
- Scheiner, A. C., Scuseria, G. E., Rice, J. E., Lee, T. J. and Schaefer III, H. F. (1987). Analytic evaluation of energy gradients for the single and double excitation coupled cluster (CCSD) wave function: theory and application, *J. Chem. Phys.* **87**, 5361–73.
- Schrödinger, E. (1926). Quantisierung als Eigenwertproblem, *Ann. Physik* **80**, 437–90.
- Sekino, H. and Bartlett, R. J. (1984). A linear response, coupled-cluster theory for excitation energy, *Int. J. Quantum Chem., Quantum Chem. Symp.* **18**, 255–68.
- Sekino, H. and Bartlett, R. J. (1986). Nuclear spin–spin coupling constants evaluated using many body methods, *J. Chem. Phys.* **85**, 3945–9.
- Sekino, H. and Bartlett, R. J. (1993). Molecular hyperpolarizabilities, *J. Chem. Phys.* **98**, 3022–37.
- Sekino, H. and Bartlett, R. J. (1999). On the extensivity problem in coupled-cluster property evaluation, *Adv. Quantum Chem.* **35**, 149–73.
- Shavitt, I. and Redmon, L. T. (1980). Quasidegenerate perturbation theories. A canonical van Vleck formalism and its relationship to other approaches, *J. Chem. Phys.* **73**, 5711–7.
- Siegbahn, P. E. M. (1978). Multiple substitution effects in configuration interaction calculations, *Chem. Phys. Lett.* **55**, 386–94.
- Sinha, D., Mukhopadhyay, S. and Mukherjee, D. (1986). A note on the direct calculation of excitation energies by quasi-degenerate MBPT and coupled-cluster theory, *Chem. Phys. Lett.* **129**, 369–74.
- Stanton, J. F. (1993). Many-body methods for excited state potential energy surfaces. I. General theory of energy gradients for the equation-of-motion coupled-cluster method, *J. Chem. Phys.* **99**, 8840–7.
- Stanton, J. F. (1994). On the extent of spin contamination in open-shell coupled-cluster wave functions, *J. Chem. Phys.* **101**, 371–4.

- Stanton, J. F. (1997). Why CCSD(T) works: a different perspective, *Chem. Phys. Lett.* **281**, 130–4.
- Stanton, J. F. and Bartlett, R. J. (1993a). The equation of motion coupled-cluster method. A systematic biorthogonal approach to molecular excitation energies, transition probabilities, and excited state properties, *J. Chem. Phys.* **98**, 7029–39.
- Stanton, J. F. and Bartlett, R. J. (1993b). A coupled-cluster based effective Hamiltonian method for dynamic electric polarizabilities, *J. Chem. Phys.* **99**, 5178–83.
- Stanton, J. F. and Gauss, J. (1994). Analytic energy derivatives for ionized states described by the equation-of-motion coupled cluster method, *J. Chem. Phys.* **101**, 8938–44.
- Stanton, J. F. and Gauss, J. (1995). Many-body methods for excited state potential energy surfaces. II. Analytic second derivatives for excited state energies in the equation-of-motion coupled cluster method, *J. Chem. Phys.* **103**, 8931–43.
- Stanton, J. F. and Gauss, J. (1999). A simple scheme for the direct calculation of ionization potentials with coupled-cluster theory that exploits established excitation energy methods, *J. Chem. Phys.* **111**, 8785–8.
- Stanton, J. F. and Gauss, J. (2000). Analytic second derivatives in high-order many-body perturbation and coupled-cluster theories: computational considerations and applications, *Int. Rev. Phys. Chem.* **19**, 61–95.
- Stanton, J. F., Gauss, J. and Bartlett, R. J. (1992). On the choice of orbitals for symmetry breaking problems with application to NO₃, *J. Chem. Phys.* **97**, 5554–9.
- Stanton, J. F., Gauss, J., Watts, J. D., Lauderdale, W. J. and Bartlett, R. J. (1992). The ACES II program system, *Int. J. Quantum Chem., Quantum Chem. Symp.* **26**, 879–94.
- Sternheimer, R. M. and Foley, H. M. (1953). Nuclear quadrupole coupling in the Li₂ molecule, *Phys. Rev.* **92**, 1460–8.
- Stevens, R. M., Pitzer, R. M. and Lipscomb, W. N. (1963). Perturbed Hartree–Fock calculations. I. Magnetic susceptibility and shielding in the LiH molecule, *J. Chem. Phys.* **38**, 550–60.
- Stolarczyk, L. Z. and Monkhorst, H. J. (1985). Coupled-cluster method in Fock space. I. General formalism, *Phys. Rev. A* **32**, 725–42.
- Swain, S. (1977). Continued fraction solutions in degenerate perturbation theory, *J. Phys. A: Math. Gen.* **10**, 155–65.

- Szabo, A. and Ostlund, N. S. (1982). *Modern Quantum Chemistry: introduction to Advanced Electronic Structure Theory* (Free Press, New York).
- Szalay, P. G. and Bartlett, R. J. (1992). Alternative ansätze in coupled-cluster theory. IV. Comparison for the two-electron problem and the role of the exclusion principle violating (EPV) terms, *Int. J. Quantum Chem., Quantum Chem. Symp.* **26**, 85–106.
- Szalay, P. G. and Bartlett, R. J. (1994). Analytical energy gradients for the two-determinant coupled cluster method with application to singlet excited states of butadiene and ozone, *J. Chem. Phys.* **101**, 4936–44.
- Szalay, P. G. and Gauss, J. (1997). Spin-restricted open-shell coupled-cluster theory, *J. Chem. Phys.* **107**, 9028–38.
- Szalay, P. G. and Gauss, J. (2000). Spin-restricted open-shell coupled-cluster theory for excited states, *J. Chem. Phys.* **112**, 4027–36.
- Szalay, P. G., Nooijen, M. and Bartlett, R. J. (1995). Alternative ansätze in single reference coupled-cluster theory. III. A critical analysis of different methods, *J. Chem. Phys.* **103**, 281–98.
- Tam, M. C., Russ, N. J. and Crawford, T. D. (2004). Coupled cluster calculations of optical rotatory dispersion of (*S*)-methyloxirane, *J. Chem. Phys.* **121**, 3550–7.
- Thouless, D. J. (1960). Stability conditions and nuclear rotations in the Hartree–Fock theory, *Nucl. Phys.* **21**, 225–32.
- Tobita, M., Perera, S. A., Musiał, M., Bartlett, R. J., Nooijen, M. and Lee, J. S. (2003). Critical comparison of single-reference and multi-reference coupled-cluster methods: geometry, harmonic frequencies, and excitation energies of N₂O₂, *J. Chem. Phys.* **119**, 10713–23.
- Trucks, G. W., Noga, J. and Bartlett, R. J. (1988). Convergence of the coupled-cluster singles, doubles and triples method, *Chem. Phys. Lett.* **145**, 548–54.
- Urban, M., Neogrády, P. and Hubač, I. (1997). Spin adaptations in the open shell restricted coupled cluster theory with a single determinant restricted Hartree–Fock reference, in *Recent Advances in Coupled-Cluster Methods*, ed. R. J. Bartlett (World Scientific, Singapore), pp. 275–306.
- Urban, M., Noga, J., Cole, S. J. and Bartlett, R. J. (1985). Towards a full CCSDT model for electron correlation, *J. Chem. Phys.* **83**, 4041–6. Erratum (1986). *J. Chem. Phys.* **85**, 5383.
- Van Vleck, J. H. (1929). On σ -type doubling and electron spin in the spectra of diatomic molecules, *Phys. Rev.* **33**, 467–506.

- Van Voorhis, T. and Head-Gordon, M. (2000). Benchmark variational coupled-cluster doubles results, *J. Chem. Phys.* **113**, 8873–9.
- Watts, J. D. and Bartlett, R. J. (1990). The coupled-cluster single, double, and triple excitation model for open-shell single-reference functions, *J. Chem. Phys.* **93**, 6104–5.
- Watts, J. D. and Bartlett, R. J. (1994). Coupled-cluster singles, doubles, and triples calculations with Hartree–Fock and Brueckner orbital reference determinants: a comparative study, *Int. J. Quantum Chem., Quantum Chem. Symp.* **28**, 195–203.
- Watts, J. D., Gauss, J. and Bartlett, R. J. (1992). Open-shell analytical energy gradients for triple excitation many-body, coupled-cluster methods: MBPT(4), CCSD+T(CCSD), CCSD(T), and QCISD(T), *Chem. Phys. Lett.* **200**, 1–7.
- Watts, J. D., Gauss, J. and Bartlett, R. J. (1993). Coupled-cluster methods with noniterative triple excitations for restricted open-shell Hartree–Fock and other general single determinant reference functions. Energies and analytical gradients, *J. Chem. Phys.* **98**, 8718–33.
- Watts, J. D., Urban, M. and Bartlett, R. J. (1995). Accurate electrical and spectroscopic properties of $X^1\Sigma^+$ BeO from coupled-cluster methods, *Theor. Chem. Accts.* **90**, 341–55.
- Wick, G. C. (1950). The evaluation of the collision matrix, *Phys. Rev.* **80**, 268–72.
- Wigner, E. (1935). On a modification of the Rayleigh–Schrödinger perturbation theory, *Math. Naturwiss. Anz. Ungar. Akad. Wiss.* **53**, 477–82.
- Wilson, S. (1979). Diagrammatic perturbation theory: the contribution of triply excited states to correlation energies, *J. Phys. B* **12**, L657–60. Erratum (1980). *J. Phys. B* **13**, 1505.
- Živković, T. P. (1977). Existence and reality of solutions of the coupled-cluster equations, *Int. J. Quantum Chem., Quantum Chem. Symp.* **11**, 413–20.
- Živković, T. P. and Monkhorst, H. J. (1978). Analytical connection between configuration-interaction and coupled-cluster solutions, *J. Math. Phys.* **19**, 1007–22.

Author index

- Adamowicz, L., 365, 400, 496
 Adams, B. G., 263, 410, 496
 Ahlrichs, R., 163, 496
 Allen, W. D., 474, 502
 Arponen, J. S., 327, 367, 496
 Auer, A. A., 346, 429, 496, 504

 Baker, H. F., 293, 496
 Balková, A., 410, 411, 474, 496, 497
 Bandyopadhyay, D., 488, 504
 Bartlett, R. J., 1, 11, 80, 129, 153, 154, 156,
 159, 160, 162–164, 182, 185, 202, 227,
 263, 301, 315, 316, 318–321, 324–328,
 336, 342–344, 346, 352, 361, 364, 365,
 367, 387, 396, 400, 402, 407, 410–414,
 417, 421–423, 426–429, 431, 436, 437,
 441–448, 450, 452–454, 460, 461, 471,
 474, 477, 480, 493–498, 501–504, 507,
 508, 510–519
 Baumgartner, G., 346, 496
 Bauschlicher Jr, C. W., 342, 498, 499
 Bernholdt, D. E., 346, 496
 Berthier, G., 162, 511
 Bethe, H. E., 25, 499
 Bibireata, A., 346, 496
 Binkley, J. S., 12, 80, 499, 515
 Bishop, R. F., 327, 496
 Bloch, C., 52, 186, 187, 464, 499
 Bomble, Y. J., 429, 499
 Brändas, E. J., 185, 497, 499
 Brandow, B. H., 121, 165, 198, 499
 Brillouin, L., 33, 499
 Brown, F. B., 474, 515
 Brueckner, K. A., 1, 41, 53, 172, 499
 Bruna, P. J., 162, 500
 Buenker, R. J., 162, 500
 Burton, P. G., 162, 500
 Byers-Brown, W., 365, 400, 504

 Campbell, J. E., 293, 500
 Čásky, P., 474, 504, 514
 Chan, G. K.-L., 343, 344, 500
 Chattopadhyay, S., 472, 500

 Chaudhuri, R., 477, 485, 500
 Chiles, R. A., 420, 500
 Cho, R. W. H., 429, 514
 Choppella, V., 346, 496
 Christiansen, O., 419, 444, 456, 495, 500, 506
 Čížek, J., 2, 41, 91, 106, 134, 162, 184, 263,
 301, 348, 350, 402, 407, 500, 514
 Cociorva, D., 346, 496
 Coester, F., 2, 501
 Cole, S. J., 153, 154, 163, 164, 315, 318, 320,
 321, 497, 519
 Comeau, D. C., 431, 501
 Crawford, T. D., 426, 427, 453, 501, 518

 Dalgaard, E., 431, 454, 501
 Dalgarno, A., 365, 400, 501
 Datta, B., 472–474, 510
 Daudey, J.-P., 490, 491, 501, 510
 Davidson, E. R., 12, 161, 162, 435, 501, 508
 de Merás, A. S., 453, 461, 506
 Dirac, P. A. M., 1, 501
 Ditchfield, R., 387, 402, 501
 Dunning Jr, T. H., 344, 501
 Durand, Ph., 490, 491, 510
 Dykstra, C., 420, 500
 Dyson, F. J., 1, 501, 502

 Emrich, K., 431, 502
 Epstein, P. S., 80, 502
 Epstein, S. T., 365, 400, 456, 504
 Ermler, W. C., 153, 154, 163, 164, 497, 516
 Evangelista, F. A., 474, 502

 Fan, P.-D., 429, 503
 Feynman, R. P., 1, 502
 Foley, H. M., 365, 400, 518
 François, J. P., 142, 510
 Frantz, L. M., 1, 165, 167, 502
 Freeman, D. L., 167, 175, 503

 Gao, X., 346, 496
 Gauss, J., 316, 319, 343, 344, 351, 352, 365,
 387, 396, 402, 410, 412, 414, 417, 421,

- 429, 441, 444, 445, 448, 499, 500, 502, 506, 508, 517–519
 Gerratt, J., 390, 393, 502
 Gijbels, R., 162, 510
 Goldstone, J., 1, 53, 152, 172, 175, 499, 503
 Goscinski, O., 185, 499, 503
 Grabowski, I., 421, 429, 430, 497, 505
 Gwaltney, S. R., 428, 503
- Hald, K., 444, 508
 Handy, N. C., 129, 315, 316, 342, 400, 421, 498, 503, 515
 Haque, M. A., 485, 503
 Harris, F. E., 167, 175, 503
 Harrison, R., 346, 496
 Hättig, C., 456, 500
 Hausdorff, F., 293, 503
 Head-Gordon, M., 129, 301, 315, 316, 319, 327, 421, 429, 503, 514, 515, 519
 Helgaker, T., 402, 419, 502, 506
 Heully, J.-L., 490, 501
 Hirao, K., 432, 503, 512
 Hirata, S., 346, 414, 421, 429, 441–444, 446–449, 497, 503, 504
 Hirschfelder, J. O., 365, 400, 504
 Horowitz, J., 52, 186, 499
 Hose, G., 227, 504
 Hsieh, H. C., 153, 154, 163, 164, 497
 Hubač, I., 351, 352, 474, 504, 513, 514, 519
 Hubbard, J., 1, 504
 Huby, R., 41, 504
 Hugenholtz, N. M., 1, 118, 165, 504
 Hylleraas, E. A., 25, 504
- Ivanov, S., 421, 497
- Jana, D., 488, 504
 Jankowski, K., 263, 429, 430, 474, 496, 505, 506
 Janssen, C. L., 346, 505
 Jayatilaka, D., 352, 505
 Jeziorski, B., 227, 301, 465, 505, 514, 515
 Jordan, P., 1, 505
 Jørgensen, P., 361, 367, 419, 431, 444, 453, 456, 461, 495, 500, 505, 506, 508
- Kaldor, U., 227, 504, 505
 Kállay, M., 342–344, 346, 429, 499, 500, 506
 Karplus, M., 456, 508
 Kelly, H. P., 1, 162, 506
 Klein, O., 1, 505
 Knowles, P. J., 342, 498
 Kobayashi, R., 419, 453, 461, 506
 Koch, H., 367, 419, 431, 444, 453, 461, 495, 500, 506
 Koch, S., 54, 163, 475, 506, 508
 Kohn, W., 413, 506
 Kowalski, K., 429, 430, 505, 506, 514
 Krishnamoorthy, S., 346, 496
 Krishnan, R., *see* Raghavachari, K.
 Krishnan, S., 346, 496
- Krogh, J. W., 343, 344, 507
 Krylov, A. I., 441, 462, 507
 Kucharski, S. A., 202, 227, 315, 321, 324–328, 336, 342, 344, 411, 426–428, 437, 444, 445, 471, 497, 498, 507, 508, 512
 Kümmel, H., 2, 501
 Kutzelnigg, W., 8, 54, 163, 327, 475, 496, 506–508
 Kvasnička, V., 52, 508
- Laidig, W. D., 365, 400, 496
 Lam, C.-C., 346, 496
 Langhoff, P. W., 456, 508
 Langhoff, S. R., 161, 342, 498, 508
 Larsen, H., 444, 508
 Lauderdale, W. J., 410, 414, 417, 502, 508, 518
 Lee, J. S., 448, 518
 Lee, T. J., 352, 365, 505, 508, 516
 Lee, Y. S., 315, 508
 Levinson, C. A., 1, 499
 Levy, B., 162, 511
 Li, X., 346, 351, 410, 466, 467, 469, 471, 472, 508, 509, 514
 Lindgren, I., 2, 52, 186, 187, 198, 478, 481, 482, 509
 Lipscomb, W. N., 390, 518
 Lischka, H., 163, 496
 London, F., 387, 402, 509
 Löwdin, P.-O., 8, 413, 418, 419, 509, 510
 Lu, Q., 346, 496
- Mahapatra, U. S., 472–474, 500, 510
 Malinowski, P., 490, 511
 Malrieu, J.-P., 490, 491, 501, 510
 Manne, R., 167, 172, 173, 510
 March, N. H., 53, 69, 510
 Martin, J. M. L., 162, 510
 Meissner, L., 162, 444, 480, 490, 492, 510, 511
 Meunier, A., 162, 511
 Meyer, W., 162, 511
 Mills, I. M., 390, 393, 502
 Mills, R. L., 1, 165, 167, 502
 Møller, C., 80, 511
 Monkhurst, H. J., 167, 175, 227, 361, 429–431, 465, 490, 501, 503, 505, 511, 518, 520
 Morrison, J., 2, 52, 187, 481, 509
 Mukherjee, D., 11, 255, 472–474, 477, 478, 480, 485, 488, 500, 503, 504, 510, 511, 513, 517
 Mukhopadhyay Jr, D., 485, 500, 511
 Mukhopadhyay, S., 478, 480, 517
 Musiał, M., 328, 336, 342, 343, 344, 407, 410, 429, 437, 444, 445, 448, 471, 493–495, 497, 507, 511, 512, 518
- Nakatsuji, H., 431, 432, 503, 512
 Neogrády, P., 351, 352, 513, 519
 Nesbet, R. K., 80, 418, 419, 513
 Noga, J., 315, 316, 318, 320, 321, 327, 361, 362, 411, 497, 498, 513, 519
 Nooijen, M., 11, 255, 346, 367, 414, 429,

- 441–448, 454, 460, 461, 490, 496, 503,
504, 511, 513, 514, 516, 518
- Ohta, K., 432, 512
- Olsen, J., 343, 344, 444, 495, 500, 506–508
- Ostlund, N. S., 2, 3, 518
- Pal, S., 477, 513
- Paldus, J., 2, 41, 91, 106, 134, 184, 263, 301,
346, 351, 402, 410, 425, 429, 430, 466,
467, 469, 471, 472, 474, 496, 500, 501,
505, 508, 509, 514, 515
- Perera, S. A., 448, 454, 460, 461, 514, 516, 518
- Petraco, N. D. K., 471, 514
- Peyrimhoff, S. D., 162, 500
- Piecuch, P., 429, 430, 503, 514
- Pittner, J., 474, 504, 514
- Pitzer, R. M., 346, 390, 496, 518
- Plesset, M. S., 80, 511
- Pluta, T., 387, 514
- Pople, J. A., 12, 80, 129, 162, 301, 315, 316,
319, 421, 499, 503, 514, 515
- Pulay, P., 393, 515
- Purvis III, G. D., 11, 153, 154, 156, 160, 163,
164, 263, 422, 423, 441, 474, 497, 498,
515
- Raghavachari, K., 129, 162, 301, 315, 316, 319,
421, 503, 514, 515
- Raimes, S., 53, 515
- Ramanujam, J., 346, 496
- Rayleigh, Baron, 37, 515
- Redmon, L. T., 46, 517
- Reid, C. E., 185, 515
- Rendell, A. P., 365, 508
- Replogle, E. S., 421, 515
- Rice, J. E., 365, 516
- Rittby, M., 410, 414, 441, 477, 513, 516
- Rosenberg, B. J., 163, 164, 516
- Rozyczko, P. B., 454, 460, 461, 516
- Russ, N. J., 453, 518
- Ruud, K., 402, 502
- Sadayappan, P., 346, 496
- Sadlej, A. J., 387, 514
- Salpeter, E. E., 25, 499
- Salter, E. A., 364, 365, 367, 400, 516
- Sambe, H., 456, 516
- Sampanthar, S., 53, 69, 510
- Sandars, P. G. H., 192, 195, 198, 516
- Sasaki, F., 12, 516
- Schaefer III, H. F., 346, 365, 400, 474, 502,
503, 505, 516
- Scheiner, A. C., 365, 516
- Schrödinger, E., 37, 516
- Scuseria, G., 365, 516
- Seeger, R., 12, 80, 162, 515
- Sekino, H., 402, 422, 423, 431, 441, 450, 454,
461, 498, 501, 515–517
- Sham, L. J., 413, 506
- Shamasundar, K. R., 11, 255, 513
- Shavitt, I., 46, 80, 153, 154, 156, 159, 160,
162–164, 182, 185, 263, 497, 498, 514,
516, 517
- Shepard, R., 474, 515
- Sibiryakov, A., 346, 496
- Siegbahn, P. E. M., 162, 517
- Silver, D. M., 1, 498
- Silver, D. W., 12, 162, 501
- Simons, J., 361, 505
- Sinha, D., 477, 478, 480, 500, 513, 517
- Snijders, J. G., 445, 513
- Staemmler, V., 163, 496
- Stanton, J. F., 352, 396, 410, 414, 417, 421,
422, 423, 426, 427, 429, 431, 436, 441,
444, 445, 448, 453, 460, 498, 499, 501,
502, 508, 517, 518
- Sternheimer, R. M., 365, 400, 518
- Stevens, R. M., 390, 518
- Stewart, A. L., 365, 400, 501
- Stolarczyk, L. Z., 490, 518
- Surján, P. R., 342, 346, 506
- Swain, S., 186, 518
- Szabo, A., 2, 3, 518
- Szalay, P. G., 351, 367, 410, 441, 518
- Takahashi, M., 429, 514
- Tam, M. C., 453, 518
- Taylor, P. R., 342, 498, 499
- Thouless, D. J., 257, 300, 413, 419, 518
- Tobita, M., 448, 518
- Trucks, G. W., 129, 316, 319, 327, 364, 365,
367, 400, 421, 497, 503, 515, 516, 519
- Urban, M., 301, 315, 318, 320, 321, 351, 352,
361, 362, 513, 519, 520
- Van Vleck, J. H., 46, 519
- Van Voorhis, T., 327, 519
- Watts, J. D., 301, 316, 319, 327, 365, 410, 412,
414, 417, 421, 497, 498, 502, 508, 518,
519
- Wick, G. C., 1, 68, 519
- Wigner, E. P., 1, 24, 33, 505, 519
- Wilson, S., 153, 154, 519
- Włoch, M., 437, 444, 507
- Young, W. H., 53, 69, 510
- Živkovič, T. P., 429, 430, 520

Subject index

- A and B matrices**, 392, 400–404, 425–426
 - complex case, 393, 402–404
- annihilation operator, 55–67
 - pseudo-, 72
- active holes, 476, 489
- active particles, 476, 489
- anticommutation relations, 57–59
- antisymmetrized Goldstone diagrams (ASGs), 121–123
 - energy, third-order
 - canonical HF case, 133
 - non-HF case, 133
 - energy, fourth-order
 - single-excitation diagrams, 142
 - double-excitation diagrams, 142
 - triple-excitation diagrams, 143
 - quadruple-excitation diagrams, 144
- QDPT level-shift operator
 - second-order, 206
 - third-order, 221
 - folded, 224
- QDPT wave operator
 - second-order, 208, 209
- wave function, second-order
 - canonical HF case, 137
 - non-HF case, 138
- antisymmetrizer, 4
- ASG, *see* antisymmetrized Goldstone diagrams
- atomic units, 2, 64
- avoided crossings, 491
- B-CC**, *see* Brueckner-orbitals CC
- Baker–Campbell–Hausdorff expansion, 293
- basis set
 - complete, 387
 - complex, 402
 - derivative integrals, *see* derivative integrals
 - perturbed, 387, 390, 392, 394–399, 404–405
- Bloch equation, 52, 186
 - generalized, 52, 186, 463–465
 - alternative forms, 464, 465
 - derivation, 187–188
 - in Fock-space MRCC, 483–488
 - matrix form, 189–191
 - normal-product form, 194–195
 - order-by-order expansion, 189
 - schematic representation, 198–203
 - secondary term, 200
 - with folded resolvent lines, 202
- bond breaking, 185, 427, 429, 441, 447–448, 462
- bonnes fonctions*, 187, 464, 472
- bracket insertion, *see* insertion
- Brillouin theorem, 9, 132, 237
 - inapplicable to ROHF, 132, 300
- Brillouin–Wigner perturbation theory (BWPT), 33–34
 - non-extensivity, 34–36
- Brueckner orbitals, 10, 413, 418–421
 - advantages, 420–421
 - conditions, 419
 - iterative process, 419–420
 - stationarity condition, 419
- Brueckner-orbitals CC (B-CC), 421
 - broken-symmetry cases, 421
- BWPT, *see* Brillouin–Wigner perturbation theory
- C-conditions, 466–467
- CC, *see* coupled cluster
- CCD (CC doubles), 163, 258–271, 342
 - algebraic derivation, 263–271
 - amplitude equations, 288–289
 - iterative solution, 290
 - configuration-space derivation, 258–263
 - diagrammatic derivation, 279–291
 - linearized, 263
- CCSD (CC singles and doubles), 163, 299–308, 342, 343, 425
 - computational cost, 308
 - equations, 301
 - linearized, 375
 - role of \hat{T}_1 , 300–301
 - role of the **A** and **B** matrices, 425
 - \hat{T}_1 equations, 304

- ASG diagrams, 302
- generation of ASG diagrams, 303
- \hat{T}_2 equations, 307
 - ASG diagrams for \hat{T}_1 contributions, 305
 - generation of ASG diagrams for \hat{T}_1 contributions, 306
- CCS (CC singles), 442
- CCSDT (CC singles, doubles and triples), 308–321, 342, 343
- CCSD(T), 319–320, 342, 343
- CCSD[T], 317–319
- CCSDT-1, 163, 315–321, 342
 - computational cost, 316
 - iterative procedure, 316, 317
- CCSDT-2, 320
 - computational cost, 321
- CCSDT-3, 320–321
 - computational cost, 321
- CCSDT- n , comparison of included terms, 321
- computational considerations, 315–318
- computational cost, 316–317
- equations, 309
- ACCS(D)(T), 426, 427
- role of \hat{T}_3 , 308–309
- \hat{T}_1 equations, 310
 - ASG diagram for \hat{T}_3 contributions, 310
- \hat{T}_2 equations, 311
 - ASG diagrams for \hat{T}_3 contributions, 310
- \hat{T}_3 equations, 313
 - ASG diagrams, 312
 - perturbation-theory order of terms, 314
- CCSDTQ, 321–328, 342, 343, 381
- CCSDT(Q_f), 343
- CCSDT[Q], 342
- CCSDTQ-1, 322–325, 342
 - computational cost, 325
- CCSDTQ-2 approximation, 325
- computational cost, 325
- equations, 321–322
- factorized quadruples (Q_f) approximations, 325–328
- ACCS(D)(Q_f) approximation, 427–428
- \hat{T}_2 equations
 - ASG diagram for \hat{T}_4 contributions, 322
- \hat{T}_3 equations, 322
 - ASG diagram for \hat{T}_4 contributions, 322
- \hat{T}_4 equations
 - ASG diagram, 323
- CCSDTQP, 342–344
- CCSDTQPH, 343, 344
- CI, *see* configuration interaction
- CID (CI doubles), 13, 159, 163, 342
- CIS (CI singles), 10
- CISD (CI singles and doubles), 9, 159, 163, 342
 - quadratic, 301
 - with Davidson correction, 163
- CISDT, 159, 342
- CISDTQ, 159, 342
- CISDTQP, 342, 471
- cluster operators, 255–258
 - amplitudes, 255–258
 - diagrammatic representation, 273–275, 285
 - in state-universal MRCC, 465
 - relative importance of \hat{T}_n contributions, 308–309
- CMS, *see* model space, complete
- commutator
 - simplification, 293
 - vacuum expectation value, 101
- computational results
 - C_2 excitation energies by IH-CC and EOM-CC, 495
 - C_2 ionization potentials by IP-EOM-CC, 446, 447
 - CH^+ electron affinities by EA-EOM-CC, 446, 448
 - CH^+ excitation energies by EE-EOM-CC, 441–442
 - CH_2 excitation energies by EE-EOM-CC, 443
 - CN electron affinity by GMBPT and CCSD, 417
 - comparison with experiment, limitations, 444
 - comparison with full CI, 340–346, 442–444, 447, 448, 495
 - advantages, 444
 - FH and H_2O by CI, MBPT and CC, 342
 - H_2O excitation energies by IH-CC and EOM-CC, 495
 - H_2O in 39-STO basis, 153–156, 159–164
 - H_2O in SU-CC, 471
 - N_2 dissociation with RHF and UHF references, 343–344
 - N_2 excitation energies by IH-CC and EOM-CC, 495
 - N_2 potential-energy curves, 345
 - Ne excitation energies by IH-CC and EOM-CC, 495
 - using full-CI Hamiltonian matrix, 444
- configuration interaction (CI), 9–10
 - extensivity correction
 - dressings, 490
 - quadruples, 162
 - full CI, 10, 159, 340–346, 430
 - multireference, 8, 490
 - MRCISD, 472
 - non-extensivity, 12, 161
 - quadratic CISD, 301
 - relationship to RSPT, 159–164
- configuration state functions, 472
- conjugate diagrams, 134, 135, 142, 416
- connectivity conditions, *see* C-conditions
- continued fractions, 185
- contractions, 68–69
 - diagrammatic representation, 92–95
 - relative to Fermi vacuum, 74–75
- core ionization, 488

- core states, 192, 193, 228
- correlation energy, 8, 85, 131, 153
 - derivative, 396–405
 - imaginary component, 401
- Coulomb integral, 7
- Coulomb operator, 7, 76
- coupled cluster, 251–430
 - CC effective Hamiltonian (\mathcal{H}), 292
 - connected form, 294
 - diagrams and intermediates, 328–340
 - simplification, 293–294
 - CC energy functional (\mathcal{E}), 366–367
 - as basis for noniterative approximations, 426–429
 - stationarity condition, 366–367
 - computational considerations, 411
 - diagrams
 - general form, 295
 - rules of interpretation, 296
 - systematic generation, 297–299
 - doubles model, 258
 - effective Hamiltonian incorporating \hat{T}_1 (\tilde{H}), 418–419
 - diagrammatic representation, 418–419
 - iterative process, 419
 - energy, 302
 - complex case, 401
 - energy derivative, 396–405
 - imaginary component, 401
 - equations, 258–328
 - characteristics, 254
 - complex solutions, 429
 - connected form, 292–295
 - nature of solutions, 429–430
 - number of solutions, 430
 - relationship of solutions to full CI, 429, 430
 - standard solution, 429
 - systematic derivation, 292–328
 - exponential *Ansatz* and extensivity, 254–255
 - foundations, 251–291
 - full CC, 430
 - history, 2
 - Λ -based noniterative approximations, 426–429
 - orthogonally spin-adapted, 410
 - relationship to MBPT, 272–279
 - factorization of disconnected diagrams, 275–279
 - relative importance of \hat{T}_n contributions, 308–309
 - role of single excitations, 300–301
 - wave function, 254–258
 - with arbitrary reference function, 411–414
- coupled-cluster linear response, 431
- coupled-perturbed Hartree–Fock (CPHF), 387–393
 - complex case, 402
- CPHF, *see* coupled-perturbed Hartree–Fock creation operator, 55–67
 - pseudo-, 72
- Davidson correction, 161–163
- DEA-EOM-CC, *see* equation-of-motion CC, double electron attachment
- degenerate perturbation theory, 186
- denominator, *see* resolvent
- density matrix, 352–361
 - diagrammatic representation, 355–361
 - energy weighted, 394
 - one-body, 352
 - diagrams for ph terms, 357
 - diagrams for pp terms, 358
 - MBPT diagrams, 360
 - relaxed, 386, 401, 426
 - response, *see* response density matrix
 - response treatment, 381–385
 - transition, 436
 - two-body, 353–355
- density-functional theory, 413
- derivative integrals, 391, 392, 396
 - avoiding transformation, 391, 395, 404–405
- destruction operator, *see* annihilation operator
- diagram summation techniques, 177–180
- diagrammatic methods, 90–164
 - history, 1
- diagrammatic notation, 90–129
 - CC, 273–275
 - CC effective Hamilton, 328
 - EOM-CC, 437
 - Λ operator, 368
 - QDPT, 195–198
 - reduced density matrix, 340, 355–361
- DIP-EOM-CC, *see* equation-of-motion CC, double ionization potentials
- dipole moment, 362, 450
- dipole operator, 436
- dipole polarizability, 362, 450
- dipole strength, 436, 461
- direct CI, 472
- disconnected clusters, 15
- disconnected diagrams, 136, 137
- \mathcal{E} , *see* coupled cluster, CC energy functional
- EA-EOM-CC, *see* equation-of-motion CC, electron attachment
- EE-EOM-CC, *see* equation-of-motion CC, excitation energies
- effective Hamiltonian
 - incorporating \hat{T}_1 (\tilde{H}), 418
 - of CC (\mathcal{H}), 292
 - for model state α (\mathcal{H}^α), 468
 - of QDPT and MRCC (\hat{H}^{eff}), 51, 187, 188, 194, 465
 - in valence-universal MRCC, 477
- electron affinities, *see* equation-of-motion CC, electron attachment
- electron correlation, 7–9, 16
 - dynamic, 8, 462
 - nondynamic, 8, 462
- electron-repulsion integral, 65, 111
 - antisymmetric, 63, 65, 111, 182–184
 - spin-free, 182–184

- EOM-CC, *see* equation-of-motion CC
- Epstein–Nesbet partitioning, 80
- EPV terms, *see* exclusion-principle violating terms
- equation-of-motion CC, 431–461
 - biorthogonality relationship, 434
 - CI-like character, 433, 435
 - computational considerations, 446
 - de-excitation operator (\hat{L}_k), 434
 - left eigenfunctions of \mathcal{H} , 434
 - diagrammatic notation, 437–440
 - double arrows, 196
 - double electron attachment, 446–448
 - double ionization, 446
 - EA-EOM-CCS, 448
 - EA-EOM-CCSD, 448
 - EA-EOM-CCSDT, 448
 - EA-EOM-CCSDT-3, 448
 - EE-EOM-CCS, 442, 443
 - EE-EOM-CCSD, 442, 443
 - inadequacy for doubly excited states, 442, 444
 - EE-EOM-CCSDT, 442, 443
 - EE-EOM-CCSDT-3, 442, 443
 - EE-EOM-CCSDTQ, 443
 - EE-EOM-CCSDTQP, 443
 - electron attachment, 445–449
 - diagrammatic equations for
 - EA-EOM-CCSDT, 447
 - electron-attachment operator (\hat{R}), 445
 - energy derivatives, 444
 - EOM-CC *Ansatz*, 432–436
 - EOM-CC equations, 435
 - excitation energies, 437–444
 - algebraic EE-EOM-CCSDT equations, 439
 - diagrammatic equations for
 - EE-EOM-CCSDT, 437–440
 - left-eigenfunction equation, 440
 - excitation operator (\hat{R}_k), 433
 - right eigenfunctions of \mathcal{H} , 433
 - excited-state properties, 436
 - frequency-dependent properties, 454–461
 - higher-order properties, 449–454
 - initial state, 432
 - ionization potentials, 445–449
 - as limits of Rydberg series, 445
 - diagrammatic equations for
 - IP-EOM-CCSDT, 446
 - ionization operator, 445
 - IP-EOM-CCS, 447
 - IP-EOM-CCSD, 445, 447
 - IP-EOM-CCSDT, 445, 447
 - IP-EOM-CCSDT-3, 447
 - IP-EOM-CCSDTQ, 447
 - IP-EOM-CCSDTQP, 447
 - similarity-transformed, 448
 - target state, 432
 - unbalanced truncation, 444
 - VU-CC analogy, 488–490
- equivalent diagrams, 112, 115
- exchange integral, 7
- exchange operator, 7, 76
- excitation energies, *see* equation-of-motion CC, excitation energies
- exclusion-principle-violating (EPV) terms, 150–156
 - conjoint, 151, 155, 156
 - disjoint, 151, 155, 156
 - in expectation values, 349, 350
- expectation value
 - CC wave function, 347–352
 - one-body operator, 352–354
 - two-body operator, 353–355
- extensivity, 11–15, 156–157
 - disconnected clusters, 15–17
 - exponential *Ansatz*, 254–255
 - lack of in truncated CI, 12
 - N He atoms, 12–15, 34–36, 45–46
 - unlinked diagrams, 156–159
- extrapolation techniques, 185
- factorization of quadruple-excitation diagrams, 180–182
- factorization theorem, 158, 165–172
- factorized-denominator diagrams, 416
- FCC, *see* coupled cluster, full CC
- FCI, *see* configuration interaction, full CI
- Fermi level, 72
- Fermi vacuum, 72
 - in Fock-space MRCC, 475
 - in Hose–Kaldor approach, 227
 - in QDPT, 192–194
- Fock operator, 4, 7, 76
 - normal-product form, 85, 280
 - perturbed, 386–387
- Fock space, 54, 445, 475
 - sectors, 476
- Fock-space MRCC, 463, 475–495
 - intermediate Hamiltonian, *see* intermediate-Hamiltonian MRCC
 - valence universal, *see* valence-universal MRCC
- folded diagrams, 200, 201, 215–220
- folded resolvent lines, 202, 210–211
 - denominator, 202
- Fourier series, 456–458
- FS-CC, *see* Fock-space MRCC
- gauge-including atomic orbitals (GIAOs), 402, 403
- GIAO, *see* gauge-including atomic orbitals
- GMBPT, *see* many-body perturbation theory, generalized
- Goldstone diagrams, 111–113, 119
 - antisymmetrized, *see* antisymmetrized Goldstone diagrams
- Green’s function methods, 445
- \mathcal{H} , *see* coupled cluster, CC effective Hamiltonian
- \tilde{H} , *see* coupled cluster, effective Hamiltonian incorporating \hat{T}_1

- \hat{H}^{eff} , *see* effective Hamiltonian, of QDPT and MRCC
- \hat{H}^{int} , *see* intermediate Hamiltonian
- half-vertices, 111
- Hamiltonian, 9, 18
 - normal-product form, 83–85, 280–281
 - partitioning, 75–80
 - zero-order, 18, 75
- Hartree–Fock
 - gradients, *see* reference function, derivative
- Hartree–Fock (HF) theory, 4
 - average-interaction approach, 6–7
 - canonical, 4, 133
 - multiconfigurational, 6
 - noncanonical, 128, 129, 132, 133, 411
 - restricted, 5, 257, 343
 - open-shell, 5, 10, 257, 300, 316, 406, 410, 413–414, 417–418, 421–425, 431
 - open-shell high-spin case, 185, 410, 424
 - unrestricted, 5, 183, 257, 343, 386, 406, 417–418, 421–425, 431
 - high-spin case, 185, 410
- Hellmann–Feynman theorem, 362, 366, 367, 394, 395
- HF, *see* Hartree–Fock
- Hilbert space, 54
- Hilbert-space MRCC, 463, 465–474
 - state-specific, *see* state-specific MRCC
 - state-universal, *see* state universal MRCC
- HK, *see* Hose–Kaldor approach
- hole lines, 197
- hole states, 72
- Hose–Kaldor approach, 227–250
 - cancellations, 235–236
 - classification of one-electron states, 228
 - diagrams, first-order, 230–232
 - diagrams, second-order, 232, 236
 - disconnected diagrams, 235
 - Fermi-vacuum states, 227
 - level-shift operator, second-order ASG skeletons, 233
 - level-shift operator, third-order, 236–250
 - contribution status of diagrams, 242–250
 - contribution status of skeletons, 242–250
 - linked ASG skeletons, 239–242
 - linked Hugenholtz skeletons, 238
 - representative classes, 237
 - unlinked ASG skeletons, 243–245
 - unlinked Hugenholtz skeletons, 239
 - model states, 228
 - one-electron interaction, 228–230
 - wave operator, second-order ASG skeletons
 - for principal term, 234
 - for renormalization term, 234
- HS-CC, *see* Hilbert-space MRCC
- Hugenholtz diagrams, 118–123, 125–128
 - CC, 285
 - fourth-order energy
 - canonical HF case, 141
 - non-HF case, 146
 - QDPT level-shift operator
 - second-order, 206
 - third-order, 223
- Hugenholtz skeletons, 120
 - classification, 139
 - connection patterns, 139
 - conversion to ASG skeletons, 238–242
 - fourth-order
 - canonical HF case, 140
 - non-HF case, 145
- Hylleraas variation principle, 25–27
- hyperpolarizability, 362, 450
- IH, *see* intermediate Hamiltonian
- IH-CC, *see* intermediate-Hamiltonian MRCC
- IMS, *see* model space, incomplete
- independent particle approximation, 3–7
- insertion, 139, 148, 153, 158, 166, 172
- interaction line, *see* vertex
- interchange theorem, 365, 393, 396, 400, 401
- intermediate Hamiltonian (IH), 490
- intermediate-Hamiltonian MRCC, 463, 490, 494
 - augmented model space, 491
 - diagrammatic representation, 494
 - excitation energies
 - comparison of results, 495
 - function-space partitioning, 491
 - IH-CCSD, 494
 - IH-CCSDT, 495
 - diagrammatic representation, 494
 - intermediate space, 491
 - main model space, 491
 - projectors on subspaces, 491
 - similarity transformation method, 492–494
- intermediate normalization, 20, 186, 463
 - in valence-universal MRCC, 477, 480
- intruder states, 193, 466, 472, 490–491
- ionization potentials, *see* equation-of-motion CC, ionization potentials
- IP-EOM-CC, *see* equation-of-motion CC, ionization potentials
- Jeziorski–Monkhorst *Ansatz*, 465, 473
- Kohn–Sham reference state, 413
- Koopmans’ theorem, 447, 448
- ladder diagrams, 116, 120, 142, 177
- Λ equations, 375
 - diagrams for Λ_1 equations, 370
 - diagrams for Λ_2 equations, 372
 - diagrams for Λ_3 equations, 374
 - disconnected diagrams, 371–373
 - disconnected term, 369
 - effective-Hamiltonian form, 376–379
 - correspondence table, 378
 - diagrams for Λ_1 equations, 376
 - diagrams for Λ_2 equations, 377
 - diagrams for Λ_3 equations, 377
 - \hat{T} -free form, 379, 380
 - correspondence table, 379

- Λ equations, 367
- Λ operator, 365, 366
 - diagrams, 368
 - relationship to \hat{T}^\dagger , 374–375
- level-shift operator (\hat{W}), 49, 188
 - diagrams, 203–227
 - first order, 203
 - schematic, 196
 - second-order, 205–207
 - third-order, 220–225
 - modified, 194
- Li–Paldus approach, *see* state-universal MRCC
- linked diagrams, 1, 136
 - in QDPT, 198
- linked-diagram theorem, 2, 139, 152–153, 158–159
 - proof, 165–176
- London orbitals, *see* gauge including atomic orbitals
- magnetic perturbation, 402, 403
- magnetic susceptibility, 402
- many-body methods
 - history, 1
 - motivation, 10–11
- many-body perturbation theory energies
 - fourth-order
 - principal term, 138
 - renormalization term, 139
 - generalized (GMBPT), 418
- many-body perturbation theory (MBPT), 153, 156
 - comparison with CC, 341–344
 - computational aspects, 177–184
 - diagram summation techniques, 177–180
 - energy, third-order, 132
 - EPV terms, 154–156
 - generalized (GMBPT), 129, 411, 414
 - history, 1
 - relationship to CI, 159–164
- many-body perturbation theory energies
 - first-order, 131
 - second-order, 131–132, 154, 163, 342
 - comparison with CI, 159
 - third-order, 134, 154, 163, 342
 - comparison with CI, 159
 - fourth-order, 138–152, 154, 163, 342
 - approximation of CI, 160
 - ASG diagrams for principal term, 140, 144
 - cancellation of unlinked diagrams, 146–150
 - Hugenholtz diagrams for principal term, 141
 - Hugenholtz skeletons for principal term, 140
 - in canonical HF case, 139–144
 - linked quadruples contribution, 154
 - non-HF case, 144–146
 - principal term, 146, 154
 - renormalization term, 138, 154
 - role of EPV terms, 150, 156
 - singles contribution, 154
 - doubles contribution, 154
 - triples contribution, 154
 - without triples, 163, 342
 - fifth-order, 342
 - sixth-order, 342
- many-body PT wave functions
 - first-order, 135–136
 - second-order wave function, 136–138
- matrix elements
 - evaluation, 86–89
 - of operator products, 102–105, 118–123
- MBPT, *see* many-body perturbation theory
- MBPT(4)SDQ, *see* many-body perturbation theory energies, fourth-order without triples
- MBPT(n) ($n = 2, 3, \dots$), *see* many-body perturbation theory energies
- MCHF, *see* Hartree–Fock theory, multiconfigurational
- MCSCF, *see* self-consistent field, multiconfigurational
- MO coefficients, *see* transformation matrix
- model functions, *see* model states
- model space, 51, 186
 - complete, 193, 466
 - disadvantages, 193, 466, 490–491
 - in valence-universal MRCC, 477
 - in Hose–Kaldor approach, 228
 - selection, 228
 - in QDPT, 192–194
 - in state-universal MRCC, 465–467
 - in valence-universal MRCC, 475
 - incomplete, 466
 - in QDPT, 227–250
 - in valence-universal MRCC, 477
 - quasicomplete, 480
- model states, 51, 186
- Møller–Plesset partitioning, 80
- Møller–Plesset perturbation theory, 80
- MRCC, *see* multireference coupled cluster
- MRCI, *see* configuration interaction, multireference
- multiplicity, *see* spin multiplicity
- multireference coupled cluster, 462–495
- multireference methods, 6, 11, 431
 - configuration interaction, *see* configuration interaction, multireference
 - coupled cluster, *see* multireference coupled cluster
 - perturbation theory, *see* quasidegenerate perturbation theory
- N He atoms example
 - in BWPT, 34–36
 - in CC, 251–254
 - in CI, 12–15
 - in MBPT, 157–159
 - in RSPT, 46
- N -dependence of diagrams, 157–159

- natural orbitals, 10, 413
- non-HF case, 129, 132, 133, 136, 138, 144–146
- normal order, *see* normal product
- normal product, 67–68
 - relative to Fermi vacuum, 74–75
 - with contractions, 69
 - relative to Fermi vacuum, 75
- notation, 2–3
 - excitation level, 3
- nuclear magnetic resonance (NMR) chemical shifts, 402
- nuclear magnetic shielding, 402
- Ω , *see* wave operator
- one-body basis, 54
- one-body operators
 - diagrammatic representation, 92–100
 - product, 100–105
- one-body states
 - core, 193
 - valence, 193
 - virtual, 5, 193
- open-shell perturbation theory, *see* degenerate perturbation theory
- open-shell states, 185, 410
 - difficulties for single-reference methods, 431–432, 462
 - high-spin, 185, 410
 - in state-universal MRCC, 471
 - in valence-universal MRCC, 475
 - low-spin, 185, 410, 440
 - EOM-CC, 441
 - open-shell singlets, 185, 410
 - EOM-CC, 440–441
 - zero-order approximation, 440
- ROHF, 5
- spin-multiplicity monitoring, 421–425, 441
- UHF, 5
- operators
 - hole–hole, 94
 - hole–particle, 98
 - normal-product form, 80–83
 - one-body, 80–81
 - two-body, 81–83
 - not in normal-product form representation, 123–128
 - particle–particle, 92
 - particle–hole, 97
 - representation, 59–65
 - invariance under unitary transformation, 65–67
- orbital energy, 5, 75, 76
- orbital relaxation, 385–396, 425, 488
- orbitals
 - including spin, *see* spinorbitals
 - localized, 5, 411
 - spatial, 5, 182–184, 407–410
- orthogonal space, 186
- particle lines, 197
- particle states, 72
- passive lines, 197, 204
- perturbation operator, 19, 75–78
 - GMBPT, 412
 - normal-product form, 83–85, 194–195
 - periodic, 455
 - RSPT, 128–129
- perturbation theory
 - many-body, *see* many-body PT
- perturbation theory (PT)
 - convergence, 11, 194
 - diagrammatic expansion, 130–164
 - formal, 18–53
 - general derivation, 29–33
 - other approaches, 53
 - similarity transformation, 46–53
 - time-dependent, 454–461
- phase factor, 106–111
 - in QDPT, 211–215
- physical vacuum, 67, 72
- Planck's constant, 3
- polarizability
 - frequency-dependent, 459–461
 - tensor, 362
- potential-energy curve, 344, 345
- potential-energy surface, 5, 344, 431, 462
 - appropriateness of SS-CC, 472
 - discontinuities, 491
 - gradient, 361, 363, 365, 381, 387–405, 448
 - Hessian, 361, 381
- principal term of m th-order energy, 39
- projection operator, 27–29
 - on complementary space, 463
 - on model space, 186, 463
 - on orthogonal space, 186
 - sector projectors, 476
- properties
 - as energy derivatives, 361–365
 - vs. as expectation values, 362–363
 - excited states, 436
 - frequency-dependent using EOM-CC, 454–461
 - higher-order, 362
 - using EOM-CC, 449–454
 - in CC theory, 347–405
 - response treatment, 361–365
- pseudolinearity, 329, 376
- QCISD, *see* configuration interaction, quadratic
- QDPT, *see* quasidegenerate perturbation theory
- QHF, *see* quasi-Hartree–Fock theory
- QRHF, *see* quasi-Hartree–Fock theory, restricted
- quadruples corrections, 162
- quasidegenerate perturbation theory (QDPT), 51, 185–250
 - classification of one-electron states, 193
 - convergence, 194

Padé approximants, 185

particle–hole formalism, 71–75

- diagrammatic notation, 195–198
- folded diagrams, 215–220, 225, 226
 - schematic representations, 215–217, 225, 226
- formal, 185–191
- incomplete model space, *see* Hose–Kaldor approach
- schematic representations, 198–203, 205, 207
- similarity transformation, 46–53
- quasienergy, 455
- quasi-equivalent external lines, 283
- quasi-Hartree–Fock (QHF) theory, 395
 - restricted, 410, 414
- quasiloop, 135
- quasi-operator, 72
- Rayleigh–Schrödinger perturbation theory, 18–27, 37–40
 - bracketing procedure, 41–42
 - extensivity, 45–46
 - fourth-order energy
 - renormalization term, 39
 - non-diagonal case, 40–41
 - summary of formal results, 43–44
- reaction operator, *see* level-shift operator
- reference energy, 73, 79
 - derivative, 393–396
- reference function
 - perturbed, 385–396
- reference state, 71–73, 78
 - arbitrary, 411–415
 - Kohn–Sham determinant, 413
 - non-diagonal case, 40–41, 415
 - QRHF, 414
 - ROHF, 413–414
- renormalization term, 34, 39, 139, 146–150
 - representation by insertion, 139
- resolvent, 31–32, 130
 - denominator, 39
 - and folded resolvent lines, 202
 - effective (\mathcal{R}), 364
 - EOM-CC states, 452
 - frequency-dependent, 460
 - line, 130–131, 149
 - folded, 202
 - non-diagonal case, 40
 - quasidegenerate case, 52, 189
- resonance, 458
- response density matrix, 381–385
 - anti-Hermitian part, 403
 - asymmetry to time inversion, 382
 - excited states, 436
 - Hermitian average, 401
 - non-Hermiticity, 382–385, 399–400
 - one-body, 381–383, 396
 - diagrams, 381–382
 - two-body, 383, 396
 - diagrams, 384
 - permutational symmetry, 383
- RHF, *see* Hartree–Fock theory, restricted
- ring diagrams, 117, 120, 142
- ROHF, *see* Hartree–Fock theory, restricted, open-shell
- RSPT, *see* Rayleigh–Schrödinger perturbation theory
- Rydberg states, 445
- \tilde{S} operator, *see* valence-universal MRCC, auxiliary operator
- SCF, *see* self-consistent field
- Schrödinger equation
 - connected form, 295
 - normal-product form, 85, 280
 - time-dependent, 455
- second quantization, 54–89
 - history, 1
- sectors of rock, space, 445, 473–477, 486, 493
- self-consistent field, 4
 - multiconfigurational, 6
- semicanonical transformation, 129, 315, 413–415
- size extensivity, *see* extensivity
- size-consistency, 12
- Slater determinants, 4
 - diagrammatic representation, 91–92
- SOS form, *see* sum over states form
- spin
 - eigenvalues, 422
 - expectation value, 422
 - computation, 422–425
 - projected value, 422
 - raising and lowering operators, 423
- spin contamination, 417, 421
- spin-flip CC, 441, 462
- spin multiplicity, 421
 - monitoring, 421–425
- spin summations, 182–184
 - in CC, 406–411
 - Brueckner orbital case, 410
 - diagrams for CCD, 407
 - low-spin open-shell case, 410
 - orthogonally spin-adapted case, 410
 - QRHF case, 410
 - ROHF case, 410
 - UHF case, 410
- spinorbital basis, *see* one-body basis
- spinorbitals, 4, 182–184
 - canonical HF, 5
 - localized, 5, 411
 - noncanonical HF, 5
 - semicanonical, 129, 315
- SRCC, *see* coupled cluster
- SS-CC, *see* state-specific MRCC
- state-specific MRCC, 463, 471–474
 - Brillouin–Wigner form, 474
 - comparison of results, 474
 - equations, 473–474
 - extensivity, 474
 - redundancy, 473
 - sufficiency conditions, 473, 474
- state-universal MRCC, 463, 465–471
 - coupling term, 469

- diagrammatic notation, 467
- disconnected clusters, 467
- equations, 468–469
- extensivity, 467
- internal excitations exclusion, 465
- local active spinorbitals, 467
- matrix elements, 469–471
- STEOM-CC, *see* equation-of-motion CC, similarity-transformed
- SU-CC, *see* state-universal MRCC
- sum-over-states (SCS) form, 449, 454, 460
- symmetry-adapted cluster CI, 431
- symmetry breaking, 5, 402, 431
- symmetry restriction, 5
- \hat{T}_1 operator
 - alternative treatment, 418–421
 - role, 300–301, 425–426
- terminology, 3
- Thouless theorem, 257, 300, 413, 414, 419
- time axis, 90, 91
- time ordering, 90–91
- transformation matrix, 51, 53, 187, 387, 464, 473
 - perturbed, 388
- transition moment, 436
- two-body operators
 - diagrammatic representation, 111–129
 - product, 113–118
- UHF, *see* Hartree–Fock theory, unrestricted
- unlinked diagrams, 125, 128, 136, 139, 146–150, 156–159, 172
 - and extensivity, 156–159
 - in QDPT, 198
- unlinked skeletons, 139
- unrestricted summation, 104, 115
- vacuum expectation value, 67, 70, 113–118
- vacuum gap, 125, 140
- valence lines, 195
 - folded, 199
- valence states, 192, 193, 228
- valence-universal MRCC, 475–490
 - auxiliary operator (\tilde{S}), 478–483
 - diagrammatic representation, 480
 - normal order of products, 480–482
 - Bloch equations, 483–488
 - diagrammatic representation, 484, 485, 487
 - hierarchical solution, 485
 - effective Hamiltonian, 477
 - diagrammatic representation, 486
 - EOM-CC analogy, 488–490
 - factorization of disconnected diagrams, 480–482
 - intermediate normalization validity, 477, 480, 487
 - model space, 475
 - complete, 486
 - incomplete, 487
 - quasicomplete, 480
 - sector projectors, 476
 - spectator amplitude, 488
 - selective summation, 488
 - subsystem embedding condition, 485, 486
 - consistency requirement, 487
 - wave operator, 477–483
 - simplifications, 482–483
- vertex
 - one-body, 93
 - interpretation, 95–97
 - two-body, 111, 118
 - interpretation, 111–113, 119, 121
- virtual states, 192, 193, 228
- VU-CC, *see* valence-universal MRCC
- \hat{W} operator
 - in MBPT and CC, 84, 280
 - in QDPT and MRCC, *see* level-shift operator
 - in single-reference RSPT, 38
- wave operator (Ω), 48, 51, 53, 186, 254, 433, 463–464
 - diagrams, 203–227
 - first-order, 204–205
 - schematic, 197
 - second-order, 207–211
 - third-order, 225–227
 - in state-specific MRCC, 472
 - in state-universal MRCC, 465
 - in valence-universal MRCC, 475, 477–483
- weight factor, 112, 115
 - in QDPT, 211–215
- Wick's theorem, 69–70
 - generalized, 85–86
 - proof, 70–71
 - relative to Fermi vacuum, 74–75
- Wigner's $2n + 1$ rule, 24–25, 327
- Z-vector method, *see* interchange theorem
- zero-order approximation, 6
 - in QDPT, 203
 - multiconfigurational, 6
- zero-order energy, 79
- zero-order function, *see* reference state